

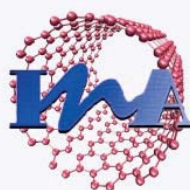


NANOSPAIN 2009

Zaragoza (Spain) March 9-12, 2009

PHANTOMS
foundation

UAM
UNIVERSIDAD AUTONOMA
DE MADRID



CEM
CENTRO ESPAÑOL
DE METROLOGIA

ibec Institute for bioengineering
of Catalonia

DONOSTIA INTERNATIONAL
PHYSICS CENTER



U
UNIVERSITAT DE BARCELONA
B

CSIC
CONSEJO SUPERIOR DE INVESTIGACIONES CIENTÍFICAS

FCT Fundação para a Ciência e a Tecnologia
MINISTÉRIO DA CIÊNCIA, TECNOLOGIA E ENSINO SUPERIOR Portugal

NanoSciences
GRAND SUD - OUEST



Edited by



Parque Científico de Madrid - Pabellón C – 1ª Planta
Ctra. Colmenar Viejo Km. 15
Campus de Cantoblanco – Universidad Autónoma de Madrid
28049 Madrid, Spain
Fax: +34 91 497 3471
E-mail: antonio@phantomsnet.net
WEB: <http://www.phantomsnet.net>

Efficient MVL Circuit Design with Use of p-CNTFETs and n-CNTFETs

S. Abdollahvand, E. Shahamatnia

Islamic Azad University, Science & Research Branch,

Daneshgah Sq., Chahardivari Ave., Tehran, Iran

S.Abdollahvand@sr.iau.ac.ir

Introduction

As the miniaturization of silicon based circuits reaches its physical limits, the exigency of substitute technologies emerges. Special characteristics of CNT such as high mobility of electrons, ballistic transport and high I_{on} - I_{off} ratio, has introduced it as an appropriate successor to silicon MOSFET. Whereas the threshold voltage cannot be decreased deliberately due to the scaling limitations of MOSFETs, in CNTFETs different threshold voltages can be obtained simply by defining different nanotube diameters because the threshold voltage is in reverse proportion with the nanotube diameter [1]. This feature of carbon nanotubes has been exploited in implementation of multiple valued logic (MVL) circuits. One of the principal ways in MVL circuit implementation is by using basic operators such as tsum, literal, min and max. In [2] we introduced a new approach for ternary Galois field design that employed different paths to obtain different logic levels and showed that this approach is more efficient than using basic MVL operators. In [3] we presented another design for Galois field which employed sharing paths method to obtain output logical levels. In this paper we propose a CNTFET design for multiplication and addition circuits that not only take advantages of these two but also further reduces the number of transistors by the idea of bridging a resistor between CNTFETs.

The Circuits Functionality

In this section we specify the proposed design of ternary multiplication and addition operators using CNTFETs. In our implementation, supply voltage has been chosen to be 1.5V (V_{DD}) which ensures sufficient static noise margin. This implementation consists of both p-CNTFETs and n-CNTFETs with two different diameters, 1.4nm and 0.5nm. These nanotube transistors have the corresponding threshold voltages $V_{th1} = 300\text{mV}$ and $V_{th2} = 840\text{mV}$ respectively. Input voltage values for logics 0, 1 and 2 are $V_{in} < V_{th1}$, $V_{th1} < V_{in} < V_{th2}$ and $V_{th2} < V_{in}$ respectively. Speaking in the ternary logic, if output voltage lies between 0 to $\frac{V_{DD}}{3}$ then the output will be logic 0, and in case that output voltage lies between $\frac{V_{DD}}{3}$ to $\frac{2V_{DD}}{3}$ then the output will be logic 1, and if the output voltage is greater than $\frac{2V_{DD}}{3}$ then the output will be logic 2.

Figure 1 shows the circuit realization of addition and multiplication operations. In both circuits, output is set to logic 0 using the pull up network. In the pull down network, resistor paths set the circuit output to logic 1 by voltage division and the non-resistor paths set the output to logic 2. According to the special arrangement of CNTFETs and their specific threshold voltages, in multiplication circuit, fig.1 (a), if at least one of the input values is zero then all the transistors will go off and the circuit output will be zero. When the output is to be logic 1, the voltage is divided between R and R_1 . For example if inputs $a=b=2$ then the transistors T_1 and T_6 goes on and the output voltage range is as expressed by Eq.1. Since the R_1 plays a rule only when the output is logic 1, by solving the Eq.1 the relation between R and R_1 is obtained by Eq.2. In cases that inputs are $a=1$, $b=2$ or when $a=2$, $b=1$, then the transistors T_1, T_2, T_3 or T_4, T_5, T_6 will go on and the non-resistor path will be active. Hence the Z will be completely discharged and this brings the output of the circuit to logic 2. The functionality of addition circuit, fig.1 (b), can be analyzed in a similar way.

$$\frac{V_{DD}}{3} \leq V_{DD} \frac{R_4}{R+R_1} \leq \frac{2V_{DD}}{3} \quad (\text{Eq. 1})$$

$$\frac{R}{2} \leq R_1 \leq R \quad (\text{Eq. 2})$$

Conclusion

In this paper we have introduced an efficient novel design for CNTFET ternary multiplication and addition circuits which by using resistor(s) (R_1) between transistors as the bridge, makes it possible to reduce the total number of transistors. The proposed approach can be applied to design efficient higher radix MVL circuits.

In [4] multiplication and addition circuits have been designed by use of CNTFET multiplexers. The techniques employed in our proposed design along with exploiting the relationship between V_{th} and nanotube diameter, have made it an efficient design which uses the minimum number of transistors. The number of transistors in multiplication and addition circuits of [4] is 16 each, but in our design these numbers are 8 and 14 respectively. It should be noted that according to [1], the NOT gate is made up of two CNTFETs.

References:

- [1] A.Raychowdhury, K.Roy, IEEE International Symposium on Multiple-Valued Logic, No. **34**, (19-22 May 2004), pp:14-19.
- [2] S. Abdollahvand, E.Shahamatnia, P.Keshavarzian and K.Navi, ANSI Journal of Applied Science, Submitted May 2008, Accepted for publication in upcoming issue.
- [3] S.Abdollahvand, E.Shahamatnia and K.Navi, 2nd International Congress on Nanoscience & Nanotechnology(ICNN), (28-30 Oct. 2008).
- [4] N.Al-Rabadi.A, ELEC.ENERG, **2** (2007), pp. 175-186.

Figures:

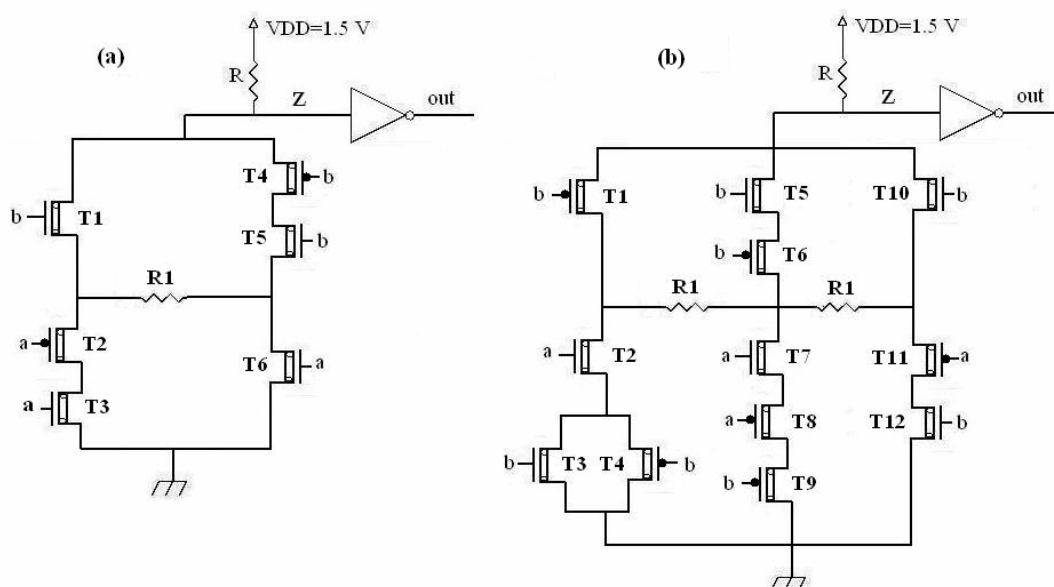


Fig.1. (a): GF(3) multiplication circuit using CNTFETs. The diameter of transistors T1 and T6 is 0.5nm and the diameter of the other transistors is 1.4nm. Resistors R and R₁ are 100k Ω . (b): GF(3) addition circuit using CNTFETs. The diameter of transistors T1, T2, T3, T4, T10 and T11 is 0.5nm and the diameter of the other transistors is 1.4nm. Resistor

PREPARATION AND EVALUATION OF ALGINATE-METHOTREXATE MICROSPHERES

Saba afifi, Shohre Alipour.S, Hashem Montaseri

Department of Pharmaceutics, Faculty of Pharmacy, Shiraz University of Medical Sciences, P.O. Box 71345-1583, Shiraz, Iran
Saba_afifi@yahoo.com

Introduction:

Recently, much research has been focused on degradable polymer microspheres for drug delivery. Administration of chemotherapeutic agents such as methotrexate via such systems is advantageous. Because microspheres can be ingested or injected; they can be tailored for desired release profiles and in some cases even provide organ-targeted release. So lower dosed and less frequent injections as a result of localized therapy and controlled release make a microspheres drug delivery system a good candidate for cancer therapy. Among the wide spectrum of polymers, alginate is so popular because of its safety, biocompatibility, biodegradability and non-immunogenicity.

Experimental Method:

In this study we have used emulsification- internal gelation method. The alginate microspheres were produced by cross-linking alginate globules dispersed in a continuous organic phase using various concentrations of calcium chloride solution. Different parameters in formulation have been studied such as alginate type (low viscosity & medium viscosity) and concentration (1-5%), calcium concentration (0.25-3.5%), surfactant concentration (1-3%) and curing time. Microspheres' size was determined by laser diffraction particle size analyzer. The size of microspheres and amount of drug loaded was the comparison factor for different formulations. The encapsulation efficiency was determined by HPLC method.

Results and Discussion:

The formulation containing a mixture of 0.5%HPMC and 4.5% alginate cured in 0.75% calcium chloride for 20 minutes was chosen as the best formula regarding the particle size and the loading efficiency. The resulting microspheres had a volume mean diameter of 6 μm and loading efficiency of about 20%.

Key words: methotrexate, alginates, Microspheres

References:

- [1] Anamika Roy, J. Bajpai, A.K. Bajpai ,Dynamics of controlled release of chlorpyrifos from swelling and eroding biopolymeric microspheres of calcium alginate and starch *Carbohydrate Polymers, In Press.*
- [2] Chaoyang Wang, Hongxia Liu, Quanxing Gao, Xinxing Liu, Zhen Tong, Alginate–calcium carbonate porous microparticle hybrid hydrogels with versatile drug loading capabilities and variable mechanical strengths *Carbohydrate Polymers, Volume 71, Issue 3, 8 February 2008, Pages 476-480.*

- [3] Susana Martins, Bruno Sarmento, Eliana B. Souto, Domingos C. Ferreira , Insulin-loaded alginate microspheres for oral delivery – Effect of polysaccharide reinforcement on physicochemical properties and release profile *Carbohydrate Polymers*, Volume 69, Issue 4, 2 July 2007, Pages 725-731.
- [4] R. Rastogi, Y. Sultana, M. Aqil, A. Ali, S. Kumar, K. Chuttani, A.K. Mishra, Alginate microspheres of isoniazid for oral sustained drug delivery *International Journal of Pharmaceutics*, Volume 334, Issues 1-2, 4 April 2007, Pages 71-77.
- [5] Renu Singh Dhanikula, Patrice Hildgen ,Influence of molecular architecture of polyether-co-polyester dendrimers on the encapsulation and release of methotrexate *Biomaterials*, Volume 28, Issue 20, July 2007, Pages 3140-3152
- [6] A. Lebugle, A. Rodrigues, P. Bonnevalle, J. J. Voigt, P. Canal, F. Rodriguez, Study of implantable calcium phosphate systems for the slow release of methotrexate *Biomaterials*, Volume 23, Issue 16, August 2002, Pages 3517-3522

A NOVEL APPROACH FOR MANY-ELECTRON TRANSPORT IN NANO-ELECTRONIC DEVICES WITH FULL COULOMB INTERACTION

G. Albareda and X. Oriols

Departament d'Enginyeria Electrònica, Universitat Autònoma de Barcelona, 08193

Bellaterra, Spain

guillem.albareda@uab.es

The exact computation of a system of interacting electrons is an extremely complicated issue because the motion of one electron depends on the positions of all others (i.e. particles are correlated). Thus, the prediction of the collective behaviour of many electrons is still a very active field of research in nano-electronics, quantum chemistry, nano-biology, quantum computing, etc. The accurate treatment of the electron-electron correlations in nanoelectronic devices is even a more difficult task because we deal with non-equilibrium open systems.

In this conference, we will present a novel approach for the accurate treatment of electron-electron correlations in many-electron open systems without any perturbative or mean-field approximation [1,2]. In particular, a set of $N(t)$ particles with full Coulomb interaction inside an open system is described by the following many-particle Hamiltonian [2]:

$$H(\vec{r}_1, \dots, \vec{r}_{N(t)}, \vec{p}_1, \dots, \vec{p}_{N(t)}, t) = \sum_{k=1}^{N(t)} \left\{ K(\vec{p}_k) + q_k \cdot W_k(\vec{r}_1, \dots, \vec{r}_{N(t)}, t) - \frac{1}{2} \sum_{\substack{j=1 \\ j \neq k}}^{N(t)} q_k \cdot V(\vec{r}_k, \vec{r}_j) \right\} \quad (1)$$

where $K(\vec{p}_k)$ represents the kinetic energy of the k th electron, $V(\vec{r}_k, \vec{r}_j)$ refers to the exact Coulomb interaction between the j th and k th electrons, and the term $W_k(\vec{r}_1, \dots, \vec{r}_{N(t)}, t)$ is a particular solution of the Poisson equation taking into account all charges excepting that of the k th electron. Notice that the position and momentum, \vec{r}_k and \vec{p}_k , in the Hamiltonian (1) can be either classical variables or quantum operators. Classically, the solution of the many-particle Hamiltonian (1) is obtained via a coupled system of Newton-like equations with a different electric field for each particle [2]. The quantum mechanical solution of (1) is achieved by using a quantum trajectory algorithm that includes exchange interaction [1]. The boundary conditions of the Hamiltonian (1) on the borders of the open system (in the real 3D space representation) include the Coulomb interaction between particles inside and outside of the open system [2]. The many-particle Hamiltonian provides the same electrostatic description obtained from the image-charge method, but it has the fundamental advantage that it can be directly implemented into realistic (classical or quantum) electron device simulators via a 3D Poisson solver. The merit of the quantum solution is certainly remarkable because the computational burden associated with the direct (i.e. without any approximation) solution of the many-particle wave-function is only accessible for very few (2,3..) electrons [3].

In this conference, we will show the computational viability of building a powerful time-dependent nanoscale device simulator from our many-particle algorithm [1,2]. We will present the numerical computation of the DC behaviour for a (classical) double gate field effect transistor (1D DG-FET) and a (quantum) resonant tunnelling diode (RTD). The numerical results from (1) will be compared with those computed from time-dependent mean-field algorithms showing important quantitative differences (see Figs. 1-4). We will also discuss the role of the electron-electron correlations on the frequency-dependent performance of nanoelectronic devices and on its electric power (see Fig. 5). In particular, power consumption has been identified recently by the IRTS [4] as one of the top three overall challenges that will drive nanoelectronic industry for next years. We notice that electric power is directly proportional to the force “felt” by each electron. This force does not depend on an average (mean) electric field, but on the gradient of the term $W_k(\vec{r}_1, \dots, \vec{r}_{N(t)}, t)$, in (1), which

discounts the effect of the k th electron on itself. The mean-field approximation of the electron-electron interaction gives an important error when computing the electric power of nanoelectronic devices (the single-transistor error drawn in fig. 5 has to be multiplied by the number of transistors in present-day CPUs).

In conclusion, within the effective mass approximation, a novel approach for the DC/AC current, noise, and power predictions of nanoelectronic devices with full Coulomb (and exchange) interaction will be presented. Classical and quantum examples for two different nanoelectronic devices demonstrate the computational viability of our many-particle algorithm which is able to treat electron dynamics without any (mean-field or perturbative) approximation in the description of the electrostatic and exchange interactions for a larger number (≈ 50) of transport electrons [1,2].

References:

- [1] X. Oriols, Phys. Rev. Lett. 98, 066803 (2007).
- [2] G. Albareda, J. Suñe and X. Oriols, Phys. Rev. B, in press, (2009).
- [3] "It would indeed be remarkable if Nature fortified herself against further advances in knowledge behind the analytical difficulties of the many-body problem". Max Born, 1960.
- [4] International Technology Roadmap for Semiconductors, 2008 Update.

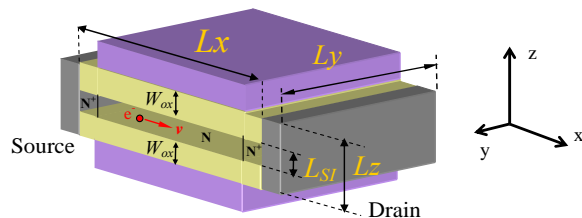


Figure 1: Schematic representation of the 1D DG-FET.

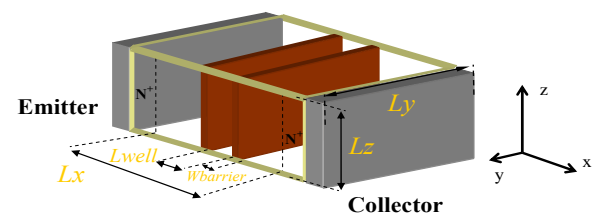


Figure 3: Schematic representation of the RTD.

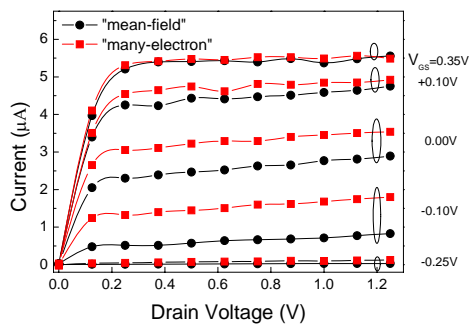


Figure 2: Average current for the 1D DG-FET of Fig. 1, using the many-electron and mean-field algorithms. The open ellipses include results with the same gate voltage indicated on the right.

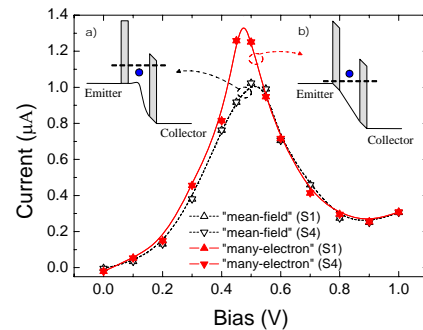


Figure 4: Average current through surfaces S1 (emitter surface) and S4 (collector surface) for the RTD of Fig. 3 as a function of bias, using the many-electron (solid symbols) and mean-field (open symbols) algorithms (lines are a visual help). Non-uniform voltages steps are used to focus on the resonant region. Insets show schematically the effect of an electron crossing an "empty" well on its own electrostatic potential using the mean-field a) or the many-electron b) approaches.

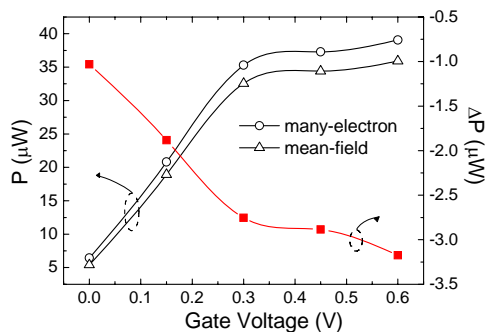


Fig. 5. Time averaged values for the electric power computed from the many-electron method and the mean-field approach in a bulk DG-FET. Differences between time averaged powers, $\langle P \rangle_{\text{mean-field}}$ and $\langle P \rangle_{\text{many-electrons}}$, are also presented. Results are presented per transistor.

Vortex dynamics and vortex lattice reconfiguration in superconducting-magnetic hybrids.

Alejandro Alija¹, David Pérez de Lara², Elvira M. González², José I. Martín¹, María Vélez¹, José M. Colino³, José V. Anguita⁴ José L. Vicent².

1. Depto. Física, Universidad de Oviedo - CINN, Oviedo, Asturias, Spain.
2. Depto. Física de Materiales, Universidad Complutense de Madrid, Spain.
3. Dpto. Física Aplicada, Universidad de Castilla - La Mancha, Ciudad Real, Spain
4. Instituto de Microelectrónica de Madrid (CNM-CSIC), Spain.

alija@condmat.uniovi.es

The study of vortex dynamics in type-II superconductors is a challenging field because of the mixed state presents a rich variety of behaviors [1,2]. Interactions between vortices and intrinsic or artificial pinning centers have been the subject of many studies. In this work, amorphous superconducting films (Mo_3Si) have been grown on top of array of nano-metric magnets. These periodic magnetic centers (Fig.1) have been fabricated on Si substrates by Electron Beam Lithography and sputtering techniques. In the mixed state, the competition between the intrinsic and random pinning potential of the superconducting film and the artificial induced periodic pinning potential governs the vortex lattice behavior [3,4]. A classical tool to explore this competition is given by magneto-resistance measurements. The dc measurements were performed in a liquid He^4 cryostat with a superconducting magnet up to 5T. The magnetic field is always applied perpendicular to the substrate and a $40\mu\text{m}$ wide bridge was used to carry out the resistance measurements (see Fig.2). Close to critical temperature, the periodic potentials could overcome the random potentials, then the vortex lattice dynamics shows collective effects which are related with the array dimension and symmetry. The periodicity in the minima in figures 3 and 4 is related to the corresponding matching field to pin the vortex lattice with the artificial pinning lattice. We will show in these hybrid systems, i.e. $\text{Mo}_3\text{Si}/80\text{ nm Ni dots}$, enhancements of these matching effects between the vortex lattice and the array unit cell, and different vortex lattice configurations respect to other systems made of superconducting Nb films.

This work was partially support by the Spanish Ministerio de Ciencia e Innovación by grants NAN2004-09087, FIS2005-07392, FIS2008-06249, Consolider CSD2007-00010, CAM grant S-0505/ESP/0337, Fondo Social Europeo and Junta de Comunidades de Castilla-La Mancha Grant No. PAI08-0067-2673 and FICYT contracts No. BP06-109 and No. IB08-106.

References:

- [1] AM Campbell and JE Evetts, Adv. Phys. 21 (1972) 199
- [2] G Blatter et al, Rev. Mod. Phys. 66 (1994) 1125
- [3] JI Martín et al, Phys. Rev. Lett. 79 (1997) 1929
- [4] JE Villegas et al, Science 302 (2003) 1188

Figures:

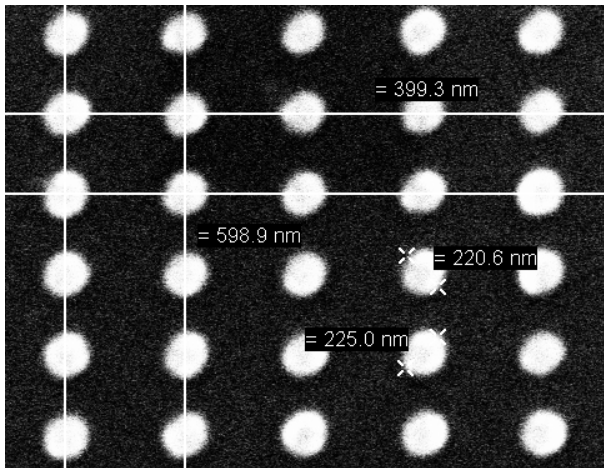


Fig.1. Scanning electron microscope image of 220 nm diameter, 80 nm thick Ni dots in 400 x 600 nm lattice in $100 \mu\text{m}^2$ square array.

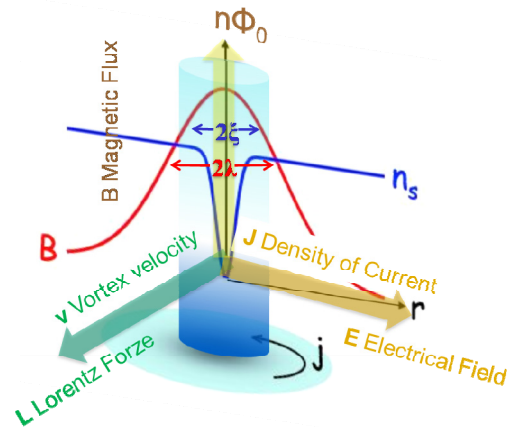


Fig.2. Individual superconductor vortex scheme. The Lorentz Force appears as a consequence of a driven current applied perpendicular to the magnetic flux which is trapped into the vortex.

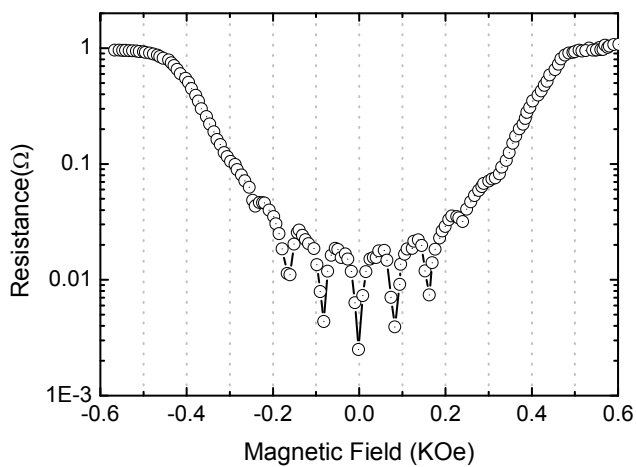


Fig.3. 100 nm Nb film ($T_c = 8.2\text{--}8.7 \text{ K}$) on top of 80 nm thick, Ni dots in 400 x 600 nm lattice.

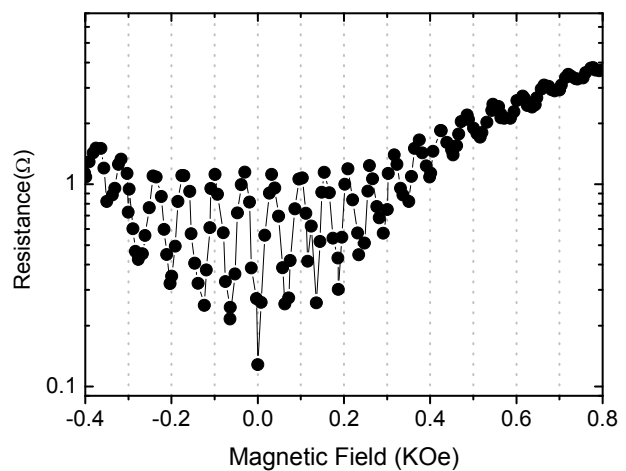


Fig.4. 100 nm Mo_3Si film ($T_c = 7.3\text{--}7.5 \text{ K}$) on top of 80 nm thick, Ni dots in 400 x 600 nm lattice.

LATERALLY COUPLED IN(Ga)As QUANTUM DOT PAIRS ON GaAs NANOHOLES

P. Alonso-González, J. Martín-Sánchez, Y. González, B. Alén, D. Fuster and L. González*
palonso@imm.cnm.csic.es

Abstract:

The formation of coupled QD permits a precise study of coupling and coherence strictly necessary for the creation of new functional units in the field of quantum computing and communication. In this way, vertically stacked self assembled QD has been well studied during the last years permitting a direct observation of controlled coupling between two QD [1]. For applications, however, the development of a lateral configuration of coupled nanostructures is highly desirable as it would extend the possible quantum coupling in two dimensions. Besides, it would facilitate the gating technology for the electrical control of the quantum light emission. Experimentally, laterally coupled pairs of QD have been recently achieved [2] by using a fabrication method based on the growth selectivity of QD inside previously *in situ* etched nanoholes. In this sense, droplet epitaxy technique has emerged as an analogous *in situ* fabrication strategy that permits to obtain low density nanoholes templates on GaAs substrates directly in a self-assembled way. In particular, by means of InAs selective growth at these nanoholes, it has been possible to form different nanostructures distributions [3,4] that present good optical properties at the single nanostructure level [5]. Moreover, the capping process of these nanostructures eventually results in the formation of mounds that are spatially located over the buried QD [4]. This effect, which permits the posterior top surface addressing of the active nanostructures, is highly useful for new quantum optoelectronics devices fabrication.

In this work we have studied the formation of low density lateral pairs of InAs QD ($2 \times 10^8 \text{ cm}^{-2}$) on GaAs templates consisting on nanoholes formed by GaAs droplet epitaxy. Our results show that the As_2 pressure used during InAs growth is a key parameter that permit to control the formation of either single QD or pairs of QD inside the nanoholes. Under the appropriate conditions we can obtain a 98% of nanoholes occupancy by QD pairs. The photoluminescence (PL) emission of the ensemble of lateral pairs of QD, in particular emission peak and full width at half maximum (FWHM) as a function of excitation intensity and temperature, has revealed typical signature previously reported for lateral coupled quantum systems [6].

References:

- [1] A. U E. A. Stinaff, M. Scheibner, A. S. Bracker, I. V. Ponomarev, V. L. Korenev, M. E. Ware, M. F. Doty, T. L. Reinecke, and D. Gammon, *Science* **311**, (2006) 636.
- [2] G.J. Beirne, C. Hermannstädter, L. Wang, A. Rastelli, O. G. Schmidt, and P. Michler, *Phys. Rev. Lett.* **96**, (2006) 137401.
- [3] Zh. M. Wang, B. L. Liang, K. A. Sablon, and G. J. Salamo, *Appl. Phys. Lett.* **90**, (2007) 113120.
- [4] P. Alonso-González, D. Fuster, L. González, J. Martín-Sánchez, and Y. González, *Appl. Phys. Lett.* **93**, (2008) 183106.
- [5] P. Alonso-González, B. Alén, D. Fuster, Y. González, L. González, and J. Martínez-Pastor, *Appl. Phys. Lett.* **91**, (2007) 163104.
- [6] B. L. Liang, P. S. Wong, N. Nuntawong, A. R. Albrecht, J. Tatebayashi, T. J. Rotter, G. Balakrishnan, and D. L. Huffaker, *Appl. Phys. Lett.* **91**, (2007) 243106.
- [7] T. v. Lippen, A. Yu. Silov, and R. Nötzel, *Phys.Rev.B* **75**, (2007) 115414.

Figures:

Figure 1

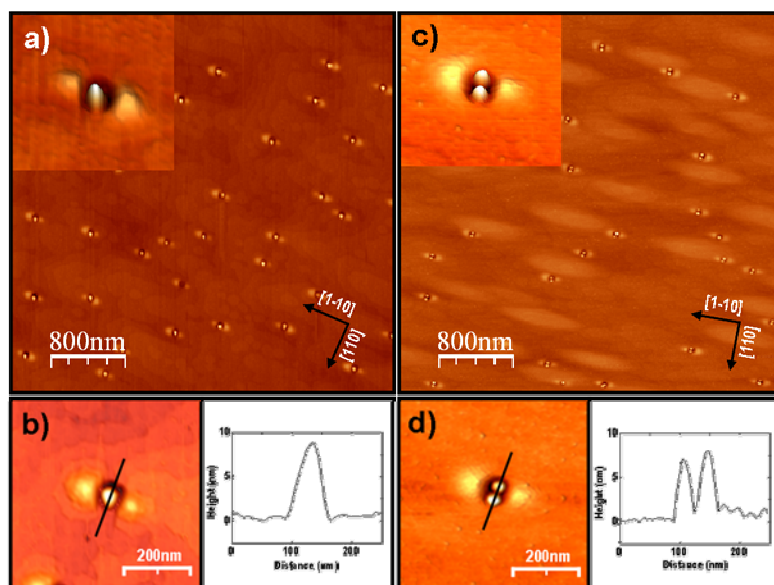


Figure 1: AFM topographic images showing the single (Figure 1a and 1b) and double configuration (Figure 1c and 1d) of InAs quantum dots depending on the As_2 pressure used during InAs deposition.

Figure 2

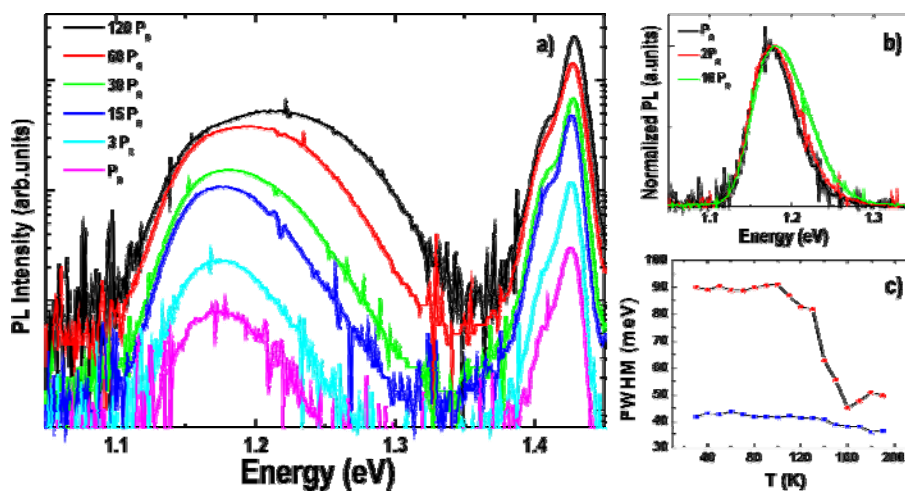


Figure 2: Macro-PL spectra showing typical phenomena of quantum coupling between QD. a) and b) PL asymmetric broadening as depending on the excitation power. c) Unusual behaviour of the FWHM with increasing T for QD molecules (red circles) as compared to single QD (blue squares).

Acknowledgements:

The authors gratefully acknowledge the financial support by the Spanish MEC (TEC-2005-05781-C03-01/-03, NAN2004-09109-C04-01/-03, Consolider-QOIT CSD2006-0019), CAM (S-505/ESP/000200), JA (TEP383) and by the European Commission through SANDIE Network of Excellence (No. NMP4-CT-2004-500101). P.A.G. thanks the I3P program.

METALORGANIC NANOSTRUCTURES: 2D- EXTENDED STRUCTURES

*L. Álvarez, R. Caillard, J.A. Martín-Gago and J. Méndez
Instituto de Ciencia de Materiales de Madrid (CSIC), Cantoblanco 28049 Madrid.
lualpima@icmm.csic.es*

ABSTRACT:

Nanotechnology is being developed as a new and very promising field of science. Very different kinds of nanomaterials are studied nowadays all around the world, looking for new materials which combine properties and applications. For example, hybrid materials obtained by a combination of inorganic and organic units, present properties and applications derived from their mixed nature [1] resulting metalorganic nanostructures, with different electronic properties than the original organic molecules.

In this work, we present a summary of nanostructuring phenomena using self-organizing strategies for structuring materials in the nanoscale range. We have studied by STM the structures resulting from the combination of iron atoms and organic molecules of PTCDA on a gold substrate. These metalorganic compounds presumably combine the properties of its components. By choosing the growth conditions (substrate temperature and adsorbates quantities) we can control the structural order and form different stable nanostructures. Previously reported nanostructures [2], organic nanodots and molecular chains, result from linking PTCDA molecules with iron atoms, and present a modified electronic structure different than the one observed for the organic material. Next structure is the “ladder-like”, resulting from two chains connected by perpendicular PTCDA molecules like the rungs of a ladder. These ladder structures can be extended over the entire surface. Figure 1 shows a STM image corresponding to a 0.9ML growth of this metalorganic 2D- structure. The image shows several domains of this “extended-ladder” structure, where the PTCDA molecules are clearly distinguished. This structure is stabilized by the iron, as it is never observed without the iron. The model for this structure suggests one iron atom per PTCDA molecule.

We have checked the stability of this structure by exposing it to oxygen atmosphere and annealing it at 420K, and no substantial changes have been observed. Finally, we have extended the growth for more than the monolayer, 1.4ML, where order at the second layer has been observed.

References:

- [1] For a review on hybrid materials see for example the special issue: *Journal of Materials Chemistry* **15** (2005).
- [2] J. Méndez, R. Caillard, R. Otero, N. Nicoara, and J.A. Martín-Gago, *Advanced Materials* **18** (2005) 2048-2052.

Figures:

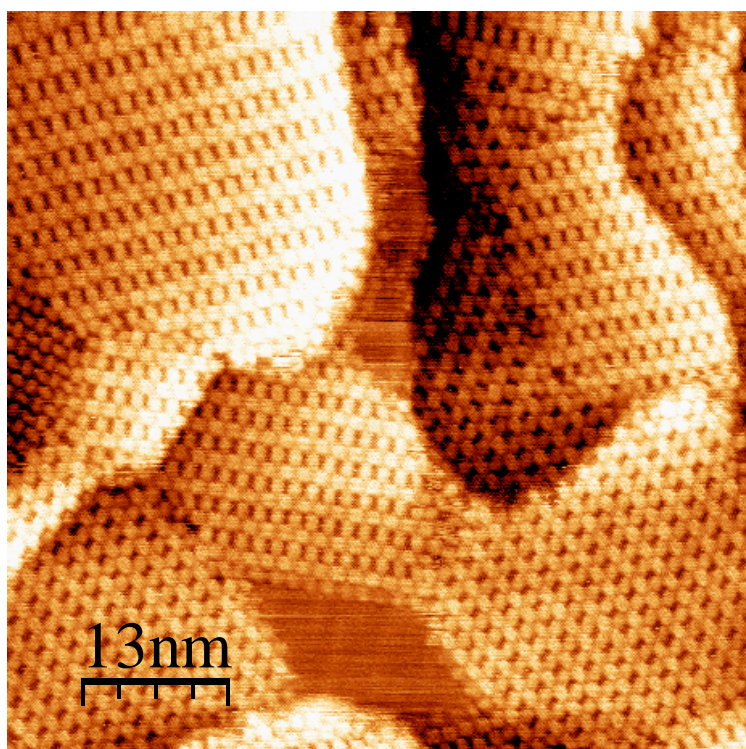


Figure 1. STM image of a gold substrate covered with 2D- metalorganic structures combining PTCDA organic molecules and iron atoms. It is remarkable that this structure is not observed in pure PTCDA growth.

**Characterization of self-assembled nanostructures exhibited by model
recombinant Elastin-like polymer E₅₀A₄₀.**

*Álvarez-Mateo, R., Ribeiro, A., R., Arias, F. J., Alonso, M., Rodríguez-Cabello, J.C.
CIBER-BBN, BIOFORGE (Group for Advanced Materials and Nanobiotechnology)
University of Valladolid, Valladolid, Spain.
Email: roca@bioforge.uva.es
Email: ramateo@bioforge.uva.es*

Genetically engineered Elastin-like polymers (ELP's) are interesting biomaterials [1]. The structure of ELP's is generally based on the repetition of the following pentapeptide sequence (VPGVG)_n where V, P, G: valine, proline and glycine, respectively. Recombinant techniques and protocols allowed us the bioproduction of monodispersed ELP's polymers that exhibit an absolute control of amino acid sequence and molecular weight [2]. Outstandingly, self-assembly properties have been attributed to these materials as function of pH, temperature (amongst other). Recently, ELP's have been envisaged for biotechnological applications such as drug delivery, and tissue engineering. Here, we would like to present our research efforts on the investigation of the structure-properties relationship exhibited by a novel ELP [(VPGVG)₂-(VPGEG)₅-(VPGVG)₂]₁₀-(VPAVG)₄₀ (E₅₀A₄₀), where A is alanine and E is glutamic acid.

E₅₀A₄₀, has the structure of an amphiphilic di-block copolymer because its structure comprises two blocks that differ in polarity. The block that contains glutamic acid residues (E) plays the role of hydrophobic block, specially at those pHs where the carboxyl group of the E side-chain is deprotonated and, therefore, negatively charged (pH>4.5). The other block exclusively exhibits non polar side chain in its amino acids, and therefore acts as a hydrophobic block.

The self-assembly features exhibited by E₅₀A₄₀ have been investigated first by calorimetric techniques such as DSC and TMDSC as way to determin the range of pH and temperature in which the system is functional [3]. In addition, the structure exhibited by E₅₀A₄₀ in the condensed phase has been directly visualized by transmission microscopy (Cryo-TEM)[4]. In this respect, globular structures that resemble micelles have been identified and measured. Furthermore, correlation of the globular assemblies observed with the temperature of the medium has been carried out by dynamic light scattering (DLS). Finally, a complete discussion on the self assembly properties exhibited by E₅₀A₄₀ as function of temperature together with possible applications for biopolymer E₅₀A₄₀ will be given.

References:

1. Rodríguez-Cabello; J. C., J. Reguera; Girotti, A.; Alonso, M.; Testera, A. M. *Prog. Polym. Sci.* **2005**, 30, 1119-1145.
2. Rodríguez-Cabello, J. C.; Reguera J.; Girotti A.; Arias, F. J.; Alonso, M. *Adv. Polym. Sci.* **2006**, 200, 119-167.
3. J.C. Rodríguez-Cabello, J. Reguera, M. Alonso, T.M. Parker, D.T. McPherson, D.W. Urry. *Chem.Phys. Lett.* **2004**, 388 (1-3), 127-131.
4. Jun Hong Yao, Khine Yi Mya, Xu Li, Manoj Parameswaran, Qing-Hua Xu, Kian Ping Loh, and Zhi-Kuan Chen, *J. Phys. Chem. B* **2008**, 112, 749-755

The Production Mechanism of Al_2O_3 - ZrO_2 Nanopowder Via Metal-Containing Polymer Precursors

Ahmad Amirshaghghi, Mehrdad Kokabi, Fatemeh Pashaei Sourbaghi*

Polymer Engineering Group, Chemical Engineering Department, Faculty of Engineering, Tarbiat Modares University (TMU), PO Box 14115-143, Tehran, Islamic Republic of Iran.

mehrir@modares.ac.ir

Thermal transformations of metal-containing monomer (MCM) are of interest at least for two reasons: first, the study of thermal decay of MCM and its transformation products makes it possible to evaluate MCM thermal stability and its role in solid state polymerization processes. Second, an investigation of MCM thermal decay is of interest in connection with the preparation of highly dispersed nano-sized metal oxide (or metal) particles stabilized in the polymer matrix. In distinction to the other known approaches, this method could successfully combine the processes of synthesis and chemical passivation of nano-sized particles. Besides, it is an important step towards solving the problem of preparing perfect composite nanopowders.

The main objective of this work was investigation the production mechanism of Al_2O_3 - ZrO_2 nanopowder through the polyacrylamide gel-net method. The monomers acrylamide, N,N' -methylene-bis-acrylamide, persulphates and N,N,N',N' -tetra methyl ethyl diamine were used to obtain gel at 4 °C. These polymer networks trapped and coordinated particles so that inhibited aggregation of Al_2O_3 - ZrO_2 , improved homogeneity, decreased agglomeration and produced narrow particle size distribution.

The Al_2O_3 - ZrO_2 nanopowders were obtained by heat treatment of precursor up to 1300 °C. Complex between monomer and ions were identified by UV-VIS and FTIR spectroscopy (Figs. 1,2,3 and 4). Particle morphology and phase transformation during heat treatment were studied by scanning electron microscopy (SEM) and X-ray diffractometry (XRD), respectively (Figs. 5 and 6). The nanopowders showed a spherical shape with particle size between 40 and 70 nm.

References:

- [1] Pittman, Charles U. Carraher, Charles E. Zeldin, M. Sheats, John E. Culbertson, Bill M. Metal-containing polymer materials. Plenum Press. New York and London 1996.
- [2] Sarkar, D. Adak, S. Mitra, N. K., Composites, **Part A 38**, 2007, 124.
- [3] Sarkar, D. Mohapatra, D. Ray, S. Bhattacharyya, S. Adak, S. Mitra, N. Ceram. Int., **33**, 2007, 1275.

Figures:

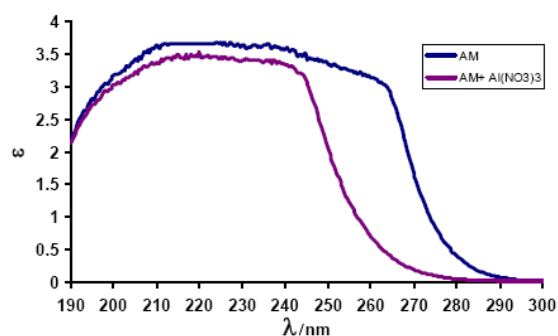


Fig 1. The UV-vis spectra of the aqueous solution of AM and AM/Al(NO₃)₃

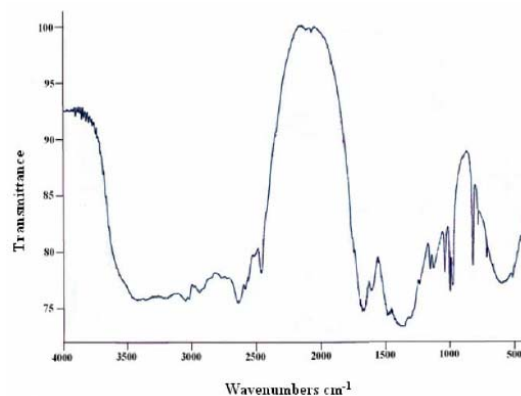


Fig. 4. Infrared spectrum of coordinated ions with polyacrylamide gel.

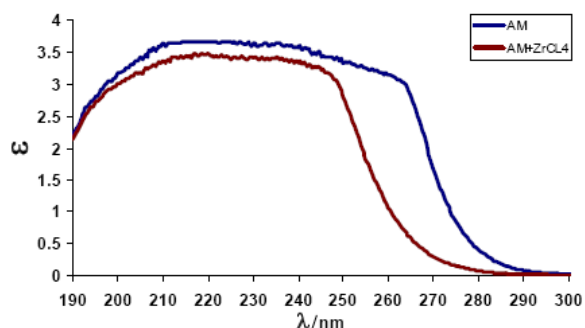


Fig 2. The UV-vis spectra of the aqueous solution of AM and AM/ZrCl₄

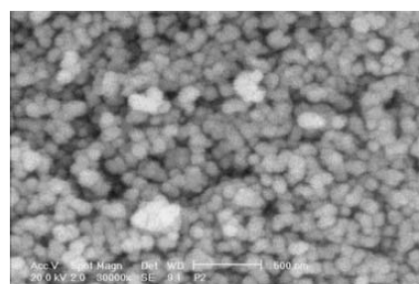


Fig. 5. SEM image of the Al₂O₃-ZrO₂ nanopowder.

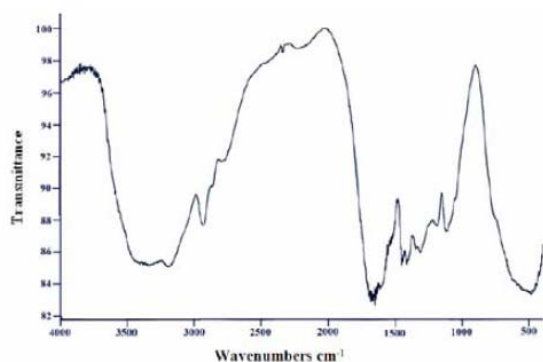


Fig. 3. Infrared spectrum of polyacrylamide gel.

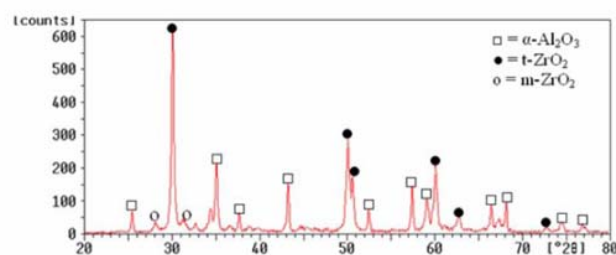


Fig. 6. XRD pattern of Al₂O₃-ZrO₂ nanopowder heat treated at 1300 °C for 1h.

NANOMEDICINES –A DYNAMIC INNOVATION IN MEDICAL SCIENCE

Ms. Deepa Grover ,Ms. Preeti Aneja

Department of Applied Science and humanities, Haryana Engineering College, Jagadhri

Deepa2805grover@gmail.com , preetianeja11@gmail.com

Abstract

Nanomedicine may be defined as the monitoring, repair, construction, and control of human biological systems at the molecular level, using engineered nanodevices and nanostructures. Nanomedicine is, in a broad sense, the application of nanoscale technologies to the practice of medicine, namely, for diagnosis, prevention, and treatment of disease and to gain an increased understanding of complex underlying disease mechanisms. Scientists and engineers believe nanotechnology can be used to benefit human health now and in the future through applications such as better filters for improving water purification, more effective methods of delivering drugs in medicine and new ways of repairing damaged tissues and organs. Nanomedicine is an exciting research area and raises not only high expectations for future health care, cosmeceuticals and other applications, but also some concerns. As the science and technology of nanomedicine speed ahead, ethics, policy and the law are struggling to keep up .Nanotechnology could also be potentially beneficial for the environment, according to the scientists, through the use of nanomaterials, for example, to create fuel cells and photovoltaic cells, or to remove heavy metals, cyanide and other substances that damage the environment. Overall nanotechnology could be used to develop industrial processes that make more efficient use of resources and generate less waste. However, some nanotechnology experts believe that more assessments need to be made of the potential risks to human health posed by nanotubes and other nanoparticles, which may have the potential to be hazardous in unpredictable ways It is important to proactively address the ethical, social and regulatory aspects of nanomedicine in order to minimize its adverse impacts on the environment and public health and also to avoid a public backlash. In order to achieve

acceptance of the expected technological benefits by the public, their impact on individuals and the society should openly be discussed

Key words: nanomedicines, nanodevices, nanomaterials, nanoparticles

Ferromagnetic resonance study of Fe/FePt coupled films with perpendicular anisotropy

Arlete Apolinario¹, D.S. Schmool¹, N. Sousa¹, F. Casoli², F. Albertini² and H. Kachkachi³

¹Department of Physics and IN-IFIMUP, University of Porto, Rua do Campo Alegre 687, 4169 007, Porto, Portugal

²IMEM – CNR, Parco Area delle Scienze 37/A, Parma, Italy

³Université de Perpignan, Perpignan, France

arletteapolinario@gmail.com

dschmool@fc.up.pt

The magnetic interaction between hard and soft magnetic materials is of current technological interest due to their potential for applications in magnetic storage devices. Such systems are referred to as “exchange springs” [1]. We have studied exchange coupled FePt/Fe magnetic layers using the technique of ferromagnetic resonance (FMR). The FePt layers show strong uniaxial perpendicular anisotropy, growing in the L1₀ epitaxial phase on MgO (100). We have considered the case for two thicknesses of Fe; 2 nm and 3.5 nm, which exhibit rigid magnet and exchange-spring behaviour. All FePt thicknesses are limited to 10 nm. The FMR results display multi-peaked spectra, where we have identified three Fe resonance lines in the rigid magnet sample and an extra two in the exchange spring sample [Fig.1(a)]. Angular FMR studies show a strong uniaxial anisotropy induced in the Fe layer via the strong exchange coupling with the FePt film. An additional uniaxial component is also observed with an easy axis inclined by about 50° from the film normal. Supplementary magnetic measurements have been used to aid with the magnetic characterisation. In this paper we discuss the elements of the theory of FMR in these exchanged coupled systems. We have developed a model of FMR for these exchange coupled systems, which is based on the magnetic free energy of the coupled layers and is required to interpret the angular dependence of the resonance fields. For this we start by applying the model by Asti *et al.* [3]. In our theoretical modelling we have carried out both analytical and numerical simulations in order to aid with the interpretation of our experimental results. Since our FMR data only measure the Fe (soft) magnetic layer, we only need consider this in our analysis, where the effect of the FePt (hard) layer is to exchange couple with the Fe film effectively pinning the interface spins. To do this we have firstly evaluated the analytical and numerical equilibrium conditions of the Fe spins as a function of distance within the layer. In the numerical minimization model, the software minimizes the free energy of the system using Monte Carlo method. It creates an array of spins in which the first one (at the Fe/FePt interface) is fixed in the perpendicular direction [Fig.1(b)]. All other spins have a random direction and the system has an initial magnetic free energy. We then minimize the free energy on a spin by spin basis in order to evaluate the equilibrium orientation as a function of position. The coupled spins have a perpendicular (uniaxial) anisotropy in the FePt film, shape anisotropy with easy axes on the plane in the Fe film. The simulations reveal a 90 degree domain wall which moves up and down with the application of an external magnetic field.

References:

- [1] E. F. Kneller and R. Hawig, "The exchange-spring magnet: A new material principle for permanent magnets," IEEE Trans. Magn., (1991) 27, 3588.
- [2] D. S. Schmool et al. "Ferromagnetic resonance study of Fe/FePt coupled films with perpendicular anisotropy", IEEE Trans Magn (2009), 44 3087 .

[3]- G.Asti, M. Ghidini, R. Pellicelli, C. Pernechele, and M. Solzi, PRB, **Magnetic phase diagram and demagnetization processes in perpendicular exchange-spring multilayers** (2006) 73, 094406.

Figures:

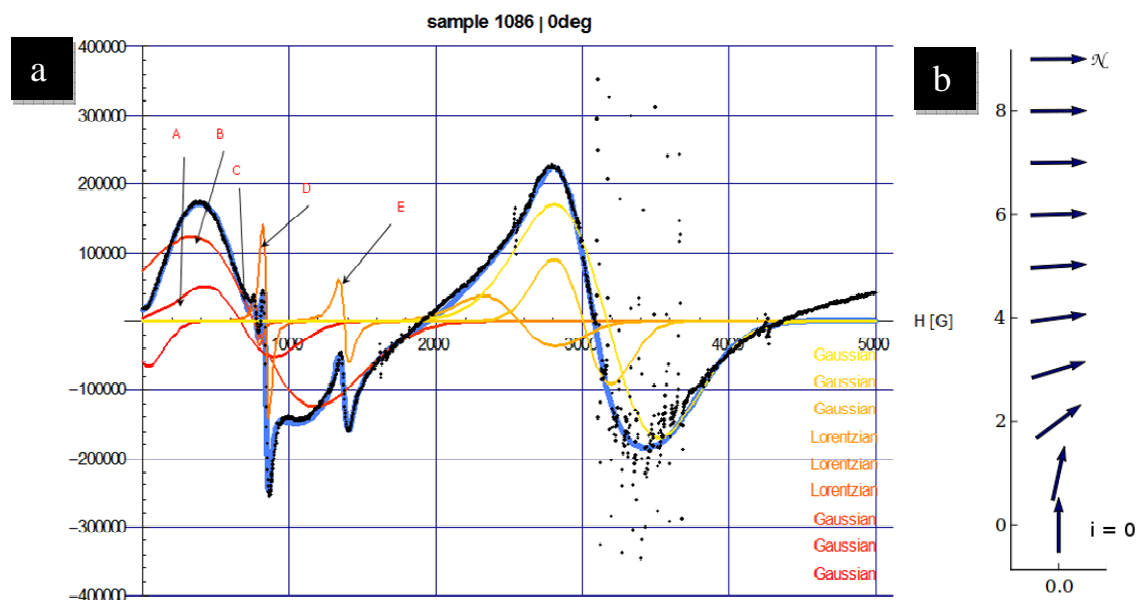


Fig. 1: (a) FMR spectrum of sample with the different resonances marked – A to E. Experimental data shown as dark blue dots and result from the fit marked with light blue line; (b) Result of the theoretical simulation of 10 array of spins exchanged coupled.

SYNTHESIS OF NANOCAPSULES CONTAINING ALMOND OIL BY MINIEMULSION POLYMERIZATION

Francisca Arán Ais¹, Ana M. Torró Palau¹, César Orgilés Barceló¹, Katharina Landfester²
¹ INESCOP. Footwear Research Institute. Polígono Industrial Campo Alto, s/n. P.O. Box 253.
03600 Elda (Alicante), Spain. aran@inescop.es

² Organic Chemistry III Institute. University of Ulm (Germany) and Max Planck Institute for
Polymer Research, Ackermannweg 10, 55128 Mainz (Germany)

Introduction

The situation of the shoe industry today makes it necessary for new materials and concepts to be found, to be used as differentiating elements against competitors and that make products stronger in terms of quality, personal hygiene and safety or respect for the environment. In this sense, microencapsulation presents a new option for the shoe industry as its application can transform traditionally used materials or products into smart materials or products capable of interacting with feet. They can improve quality of life by incorporating different therapeutic products for foot care such as essential oils properly dosed. The microencapsulation of active substances to be incorporated in different footwear components in order to obtain an “active shoe” presents an opening up of a new way of innovation.

Actually, in this study polystyrene nanocapsules containing almond oil were synthesized by a direct miniemulsion polymerization process (O/W) to be applied to footwear materials (lining, insoles, etc.). Sweet almond oil is a natural moisturizing agent very often used in the cosmetic industry due to its high content of essential oils content such as oleic and linoleic oils. Because it is not greasy, it is absorbed quickly. In this case, the nanocapsule can act as nanocontainer in order to retain the liquid and therefore to prevent it from leaking into the continuous phase. In addition, nanocapsules formation improves the oil stability, reduces its evaporation rate and it allow a release control when are applied on a substrate.

Nanocapsules are generally considered as spherical, hollow structures with an average diameter of less than 1 μm . Typically, the capsule consists of a polymeric wall with a thickness in the nanometer region, filled with an oil. To enable a stable dispersion, the capsule is stabilized by surface charges or by absorption of an amphiphile. The approach to synthesize nanocapsules is based on the principle of miniemulsion using the differences of interfacial tension and the phase separation process during polymerization to obtain a nanocapsule morphology. A miniemulsion polymerization is described that yields an encapsulation of a nonsolvent hydrocarbon by the polymer being formed. Using this process, it is possible to prepare latex particles having voids with facile control of the particle diameter, void fraction and structure. The process initially involves polymerizing a monomer in a dispersed hydrocarbon-monomer mixture which phase-separates during the polymerization. This phase-separated polymer subsequently serves as a locus for polymerization. The morphology of the demixing structure is determined by the type of surfactant chosen, the polarity of the monomer, and the choice of hydrophobe.

In this paper, different monomer/almond oil ratios as well as different amounts of the surfactant (SDS) were applied to obtained nanocapsules and their effects on the morphology of capsules were investigated by different experimental techniques for footwear applications.

Experimental

Polystyrene nanocapsules containing almond oil were prepared by the convenient one-step direct miniemulsion (O/W) polymerization. Aqueous miniemulsion was obtained by mixing

monomer (styrene), almond oil and initiator (2,2'-azobis(2-methylbutyronitrile)), and then adding the solution to an aqueous solution of surfactant (SDS) and water, followed by ultrasonification. The polymerization was started by heating to 72 °C and kept at this temperature overnight. After polymerization, the samples were freeze-dried.

After that, the miniemulsions and nanocapsules obtained were analysed by different experimental techniques: The solid content was measured gravimetrically and the average particle size by means of dynamic light scattering (DLS). For morphological characterization, transmission electron microscopy (TEM) was carried out. The average molecular weights of the polymers were determined by gel permeation chromatography. Chemical properties were analysed by FTIR spectroscopy and ¹HNMR. Finally, the glass transition temperatures were measured by differential scanning calorimetry (DSC) and the thermal degradation by thermogravimetry.

Results and discussion

The styrene concentration as monomer in the oil phase as well as the surfactant (SDS) concentration in the aqueous phase, determined the morphology of the nanocapsules containing almond oil. Nanocapsules showed a core/shell structure analysed by transmission electron microscopy (TEM) with average diameter of 75-150 nm depending on the monomer/oil ratio and the surfactant concentration.

According to the results obtained an increase in the surfactant concentration in the aqueous phase, as well as, an increase in the monomer concentration in the oil phase produced a decrease in the nanocapsules average size and an increase in the molecular weight of shell polystyrene. This increase is due to a similar cohesion energy between the polymer and the almond oil and therefore the morphology of the nanocapsules is determined by the parameters that affect the interfacial tension.

PS nanocapsules containing different amounts of almond oil was studied under nitrogen atmosphere by TGA. A degradation process in a two steps process is observed and an increase in the thermal stability of the almond oil occurs when the oil is encapsulated.

Acknowledgments: This work has been partially financed by the Spanish Ministry of Education and Science (project MAT2007-65372).

References:

- [1] N. Bechthold, F. Tiarks, M. Willert, K. Landfester, M. Antonietti, *Macromolecular Symposia*, **151** (2000) 549.
- [2] K. Landfester, N. Bechthold, F. Tiarks, M. Antonietti. *Macromolecules* **32** (1999) 2679.
- [3] P. J. Doping, R. Atkin, B. Vicent, P. Bouillot. *Langmuir*, **20** (2004) 11374.
- [4] F. Tiarks, K. Landfester, M. Antonietti. *Langmuir* **17** (2001) 908.

AC electrical properties characterization of Polyaniline-Fe₃O₄ nanocomposite

A. C. V. de Araújo^{1}, R. J. de Oliveira¹, S. Alves Jr.¹ and W. M. de Azevedo¹*

Universidade Federal de Pernambuco-, Departamento de Química Fundamental, Av. Prof. Luiz Freire S/N, Recife-PE, Brazil

acva@nlink.com.br

Composites materials obtained by the combination of conducting polymers and magnetic oxides presents an organized structure and provide functional hybrid materials with interesting properties. Among the conducting polymers, polyaniline (PANI) has attracted particular interest due to the fact that its electrical and optics properties can be reversibly controlled by changing the oxidation state of the main chain and by protonating the imines nitrogen atoms¹.

Dielectric spectroscopy has been found to be a valuable experimental tool for understanding the phenomena of charge transport in conducting polymers², using experimental information like *ac* conductivity, dielectric relaxation and photoconductivity³. In this work, we report the studies on electrical properties of polyaniline-Fe₃O₄ nanocomposites. These nanocomposites were obtained according to methodology previously reported⁴, and shown in figure 1(a) and 1(b). The particle average size was found to be around 25-30 nm. The Nyquist diagram shows a large semicircle and a part of a semicircle in the high frequency limit. The major semicircle corresponds to the interfaces response, while the minor is related to the bulk effect. By using a R(RC)(RQ) equivalent circuit to model the magnetite nanocomposite sample, the grain and boundary grain conductivities, $\sigma_g = 5.0 \cdot 10^{-5} \text{ S cm}^{-1}$ and $\sigma_{gb} = 8.6 \cdot 10^{-7} \text{ S cm}^{-1}$, was obtained respectively. The *dc* conductivities for pure magnetite were around $10^{-6} \text{ S cm}^{-1}$ and for the nanocomposites around $10^{-5} \text{ S cm}^{-1}$. Partial overlap occurs in the graphics of Z'' , imaginary impedance, and M'' , electric modulus, (fig.1(c)), confirming the long range conducting mechanism attributed to PANI in the composites. There is no overlap for the magnetite, indicating that its conductivity is dominated by localized relaxations due to the electron hopping between Fe³⁺ and Fe²⁺ sites. The *ac* conductivities of the composites, present metallic response (Drude model) for frequencies below the critical frequency. It's attributed to the PANI electrical character.

References:

- [1] Falcão E. H. L., Azevedo W. M., Synth. Met.; 128 (2002) 149.
- [2] Kivelson S., Phys. Rev. B; 25 (1982) 3799.
- [3] Mammone R. J.; Binder M.; J. Electrochem. Soc.; 137 (1990) 2135.
- [4] De Araújo A. C. V., Alves Jr. S., Azevedo W. M.; Adv. Sci. Technol. 54 (2008) 325.

Figures:

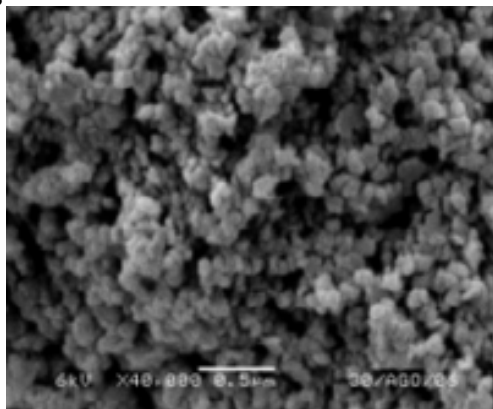


Fig. 1 (a): SEM image of magnetite nanoparticles.

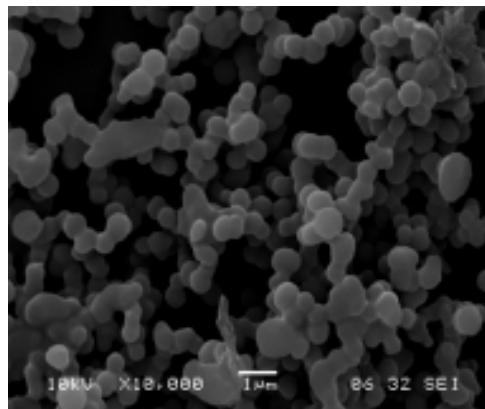


Fig. 1 (b): SEM image of nanocomposite.

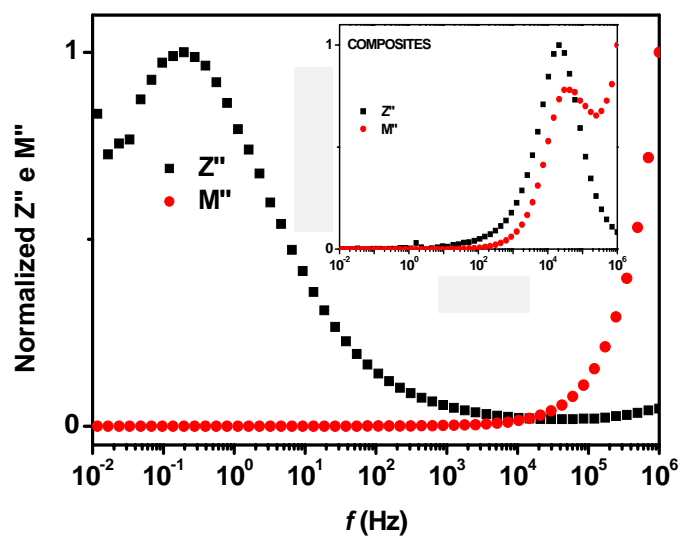


Fig. 1 (c): Z'' and M'' of magnetite and composite (insert).

EFFECT OF NANOPARTICLE VOLUME CONCENTRATION IN LAMINAR JET

Taher Armaghani^a, Mohammad Javad Maghrebi^a, Farhad Talebi^b

^aThe Faculty of Mechanical Engineering, Shahrood University of Technology, Shahrood, Iran

^bThe Faculty of Mechanical Engineering, Semnan University, Semnan, Iran,

taherarmaghani@yahoo.com

Jet flow with desired physical conditions thought lots of applications in industrial and scientific scope has been the most important subjects in fluid mechanic and from appearance of fluid mechanic theory; many researchers have attended this subject.

In this paper, direct numerical solution two dimensional incompressible jet flows is performed.

We replaced the base fluid properties with nanofluid that contain nanoparticle and base fluid. Nanoparticle in this study is Al_2O_3 and the basefluid is water.

In this study the following non-dimensional equation are solved :

$$\nabla \cdot \vec{U} = 0 \quad (1)$$

$$\frac{\partial \nabla^2 \vec{U}}{\partial t} = -\nabla \times (\nabla \times \vec{H}) + \frac{1}{Re} \nabla^4 \vec{U} \quad (2) \quad \text{in there } \vec{H} = (H_1, H_2, H_3) = \vec{U} \times \vec{\omega} \quad (3)$$

$$\frac{\partial T}{\partial t} + \vec{U} \cdot (\nabla T) = \frac{1}{Pe} (\nabla^2 T) \quad (4)$$

The equation (2) used by many investigators including Maghrebi[1] is the vorticity form of Navier stokes equation.

The governing equations are discretized in the streamwise direction (x), using a sixth order compact finite difference scheme, and in the cross-direction (y) using a mapped compact finite difference scheme[2]. A cotangent mapped of $y = -\beta \cot(\pi\zeta)$ [3] is used to relate the computational domain $0 \leq \zeta \leq 1$ to the physical domain in the double infinit interval of $-\infty \leq y \leq \infty$. The compact third order of Runge-Kutta method [4] is used for the time-advancement of the simulation. The inlet boundary condition is the Dirichlit and Neumann condition; The convective outflow boundary condition is employed to create a non-reflective type boundary condition at the outlet[1]. An inviscid (Stuart flow)[5] and a completely viscose solutions of the Navier Stokes equations are used for verification of the numerical simulation. The numerical results show a very good accuracy and agreement with exact solution of the Navier Stokes equation[1].

For nanofluid(Al_2O_3 -water) the following equation are used. these equations, introducing the effective properties, were used by maiga[6]

$$\rho_{nf} = (1 - \phi)\rho_{bf} + \phi\rho_p \quad (5) \quad (cp)_{nf} = (1 - \phi)(cp)_{bf} + \phi(cp)_p \quad (6)$$

$$\mu_{nf} = (123\phi^2 + 7.3\phi + 1)\mu_{bf} \quad (7) \quad k_{nf} = (4.97\phi^2 + 2.72\phi + 1)k_{bf} \quad (8)$$

In these equation ρ, μ, cp, k refers to density, viscosity, specific heat, conductivity respectively where ϕ refers to nanofluid volume concentration. and sub scrips nf, bf, p refers to nanofluid, base fluid and particle respectively.

Figure (1,2) show the validity the result with Stuart flow and Navier Stokes equation.

Figure (3) show the velocity time histories for U component without noise and without nanoparticle.

Figure (4) show the temperature time histories without noise and without nano particle.

Figure (5) show the effect of nanoparticle volume concentration in Thermal cross-stream

diffusion depth the figure result that ϕ increase the Thermal cross-stream diffusion depth increase .Figure (6) show the effect of nanoparticle volume concentration in Hydrodynamic cross-stream diffusion depth the figure result that ϕ increase the Hydrodynamic cross-stream diffusion depth increase. Figure (7) show the effect of nanoparticle volume concentration in thermal streamwise diffusion depth . Figure (8) show the effect of nanoparticle volume concentration in hydrodynamic streamwise diffusion depth .

References:

- 1-M.J. Maghrebi, "A Study of Evolution of Intense Focal Structures in Spatially-Developing Three-Dimensional Planer Wake", PhD thesis, Department of Mechanical Engineering, Monash University, Melbourne, Australia,1999.
- 2- S.K. Lele, "Compact Finite Difference Scheme with Spectral-Like Resolution", Journal of Computational Physics, 103, 16-12, 1992.
- 3- M.J. Maghrebi, "Orr Summerfield Solver Using Mapped Finite Difference Scheme for Plane Wake Flow",.
- 4- A. Wray & M.Y. Hussaini, "Numerical Experiments in Boundary Layer Stability", Proc. R. Soc. Lond. A, vol. 392, pp 373-389, 1984.
- 5- J. T. Stuart. On finite amplitude oscillations in laminar mixing layer. Journal of fluid mechanics. 29.(3) pp 417-440. 1967.
- 6-S.E.B.maiga et all , "Heat transfer enhancement by using nanofluids in forced convection flows".Internal Journal of Heat and Fluid flow 26(2005)530-546

Figures:

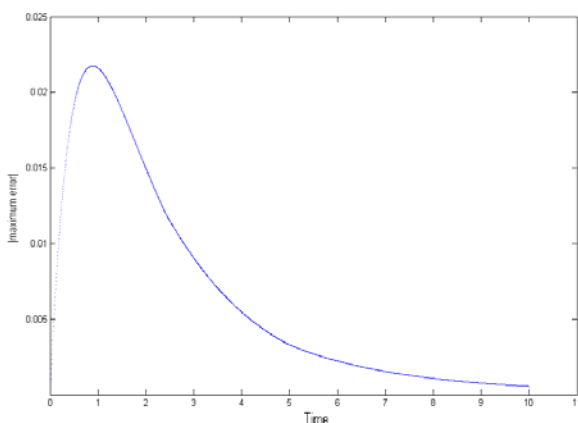


Figure 1.maximum error in 2D solution

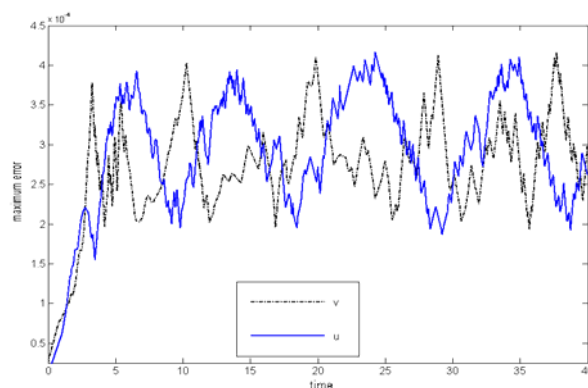


Figure2.maximum error for Stuart flow

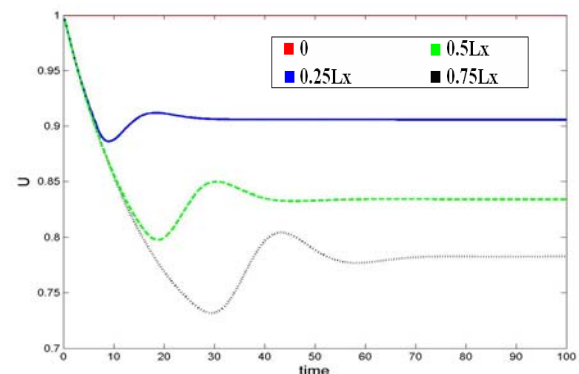


Figure 3.U velocity time history of numerical simulation

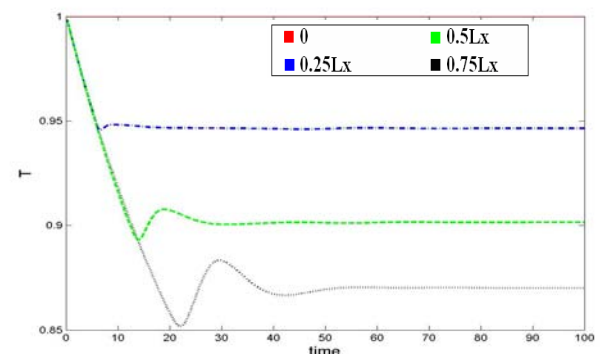


Figure4 temperature time history of numerical simulation

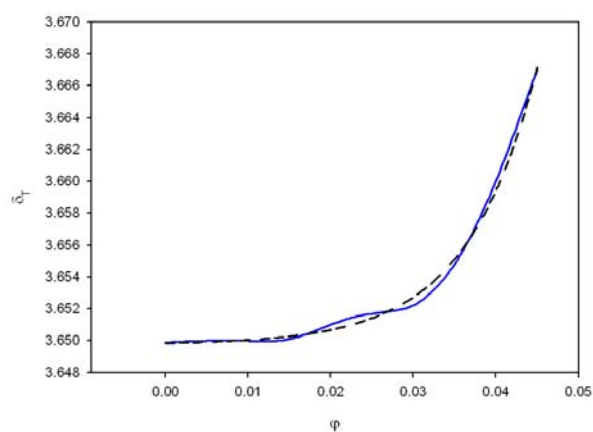


Figure5. effect of nanoparticle volume concentration
in δ_T at time=100, $x=0.75Lx$

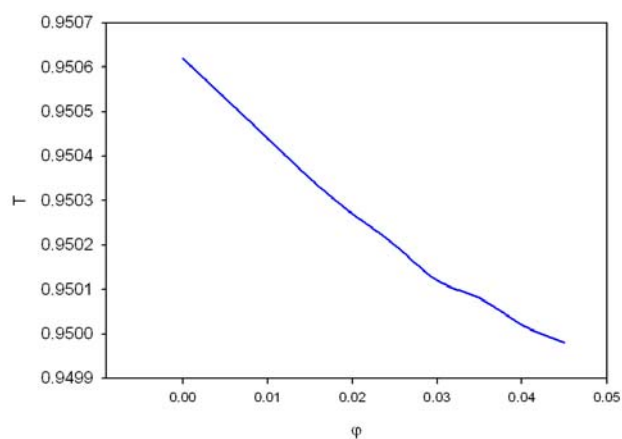


Figure7.temperature at time=100, $y=0, x=0.75Lx$

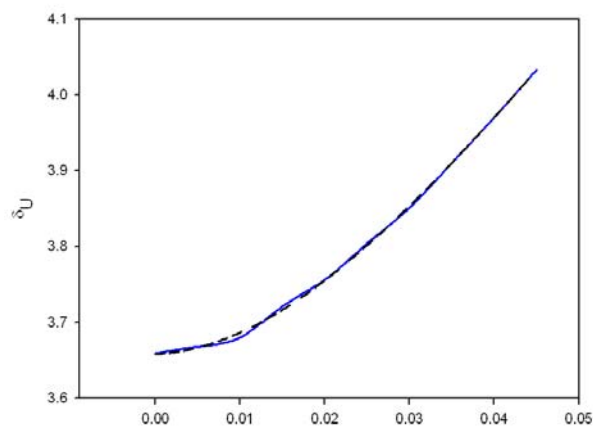


Figure6. effect of nanoparticle volume concentration
in δ_U at time=100, $x=0.75Lx$

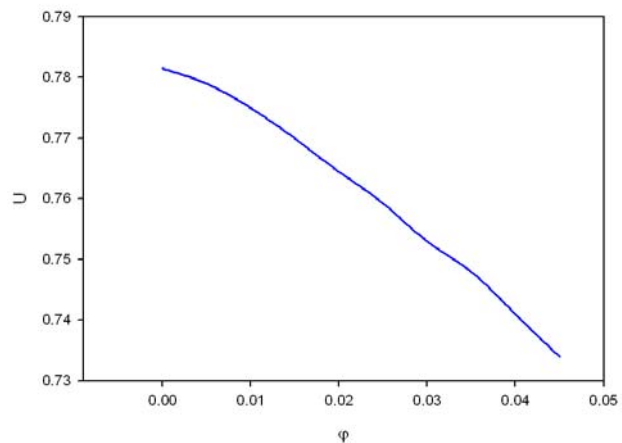


Figure7.U velocit.temperature at time=100,
 $y=0, x=0.75Lx$

Dendritic cell uptake of magnetic nanoparticles for magnetic hyperthermia

Laura Asín Pardo¹, Iván Marcos Campos^{1,2}, Teobaldo Enrique Torres¹, Gerardo F. Goya¹, Clara Marquina³, Alejandro Tres Sanchez^{1,2}, Ricardo M. Ibarra¹.

1-Aragon Institute of Nanoscience (INA), Pedro Cerbuna 12, University of Zaragoza, Spain

2- Lozano Blesa University Hospital, Oncology Service, Zaragoza, Spain

3- Aragon Institute of Materials Science (ICMA), University of Zaragoza, Spain
lasin@unizar.es

Dendritic cells (DCs) are the most important antigen presenting cells (APCs) and as its prime function play a key role in both innate and adaptive immune response. Dendritic cells and endothelial cells are closely related and *in vitro* studies have demonstrated that monocytes and dendritic cells transdifferentiate into endothelial cells in the presence of proangiogenic factors as vascular endothelial growth factor (VEGF). Vasculogenesis, which is the recruitment of endothelial progenitor cells circulating in peripheral blood, contribute to the neovascularization, a cardinal process for the tumor surviving.

Our main aim in this project is to vectorize dendritic cells, previously charged with magnetic nanoparticles (MNPs), to tumor microenvironment to become part of the new vessels by vasculogenesis. Once there, applying an alternate magnetic field we can rise the temperature of the cells causing their destruction and subsequently the damage of the vessels avoiding the nutrition of the tumor and its regression or death.

The particles used in these experiments consist of a magnetite core covered by dextran and functionalized with COOH- groups at the surface. A second type of NPs composed of a latex nucleus and fluorescent markers at the surface were used to verify the distribution within the cells using confocal microscopy (see figure). Both of them have the same hydrodynamic ratio of 250 nm and COOH- surface groups. We have investigated the internalization of magnetic nanoparticles (MNPs) into DCs and analyzed the viability of the cells after having been cultured with MNPs. After cheking that the particles have no toxic effect on the cells we have undergone the cells to an external alternate magnetic field and measure the cell viability using three different methods: Trypan Blue, MTT and Flow Cytometry. High levels of cell death (up to 90%) were observed after application of magnetic fields, only for those cells that were previously loaded with MNPs. The quantification of the MNPs into the DCs has been done using a SQUID (Superconducting Quantum Interference device).

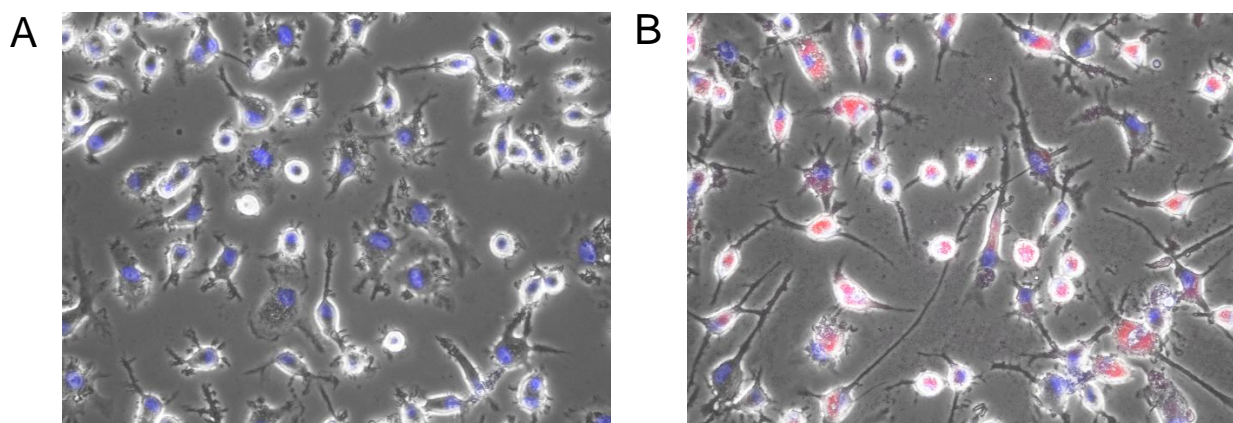
Current projects and activities:

- (1) Proyecto Multidisciplinario: “Vectorización de Nanoparticulas Magnéticas a través de células dendríticas y su utilización em Hipertermia Magnética para Terapia Oncológica.” Diputacion General de Aragon (DGA).
- (2) Consolider-Ingenio2010. “Nanobiomed: Nanotechnologies in Medicine” MICINN.

References:

- (1) Hart DN. *Blood*. **Dendritic cells: unique leukocyte populations which control the primary immune response.**1997; 90:3245-87.
- (2) Banchereau J, Steinman RM. *Nature*. **Dendritic cells and the control of immunity.**1998; 392:245-52.
- (3) Fernandez Pujol B, Lucibello FC, Zuzarte M, Lütjens P, Müller R, Havemann K. *Eur J Cell Biol*. **Dendritic cells derived from peripheral monocytes express endothelial markers and in the presence of angiogenic growth factors differentiate into endothelial-like cells.** 2001 Jan; 80(1):99-110.
- (4) Jordan A, Scholz R, Wust P, Föhling H, Krause J, Wlodarczyk W, Sander B, Vogl T, Felix R. *Int J Hyperthermia*. **Effects of magnetic fluid hyperthermia (MFH) on C3H mammary carcinoma in vivo.** 1997 Nov-Dec;13(6):587-605
- (5) Goya GF, Marcos-Campos I, Fernández-Pacheco R, Sáez B, Godino J, Asín L, Lambea J, Tabuenca P, Mayordomo JI, Larrad L, Ibarra MR, Tres A. *Cell Biol Int*. **Dendritic cell uptake of iron-based magnetic nanoparticles.** 2008 Aug;32(8):1001-5.

Figures:



Fluorescent microscopy of DCs seeded on fibronectin- coated coverslips and stained with DAPI (BLUE) which is a nucleus dye. **A:** DCs without NPs. **B:** DCs having been cultured overnight with fluorescent NPs-Rhodamine (RED).

NON-COVALENT FUNCTIONALIZATION OF CARBON NANOTUBES WITH GLYCOLIPIDS: GLYCONANOMATERIALS WITH SPECIFIC LECTIN-AFFINITY

*Mohyeddin Assali^a, Manuel Pernía Leal^a, Inmaculada Fernández^b, Rachid Baati^c, Charles Mioskowski^{‡c} and Noureddine Khiar^{*a}*

^a*Instituto de Investigaciones Químicas, C.S.I.C-Universidad de Sevilla, c/. Américo Vespucio, 49, Isla de la Cartuja, 41092, Sevilla, Spain.*

^b*Departamento de Química Orgánica y Farmacéutica, Facultad de Farmacia, Universidad de Sevilla, 41012, Sevilla, Spain*

^c*Laboratoire de Synthèse Bio-Organique, Faculté de Pharmacie UMR 7175-LC1, Université Louis Pasteur de Strasbourg, 74 route du Rhin, 67401, Illkirch-Graffenstaden, France*

mohyeddin@iiq.csic.es

The utilization of a nanomaterial wrapped in biologically relevant molecules to study and solve biomedical problems is a new and stimulating field of research.¹ One of the most salient features of using nanomaterials, such as nanoparticles, nanorods, nanowires and carbon nanotubes in biology is their ability to carry multiple copies of a single drug or various active principles with different, ideally synergistic, modes of action.² Consequently, those diseases or biological processes whose biological targets require a multivalent display of the active epitope, are expected to benefit from the application of a nanometric platform. Illustrative examples of such events are those mediated by carbohydrates, which include cell adhesion, inflammation, tumour cell metastasis, and pathogen infections.³ It has been shown that the weak interaction between an individual ligand and the corresponding specific lectin is compensated by the multivalent display of carbohydrates through the so called cluster effect.⁴ On the other hand, single-walled carbon nanotubes (SWCNTs) as interesting 1D nanomaterials, are actually being actively investigated as vehicles for the in vivo smart delivery of biologically relevant cargoes including drugs, proteins, and nucleic acids, as nanometric sensors, and for cancer treatment.⁵

In this study, we disclose our results on the utilization of carbon nanotubes as molecular platforms for a multivalent presentation of biologically relevant saccharide epitopes. Our strategy is based on the utilization of neutral pyrene functionalized neoglycolipids **I**⁶ that interact with a CNT's surface giving rise to a nanometric material with a multivalent display of carbohydrates, much like the glycocalyx on the cell surface.⁷

The characterization of SWCNT-Py-PEG-Lac-**5**/Py-PEG-Man-**6** as well as MWCNT-Py-PEG-Lac-**5**/Py-PEG-Man-**6** aggregates is carried out by transmission electron microscopy (TEM).

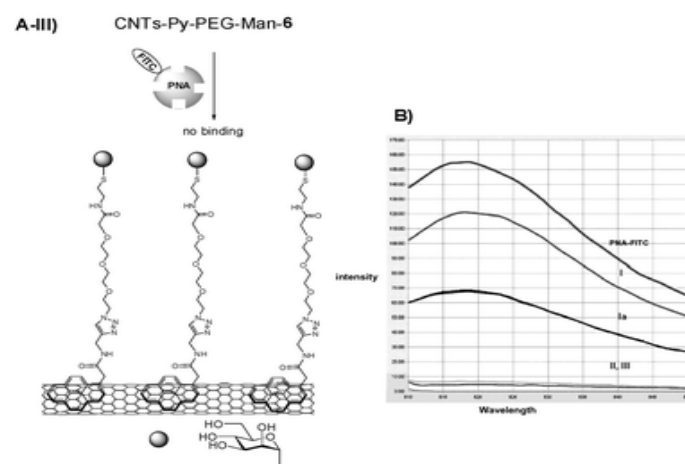
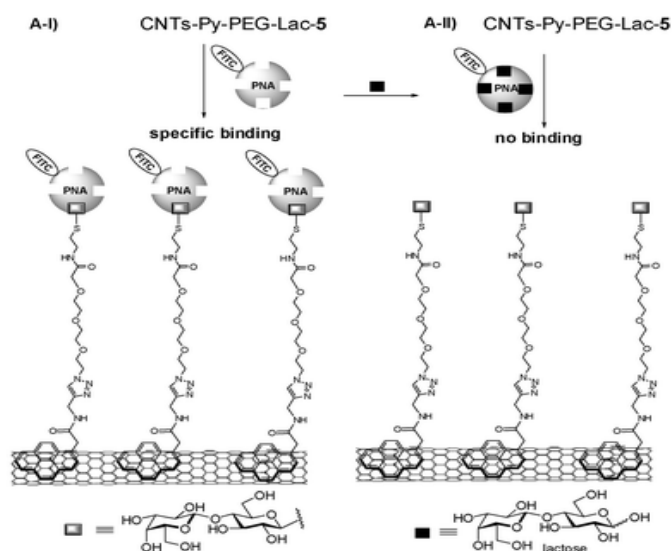
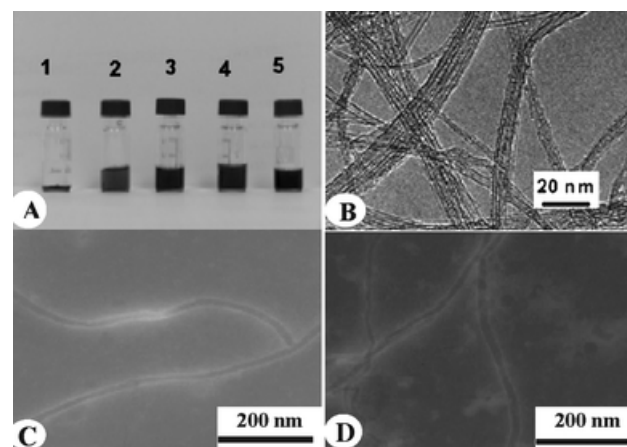
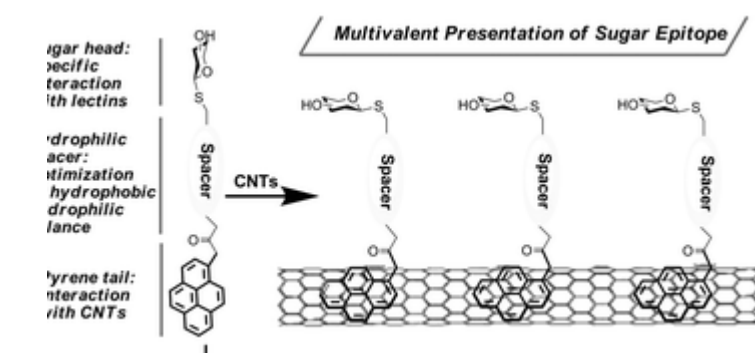
In order to study this specific binding feature, critical for future biological applications of the prepared bio-nanomaterials, we make use of the known sugar-lectin specificity.⁸

In summary, we have developed a mild and practical non covalent approach for the functionalization of carbon nanotubes. The obtained aggregates with a multivalent sugar exposition on their surface are able to engage specific ligand-lectin interactions similar to glycoconjugates on the cell membrane.

References:

- [1] R. F. Service, *Science*, 2005, **310**, 1132
 [2] I. Brigger, C. Dubernet and P. Couvreur, *Adv. Drug Deliv. Rev.*, 2002, **54**, 631
 [3] R. A. Dwek, *Chem. Rev.*, 1996, **96**, 683
 [4] M. Mamen, S. K. Choi and G. M. Whitesides, *Angew. Chem. Int. Ed.*, 1998, **37**, 2754
 [5] D. Pantarotto, J. Briand, M. Prato and A. Bianco, *Chem. Commun.*, 2004, 16
 [6] R. J. Chen, Y. Zhang, D. Wang and H. Dai, *J. Am. Chem. Soc.*, 2001, **123**, 3838
 [7] X. Chen, U. C. Tam, J. L. Czapinski, G. S. Lee, D. Rabuka, A. Zettl and C. R. Bertozzi, *J. Am. Chem. Soc.*, 2006, **128**, 6292
 [8] S. A. Lasky, *Ann. Rev. Biochem.*, 1995, **64**, 113

Figures:



NANOSTRUCTURED LARGE-PORE SILICA NANOMATERIALS FOR DRUG RELEASE

Daniel Carmona, Francisco Balas and Jesús Santamaría

Dpto. Ingeniería Química y Tecnologías del Medio Ambiente,

*Universidad de Zaragoza – Instituto de Nanociencia de Aragón (INA), c/ Pedro Cerbuna 12,
50009 Zaragoza (Spain), and*

*Networking Research Center for Bioengineering, Biomaterials and Nanomedicine (CIBER-
BBN), c/ María de Luna 11, 50018 Zaragoza (Spain)*

dacarmon@unizar.es

The ceramics for medical practice have been traditionally classified into two main groups, those inert materials such as alumina, zirconia or carbon and those that undergo a specific interaction with the physiological environment when implanted leading to material integration in the living tissue [1]. In the latter years, it has been also reported that silica-based ordered mesoporous materials with certain porous frameworks can be used as biomaterials with both bioactivity and controlled drug delivery ability [2].

However, the adsorption of biological molecules, such as oligopeptides, requires tailoring the interaction between matrix and adsorbed molecules for avoiding the modification of their active centres. The present work is focused in developing cage-like mesoporous structures for an enhanced drug loading. For this purpose, SBA-16 and FDU-12 nanostructured silica-based materials were synthesized by templating and further functionalized by means of post-synthesis grafting of chloropropyl and aminopropyl groups. As an adsorption model, the well known anti-inflammatory drug ibuprofen (ibu) is chosen for study.

Pure silica SBA-16 and FDU-12 nanostructures were synthesised as it was previously reported [3,4]. The functionalization of silica materials was performed by post-synthesis reaction either with 3-chloropropyl trimethoxysilane ((OMe)₃SiC₂H₂Cl) or with 3-aminopropyl triethoxysilane ((OEt)₃SiC₂H₂NH₂) in refluxing toluene under Ar gas. Materials were loaded with ibuprofen by soaking 100 mg of material in saturated drug water/ethanol (1/2) solutions. The drug release tests were carried out in phosphate buffer solution (PBS) at pH 7.25.

N₂ adsorption isotherms show the reduction of both the pore volume after functionalization, which goes together with by the decrease on the lattice parameters of the hexagonally ordered array of mesopores. Moreover, the small-angle X-ray scattering (SAXS) studies prove the spherical arrangement of nanopores since the Porod's region shows a q^{-4} dependence with the scattered intensity [5] modification on the nanoporous structure of the materials when submitted to the functionalization process, which points to the formation of opener pore frameworks

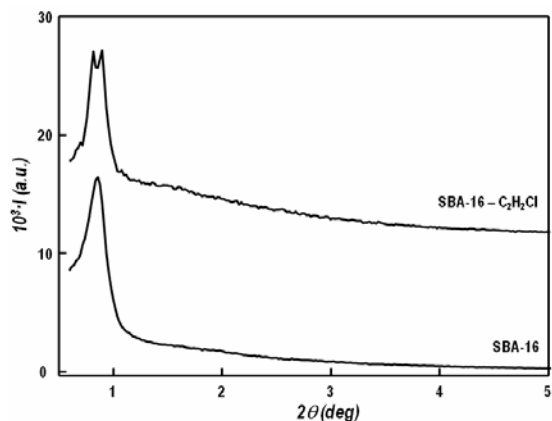
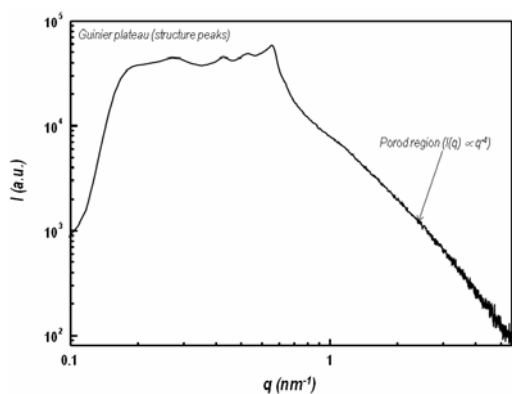
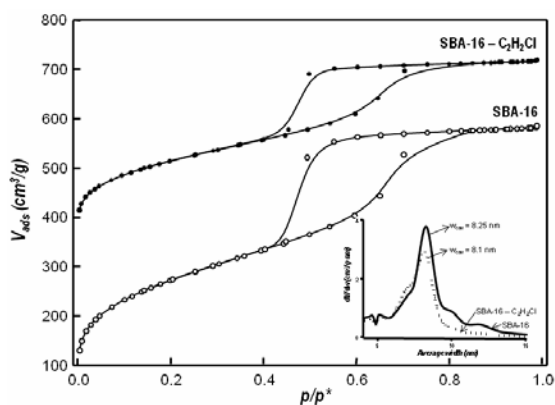
Analysis by FTIR confirmed the grafting on the surface of the organic amine, where the bands of the CH group (ν_{CH}) and NH group (ν_{NH}) stretching modes were detected.

Maximum load of ibuprofen on the unfunctionalized silica surfaces was almost twice smaller than for functionalized materials. When loaded materials are exposed to releasing environments, the amino acid is slowly delivered to media as a function of the electrostatic interaction between molecule and substrate. Ordered mesoporous silica materials can be employed for loading peptides with diverse biological applications. Functionalization with the appropriate functional group assures the retaining of peptide as well as its controlled release to environment.

References:

- [1] Vallet-Regí M et al. J Mater Chem, 15 (2005) 1.
 [2] Vallet-Regí M, Balas F. Open Biomed Eng J, 2 (2008) 1.
 [3] Yu T et al. J Phys Chem B, 110 (2006) 21467.
 [4] Kleitz F et al. Langmuir, 22 (2006) 440.
 [5] Feigin LA et al. Structure analysis by small angle X-ray and neutron scattering. (Plenum Press, 1987)

Figures

**Figure 1.** XRD patterns for SBA-16 and SBA-16-C₂H₂Cl materials**Figure 2.** SAXS Guinier plots of for SBA-16 materials**Figure 3.** N₂ sorption isotherms and the DFT pore size distributions for SBA-16 and SBA-16-C₂H₂Cl materials (isotherms are deliberately shifted for clarity)

X-RAY ABSORPTION SPECTROSCOPY FOR CHARACTERIZING IRON OXIDE NANOPARTICLES

Francisco Balas¹, Cristina Piquer², Daniel Carmona¹, Roberto Boada², Jesús Santamaría¹ and Jesús Chaboy²

¹Dpt. Ingeniería Química y TMA. Universidad de Zaragoza – Instituto de Nanociencia de Aragón

²Instituto de Ciencia de Materiales de Aragón, CSIC – Universidad de Zaragoza

fbalas@unizar.es; cpiquer@unizar.es

Iron oxide nanoparticles are nowadays being used for a myriad of applications from nanoelectronics to biomedicine, due to both to their interesting magnetic and biocompatible characteristics. It is a matter of fact that the oxidation state of Fe ions in the nanostructures determines the final magnetic and biological properties of iron oxide nanoparticles [1-2]. Moreover, the shape and size of nanoparticles also plays an important role in the final applications of the synthesized materials. There are a large number of physical and chemical procedures that has been used for studying the actual state of Fe, the crystal structure, shape and particle size in iron oxide nanomaterials. Nevertheless, the common techniques are not able to determine the actual structure and composition of nanoparticulate iron oxides.

In the present work, the use of the X-ray absorption spectroscopy, XAS, for determining the oxidation state of iron oxide nanoparticles is proposed. Atomic-selective information can be obtained by means of the XAS technique. The near-edge region of the XAS spectrum, extending over the first 10 eV above the threshold, carries information about the electronic structure of the absorbing atom. In contrast, the high energy region of the spectrum (EXAFS) is mainly related to the local structure around the absorbing atom.

We have performed a detailed XAS study at the Fe K-edge in nanoparticulate systems with different chemical composition, crystal structure and magnetic properties; iron oxyhydroxide (FeOOH) and magnetite (Fe₃O₄). The objective is to determine the actual chemical composition by direct comparison of the experimental XAS spectra to those obtained for bulk reference materials [3].

The Fe₃O₄@TREG (TREG) nanoparticles were obtained by the decomposition of Fe(acac)₃ with lauric acid and laurilamine in octyl ether at 290°C for 3 h. The nanoparticles were subsequently separated by solvent exchange using tetraethylene glycol (TREG). On the other hand, FeOOH nanoparticles (MAG1) were synthesized using by mixing of FeCl₃·9H₂O in a oleic acid and oleylamine in phenyl ether under stirring, followed by reaction with propylene oxide at 90°C. The solid is separated, washed and dried at 200°C. The XRD prove that the structures are alternatively a mixture of FeOOH and γ -Fe₂O₃ and Fe₃O₄. Moreover, ⁵⁷Fe Mossbauer measurements also confirm that samples are nanoparticulate iron oxides.

XAS experiments were performed at the BM25A SPline beamline of the ESRF. Measurements were performed at room temperature in the transmission mode on homogeneous thin layers of the powdered samples at the Fe K-edge. The absorption spectra were analyzed according to standard procedures: the background contribution from previous edges was fitted with a linear function and subtracted from the experimental spectrum. Then, XANES spectra were normalized to the absorption coefficient at high energy to eliminate the thickness dependence.

The XAS spectrum of sample TREG has been compared to those of bulk magnetite and maghemite in Fig. 1. As we can see, the XAS spectrum of TREG and bulk maghemite are virtually identical. This demonstrates that maghemite is the main crystal phase in the TREG nanoparticles and, furthermore, Fe³⁺ ions are predominant. On the other hand, the XAS spectra of MAG1 has been compared to those of bulk magnetite, maghemite and goethite in

Fig. 2. In this case, the XAS spectrum of MAG1 resembles more to goethite than to the other oxides.

In summary, these results show that XAS is a powerful technique for determining the actual crystal structure and chemical state of iron oxide nanoparticles.

References:

[1] Biddlecombe BG, et al. *J. Mater. Chem.* **11** (2001) 2937.

[2] Si S, et al. *Chem. Mater* **16** (2004) 3489.

[3] Wilke M. et al. *Am. Miner.* **86** (2001) 714.

Figures:

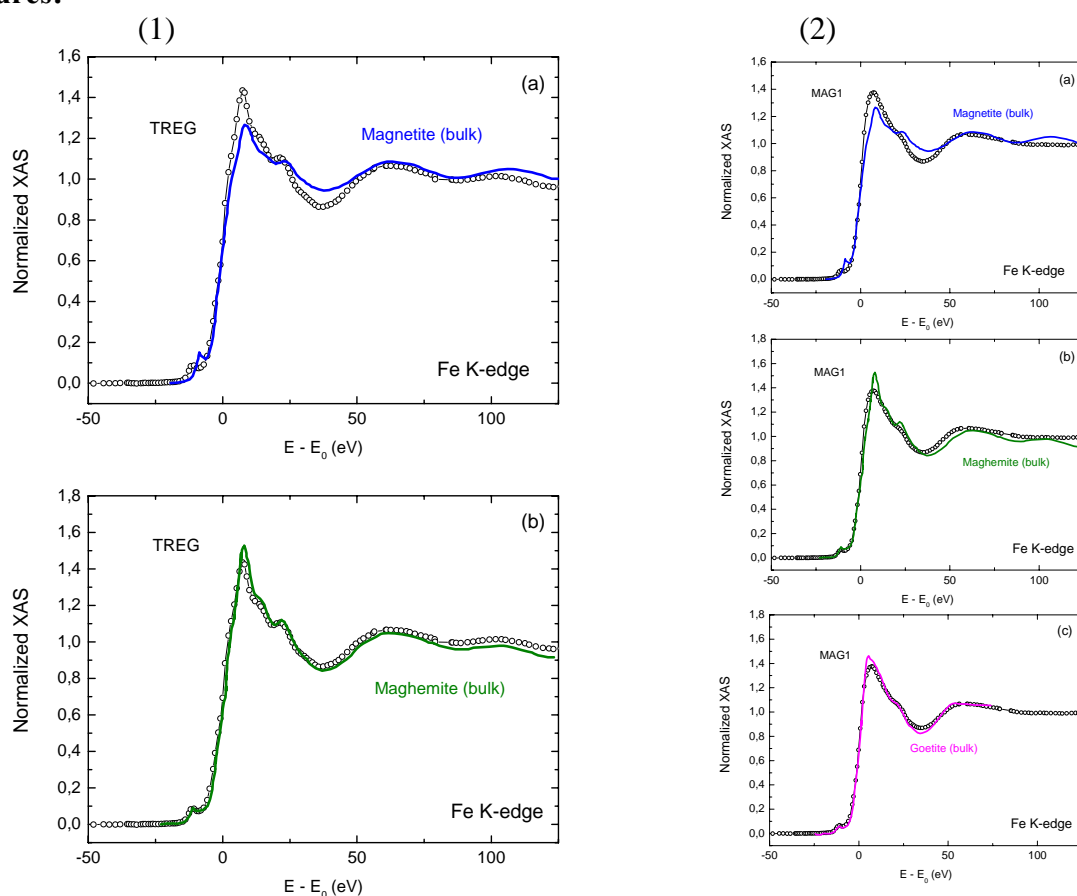


Figure 1. (color online) Comparison of the Fe K-edge XAS spectra of sample TREG and (a) bulk magnetite, and (b) bulk maghemite.

Figure 2. (color online) Comparison of the Fe K-edge XAS spectra of sample MAG1 and (a) bulk magnetite, (b) bulk maghemite, and (c) bulk goethite.

GOLD NANOPARTICLES-INDUCED ENHANCEMENT OF THE ANALYTICAL RESPONSE OF AN ELECTROCHEMICAL BIOSENSOR BASED ON A NEW ORGANIC-INORGANIC HYBRID COMPOSITE MATERIAL

M. Barbadillo Pérez de Ayala^{a}, E. Casero^a, M.D. Petit-Domínguez^a, F. Pariente^a, E. Lorenzo^a, L. Vázquez^b*

^aDepartamento de Química Analítica y Análisis Instrumental. Universidad Autónoma de Madrid. Campus de Cantoblanco. 28049 Madrid. Spain.

^bInstituto de Ciencia de Materiales de Madrid (CSIC). 28049 Madrid. Spain.

**e-mail: martabpda@hotmail.com*

Design and development of sensors based on enzyme immobilization onto transducer surfaces is of great interest in the field of bionanotechnology, mainly due to its potential applications in the development of analytical devices. In general, the retention of the enzymatic activity after the immobilization process is one of the most important issues in this field because the interaction between the enzyme and the solid surface can induce conformational changes in the adsorbed enzymes. The alteration of the three-dimensional conformation leads to a diminution of the catalytic activity. In this sense, the use of a polymeric network generated by sol-gel technology can be used as a strategy to provide a biocompatible environment for enzyme protection exhibiting additional advantages such as simplicity of preparation, physical rigidity, renewable surface and tuneable properties [1-2]. Moreover, the integration of nanomaterials into (bio)sensors has become an attractive method for improving the properties of the resulting analytical device. From a practical point of view, gold nanoparticles (AuNPs) are widely used due to their interesting physicochemical properties, including i) a large surface area, ii) an excellent biocompatibility and iii) highly attractive catalytic properties toward several compounds as a consequence of an enhancement of the electrical communication with the electrode surface [3]. These characteristics made this nanomaterial suitable to immobilize biomolecules, particularly enzymes, allowing the retention of the biological activity for a long period of time.

In the present work, we describe the preparation and characterization of a new organic-inorganic hybrid composite material from a three dimensional silica polymer network, obtained by means of the sol-gel technology using tetraethoxysilane (TEOS) as precursor. The final properties of the sol-gel matrix play a key role in the biosensor performance and can be easily controlled by varying some parameters such as the precursor type or the preparation conditions (pH, ratio of compounds, etc). This matrix provides an excellent network allowing the encapsulation of the different biosensor components: a biosensing molecule (glucose oxidase, GOx was chosen as a model), gold nanoparticles (AuNPs) and graphite powder (C). The resulting sol-gel / glucose oxidase / gold nanoparticles / graphite powder (TEOS/GOx/Au-NPs/C) hybrid material benefits from the advantages of their different components, giving rise to a material particularly attractive for electrochemical biosensor preparation.

We have used as a surface characterization technique the Atomic Force Microscopy (AFM) since it allows us to assess the influence of the nanoparticle addition on the electrode nanomorphology [4-5]. Thus, we have studied by AFM operating in tapping mode in ambient conditions the surface morphology of the different systems despite the micro-roughness of some of them. We have measured areas from 64 nm² down to 0.25 nm² in order to characterize their roughness at the nanoscale. For the carbon-based electrodes, we addressed special emphasis to resolve the surface structure at atomic resolution. In contrast, for the enzyme-containing systems AFM was used to map the protein surface coverage and homogeneity. Figures A and B show AFM images of relative large and small areas, respectively, of the surface of a TEOS/GOx/Au-NPs/C electrode. The rounded structures seen in B correspond to the globular GOx enzymes and aggregates covering the electrode surface. Phase-contrast images were also acquired in order to gain further sensitivity to be able to distinguish soft and hard nanodomains within the sampled areas. Finally, we also performed preliminary force curve analysis on the different systems.

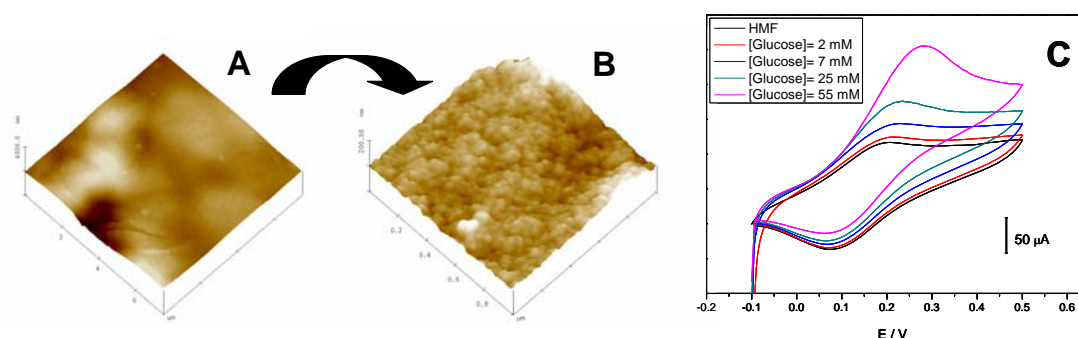
Finally, the designed material was applied to the determination of glucose in presence of hydroxymethylferrocene (HMF) as a redox mediator. The system exhibits a clear electrocatalytic activity towards glucose (see Figure C), allowing its determination at 200 mV versus SCE. with a good operational performance.

Acknowledgements: This work has been supported by *Comunidad de Madrid/Universidad Autónoma de Madrid* (Project N° CCG08-UAM/SEM-4074 and the *Ministerio de Ciencia e Innovación* (Project No. CTQ2008-05775 and FIS2006-12253-C06-03).

References:

- [1] Lev, O., Tsionsky, L., Ravinovich, V., *Analytical Chemistry* **67**(1) (1995) 22A-30A.
- [2] Dave, B.C., Dunn, B., Valentine, J.S., Zink, J.I., *Analytical Chemistry* **66**(22) (1994) 1120A-1127A.
- [3] Fendler, J.H., (Ed.), "Nanoparticles and Nanostructured Films" (1998) Weinheim, VCH.]
- [4] Chiorcea-Paquim, A.M., Pauliukaite, R., Brett, C.M.A., Oliveira-Brett, A.M., *Biosensors and Bioelectronics* **24** (2008) 297-305.
- [5] Pauliukaite, R., Chiorcea-Paquim, A.M., Oliveira-Brett, A.M., Brett, C.M.A., *Electrochimica Acta* **52** (2006) 1-8.

Figures:



**Structure, morphology and optical properties of $V_xMo_{1-x}O_2$ thermochromic coatings
synthesized by DC reactive magnetron sputtering**

C. Batista, V. Teixeira, R. M. Ribeiro

University of Minho, Department of Physics, Campus de Gualtar, 4710-057 Braga, Portugal

cbatista@fisica.uminho.pt

The latest approach on the improvement the energy efficiency of buildings is based on the use of thermochromic coatings on so-called “smart” windows. These coatings possess the ability of changing their optical properties as a consequence of a reversible structural transformation when going through a critical temperature. Vanadium dioxide is an example of a transparent thermochromic material which is a promising candidate for this kind of application. The change on its optical and also electrical properties takes place at 68°C as a result of a first-order structural transition, known as Mott transition [1], going from a monoclinic to a tetragonal phase on heating. The low temperature semiconducting phase which is transparent to radiation in the visible and infrared wavelength range maximizes the heating due to blackbody radiation, while the metallic high temperature phase blocks the infrared radiation and maintains at the same time the transparency required, in the visible range, to keep an environment of natural light. A transition temperature of 68°C is too high for this application and must therefore be reduced. Tungsten-doping of VO_2 has demonstrated to decrease the transition temperature in the greatest extent, when compared with other metals, and has therefore been the focus of most of the research [2].

In this study, we have prepared Mo-doped VO_2 thin films onto SiO_2 -coated float-glass substrates by reactive direct current (DC) magnetron sputtering. The films were characterized in terms of crystal structure and texture by x-ray diffraction (XRD) and the morphology of the surface has been analyzed by scanning electron microscopy (SEM) and atomic force microscopy (AFM). The optical/thermochromic behavior of the different films has been studied by optical spectrophotometry in the UV-VIS-NIR range. The relationship between the contents of substitutional Molybdenum in VO_2 solid solution and the semiconductor-metal transition temperature has been established. Moreover, the influence of dopant concentration on the transition hysteresis and IR modulation efficiency is demonstrated.

References:

- [1] A. Zylbersztejn and N.F. Mott, Physical Review B 11 (1975) 4383-4395.
- [2] I.P. Parkin and T.D. Manning, Journal of Chemical Education 83 (2006) 393-400.

STM manipulation of molecular moulds on metal surfaces

Youness BenJalal ³, *Xavier Bouju* ², *Mohamed Hliwa* ^{2,3}, *André Gourdon* ², *Christian Joachim* ², *Nataliya alashnyk* ¹, *Miao Yu* ¹, *Wei Xu* ¹, *Regis Barattin* ², *Erik Lægsgaard* ¹, *Ivan Stensgaard* ¹, *Trolle R. Linderoth* ¹ and *Flemming Besenbacher* ¹
¹ Interdisciplinary Nanoscience Center (iNANO) and Department of Physics and Astronomy, University of Aarhus, Ny Munkegade, 8000 Aarhus C, Denmark
² Nanoscience group, CEMES-CNRS, 29 rue Jeanne Marvig, 31055 Toulouse, France
³ Faculté des Sciences Ben M'Sik, Université Hassan II-Mohammédia, BP 7955, Sidi Othman, Casablanca, Morocco
benjalal@cemes.fr

Molecular Landers are a class of compounds in which an aromatic board is decoupled from the underlying substrate via bulky spacer groups. They have attracted considerable attentions as molecular wires, light-driven nanocars, in particular due to the special capability by trapping metal atoms beneath into nanostructures[1,2]. However, except those pure-ordered short Lander chains, the attempt on 1D assembly of the Lander moulds has been only succeeded when applying special templates which unfortunately limits the future application.

By means of scanning tunneling microscopy (STM) imaging and manipulation, the morphology and anchoring of a specially designed Lander-type molecule, bis(diaminotriazine) (DAT, C₆₄H₆₈N₁₀) (Fig. 1(a)) is studied on Cu(110) and Au(111) surfaces under ultrahigh vacuum (UHV) conditions. Different electronic contact configurations of individual DAT molecules at step edges of Cu(110) substrate can be achieved and modified in a controlled manner by STM manipulation, including lateral translation, rotation, and pushing the molecule to an upper terrace. Through the comparison of manipulation of individual DAT on Cu(110) and Au(111) surfaces, we probe the qualitative molecule-substrate interaction directly, indicating that the diffusion barrier of single DAT molecules on Au(111) is smaller than that on Cu(110) and providing relevant information to the substrate selection for the self-assembly of DAT.

Fig. 1(b) presents a high-resolution STM image of a DAT molecule on Cu(110), showing four bright lobes in a rectangular shape (11.0 Å × 6.5 Å), and some sub-protrusions in the centre. The same morphology of the DAT molecule is depicted on the Au(111) surface (Fig. 2(b)). We tentatively interpret that each bright lobe corresponds to tunneling through one of the four *tert*-butyl groups, while the sub-protrusions may be attributed to the hexa-phenyl rings, which are connected with the central benzene by σ bonds. There is, however no obvious feature in the recorded STM images that can be attributed to the diamino-pyridine group. Theoretical simulations have been performed using elastic-scattering quantum chemistry (ESQC) [3] after having relaxed the molecule on the surface with molecular mechanics MM4(2003) code [4]. The STM images are compared with theoretically calculated STM images using the ESQC approach. From Figure 1(c) and Figure 2(c), it is seen that the contribution of diamino-pyridine groups to the tunneling current is apparently minor, consistent with the experimental findings, which confirms the interpretation above of the individual DAT molecule. Taking into account the electronic gap of DAT (2.05 eV), a calculation of the different molecular orbital shows that the highest occupied molecular orbital is imaged at the operating energy.

Lander B consists of a central polyaromatic unit, two imide functional groups on opposite sides and four *di-tert-butyl-phenyl* (DTP) spacer legs (Figure 3(c)). Figure 3(a) and 3(c) present the experimental and simulated STM images of a single Lander B molecule respectively, which are nicely consistent with each other. The dimension of the four bright

protrusions is approximately 14.5 Å long and 9.5 Å wide, attributed to tunneling through the DTP groups. Since the molecular core is lifted away the substrate (Figure 3(d)), its contribution to the tunneling current is rather minor. Similar to Lander A, the imide groups of Lander B also allow the HB between neighboring molecules, where the neighboring Lander B adopts a head-to-tail arrangement. The double N-H...O HB between imide functional groups.

References:

- (1) Rosei, F.; Schunack, M.; Jiang, P.; Gourdon, A.; Lægsgaard, E.; Stensgaard, I.; Joachim, C.; Besenbacher, F. *Science* **2002**, *296*, 328-331.
- (2) Schunack, M.; Rosei, F.; Naitoh, Y.; Liang, P.; Gourdon, A.; Lægsgaard, E.; Stensgaard, I.; Joachim, C.; Besenbacher, F. *J. Chem. Phys.* **2002**, *117*, 6259-6265.
- (3) Sautet P.; Joachim C. Calculation of the benzene on rhodium STM images. *Chem. Phys. Lett.* **1991**, *185*, 23-30.
- (4) Allinger N. L.; Chen K.; Lii J.-H. An improved force field (MM4) for saturated hydrocarbons. *J. Comput. Chem* **1996**, *5-6*, 642-668.

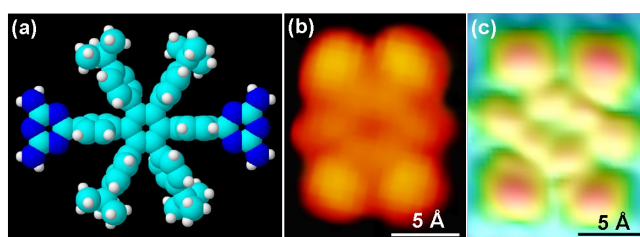


Figure 1: (a) Space-filled model of bis(diaminotriazine) (DAT) molecule ($C_{64}H_{68}N_{10}$). It consists of a benzene ring connected with four *tert*-butyl groups and two diamino-pyridine groups by σ bonds, where the carbon, hydrogen and nitrogen atoms are represented in pale blue, white and blue, respectively. (b) A typical high-resolution STM image of a DAT molecule on Cu(110). (sample voltage, -1.73V; tunneling current, -0.66 nA) (c) ESQC-simulated STM image of the DAT on Cu(110) as the same tunneling conditions as the experimental result in (b).

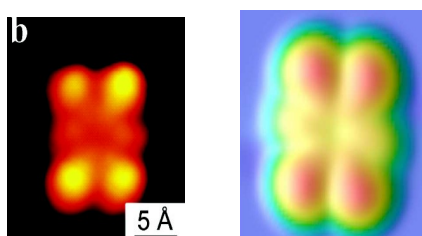


Figure 2: (b) A high-resolution STM image of a single Lander A (DAT) on Au(111). ($I_t=0.32$ nA, $V_t=1487$ mV). (c) EHMO-ESQC simulated image of Lander A on Au(111) at the same tunneling conditions as in panel (b).

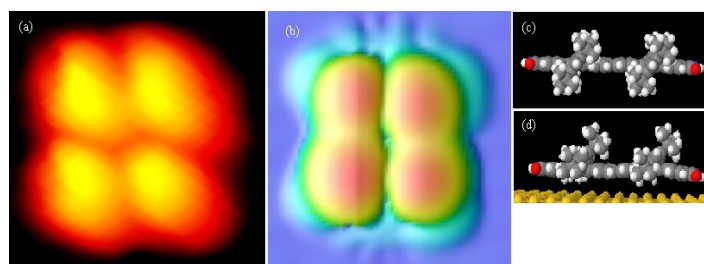


Figure 3 : (a) A high-resolution STM image of a single Lander B on Au(111). ($I_t=0.26$ nA, $V_t=1239$ mV). (b) ESQC-MM4 simulated image at the same tunneling conditions as in panel (a). (c) The anticipated model of space-filling Lander B. Carbon, hydrogen, oxygen and nitrogen atoms are represented in grey, white, red and blue, respectively. (d) A side-view model of Lander B on a substrate, showing the molecule is lifted away from the surface.

Synthesis and magnetic properties of CoFe_2O_4 spinel with nanometric size.

V. Blanco¹, M. J. Torralvo¹, R. Sáez¹, E. Legarra², F. Plazaola²

¹*Depto. Química Inorgánica, Facultad Ciencias Químicas, Universidad Complutense, 28040 Madrid, Spain.*

²*Depto. Electricidad y Electrónica, UPV/EHU, Aptdo. 644, 48080 Bilbao, Spain.
veronicabg@quim.ucm.es*

There is a growing interest in nanomaterials as they present different properties than their bulk counterparts. This fact makes possible to have a new variety of technological applications of these materials. In this work, nanosized spinel with different magnetic properties to their bulk counterparts, have been prepared.

Two samples of CoFe_2O_4 with different particle size were synthesized by the solvothermal method. Firstly, stoichiometric amounts of iron nitrate and cobalt nitrate were dissolved in water (for the 20 nm sample) or ethylenglycol (in the case of the 6 nm sample) and later, KOH was added as precipitant agent. The resultant mixture was transferred into an autoclave to be treated at 180° C for several hours (1).

X-ray diffraction data reveal that pure CoFe_2O_4 with spinel structure was obtained in both cases. It can be seen in the TEM images that both samples present homogenous particle size and polyhedral shape. It is worth noting that in the case of the sample with bigger particle size, well defined octahedral were obtained (see figure 1).

Different magnetic data depending on the particle size of the Co-ferrite were obtained and indicate that both samples behave as superparamagnetic. It can be seen that the coercive field increases as the particle size does as well as the blocking temperature corresponding to the maxima seen in the susceptibility curve (see figure 2). Mössbauer spectroscopy study confirms this behaviour showing a sextet structure below the blocking temperature, and a doublet above this temperature according to the previous work done by Manova et al. (2).

References:

- [1] R. Saez Puche, M. J. Torralvo Fernandez, V. Blanco Gutierrez, R. Gomez, V. Marquina, M. L. Marquina, J. L. Mazariego, R. Ridaura, Bol. Soc. Esp. Ceram.V., **47**, 3 (2008) 133.
- [2] Manova et al., Chem. Mater., **16**, 26 (2004) 5689.

Figures:

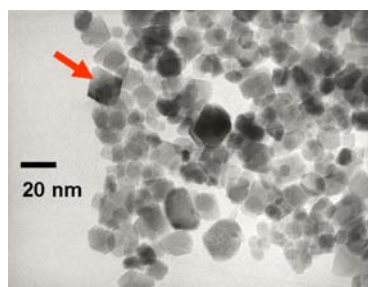


Fig. 1 Octahedral particles of Co-ferrite obtained by hydrothermal method.

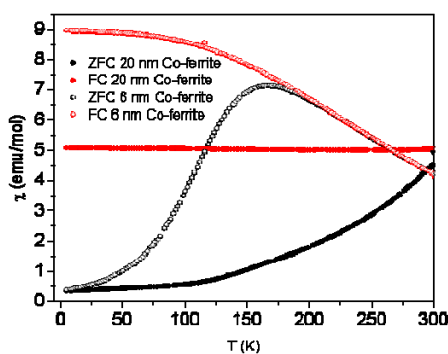


Fig. 2 Magnetic susceptibility for samples of CoFe_2O_4 with 20 nm and 2 nm particle size.

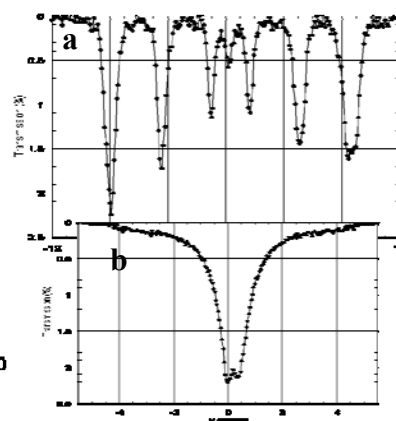


Fig. 3 Mössbauer spectra for 2 nm Co-ferrite at 55 K (a.) and room temperature (b.).

AN ELECTROCHEMICAL NANOSTRUCTURED APTAMER BIOSENSOR-BASED SANDWICH ASSAY FOR DETECTION OF C REACTIVE PROTEIN (CRP) AND OCHRATOXINE A (OTA)

L.Bonel*, JC.Vidal, P.Duato and JR.Castillo

Institute of Environmental Sciences (IUCA)

Analytical Spectroscopy and Sensors Group (GEAS)

University of Zaragoza. Ciudad Universitaria (50009) ZARAGOZA. Spain

**lbonel@unizar.es*

Detection and quantification of C-reactive protein (CRP) in an easy, cheap, and fast way can improve clinical diagnostics in order to prevent serious inflammatory states [1]. The CRP reference concentration of healthy subjects is < 5 mg/l in serum and the clinical range of interest is 1-500 mg/l [2]. The few proposed biosensors for CRP detection employ antibodies as bio-recognition elements, whereas few papers are based on the use of aptamers [3-5].

We have developed, optimized and validated, an electrochemical aptamer-based nanostructured sandwich aptasensor performed on magnetic nanoparticles for detection of CRP in serum samples.

This aptasensor involves the use of screen-printed electrodes for the transduction step and the use of another physical support for the affinity reaction.

Magnetic nanoparticles are available with a wide variety of surface functional groups and size and have the possibility of reaction kinetics similar to those found in free solution. Graphite and magnetic nanoparticles represent the most commonly used beads in bioelectroanalytical systems. Magnetic nanoparticles respond to an applied magnetic field and re-disperse upon removal of the magnet. They consist of 36–40% magnetite dispersed within a copolymer matrix consisting of styrene and divinylbenzene. Their binding capacity varies with the bead size, composition and the size of the binding ligand. There is a general consensus that the use of magnetic beads greatly improves the performance of the immunological reaction, due to an increase in the surface area, as well as the faster assay kinetics achieved because the beads are in suspension and the analytical target does not have to migrate very far

The designed aptasensor is based on the use of two surfaces, magnetic nanoparticles for immunoassay and screen-printed electrodes for electrochemical transduction, giving the best analytical performances in terms of sensitivity and speed of the analysis.

After the assay, the modified magnetic beads were captured by a magnet on the surface of a graphite working electrode and the electrochemical detection was thus achieved through the addition of the AP substrate (α -naphthyl-phosphate) and α -naphthol produced during the enzymatic reaction was detected using differential pulse voltammetry (DPV).

The LOD and LOQ calculated in CRP free serum were 0.2 and 6 mg/l respectively and the average coefficient of variation (ACV) was 8 %. The LOD found was comparable with the reported by ELISA and it was much lower than the clinically useful borderline value (8 mg/l). Finally, this approach was applied to the analysis of some serum samples and it resulted as a promising tool to predict the risk of a possible disease with CRP levels

Additionally, we are going in this communication to explain the nanostructured design developed using a selective aptamer for Ochratoxine A (OTA), but in this case the magnetic beads weren't used as solid support. OTA-BSA conjugated was immobilized onto screen printed electrodes (SPCEs) and then the aptamer biotinylated was added onto surface. Finally, Alkaline Phosphatase-ExtraAvidin was used as enzymatic conjugate in the electrochemical detection step. We will present this new aptasensor for OTA with good analytical performances to determine this mycotoxine in foods and beverages.

References:

- [1] M. Ramada, A. Shrive, D. Miles, J. Volanakis, L. Delucas, T. Greenhough, *Acta Crystallographica*, **58** (2002) 992-1001
- [2] C. Burtis, E. Ashwood, D. Bruns, *Testbook of Clinical Chemistry and Molecular Diagnostics*, 4th ed, Elsevier Saunders 2006, USA.
- [3] K. Pagana, T. Pagana, *Manual of Diagnostic and Laboratory Tests*, 3th ed, Mosby Elsevier, 2006, USA.
- [4] A. Bini, S. Centi, S. Tombelli, M. Minunni, M. Mascini, *Analytical and Bioanalytical Chemistry*, **390** (2008) 1077-1086
- [5] J. Pultar, U. Sauer, P. Dommanich, C. Preninger, *Biosensors and Bioelectronics*, 2008. doi: 10.1016/j.bios.2008.08.052

NANO-CONFINEMENT OF WATER IN SILICALITE AND $\text{AlPO}_4\text{-5}$ ZEOLITES: INVESTIGATION OF THE STRUCTURE AND THE DYNAMICS BY MOLECULAR MODELLING

Patrice Bordat, Pierre-André Cazade, Isabelle Baraille and Ross Brown
Institut pluridisciplinaire de recherche sur l'environnement et les matériaux,
UMR 5254 du CNRS et de l'Université de Pau et des Pays de l'Adour,
Avenue Pierre Angot, 64053 Pau cedex, France
patrice.bordat@univ-pau.fr

While silicas are among the chemically simplest of minerals, their structure and dynamics are fascinatingly rich and varied, thanks in part to the subtle interplay of the rigidity of the SiO_4 units and to the flexibility introduced by their association in networks of corner- or edge-sharing tetrahedra. The balance of forces in porous polymorphs like zeolites is even more delicate, so that their phase transition may depend on the presence of defects [1] or occluded molecules, as when adsorption of *p*-xylene in H-ZSM-5 determines a transition from monoclinic to orthorhombic [2]. The framework flexibility is thus an important parameter in problems of molecular adsorption and diffusion in zeolites.

The affinity of zeolites for water is also very varied, depending on the amount and the type of the defects. A perfect silicalite (without structural defects and aluminium) is very hydrophobic while synthesized silicalites are from slightly hydrophobic to very hydrophilic [3]. On the contrary, perfect $\text{AlPO}_4\text{-5}$ is very hydrophilic, as is faujasite NaY, containing aluminium and Na^+ counter-ions.

Molecular dynamics is a useful tool to investigate these materials, either empty or mixed with organic adsorbates, at the nanometric scale. Nevertheless, most simulations:

- assume rigid frameworks ignoring then the flexibility issue,
- poorly represent the inorganic-organic interactions because of the incompatibility of the large charges in oxide models ($q_{\text{Si}} > 2e$) [4] compared to those in typical molecular force fields ($q < 0.5e$).

We provide a new force field for silicas, able to describe their structure and their dynamics and compatible with the molecular interactions with organic systems. We will show that the new force field is valid either for dense silicas like α -quartz or α -cristobalite, or for microporous silica like silicalite. The new force field describes well the affinity of silicalite for water, which will be compared to the adsorption of water in $\text{AlPO}_4\text{-5}$.

This study is a necessary preliminary step before encapsulating organic molecules of interest in both hydrophilic and hydrophobic microporous silicas and looking at their adsorption sites and their diffusion.

References:

- [1] G. Artioli, C. Lamberti and G. L. Marra, *Acta Cryst. B*, **56** (2000) 2.
- [2] H. van Koningsveld, F. Tuinstra, H. van Bekkum and J. C. Jansen, *Acta Cryst. B*, **45** (1989) 423.
- [3] V. Bolis, C. Busco and P. Ugliengo, *J. Phys. Chem. B*, **110** (2006) 14849.
- [4] B. W. H. van Beest, G. J. Kramer and R. A. van Santen, *Phys. Rev. Lett.*, **64** (1990) 1955.

THE AGGREGATION OF SUPERPARAMAGNETIC PARTICLES IN A FERROFLUID

Stanislav Čampelj¹, Marko Jagodič², Alenka Mertelj¹, Zvonko Jagličić², Darko Makovec¹

¹*“Jožef Stefan” Institute, Jamova 39, Slovenia*

²*Institute of Mathematics, Physics and Mechanics, Jadranska 19, Slovenia*

stanislav.campelj@ijs.si

Stable colloidal suspensions of magnetic nanoparticles called ferrofluids have attracted a lot of attention in recent years, since they can be used in numerous technological and medical applications [1-3]. For biomedical applications aqueous-based ferrofluids are being tested. Besides the requirements concerning their non-toxicity and biocompatibility, their behaviour in a magnetic field is also of great importance. Under the influence of an external magnetic field, the nanoparticles of the ferrofluid undergo a major change in their ordering, forming agglomerates, which can lead to a phase separation. The transformations in the ordering of the nanoparticles in the ferrofluid and phase separation have a drastic effect on the rheological properties of the ferrofluid.

In the absence of a magnetic field the thermal energy, kT , prevails over the dipole-dipole interaction between superparamagnetic nanoparticles. As a result, the nanoparticles remain separated and suspended in a carrier liquid. A drastic change in their ordering occurs when they are exposed to a magnetic field. The dipole-dipole interactions prevail over kT and the nanoparticles start to form chain-like agglomerates. This agglomeration leads to a phase separation, resulting in two phases: the “liquid phase”, containing a larger content of the nanoparticles; and the “gas phase”, with a lower content of nanoparticles. The transition is usually described by the van der Waals “gas-liquid” phase transition [4-6].

In this work, the process of agglomeration was studied in a ferrofluid prepared by dispersing superparamagnetic nanoparticles of maghemite in water, using citric acid as the surfactant. The nanoparticles were 14 nm in diameter, with a saturation magnetization of 66 emu/g. The ferrofluid contained from 0.5 to 1.7 wt.% of magnetic phase.

The changes in the internal structure caused by the ordering of the nanoparticles in ferrofluids under the influence of an external magnetic field were studied with measurements of the rheological properties as a function of field strength, with dynamic light scattering (DLS), and with magnetic measurements. The rheological measurements showed the influence of the magnetic field on the rheological behaviour of the ferrofluid. With an increasing magnetic field, first the viscosity increases, as the character of the ferrofluid changes from a sol to a gel. At even higher magnetic fields, the gel transforms back to a sol and the viscosity decreases. These changes can be attributed to a gradual change in the ordering of the nanoparticles. In parallel, the changes in the internal structure during the process of phase separation were studied using DLS. The internal structures appearing in the ferrofluid were observed using an optical microscope. The magnetic interactions between the nanoparticles originating from the formation of the internal structure as a function of the magnetic field were also studied, using measurements of magnetization under zero field and field cooling (ZFC/FC) conditions. The ZFC/FC measurements showed an increase in the saturation magnetization at the blocking temperature, depending on the strength of the magnetic field at which the sample was frozen. The increase in the magnetization can be explained by the agglomeration of the particles. Once the particles come into close proximity, the coupling of the magnetic moments occurs, which increases the initial ($H=0$) susceptibility of the nanoparticles. The process was found to be totally reversible. When the magnetic field is cancelled, the magnetization reduces back to

the original value, indicating that the particles in the formed agglomerates do not come into direct contact.

References:

- [1] Z. Ma, Y. Guan, H. Liu, J. Magn. Magn. Mater., **301** (2006) 469
- [2] Q. A. Pankhurst, J. Connolly, S. K. Jones, J. Dobson, **36** (2003) R167
- [3] R. E. Rosensweig, Ferrohydodynamics, Dover Publications Inc., Mineloa, New York (1985)
- [4] A. Yu. Zubarev, L. Yu. Iskakova, Physica A, **335** (2004) 325
- [5] A. Yu. Zubarev, L. Yu. Iskakova, Physica A, **343** (2004) 65
- [6] A. F. Pshenichnikov, J. Magn. Magn. Mater, **145** (1995) 319

Figures:

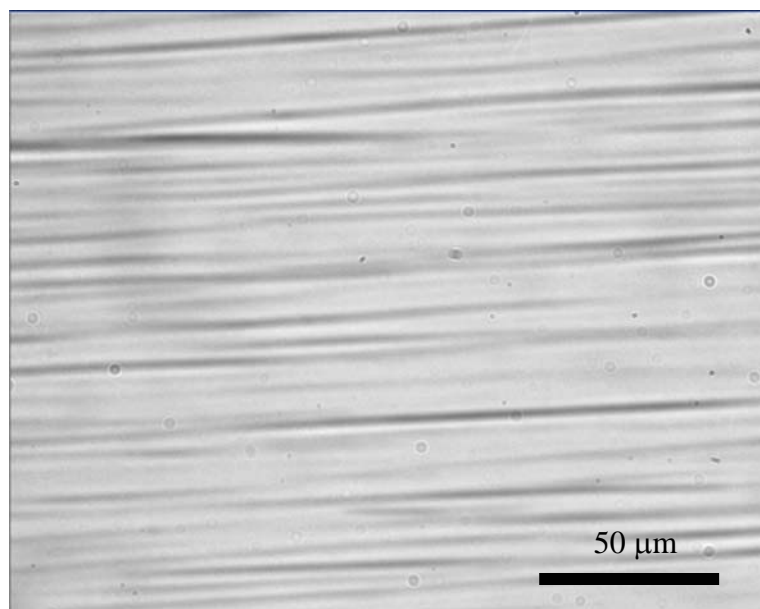


Figure 1: Micrograph shows phase separation into “liquid phase”, containing a larger content of the nanoparticles (darker areas), and the “gas phase”, with a lower content of nanoparticles (lighter areas) in the ferrofluid under the influence of a 270 mT magnetic field.

Pd Nanoparticles Deposited in Multiwalled Carbon Nanotubes as Catalysts for C-C Coupling Reactions

Manoli Cano^a, Ana M. Benito^a, Wolfgang K. Maser^a, Esteban Urriolabeitia^b

a Instituto de Carboquímica, CSIC, Zaragoza, E-50018, Spain

b Dept Compuestos Organometálicos, Instituto de Ciencia Materiales Aragon, CSIC-Univ. Zaragoza, E-50009 Zaragoza, Spain

mcanogaley@icb.csic.es

Metal nanoparticles are objects of great interest for an enormous number of applications in many fields such as electronics, optoelectronics, biology and catalysis (1,2). In catalysis, the large surface area-to-volume ratio of nanoparticles allows their effective utilization. In this context, catalyst support plays an important role on both catalytic activity and stability. Without suitable support metal particles aggregate, reducing surface area and restricting control over particle size. To overcome this problem several supports have been essayed to immobilize catalytic nanoparticles, e.g. carbon, metal oxides and zeolites (3). Carbon Nanotubes (CNTs) have proven to be a good alternative allowing small and highly dispersed nanoparticles in its structure (2).

In this work, palladium nanoparticles supported on carbon nanotubes were evaluated as catalyst for relevant C-C coupling reactions, for instance in Heck or Suzuki couplings (4).

Palladium nanoparticles were deposited by in-situ decomposition of a palladium complex, tris(dibenzylidenacetone) dipalladium (0), in presence of multiwalled carbon nanotubes under inert atmosphere in toluene. Characterization of the Pd-CNTs catalyst by TEM, SEM, DRX, ICP and elemental analysis was carried out. Homogeneous distribution of Pd nanoparticles on the carbon nanotubes sample, with sizes in the range 4-6 nm were obtained (Fig. 1).

The Pd-loaded CNTs material was used as catalyst for CC couplings between iodobenzene and methyl acrylate (Fig.2) or phenylboronic acid under Ar atmosphere. High yields were obtained, showing the high catalytic activity of the prepared catalysts. Characterization of the catalyst before and after the reaction was carried out.

References:

- [1] Drake C, Deshpande, S, Bera, D, Seal, S., International Materials Reviews, 52 (2007) 5
- [2] Anson, E. Lafuente, E. Urriolabeitia, E.P. et al., J. of Alloys and Compounds, 436 (2007) 294
- [3] a) Liu Z., Ling, X.Y.; Su, X.; Lee, J. Y. J. Phys. Chem. B 108 (2004) 8234; b) Mallick, K.; Scurrel, M.S. Appl. Catal. A. 253 (2003) 527; c) Sun C.; Peltre, M. J.; Briend, M., Blanchard, J. et al. Appl. Catal. A. 245 (2003), 245.
- [4] N. Karousis, G. Tsotsou, F. Evangelista et al. J. Phys. Chem. C 2008, 112, 13463-69.

Figures:

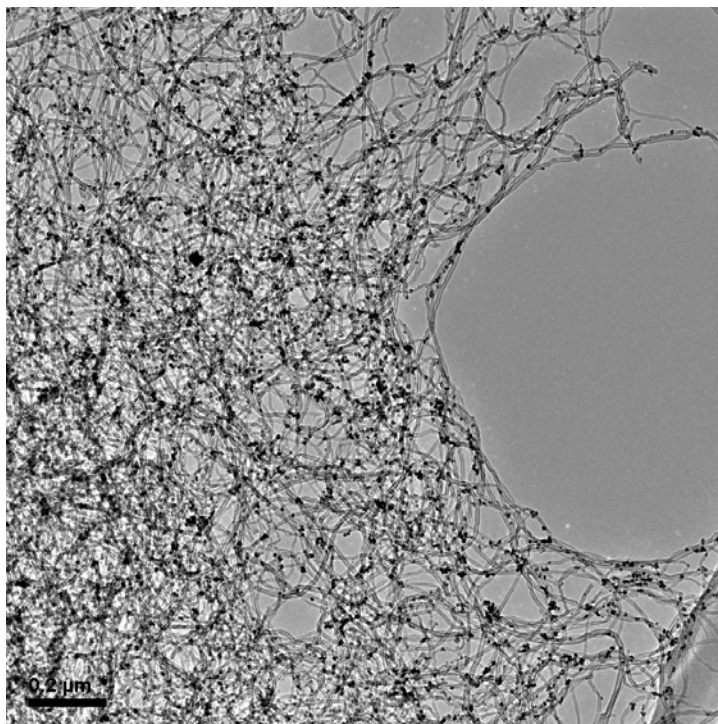


Fig. 1 TEM image of MWNTs loaded of palladium nanoparticles

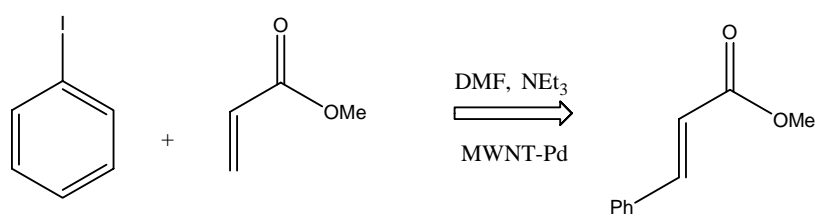


Fig. 2 Heck reaction with MWNT-Pd

NANOTOXICOLOGY: EXPLORING NEW PARADIGMS IN TOXICOLOGY

Eudald Casals, Edgar Gonzalez, Lorena García, Joan Comenge, Neus Bastús, Inge Nelissen, Tobias Pfaller, Geja Oosting, Albert Duschl, and Victor Puntès.

*Institut Català de Nanotecnologia, Campus UAB, Edifici Q (ETSE), 08193 Bellaterra, Spain
eudald.casals.icn@uab.es*

Nanotechnology offers promising opportunities in new materials and biomedical applications among others. The human exposure to larger amounts of naturally produced or intended (chemically or physically prepared) nanoparticles (NP) will become inevitable and previously uncertain risks must be evaluated. As a result, nanotoxicology research is now gaining attention¹. The aim of this work is to tackle the study from a holistic perspective, regarding nanomaterials features that can be named as the NP full life cycle, i.e. how they behave far from the synthesis when they are dispersed in the exposure media and finally exposed to humans and environment².

It is well known that colloidal particles are systems out of chemical equilibrium, in a metastable phase. Their final fate is the desintegration or agglomeration towards more stable phases. Thus, characterization of NP once produced, as used (administered or other mechanisms of human exposure) and after using is required since physico-chemical changes occur while in solution, what may have a significant impact on observed toxicological responses that go far from the classical paradigms of toxicology. In this scenario we focus our attention on:

Stability of NP: The proper interaction of the NP with biological entities will depend on the stability of the NP in biological media. Consequences of this are of great interest, for instance the higher cytotoxicity of unstable colloidal preparation of NPs are not due to the material but rather its physical state.

The surface of NP: While much of the NPs function is due to their core structure, the surface coating defines much of their bioactivity. NP never travel alone, but they are constantly surrounded by an intended (for further application) or spontaneous due to the environment (the protein-corona³) coating. Consequences of this can be the different final bioactivity of NP of the same element depending on among others: 1) Their surface charge: Obviously “positive” NP attach predominantly negative biological surfaces as cell membranes, leading to cell death. 2) The spontaneous coating is not immediate but develops as time progresses with the possibility of different responses at different moments of the exposure.

The core of NP: Not for the composition of the NP itself because can be inert or toxic regarding their surface structure as mentioned above but for the release of cations that NP experiment in their full life cycle. Initially, not all of the precursor reagent used to synthesize NP is transformed. After synthesis, additional leakage of cations is observed, usually the leakage is fast in the first few days and then more slowly in the latter days (1% in 100 days of exposure of NP to Cell Culture Medium supplemented with serum). We have observed this pattern for Oxides NP (CeO₂, Fe₃O₄, CoO) and Metallic NP (Au, Ag, Pt), and similar data are being published for Quantum Dots (CdSe) and Carbon Nanotubes⁴. And this release must be taken into account regarding the toxicity of the material.

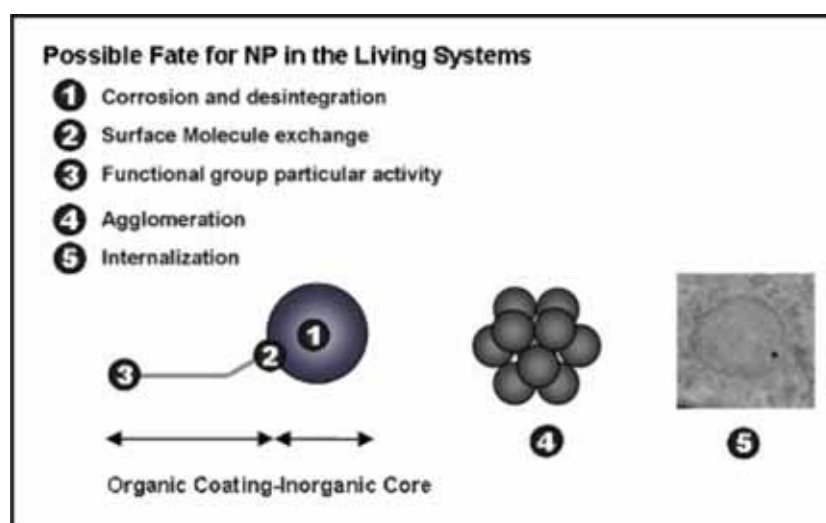
New paradigms in Nanotoxicology: Obviously cells death in the presence of inorganic NP is not the only factor to examine. Other important consideration such as the immunomodulatory effects must be also studied. While inorganic matter is known to be not toxic sometimes, immunogenic leading to sarcoidosis, granulomatosis, asbestosis, silicosis and others are. However in nanometric sizes particles will not follow such pattern since they are easily phagocyted. This new pattern of immune response caused by NP can lead to the possibility of tuning this response⁵.

The co-stimulatory effects⁶ of NP when they are not toxic for healthy organisms but hazardous in some compromised states should suggest the needs to focus on the efforts on studying nanotoxicology in a more compromised cases.

The effect of the solvent itself -where there are presence of stabilizers, surfactants and other molecules required for the NP synthesis – must be considered and not only used as a control.

Many times the toxic effect is performed as a “catalytic-like” that means inorganic NPs are not deactivated when killing the cell (for instance making a hole in cell membrane due to the positive surface charge) and introducing the concept of single particle lethality where in the worse –imaginary- scenario one nanoparticle could kill an organism made of millions of cells.

We work on all these aspects and our results and conclusions will be exposed and discussed.



Regarding the reactivity of a NP inside a biological system one have to take into account: i) degradation of their inorganic core, ii) the surface-molecule substitution and molecule release (phenomenon which can be used at the advantage of the researcher), iii) the particular coating molecule reactivity, iv) NPs stability and agglomeration and the v) NPs internalization.

References:

- [1] Bastus, N. Casals, E. Vazquez-Campos, S and Puentes, V. *Reactivity of engineered inorganic nanoparticles and carbon nanostructures in biological media*. **Nanotoxicology** 2 (2008) 99-112.
- [2] Casals, E. Vazquez-Campos, S. Bastus, N and Puentes, V. *Distribution and potential toxicity of engineered inorganic nanoparticles and carbon nanostructures in biological systems*. **TrAC, Trends Anal. Chem.** 27 (2008) 672-683.
- [3] Cedervall, I. Lynch, S. Lindman, T. Berggard, E. Thulin, H. Nilsson, K. A. Dawson and S. Linse. *Understanding the nanoparticle-protein corona using methods to quantify exchange rates and affinities of proteins for nanoparticles*. **PNAS**. 104 (2007), 2050-2055.
- [4] Kirchner, C. Liedl, T. Kudera, S. Pellegrino, T. Muñoz, A. Hermann, M. Gaub, E. Stozle, S. Fertig, N and Parak, W.J. *Cytotoxicity of Colloidal CdSe and CdSe/ZnS Nanoparticles*. **Nano Lett.** 5 (2005) 331-338
- [5] Bastús, N. Sánchez-Tilló, E. Pujals, S. Farrera, C. Kogan, M. Giralt, E. Celada, A. Lloberas, J. and Puentes, V. *Peptides Conjugated to Gold Nanoparticles Induce Macrophage Activation*. **Molecular Immunology** in press (2008).
- [6] Pfaller, T. Puentes, V. Casals, E. Duschl, A and Oostingh, G. *The impact of experimental design and cell choice for the analysis of immunomodulatory effects of engineered inorganic nanoparticles*. **Nanotoxicology** in press (2008).

ULTRATHIN HEMATITE AND GOETHITE-HEMATITE CORE-SHELL NANORODS AND COMPOSITE NANOWIRES BY ELECTROSPINNING

Sara Cavaliere-Jaricot, Arnaud Brioude, Philippe Miele

*Laboratoire des Multimatériaux et Interfaces UMR 5615 CNRS - Université Lyon 1,
Université de Lyon - 43 bd du 11 Novembre 1918, F-69622 Villeurbanne, France.*

sara.cavaliere-jaricot@univ-lyon1.fr

Hematite (α -Fe₂O₃) is an environmentally friendly, low cost, high resistant to corrosion and versatile material with n-type semiconducting and magnetic properties. Due to such stability and electronic properties, this oxide has various applications in several fields as catalyst, photocatalyst, photoelectrode, battery electrode, gas sensor, pigment and magnetic material.

Considerable interest has been devoted toward hematite nanostructures of various morphologies because of the novel size- and shape-dependent chemical and physical properties appearing at the nanoscale. A variety of physical and chemical strategies have been developed for the synthesis of size-controlled hematite 1D nanostructures: pulsed laser deposition (PLD), metal-organic chemical vapor deposition (MOCVD), hydrothermal synthesis, microwave assisted hydrothermal synthesis, sol-gel process, template-assisted synthesis, iron-water vapor reaction, forced hydrolysis, and micellar synthesis [1-4]. Such synthesis routes involved the introduction of surfactants or shape control ions, high temperatures, precursor calcination steps, and are often time-consuming. Furthermore, it still remains a challenge to develop simple and mild routes to synthesize nanorods with ultra-thin diameters.

One-dimensional α -Fe₂O₃ nanorods with very small diameter of about 10 nm and length between 100 to 200 nm (Figure 1) were synthesized in aqueous solution at low temperature with a simple and rapid method based on the oxidation of Fe₃O₄ nanoparticles at acidic pH, without using surfactants [5]. HRTEM (High Resolution Transmission Electron Microscopy) also showed the presence of core-shell structures (Figure 2). The core phase is goethite (α -FeOOH) with the typical $d(110)=4.18\text{\AA}$ (JCPDS n°81-0464) interplanar distance and the shell is composed of hematite layers with the typical $d(104)=2.703\text{\AA}$ interplanar distance (JCPDS n°33-0664). It is likely to think that the formation mechanism of the core-shell structures involves the heterogeneous nucleation of hematite on initially precipitated goethite cores. For thinner nanorods, we can assume that the goethite phase has been totally transformed into hematite one.

Optical characterization of such 1D nanostructures was performed by Raman and UV-vis spectroscopy (Figure 2) and will be furthermore discussed in more detail.

As an interesting issue, such nanomaterials are incorporated in a polymer matrix (PAN, polyacrylonitrile) and nanowires are obtained by the electrospinning method (Figure 3). Such nanocomposite materials can have applications in gas sensing and depollution.

References:

- [1] Z. Zhong, J. Ho, J. Theo, S. Shen, A. Gedanken, Chem. Mater. **19** (2007) 4776.
- [2] X. Zhang, Q. Li, Mater. Lett. **62** (2008) 988.
- [3] Y. Zhao, C.W. Dunnill, Y. Zhu, D.H. Gregory, W. Kockenberger, Y. Li, W. Hu, I. Ahmad, D.G. McCartney, Chem. Mater. **19** (2007) 916.
- [4] W. Zhou, K. Tang, S. Zeng, Y. Qi, Nanotechnology **19** (2008) 065602.
- [5] S. Cavaliere-Jaricot, A. Brioude, P. Miele, Langmuir, accepted.

Figures:

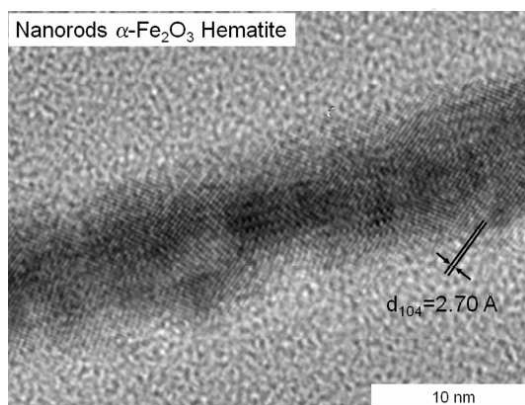


Figure 1. HRTEM micrograph of hematite nanorods with diameter less than 10 nm.

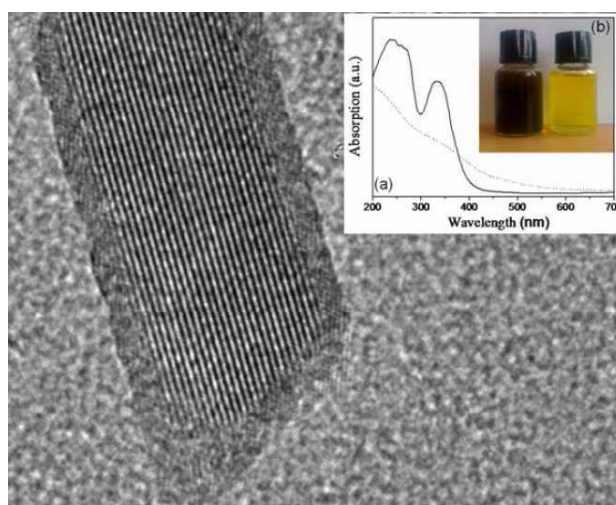


Figure 2. HRTEM micrograph of a core-shell goethite-hematite nanorod. In the inset: (a) UV-vis absorption spectra of the as-prepared solutions. (b) Optical images of the magnetite precursor solution (left side) and of the brilliant yellow hematite rods solution (right side).

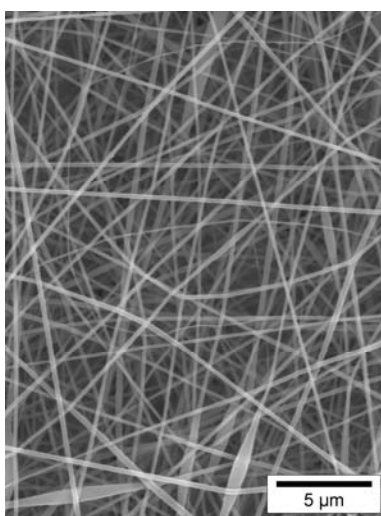


Figure 3. SEM image of composite nanomaterials/PAN nanowires obtained by the electrospinning technique.

PREPARATION AND PROPERTIES OF NANOSTRUCTURED HYDROGENATED CARBON THIN FILMS

F. Cerny, V. Jech and S. Konvickova

Czech Technical University, Technicka 4, 16607 Prague, Czech Republic

Frantisek.Cerny@fs.cvut.cz

The nanostructured or amorphous carbon materials containing less than 1% hydrogen (designated a-C or taC—for "tetrahedral carbon") may contain 85% or more sp^3 type C bonds (sp^3 hybridized carbon) and show attractive, diamond-like physical and mechanical properties; other such materials containing up to ca. 50 at.% hydrogen (hydrogenated carbon designated a-C:H) typically contain sp^3 fractions smaller than 50%. In both cases, the remainder is made up mainly of sp^2 type C bonds forming graphitic structure when clustered. Some confusion arises from the circumstance that both these forms are often termed DLC (Diamond-Like Carbon). Hydrogenated amorphous carbon coatings describe a large class of different coatings with properties ranging from relatively soft to extremely hard, from highly amorphous to more graphitic-like and from high to low hydrogen contents, as well as any combination of these [1,2]. As indicated by some new applications, the potential of a-C:H films today extends far beyond their already undisputed application areas [3]. This gave the basic impetus for examining PACVD (Plasma Assisted Chemical Vapour Deposition) coatings of the a-C:H type in the present study.

The a-C:H films were prepared by PACVD from methane precursor in the presence of hydrogen and/or argon (all min. 99.99% purity). The heart of the apparatus was a tubular reactor with capacitor type arrangement of electrodes, also permitting heating or conversely, at least partial cooling of the samples.

Two variants of plasma generation were used: (i) plasma generated by radio-frequency (rf) discharge (at 13.56 MHz and 2-10 W/cm² power density), and (ii) plasma generated by direct current (dc) discharge (at current densities of 1.2, 2.4, and 3.6 mA/cm²).

In the case of rf plasma the film growth rate as function of electrode bias and function of temperature and the effect of heat treatment of the films (annealing at 400-900°C/Ar) on film structure as reflected by the progress of the Raman spectra were studied.

The experiments conducted to establish the film growth rates at room (or moderately increased) temperature made use of Si substrates and were always begun at 25°C; but not even the water-cooled substrate holder succeeded in preventing a mild increase in temperature (up to ca. 50°C) due to the effect of the impinging ions during the course of deposition. The substrate bias voltage was pre-set to values ranging from -100 to -700 V to achieve ion bombardment of the growing film. At least three samples at each bias were prepared and examined.

a-C:H films deposited on Si (111) substrates were also used to study of effect of the thermal treatment of the films. These samples were annealed at 100-900°C, always for 30 minutes under argon. The experiments aiming to establish the film growth rates at elevated temperature were run at 50-500°C, at 100 and 200 V negative bias.

The a-C:H films deposited in dc plasma were produced in the same way and in the same apparatus as those deposited in rf plasma. The films were deposited on Si (111) substrate at room temperature (here the substrate had less tendency to heat up than in the case of rf plasma), at various negative dc bias values of 400-1000 V. The dependence of microhardness of the a-C:H films on the bias voltage was measured.

Experiments directed on applications of a-C:H films for power diodes were also carried out with both modification of PACVD method (rf and dc).

Film growth rate. The film deposition rate increases linearly with bias voltage within the entire bias range studied; raising the negative bias by 100 V will increase the film growth rate by ca. 10 nm/min.

The film growth rate decreases with increasing deposition temperature (within the range of up to 500°C). It appears that factors responsible for the gradual decline in growth rate observed on increasing the temperature of deposition may also include the etching effect of hydrogen (contained in the reaction atmosphere) on the removal of the graphitic form of carbon (as hydrogen will combine readily with graphitic carbon, the content of which increases with increasing temperature).

Effect of heat treatment. The effect of heat treatment of the a-C:H films prepared at a given electrode bias voltage and subsequently annealed at different temperature for 30 min. in an argon atmosphere was followed mainly by investigation of qualitative assessment of the shares of the "disorder" and the graphitic components in the Raman spectra. The Raman spectra obtained for films deposited on Si(111) indicate that the peak located around 1330 cm⁻¹ (peak D – disorder) becomes more pronounced as the annealing temperature grows higher.

Refraction index. The refraction index of the a-C:H films deposited at -250 V and 20-50°C kept decreasing moderately with increasing annealing temperature (at 100-500°C/30 min./Ar). For the temperature range in question it varied within the range of 2.1-2.4.

Morphology and adhesion. The a-C:H films applied onto polished silicon exhibit a smooth surface with no visible signs of disturbed morphology. The a-C:H films are known to exhibit high levels of internal stress. They often develop cracks even during deposition, and tend to peel off. Therefore, film adhesion was examined by microscopy and by indentation. It has been ascertained that the susceptibility to cracking is greater on metallic substrates than on Si, and grows more serious with increasing electrode bias voltage. It was in particular the a-C:H films of thicknesses greater than 250 nm which cracked if deposited on metallic substrates at negative bias exceeding 200 V. Peeling of the a-C:H films on samples showing poor adhesion can be observed even at low magnification. When an indenter is applied against the film surface, the cracks produced propagate in directions away from the point of indentation.

Films prepared in dc plasma. It has been found that the a-C:H films prepared in dc plasma had much better adhesion to substrate than those produced in rf plasma; the former films had much lower internal stress. Whereas with the rf plasma films the problem of poor adhesion tended to crop up as early as at 300-500 nm thickness, films showing good adhesion to Si substrates even at 1-2 µm thickness could conveniently be prepared in the dc plasma. The dc plasma suffers from the drawback that—and this is important in the deposition of insulating films—the film deposition rate would gradually fall off nearly down to zero as the films are built up to greater thickness. Also the microhardness of the a-C:H films prepared in dc plasma is lower than in the case of rf plasma probably because of lower internal stress. Microhardness grew moderately with increasing bias: for films deposited in dc plasma it was highest at the negative bias of 1000 V. The films deposited at 300 V negative bias were rather soft.

Applications of a-C:H films for power diodes. An experiment was carried out relating to the design of power diodes: the P-N junction was passivated by applying precisely a-C:H film prepared at room temperature. The characteristics of diodes provided with a-C:H film prepared in rf plasma and in dc plasma were measured. The experimental data confirm that both rf and dc plasma produced passivation films are sufficiently insulating at voltages up to ca. 2200 V and 2500 V, respectively. So next potential application of a-C:H films: The a-C:H films can be designed for the passivation of the P-N junction of power diodes.

Acknowledgement. This research has been supported by the FP6 Integrated Project Napolyde (EU contract N° 515846, NMP2-CT-2005-515846) and by the Czech Ministry of Education project "Transdisciplinary research in Biomedical Engineering II" No. MSM 6840770012.

References:

- [1] U. Müller and R. Hauert, Surface and Coatings Technology, **174-175** (2003) 421.
- [2] I. Landor, A. Sosna, P. Vavrik, C. Povysil and D. Jahoda, Chir Organi Mov., **82** (1997) 381.
- [3] Y. Lifshitz, Diamond and Related Materials, **8** (1999) 1659.

SPIN OF HOLE: A NEW PARADIGM IN QUANTUM COMPUTATION ?

*B. Eble(1), C. Testelin(1), P. Desfonds(1), F. Bernardot(1), T. Amand (2), A. Balocchi(2),
A. Miard(3), A. Lemaitre(3), X. Marie(2) and M. Chamarro(1)*

(1) Institut des Nanosciences de Paris, Université P. et M. Curie, CNRS-UMR7588, Paris, F-75015 France

(2) Laboratoire de Physique et Chimie des Nano-Objets, INSA-CNRS-UPS, 135 avenue de Rangueil, 31077 Toulouse Cedex 4, France

(3) Laboratoire de Photonique et Nanostructures, CNRS, Route de Nozay, F-91460 Marcoussis, France

maria.chamarro@insp.jussieu.fr

The electron and the hole, a vacancy of electron, are particles with opposite charge governing semiconductor properties. Both of them carry a magnetic moment, their spin. Since fifteen years, physicians try to add new functionalities to the electronic via the manipulation of this purely quantum property. Recently, the spin of a single electron localised in nanometre scale has been proposed as a good candidate for the fundamental logical unit in a quantum computer, a qubit[1,2]. The ultimate limit for this application has been investigated experimentally and determined to be the coupling of the electron spin to nuclear spins[3,4]. For hole, this coupling is expected to be much weaker than for electrons since the p-symmetry of valence band[5]. Up to now, not experimental evidence of hole-nuclear coupling has been obtained because the spin-orbit coupling is dominant in bulk and quantum well semiconductor structures and govern its spin relaxation dynamics.

We have measured the carrier spin dynamics quantum dots by pump-probe photo-induced circular dichroism and time-resolved photoluminescence experiments. We show that the hole spin dephasing is controlled by the hyperfine interaction between hole and nuclear spins. In the absence of external magnetic field, we find a characteristic hole spin dephasing time of 15 ns, in close agreement with our calculations based on dipole-dipole coupling between the hole and the quantum dot nuclei.

The effect of this hyperfine interaction on the hole spin relaxation time can be efficiently suppressed by an external magnetic field provided that it is larger than the fluctuations of the effective nuclear field acting on the hole spin. We have shown that this field is of the order of a few mT, which is one order of magnitude smaller than the magnetic field required to screen the interaction of an electron with the nuclear spins in the same dots. This nuclear induced hole spin dephasing, which has not been measured before in semiconductors, must be taken into account in future nanoscopic hole-spin-based quantum devices.

References:

- [1] Loss, D. and DiVincenzo, D. Quantum computation with quantum dots, *Phys. Rev. A* **57**, 120-126 (1998).
- [2].-Awschalom, D. D., Loss, D. and Samarth N. (eds), *Semiconductor Spintronics and Quantum Computation* (Springer, Berlin, 2002)..
- [3] Merkulov I.A., Efros Al L. and Rosen M., Electron spin relaxation by nuclei in semiconductor quantum dots, *Phys. Rev. B* **65**, 205309,(2002).
- [4] Braun P.-F et al., Direct Observation of the Electron Spin Relaxation Induced by Nuclei in Quantum Dots, *Phys. Rev. Lett.* **94**, 116601 (2005)
- [5] Gryncharova E.I. and Perel V.I., Relaxation of nuclear spins interacting with holes in semiconductors, *Sov. Phys. Semicond.* **11**, 997 (1977).

Figures:

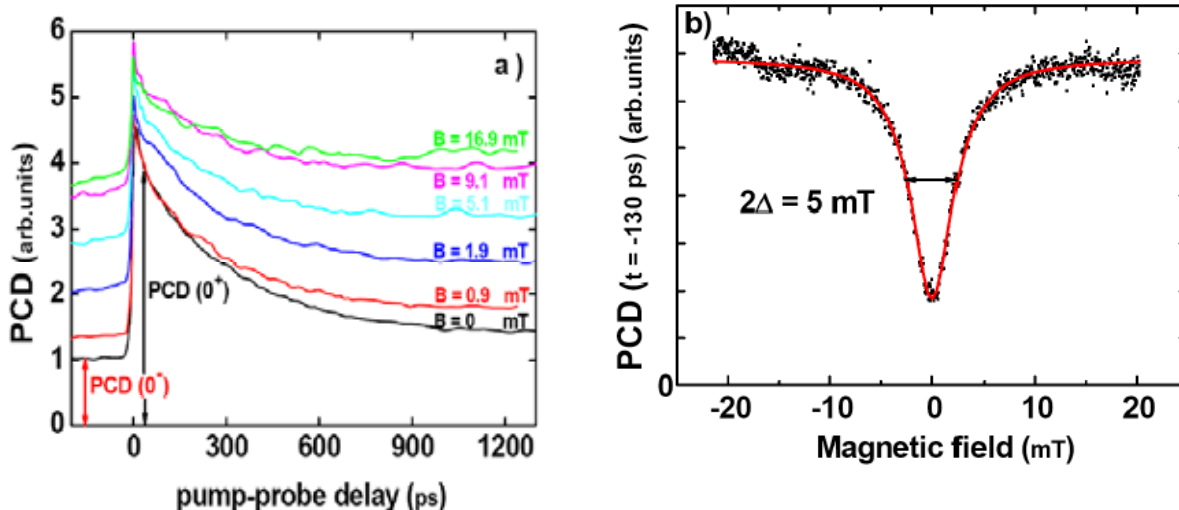


Figure 1 a) Photoinduced circular dichroism (PCD) signal of p-doped InAs/GaAs quantum dots as a function of the pump-probe delay, for different values of the external magnetic field B applied along the sample growth axis (z-direction). The pump and probe beams are tuned to 1.35 eV. The zero-signal level is the same for all displayed curves. $T = 2$ K. We clearly see in this figure that the amplitude of the PCD signal for $t < 0$ increases significantly with the increase of B .

Figure 1b). PCD amplitude (full square) at negative pump-probe delay $t = -130$ ps (i.e. $t \approx 13$ ns after the previous pump pulse) versus the applied longitudinal magnetic field. PCD signal at negative delay is related to the polarization of resident holes in the sample. The data are normalized to unity for the highest magnetic field. The solid line is a Lorentzian fit of the PCD signal. The striking feature is that a small external field has a dramatic impact on the resident hole spin polarization.

DO ALL CADHERINS BIND THROUGH THE SAME ADHESIVE INTERFACE?

Chevalier Sébastien, Courjean Olivier, Feracci Hélène[‡]

*Centre de Recherche Paul Pascal (CNRS, UPR 8641), Université Bordeaux 1, Avenue du Dr
A. Schweitzer, 33600 PESSAC, France*

[‡]feracci@crpp-bordeaux.cnrs.fr

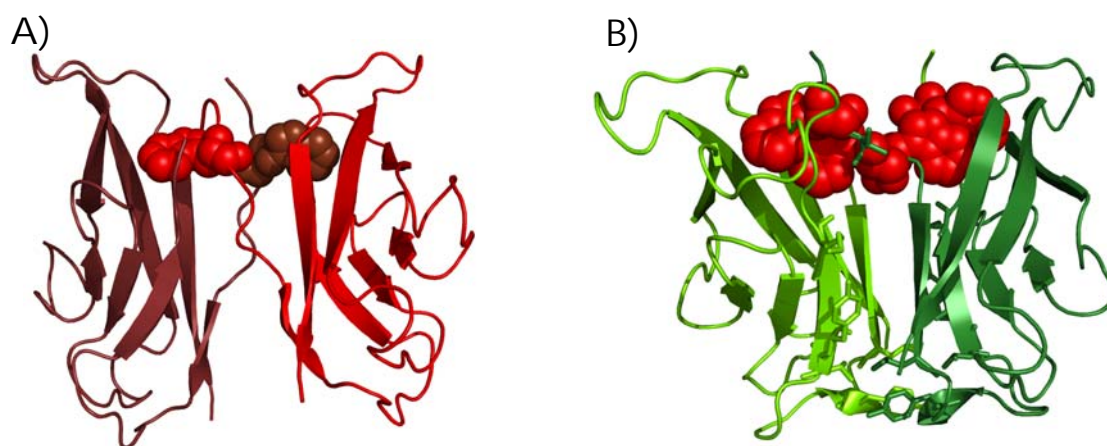
Classical cadherins are cell surface transmembrane glycoproteins involved in cell to cell adhesion. They play important roles in tissue morphogenesis and in the maintenance of tissue architecture in adults. In addition to their structural function, cadherins contacts are actively remodeled and impact cell movement and migration. Moreover, changes in cell-cell adhesion accompany the transition from benign tumor to invasive malignant cancer, and the subsequent metastatic dissemination of tumor cells.

Our aim is to better understand how cadherins regulate cell contacts stability, as well as numerous intracellular signaling pathways. We choose to focus on two cadherins, E(epithelial)-cadherin that is a tumor suppressor, and cadherin-11, as prototypes of type I and type II classical cadherins respectively. Switching between E- and -11 cadherin is often observed in many epithelial cancers. Since the extracellular domain (EC) is crucial for regulating specific Ca^{2+} -dependent homotypic interactions [1], we recombinantly expressed EC domains of E-cadherin and cadherin-11. The E-cadherin [2] and cadherin-11 (unpublished data) fragments retain biological activity when chemically immobilized on glass beads. Individual E-cadherin trans interaction was then analyzed using biophysical approaches such as Laminar Flow Chamber [3]. Our recent studies revealed the importance of the N-terminal beta strand exchange in type I cadherins trans interaction, and the major role played by a key amino acid: the Tryptophan 2 (Trp2). Cristallographic studies revealed that, except for 2 Tryptophan residues in position 2 and 4 instead of one, the homophilic adhesive interface of type I and type II cadherins is very similar suggesting a similar interaction model [4]. Interestingly, our recent dynamic studies combined with molecular biology techniques strongly suggest that despite these similarities, E-cadherin and cadherin-11 interact with completely different adhesive mechanisms. Comparison of the kinetics parameters between E- and -11 cadherins at the single molecule level reveals that type I and type II cadherins have different interaction properties which should help understanding differences in their biological roles (in preparation).

This work was supported by grants from the Association pour la Recherche sur le Cancer, Fondation pour la Recherche Médicale, Ligue Contre le Cancer Dordogne, and the Région Aquitaine.

References:

- [1] Perret E, Leung A, Feracci H, Evans E, *PNAS*, **Vol 101** (2004) 16472-16477.
- [1] Perret E, Leung A, Morel A, Feracci H, Nassoy P, *Langmuir*, **Vol 18** (2002) 846-854.
- [2] Perret E, Benoliel A-M, Nassoy P, Pierres A, Delmas V, Thiery J-P, Bongrand P, Feracci H, *EMBO Journal*, **Vol 21** (2002) 2537-2546.
- [4] Patel S, Ciatto C, Chen C-P, Bahna F, Rajebhosale M, Arkus N, Schieren I, Jessel T, Honig B, Price S, Shapiro L, *Cell*, **Vol 124** (2006) 1255-1268.

Figure:

Structural images of A) Type I (Boggon & al., Science, 2002) and B) Type II (Patel & al., [4]) classical cadherins adhesive interfaces. Residues highlighted are Trp2 for type I and Trp2 and 4 for type II cadherins docked in their hydrophobic pocket

Focused-Electron/Ion-Beam-Induced nanodeposits studied with Transmission Electron Microscopy

^{1,3}R. Córdoba, ^{2,3}J. M. De Teresa, ^{1,2,3}A. Fernández-Pacheco, ^{1,3}P. Strichovanec, ^{1,2,3}M.R. Ibarra

¹ *Instituto de Nanociencia de Aragón, Universidad de Zaragoza, Zaragoza, 50009, Spain*

² *Instituto de Ciencia de Materiales de Aragón, Universidad de Zaragoza-CSIC, Facultad de Ciencias, Zaragoza, 50009, Spain*

³ *Departamento de Física de la Materia Condensada, Facultad de Ciencias, Zaragoza, 50009, Spain*

rocorcas@unizar.es

Focused-Electron/Ion-Beam-Induced Deposition (FEBID and FIBID respectively) of metallic materials is one major application of “Dual Beam” systems, which integrate electron and ion columns. FEBID and FIBID allow local deposition in the targeted place with controllable nanometric lateral size and thickness [1]. FEBID and FIBID of materials is a Chemical Vapour Deposition (CVD) induced by focused electron and ion-beam, respectively [2, 3].

Previous studies on FEBID Pt deposits have shown the decrease of the deposition rate as a function of the beam energy [2-4]. However in the case of FIBID Pt deposits, the deposition rate was found to vary little [2-4]. The microstructure of the Pt deposits have been studied by means of transmission electron microscopy (TEM) [4]. These studies showed that the deposits consist of Pt-rich inclusions in a carbonaceous matrix.

In this contribution we present a systematic study of the volume per dose and microstructure of FEBID and FIBID Pt nanodeposits as a function of the beam energy and current [5]. Our experiments were performed in a Dual Beam equipment (Nova 200 NanoLab). For Pt deposition, an automatized gas-injection system (GIS) was used with $(\text{CH}_3)_3\text{Pt}(\text{CpCH}_3)$ as the precursor material. The volume per dose was calculated after performing cross-sections of the deposited material measuring the deposit thickness. Finally, the microstructure was investigated on Pt nanodeposits grown on Cu TEM grids with a supporting carbon membrane and by inspection of a typical < 100nm thin lamella prepared after deposit growth by HRTEM (JEOL 2010F, 200 kV).

The volume per dose (FEBID) dramatically decreases by a factor four as a function of the incident electron-beam energy as shown in fig. 1(a). This can be explained by the decrease in the amount of secondary electrons reaching the sample surface. For FIBID, the volume per dose increases as a function of the incident ion-beam energy as illustrated in fig. 1(b), which would be explained by the slight changes in the energy dependence of the secondary electron yield. In the inset of fig. 1(b) for deposits at 10 kV, the volume per dose decreases as a function of the beam current, which is explained by the lack of full refreshment of the precursor molecules adsorbed to the sample surface at high beam currents. For the microstructure study of the Pt nanodeposits, two different methodologies have been followed. First, several lamellae were prepared out of the deposits grown on Si substrates. Second, the FEBID and FIBID Pt deposits (thickness in the range 20-50 nm) were directly grown on Cu TEM grids with a supporting carbon membrane. Both approximations show a similar microstructure, formed by independent Pt nanocrystals (3-5 nm) embedded in an amorphous carbon matrix (see fig. 2).

References:

- [1] L. A. Giannuzzi and F. A. Stevie, Introduction to Focused Ion Beams, Boston, 2005.
- [2] I. Utke, P. Hoffmann, J. Melngailis, J. Vac. Sci. Technol. B, **26** (2008) 1197-1276.
- [3] W.F. van Dorp and C.W. Hagen, J. Appl. Phys., **104** (2008) 081301-081342.
- [4] R.M. Langford, T-X. Wang, and D. Ozkaya, Microelectron. Eng., **84** (2007) 784-788.
- [5] J.M. De Teresa, et al, submitted to Journal of Nanomaterials.

Figures:

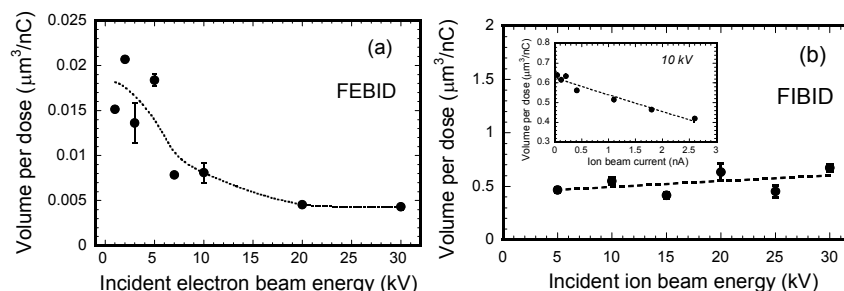


Figure 1: Average volume per dose versus incident electron beam energy in the investigated Pt deposits by FEBID (a) and by FIBID (b). The inset shows the volume per dose versus ion beam current in the investigated FIBID deposits at fixed incident beam energy of 10 kV.

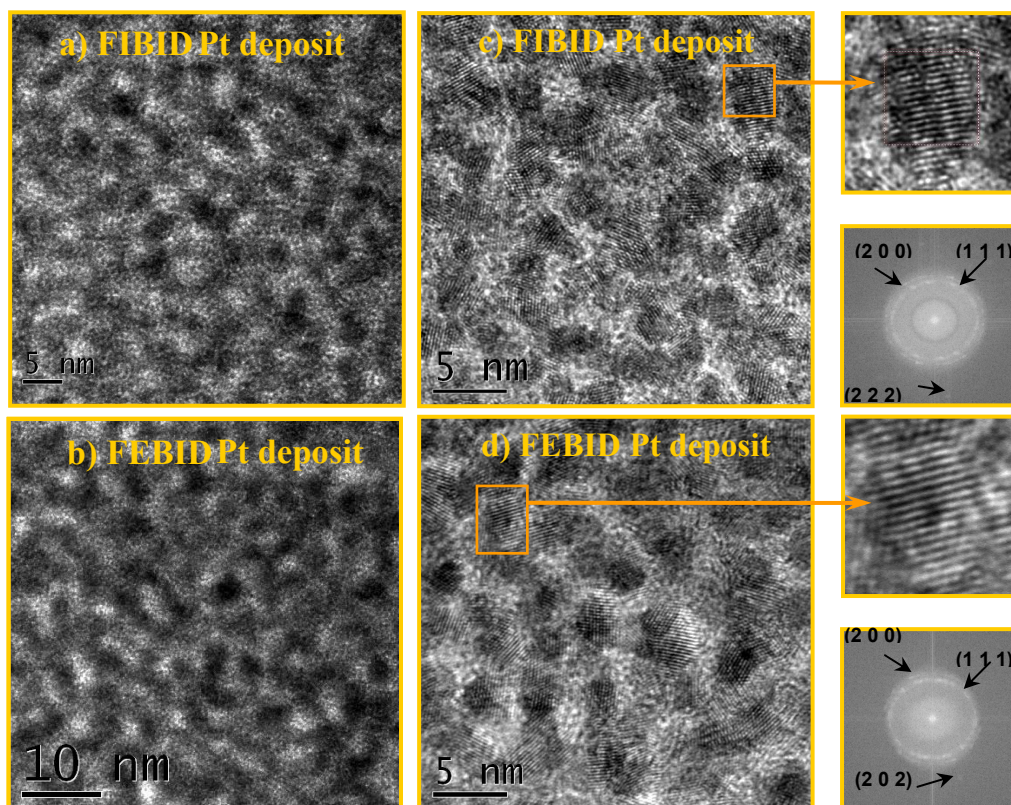


Figure 2: HRTEM images obtained out of lamellae fabricated respectively from a Pt nanodeposit by FIBID (a) and by FEBID (b), in both cases grown at 5 kV beam energy. HRTEM images of a Pt nanodeposit by FIBID (c) and FEBID (d), in both cases grown at 30 kV beam energy on top of a TEM Cu grid covered with a thin supporting holey carbon membrane. One Pt grain has been selected in each case for magnification and clear observation of the corresponding atomic planes. The Fast-Fourier-Transform of the full image gives diffraction spots that correspond to the (200), (111), (222) and (202) atomic planes of fcc Pt.

Silica coating of FeCo magnetic nanoparticles in non-alcoholic media

Alfonso Cornejo^a, Nancy El-Hawi^a, Céline Nayral^a, Fabien Delpech^a, Bruno Chaudret^{a,b}

a) Laboratoire de Chimie et Physique des Nano-Objets, Dpt. de Génie Physique, INSA, 135 av. de Rangueil, 31077 Toulouse, France. b) Laboratoire de Chimie de Coordination du CNRS, 205 route de Narbonne, 31077 Toulouse, France

Contact: alfonso.cornejo@insa-toulouse.fr, celine.nayral@insa-toulouse.fr, fdelpech@insa-toulouse.fr

During the last years magnetic nanoparticles (MNPs) have offered promises in local hyperthermia and in application in magnetic targeted drug delivery. Local hyperthermia depends on specific loss power (SLP) of the MNP which scales with the saturation magnetization (Ms) of the magnetic material¹. Magnetic hyperthermia uses vectorised MNPs to heat cancerous regions in an alternative magnetic field. Metallic MNPs have larger magnetic moments than oxides, allowing similar heating while using lower concentrations. However these particles are highly sensitive to oxidation (caused by oxygen and water), and thus, magnetic properties are easily lost. Some attempts to protect MNPs such as coating Fe ones with SiO₂ have been made, however drastic reaction conditions such as using H₂ at 800°C or H₂ and acetylene at 400°C were required².

One suitable coating to render FeCo nanoparticles biocompatible and easy to functionalize would be a silica shell which could prevent the formation of oxides. Up to date, some methods have been developed for coating ferrite³ or cobalt ferrite^{4,5} nanoparticles with a controlled thickness shell of silica by using slight modifications of the Stöber sol-gel method in alcoholic media⁶, but coating of metallic FeCo MNPs has not been described yet.

Our group has been working during the last years in the synthesis of FeCo MNPs⁷ and in the synthesis of SiO₂ nanoparticles in non-alcoholic media⁸. Here we will present the application of these synthetic methods to the coating of FeCo nanoparticles with silica in non-alcoholic media (figure 1). Resulting FeCo/SiO₂ MNPs keep original magnetic properties (Ms and coercitivity) depending on the synthetic conditions.

We will also show the influence of parameters (such as solvent, temperature, reagents ratio, stabilizing agents, dispersion of FeCo and thermal treatment after synthesis) on the size of the FeCo/SiO₂ agglomerates (figure 2) and/or on the magnetic properties of the resulting solid.

Finally, we will show some examples of MNPs and MNPs/SiO₂ exposed to air and the stability (or not) of their magnetic properties depending on the synthetic method.

(1) Habib, A. H.; Ondeck, C. L.; Chaudhary, P.; Bockstaller, M. R.; McHenry, M. E. *Journal of Applied Physics* **2008**, *103*.

(2) Tang, N. J.; Chen, W.; Zhong, W.; Jiang, H. Y.; Huang, S. L.; Du, Y. W. *Carbon* **2006**, *44*, 423-427.

(3) Lu, Y.; Yin, Y. D.; Mayers, B. T.; Xia, Y. N. *Nano Letters* **2002**, *2*, 183-186.

(4) Phan, N. T. S.; Gill, C. S.; Nguyen, J. V.; Zhang, Z. J.; Jones, C. W. *Angewandte Chemie-International Edition* **2006**, *45*, 2209-2212.

- (5) Yoon, T. J.; Kim, J. S.; Kim, B. G.; Yu, K. N.; Cho, M. H.; Lee, J. K. *Angewandte Chemie-International Edition* **2005**, *44*, 1068-1071.
- (6) Stöber, W.; Fink, A.; Bohn, E. *Journal of Colloid and Interface Science* **1968**, *26*, 62-69.
- (7) Desvaux, C.; Amiens, C.; Fejes, P.; Renaud, P.; Respaud, M.; Lecante, P.; Snoeck, E.; Chaudret, B. *Nature Materials* **2005**, *4*, 750-753.
- (8) El-Hawi, N.; Delpech, F.; Nayral, C. **2007**; *French Patent*, **07/08107**.

Figure 1. Synthesis of FeCo MNPs (1) and coating with SiO₂ (2).

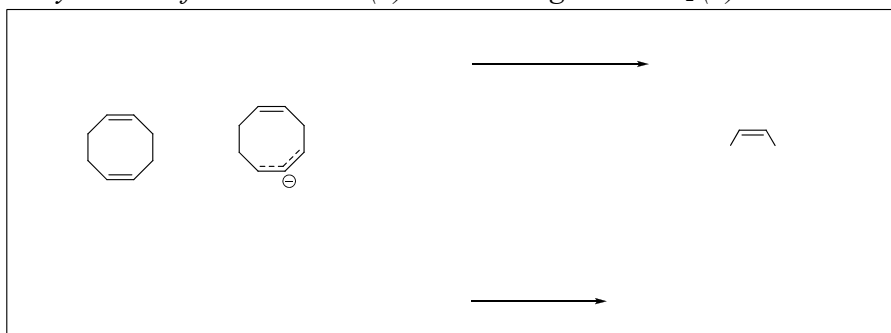
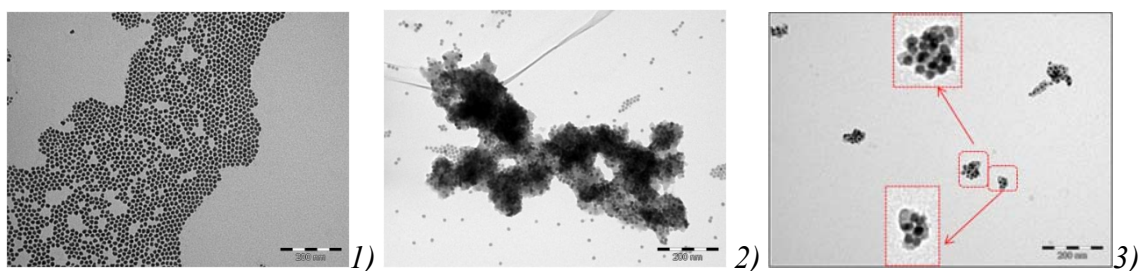


Figure 2. Selected TEM images of FeCo (1), and FeCo@SiO₂ before optimization of the coating method (2) and after (3)



COD:

CO

InP/MS core/shell nanocrystals (M = Zn, Cd) : synthesis, surface chemistry and luminescence

CROS-GAGNEUX Arnaud^{1,2}, CORNEJO Alfonso^{1,2}, DELPECH Fabien^{1,2}, NAYRAL Céline^{1,2}, et CHAUDRET Bruno³

¹ Université de Toulouse, UPS, INSA, LPCNO (Laboratoire de Physique et Chimie des Nano-Objets), 135, avenue de Rangueil ; F-31077 Toulouse, France

² CNRS, LPCNO (Laboratoire de Physique et Chimie des Nano-Objets), UMR 5215, F-31077 Toulouse, France

³ CNRS, LCC (Laboratoire de Chimie de Coordination), UPR 8241, 205 route de Narbonne, F-31077 Toulouse, France

Contact: a_cros@insa-toulouse.fr, cnayral@insa-toulouse.fr, fdelpech@insa-toulouse.fr

Semi-conductor nanocrystals have attracted much attention in the last years because of their unique optical properties. In particular, they have emerged as valuable alternative to organic dyes in bioimaging applications and cancer detection. Among them, II-VI semi-conductor type such as CdSe quantum dots (QD) are the most documented ones [1] but a widespread replacement of organic fluorophores is hindered by (i) the inherent cytotoxicity of the individual ions [2] and (ii) the strong absorption of organic tissues and blood of the emitted QD photons (UV-vis spectral range). In this context, III-V type materials appear as potential better candidates because they could offer near infrared emission suitable for in vivo bioimaging without intrinsic toxicity.

We present here, the InP QD synthesis using an organometallic route that involves indium carboxylates as precursors and fatty acids as stabilizers in non-coordinating solvent [3]. The NMR study of these QDs will be detailed, allowing a comprehensive description of their surface state that play a determining role in the size control and photoluminescence (PL) properties of these objects.

The second part deals with the coverage of the InP core with a II-VI semi-conductor shell (CdS or ZnS) [4]. This modification sensibly enhances the PL quantum yield and a shift of the PL wavelength.

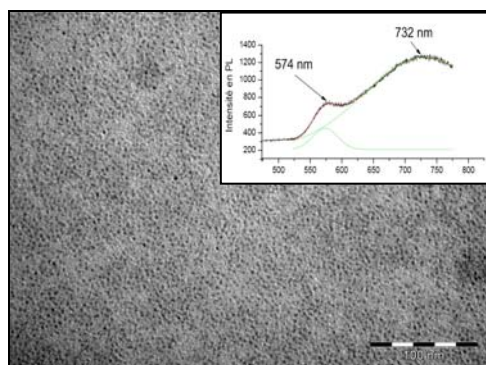


Fig 1. Transmission electronic microscopy image and photoluminescence spectrum of InP QDs.

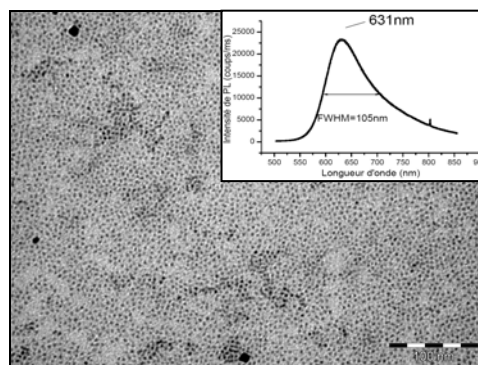


Fig 2. Transmission electronic microscopy image and photoluminescence spectrum of InP/CdS QD.

The water-soluble version of InP/CdS has been obtained by substitution of the surface ligands by mercapto-acetic acid [5] while keeping preserved the PL properties.

[1] A.M. Smith, S.D. Dave, S. Nie, L. True, X. Gao, *Exp. Rev. Mol. Diag.*, **6(2)** (2006), 231.

[2] A.M. Derfus, W.C.W. Chan, S.N. Bhatia, *Nano Lett.*, **4** (2004) 11.

[3] a) D. Battaglia, X. Peng, *Nano Lett.*, **2** (2002), 1027. b) D. Battaglia, X. Peng, *J. Am. Chem. Soc.*, **129** (2007), 15432.

[4] D.W. Lucey, D.J. Macrae, P.N. Prasad, O.T. Beachley, *WO2005/002007A2*.

[5] N. Pradhan, D.N. Battaglia, Y.C. Liu, X.G. Peng, *Nano Lett.*, **7** (2007), 312.

SYNTHESIS AND CHARACTERIZATION OF FERRITIN DIMERS: A NEW APPROACH TOWARDS MULTIFUNCTIONAL MATERIALS

Anabel Lostao^{1,4}, Rocío de Miguel¹, Chiara Carbonera², Marta Martínez-Júlvez^{1,3}, Carlos Gómez-Moreno^{1,3}, M^a José Martínez², Fernando Luis^{2*}

¹Instituto de Nanociencia de Aragón (Universidad de Zaragoza)

²Instituto de Ciencia de Materiales de Aragón (CSIC-Universidad de Zaragoza) y
Departamento de Física de la Materia Condensada, Universidad de Zaragoza, Pedro
Cerbuna 12, 50009 Zaragoza, Spain

³Departamento de Bioquímica, Universidad de Zaragoza, Pedro Cerbuna 12, 50009
Zaragoza, Spain

⁴Fundación ARAID, Zaragoza, Spain

fluis@unizar.es

Biological moulds, such as apoferritin, can be used to synthesize nanoparticles [1]. This biomimetic approach offers a number of advantages over other synthetic methods. Worth mentioning, among them, are the good homogeneity in the size and shapes of these moulds and the possibility of functionalizing the biological envelope with different chemical groups. Apoferritin robustness against relatively large variations in temperature and pH enables the synthesis of a variety of inorganic materials, from magnetic oxides such as γ -Fe₂O₃ [1] and Gd complexes [2], to metals (Cu [3], Ni, Cr [4], etc) and even semiconductors as CdS [5] or CdSe [6]. For this reason, ferritin-based nanoparticles are seen as promising materials for a vast number of applications. The versatility of ferritin as a mould could also be advantageously employed to obtain multifunctional materials, by e.g. linking together ferritin molecules with different functionalities (e.g. a large magnetic moment in one monomer plus an optically active centre in the other). Although ferritin dimers and higher oligomers are present in solution [7], these molecular associations are mainly composed of reversible dimers with very weak interaction [8]. Here, as a first step, we report the synthesis and purification of dimers of natural ferritin molecules bound covalently by chemical linkers.

Ferritin molecules were covalently bound using the cross-linking agent sulfo-LC-SPDP, a sulfonated and longer analog of SPDP. This heterobifunctional cross-linker contains an amine-reactive N-hydroxysuccinimide (NHS) ester that reacts with lysine residues to form a stable amide bond. The other end of the spacer arm is terminated in the pyridyl disulfide group that reacts with sulfhydryls to form a reversible disulfide bond. Different portions of functionalized ferritin were made to react in 1:1 stoichiometry, favoring the production of dimers. The chromatogram (Figure 1) showed three well defined peaks, the first corresponding hypothetically to dimers, the second to monomers and the third to non-reacted SPDP.

The fractions of the sample containing respectively ferritin monomers (peak 2 in Fig. 1) and dimers (peak 1 in Fig. 1) were further investigated by AFM. Typical images are shown in Fig. 2. The peak attributed to ferritin shows well-separated, 20-40 nm wide, molecules with an apparent height of 10 ± 2 nm. The apparent width is considerably larger than the true dimension due to tip broadening. Dimers show 40-80 nm width and approx the same height as monomers, indicating that the conformation of the protein has not been altered during dimerization. Further evidence of the formation of stable dimers is provided by the magnetic characterization of aqueous solutions of the two samples. As T decreases, the susceptibility of the monomers and dimers shows the typical drop or “superparamagnetic blocking” that is also observed in natural ferritin samples [9]. However, the blocking temperature of the dimers is higher, by more than a 50 percent, than the blocking temperature of the monomers. It is well known that the dipolar interactions between magnetic nanoparticles can modify, often

increase, the energy barriers for the magnetization reversal [10] thus leading to an increase in T_b , as observed here. In fact, these artificially engineered ferritin dimers provide model systems to investigate how interparticle interactions modify the magnetic memory of nanoparticles.

In conclusion, we have achieved the synthesis of covalently bound natural ferritin dimers, which are stable in solution. These materials open the door to the design of biocompatible multifunctional nanomaterials, e.g. by the combination of two ferritin monomers encapsulating nanoparticles of two different compounds. This work is currently underway.

This research has been funded under Project NABISUP from DGA.

References:

- [1] M. T. Klem, M. Young, and T. Douglas, *Materials Today*, September (2005) 28.
- [2] P. Sánchez et al., *Dalton Transactions* **5**, 800-804 (2009).
- [3] N. Gálvez, P. Sánchez, J. M. Domínguez-Vera, *Dalton Transactions*, **15** (2005) 2492.
- [4] M. Okuda, K. Iwahori, I. Yamashita, H. Yoshimura, *Biotechnology and Bioengineering*, **84** (2) (2003) 187.
- [5] K K W Wong and S. Mann, *Advanced Materials* **8**, 928 (1996).
- [6] I. Yamashita, J. Hayashi, and M. Hara, *Chemistry Letters* **33**, 1158-1159 (2004).
- [7] D.N. Petsev, B.R. Thomas, S. Yau, P.G. Vekilov, *Biophys J.*, **78**(4) (2000) 2060-9.
- [8] D. Yang, K. Matsubara, M. Yamak, S. Ebina, K. Nagayama. *Biochim Biophys Acta*, **1206**(2) (1994) 173-179.
- [9] H. Kilcoyne and R. Cywinski, *J. Mag. Mag. Mater.*, **1466** (1995) 140-144.
- [10] F. Luis, et al., *Phys. Rev. Lett.*, **88** (2002) 217205.

Figures:

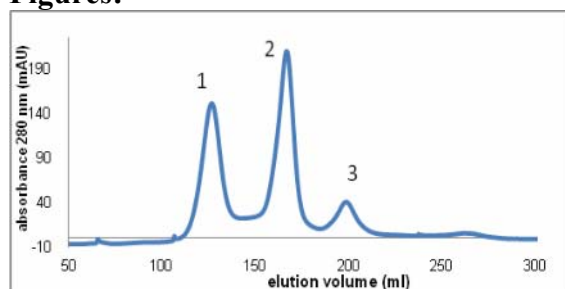


Fig. 1. Chromatogram following absorbance at wavelength 280 nm vs volume corresponding to the separation of dimers from monomers by size exclusion chromatography. From right to left the molar mass grows.

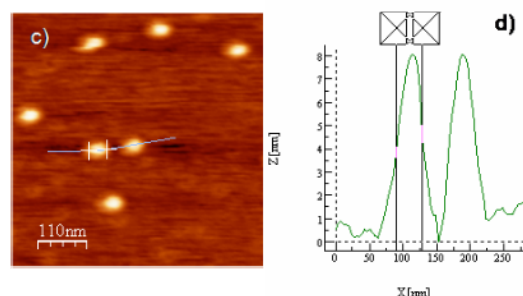
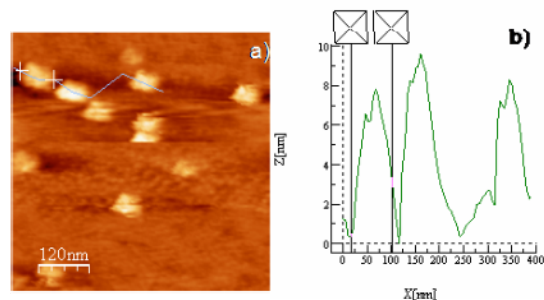


Fig. 2. AFM images in Jumping Mode of a characteristic region of the sample taken in contact conditions in acetate / glycine buffer, pH 4. a) sample from Peak 2; b) profile of the dimerized protein from a); c) sample from Peak 1; d) profile of the monomer protein from c).

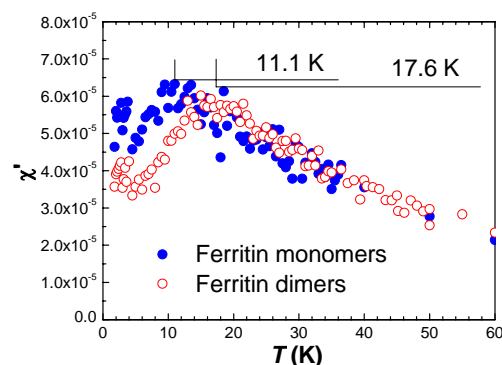


Fig. 3. Ac susceptibility data measured on aqueous solutions of ferritin monomers and dimers.

NANOSCALE IRREGULARITY EFFECTS IN THE FIELD EMISSION OF METAL SURFACES.

T. Albuquerque¹, F. Borondo¹, R. M. Benito², R. F. S. Andrade³

¹ *Departamento de Química and Instituto Mixto de Ciencias Matemáticas CSIC-UAM-UC3M--UCM, Universidad Autónoma de Madrid, Cantoblanco, 28049 Madrid, Spain.*

² *Grupo de Sistemas Complejos, Departamento de Física y Mecánica, ETSI Agrónomos, Universidad Politécnica de Madrid, Ciudad Universitaria, 28040 Madrid, Spain.*

³ *Instituto de Física, Universidade Federal da Bahia, Campus Universitário da Federação, 40210--340, Salvador, BA, Brazil.*

t.albuquerque@uam.es

Present vacuum microelectronics technology (VMET) is a field that has gained a great and sustained impulse during the last few decades. Electrons emitted from very sharp tips, as a result of an externally applied electric field, which is a consequence of a potential bias, tunnel through a potential energy barrier, resulting in an electric current. Since some applications require strong electric currents under low voltages, investigations of low work-function materials or structures are of great practical importance. The next generation of such electron emitters requires a fine tuning of several parameters such as material work-function, surface structure, field strength, and temperature, in order to warrant that most part of the emission originates from electronic energy levels in the vicinity of the potential barrier.

Some results [1,2] suggest that a substantial reduction in the emitting field can be achieved by using cathode surfaces with fractal structure of increasing self-similarity. In previous works, [3,4] some of us explored the scaling behavior of equipotential surfaces in an electric field generated by conductors with fractal geometry. The results were analyzed for models of $D+1$ dimensions, with $D=1,2$.

The purpose of this work is to present a theoretical analysis of the influence of the irregular structure of cold emitted conductors on the emission properties. First, we discuss the connection between the geometrical properties of the emitter surface generated by **fBm** algorithm [5], fractal dimension d_f , roughness W , and the local intensity of electric field. Our results suggest that the fractal dimension may be related to the field amplification factor, while the total emission current is determined by the roughness of the surface [5]. These results were supported by the analysis of the Fowler plots (FP), which relates the average emission current, $\langle J \rangle$, with respect to the anode potential (see Fig. 1). Also, it is possible to observe the relation between the effective field amplification and the irregularities at nanometric scales by performing a comparison between the electric field intensity and local roughness distributions. We believe that these results can help to explain some differences between theoretical calculations with smooth geometries and experimental studies, which predict high values of the field amplification factor and very small values of effective emitting area.

In addition, we investigate, the case of a metallic cathode surface composed by an “array” of nanopyrimal structures*. It is possible to determine the influence, on the emission properties, of parameters like the distance anode-cathode and number of pyramids per unit of area of the underlying surface. The results demonstrate that the inter-pyramidal distance (δ), exhibits an important effect in the optimisation of the maxima field amplification factor (γ^{\max}) (see Fig. 2).

* These analyses were done in collaboration with Profs. Caio Castilho and Fernando Mota, of the Physics and Materials Surfaces's Group of Universidade Federal da Bahia, Brazil.

References:

- [1] V. A. Solntsev , A. N. Rodionov, Solid-State Electronics, **45**, 853 (2001) .
- [2] T. Habermann, A. Gohl, D. Nau, M. Wedel, G. Muller, M.Christ, M. Schreck, B. Stritzker, Proceedings of the 10th International Vacuum Microelectronics Conference IVMC, p.156 (1997).
- [3] T. A. de Assis, F. B. Mota, J. G. V. Miranda, and R. F. S. Andrade, H. de O. Dias Filho, C. M. C. de Castilho, J. Phys.: Condens. Matter **18**, 3393 (2006).
- [4] T. A. de Assis, F. B. Mota, J. G. V. Miranda, R. F. S. Andrade, C. M. C. de Castilho, J. Phys.: Condens. Matter **19**, 476215 (2007).
- [5] T. A. de Assis, F. Borondo, R. M. Benito, R. F. S. Andrade, Phys.: Rev. B, **78**, 235427 (2008).

Figures:

Fig1.: Fowler-Nordheim plot, representing how the average current density depends on the anode electric potential. Circles, triangles, squares and diamonds represent the emission surfaces in descending order of roughness.

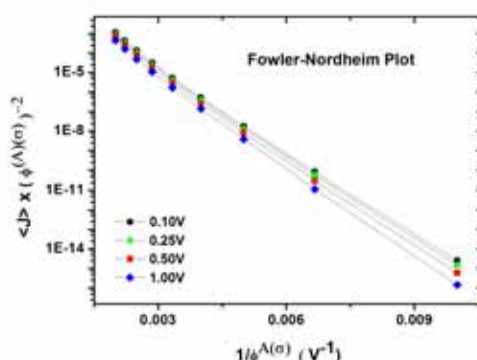
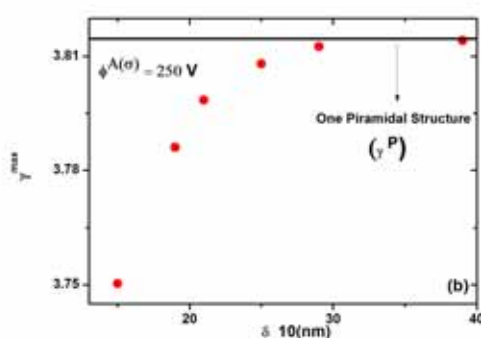


Fig2.: Maxima field amplification factor, γ^{\max} , as a function of inter-pyramidal distance δ . In this case, we considerate the cathode formed by 16 pyramidal structures in a regular disposition, and the anode potential 250V. The horizontal line indicates the value of the maxima field amplification factor on top of an isolated pyramidal structure.



IMMOBILIZATION OF LABELED GLUCOSE OXIDASE TO MAGNETIC NANOPARTICLES FOR DEVELOPMENT OF A GLUCOSE NANOBIOSENSOR

M. del Barrio^{1,2}, S. Puertas², V. Graziú², S. de Marcos^{1,2}, J. M de la Fuente² and J. Galbán^{1,2}

¹GBA (Analytical Biosensors Group), Analytical Chemistry Department, Faculty of Science, University of Zaragoza. ²INA (Institute of Nanoscience of Aragón), University of Zaragoza.

Pedro Cerbuna 12, 50009, Zaragoza, Spain

mdbarrio@unizar.es

In recent years our research group has developed new alternatives for fluorescence enzymatic determinations. The methods are based on the alteration of the enzyme fluorescence during its reaction with the substrate, which is proportional to the concentration of the corresponding analyte. Chemically modified glucose oxidase (GOx) with fluorophores has been used in order to work in spectral areas where organic interferences were minimized and to make possible *in vivo* determinations. In previous work the research group has proposed the use of labeled GOx with a fluorescein derivative for the direct determination of glucose in serum[1]. In this work we present first results obtained using GOx covalently linked to bis(2,2'-bipyridine)-4'-methyl-4-carboxybipyridine-ruthenium N-succinimidyl ester-bis(hexafluorophosphate) (Ru). Because of his long fluorescence lifetime this a very interesting fluorophore.

Magnetic nanoparticles could be used as a subcutaneous support for non-invasive nanobiosensor. They can be channelled in a biological fluid and directed by the action of an external magnet to low tissue thickness, without any deterioration in the body. Nanoparticles used in this work consist of a magnetite core which is covered with hydrophilic polymers containing amino terminal groups used for linking to biomolecules.

The immobilization of GOx-Ru to nanoparticles was done via reductive amination through the amino terminal groups of nanoparticles and aldehyde groups, previously generated by oxidation of polysaccharide chains of GOx with periodate[2]. Enzyme molecules retained their enzymatic activity after immobilization and the change of fluorescence during the reaction was observed. Fluorescence lifetimes measurements are being carried out in order to both, nanoparticles characterization and scattering problems correction.

Acknowledgements: This work was supported by the Ministry of Science and Innovation (MICINN) of Spain within the project CTQ 2008-06751-C02-01 which is gratefully acknowledged. JMF thanks ARAID for financial support.

References:

- [1] Sierra, JF; Galbán, J; de Marcos, S, et al. *Analytica Chimica Acta* 414 **1-2** (2000) 33-41
- [2] Sun, YY; Yan, F; Yang, WW, et al. *Analytical and Bioanalytical Chemistry* 387 **4** (2007) 1565-1572

SILVER NANOSHELLS: SYNTHESIS, PLASMONIC PROPERTIES AND PROSPECTS IN CANCER THERAPY

O. V. Dementieva¹, M.E. Kartseva¹, M.A. Filippenko¹, E.M. Sedykh², L.N. Bannykh², B.Ya. Kogan³, N.V. Andronova⁴, R.I. Yakubovskaya⁵, A.A. Pankratov⁵, V.M. Rudoy¹

¹ *A.N. Frumkin Institute of Physical Chemistry and Electrochemistry of RAS,
31 Leninsky prospect, 119991, Moscow, Russia*

² *V.I. Vernadsky Institute of Geochemistry and Analytical Chemistry of RAS,
19 Kosygin street, 119991, Moscow, Russia*

³ *FGUP "GNC NIOPIK", ¼ B. Sadovaya street, 123995, Moscow, Russia*

⁴ *N.N. Blokhin Russian Cancer Research Center of RAMS,
24 Kashirskoe Sh., 115478 Moscow, Russia*

⁵ *P.A. Gertsen Moscow Research Oncological Institute,
3Second Botkinsky proezd, 125284 Moscow, Russia
dema_ol@mail.ru*

Composite nanoparticles with dielectric cores and gold or silver shells, possessing unique optical properties, are of growing interest from the point of view of their potential use in medicine, in particular, in diagnostics and therapy of tumors.

As far as we know, only the particles with Au shells, the synthesis of which have been developed well enough for today, have been used in occasional studies till now (including *in vivo* ones) [1]. At the same time a much greater interest is attracted by similar Ag-based composite particles. It is caused by unique bactericidal properties of silver and its significantly larger resonant absorption cross section (in comparison with gold). However, the reproducible synthesis of such structures is a rather difficult problem which has not been solved completely.

In this work, results concerning the silver nanoshell's synthesis on various cores are presented. Moreover, the optical properties of such nanoshells as well as the possibility of their application to laser hyperthermia of tumors are discussed.

The general scheme of core/shell nanostructures synthesis is represented in Fig. 1.

The possibility of the synthesis of continuous silver shells on spherical SiO₂ particles and spindle-shaped particles of iron hydrous oxide is demonstrated for the first time. The procedure consists in the enlargement of preadsorbed seeding Au or Ag nanoparticles in the solution containing silver nitrate and ascorbic acid.

It is shown that, for such composite structures, the maximum of surface plasmon resonance lies in the range of 600–1200 nm, i.e., its significant bathochromic shift takes place relatively to the position, characteristic for spherical silver nanoparticles (Fig. 2).

Procedure of the surface modification of core/shell nanoparticles with thiolated poly(ethylene glycol) (PEG) has been realized which provides high nanoparticle's aggregative stability in strong electrolyte (NaCl) solutions.

Quantitative information about the redistribution dynamics (on the time scale from 2 min to 24 h) of the PEG-conjugated composite SiO₂-core/Ag-shell particles between various organs and tissues of tumor-bearing mice has been obtained after particles intravenous injection in the form of colloid solution. It is revealed that such conjugated particles are characterized

rather long circulation time in blood; moreover, their high-selective accumulation in tumor takes place.

Preliminary *in vivo* experiments show that PEGylated silver nanoshells are effective sensibilizers in pulse-laser hyperthermia of tumors.

References:

[1] Loo C., Lin A., Hirsch L., Lee M.-H., Barton J., Halas N., West J., Drezek R., *Technology in Cancer Research & Treatment*, **1** (2004) P. 33.

Figures:

Fig. 1. General scheme of core/shell nanoparticles' synthesis.

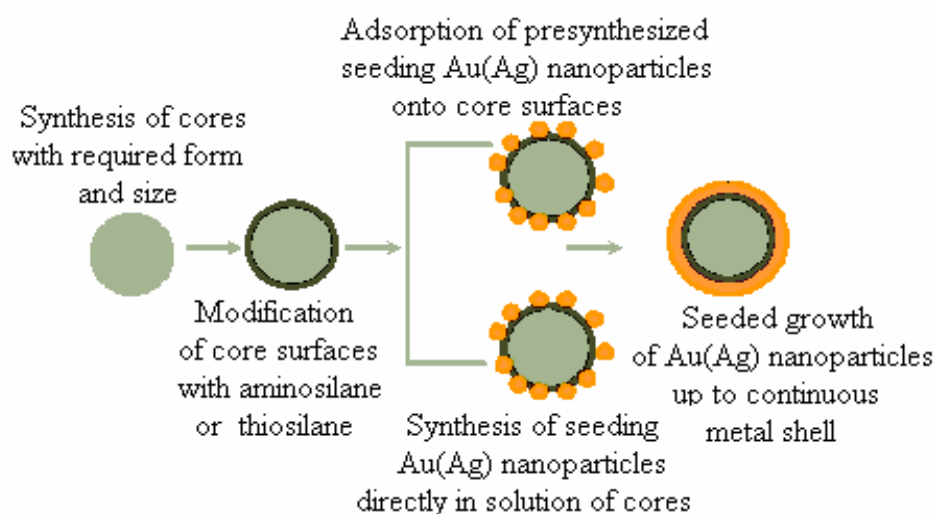
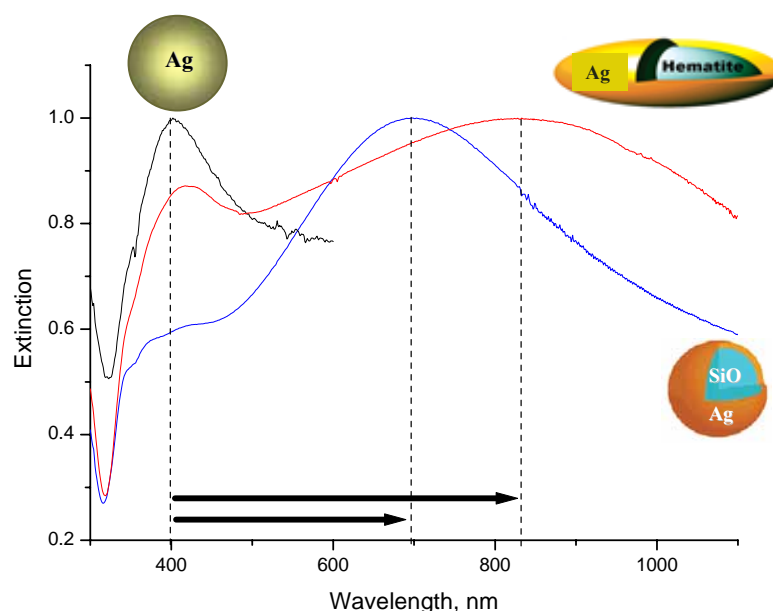


Fig. 2. Extinction spectra of silver-based nanostructures.



Acknowledgements:

This work was supported by the Program of Moscow Government "Development and practical realization in public health services of new methods and means of preventive maintenance, diagnostics and treatment of oncological, infectious and other dangerous diseases" for 2007-2009.

INTRACELLULAR BIOSYNTHESIS OF SILVER NANOPARTICLES USING *STREPTOMYCES* SPECIES

¹Sapkal M.R., ²Sapkal R.T. and ³Deshmukh A.M.

¹Department of Microbiology B.D. College, Patan, Dist-Satara(M.S.)415206. INDIA.

²Department of Physics . T.C.College Baramati, Dist Pune (M.S.) INDIA.

³Department of Microbiology Dr. Babasaheb Ambedaka Marathawada University,
Aurangabad Subcentre Osmanabad, 413501(M.S.)

Abstract

The development of ecofriendly, reliable process for the synthesis of nanomaterials using microorganisms is an important aspect. We have concentrated on the use of actinomycetes in the intracellular biosynthesis of silver nanoparticles . It was observed that when different species of *Streptomyces* viz *Streptomyces rameus* NBR and *Streptomyces* sp. LD021 were exposed to aqueous 10^{-3} M AgNO₃ solution at $28^{\circ}\text{C} \pm 0.5^{\circ}\text{C}$ for 72 hours under optimum conditions, they synthesize silver nanoparticles intracellularly. Particle size is in the range of 12 to 22 nm. The characterization of nanoparticles was carried out by using UV Visible spectrophotometer, XRD, SEM techniques.

Key words: Intracellular silver nanoparticles, *Streptomyces*,

MC SIMULATION OF WATER MENISCUS IN NANOCONTAINERS: EXPLAINING THE COLLAPSE OF VIRAL PARTICLES DUE TO CAPILLAR FORCES.

M. Douas^{1,2*}, P.A. Serena², M.I. Marqués¹, C. Carrasco³, P. J. de Pablo³, R. Miranda⁴, J. L. Carrascosa⁴, M. Castellanos⁵, M. G. Mateu⁵

¹ *Departamento de Física de Materiales, C-IV, Facultad de Ciencias, Universidad Autónoma de Madrid, 28049 Madrid, Spain.*

² *Instituto de Ciencia de Materiales de Madrid, Consejo Superior de Investigaciones Científicas, Campus de Cantoblanco, 28049 Madrid, Spain..*

³ *Departamento de Física de la Materia Condensada C-III, Facultad de Ciencias, Universidad Autónoma de Madrid, 28049 Madrid, Spain.*

⁴ *Departamento de Estructura de Macromoléculas, Centro Nacional de Biotecnología, Consejo Superior de Investigaciones Científicas, Campus de Cantoblanco, 28049 Madrid, Spain...*

⁵ *Centro de Biología Molecular Severo Ochoa, Consejo Superior de Investigaciones Científicas-Universidad Autónoma de Madrid, Campus de Cantoblanco, 28049 Madrid, Spain..* Presenting

*e.mail: maysoun.douas@icmm.csic.es

The study of properties of water confined in complex systems is relevant to many important processes ranging from industrial applications (water membranes, filtering, etc) to biological processes (protein folding, ionic transport through membranes,...) [1]. Changes in thermodynamics, phase behavior and the molecular mobility of water have been observed upon confinement [2]. These changes are strongly dependent on the nano-container properties. In particular, very recently [3-4] we have reported, using atomic force microscopy (AFM), that remarkable structural modification takes place during the desiccation processes on individual particles of the bacteriophage $\phi 29$ and the minute virus of mice (MVM). In both cases the genomic DNA was ejected from the viral capsid (see Figure 1). However, while the structural integrity of the minute virus of mice was essentially preserved, the $\phi 29$ capsid underwent a wall-to-wall collapse. These results points towards the important role played by the capillary forces of water confined inside the viruses. In fact, the desiccation process of an empty viral particle (nano-container) is associated to the formation of internal water menisci with shape (exposed area and curvature) determined by the capsid geometry.

In order to study the way in which the water menisci evolves during the desiccation process of viral particles we have simulated the water+capsid system using a lattice gas model that mimics the gas-liquid phase transition in water. This model has been previously used to study the geometry of the water meniscus formed between an atomic force microscope tip and a substrate [5]. Averaged Monte Carlo (MC) simulations of the water meniscus evolution have been carried out for two types of viruses' cavities: an asymmetric one with a single channel and a symmetric one with pores at every fourfold symmetry axis. The MC simulations describe the formation of an asymmetric water meniscus for the virus with a single hole ($\phi 29$) whereas, for the virus with a symmetric location of the pores (MVM), the water bridge formed is symmetric and capillary forces could cancel one another (see Figure 2). These differences could explain the wall-to-wall collapse noticed for $\phi 29$ viral capsids. In order to determine these forms, the future work is based on a accurate determination of the water meniscus profile for each step of the desiccation process. Characterization of the profile will be performed by fitting to geometric parameters like Kelvin's radius [6].

References:

[1] Special issue on nanoconfined water. J. Phys. Condens. Matter. 16 (2004) pp.S5257-S5470.

- [2] See f.i. M. Rovere (ed.) J. Phys.: Condens. Matter 16, (45), (2004) 1.
- [3] C. Carrasco, M. Douas, R. Miranda, M. Castellanos, P.A. Serena, J.L. Carrascosa, M.G. Mateu, M.I. Marqués, P.J. de Pablo, PNAS (accepted).
- [4] P.A. Serena, M. Douas, M.I. Marqués, C. Carrasco, P. J. de Pablo, R. Miranda, J. L. Carrascosa, M. Castellanos, M. G. Mateu PSS (accepted).
- [5] J. Y. Jang, G.C. Schatz, M.A. Ratner, Phys. Rev. Lett. 92, (8), (2004) 085504.
- [6] E.Sahagún, P.García –Mochales, G.M.Sacha and J.J. Sáenz, PRL 98 (2007) 176106

Figure 1. MVM (Left) and $\phi 29$ (Right) viral particles after de-wetting processes with their respective DNA ejected from the capsids.

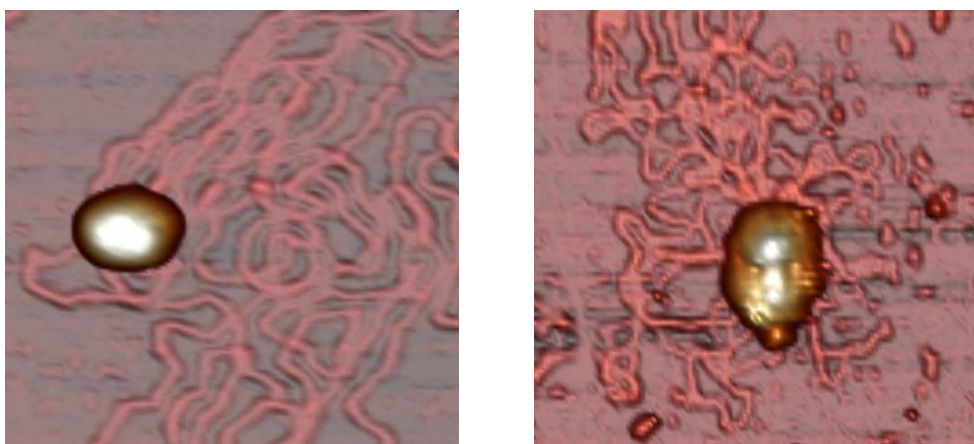
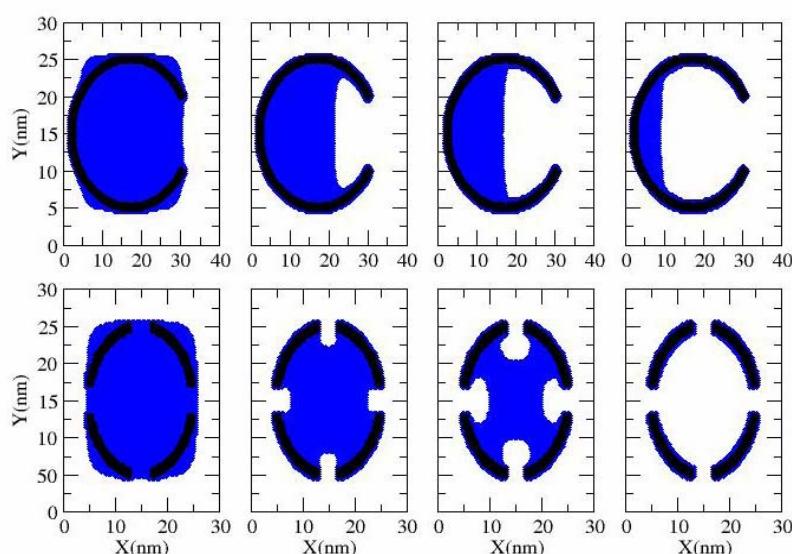


Figure 2. Numerical simulation of a desiccation process for asymmetric (upper panel) and symmetric (lower panel) virus cavities. Monte Carlo steps considered are 200, 600, 800, 1100 (upper panel from left to right) and 200, 400, 500, 700 (lower panel from left to right). Every lattice site with averaged water occupation probability $n(i,j) > 0.5$ is represented with a blue point. Points belonging to the virus cavity are represented with a black line.



AMPEROMETRIC IMMUNOSENSORS FOR OCHRATOXIN A (OTA) BASED ON SCREEN PRINTED ELECTRODES (SPCES) NANOSTRUCTURED WITH GOLD NANOPARTICLES

P. Duato, J.C. Vidal, L. Bonel and J.R. Castillo

Institute of Environmental Sciences (IUCA)

Analytical Spectroscopy and Sensors Group (GEAS),

University of Zaragoza, Ciudad Universitaria, 50009, Zaragoza, Spain

pduato@unizar.es

Ochratoxin A (OTA) is a mycotoxin with nephrotoxic, teratogenic, carcinogenic and immunotoxic activity in human and animals. OTA occurs in several foodstuffs such as cereals, coffee beans, nuts and cocoa. There are very strict mycotoxin regulations all over the world [1].

Chromatographic analytical methods available for the analysis of mycotoxins in food , beverages, and foodstuffs are usually validated by AOAC International Official Methods of Analysis [2].

The direct voltammetric analysis of OTA is possible [3], but the oxidation of this molecule needs a very high potential (+1.5 V). Besides, sensitivity is low, and then the direct amperometric determination of OTA is not suitable at the level of low ppb required. For these reasons the use of immobilized antibodies is more convenient when amperometric transducer are used

We are developing a rapid and sensible OTA immunosensors using advantages of the immunochemical assay and the nanostructured screen-printed technology. We have studied the influence of gold nanoparticles (AuNP, 20 nm. diameter) directly immobilized on screen printed graphite electrodes (SPCEs) made in our lab in order to increase the analytical signal obtaining higher voltammetric currents in the detection step. The Quartz Crystal Microbalance (QCM) was used to demonstrated that the nanofunctionalization process with AuNP increases the real sensing surface of the quartz crystal device

The use of AuNP as versatile and efficient substrates for the immobilization of antibody or antigen showed not only enhance the amount of antibodies or antigens immobilized on the electrode sensing surface, also preserve the activity of the immobilized biomolecules. Nanometer-size (20nm) AuNPs exhibit excellent catalytic activity and these AuNPs have a relative high surface area-to-volume ratio.

We used indirect immunoassays in a competitive way by immobilizing OTA-BSA (ochratoxin A with serum albumin bovine) conjugate on the SPCEs and using alkaline phosphatase (AP) or horse-radish peroxidase (HRP) as transduction enzymes labelled to secondary anti-IgG antibodies to generate the amperometric signal. Also we used bovine serum albumin (BSA) for blocking and avoiding unspecific adsorption.

The electrochemical substrate for generating the amperometric signal was 1-naphtil phosphate for AP and hydroquinone/H₂O₂ for HRP. The enzymatic product of both reactions was detected by differential pulse voltammetry (DPV).

The designed immunosensors were compared with spectrophotometric ELISAs (enzyme-linked immunosorbent analysis) using 4-nitronaphtyl phosphate as enzymatic substrate and

measuring the UV-VIS molecular absorbance of 1-nitronaphthol at a wavelength of 405 nm obtaining good validation analytical results.

Besides, the analytical results were validated with official methods based on HPLC with fluorescence detection. Regeneration of the immunosensor surfaces has been studied. And the SPCEs with AuNPs were observed by Scanning Electron Microscopy (SEM) in order to characterize their nanostructured surface. In conclusion, *SPCEs* immunosensors for OTA allow the quick and specific determination of this mycotoxin at the ppb levels. The formation of a layer of nanostructured particles (AuNPs) increased the sensitivity of the transduction process in this new OTA amperometric immunosensors.

This work has been financed by the Aragon Government (Science, Technology and University Department) with Project PM 027/2007. Patricia Duato thanks ACP S.A. a research grant.

References:

- [1] Egmond H.P. et al, Analytical Bioanalytical Chemistry, **389** (2007) 147.
- [2] Trucksess M.W., Journal of AOAC Int., **89** (2006) 270.
- [3] Oliveira S.C.B. et al., Analytica Chimica Acta, **588** (2007) 283.

MAGNETIC FORCE MICROSCOPY OF MIXED SYSTEMS: DOES IT WORK?

*Cristina S. Neves^a, Pedro Quaresma^{a,b}, Patrícia A. Carvalho^c,
João Pedro Araujo^d, Peter Eaton^{a*} and Eulália Pereira^a*

^a REQUIMTE/Faculdade de Ciências, Universidade do Porto, R. Campo Alegre 687, 4169-007 Porto, Portugal

^b CIGMH/Departamento de Ciências da Vida, FCT-UNL, 2829-516 Caparica, Portugal

^c Departamento de Engenharia de Materiais, IST, Av. Rovisco Pais 1049-100 Lisboa, Portugal

^d IFIMUP, R. Campo Alegre, 678, 4169-007 Porto, Portugal

* Corresponding author: peter.eaton@fc.up.pt

Magnetic force microscopy (MFM) is a variant of atomic force microscopy (AFM), in which a probe with a magnetic coating is used, conferring sensitivity to the magnetic fields of the sample. In order to obtain useful information, it is necessary to separate the magnetic forces acting on the probe from short and long range non-magnetic forces. A variety of methods have been described, but in the most commonly employed configuration, the surface topography is measured by normal AFM methods, followed by lifting the probe from the surface, and scanning at a fixed height above the sample, in order to remove short-range nonmagnetic forces acting on the probe. The magnetic fields are detected by measuring the phase shift of the oscillating probe (this is the so-called lift mode). This technique is widely employed to study large (>50nm) magnetic domains in flat surfaces, and provides useful information under these circumstances.

Recent work has established that this method may also be appropriate to characterise the magnetic properties of superparamagnetic nanoparticles [1], although work on using MFM to characterize nanoparticles has been scarce until now, presumably due to the difficulties in detecting very small magnetic domains with this technique [2]. Unfortunately, there are a large number of difficulties with this technique, not least of which is uncertainty about the actual mechanism of contrast formation [3, 4]. In practical terms, for MFM imaging of MNPs in ambient conditions the major problem is the existence of non-magnetic forces, which can give rise to contrast in the phase-shift images, even without any magnetic interaction [2, 5]. The work described in this poster was carried out in order to determine whether the contrast seen in lift mode MFM is really of magnetic origin. Furthermore, we aimed to use MFM to differentiate between magnetic and nonmagnetic materials, and ultimately enable measurement of properties of MNPs on a single particle level. In order to help us to understand better the response of MFM under these conditions, we have applied it to the study of a range of both magnetic and nonmagnetic nanoparticles.

Magnetic particles of about 10 nm diameter produced by thermal decomposition of iron precursors were studied by lift mode MFM under an external magnetic field. By the measurement of phase shift at different lift heights, the expected dependence of the phase shift vs lift height was verified. Furthermore, in order to test the ability to distinguish magnetic interactions from non magnetic ones a mixture of Au nanoparticles (17 nm) and Fe₃O₄ nanoparticles (33 nm) was imaged. Signal decay vs distance was verified as well as the inversion of the phase signal when comparing Au nanoparticles with Fe₃O₄ nanoparticles showing that a distinguishable response between the two materials could be observed. The samples were examined both in the presence and absence of an external magnetic field, further enabling our understanding of the mechanisms of contrast formation by this technique. The results of the study increase our comprehension of MFM, and allow the use of this technique to probe the magnetic properties of magnetite-based nanoparticles, enabling further study in more complex systems in the future.

References:

- [1] S. Schreiber, M. Savla, D. V. Pelekhov, D. F. Iscru, C. Selcu, P. C. Hammel and G. Agarwal, *Small* **4(2)** (2008) 270.
- [2] M. Rasa, B. W. M. Kuipers and A. P. Philipse, *Journal of Colloid and Interface Science* **250(2)** (2002) 303.
- [3] R. Proksch, *Current Opinion in Solid State & Materials Science* **4(2)** (1999) 231.
- [4] T. E. Schaffer, M. Radmacher and R. Proksch, *Journal of Applied Physics* **94(10)** (2003) 6525.
- [5] A. Schwarz and R. Wiesendanger, *Nano Today* **3(1-2)** (2008) 28.

Figures:

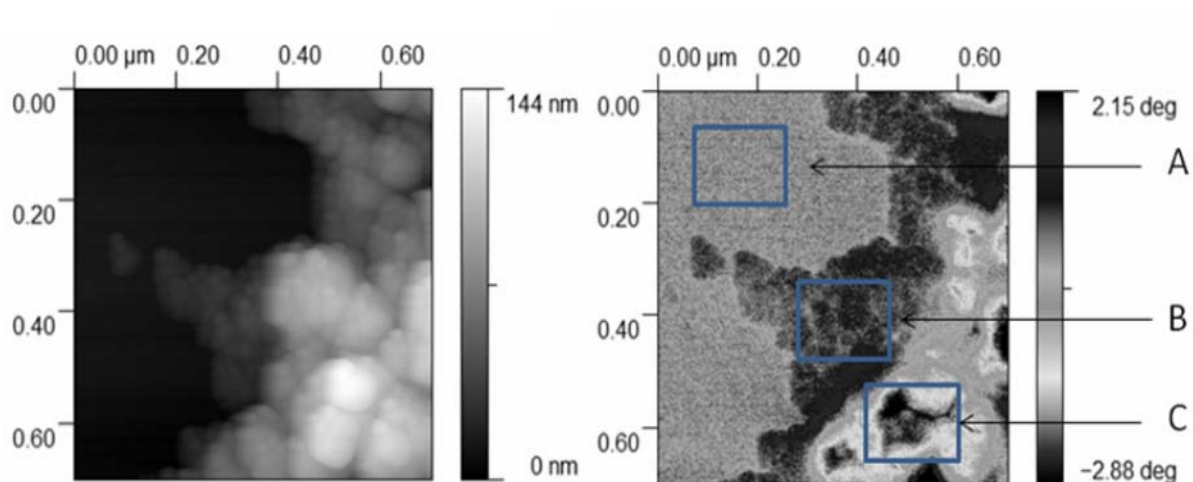


Figure 1 – Left: AFM height image of a mixture of gold and magnetite nanoparticles. Right: MFM phase shift of the same area measured in lift mode, showing contrast between mica substrate (A), gold (B) and magnetite (C) nanoparticles.

Acknowledgments

The authors would like to thank FCT (Fundação para Ciência e Tecnologia) through projects PTDC/BIO/66514/2006; PTDC/QUI/64484/2006 and PTDC/SAU-BEB/66511/2006, and SFRH/BD/28209/2006 to Pedro Quaresma.

Infrared and Raman spectroscopy investigations on SiO₂-P₂O₅ sol gel powders

B.Sava¹, A.Diaconu¹, D.Ursu¹, M.Elisa², I.Feraru², I.C.Vasilu²

¹National Institute of Glass S.A., 47 Th.Pallady Ave., 032258, Bucharest, Romania

²National Institute of R&D for Optoelectronics INOE 2000, 409 Atomistilor Str., 77125, Magurele, Romania

Contact: astatin18@yahoo.com

The purpose of the study is to investigate the influence of the precursors, pH of the solution and temperature on the gelation time of the samples from the SiO₂-P₂O₅ system. Tetraethoxysilane (TEOS) was used as precursor for SiO₂ and triethylphosphate (TEP) or phosphoric acid for P₂O₅, together with water as reagent for hydrolysis reaction and ethylic alcohol as solvent [1-5]. The pH of the sols was modified by adding 0.1 N HCl, in the case of TEP and 1.25 wt. % NH₃, in the case of H₃PO₄. The samples have been prepared starting from P₂O₅/SiO₂ = 1/10 molar ratio, H₂O/TEOS = 1; 2; 3 mass ratios and C₂H₅OH/TEOS = 1 mass ratio. We prepared silico-phosphate samples in the pH domain 1.5-3.5 and we observed that in all the cases, the lowest gelation time was found in the pH range of 3.5-4.5. We found that for the same pH value, the samples prepared with H₃PO₄ had a lower gelation time (few days) when compared to the samples prepared with TEP (weeks), explainable by the low rate of the hydrolysis and condensation reactions of TEP [6]. When the amount of water was increased, the gelation time increased in the case of samples prepared with H₃PO₄ and it was not significantly changed for the samples prepared with TEP. The increasing of the solution temperature up to 41-42°C yielded a decreasing of the gelation time (hours), especially for the samples prepared with H₃PO₄ when compared to those with TEP. In all the cases, the increased amount of water resulted in an increasing of the gelation time, even the temperature was raised.

FTIR and Raman spectroscopy characterizations have been performed aimed at getting information about the structural changes in the case of the samples dried in air and also for those heated at 100°C for 10 hours. Vibration modes specific for Si-O-Et, Si-OH, hydrogen bonds, H₂O and combined vibrations have been observed, which are in agreement with those revealed in [7].

References:

- [1] T.Uma, M.Nogami, Chem.Phys.Chem., **8** (15), (2007), p.2227-2234
- [2] L.C.Klein, Mater. Sci., **20** (1), (2002), p.81-93
- [3] Ph. Massiot, M. A. Centeno, M. Gouriou, M. I. Domínguez and J. A. Odriozola, J. Mater. Chem., **13** (2003), p.67 - 74, DOI: 10.1039/b208698k
- [4] J.D.Matthews, C.Powell, N.Borrelli, J.Am.Ceram.Soc., **88** (9), (2005), p.2455-2441
- [5] D.Predoi, V.Kuncser, M.Zaharescu, W.Keune, B.Sahoo, M.Valeanu, M.Crisan et.al, Phys.Stat.Sol.C, **1** (12), (2004), p.3507-3510
- [6] S.G.Kosinski, D.M.Krol, J.of Non-Cryst.Solids, **105** (1988), p.45
- [7] S.P.Tung, B.J.Hwang, J. Membr. Sci., **241** (2004), p.315-323

Figures: Bellow, we present FTIR spectra (fig.1) for two samples: 1 and 6, which has the lowest gelation time, within a series of 30 silico-phosphate sol gel samples, numbered from 1 to 30.

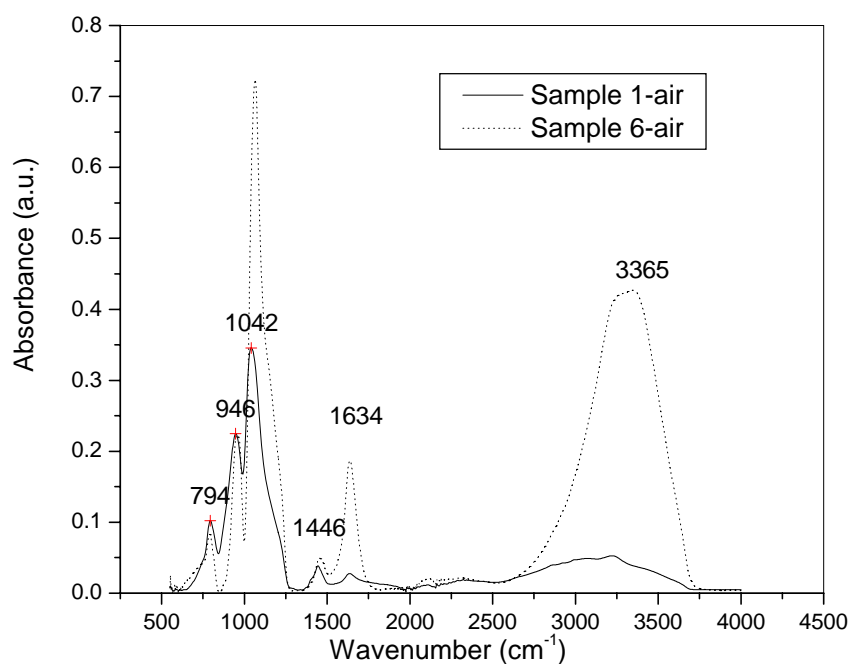


Fig.1 FTIR spectra of samples 1 and 6, dried in air

Sample 1: TEOS used as precursor for SiO₂; H₃PO₄ used as precursor for P₂O₅; P₂O₅/SiO₂ = 1/10 molar ratio; H₂O/TEOS = 1; C₂H₅OH/TEOS = 1 mass ratio; pH=3,5

Sample 6: TEOS used as precursor for SiO₂; H₃PO₄ used as precursor for P₂O₅; P₂O₅/SiO₂ = 1/10 molar ratio; H₂O/TEOS = 2; C₂H₅OH/TEOS = 1 mass ratio; pH=3,5

Pt-ZY and Pt-ZSM-5 as potential catalysts for VOCs elimination in a microchannel reactor

Miguel Escuin, Nuria Navascués, Yolanda Rodas, Victor Sebastián, Oscar del la Iglesia, Reyes Mallada, Silvia Irusta and Jesus Santamaría.

Department of Chemical and Environmental Engineering and Nanoscience Institute of Aragon, University of Zaragoza, 50009, Zaragoza

miguelescuin@gmail.com

Volatile organic compounds, VOCs, include a variety of chemicals with very low vapour pressure, i.e. 0.01kPa, at room temperature, some of which may have short and long adverse effects in health and the environment, indoor and outdoor. The VOCs oxidation reaction can represent a good method to eliminate them, especially when their concentration is in the ppm range. The challenge is to achieve a high conversion at low temperatures to optimize energy consumption, by using the appropriate catalyst and reactor. The oxidation of VOCs, in particular benzene and hexane, using a nanoporous Pt-zeolite catalyst either in a fixed bed or a microreactor is carried out.

Zeolites are especially interesting candidates as catalyst supports, due to its ability to grow as films on a variety surfaces and their high ion exchange capacity (e.g. Pt). In addition, the large ratio of zeolite coated microchannels provides an excellent contact between reactants and catalyst [2]. In Pt-zeolites, platinum provides the catalytic activity.

On the other hand, microchannel reactors, that could be defined as three-dimensional structures with inner dimensions in the range of 10 to 100 microns offer many advantages over convectional reactors. Their high surface area to volume ratio, with values between 10000 and 50000 m²•m⁻³, enhances their mass and heat transport properties, and make them ideal candidates for process intensification. Mass transfer processes can be accelerated considerably in microreactors because of their small dimensions so it is possible to strongly reduce diffusion times. The high heat transfer coefficient allows, for instance, carrying out highly exothermic reactions under near isothermal conditions and avoiding hot spots.

In this work, Pt-ZY and Pt-ZSM-5 have been synthesized as powder or coated in microchannel reactors. Both types of materials have been evaluated for the catalytic combustion of hexane at low concentration, 200ppm.

Experimental

The synthesis of the zeolite layer on the microchannels was carried out by a seeded (secondary) growth method. A 5wt.% seeds suspension of zeolite (ZSM-5 or ZY) was deposited in the microchannels, after that the stainless steel plates were placed vertically in the autoclave with the synthesis gel. The molar composition of ZY and ZSM-5 gel was 17Na₂O:12,8SiO₂:1Al₂O₃:975H₂O and 21SiO₂:3NaOH:0,102Al₂O₃:1TPAOH:MH₂O (M=1974) respectively. The synthesis was carried out at 90 °C for 24 h in the case of ZY and 150 °C for 12 h for the ZSM-5 microreactor. Pt was introduced into the framework by convectional ion-exchange method with an aqueous [Pt(NH₃)₄](NO₃)₂ solution. Pt-ZY powder was prepared from commercial NaY zeolite by the same ion exchange method. Pt-ZSM-5 powder was prepared starting from a more concentrated gel than the used for microreactor (M=987), and the synthesis was carried out at 175 °C for 8 h-

Hexane oxidation was carried out in a conventional fixed bed reactor: The reactive flow was composed of air and 200 ppm of gaseous hexane. The flow rate through the reactor was set to produce a space velocity between 60000 and 240000 ml.h⁻¹.g⁻¹.

Results and discussion

Hexane oxidation curves versus temperature are presented in Fig. 1 and Fig. 2. The observed products are only carbon dioxide and water indicating complete combustion occurring during the reaction.

Fig. 1 shows catalytic activity of Pt-ZY and Pt-ZSM-5 with a 0,69 % and 2 % of Pt respectively. Despite that Pt-ZY have less amount of Pt, it reached 50 % of conversion at a temperature 30 °C lower than Pt-ZSM-5. It is necessary to increase the temperature up to 350°C, with Pt-ZSM-5 catalysts, in order to obtain the complete conversion of hexane. Pt-ZY is more active for catalysis than Pt-ZSM-5

Fig. 2 shows catalytic activity of Pt-ZY with a 3,6 % and 1,7 % of Pt. In both catalysts Pt(3.6 wt%)/Y and Pt(1.7 wt%)/Y, the oxidation of hexane reached 50% of conversion at 164 °C for the lower value of GHSV.

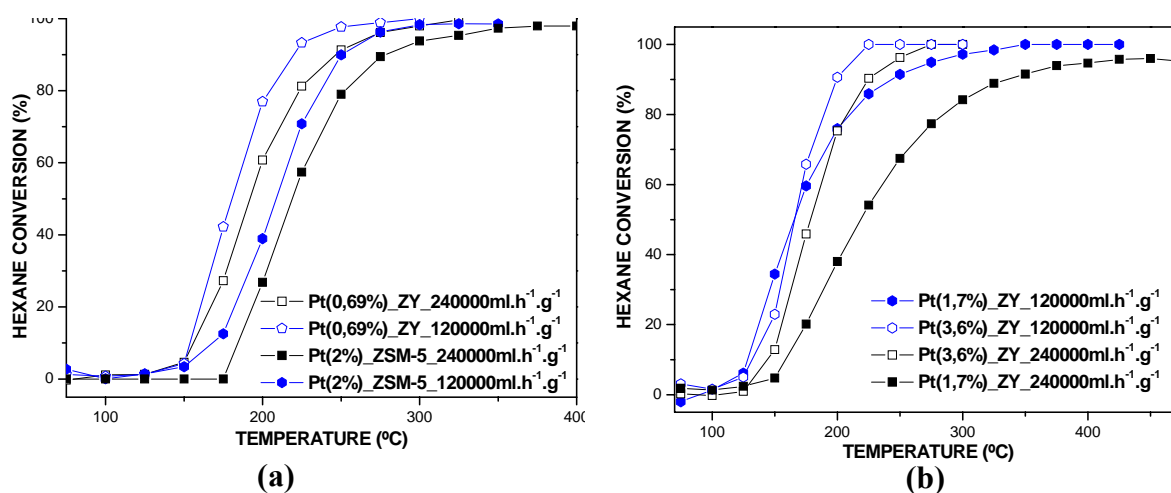


Figure 1. Hexane conversion curves versus temperature: a) Catalytic activity of Pt(2%)-ZSM-5 and Pt(0,69%)-ZY. b) Catalytic activity of Pt/Y solids with different amount of Pt. Hexagon symbols: GHSV = 120,000 ml.h⁻¹.g⁻¹, square symbols: GHSV = 240,000 ml.h⁻¹.g⁻¹.

The effect of the space time in conversion is less pronounced for the Pt(3.6 wt%)/Y, compared to the Pt(1.7 wt%)/Y. The latter could not achieve a 100% conversion at the highest GHSV value.

It is important to note that in all cases the total conversion is achieved at relatively low temperatures compared to published results. Furthermore, it is foreseen that the use of these zeolites in a microchannel reactor would decrease, even more, this temperature as it was observed for other reactions [3].

References:

- [1] Saravanan, V., Rajamohan, N., Treatment of xylene polluted air using pressmud-based biofilter, *Journal of Hazardous Materials*, 162 (2009) 981-988.
- [2] Lai, S.M., Ng, C.P., Martin-Aranda, R., Yeung, K.L., Knoevenagel condensation reaction in zeolite membrane microreactor, *Microporous and Mesoporous Materials*, 66 (2003) 239–252.
- [3] O. de la Iglesia, V. Sebastián, R. Mallada, G. Nikolaidis, J. Coronas, G. Kolb, R. Zapf, V. Hessel, J. Santamaría. Preparation of Pt/ZSM-5 films on stainless steel microreactors. *Catal. Today*, 125, (2007), 2-10.

CRITICAL SLOWING DOWN OF THE SPIN RELAXATION IN NANOCLUSTERED FE-AL-B ALLOYS

D. Alba Venero¹, L. Fernández Barquín¹, J. A. de Toro, J. M. Riveiro²

¹Depto. CITIMAC, F. Ciencias, Universidad de Cantabria, Santander 39005, Spain

²Depto. Física Aplicada, Universidad de Castilla-La Mancha, Campus Universitario, Ciudad Real 13071, Spain

barquinl@unican.es

A vast number of heterogeneous magnetic systems, which are the subject of present scientific and technological attention, display disordered magnetic arrangements as a result of spatial and/or anisotropy randomness and competition between interactions of different sign. The magnetic relaxation of atomic spins (or the macrospin of nanoparticles) slows down upon cooling and, under certain conditions, finally collectively freeze in a spatially uncorrelated magnetic configuration, called the spin-glass (or superspin-glass) state [1-4]. The superspin freezing temperature will depend on the particle size and concentration, and also on the matrix nature [2]. The terms *superspin-glass* (SSG), or *superferromagnet*, were coined analogously to the older term *superparamagnetism*: the prefix “super” expresses the substitution of the atomic spin by a particle magnetic moment of several hundreds/thousands Bohr magnetons, with the particle ensembles retaining, nonetheless, the essential magnetic behavior of the corresponding atomic-spin scenario (paramagnetism, ferromagnetism, or spin-glass), only with higher transition temperatures from the collective low temperature states to the superparamagnetic regime [4]. These terms have been applied in relatively different solids such as ultrafine monodispersed Fe-C particles [5] and Co₈₀Fe₂₀/Al₂O₃ discontinuous multilayers [6]. Recently, it has been shown that Fe-based alloys (around 30% Fe) obtained by milling exhibit SSG behavior [7-10], where the cluster diameter was estimated to be as small as 1 nm, similarly to other less Fe-concentrated alloys.

A highly disordered alloy of Fe₃₅Al₅₀B₁₅ has been produced by milling under vacuum for 840 hours, with the X-ray diffraction pattern showing only two broad peaks. The AC-susceptibility shows sharp maxima around 20 K (21 K) in the real (complex) components. Those are due to spin freezing, and shift up in temperature when the frequency is increased. The magnetic dynamics is accounted for by a critical slowing down with $z\nu = 8.0(4)$ and $T_0 = 19.8(2)$. The large dynamic exponent $\beta = 1.3(1)$ is an indication of a non-conventional transition. The non-linear susceptibility reveals a peak with $\gamma = 1.2(4)$ which is affected by the oscillating $h < 5$ Oe and biasing ($H_{DC} \leq 40$ Oe) fields. The results are interpreted in terms of the collective blocking of very fine Fe-rich magnetic particles resulting from an incomplete compositional homogenization

References:

- [1] J. A. Mydosh, *Spin Glasses: an experimental approach* (Taylor and Francis, 1993).
- [2] S. Bedanta and W. Kleemann, *J. Phys. D: Appl. Phys.* **42** (2009) 13001.
- [3] S. Mørup, M. B. Madsen, J. Franck, J. Villadsen, and C. J. W. Koch, *J. Magn. Magn. Mat.* **40** (1983) 163.
- [4] J. L. Dormann, D. Fiorani and E. Tronc, *Ad. Chem. Phys.* **98** (1997) 283.
- [5] C. Djurberg, P. Svedlindh, P. Nordblad, M. F. Hansen, F. Bødker and S. Mørup, *Phys. Rev. Lett.* **79** (1997) 5154; M. F. Hansen, P. E. Jönsson, P. Nordblad and P. Svendinh, *J. Phys.: Condens. Matt.* **14**, (2002) 4901.
- [6] X. Chen, S. Bedanta, O. Petravic, W. Kleemann, S. Sahoo, S. Cardoso and P. P. Freitas, *Phys. Rev. B* **72** (2005) 214436.
- [7] J. A. De Toro, M. A. López de la Torre, J. M. Riveiro, R. Sáez Puche, A. Gómez-Herrero, and L. C. Otero-Díaz, *Phys. Rev. B* **60** (1999) 12918.

- [8] J. A. De Toro, M. A. López de la Torre, M. A. Arranz, J. M. Riveiro, J. L. Martínez, P. Palade and G. Filoti, *Phys. Rev. B* **64** (2001) 94438.
- [9] J. A. De Toro, M. A. López de la Torre, J. M. Riveiro, J. Bland, J. P. Goff and M. F. Thomas, *J. Appl. Phys.* **91** (2002) 8396.
- [10] J. A. De Toro, M. A. López de la Torre, J. M. Riveiro, A. Beesley, J. P. Goff and M. F. Thomas, *Phys. Rev. B* **69** (2004) 224407.
- [11] L. Fernández Barquín, R. García Calderón, B. Farago, J. Rodríguez-Carvajal, A. Bleloch, D. McComb, R. Chater, and Q. A. Pankhurst, *Phys. Rev. B* **76** (2007) 172404.
- [12] D. H. Ucko, Q. A. Pankhurst, L. Fernández Barquín, J. Rodríguez Fernández, and S. F. J. Cox, *Phys. Rev. B* **64** (2001) 10433.

IMMOBILIZATION OF A LASER-DYE ON GOLD NANOPARTICLES. ANALYTICAL APPLICATIONS

Edgar Alonso-Reynoso¹, Alfonso Fernández-González², Ignacio Rivero-Espejel³
Marta Elena Díaz García²

¹On leave from the Technological Institute of Tijuana, Baja California, México.

²Department of Physical and Analytical Chemistry, University of Oviedo, Spain.

³Technological Institute of Tijuana, Baja California, México.

medg@uniovi.es

In the recent years, the synthesis, characterization and exploitation of noble metal nanoparticles have become a very active research field. Gold nanoparticles exhibit optical properties different from those of metal ions in solution. These nanoparticles may be easily functionalized in order to interact with chemical species of analytical concern, such as amino acids or amines [1,2].

Gold nanoparticles are conventionally functionalized by exploiting the high affinity between sulphur and gold atoms. So, mercapto-compounds are commonly used to provide gold nanoparticles with carboxylic (e.g. mercaptoundecanoic acid) or amine (e.g. cysteamine) moieties, among others. However, there are compounds, like cyanide, that also exhibit a high affinity against gold. In this work, we took advantage from this to study the binding of a cyane-containing laser fluorescent dye (4-(Dicyanemethylene)-2-methyl-6-[*p*-(dimethylamine)styryl]-4*H*-piran, DCM) on gold nanoparticles (DCM-GNPs).

The interaction between the dye and the gold nanoparticles was studied using several analytical techniques, such as Visible-UV Spectrometry, Fluorescence Spectrometry, Infrared Spectrometry, Nuclear Magnetic Resonance and X-ray Photoelectron Spectrometry that provided interesting information about that interaction.

Experimental conditions for the displacement of DCM from the DCM-GNPs surface by cyanide ions were studied. In Figure 1, the spectral changes upon cyanide additions to a solution containing DCM-GNPs are observed. The potential application of the approach for cyanide determination is outlined.

References:

- [1] Du B., Li Z., Cheng Y., Talanta **75** (4) (2008) 959-964.
- [2] Daniel M.C., Astruc D., Chem. Rec **104** (2004) 293-346.

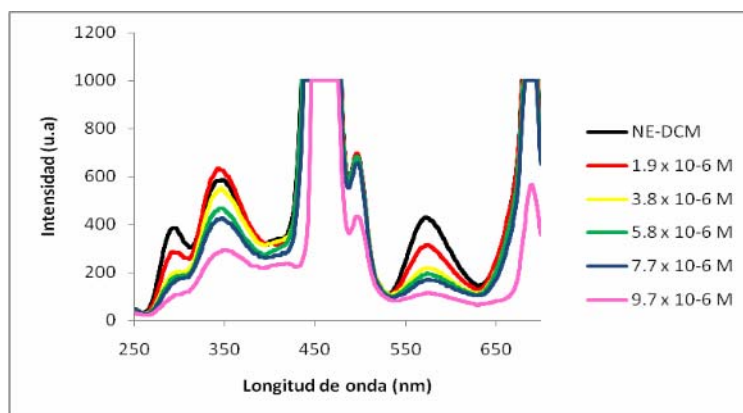


Figure 1- Interaction of CN⁻ anion with dye-functionalized GNPs.

MAGNETIC PROPERTIES OF COBALT NANODEPOSITS CREATED BY FOCUSED ELECTRON BEAM INDUCED DEPOSITION

^{1,2}A. Fernández-Pacheco, ²J. M. De Teresa, ¹R. Córdoba, ^{1,2}M.R. Ibarra, ³D. Petit, ³D.E. Read, ³H.T. Zeng, ³L. O'Brien, ³E.R. Lewis, ³R.P. Cowburn

¹ Instituto de Nanociencia de Aragón, Universidad de Zaragoza, Zaragoza, 50009, Spain

² Instituto de Ciencia de Materiales de Aragón, Universidad de Zaragoza-CSIC, Facultad de Ciencias, Zaragoza, 50009, Spain

³ Nanoscale Magnetism Group, Department of Physics, Blackett Laboratory, Imperial College London, Prince Consort Road, London SW7 2BW, United Kingdom

fpacheco@unizar.es

The **local deposition of materials using a focused electron beam in the presence of a gas precursor (FEBID)** is a well-known technique used for the mask-less fabrication of structures with nanometer resolution, with a wide range of applications [1]. The possibility of growing nanometric magnetic materials is especially attractive, since it widens the applications to fields such as magnetic storage or magnetic sensing, among others. However, long-standing problems exist for this kind of deposits, associated with the, in general, organo-metallic nature of the precursor gas. The low efficiency of the process for decomposing the precursor molecules gives as a result a predominant C-content composition, with low metallic percentages. As a result, the electrical transport properties show non-metallic behaviour, with resistivities orders of magnitude larger than the bulk value [1].

In this contribution we characterize magnetically **Co nanowires** (NWs) created by FEBID by means of magnetotransport measurements [2], as well as by spatially resolved magneto-optical Kerr effect (MOKE) [3].

By magnetotransport measurements of individual NWs, together with EDX analysis, we have studied the importance of the growth conditions in the quality of the NWs, finding that at high beam currents (figure 1a), the deposits are highly pure (around 95% of atomic cobalt) and their resistivity is about 40 $\mu\Omega\text{cm}$ at room temperature, with metallic temperature dependence. Magnetoresistance (MR) measurements in different configurations are used to study how the magnetization (*M*) is aligned in the NWs (see insets figure 1). We find that the shape anisotropy dominates the direction of *M*. Coherent rotation seems to be the mechanism for reversal when the field is applied perpendicular to the NW axis and the substrate plane, because of the NW dimensions. From the saturation field in this configuration we deduce a saturation magnetization value of $1329 \pm 20 \text{ emu/cm}^3$, very close to the bulk value of pure Co. We have studied in detail other aspects of the magnetism of the NWs by measuring the Hall effect and the Planar Hall effect as a function of temperature. Similar magnetotransport properties have been previously observed in polycrystalline Co NWs fabricated by Electron Beam Lithography [4], demonstrating the high quality of these FEBID structures. These high quality properties sharply contrast with NWs grown at lower beam currents (figure 1b), with resistivities 300 times larger at room temperature, semiconducting behaviour, and MR ratios one order of magnitude smaller than those found for the nanowires grown under high currents. We associate the important differences found as a function of the beam with a heating effect process during deposition, a crucial point in FEBID processes [1].

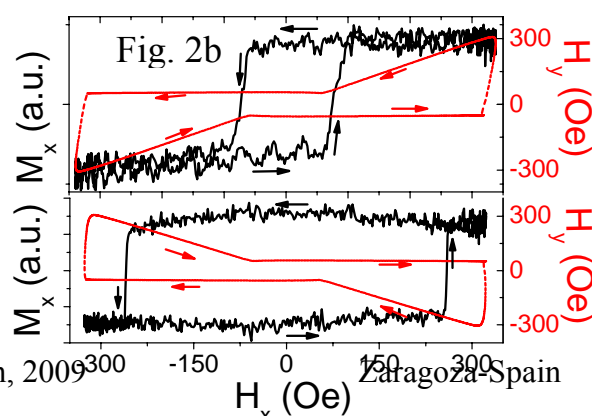
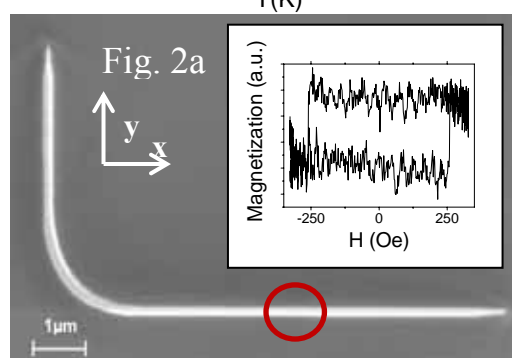
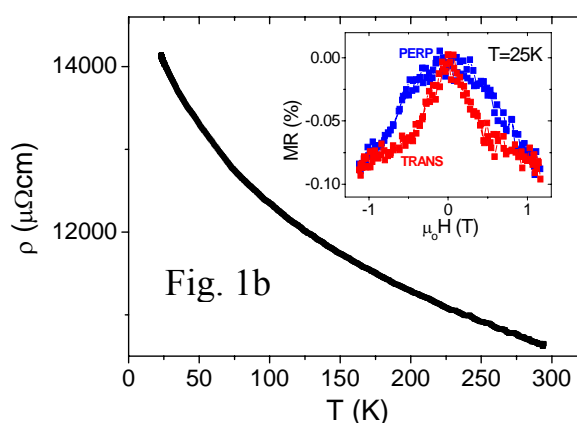
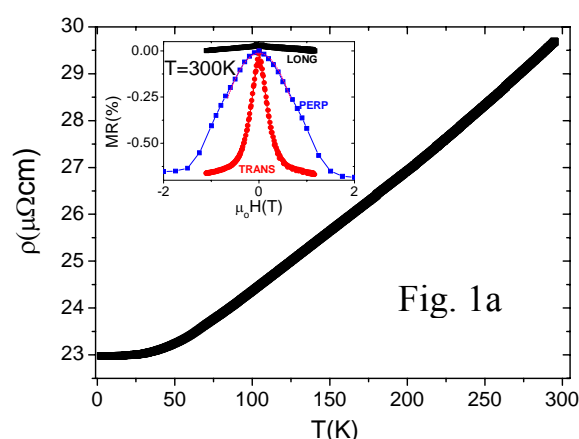
We have also studied the domain wall (DW) conduit properties of FEBID-Co NWs [5], i.e., the possibility to displace DWs at much lower magnetic fields than are needed to nucleate

new domains. Controlling the switching of nanometer sized elements is the subject of intense research due to their potential applications in fields such as spintronic logic [5] or DW based memory devices [6]. Most of the work to date in this field has been done on permalloy NWs. We show in this work that FEBID Co is a good alternative for such applications. For this study we have fabricated L-shaped NWs for several aspect ratios (see figure 2a). The component of the magnetization along the x axis was determined by measuring the longitudinal Kerr effect. A typical hysteresis loop is shown in the inset of figure 2a, corresponding to a single-sweep cycle. The sensitivity in this MOKE setup allows a clear observation of the magnetic switching even in a single-shot measurement. By applying different in-plane magnetic field sequences (red dashed lines in figure 2b), the magnetization of the structure (solid black lines in figure 2b) is initialized in a different magnetic configuration. The initial magnetic configuration is achieved by placing (or not) a domain wall at the corner of the L-shape. The initial state determines the magnetization reversal mechanism, which allows the measurement of the domain wall propagation (figure 2b-up) or nucleation (figure 2b-down) field respectively. Significant differences are found for the fields necessary to reverse the magnetization, if a DW is initially present, or not, in the nanostructure. This demonstrates the conduit properties of the Co FEBID nanowires.

References:

- [1] I. Utke, P. Hoffmann, J. Melngailis, J. Vac. Sci. Technol. B **26** (2008) 1997.
- [2] A. Fernández-Pacheco, J.M. De Teresa, R. Córdoba, M.R. Ibarra, J. Phys. D: Appl. Phys., in press
- [3] A. Fernández-Pacheco et al, submitted to Appl. Phys. Lett.
- [4] B. Leven, G. Dumpich, Phys. Rev. B **71** (2005) 064411
- [5] D. A. Alwood, G. Xiong, C.C. Faulkner, D. Atkinson, D. Petit, R.P. Cowburn, Science **309** (2005) 1688
- [6] S. S. P. Parkin, U.S. Patents No. 6,834,005, 6,834,005, 6,898,132, 6,920,062, 7,031,178, and 7,236,386 (2004 to 2007)

Figures:



pH-Switched Adsorption of Cytochrome c to Self-Assembled Monolayers on Gold Surfaces and Nanoparticles

Inês Gomes,^a Maria F. Feio,^b Krisztina István,^b Nuno C. Santos,^c Peter Eaton,^b Eulália Pereira,^b and Ricardo Franco^a

^aREQUIMTE, Departamento de Química, Faculdade de Ciências e Tecnologia, Universidade Nova de Lisboa, 2829-516 Caparica ^bREQUIMTE, Departamento de Química, Faculdade de Ciências da Universidade do Porto, 4169-007 Porto ^cInstituto de Medicina Molecular, Faculdade de Medicina da Universidade de Lisboa, 1649-028 Lisboa, r.franco@dq.fct.unl.pt

Understanding nanoparticle-biomacromolecule interactions is important in the design of nanotechnology-based biosensors, diagnostic agents and novel materials. In this context, monolayer-capped gold nanoparticles (AuNP) provide an suitable scaffold for developing biomarker platforms due to their unique optical properties, robustness, and high surface areas [1,2]. In this work, the adsorption characteristics of horse heart cytochrome c (HCc) onto mercaptoundecanoic acid (MUA)-capped AuNP and also on self-assembled monolayers of MUA on gold surfaces were studied by quartz crystal microbalance, atomic force microscopy, UV-visible spectroscopy and ζ -potential.

To follow the formation of bionano-conjugates of HCc on citrate-capped AuNP; or on MUA-capped AuNP, a previously developed method based on ζ -potential measurements was used [3]. Analysis of the obtained Langmuir isotherms allowed concluding that HCc adsorption to AuNP is thermodynamically favored in the presence of a MUA capping in relation to citrate capping (Figure 1). UV-visible data on both types of bionano-conjugates show aggregation as a function of the solution pH, inducing a shift of the AuNP plasmon band corresponding to a red-to-blue color change in the solution. Both bionano-conjugates aggregate at around pH 6.2, whereas citrate- or MUA-capped AuNPs pH values correspondent to the pKa value of the capping species. These aggregation results were confirmed by ζ -potential determinations.

Quartz crystal microbalance provided quantitative information regarding the adsorption of HCc onto a bare gold surface and a MUA self-assembled monolayer on gold. Results of experiments carried out with this pseudo-two dimensional system at pH 7.4 and 4.5 showed an increase in protein adsorption at the higher pH. This increase is threefold higher when a MUA self-assembled monolayer is present, comparatively with the bare surface. Atomic force microscopy studies of this system in solution provided images showing the distribution of individual protein molecules adsorbed onto the surfaces (Figure 2).

In conclusion, the interaction of HCc with MUA-capped nanoparticles and surfaces is mainly of an electrostatic nature, and pH can be used as an adsorption modulator, with a “switching” pH value for protein adsorption.

References:

- [1] Baptista, P.; Pereira, E.; Eaton, P.; Doria, G.; Miranda, A.; Gomes, I.; Quaresma, P.; Franco, R. *Analytical and Bioanalytical Chemistry*, **391** (2008) 943.
- [2] You, C.-C.; Verma, A.; Rotello, V. M. *Soft Matter*, **2** (2006) 190.
- [3] Gomes, I.; Santos, N. C.; Oliveira, L. M. A.; Quintas, A.; Eaton, P.; Pereira, E.; Franco, R. *Journal of Physical Chemistry C*, **112** (2008) 16340.

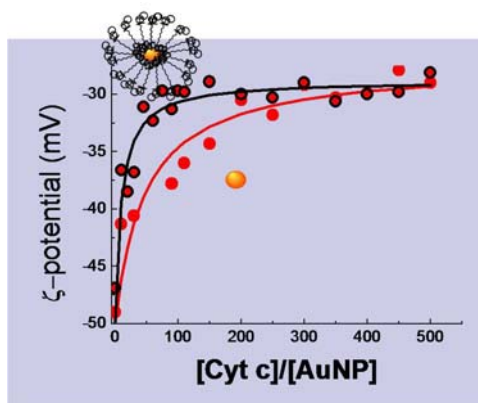


Figure 1 – Cytochrome c adsorption to citrate- and MUA-capped AuNPs as determined by ζ -potential

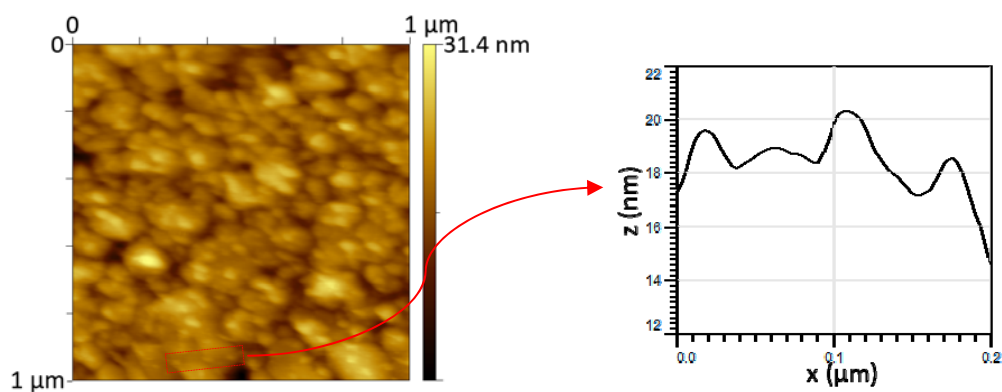


Figure 2 – Atomic Force Microscopy of a gold crystal surface with Cytochrome c deposited over a MUA self-assembled monolayer (pH 7.4; in buffer). The marked region is shown in the height profile, indicating 3 absorbed protein molecules.

Structural, magnetic and magnetotransport characterization of Fe/MgO granular multilayers

*A. García-García^{2,3}, A. Vovk^{1,3,6}, J. A. Pardo^{1,4}, P. Štrichovanec¹, C. Magén^{1,5}, E. Snoeck⁵,
P. A. Algarabel^{2,3}, J. M. De Teresa^{2,3}, L. Morellón^{1,2,3}, and M. R. Ibarra^{1,2,3}*

1 Instituto de Nanociencia de Aragón, Universidad de Zaragoza, 50009-Zaragoza, Spain

2 Instituto de Ciencia de Materiales de Aragón, Universidad de Zaragoza-CSIC, 50009-Zaragoza, Spain

3 Departamento de Física de la Materia Condensada, Universidad de Zaragoza, 50009-Zaragoza, Spain

4 Departamento de Ciencia y Tecnología de Materiales y Fluidos, Universidad de Zaragoza, 50018-Zaragoza, Spain

5 Centre d'Elaboration de Matériaux et d'Etudes Structurales, CNRS, 31055-Toulouse, France

6 Institute of Magnetism NAS of Ukraine, 36-b Vernadsky blvd., 03142, Kyiv, Ukraine

Magnetic granular solids consist of nanometer-sized magnetic particles embedded in an immiscible insulating or metallic medium. The spin-dependent transport in these materials is of particular interest for magnetoelectronic applications, such as sensors, read heads and nonvolatile memories¹. In this work we report the structural, magnetic and magnetotransport characterization of $[\text{Fe}(t)/\text{MgO}]_N$ multilayers with nominal Fe layer thickness t near percolation threshold ($t \sim 0.8$ nm).

Granular multilayers $[\text{Fe}/\text{MgO}]_N$ were prepared on glass substrates by sequential Pulsed Laser Deposition (PLD). A 3 nm buffer layer of MgO was deposited on the glass substrates. The total amount of Fe was preserved between samples by choosing the number of bilayers N , while the nominal thickness of MgO layers was fixed at 3 nm.

Specular X-ray reflectivity profiles of the multilayers show well defined first and second order Bragg peaks, and Kiessig fringes, indicating a high degree of structural periodicity of the samples [FIG.1]. TEM micrographs [FIG.2] show that the structure of each Fe layer evolves from continuous film to an ensemble of granules through multiple percolation structures with decreasing t .

A transition from ferromagnetic for $t > 0.81$ nm to superparamagnetic (SPM) for $t \leq 0.61$ nm behaviour upon decreasing iron concentration is observed. Zero Field Cooled (ZFC) and Field Cooled (FC) susceptibility measurements show clearly irreversible behaviour for SPM samples below bifurcation temperature (T_b). The values of T_b increase with t indicating growth of the average particle size.

For the films with $0.40 \text{ nm} \leq t \leq 0.61 \text{ nm}$ the particle size distribution (PSD) was estimated from fitting M vs. H curves at different temperatures above T_b using weighted Langevin functions and an approach of log-normal distribution of particle sizes [FIG.3]. The values of average particle size obtained from magnetic data fittings correlates with those from plan-view high resolution-TEM micrographs of MgO/Fe/MgO trilayers deposited on carbon grids with the same Fe:MgO ratios.

The magnetoresistance ($\text{MR} = [\rho(H) - \rho(0)] / \rho(0)$, where $\rho(0)$ and $\rho(H)$ are the resistivity of the film in zero and in applied magnetic field, respectively) was measured with magnetic field in the films plane and parallel (L-geometry) and perpendicular (T-geometry) to the applied current in temperature range 10 – 300 K and in magnetic field up to 18 kOe. An isotropic MR $\sim 3\%$ at room temperature was found for the films with $t \leq 0.61$ nm [FIG.4]. The temperature dependence of resistance for this film follows the behaviour $\rho(0) \sim \exp(2 \cdot E_c / k_B T)^{0.5}$ indicating tunnelling type of conductance [FIG.5]. Here E_c is an activation energy necessary to create a pair of charged particles during thermally activated and/or bias assisted tunneling process in a system with distribution of particle sizes and interparticle distances, k_B is Boltzmann constant and T is temperature. Thus MR is due to spin-polarized electron tunnelling between neighboring SPM granules¹. An enhanced MR is observed

[FIG.6] at low temperatures indicating higher-order tunnelling processes between large particles mediated by small ones as T decreases². For the films with $t > 0.81$ nm an anisotropic MR for L-geometry measurements is observed. This confirms the formation of continuous Fe layers in the films³.

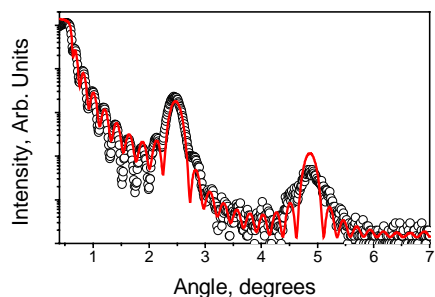


Fig. 1 X-ray reflectivity measured in the sample with nominal Fe thickness $t=0.81$ nm (open circles) and fitted reflectivity (solid line).

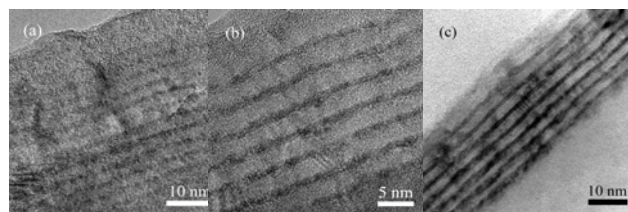


Fig. 2 Cross section TEM images of selected MgO/Fe specimens with increasing thickness (a) $t=0.4$ nm, (b) $t=0.81$ nm and (c) $t=1.25$ nm.

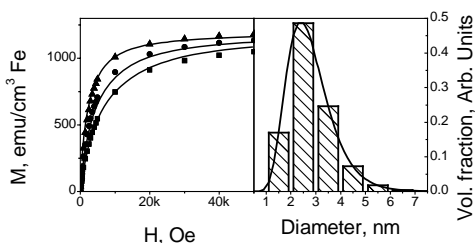


Fig. 3 Fitting of the hysteresis loops of the layered granular films Fe (0.61 nm)/MgO (3 nm) at 100 K (square), 200 K (circle) and 295 K (triangle) (left panel) and calculated particle sizes distribution (right panel).

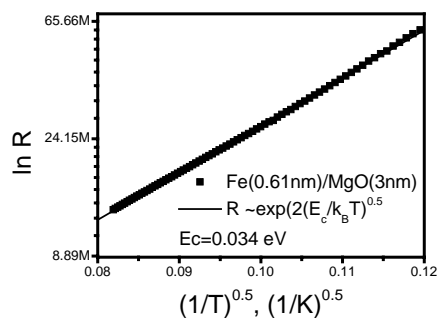


Fig. 5 Temperature dependence of resistance for Fe(0.61 nm)/MgO(3 nm) film. Solid line presents results of the experimental data fitting using $\ln(\rho) \sim (E_c/T)^{0.5}$ model.

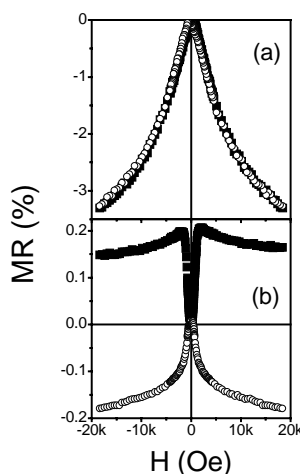


Fig. 4 Dependencies of MR on applied magnetic field for films Fe(0.61 nm)/MgO(3 nm) (a) and Fe(0.81 nm)/MgO(3 nm) (b). Measurements in L- (solid squares) and T- (open circles) geometries at room temperature.

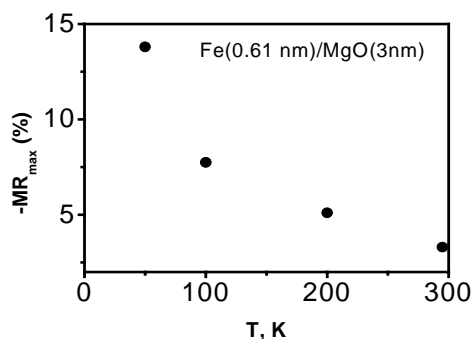


Fig. 6 Temperature dependence of MR for Fe(0.61 nm)/MgO(3 nm) film in magnetic field of 18 kOe, T-geometry.

References

- [1] H. Fujimori et al., J. Magn. Magn. Mater. **304**, 32 (2006)
- [2] S. Mitani et al., Phys. Rev. Lett. **81**, 2779 (1998)
- [3] A. Vovk et al., J. Appl. Phys., **91**, 10017 (2002)

Nanoengineering the growth of a carbon nanofiber layer on micro-structured reactors

Pedro Ruiz-Cebollada, L. Martínez-Latorre, E.García-Bordejé

Instituto de Carboquímica (C.S.I.C.), Miguel Luesma Castán 4, 50015 Zaragoza, Spain

Tel: +34 976733977; Fax: +34 976733318, e-mail: jegarcia@icb.csic.es

Background

Microreactors share some common properties with other structured reactors, such as low pressure drop. Besides, its channel diameter ($< 1\text{mm}$) enhances mass and heat transport, enabling isothermal operation, improved selectivity and security [1]. To increase the catalytic surface area of microreactor, one option would be filling the microchannels with catalytic material. However, this will increase substantially the pressure drop. Thus, the best option is coating the microchannel walls by a well-adhered catalyst layer because it keeps a low fluidic resistance.

CNF and CNT hold many promises as catalyst support [2]. For instance, some gas-phase reactions benefit from the use of graphitic materials as catalyst support [3]. Furthermore, graphitic nanomaterials by themselves have outstanding performance in dehydrogenations reactions [4-5]. Unlike metal oxide support, CNF form aggregates with high surface areas, high mesopore volumes and low tortuosity. This is favourable for diffusion of liquids to catalytic sites, while keeping low pressure drop.

Nevertheless, CNFs in powder form have some drawbacks such high-pressure drop, plugging and flow maldistribution for fixed bed operation, and agglomeration and difficulty of filtration due to the formation of fines for slurry phase operation. The attachment of CNF to structured reactors would circumvent these drawbacks.

CNF coated microreactors must be endowed with good activity and durability to be competitive with conventional technology. To this end, catalytic coating must exhibit a good adhesion to substrate, open porosity (mesoporosity) to enhance the diffusion of reactants, uniform thickness of CNF layer, good mechanical strength and control over the microstructure of CNFs. The good mechanical stability of CNF inside microchannels is crucial to prevent channel blocking by loose CNFs.

In this work, we study the conditions for the growth of a well-adhered layer of carbon nanofibers (CNF) on microreactors via catalytic decomposition of hydrocarbon. The CNF coating properties have been optimised by studying different variables such as pretreatment of microreactor substrate, reaction temperature, hydrocarbon and addition of H_2 . To our knowledge, it is reported the coating with carbon nanomaterials of silica microreactors [6-7], but there is no report of coating stainless steel microreactors. The catalytic microreactor is intended as e.g. for in-situ H_2 generation from NH_3 decomposition to feed a fuel cell in portable applications.

Experimental

We have coated stainless steel microreactor with a CNF layer by the following procedure. First, coating the stainless steel microreactor with a well-adhered alumina layer. Subsequently, Ni catalyst was impregnated via electrostatic interaction of alumina coating with a nickel solution at neutral pH. Finally, we have grown a CNF layer over microreactors via catalytic chemical vapour deposition (CCVD) of methane or ethane. The techniques used for characterization of CNF layer comprise SEM-EDX, XRD, Raman spectroscopy, TEM, Temperature programmed oxidation and N_2 adsorption.

Results

Figure 1 displays picture of the microreactor platelets after different preparation stages. Figure 1c shows the microchannels covered by a CNF layer (back colour). After CNF growth, the microreactor exhibited a complete coating with CNFs of uniform size (figure 2).

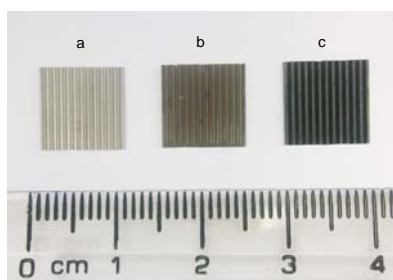


Figure 1. microreactor platelets corresponding to several preparation steps. (a) as-received platelet, (b) platelet after thermal treatment and alumina coating, (c) platelet after CNF growth

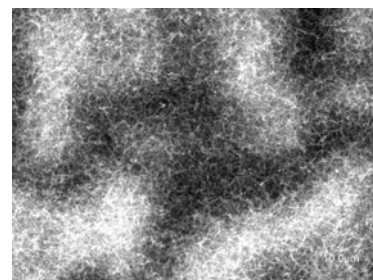


Figure 2. Top view of a microreactor channel coated with the nanofibers

The grown CNFs are of the fishbone type. This kind of nanofibers exposes numerous graphene edges. The presence of these edges has been reported to be beneficial for catalysis [8] because graphene edges can be functionalised to disperse catalyst particles. Figure 3 shows a representative Raman spectra. The D band is the disordered induced band. The presence of this band is an indication of CNF exposing graphene edges or defective graphitic structure. Depending on the growth conditions (hydrocarbon, the hydrocarbon:H₂ ratio, growth temperature), we obtained different CNF yields, CNF thicknesses and type of carbonaceous products in terms of graphiticity and morphology. When the growth temperature increases, the graphiticity increases accordingly, regardless the hydrocarbon. Additionally, increasing temperature also leads to less uniformity in the morphology of nanocarbons. At the highest temperatures metal dusting occurs. These fragments of metals from microreactor walls catalyse the growth of different nanocarbon structures. This also leads to a non uniform growth, with some carbon protrusions plugging some microchannels. For the optimised CNF coating, the weight loss after drop test was negligible (< 5 wt%). This good adhesion was confirmed by SEM characterisation. This technique revealed a complete coverage of the channels by CNFs. Figure 4 shows a detail of the CNF layer, which shows the tight contact between the CNF layer and the microchannel wall.

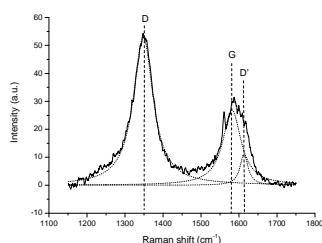


Figure 3. Raman spectra of CNFs over microreactor



Figure 4. Edge of a microreactor channel coated with CNF layer

Conclusions

Stainless steel microreactors have been coated by a uniform layer of entangled carbon nanofibers with satisfactory mechanical resistance. The CNFs have uniform size and microstructure. Thus, the CNF-microreactor has good perspectives as catalyst support or catalyst by itself.

References

- [1] G. Kolb, V. Hessel, Chemical Engineering Journal, 98 (2004) 1.
- [2] P. Serp, M. Corrias, P. Kalck, Applied Catalysis A-General, 253 (2003) 337.
- [3] R. Z. Sorensen, A. Klerke, U. Quaade, S. Jensen, O. Hansen, C. H. Christensen, Catalysis Letters, 112 (2006) 77.
- [4] J. Zhang, X. Liu, R. Blume, A. H. Zhang, R. Schlogl, D. S. Su, Science, 322 (2008) 73.
- [5] N. Keller, N. I. Maksimova, V. V. Roddatis, M. Schur, G. Mestl, Y. V. Butenko, V. L. Kuznetsov, R. Schlogl Angewandte Chemie-International Edition, 41 (2002) 1885.
- [6] N. Ishigami, H. Ago, Y. Motoyama, M. Takasaki, M. Shinagawa, K. Takahashi, T. Ikuta, M. Tsuji, Chemical Communications, (2007) 1626.
- [7] I. Janowska, G. Wine, M. J. Ledoux, C. Pham-Huu, Journal of Molecular Catalysis A-Chemical, 267 (2007) 92.
- [8] T. J. Zhao, W. Z. Sun, X. Y. Gu, M. Ronning, D. Chen, Y. C. Dai, W. K. Yuan, A. Holmen, Applied Catalysis A: General, 323 (2007) 135.

Directional effects in the scattering produced by nanosystems with double negative optical properties

Braulio García-Cámara, José María Saiz, Francisco González, Fernando Moreno

Grupo de Óptica. Departamento de Física Aplicada. Universidad de Cantabria.

Avda de los Castros s/n 39005, Santander (SPAIN)

garciacb@unican.es

This research analyzes the directional scattering behaviour of systems formed by two or three nanoparticles with given optical properties (including non-conventional ones) as a function of the geometrical properties (distance and alignment of the particles on the system). This could be a first step to the design of systems with capabilities for guiding the light at the nanoscale.

Introduction

One of the important challenges in photonics is the possibility to govern the directionality of the light at nanoscales. The efficiency of some applications based on nanoparticles or nanostructures [1, 2] can be improved significantly if we are able to control the scattered light by them. We are talking, for example, about solar cells with very high efficiency or biomedical treatments that will be able to reach a certain area, more accurately, without danger in the surroundings.

This kind of features is closer with the recent studies on nanostructured metamaterials [3]. These researches are focused on producing nanomaterials with effective optical properties that can be chosen previously, including negative-negative values (left-handed materials). The election of the optical constants of the materials allows us to manipulate the scattering behaviour of those materials, and in particular the directionality of the scattered light. In this sense, Engheta [4] proposed a first design of light nanocircuits based on these nanostructured metamaterials.

Kerker et al [5] were pioneers in the study of the scattering behaviour of small spherical particles with whatever values of the optical properties. They demonstrated that, under certain conditions for the optical constants, dipole-like particles don't scatter light in the forward or backward direction. Recently, we have shown that those conditions can be generalized to finite-size particles (nanoparticles in the visible range) and to every scattering direction [5]. In this work we study systems of two or three particles with given optical properties in order to analyze the global scattering behaviour, searching this possibility to govern the directionality of the scattered light by the system.

Description of the system

We consider systems that are formed by two or three spherical particles with different orientations and distances between them. The size of the particles is in the range of 0.01 to 0.05 times the incident wavelength, that is, nanoparticles in the visible range. The optical properties (ϵ, μ) are in such a way that each particle either scatters mainly in one direction or doesn't scatter in other one. The efficiency of the system may be increased by introducing resonant conditions in the nanoparticles.

The scattering polar diagrams of these systems can be analyzed as a function of the optical or geometrical properties in search overall directional effects.

Results

As an example, in Fig. 1 we show the scattering diagram of two nanoparticles ($R=0.01\lambda$) at a distance equal to a half of the incident wavelength ($\lambda/2$) and with optical constants such as the left one doesn't scatter in the forward direction ($\epsilon=\mu=-4.55$) and the right one doesn't scatter in the backward direction ($\epsilon=-1.06$, $\mu=-4.55$). So, both particles scatter in the direction of the gap between them. The incident light is polarized perpendicular to the scattering plane and the particles are parallel to the incident direction.

References

- [1] J.N. Anker, W.P. Hall, O. Lyandres, N.C. Shah J. Zhao and R.P. Van Duyne, Nat. Materials **7**, 442-453 (2008).
- [2] K.R. Catchpole and A. Polman, Opt. Express **16**, 21793-21800 (2008)
- [3] V. Shalaev, Nature Phot. **1**, 41-48 (2007)
- [3] M. Kerker, D.-S. Wang and C.L. Giles, J. Opt. Soc. A. **73**, 765-767 (1983)
- [4] B. García-Cámara, F. Moreno, F. González and J.M. Saiz, J. Quant. Spec. Rad. Trans. (submitted)
- [5] N. Engheta, Science **317**, 1698-1702 (2007)

Figures:

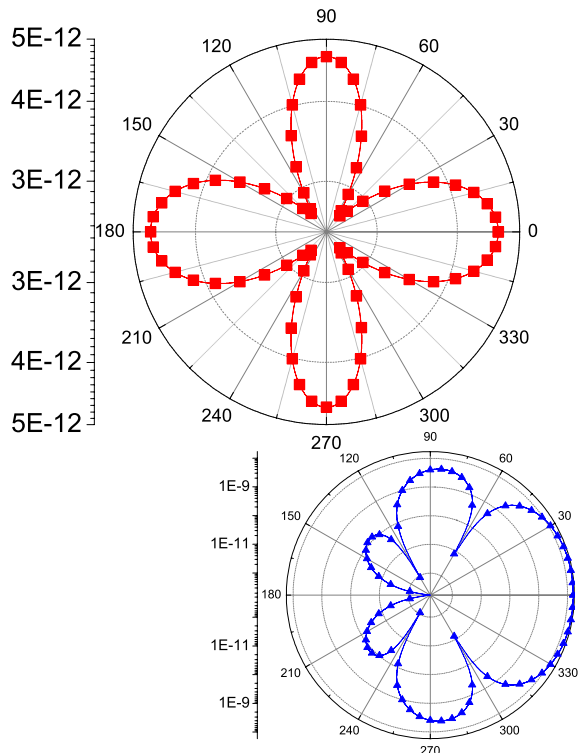


Fig.1. Scattering diagram of a system of two nanoparticles ($R=0.01\lambda$) parallel to the incident direction and separate a distance $\lambda/2$. The with chosen optical properties such as both scatter to the gap between them. A TE incident polarization is considered.

IDENTIFICATION AND CHARACTERIZATION OF ICOSAHEDRAL NANOWIRES ON FCC METALS

S. Peláez¹, C. Guerrero², R. Paredes³, P. A. Serena¹, P. García-Mochales^{4,}*

¹ *Inst. de Ciencia de Materiales de Madrid, Consejo Superior de Investigaciones Científicas (CSIC),
c/ Sor Juana Inés de la Cruz 3, Cantoblanco, E-28049-Madrid, Spain*

² *Departamento de Física, Facultad Experimental de Ciencias, La Universidad del Zulia (LUZ),
Maracaibo, Venezuela*

³ *Centro de Física, Instituto Venezolano de Investigaciones Científicas (IVIC),
Apto. 20632, Caracas 1020A, Venezuela*

⁴ *Dept. Física de la Materia Condensada, F. de Ciencias, Universidad Autónoma de Madrid (UAM),
c/ Tomas y Valiente 7, Cantoblanco, E-28049-Madrid, Spain*

* *pedro.garciamochales@uam.es*

Icosahedral or pentagonal nanowires are formed by subsequent staggered parallel pentagonal rings (with a relative rotation of $\pi/5$) connected with single atoms, showing a characteristic -5-1-5-1- ordering (see an example in Fig. 1b). Metallic nanowires are of great technological importance due to their properties and potential applications. Contrary to monoatomic chains, pentagonal nanowires are rather robust structures at relatively high temperatures and, therefore, they may consider as a promising candidate for being used as nanodevice components. Different computational works during the last decade have showed the formation of staggered pentagonal configurations on breaking nanowires of different species [1,2]. The atomic sequence -1-5-1-5- presents a fivefold symmetry with respect the nanowire axis. This symmetry does not correspond to any crystallographic FCC nor BCC structures. The -1-5-1-5- staggered nanowire configuration may be understood in terms of a sequence of interpenetrated icosahedra.

We present a computational method to identify and characterize icosahedral nanowires. This methodology also allows the determination of the pentagonal chain length as well as the number of pentagonal rings that forms it. The algorithm is based in the determination of the angular distribution of the nearest-neighbors atoms and provides a parameter ($\alpha(z)$) which compares the angular distribution of the projected nanowire atomic coordinates with that corresponding to a perfect pentagonal nanowire. This algorithm is applied along the z-coordinate of the nanowire and the result is a $\alpha(z)$ pentagonal profile of the nanowire.

We have tested (Figure 1a) the proposed algorithm for several ad-hoc ordered and disordered structures, proving that it can satisfactorily distinguish staggered pentagonal nanowires from other tubular structures. The initial ordered structures are depicted as inset in Figure 1a, and only in the case of pentagonal nanowire the parameter α takes value 0, being ~ 1 for the other structures. As the disorder increases, the α average ($\bar{\alpha}$) varies: it increases for pentagonal nanowires and slightly decreases for the other nanowires. If the disorder with respect the initial structure is strong enough, the average of α for all the test nanowires converges to a value ~ 0.9 .

The result of the algorithm applied over a simulated nanowire that presents an icosahedral structure (showed in Figure 1b) are illustrated in Figure 1c: the algorithm returns value near to 1 when is applied to the ordered regions of the nanowire, and values below 1 for the thinnest part of the nanowire. Minima of $\langle \alpha \rangle$ correspond to the position of the pentagonal rings; as they are not perfect ordered structures (but still they can be recognized as pentagons) their $\langle \alpha \rangle$ values are greater than zero. The value $\langle \alpha \rangle = 0.5$ discriminates between pentagonal and non-

pentagonal structures. As it can be seen in Figure 1a, non-pentagonal tubular structures (even with strong disorder) have a $\langle\alpha\rangle$ value higher than 0.5. The pentagonal nanowire, even with a relative strong disorder, presents a $\langle\alpha\rangle$ lower than 0.5; a disordered pentagon with $\langle\alpha\rangle > 0.5$ can not be identified as a regular pentagon. We define the pentagonal nanotube length $L_p(t)$, observed during stretching at a given time t , from the maximum and minimum z coordinates with $\langle\alpha\rangle=0.5$ as it is shown in Fig. 1c. L_p^m is the maximum value of $L_p(t)$, observed when the nanowire is about to break, and n_p is the number of pentagonal rings forming the icosahedral nanowire at its late stage (equivalent to the number of $\langle\alpha\rangle$ minima below 0.5).

The new methodology has been applied for statistically studying hundreds of breaking nanowire simulations of different metallic species (Al, Cu, Ni) at different temperatures (ranging from 4K to half of its bulk melting temperature), obtaining the maximum pentagonal length L_p^m and number of rings n_p distributions. We have compared these results with the Δt_5 distributions, already used in previous works [2] to identify the existence of pentagonal nanowires (Δt_5 is defined as the time spent by the nanowire with a cross section S_m between 6 and 4 in atomic section units). We show that the quantity Δt_5 generally underestimated the length of the icosahedral nanowire and, as consequence it is not adequate for the characterization of icosahedral nanowires.

References:

- [1] R.N. Barnet and U. Landman, Nature 387, 788 (1997); H. Mehrez and S. Ciraci, Phys. Rev. B **56**, 12622 (1997); O. Gülseren *et al.*, Phys. Rev. Lett. **80**, 2775 (1998). J. C. González *et al.*, Phys. Rev. Lett. **92**, 126102 (2004); V.K. Sutkar and D.R. Mahapatra, J. Phys.: Condens. Matter **20**, 335205 (2008); H. S. Park and J. A. Zimmerman, Scripta Materialia **54**, 1127 (2006); P. Sen *et al.*, Phys. Rev. B **65**, 235433 (2002).
- [2] P. García-Mochales, R. Paredes, S. Peláez and P.A. Serena, Nanotechnology **19**, 225704 (2008); Journal of Nanomaterials **2008**, 361464 (2008); Phys. Stat. Sol. (a) **205**, 1317 (2008).

Figures:

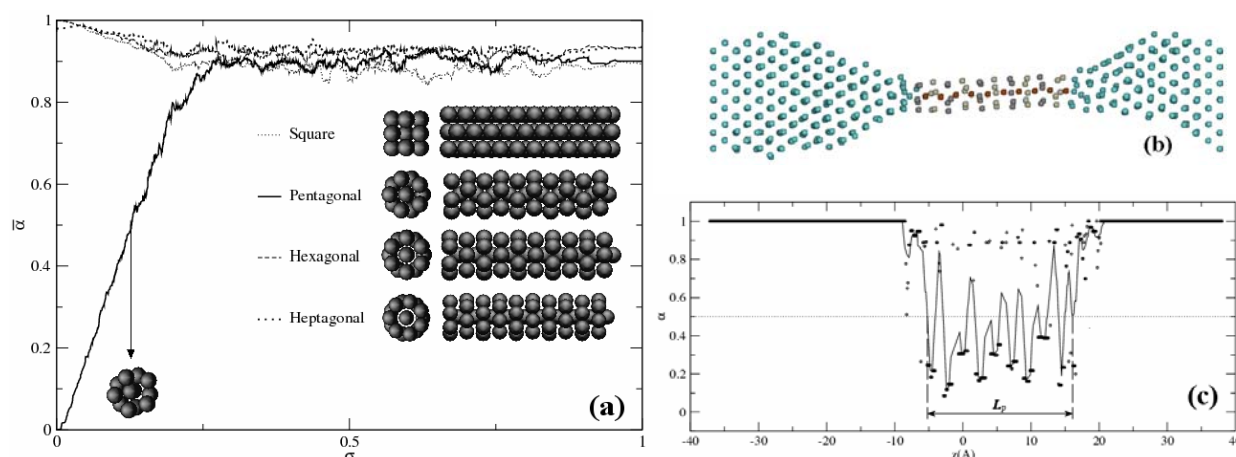


Figure 1 (a) The average of the α -parameter ($\bar{\alpha}$) versus different strengths of the disorder parameter σ for four test configurations: square nanowires with atoms sequence 5-4-5-4 taken from a FCC structure along the [100] direction; staggered pentagonal nanowires with atoms sequence 1-5-1-5; staggered hexagonal 1-6-1-6 nanowires; and staggered heptagonal nanowires with 1-7-1-7 sequence (the inset shows the perfect ordered configurations of the four test nanowires). σ is the mean atomic displacement of atoms with respect to the perfect position of the ordered configuration. The average value of α for disordered nanowires was obtained averaging over 50 configurations. (b),(c) Results from Molecular Dynamics simulations of Ni [100] nanowires containing 1029 atoms and subjected to longitudinal stretching at $T=375\text{K}$: (b) Snapshot of a nanowire formed under stretching presenting an icosahedral structure with $n_p=10$ pentagonal rings. (c) α -parameter (dots) and its average $\langle\alpha\rangle$ (solid line) along the Ni[100] simulated nanowire of Figure 1b and the icosahedral nanowire length L_p (≈ 21.1 Å). The dotted line $\langle\alpha\rangle=0.5$ is the limit value we have chosen for the identification of pentagonal structures. The minimum values of $\langle\alpha\rangle$ correspond to the position of pentagonal rings forming the icosahedral nanowire.

Effect of organo-clay on dielectric properties of silicone rubber

Nafiseh Gharavi, Mehdi Razaghi Kashani

Tarbiat Modares University, Jalale Ale Ahmad Highway, Tehran, Iran

nafiseh_gharavi@yahoo.com

Abstract. Dielectric elastomers are highly deformable smart materials capable of actuation under electric fields [1,2]. To study the effect of organically modified Montmorillonite (OMMT) on dielectric properties of silicone rubber as a commercially available dielectric elastomer, OMMT was added to this rubber at two levels of 2% and 5% using high shear mixing. Composites were characterized by X-Ray Diffraction (XRD), Scanning Electron Microscopy (SEM), and Atomic Force Microscopy (AFM). The XRD patterns showed that ordered crystallite structure of clay loses its ordered structure leading to disappearance of diffraction peaks. SEM and AFM micrographs depicted good dispersion and uniform distribution of the organo-clay. Tensile properties and dielectric properties of the composites were measured under AC electric fields, and results were compared with the reference silicone rubbers with no OMMT. It was shown that storage and loss dielectric constants of base silicone rubber increase when it is compounded with OMMT.

Experimental

Silicone rubbers used in this study were High Temperature Vulcanized (HTV) silicone rubber from Shenzhen APR (APH-20) in high consistency rubber form. The organo-clay Montmorillonite (Cloisite 15A) was obtained from Southern Clay Inc. High-shear mixing of HTV with 2% and 5% by weight OMMT was performed in a Brabender internal mixer. Then, the cross-link agent, Dicumyl Peroxide, was added to the compound on a two-roll mill in 50 °C for 20 minutes. Finally, the compound was hot pressed to complete the vulcanization process.

X-Ray diffractometer of type X' -pert by Philips was employed to study changes in crystalline structure of the organo-clay as a result of dispersion in the rubber matrix. Scanning Electron Microscopy (SEM) micrographs were obtained using XL30 apparatus from Philips with excitation voltage of 20 KV. Atomic Force Microscopy (AFM) on the surface of samples was performed using DME SPM-Prober Station 150. Mechanical properties were measured using an Instron 5565 according to standard ASTM D412. Finally, Frequency dependent dielectric properties were measured by LCR-meter apparatus produced by INSTRON.

Result and Discussion

According to Figure 1, the larger main peak related to Bragg diffraction from 001 planes in the silicate crystal cells of pure OMMT has been disappeared in composites which means either represent high level of silicate dispersion/exfoliation, or the existence of a disordered/intercalated structure of clay platelets.

Micrographs of Figures 2, taken at different magnifications for both clay contents in HTV composites, show a well distribution of small rod-shape cross-section of clay bundles, especially for 2% clay content.

Atomic Force Microscopy (AFM) was employed to confirm the degree of dispersion of OMMT in the composites. Figure 3 complements the XRD graphs in confirming that extent high-shear mixing disperse the organo-clay in the rubber matrix.

Mechanical properties, tensile strength and elongation at break, of Composites of HTV silicone rubber mixed with OMMT enhanced. These results prove fine dispersion of OMMT in HTV silicone under high-shear mixing which leads to disordered clay layers and improved mechanical properties.

The frequency dependent storage (ϵ'_r) and loss (ϵ''_r) dielectric constants for HTV silicone rubber and their composites are presented in figures 4. These figures illustrate enhancement in both ϵ'_r and ϵ''_r as a result of OMMT addition which led to additional polarization mechanisms. This includes interfacial polarization or accumulation of space-charges at the interface between rubber and heterogeneous inclusions with higher permittivity than rubber as well as distortion and amplification of electric fields around filler particles, especially flat platelets [3, 4].

Conclusion

Ionic nature and platelet shape of silicate layers in OMMT as well as large initial basal spacing and modifier concentration of Cloisite 15A used in these study, allowed for of both dielectric permittivity and loss in these composites under AC electric fields. Interlayer spacing and dispersion of clay bundles, were detected by XRD, SEM, and AFM. The results of tensile properties in uniaxial tension also proved effective dispersion of organo-clay under extensive melt mixing.

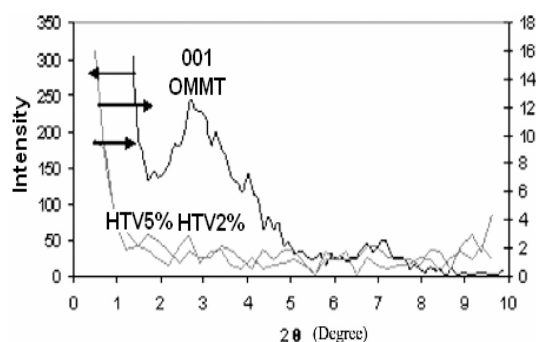


Figure 1. XRD diffractograms

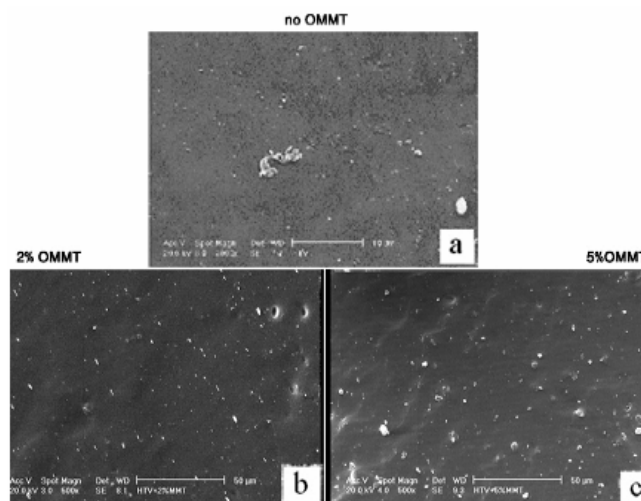


Figure 2. SEM micrographs of silicone and nanocomposites

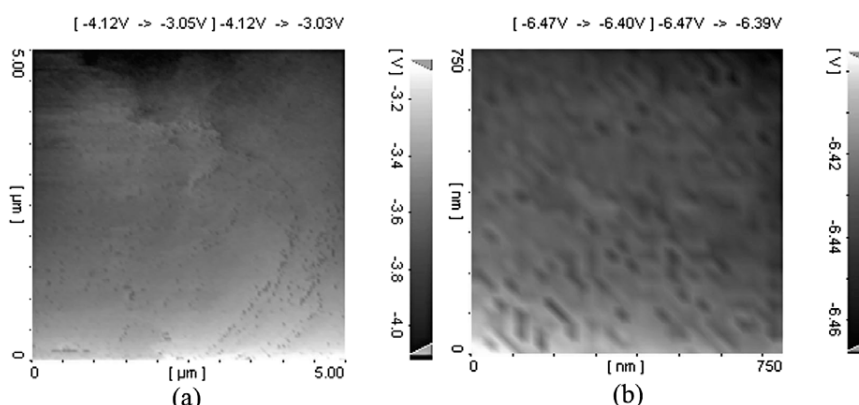


Figure 3. AFM micrographs from the surface of HTV + 5% OMMT composite at two scales: (a) 5 μm and (b) 750 nm.

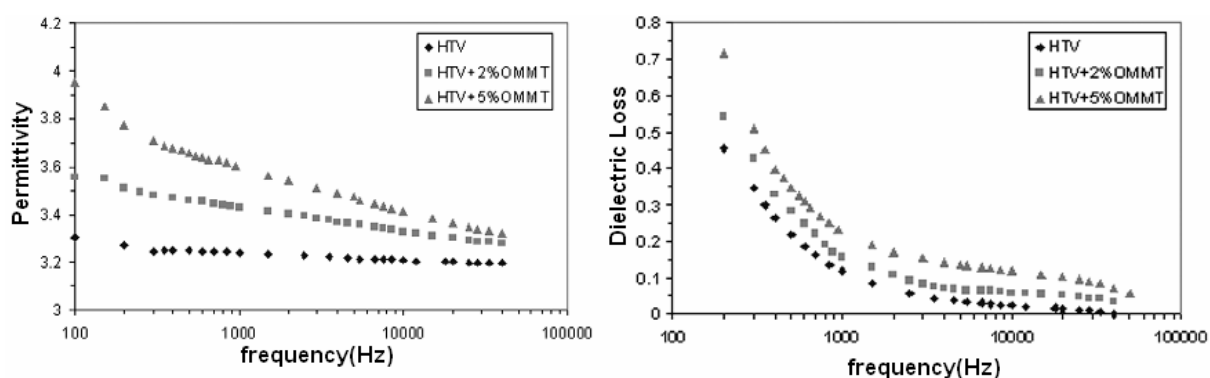


Figure 4. Effect of OMMT on dielectric permittivity and dielectric loss of HTV silicone

References

- [1] R.E. Perline, R.D. Kornbluh, *Sensors and Actuators A* 64 (1998) 77-85
- [2] R.E. Perline, R.D. Kornbluh, *Mater. Sci. Eng. C11* (2000) 89-100
- [3] B. Tareev, *Physics of Dielectrics*, 1979, Mir Publishers. Moscow
- [4] K.A. Page, K. Adachi, *Polymer* 47 (2006) 6406-6413.

CO₂ ADSORPTION BY AMINE MODIFIED MESOPOROUS SILICA MATERIALS: SYNTHESIS OPTIMIZATION

M. Gil, O. de la Iglesia, R. Mallada and J. Santamaría

Nanoporous Films and Particles Group. Institute of Nanoscience of Aragón.

Department of Chemical and Environmental Engineering.

University of Zaragoza. Pedro Cerbuna, 12 50009 Zaragoza, Spain.

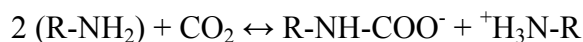
rmallada@unizar.es

CO₂ is one of the greenhouse gases whose increasing concentration in the atmosphere is proposed to have direct linkage to global warming. Large-scale separation of CO₂ by liquid phase alkylamines is the most widely developed commercial technology. However, the use of liquid amines has several disadvantages: high energy consumptions, a difficult solvent regeneration, equipment corrosion or problems with viscosity flow. Separation processes based on solid sorbents are an alternative to overcome some of these limitations [1].

The family of mesoporous materials called M41S (MCM-41, MCM-48 and MCM-50) is a subject of growing interest since they were discovered by Mobil researchers in 1992 [2]. These materials are the result of the ordering of micelles formed when a silica and surfactant solution is under proper conditions. In the case of MCM-48, the micelles are ordered in hexagonal arrays, MCM-48 has a three-dimensional cubic structure and MCM-50 has an unstable lamellar structure.

The characteristic properties of these materials are: i) a very narrow pore size distribution in the mesoporous region, typically between 2 and 4 nm, ii) a high specific surface area (1000-1500 m²/g), iii) a highly ordered structure and iv) an active surface chemistry that allows an easy modification of the properties of these solids. All of them make these materials very attractive for numerous applications such as catalysis, separations, and encapsulation of molecules.

The aim of this work is the surface modification of the MCM-48 [3] by silane coupling agents in order to improve the separations. In this work we report the MCM-48 modification with 3-aminopropyl tri-ethoxysilane (APTS), in which the amino groups will react with CO₂ as follows:



In order to locate the organic groups inside the pores of MCM-48 two different functionalization strategies have been carried out:

Method A, in which the modification is carried out in the calcined material to obtain fully functionalized pores; and Method B, that is made in the as synthesised with surfactant agent occluding mesopores to get partially functionalized pores, after functionalization the surfactant is extracted.

To optimise the reaction different variables are studied: Time of reaction, temperature of reaction and APTS concentration.

Figure 1 shows the X-ray diffractograms for MCM-48 powder as synthesized, calcined and functionalized by means of method A and B. As can be seen, structure of MCM-48 remains after both functionalization methods. Method A give rise to a displacement to higher 2θ angles in comparison to the calcined sample because of the reduction of the pore diameter produced by the APTS molecules.

CO₂ adsorption isotherms at 298 K for MCM-48 powder unmodified and functionalized by method A and B are presented in Figure 2. The sample modified with method A adsorbed a higher amount of CO₂ than the one with method B. This behavior can be explained by the higher amount of amine groups that could react with CO₂ molecules present in sample A. This was confirmed by means of elemental analysis: Sample modified by method A had 2.24 mmol NH₂/g while the one modified with method B had 1.85 mmol NH₂/g since the pores are occluded with surfactant during the reaction with APTS. Furthermore, the amount of NH₂ obtained by elemental analysis is in good agreement with the weight loss observed in TGA experiments.

The Method A sample shows a good adsorption compare to literature [1]

References:

- [1]. Harlick, P and Sayari, A. *Ind. Eng. Chem. Res.*, **46**, (2007) 446-458
- [2]. J.S. Beck, J.C. Vartuli, W.J. Roth, M.E. Leonowicz, K.D. Schmitt, C.T-W Chu, D.H. Olson, E.W. Sheppard, S.B. McCullen, J.B. Higgins and J.L. Schlenker, *J. Am. Chem. Soc.* **114** (1992) 10834-10842.
- [3] Kim, J.M., Kim, S.K. y Ryoo, R., *Chem. Commun.* (1998) 259-260

Figures:

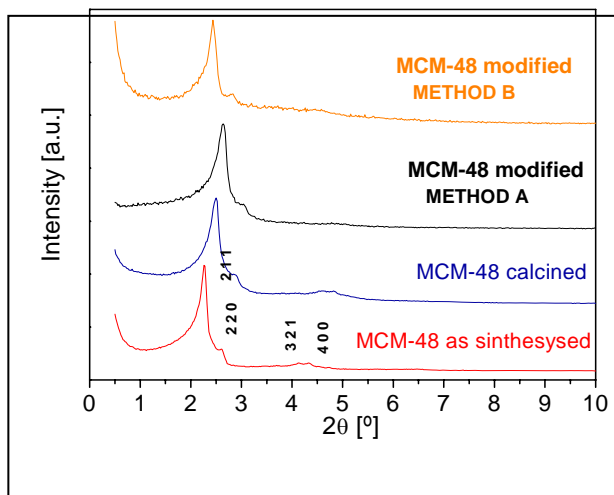


Fig. 1. X-ray diffractograms of MCM-48 powder as synthesized, calcined and modified by methods A and B.

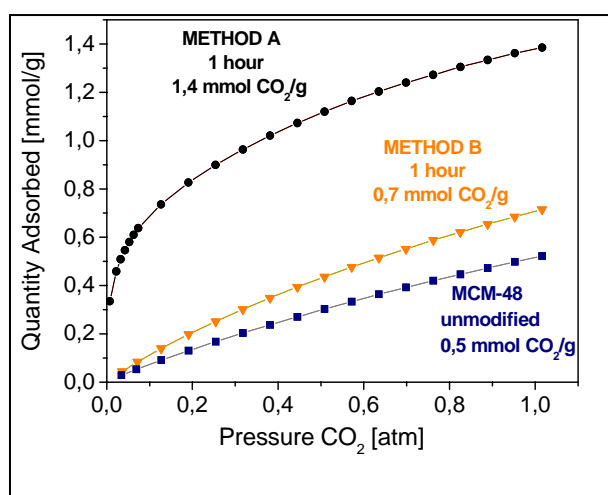


Fig. 2. CO₂ adsorption isotherms at 298 K of MCM-48 powder without modification and modified by methods A and B

THE EFFECT OF NANOCCLAY PRESENCE ON EXTENSIBILITY AND SHAPE RECOVERY OF CROSS LINKED LOW DENSITY POLYETHYLENE SHAPE MEMORY NANOCOMPOSITE

*Atefeh Golbang, Mehrdad Kokabi**

Polymer Engineering Group, Chemical Engineering Department, Faculty of Engineering, Tarbiat Modares University, P.O. Box: 14115-143, Tehran, Islamic Republic of Iran.

**mehrir@modares.ac.ir*

Shape memory polymers (SMPs) belong to a class of smart materials, which have drawn considerable research interest in recent years because of their applications in microelectromechanical systems (MEMS), actuators, self healing and health monitoring purposes, and in biomedical devices [1]. SMPs can return from their temporary shape to the original (permanent) shape after exposure to heat as an external stimulus. One of the key advantages of SMPs compared to shape-memory alloys, such as NiTi, is their ability to store and recover larger strains. The large strain capacity of SMPs is useful because it allows devices to be compacted to a fraction of their permanent size then transition to a significantly different final size and shape once stimulated. The shape change enhances the capacity to perform complex surgical procedures in restricted environments [2]. Therefore gaining larger deformation and complete shape recovery is every one favour. On the other hand, the SMPs in general exhibit lower strength and stiffness, which limits their use for many advanced applications. The low stiffness of SMPs produces only a small recovery force in the temperature change process. Thus incorporation of reinforcing fillers have been investigated in order to improve the mechanical properties and to diversify the applications of SMPs [1, 3]. Cross-linked low-density polyethylene (XLDPE), as a shape memory polymer, deforms easily above its crystalline melting point ($T_m \approx 120^\circ\text{C}$) under external force, maintains this deformation (temporary shape) by cooling and restores its original shape upon subsequent heating above its transition temperature [3].

In this work, the effect of nanoclay presence on extensibility and shape recovery of XLDPE nanocomposite was evaluated. The aim was to achieve the largest possible extension within an acceptable range of shape recovery ratio.

In our experiments deformation limits as a function of temperature was studied in rod shaped samples. The melting point of the crystalline soft segments was used as the transition temperature. The tests were carried out in different temperatures; well above (185°C) and near the transition temperature (135°C).

LDPE and 3 wt. % Cloisite 15A were melt blended in a Brabender batch mixer at 170°C . The compound was then removed from the chamber, cooled to room temperature and cut into small pieces. The x-ray diffractometry (XRD) data attributed to nanocomposite formation are compiled in Table1. The resultant nanocomposite was then mixed with 0.3 wt. % DCP and 0.1 wt. % antioxidant at 130°C . The samples were shaped into rods using a self-made set-up, Fig. 1).

The samples were uniformly heated in an oven to a temperature above its melting transition temperature in which they were extended ($T_h > T_m$), then gradually cooled to room temperature and unloaded. They were finally heated to a certain recovery temperature ($T_r = T_h$) for shape recovery observation.

From the results in Table 2, it is observed that with the addition of nanoclay, extensibility and final shape recovery slightly decreases, resulting in a drop in the shape recovery ratio. Larger deformation up to about 500% is possible in higher temperatures (well above T_m), although it leads to an incomplete shape recovery. The thermomechanical cycles (including programming, cooling, unloading and heating) shown in Table 3, resulted in an increase of irreversible strain associated with a corresponding decrease of shape recovery ratio. Higher shape recovery ratio is achieved at temperatures well above the transition temperature.

References

1. Ratna D., Karger-Kocsis J., "Recent Advances in Shape Memory Polymers and Composites: a Review", Journal of Material Science, **43**, 2008, 254–269.
2. Yakacki C.M., Willis S., Luders C., Gall K., "Deformation Limits in Shape-Memory Polymers", Advanced Engineering Materials, **10**, 2008, 112-119.
3. Rezanejad S., Kokabi M., "Shape Memory and Mechanical Properties of Cross-linked Polyethylene/clay Nanocomposites", European Polymer Journal, **43**, 2007, 2856-2865.

Table 1. The angle and layer spacing regarding the XPLE nanocomposite with 3 wt. % nanoclay

Specification	Angle in correspondence with the first peak (degree)	Basal spacing (Å)
Cloisite 15A	2.75	31.5
XLPE nanocomposite (3 wt. % nanoclay)	2.6	33.88

Table 2. Shape memory properties of samples with $T_h=T_r=185^{\circ}\text{C}$

Clay Content (wt. %)	High Extension (%)	Low Extension (%)	Shape Recovery Ratio (%)
0	407		98.7
		102.6	99.4
3	373		98.2
		94.9	99

Table 3. Thermomechanical cycles of 3 wt. % nanoclay at $T=135^{\circ}\text{C}$

No. of cycles	1	2	3	4
Shape Recovery Ratio (%)	98.1	97.3	95.4	93.2

OPTICAL DETECTION OF DNA HYBRIDIZATION ON CARBON NANOTUBES

*Mónica González^a, Alejandro Ansón^a, Ana María Benito^a, Wolfgang Maser^a, Anna Lagunas^b,
Elena Martínez^b, Maria Teresa Martínez^{a*}*

^aInstituto de Carboquímica-CSIC, Miguel Luesma Castán, 4, 50018, Zaragoza

^bInstitut de Bioenginyeria de Catalunya-IBEC, Josep Samitier, 1-5, 08028, Barcelona

mtmartinez@icb.csic.es

Single-walled carbon nanotubes (SWNTs) have outstanding properties and are being studied for applications in very different fields. One of the most promising applications is in the field of biomedicine where are being utilized as components of DNA, protein biosensors, drug delivery, gene therapy and scaffolds for neuronal growth [1].

SWNTs have protein affinity, and streptavidin non specific adsorption onto nanotubes surface has been demonstrated [2] in previous studies. Using this fact and the highly specific interaction between biotin and streptavidin, in this communication the streptavidin has been used as interlinker between SWNTs and a single stranded DNA modified with biotin. Streptavidin has been adsorbed on purified SWNTs and a single sequence of DNA (CTCGATGACTCAATGACTCG) has been attached to the SWNTs by means of biotin streptavidin bonding. Finally the hybridization with the complementary DNA sequence (CGAGTCATTGAGTCATCGAG) marked with Alexa 555 ® has been carried out (Figure 1). A control experiment has been performed by adding the complementary DNA strand labelled with Alexa 555 to the SWNTs-Streptavidin. It has been determined that the complementary sequence does not join the SWNTs when the biotin is not present.

Aqueous solutions of SWNTs with the complementary DNA sequence has been transferred to glass slide using PDMS stamp and fluorescence has been observed after DNA hybridization (Figure 2).

The possibility of using CNTs- Streptavidin as linker for DNA has been demonstrated and the optical detection of DNA hybridization has been performed. Specific bonding of complementary DNA strands can be used for optical detection of specific sequences. False positive hybridization due to non-specific adsorption of the ssDNA on the nanotubes surface has been discarded.

As SWNTs have been probed to enter the cell [3], this strategy can also be followed to detect the delivery of DNA or RNA sequences into cells.

References:

- [1] Bianco A., Kostarelos K., Partidos C.D., Prato M. *Chem. Commun.* **2005**, 571
- [2] Gonzalez M., Tort N., Benito A.M., Maser W., Marco M.P., Martínez M.T.; *J. Nanosci. Nanotechnol.* accepted January 2009.
- [3] N.W.S. Kam, T.C. Jessop, P.A. Wender, H.J. Dai; *J. Am. Chem. Soc.* **2004**, 126, 6850

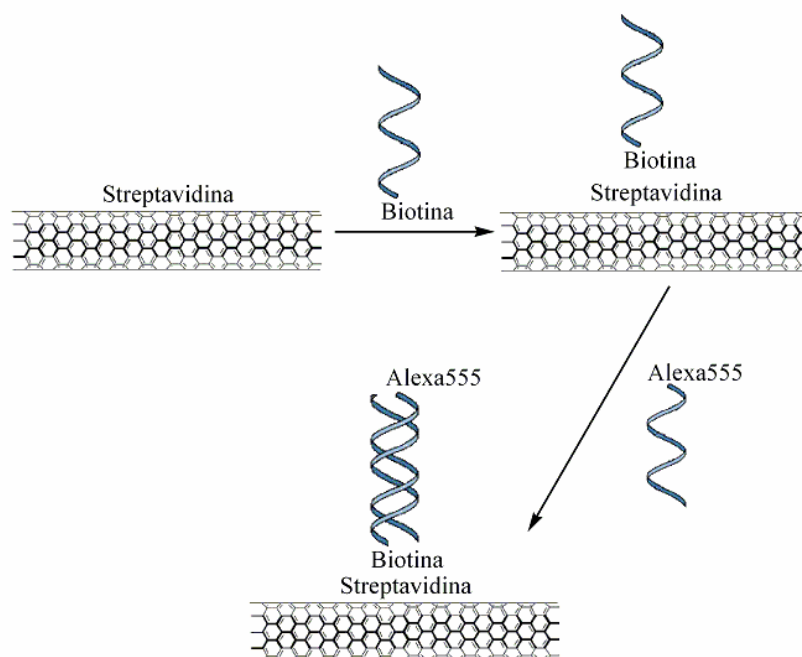
Figures:

Figure 1. Scheme of DNA hybridization on SWNTs

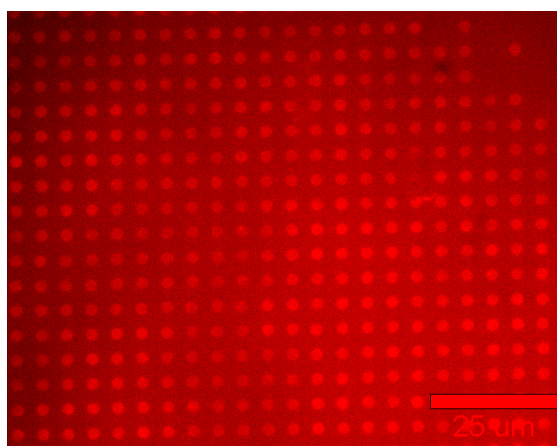


Figure 2. Fluorescent image of imprinted hybridized DNA SWNTs

PROTEIN IMMOBILIZATION METHODS FOR BIOLOGICAL ATOMIC FORCE MICROSCOPY

Rocío de Miguel¹, Marta Martínez-Júlvez^{1,2}, Carlos Gómez-Moreno^{1,2}, Anabel Lostao^{1,3}

1 Instituto de Nanociencia de Aragón, Zaragoza, Spain

2 Dept. de Bioquímica y Biol. Mol. y Cel., Universidad de Zaragoza, Zaragoza, Spain

3 Fundación ARAID, Zaragoza, Spain

aglostao@unizar.es

Atomic Force Microscopy (AFM) has been increasingly used in biological sciences and it is now established as a versatile tool to address the structure, properties and functions of biosystems. AFM is unique in that it provides 3-D images of biological structures of all kinds in their native environment with nanometer resolution. In the last years has been also applied to measure intermolecular forces using Force Spectroscopy, based on the deflection signal of the cantilever probe caused by the force between the cantilever modified with a molecule of interest and a complementary molecule on a substrate.

A crucial prerequisite for successful, reliable biological AFM is that the samples need to be well attached to a solid flat surface using appropriate, non destructive methods. Our group have designed different procedures for immobilizing proteins for different AFM studies: topography imaging, molecular recognition imaging and Force Spectroscopy. The methods have been optimized to minimize nonspecific adhesion with the tip. We have also developed procedures to control the quantity and functionality of the bound molecules.

In the case of protein-ligand recognition studies, the rupture forces are often obscure by the lack of molecular mobility, nonspecific adhesive bindings or an incorrect orientation of a molecule over the other. Our group has been using a linker molecule [1] to increase the mobility of the molecule at the tip with success and has introduced a correction in the measured force due to the angle that is created between the measured force in the normal direction of the probe and the bond direction caused by the flexibility of the spacer [2].

Typically, the immobilization of the molecules is carried out in a non-oriented manner. In some cases, this could be problematic for imaging, but can be very negative in Force Spectroscopy experiments, where an incorrect orientation of the molecule in the sample over the one at the tip makes the binding does not take place or occurs in a very small percentage of approaches, which is quite common in these experiments. In this work we introduce the factor of protein orientation to measure intermolecular forces in flavoprotein complexes. The enzyme FNR catalyses the transfer of two electrons from two independent Ferredoxin (Fd) or Flavodoxin (Fld) molecules, previously reduced by Photosystem I (PSI), to NADP⁺ in the photosynthetic chain. This reaction requires formation of a complex that allows the optimal orientation between the redox centers of both molecules for the subsequent electron transfer [3]. We have developed two strategies of oriented immobilization of FNR on mica. On the one hand, we have attached FNR oriented to its redox partners Fd or Fld that will be also oriented bound to the AFM tip. On the other hand, a double histidine mutant in FNR will favour the proper orientation in the surface to the NADP⁺ substrate that will be attached to the tip.

In summary, we have developed new strategies to control the immobilization of different proteins on substrates and tips in order to optimize imaging and Force Spectroscopy experiments. These procedures could also apply for other uses that require a precise control in immobilization.

This research has been funded under Project INTERBIONANO (BIO2006-09178-C02) from MICINN.

References:

- [1] P. Hinterdorfer, W. Baumgartner, H.J. Gruber, K. Schilcher, H. Schindler PNAS, **93** (1996) 3477-3481.
- [2] J. Sotres, A. Lostao, L. Wildling, A. Ebner, C. Gómez-Moreno, H.J. Gruber, P. Hinterdorfer, A.M. Baró, ChemPhysChem, **9** (2008) 590-599.
- [3] M. Medina, C. Gómez-Moreno, Photosynth. Res., **79** (2004) 113-131.

Figures:

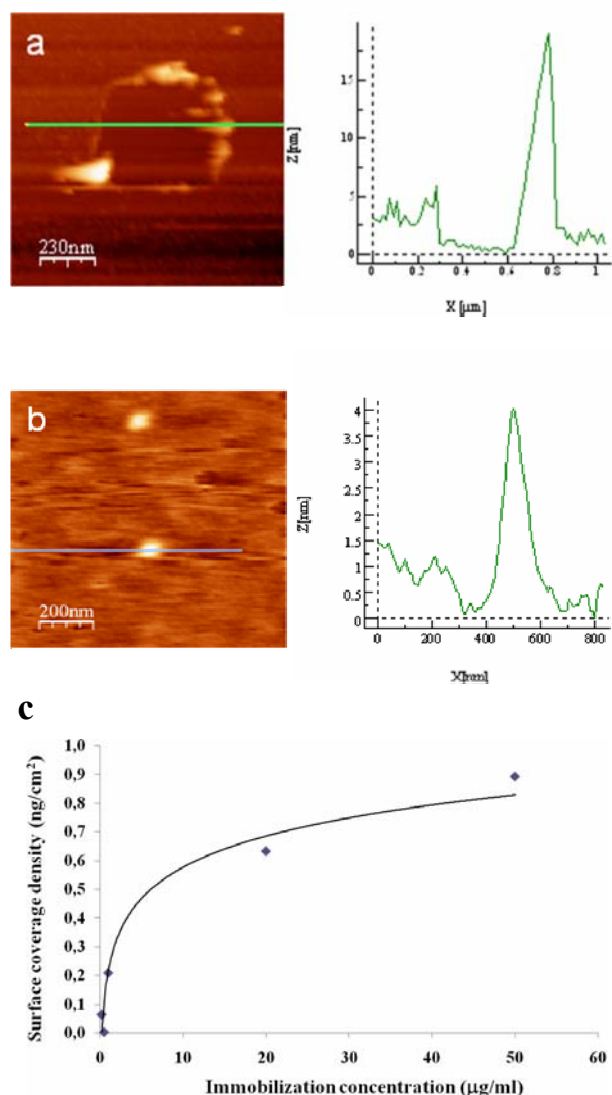


Fig. 1. Streptavidin covalently bound a) to APTES-mica through glutaraldehyde to form a monolayer and b) to thiolated mica to get resolved molecules. Samples were washed with PBST/SDS showing no unspecific tip-sample adhesion. Images taken using Jumping Mode with cantilevers of k 30 pN/nm. c) Protein concentration applied for immobilization versus immobilized protein mass for case b), obtained using a specific enzymatic assay with biotin-HRP and TMB as substrate.

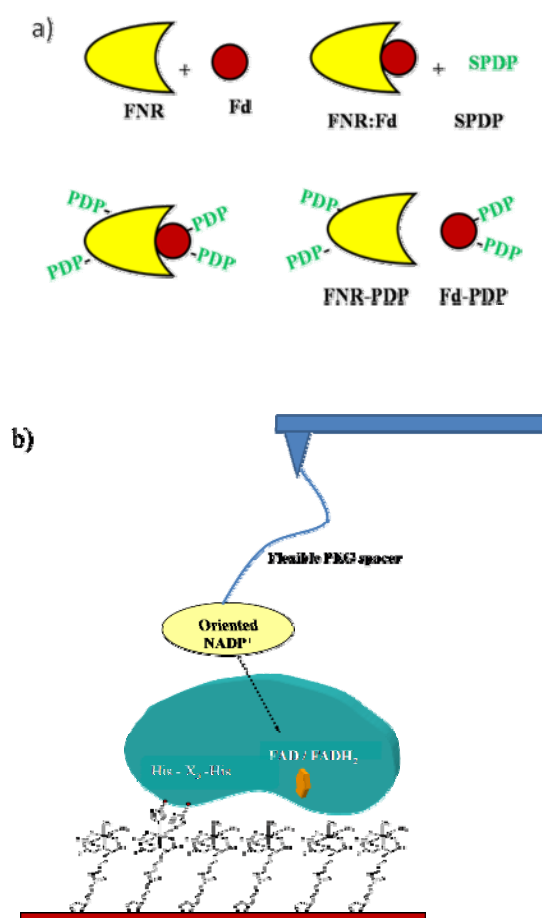


Fig. 2. Orientation strategies in the immobilization of FNR on mica to measure the unbinding force with a) its redox protein partners Fd and Fld and b) its enzymatic substrate NADP⁺.

NANOMEDICINES –A DYNAMIC INNOVATION IN MEDICAL SCIENCE

Ms. Deepa Grover ,Ms. Preeti Aneja

Department of Applied Science and humanities, Haryana Engineering College, Jagadhri

Deepa2805grover@gmail.com , preetianeja11@gmail.com

Abstract

Nanomedicine may be defined as the monitoring, repair, construction, and control of human biological systems at the molecular level, using engineered nanodevices and nanostructures. Nanomedicine is, in a broad sense, the application of nanoscale technologies to the practice of medicine, namely, for diagnosis, prevention, and treatment of disease and to gain an increased understanding of complex underlying disease mechanisms. Scientists and engineers believe nanotechnology can be used to benefit human health now and in the future through applications such as better filters for improving water purification, more effective methods of delivering drugs in medicine and new ways of repairing damaged tissues and organs. Nanomedicine is an exciting research area and raises not only high expectations for future health care, cosmeceuticals and other applications, but also some concerns. As the science and technology of nanomedicine speed ahead, ethics, policy and the law are struggling to keep up .Nanotechnology could also be potentially beneficial for the environment, according to the scientists, through the use of nanomaterials, for example, to create fuel cells and photovoltaic cells, or to remove heavy metals, cyanide and other substances that damage the environment. Overall nanotechnology could be used to develop industrial processes that make more efficient use of resources and generate less waste. However, some nanotechnology experts believe that more assessments need to be made of the potential risks to human health posed by nanotubes and other nanoparticles, which may have the potential to be hazardous in unpredictable ways It is important to proactively address the ethical, social and regulatory aspects of nanomedicine in order to minimize its adverse impacts on the environment and public health and also to avoid a public backlash. In order to achieve

acceptance of the expected technological benefits by the public, their impact on individuals and the society should openly be discussed

Key words: nanomedicines, nanodevices, nanomaterials, nanoparticles

Self-Assembly and Self-Esterification of Plant Lipids on Mica Surface

J.A. Heredia-Guerrero¹, M.A. San-Miguel², M.P. Sansom², A. Heredia³ and J.J. Benítez¹.

¹Instituto de Ciencias de Materiales de Sevilla, Centro Mixto CSIC-Universidad de Sevilla, Avda. Americo Vespuccio 49, 41092 Sevilla, Spain.

²Department of Biochemistry, University of Oxford, South Parks Roads, Oxford OXI 3QU, England.

³Departamento de Biología Molecular y Bioquímica, Facultad de Ciencias, Universidad de Málaga, E-29071 Málaga, Spain.

alejandrohg@cartuja.csic.es

Ultimate knowledge of the reaction mechanism between single molecules requests a precise recognition of their intermolecular interactions at the sub-nanometer scale. Several analysis techniques to carry out this task are currently available to researchers. Among them, scanning probe microscopies have proven to be very useful. Atomic Force Microscopy (AFM) and Scanning Tunneling Microscopy (STM), for instance, can resolve the packing structure of self-assembled layers (SAMs) of functionalized long chain alkyl molecules on a flat substrate [1,2]

9(10), 16- Dihydroxypalmitic acid (diHPA) is a particularly interesting plant poly hydroxylated fatty acid. First, because it is the main monomer of cutin, the most abundant biopolyester in nature. Secondly because the presence of a terminal and a secondary hydroxyl group in mid-chain positions provides an excellent model to study their respective intermolecular interactions in a confined phase such as self-assembled layers [3]. In this study we have combined AFM, XPS, ATR-FT-IR as well as MD simulations to conclude that the self-assembling of diHPA molecules on mica is a layer by layer process following a BET type isotherm and with the first layer growing much faster than the rest. Secondary to secondary hydroxyl interactions reinforces the cohesive energy of the monolayers while the presence of the terminal hydroxyl group is necessary to trigger the multilayered growth. Besides, XPS and ATR-FT-IR spectroscopies clearly indicate that spontaneous self-esterification occurs upon self-assembling. The esterification reaction is a pre-requisite to propose a self-assembly route for the biosynthesis of cutin in nature. Molecular dynamics simulations have shown that internal molecular reorganization within the self-assembled layers provides the right molecule to molecule orientation to facilitate the nucleophilic attack and the release of a water molecule requested by the esterification reaction.

References:

- [1] Alves, C. A.; Smith, E. L.; Porter, M. D., J. Am. Chem. Soc., **114** (1992) 1222.
- [2] Liu, G.; Salmeron, M. B., Langmuir, **10** (1994) 367.
- [3] Benítez, J. J.; Heredia-Guerrero, J. A.; Serrano, F. M.; Heredia, A., J. Phys. Chem. C **112** (2008) 16968.

Figures:

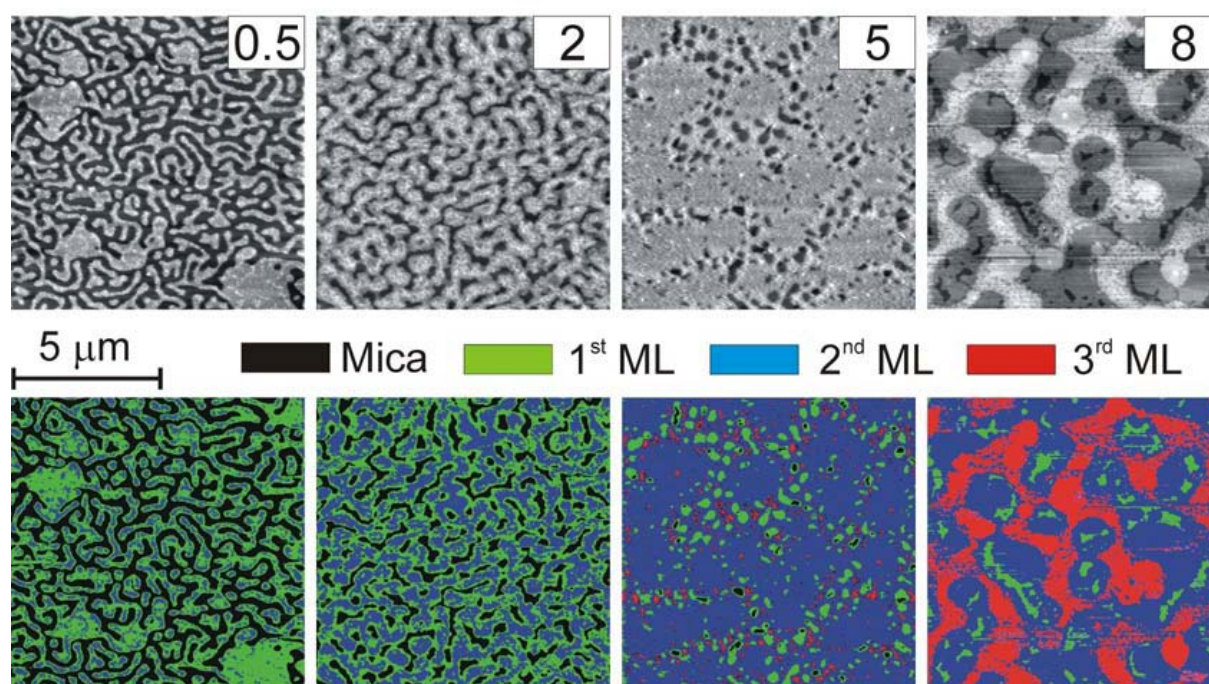


Figure 1. $10 \times 10 \mu\text{m}^2$ topographic AFM images showing the evolution of diHPA self-assembled layers on mica after preparation from 0.5, 2, 5 and 8 mM solutions. The colour coded image below is added to better distinguish mica support and 1st to 3rd diHPA monolayer regions.

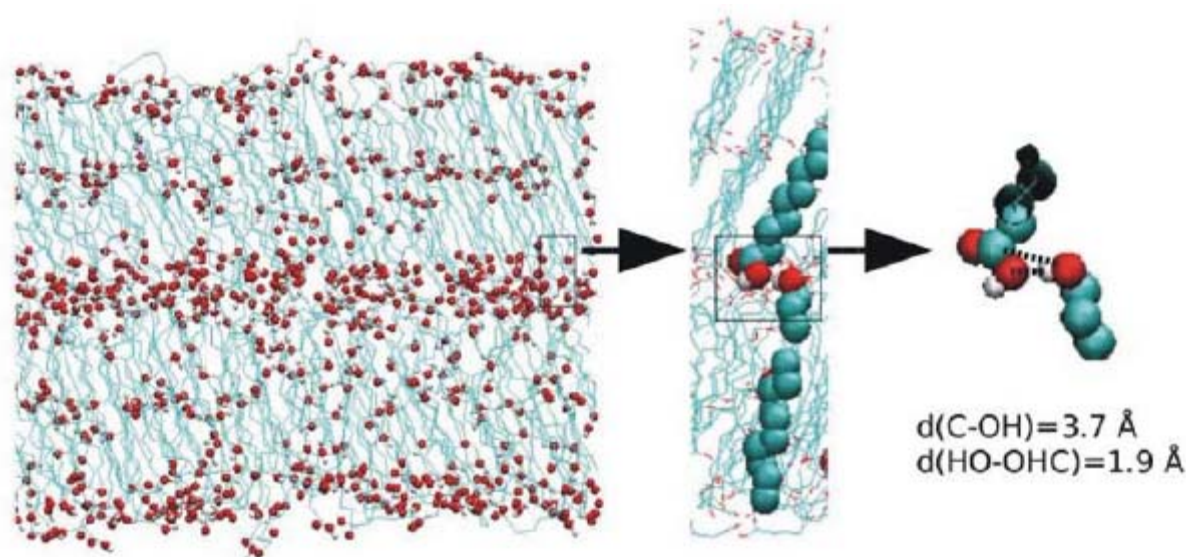


Figure 2. Molecular dynamics simulation results showing the packing structure of a bilayer of diHPA supported on mica. As seen on the magnified drawing of the first-second monolayer boundary, diHPA molecules adopt the right relative orientation to generate an esterification reaction.

Characterization of Particulate Sol-gel Synthesis of Orthorhombic LiMnO_2 and Cubic Spinel LiMn_2O_4 Via Citric Acid Assistance with Different Solvent as a Cathode Material for Lithium-ion Batteries

*Sh.Houshyarazar, M.S.Ahmadian **

Department of chemistry, University of Tarbiat moallem azarbaijan, 35Km Tabriz-Maragheh Tabriz, Iran

Shady1361_chem@yahoo.com, seyedahmadian@azaruniv.edu

Lithium batteries have the highest energy density of all rechargeable batteries and are favoured in application, where low weight or small volume are desired for example: laptop computers, cellular telephones and electric vehicles.

Recently lithium manganese oxides (LiMnO_2 and LiMn_2O_4) has attracted a great deal of attention as a promising cathode material for rechargeable lithium-ion batteries because this material is environment benign and relatively inexpensive compare with lithiated cobalt which is promising candidate material for cathodes in lithium-ion batteries. Conventionally LiMn_2O_4 and LiMnO_2 are prepared by the solid state and precipitation reaction which causes LiMn_2O_4 and LiMnO_2 powders to exhibit strongly agglomerated state and large grain size due to high temperature reaction. Therefore, post-calcination treatments such as grinding and sieving are necessary for obtaining LiMn_2O_4 and LiMnO_2 with small particle size.[1].

In this study, we report the synthesis of LiMn_2O_4 and LiMnO_2 powders with uniform nanosized particle using an aqueous solution of metal nitrates containing ethanol and distilled water as a solvent and citric acid as a chelating agent at considerably lower temperature and shorter heating time as compared with solid state reaction and other reported solution techniques. Different ratios of $\frac{\text{ethanol}}{\text{water}}$ and citric acid to metal ions (R) have been used for investigating the role of ethanol and citric acid in the formation of LiMn_2O_4 and LiMnO_2 powders. The precursor powders were heated at various temperatures for 4h under a flow of argon and air, to examine the reaction processes for the formation of the single-phase LiMn_2O_4 and LiMnO_2 powders.

For the synthesis of single – phase LiMn_2O_4 powder, homogeneity and reactivity of the precursor powder are enhanced with an increase in the amount of citric acid in the starting solution. When the amount of citric acid is low, an impurity phase, Li_2MnO_3 , is formed but this phase is observed in XRD patterns of LiMnO_2 when $R < 1$. On the other hand when the ethanol to water ratio (R') is higher than 2 only single phase of both LiMn_2O_4 and LiMnO_2 is observed.

Physical properties of these compound are discussed in the light of structural [x-ray diffraction (XRD) in Fig1. and scanning electron microscope (SEM) in Fig2.] and spectroscopic (FTIR) in Fig3. thermal behaviour of salt precursor was studied by thermogravimetric analysis (TGA) in Fig4.

References:

[1] Chung-Hsin Lu; S.K.Saha, Journal of Sol-Gel Science and Technology, **20**, (2001), 27-34

Figures:

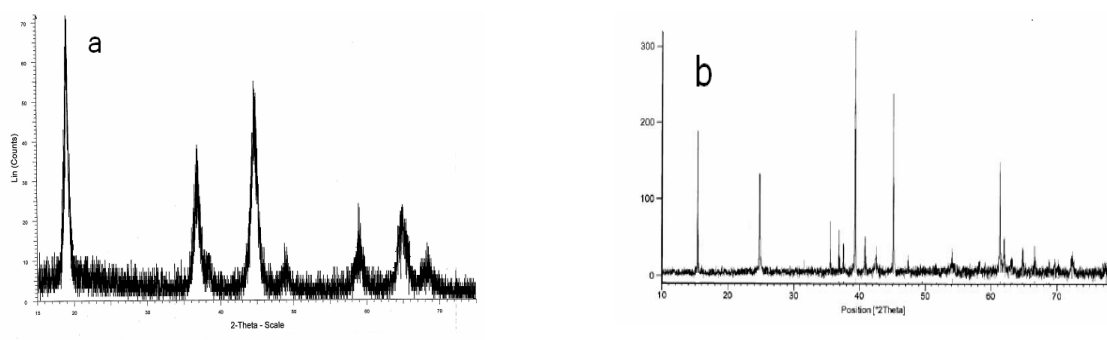


Fig 1. XRD patterns of a) LiMn_2O_4 at 400°C b) LiMnO_2 at 800°C via sol-gel method

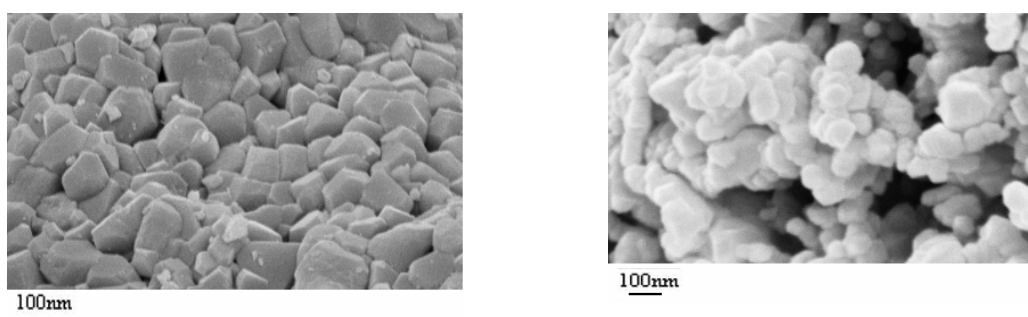


Fig 2. SEM image of a) LiMn_2O_4 b) LiMnO_2

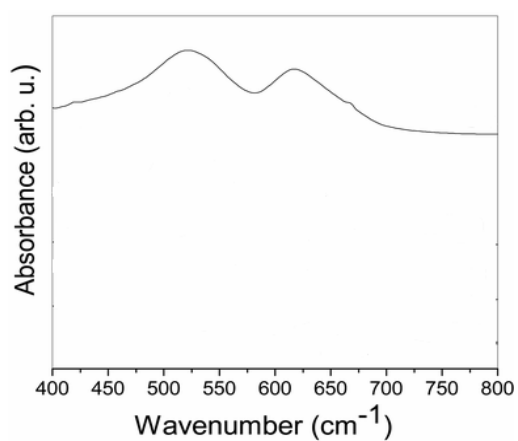


Fig 3. FTIR of the Lithium manganese oxide

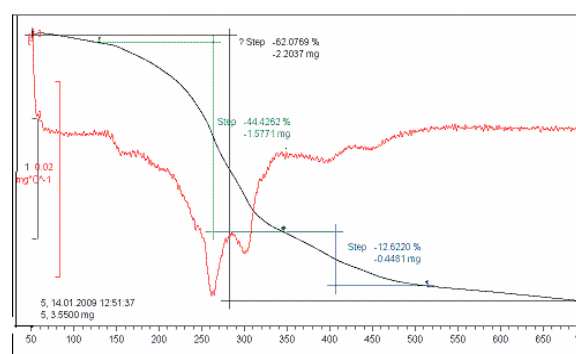


Fig 4. TGA curve for Lithium Manganese oxide

Ag Nanoparticles Functionalized with Amines and Thiols: Structural and Magnetic Characterization

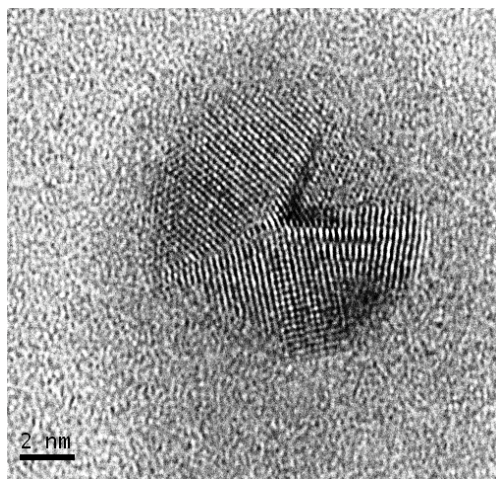
E. Goikolea^a, M. Insausti^a, J.S. Garitaonandia^a, I. Gil de Muro^a, T. Uruga^b, H. Tanida^b, F. Plazaola^a, T. Rojo^a

^a *Zientzia eta Teknologia Fakultatea, Euskal Herriko Unibertsitatea, P.O. Box 644, E-48080 Bilbao, Spain.*

^b *Japan Synchrotron Radiation Research Institute (JASRI/SPRING-8) 1-1-1 Kouto, Mikazuki, Sayo 679-5198, Japan
maite.insausti@ehu.es*

Size confinement to a nanometer scale has induced permanent magnetism in gold nanoparticles when capped with thiols [1]. The combination of particle size and the surface environment induces a strong charge transfer from the Au surface atoms to the S atoms, generating unoccupied densities of *d* states located at the Au surface atoms. These gold atoms present an intrinsic magnetic behaviour, which has been corroborated by element selective techniques such as x-ray magnetic circular dichroism (XMCD) and ¹⁹⁷Au Mössbauer spectroscopy [2]. In spite of the investigation performed with gold nanoparticles, silver ones remain to be studied. In this way we are dealing with the preparation and characterization of silver nanoparticles surrounded by different type of ligands in order to know the influence of the metal concentration and functional groups on the magnetic behaviour of the nanoparticles.

Silver nanoparticles were synthesized following the Brust method [3], which is based on the transfer of AgNO₃ from an aqueous solution to toluene using tetraoctylammonium bromide (TOAB) as the phase-transfer reagent. The reduction of the solution with aqueous sodium borohydride in the presence of dodecanethiol, octadecanethiol, dodecylamine and 1-dodecanol yields Ag-SR, Ag-oSR, Ag-NR and Ag-OR colloidal solutions, respectively. By the addition of ethanol to the suspension, only Ag-SR and Ag-oSR samples precipitate.



Colloidal solutions were studied by means of TEM and HRTEM microscopy and UV-visible microscopy. Nanoparticles present high crystalline nature and a mean size of 2.3 nm. In some cases icosahedral and Marks shapes have been observed in the samples (Fig. 1).

Figure 1. HRTEM image of Ag-NR nanoparticles.

In UV-vis spectra, a band centered at 415-445 nm appears for Ag-oSR, Ag-NR and Ag-OR samples and is associated to a plasmonic resonance characteristic of non-localized electrons. The lack or attenuation of this band in the case of Ag-SR NPs, evidences the Ag-thiol interaction.

In the cases of the solid samples, thermogravimetric measurements were performed and a content of organic matter of 22% was observed for Ag-SR NPs. Magnetic measurements of the NPs with dodecanethiol (-SR) and octadecanethiol (-oSR) were performed at 5 and 300 K, and only dodecanethiol capped NPs showed magnetic behaviour with a maximum value of 6.8 emu/g_{Ag} at 5 K.

In this way, and in order to note the influence of the length of the ligand on the interaction Ag-S in the nanoparticles XAS measurements (X-ray absorption spectroscopy) have been performed in transmission mode in Ag K-edge 25514 keV edge at BL01B1 beamline at SPring8. Figure 2 shows the XAS spectra of the measured samples. The absorption spectra of three thiol-capped samples, Ag-oSR, Ag-SR(1) and Ag-SR(2) (these last two last samples differ in the initial concentration of the metallic salt) revealed all the main features of bulk Ag. Nevertheless, owing to the reduce particle size, an overall attenuation and broadening is observed over the whole XAS spectra.

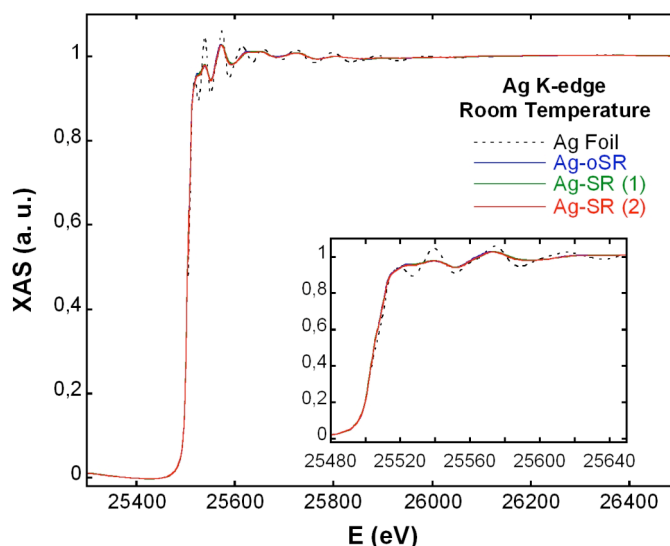


Figure 2. Ag K-edge XAS spectra for three thiol-capped Ag nanoparticle samples: Ag-oSR, Ag-SR (1) and Ag-SR (2). In the inset the attenuation of the oscillations can be better distinguished.

References:

- [1] Crespo, P.; Litrán, Rojas, T.C.; Multigner, M.; de la Fuente, J.M.; Sánchez-López, J.C.; García, M.A. *Phys. Rev. Lett.* 93 (2004) 087204.
- [2] Garitaonandia, J.S.; Insausti, M.; Goikolea, E.; Suzuki, M.; Cashion, J.D.; Kawamura, N.; Ohsawa, H.; Gil de Muro, I.; Suzuki, K.; Plazaola, F.; Rojo, T. *NanoLett.* 8(2) (2008) 661.
- [3] Brust, M.; Walker, M.; Bethell, D.; Schiffrin, D.J.; Whyman, R. *J. Chem. Soc., Chem. Commun.* 1994 (1994) 801.

IMPROVED PROCESSING OF POLYANILINE-CARBON NANOTUBE NANOCOMPOSITES VIA WATER DISPERSIONS

Pablo Jiménez, Wolfgang K. Maser, Ana M. Benito

Instituto de Carboquímica (CSIC), Miguel Luesma Castán 5, 50018 Zaragoza, Spain

pablojm@icb.csic.es

Carbon nanotubes (CNTs) had generally presented difficulties regarding its processing, mainly due to the strong interactions between individual tubes. In order to avoid this problem one of the most popular strategies is that of the chemical functionalization, covalent or non-covalent, to improve the interaction of CNTs with the environment and facilitate the separation (i.e.: dispersion) of the CNTs. Non-covalent functionalization, although it is weaker than the covalent one, has the advantage of not modifying drastically the special properties of CNTs. Conducting polymers are excellent candidates for this kind of non-covalent functionalization, that usually happens through π - π interactions. Nevertheless, up till now composites of conducting polymers and CNTs, despite its very interesting properties, have not improved significantly the processing of carbon nanotubes.

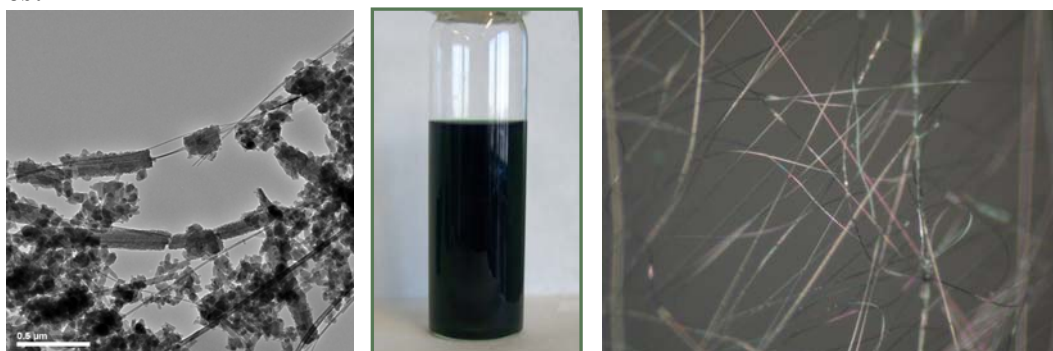
In this work we show a nanostructured composite between polyaniline (PANI) and multi-wall carbon nanotubes^[1] (MWNTs) that can be dispersed in aqueous solutions in high concentrations, which allows different kinds of processing^[2]. The content of MWNTs in these composites can be as high as 50% wt. without losing its water dispersibility. The low size of the nanostructures, the hydrophilicity of PANI in the emeraldine salt state, and the good PANI-MWNT interaction are responsible for the high stability and homogeneity of the water dispersions of the material.

Some topics related to the properties, processing and application of the material will be presented. Among the most relevant properties of the material some of them come not only from the MWNTs (electrical conductivity, thermal stability), but also from PANI (hydrophilicity, electrochemically or chemically tuneable properties, like color) and the morphology of the material (high surface area). The processing of the material could be directly done from water dispersions or via hydrophilic polymer mixtures. With these approaches this material can be processed into films or fibers, employing techniques like spin coating, inkjet printing, electrospinning, wet spinning, etc. The wide range of properties and ways of processing make this material a promising candidate in many applications in fields such as organic photoelectronics, mechanical reinforcement of plastics, chemical detection, printable circuits, smart fabrics, and so on.

References:

- [1] P. Jiménez, W.K. Maser, P. Castell, M.T. Martínez, A.M. Benito, *Macromolecular Rapid Communications*. *In Press*, DOI: 10.1002/marc.200800707 (Published Online: Jan 21 2009)
- [2] A.M. Benito, P. Jiménez, M.T. Martínez, W.K. Maser, Patent Application: P200800283

Figures:



High Performance in Self-heated Single Nanowire Based Sensors

Roman Jiménez-Díaz⁽¹⁾, J. D. Prades⁽¹⁾, F. Hernandez-Ramirez⁽²⁾, A. Cirera⁽¹⁾, A. Romano-Rodríguez⁽¹⁾, A. Cornet⁽¹⁾, J. R. Morante⁽³⁾, S. Barth⁽⁴⁾, S. Mathur^(5,6)

⁽¹⁾ MIND-IN2UB, Departament d'Electrònica, Universitat de Barcelona, C/ Martí i Franquès, 1, E-08028 Barcelona, Spain

⁽²⁾ Electronic Nanosystems, S.L., E-08028, Barcelona, Spain / M-2E

⁽³⁾ IREC, Catalonia Institute for Energy Research, E-08019, Barcelona, Spain / M-2E

⁽⁴⁾ Department of Chemistry, University College Cork, Cork, Ireland

⁽⁵⁾ Institute of Inorganic Chemistry, University of Cologne, Cologne, Germany;

⁽⁶⁾ Nanocrystalline Materials and Thin Film Systems, Leibniz Institut of New Materials, Saarbruecken, D-66123, Germany

rjimenez@el.ub.es

Research on 1-D nanomaterials is a subject of great interest due to the possibility of using them as building blocks of new devices. Basic characterization has been performed on these materials and primary integration in sensors is currently researched. In this work, we focused our attention in the modulation of the temperature of these brand new devices due to the application of controlled probing currents.

Individual nanowires are accessed by means of the fabrication of platinum nanocontacts with a Focused Ion Beam (FIB) system, following a process which combines both electron and ion assisted depositions [1]. These contacts fabricated over the nanowire and extended to pre-patterned microelectrodes allow the characterization of the sensing capabilities of the nanowire to different gas species [2] at different temperatures with the help of a furnace.

Additionally an innovative method of setting the working temperature of the device has been used recently. In these new systems, the nanowires are contacted over suspended MEMS hotplates that contain integrated heaters [3][4]. The thermal isolation and reduced dimensions of these microhotplates allow faster modulation of the working temperature with reduced power consumptions.

As chemiresistors, nanowires are elements prone to experience the Joule effect due to their small dimensions, heating themselves above working temperature. Contact degradation and device failure have been reported as a result of the high temperatures produced when uncontrolled probing currents are applied [5].

Nevertheless, the use of controlled probing currents to achieve optimal working temperatures with extremely low power consumption is an issue of great interest for the potential applications in portable and autonomous single nanowire based gas sensors.

We prove that it is possible to use this method to equal the performance of nanowires heated over microhotplates when characterizing their sensing capabilities towards NO₂, and that device preservation it is possible by controlling the probing current [6].

In summary, we demonstrate that self-heating effect can be applied to the characterization of single nanowire based gas sensors with low power consumption, presenting an importance advance in power efficiency and miniaturization.

References:

- [1] A. Vilà, F. Hernández-Ramírez, J. Rodríguez, O. Casals, A. Romano-Rodríguez, J.R. Morante and M. Abid, *Materials Science and Engineering C*, **26** (2006) 1063 – 1066.
- [2] F. Hernández-Ramírez, J. Rodríguez, O. Casals, E. Russinyol, A. Vilà, A. Romano-Rodríguez, J.R. Morante and M. Abid, *Sensors and Actuators B*, **118** (2006) 198–203.
- [3] F. Hernandez-Ramirez, J. D. Prades, A. Tarancon, S. Barth, O. Casals, R. Jimenez-Diaz, E. Pellicer, J. Rodriguez, M. A. Juli, A. Romano-Rodriguez, J. R. Morante, S. Mathur, A. Helwig, J. Spannhake, and G. Mueller, *Nanotechnology*, **18** (2007) 495501-495505.
- [4] D. C. Meier, S. Semancik, B. Button, E. Strelcov, A. Kolmakov, *Appl. Phys. Lett.*, **91** (2007) 063118-063120.
- [5] F. Hernandez-Ramirez, A. Tarancon, O. Casals, E. Pellicer, J. Rodriguez, A. Romano-Rodriguez, J. R. Morante, S. Barth, S. Mathur, *Phys. Rev. B*, **76** (2007) 085429-085433.
- [6] J. D. Prades, R. Jimenez-Diaz, F. Hernandez-Ramirez, S. Barth, A. Cirera, A. Romano-Rodriguez, S. Mathur, J. R. Morante, *Applied Physics Letters* **93** (2008) 123110.

OXIDATIVE STRESS INDUCTION IN CACO-2 CELLS BY SINGLE WALL CARBON NANOTUBES

Jos A¹, Pichardo S¹, Gutiérrez-Praena D¹, Puerto M¹, Sánchez-Granados E², Grilo A², Cameán AM¹

¹ Area of Toxicology. Faculty of Pharmacy. Profesor García González 2, 41012 Seville, Spain
angelesjos@us.es

² University Hospital Virgen de Valme. Avda. Bellavista s/n, 41014 Seville, Spain.

Carbon nanotubes (CNTs) are among the nanoparticles with higher potential for biomedical uses. They consist exclusively of carbon atoms arranged in a series of condensed benzene rings rolled-up into a tubular structure, and belongs to the third allotropic form of carbon along with graphite and diamond. CNTs can be classified in two general categories: single-walled nanotubes (SWNT) which have diameters from 0.4 to 2.0 nm and lengths in the range of 20–1000 nm, and multi-walled nanotubes (MWNT) that are bigger objects with diameters in the range of 1.4–100 nm and lengths from 1 to several μm .

CNTs have some interesting physicochemical properties such as: ordered structure with high aspect ratio, ultralight weight, high mechanical strength, high electrical conductivity, high thermal conductivity, metallic or semi-metallic behaviour and high surface area, which make CNTs a unique material with the potential for diverse applications, including biomedical [1].

Another point is the status of CNTs dispersion in solution because CNTs are highly hydrophobic [2]. Some studies show that well-dispersed SWNT is associated with lesser cytotoxicity compared with the same SWNT present in an agglomerated form [3]. This high hydrophobicity of pristine CNTs has induced the need to modify the surface chemistry of CNTs to improve their aqueous solubility, which is a very important point in terms of their subsequent potential toxicity. Thus, CNTs are functionalized to obtain more biocompatible products.

CNTs toxicity has been previously studied mainly in pulmonary and dermal cells. Some *in vitro* studies highlight that CNTs can be toxic for macrophages [4], lymphocytes [5], keratinocytes [6], type II alveolar epithelial cells [4], mesothelial cells [7], aortic smooth muscle cells [8], skin fibroblasts [9] and embryo kidney cells [10], but the gastrointestinal tract is also one of the prime targets for direct interactions with nanomaterials and studies on it are still scarce. In terms of the intracellular mechanism, oxidative stress is frequently proposed as a key mechanism of CNT-induced toxicity, usually linked to the metallic impurities of CNTs [11].

Single wall CNTs functionalized with carboxylic acid (COOH-SWCNT) have shown to induce cytotoxicity on the human intestinal cell line Caco-2 [12] with a reduction of the cell viability and cell membrane injury. The present study explores the oxidative stress as toxic mechanism involved in COOH-SWCNT observed damage in Caco cells. Cells were exposed to concentrations between 0 and 1000 $\mu\text{g/mL}$ COOH-SWCNT for 24h of exposure and the following oxidative stress biomarkers were studied: lipid peroxidation (LPO); antioxidant enzymatic activities such as catalase (CAT), superoxide dismutase (SOD), glutathione peroxidase (GPx), glutathione reductase (GR) and glutathione-S-transferase (GST); and cellular glutathione content (GSH).

Results showed that LPO significantly increased with COOH-SWCNT concentrations from 50 $\mu\text{g/mL}$ (Fig.1). Exposure to COOH-SWCNT induced CAT activity in a concentration-dependent manner up to 500 $\mu\text{g/mL}$, but with 1000 $\mu\text{g/mL}$ depletion was observed (Fig.2). SOD, GPx and GR showed a similar trend; reaching their maximum level at 100 $\mu\text{g/mL}$ (Fig.3); although the increase was not significant for GR. At higher concentrations, however, they experienced a reduction. No significant changes were observed in the activity of GST with the different concentrations of COOH-SWCNT assayed. Finally, GSH content of the cells decreased at all exposure levels but only with 1000 $\mu\text{g/mL}$ this reduction was significantly different from control values (Fig.4).

COOH-SWCNT induced oxidative stress in Caco-2 cells from 50 $\mu\text{g/mL}$. The increase in the antioxidant enzymatic activities could be due to an adaptative response of the cells to the toxic injury, whereas the depletion at the highest concentration mainly observed in CAT activity could reflect not a functional damage but a structural one, indicating a higher sensitivity of this enzyme to this compound. Further investigations are necessary to elucidate whether the oxidative stress observed is induced by the COOH-SWCNT per se or by potential metallic traces contained in the product and derived from the synthesis process.

References:

- [1] A. Bianco, K. Kostarelos, C.D. Partidos, M. Prato, *Chem. Commun.* **7** (2005) 571–577.
- [2] Dumonteil S, Demortier A, Detriche S, Raes C, Fonseca A, Rühle M, Nagy JB, J. *Nanosci. Nanotechnol.* **6** (2006) 1315–1318.
- [3] Wick P, Manser P, Limbach LK, Dettlaff-Weglikowska U, Krumeich F, Roth S, Stark WJ, Bruinink A, *Toxicol. Lett.* **168** (2007) 121–131.
- [4] Pulskamp K, Diabate S, Krug KF, *Toxicol. Lett.* **168** (2007) 58–74.
- [5] Bottini M, Bruckner S, Nika K, Bottini N, Bellucci S, Magrini A, Bergamaschi A, Mustelin T, *Toxicol. Lett.* **160** (2006) 121–126.
- [6] Zhang LW, Zeng L, Barron AR, Monteiro-Riviere NA, *Int. J. Toxicol.* **26** (2007) 103–113.
- [7] Wick P, Manser P, Limbach LK, Dettlaff-Weglikowska U, Krumeich F, Roth S, Stark WJ, Bruinink A, *Toxicol. Lett.* **168** (2007) 121–131.
- [8] Raja PM, Connolley J, Ganesan GP, Ci L, Ajayan PM, Nalamasu O, Thompson DM, *Toxicol. Lett.* **169** (2007) 51–63.
- [9] Tian F, Cui D, Schwarz H, Estrada GG, Kobayashi H, *Toxicol. In Vitro*, **20** (2006) 1202–1212.
- [10] Cui D, Tian F, Ozkan C, Wang M, Gao H, *Toxicol. Lett.* **155** (2005) 73–85.
- [11] Fenoglio I, Tomatis M, Lison D, Muller J, Fonseca A, Nagy JB, Fubini B, *Free Radic. Biol. Med.* **40** (2006) 1227–1233.
- [12] Jos A, Pichardo S, Puerto M, Sánchez-Granados E, Grilo A, Cameán AM, *Toxicol. In vitro*, **Accepted** (2009)

Figures:

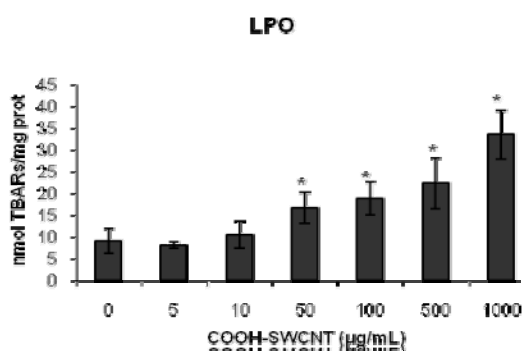


Figure 1. Lipid peroxidation (LPO) on Caco-2 cells exposed to COOH-SWCNT for 24h. The values are expressed as mean \pm S.E. LPO value is expressed as nmol TBARS/mg protein.

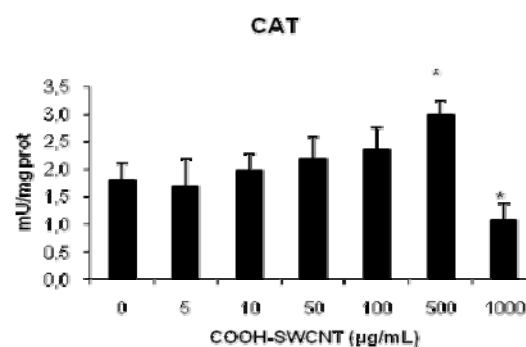


Figure 2. Catalase activity (CAT) on Caco-2 cells exposed to COOH-SWCNT for 24h. The values are expressed as mean \pm S.E. CAT activity is expressed as mU/mg protein.

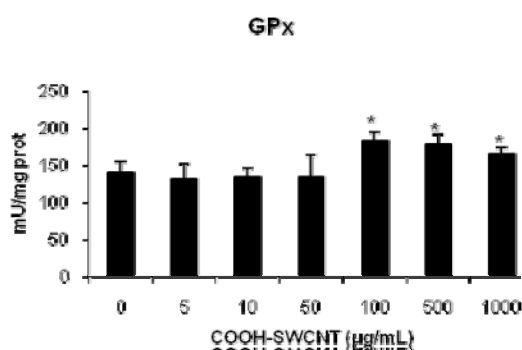


Figure 3. Glutathione peroxidase activity (GPx) on Caco-2 cells exposed to COOH-SWCNT for 24h. The values are expressed as mean \pm S.E. GPx activity is expressed as mU/mg protein.

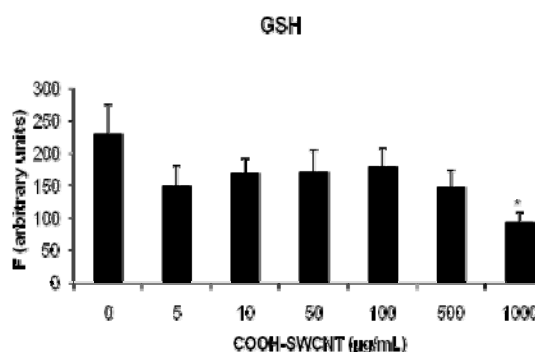


Figure 4. Glutathione (GSH) on Caco-2 cells exposed to COOH-SWCNT for 24h. The values are expressed as mean \pm S.E. GSH is expressed as arbitrary units.

*Significantly different from control ($p \leq 0.05$)

NANOTECHNOLOGY: PATHWAYS FOR ECONOMIC CHALLENGES AND SCIENTIFIC POLICIES IN SPAIN

Esteve Juanola-Feliu

CEMIC-Universitat de Barcelona, Martí i Franquès 1, Planta 2, Barcelona, Spain

ejuanola@el.ub.es

This paper analyses the state of the art for nanotechnology, focussing on the scientific and economic challenges arising from nanotechnologies and the policies that could be used to meet them in Spain.

Nanotechnology is an endless source of innovation and creativity at the intersection of medicine, biotechnology, engineering, physical sciences and information technology, and it is opening up new directions in R+D, knowledge management and technology transfer. Nanotechnology has already penetrated the market and, consequently, the competitive advantages of the more developed economies are threatened. Given the huge economic investment and cutting-edge research in the field of nanotechnology, scientific policies enhancing the cooperation-based university industry are more in demand than ever before.

Nanotechnology is expected to make a rapid impact on society [1]: creation of future economic scenarios, stimulation of productivity and competitiveness, converging technologies, and new education and human development. Evidence for the rapid impact of nanotechnology can be gleaned from figures for government investment in nanotechnology R+D activities, facilities and workforce training. The 2008 USA National Nanotechnology Initiative budget request for nanotechnology R+D across the Federal Government was over US\$1.44 billion [2]. In Europe, the VIIth Framework Programme (FP) will contribute about €600 million per year to nanotechnology research until 2013, with an additional, similar amount being provided by individual countries. This gives Europe a larger yearly spend on nanotechnology than the United States or Japan [3].

Scientific papers and patents in the nanotechnology sector have grown exponentially over the last two decades. Products based on nanotechnology are already in use and analysts expect markets to grow by hundreds of billions of euros during the present decade. After a long R+D incubation period, several industrial segments are already emerging as early adopters of nanotech-enabled products [4]; in this context, surprisingly rapid market growth is expected and high mass market opportunities are envisaged for targeted research sub-segments (Figure 1).

Nanotechnology activities in Spain are coordinated through the Ministry of Science and Innovation. The Working Program for the 2008-2011 National R&D&I and Innovation Plan has a Strategic Action called Nanoscience and Nanotechnology, New Materials and New Industrial Processes with seven actions (Human Resources, Fundamental Research Projects in R&D and Innovation, Institutional Strengthening, Infrastructures, Using Knowledge, System Articulation and Internationalization, and Networks). Actually, the other four Strategic Actions are close to the N&N activity: Healthcare, Energy and Climate Change, Telecommunications and Information Society, and Biotechnology.

In the context of European policy, N&N is a key area for the European Commission: the VIIth FP (2007-2013) provides a specific programme for Nanosciences, nanotechnologies, materials and new production technologies with a budget of €3,475 million (10.72% of the VIIth FP total budget). Moreover, several specific programmes are involved in nanoscale research, and thus the total budget invested in nanoactivities will be increased by several thousands of

€millions (Meur) coming from the following programmes: Health (6,100 Meur), Food, agriculture and biotechnology (1,935 Meur), ICT (9,050 Meur) and Energy (2,350 Meur).

The “Knowledge Regions” initiative of the VIIth FP, aimed at enhancing regional clusters, and the Spanish R&D Ingenio 2010 Programme (Consolider Program, CENIT Program and Avanza Plan), linked to regional policies that stimulate R&D activities, might achieve the ambitious objective of 2% GERD of GDP by 2010 (3% in Europe).

By the end of 2007, the NanoSpain Network was up to 234 research groups and companies accounting over 1500 researchers [5]. In 2007, there were 211 Spanish projects in the nano field (including 567 subprojects), involving 294 industries as partners or end users, as well as 5,000 researchers (2,400 doctors) [6]. Since 2004 the Spanish NanoTechnology Think Tank has sought to link public research institutions and private companies by exploiting innovative market opportunities from nanotechnologies. Over fifty applications in biomedicine and pharmacology, energy, electronics, ICT, aeronautics, chemistry and advanced materials have been launched onto the market in the search for development agreements [7]

In summary, nanotechnology is critical for the future of economic and regional competitiveness, job creation, and technological superiority. In a context of increasing R+D expenditure, scientific policies might promote the best models and practises from research, industry and financial strategies. As a result, Spain could strengthen its networks of science and technology parks, institutes and research centres, and technology platforms and incubators to meet the new scientific and market challenges.

References:

- [1] Roco M.C., Bainbridge W.S. (2005). « Social implications of nanoscience and nanotechnology: Maximising human benefit », *Journal of Nanoparticle Research*, Vol. 7, p.1-13.
- [2] NNI (2007). « Research and Development Leading to a Revolution in Technology and Industry ». National Nanotechnology Initiative, Supplement to the President’s 2008 Budget
- [3] Swarup A. (2007). « How Will Nanotech Fare in Europe? » http://sciencecareers.sciencemag.org/career_development/previous_issues/articles/2007_09_21/caredit_a0700136
- [4] Fuji-Keizai USA (2007). « Worldwide Market Research: Nanotechnology-based Product Market and Business Opportunities-Current & Future Outlook », February 2007
- [5] Fundación Phantoms (2007). «Nanociencia y Nanotecnología en España». Page 14
- [6] Spanish Strategic Action for Nanoscience and Nanotechnology, Ministry of Science and Innovation
- [7] Juanola-Feliu E. et al. (2004). « Spain Nanotechnology Think Tank 2004 », Fundación Española para la Ciencia y la Tecnología, ISBN 84-689-2723-6

Figures:

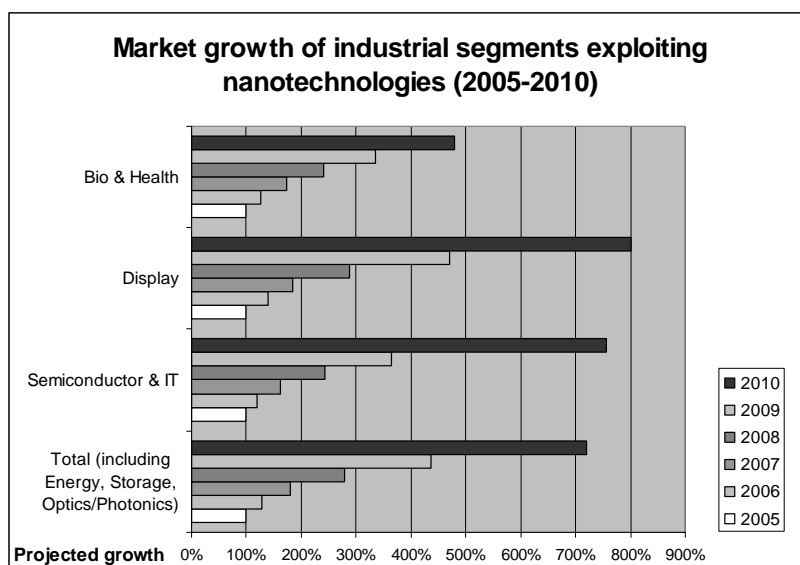


Figure 1: Chart based on Fuji-Keizai USA market research

HIGHLY ELECTRICAL CONDUCTIVE SPARK-PLASMA SINTERED CNTs-SiO₂ NANOCOMPOSITES

Mônica Jung de Andrade^{a,b}, Alicia Weibel^b, Christophe Laurent^b,
Carlos Pérez Bergmann^a, Claude Estournès^b, Alain Peigney^b

^a*Universidade Federal do Rio Grande do Sul*

Porto Alegre-RS, Brazil

^b*Institut Carnot CIRIMAT – CNRS – Université Paul Sabatier,
31062, Toulouse cedex 9, France
jung@chimie.ups-tlse.fr*

The addition of carbon nanotube (CNT) in ceramic composites is a promising field for different applications. Particularly, its huge aspect ratio and outstanding electrical properties give rises to percolation in insulating matrix at much lower content than any other additives [1]. The main challenges to obtain such composites are the dispersion of CNTs in the matrix and the densification of the final product [2,3]. In order to overcome this, we prepared CNTs-SiO₂ glass nanocomposites by sol-gel method using purified double-walled carbon nanotubes (DWCNTs) or by in-situ synthesis and then densified by Spark Plasma Sintering (SPS).

For the sol-gel preparation, purified DWCNTs were acid-functionalized and then dispersed by sonication in an acidic aqueous solution. After that, it was incorporated into an alcoholic solution containing an alkoxide silica precursor to let it gelificate. Then, the obtained xerogels were grinded and calcinated in air at 400 °C prior to its densification by SPS. These calcinated powders were densified by SPS at temperatures of 950 or 1000 °C under uniaxial pressures of 50 or 100 MPa. In order to understand the influence of the dispersion of CNTs on the electrical conductivity, studies were conducted both on suspensions of purified DWCNTs in insulating liquid (chloroform) with sonication [4] and on densified CNT-SiO₂ nanocomposites. The influence of the SPS parameters on the densification of the nanocomposites was also investigated and correlated to the electrical conductivity.

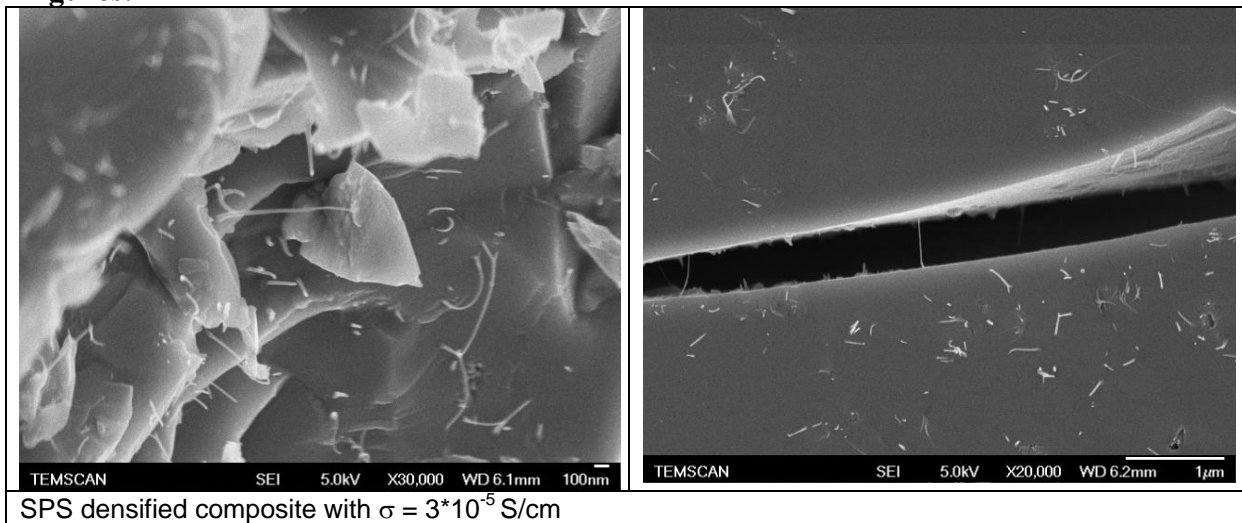
As it might be expected, the densified CNTs-SiO₂ nanocomposites have not achieved the same electrical conductivity measured on suspensions of CNTs in chloroform, whose dispersion state can be considered as the ideally case. In the other hand, highly densified and much higher electrical conductive nanocomposites were obtained than literature (6 orders of magnitude of enhancement), as far as we know [5]. A nanocomposite material prepared by the sol-gel method and densified by SPS (96.5% densification), containing less than 1% vol of C, showed an electrical conductivity of 10⁻⁴ S/cm.

References:

- [1] A. Loiseau, P. Launois, P. Petit, S. Roche, J.P. Salvetat, *Understanding Carbon Nanotubes from basics to application*; Springer, Heidelberg, **2006**, p. 24
- [2] M.J. de Andrade, M.D. Lima, C.P. Bergmann, G.O. Ramminger, N.M. Balzaretti, T.M.H. Costa, M.R. Gallas, *Nanotechnology*, **19** (2008) 265607.
- [3] M.J. de Andrade, M. Dias Lima, L. Stein, C.P. Bergmann, S. Roth, *phys. stat. sol. (b)*, **244** (2007) 4218.
- [4] M.D. Lima, M.J. Andrade, V. Skákalová, C.P. Bergmann, S. Roth, *Journal of Materials Chemistry*, **17** (2007) 4846.

[5] C.Xiang, X.Shi, Y.Pan, J.Guo, Key Engineering Materials, **280-283** (2005) 123.

Figures:



TOWARDS HETEROGENEOUS INTEGRATION WITH FUNCTIONALIZED NANOIMPRINTED POLYMER SURFACES

N. Kehagias¹, V. Reboud¹, W. Hu², N. Lu², L. Chi^{2,3}, H. Fuchs³, A. Genua⁴, J. A. Alduncín⁴,
J. A. Pomposo⁴, D. Mecerreyes⁴, I. Obieta, M. Striccoli⁶, M. Tamborra⁶, M. L. Curri⁶, A.
Agostiano^{6,7}, and C. M. Sotomayor Torres¹

1. *Catalan Institute of Nanotechnology, Campus de Bellaterra, Edifici CM7, ES 08193 - Bellaterra, Spain and
Catalan Institute for Research and Advanced Studies ICREA, 08010 Barcelona, Spain*
2. *State Key Laboratory of Supramolecular Structure and Materials, Jilin University, 130012, Changchun, P. R.
China*
3. *Physikalisches Institut and Center for Nanotechnology (CeNTech), Westfälische Wilhelms-Universität, D-
48149 Münster, Germany*
4. *New Materials Department, Centre for Electrochemical Technologies (CIDETEC), San Sebastian Technology
Park, Paseo Miramón 196, Donostia-San Sebastián 20009, Spain*
5. *Inasmet-Tecnalia, Pº Mikeletegi 2, 20009 San Sebastian, Spain*
6. *CNR IPCF Sezione Bari c/o Dipartimento di Chimica, Università di Bari, Italy*
7. *Dipartimento di Chimica, Università di Bari, via Orabona 4, I-70126 Bari, Italy*

Email: nikolaos.kehagias.icn@uab.es

Nanoimprint lithography (NIL) is an emerging nano-patterning technique with expanding number of possible applications. Although it may initially have targeted semiconductor applications an exponential increase of the use of NIL in various fields has been reported. A notable feature of NIL is its relatively low cost, which allows researchers to explore applications of nanopatterning that might have been economically unaffordable given the extraordinary cost associated with the beam based lithography process.

Printable polymers can be tailored to have a surface upon which molecules self-assemble. Furthermore, the resulting surfaces can be heterogeneously structured with or without etching away parts of imprinted polymers, in order to provide a flexible platform for structured surfaces with functional materials.

In this paper we show results of how nanoimprinted polymer surfaces could be used as templates for various applications. In particular we demonstrate multicolor emission by means of gas phase deposition of one type of dye molecule on a pre-patterned polymer substrate. The difference in color is due to the spectral shift of the dye molecules when subjected to different aggregation states (Fig. 1). In another example we illustrate that nanopatterned surfaces could be modified by growth of polymer brushes to create either hydrophobic or hydrophilic surfaces and moreover to attach to them luminescent nanocrystals.

Our results demonstrate that NIL is a feasible, high resolution and high throughput lithography technique which can be combined with other cost efficient self assembly approaches to fabricate functional devices such as biosensors and light emissive displays.

Acknowledgments: The support of the EC-funded projects NaPa (Contract No. NMP4-CT-2003-500120), PHOREMOST (FP6/2003/IST/2-511616), and NAPANIL is gratefully acknowledged. The content of this work is the sole responsibility of the authors.

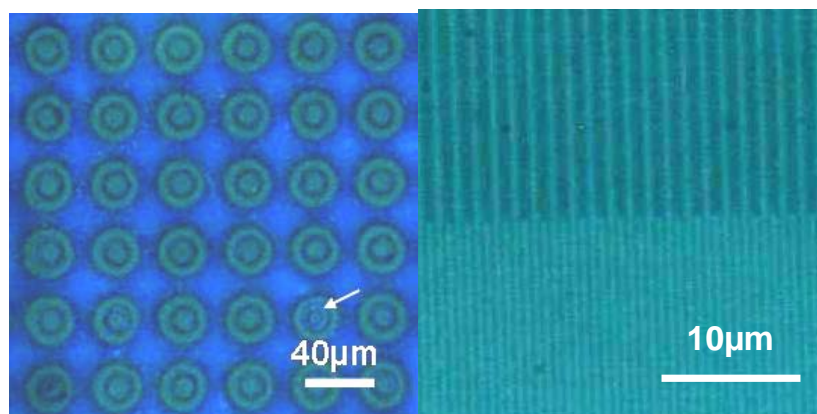


Figure 1. Fluorescence micrographs of ANP evaporated on patterned substrates with: a) 10 nm ANP on quartz/ PDMS rings and quartz discs embedded in PDMS matrix; b) 4 nm ANP on lined structure of PMMA with a resolution down to 300 nm. The colour change (420 and 490 nm) depends only on surface engineering of the PDMS layer containing the dye molecule. Parameters: evaporation rate and dye concentration.

MAGNETORESISTANCE IN POSITIVE AND NEGATIVE EXCHANGE BIAS Ni/FeF2 BILAYERED 200 NM ANTIDOTS

*M. Kovylna^{1,2}, R. Morales^{3,4}, J. Villegas⁴, M. Erekhinsky⁴, I. V. Roshchin⁴,
A. Labarta^{1,2}, I. K. Schuller⁴, and X. Batlle^{1,2}*
*Departament de Física Fonamental¹ and Institut de Nanociència i Nanotecnologia (IN2UB)²,
 Universitat de Barcelona, 08028 Barcelona, Catalonia, Spain*
Departamento de Física, Universidad de Oviedo, Oviedo 33007, Spain³
Physics Department, University of California-San Diego, La Jolla, California, USA⁴
miroslavna@ffn.ub.es

Despite the experimental and theoretical investigations, the exchange bias phenomenon (EB) in nanostructured systems remains poorly understood [1]. We used focused ion beam (FIB) lithography to prepare a series of samples of antidots of the same size and different distances in x-y directions. All of the fabrication has been performed on bilayered samples prepared by electron beam evaporation and consisted of antiferromagnetic (AF) FeF₂ (70nm), ferromagnetic (FM) Ni (50nm) and Al (4nm) as a protective layer. The square antidots with antidot size of 200 nm and x and/or y distance of 120-900 nm have been fabricated using an ion current of 30 pA. It is well known that magnetoresistance (MR) measurements can be used to determine exchange bias in thin films and nanostructures. MR was measured with the standard four terminal dc techniques in a He4 flow cryostat equipped with a superconducting solenoid. All measurements were carried out with the field applied parallel to the easy axis of the AFM and transport data were taken with the current in plane and perpendicular to the field. The resistivity was measured at 4.2 K in various field cooling conditions. The measuring field was applied along the same axis as the cooling field.

We observed three different types of behaviour: for small cooling fields, MR displays a shift towards negative field values (negative EB), while for large cooling fields the shift is positive (positive EB). In the intermediate case, we observed two MR peaks with different height and area. In the first and second case (small and large cooling fields) the reversal is sharper in the opposite field direction to the resulting shift of MR data. It is worth stressing that the switching from positive to negative EB depends on the antidote density. The positions of the MR peaks are mostly independent of the cooling field, which suggest the AF domain size is comparable to or larger than the FM domain size and that each FM domain couples only to one AF domain with a particular direction of the EB [2]. For small/large cooling fields we have only one EB direction while two appear for the intermediate cooling cases.

The funding from the Spanish MEC through a FPU grant, Spanish CICYT project MAT2006-03999 and from the Catalan DURSI (2005SGR00969) are acknowledged.

References:

- [1] O. Iglesias, A. Labarta, X. Batlle, Journal of Nanoscience and Nanotechnology (Invited Review paper), arxiv:cond-mat/067716.
- [2] O. Petravic, Z.P. Li, Igor V. Roshchin, M. Viret, R. Morales, X. Batlle, and I. K. Schuller, Appl. Phys. Lett. 87, 222509, (2005).
- I. Roshchin, O. Petravic, R. Morales, Z.P. Li, X. Batlle and I.K. Schuller, Euro. Phys. Lett. 71, 297, (2005).

Exchange bias in core/shell ferromagnetic/antiferromagnetic Co/Co-O nanoparticles of controlled size embedded in an insulating matrix

M. Kovylna^{1,2}, M García del Muro^{1,2}, Z Konstantinovic^{1,2}, M. Varela³, A. Labarta^{1,2}, and X. Batlle^{1,2}

*Departament de Física Fonamental¹ and Institut de Nanociència i Nanotecnologia (IN2UB)²,
Universitat de Barcelona, 08028 Barcelona, Catalonia, Spain*

*Departament de Física Aplicada i Òptica, Universitat de Barcelona, 08028 Barcelona, Catalonia, Spain³
miroslavna@ffn.ub.es*

Starting from the first report of exchange bias (EB) in fine particles, a huge amount of different EB system has been investigated [1]. Here we present the results of fabrication and characterization of core/shell Co/Co-O ferromagnetic/antiferromagnetic (FM/AFM) nanoparticles in an insulating zirconia matrix. These systems were prepared by pulsed laser ablation [2] at the room temperature in vacuum chamber in O₂ presence. Depending on the target component ratio, it is possible to obtain metallic particles of different sizes, above or below the percolation threshold. The samples of this study have been grown well below percolation threshold in order to exclude as much as possible the interactions between particles.

We have prepared a variety of samples at different O₂ chamber pressures (pO₂) which resulted in different core-shell ratios. It is significant that the oxide shell forms while the Co particles fly from the target to the substrate. The investigated thin films were about 200-300 nm thick and were deposited onto different substrates according to the characterization technique to be used. The magnetic properties were measured by SQUID magnetometer. As pO₂ increases, three interesting effects in zero field cooling/field cooling (ZFC/FC) and M(H) data can be observed (Fig. 1, Fig. 2): (i) the magnetization of the samples decreases due to decrease in the volume fraction of FM Co in the core of nanoparticles; (ii) the ZFC peak position moves from 6.5 K for pO₂ = 0 to 12.5 K for pO₂ = 10 · 10⁻⁷ bar, since the higher pO₂, the larger the mean particle size, while it broadens since the size distribution also broadens; (iii) the EB field first increases with increasing pO₂ (increase in the AFM shell thickness at the expense of the FM core), while it decreases at large pO₂ when the whole particle becomes AFM. Comparing the behaviour between pure AFM and core-shell particles, it is evident that the AFM nanoparticles do not present hysteresis behaviour.

The funding from the Spanish MEC through a FPU grant, Spanish CICYT project MAT2006-03999 and from the Catalan DURSI (2005SGR00969) are acknowledged.

References:

- [1] O. Iglesias, A. Labarta, X. Batlle, Journal of Nanoscience and Nanotechnology (Invited Review paper), arxiv:cond-mat/067716.
- [2] O. Petravic, Z.P. Li, Igor V. Roshchin, M. Viret, R. Morales, X. Batlle, and I. K. Schuller, Appl. Phys. Lett. 87, 222509, (2005).
- I. Roshchin, O. Petravic, R. Morales, Z.P. Li, X. Batlle and I.K. Schuller, Euro. Phys. Lett. 71, 297, (2005).

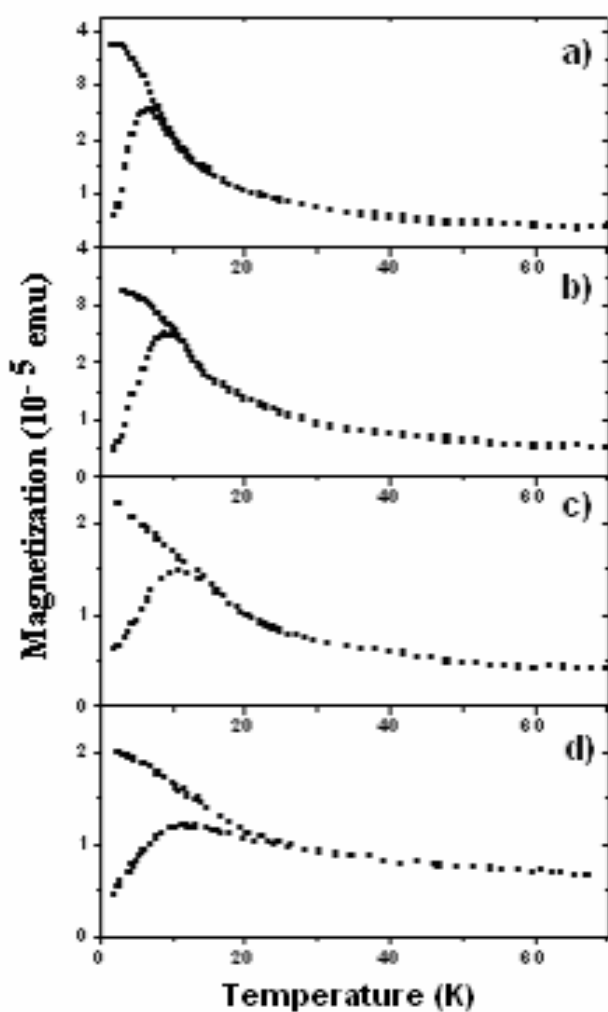


Fig. 1. Temperature dependence of the field cooled and zero field cooled magnetization. The pressure of O_2 during preparation: a) 0, b) 2.5, c) 7, and d) 10 (in units of 10^{-7} bar); Co volume fraction x_V : 0.30, 0.28, 0.27, and 0.25 correspondingly.

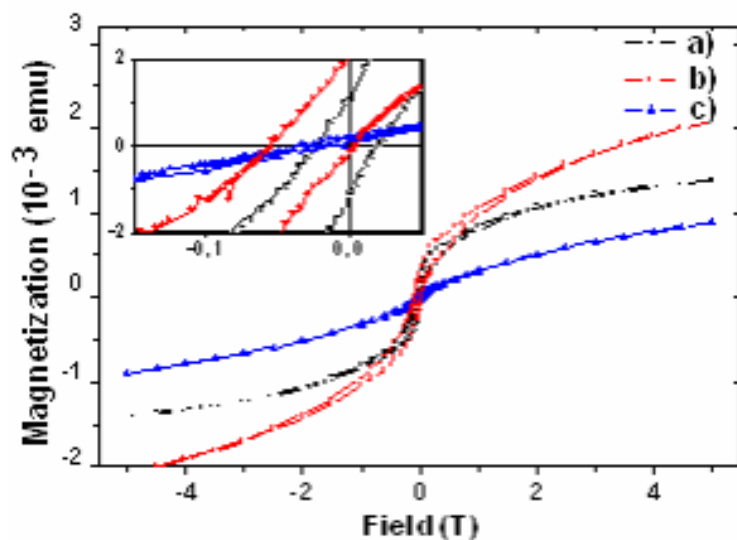


Fig. 2. Hysteresis loops.

The pressure of O_2 during preparation: a) 0, b) 0.25, c) 11 (10^{-6} bar).

The inset shows a low field magnification of the magnetization, the unit of the vertical scale is 10^{-4} emu.

Surface characterization techniques at the micro/nano scale: a complete set of tools at Parc Científic de Barcelona

María Jesús López-Bosque, Xavier Sisquella, Raúl Pérez, Marina Cazorla, Marta Poch, Sylvia Feitosa, Esther Tejeda-Montes, Andrew Bartles, Margalida Seguí, Alvaro Mata

*Nanotechnology Platform, Parc Científic de Barcelona,
Baldri Reixac 10-12, 08028 Barcelona, Spain*

mjlopez@pcb.ub.es

Characterization at the micro/nano scale is a critical step in the development of all kind of biomedical devices for biosensing and tissue engineering applications. Accurate control of the physical and chemical properties of the components and materials of these devices are directly related to their ultimate biocompatibility, bioactivity, and overall performance. Biological responses such as protein adhesion and conformation, cell attachment, morphology, proliferation, and differentiation can be modulated by controlling surface micro/nano topography and biochemistry. Nanotechnology not only allows to create well defined topographical and biochemical structures that can selectively modulate the behaviour of biological processes, but it also facilitates high-resolution surface characterizations to better identify and quantify the influence of micro and nano topography as well as surface biochemistry on specific biological components.

The Nanotechnology Platform at the Parc Científic de Barcelona (PCB) is a well established laboratory that comprises a large number of the state-of-the-art micro/nanofabrication and characterization equipment, a cleanroom facility and six laboratory technicians with extensive experience in a variety of fabrication and characterization techniques at the micro/nano scale. This abstract describes the different characterization techniques that are available at this facility, which can be used to investigate chemical and physical properties of materials and structures with micro and nanoscale resolution for a variety of biosensing and tissue engineering applications. These techniques include Time of Flight Secondary Ion Mass Spectroscopy (TOF-SIMS), Atomic Force Microscopy (AFM), High-resolution Scanning Electron Microscopy (HR-SEM), interferometric microscopy, mechanical profilometry, and surface energy analysis. Integrating SEM with AFM allows a very fine topographical characterisation expanding from the molecular to the micro scale. Furthermore, AFM can also provide physical and mechanical analysis at the molecular level, which can be correlated to the chemical and biomolecular composition of the samples. Utilization of the TOF-SIMS would allow two-dimensional analysis of elemental and molecular masses at the micro/nano scale, permitting the localization of drugs, cell signalling molecules, antibodies, nanoparticles, etc. The combination of these three techniques (TOF-SIMS, SEM, and AFM) offers a versatile and complementary repertoire for the analysis of surface properties.

The Nanotechnology Platform has at its disposal two Atomic Force Microscopes. The Molecular Force Probe (MFP-3D) from Asylum Research is an optimised AFM that measures forces at the molecular scale. Apart from analysing the atomic and molecular topography of different samples, (Figure 1a) it can characterize elastic properties of molecules such as proteins or DNA, receptor/ligand interactions, nanoindentation, and adhesion forces. The other system is the Molecular Imaging, from Scientec, which is able to increase contrast in the

amplitude and phase signals for better characterisation of molecular patterns of functionalised surfaces (Figure 1b).

Scanning Electron Microscopy permits a topographical characterisation of the surface properties with resolutions down to 5 nm. SEM provides qualitative information of the reproduction quality of the various surface patterns and textures and to study the morphological characteristics of cells on a substrate (figure 1c).

The TOF-SIMS is a mass spectrometer with a TOF detector that allows to obtain chemical maps of the surface with a 200 nm lateral resolution (figure 2), graphs of element distribution in depth (depth profiles), and compositional graphs in 3D.

Figures:



Figure 1: a) Topography image taken by an AFM of mesenchymal stem cells adhered on a glass surface; b) Phase contrast AFM image of a micro-contact printed self assembled monolayer obtained with a force modulation mode of operation; c) SEM image of cells on a microstructured polymer (Courtesy of Dr. Elena Martínez, IBEC).

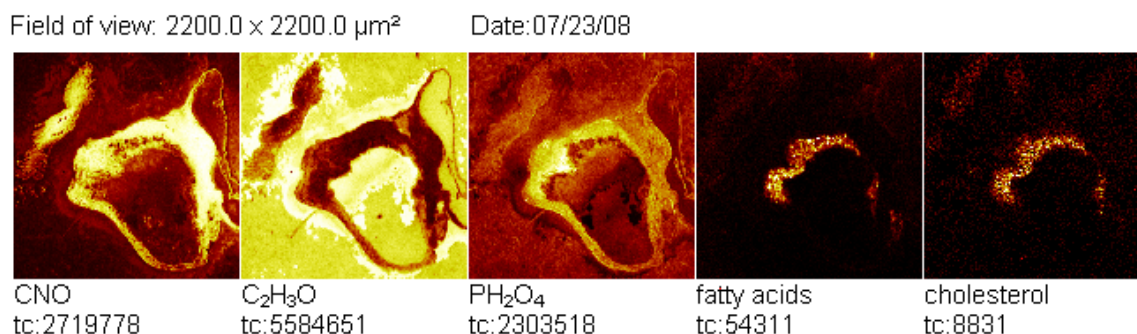


Figure 2: Surface Image of tissue cross-section of a human aorta vessel by TOF-SIMS

STRATEGIC LINES OF RENAC, NETWORK FOR APPLICATION OF NANOTECHNOLOGIES IN MATERIALS AND PRODUCTS FOR CONSTRUCTION AND THE HABITAT















Pilar Lozano, Celia Silvestre, MJ López Tendero, JM Lloris Cormano, P Calero
Aidico, Av Benjamin Franklin 17, (46918 Paterna) Valencia, Spain
nano-renac@aidico.es

RENAC is the Spanish network for application of nanotechnology in construction and habitat products. It has been established as a scientific and technological platform that primarily intends to overcome fragmentation of costly research effort by integration and generation of a knowledge base for the construction sector to meet EU objectives (sustainable development, social cohesion). The final objective is to facilitate industrial exploitation and improve the competitive position and employment prospects of the construction and habitat sectors.

RENAC has 24 members, among them 8 technology institutes that belong to REDIT: AIDICO, ITC-AICE, AIDIMA, AIMPLAS, AIDO, AIMME, ITE, and AITEX, and 16 related prestigious research groups that work with nanotechnologies and belong to universities from the Community of Valencia: Jaime I University, University of Valencia, Technical University of Valencia and University of Alicante. The multidisciplinary expertise comes from the integration of Technological Institutes groups dealing with research in different traditional materials (wood, plastic, concrete, ceramic, stone, metal) with University research groups with a recognised excellence in nanoscience fields such as interface science, nanoparticles, photovoltaic nanomaterials, nanocomposites, mesoporous materials, chemical sensors, and polymer science.

The Research Centres and the Industries have the greater opportunities to consolidate their capital in Industrial Property in the emergent stage of the development of a new technology. This will allow them to bring to the market innovating products and to avoid the dependency of external technology.

RENAC has been organized into 14 different working groups for research as well as the detection of industrial opportunities.

 AIDIMA INSTITUTO TECNOLÓGICO MUEBES, MADERA, BUAJALÉ Y AFINES	Fire resistant polymers	Photocatalytic coatings	 ITC Instituto de Tecnología Cerámica
 ITC Instituto de Tecnología Cerámica	Nanocomposites for high shear resistance.	Photovoltaic materials.	 NTC
 ITC Instituto de Tecnología Cerámica	Nanostructured coatings: ceramic/metalc ceramic	Nanocomposites for natural stone treatments	 AIDICO INSTITUTO TECNOLÓGICO DE LA CONSTRUCCIÓN
 AIDIMA INSTITUTO TECNOLÓGICO MUEBES, MADERA, BUAJALÉ Y AFINES	Nanoencapsulation for Control liberation	Surface functionalization.	 ICMUV Instituto de Cerámica y Materiales
 GRUPO DE DISEÑO Y DESARROLLO DE SENSORES UPV	Chemical sensors	Multifunctional pigments	 AIDICO INSTITUTO TECNOLÓGICO DE LA CONSTRUCCIÓN
 AIDICO INSTITUTO TECNOLÓGICO DE LA CONSTRUCCIÓN	Intelligent polymers.	Nanomaterials for Portland cement based materials.	 AIDICO INSTITUTO TECNOLÓGICO DE LA CONSTRUCCIÓN
 AIMPLAS INSTITUTO TECNOLÓGICO DEL PLÁSTICO	Conductive polymers.	Nanostructure characterization.	 ITM Instituto de Tecnología de Materiales

References:

[1] MJ Lopez-Tendero, L. E. Dominguez, J M Lloris, M Cruz, C Silvestre1,V Sanz, A Moreno RENAC: Network for the nanotechnology application in materials and products for construction and habitat. EuroNanoForum 2007 Nanotechnology in Industrial Applications. European and International Forum on Nanotechnology Düsseldorf (Germany), 19-21 June 2007 EUR 22833 PROCEEDINGS, 235-238.

MAGNETIC AGING OF SELF-ORGANIZED ARRAYS OF Co NANOPARTICLES: IS THERE A SUPERSPIN-GLASS PHASE?

F. Luis¹, R. López Ruiz¹, J. Sesé², J. Bartolomé¹, C. Deranlot³, and F. Petroff³

*¹Instituto de Ciencia de Materiales de Aragón (CSIC-Universidad de Zaragoza) y
Departamento de Física de la Materia Condensada, Universidad de Zaragoza, Pedro
Cerbuna 12, 50009 Zaragoza, Spain*

*²Instituto de Nanociencia de Aragón (Universidad de Zaragoza) y Departamento de Física de
la Materia Condensada, Universidad de Zaragoza, Pedro Cerbuna 12, 50009 Zaragoza,
Spain*

*³Unité Mixte de Physique CNRS/Thales, Route Départementale 128, 91767, Palaiseau Cedex,
France and Université Paris-Sud, 91405 Orsay Cedex, France*

fluis@unizar.es

Dense arrays of magnetic nanoparticles contain the physical ingredients that are usually met in conventional spin-glasses [1]. The unavoidable disorder in the positions and orientations of the particles leads to disorder and frustration of the dipolar interactions between their magnetic moments, which are usually dominant. However, in contrast with “canonical” spin-glasses, the slow magnetic relaxation introduced by these collective effects coexists and competes with the slow magnetization reversal associated with the anisotropy energy barriers and with the, usually large, distributions of particle’s sizes and shapes. Many experiments performed on dense nanoparticulate materials show phenomena such as the dynamical scaling of the susceptibility [2] and aging [3] that are typical of the spin-glass behaviour. Recent numerical simulations show, however, that magnetic aging is not exclusive of spin-glasses [4]. The question is, then, whether real materials show a true superspin-glass phase. In order to address this question experimentally, we have compared the magnetization dynamics of well-characterized three- and two-dimensional arrays of magnetic nanoparticles. In the latter case, theory predicts that the freezing temperature T_g vanishes, i.e. that no spin-glass phase can exist at any finite temperature [1].

Recently, we investigated interaction effects on samples of 2.6 nm Co nanoparticles prepared by sequential sputtering of Co on amorphous alumina layers [5]. Increasing the number N of $\text{Al}_2\text{O}_3/\text{Co}$ layers, it is possible to modify dipolar interactions *in a controlled and measurable way, while keeping the rest of parameters (size, magnetic anisotropy, etc) known and constant*. Here, we report results of aging experiments of the ZFC susceptibility measured with a waiting time cooling protocol (at a temperature T_w , a pause of t_w seconds is made before cooling to the lowest temperature). The susceptibility difference $\Delta\chi$ between experiments recorded after cooling without and with pause shows a peak at T_w (see Fig. 1).

We have performed aging experiments for samples with N increasing from $N = 1$ (two-dimensional limit) to $N = 20$ layers (three-dimensional limit), and as a function of all relevant parameters: waiting temperature T_w , waiting time t_w , and the applied magnetic field H . The amplitude of the aging phenomenon $\Delta\chi$ is observed to grow with time and to decrease with increasing H , suggesting that this quantity is indeed linked to the growth of magnetic correlations. However, some of our results do not agree with the interpretation based on the existence of a spin-glass phase. First, $\Delta\chi$ shows a maximum at a temperature $T_{w,\text{max}}$ that can be accounted for by the same Arrhenius’ law that holds in the superparamagnetic regime (i.e. for $T > T_g$). Second, we observe aging phenomena in 3-D samples (i.e. for $N = 20$) as well as for 2-D single layers (Fig. 2).

We have also measured the FC and remanent magnetizations, and the frequency-dependent ac susceptibility. These techniques are usually employed in the research of other (super)spin-glass systems. As for the aging phenomenon, we observe the same qualitative behaviour in two and three dimensional arrays. In particular, the critical scaling analysis of the ac susceptibility, usually known as critical slowing down, [2] holds equally well for the two limits with exactly the same “critical exponents”, as it is shown in Fig. 3.

Our main conclusion is that phenomena such as aging and the critical slowing down of the susceptibility do not provide a definite proof of the existence of a superspin-glass phase. Our work casts serious doubts on the existence of this phase and calls for alternative interpretations.

This research has been funded under Projects MAT2008/1077 from MCINN and NABISUP from DGA.

References:

- [1] J. A. Mydosh, *Spin glasses : an experimental introduction*, Taylor and Francis (London, 1993).
- [2] C. Djuberg, P. Svedlindh, P. Norblad, M. F. Hansen, F. Bodker, and S. Morup, Phys. Rev. Lett. **79**, 5154 (1997).
- [3] T. Jonsson, J. Mattsson, C. Djuberg, F. A. Khan, P. Norblad, and P. Svedlindh, Phys. Rev. Lett. **75**, 4138 (1995).
- [4] J. F. Fernández and J. Alonso, to be published.
- [5] F. Luis, F. Petroff, J.M. Torres, L. M. García, J. Bartolomé, J. Carrey, and A. Vaurès, Phys. Rev. Lett. **88**, 217205 (2002).

Figures:

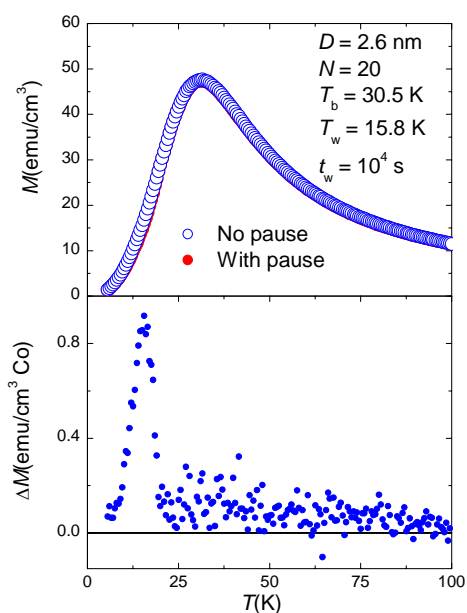


Fig. 1. Aging of the ZFC susceptibility of 2.6 nm Co nanoparticles.

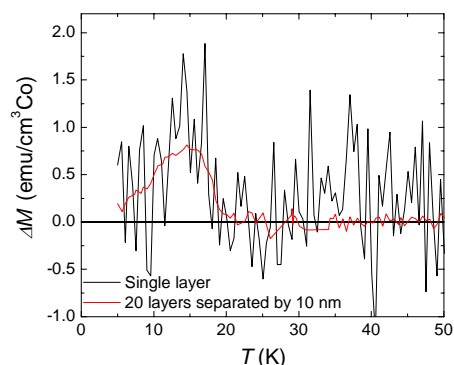


Fig. 2. Aging of the magnetization of a single layer and a multilayer of Co nanoparticles.

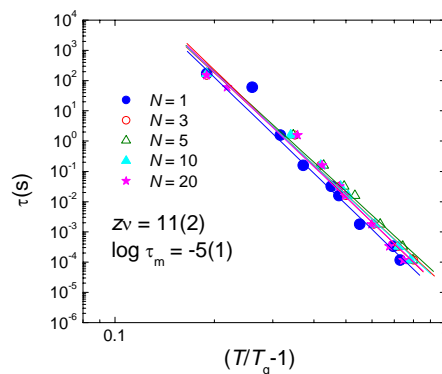


Fig. 3. Critical scaling down of the freezing temperature extracted from ac susceptibility experiments performed on samples with varying number of layers N .

Z-contrast STEM imaging of B cation ordering and microstructure of $\text{Sr}_2\text{CrReO}_6$ double perovskite thin films

*C. Magén^{1,2}, M. Varela², S. J. Pennycook²,
J. Orna^{1,3}, L. Morellón^{1,3}, P. A. Algarabel³, M. R. Ibarra^{1,3}*

¹ *Instituto de Nanociencia de Aragón, Universidad de Zaragoza, 50009 Zaragoza, Spain*

² *Oak Ridge National Laboratory, Oak Ridge TN 37831, USA*

³ *Instituto de Ciencia de Materiales de Aragón, Universidad de Zaragoza-CSIC, 50009 Zaragoza, Spain*
cmagend@unizar.es

Half-metallic compounds present a great potential for room-temperature applications at room Spintronics. Ferrimagnetic double perovskites (DP) with formula unit $\text{A}_2\text{BB}'\text{O}_6$ are candidates to exhibit half-metallicity and high Curie temperatures based on a modified perovskite structure where the $\text{BO}_6/\text{B}'\text{O}_6$ octahedra are arranged in a superstructure of two interleaving fcc sublattices antiferromagnetically coupled [1]. $\text{Sr}_2\text{CrReO}_6$ (SCRO) is a metallic ferromagnetic DP with one of the highest Curie temperature ($T_C=625$ K) [2]. SCRO has a experimental saturation magnetization of $M_S=1.38 \mu_B/\text{f.u}$ (the theoretical value is $1 \mu_B/\text{f.u}$) [3], but the existence of antisite (AS) defects at the B/B' sites can reduce this value and also destroy the half-metallic nature of the material.

The controllable growth of high-quality epitaxial films of SCRO ordered double-perovskite with high T_C and full magnetization is required for electrodes in spintronic devices [4,5,6]. In this work we report the Z-contrast STEM characterization of the chemical ordering and microstructure of epitaxial SCRO deposited on SrTiO_3 (001) substrates by pulsed laser deposition (PLD). The growth conditions can be found elsewhere [7]. High resolution scanning transmission electron microscopy (HR-STEM) were performed in the VG Microscopes HB501UX and HB603U operated at 100 kV and 300 kV, respectively and both equipped with a Nion aberration corrector.

High resolution annular dark field (ADF) STEM image of a cross section specimen of SCRO is depicted in Figure 1. In this image we can clearly perceive the cationic ordering in the B sites due to the Z-contrast. The intensity profile of the image evidences the presence of the three elements; i.e. Sr (A site), Re and Cr (B, B' sites). Figure 2 displays a Z-contrast image of the SCRO film in the proximity of the substrate, which shows an excellent epitaxial growth of the SCRO layer in the early stages of the growth and a defectless unrelaxed interphase. The epitaxy relations in this stage of growth are $\text{STO} (111) [1-10] // \text{SCRO} (111) [1-10]$. At a thickness of approximately 4-5 nm we can observe the formation of two sets of twins in the shape of planar grains parallel to the substrate plane with two alternating orientations. One corresponds with the same orientation as the substrate (i.e. the twin present in the first nanometers of the film), the other with the a axis rotated $\sim 110^\circ$ clockwise in the image. The orientation of the second set of twins corresponds to a rotation of the SCRO crystal of 180° around the (111) axis. Therefore, the epitaxy relation of the second twin with respect to the first one (i.e. with respect to the substrate is $\text{STO} (111) [1-10] // \text{SCRO} (111) [100]$. Z contrast is a powerful tool to characterize the chemical ordering in DP. The effect of the formation of twin boundaries can be observed in Figure 2(b). While in the upper boundary the B superstructure is conserved through the boundary (thick lines indicate the Re columns and thin lines are Cr columns), the lower boundary creates an AS boundary.

References:

- [1] D. Serrate *et al.*, J. Phys.: Condens. Matter **19**, 023201 (2007), and references therein.
- [2] H. Kato *et al.*, Appl. Phys. Lett. **81**, 328 (2002).
- [3] J. M. De Teresa *et al.*, Appl. Phys. Lett. **90**, 252514 (2007).
- [4] H. Asano *et al.*, IEEE Trans. Magnetics **41**, 2811 (2005)
- [5] H. Asano, N. Koduka, A. Tsuzuki, and M. Matsui, Appl. Phys. Lett. **85**, 263 (2004).
- [6] S. Geprägs *et al.*, cond-mat 2009, arXiv:0901.4499
- [7] J. Orna *et al.*, to be published in J. Magn. Magn. Mater.

Figures:

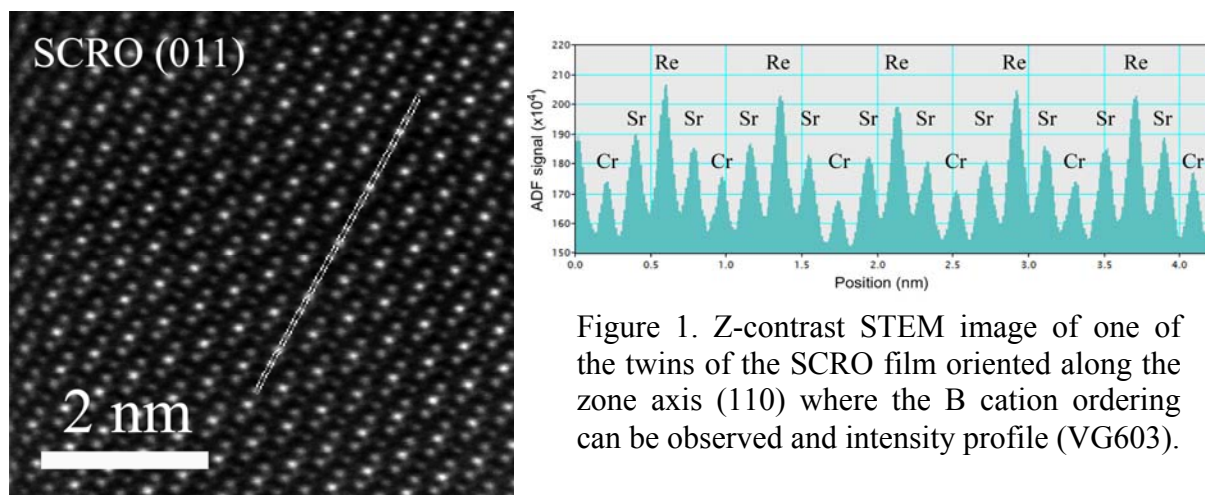


Figure 1. Z-contrast STEM image of one of the twins of the SCRO film oriented along the zone axis (110) where the B cation ordering can be observed and intensity profile (VG603).

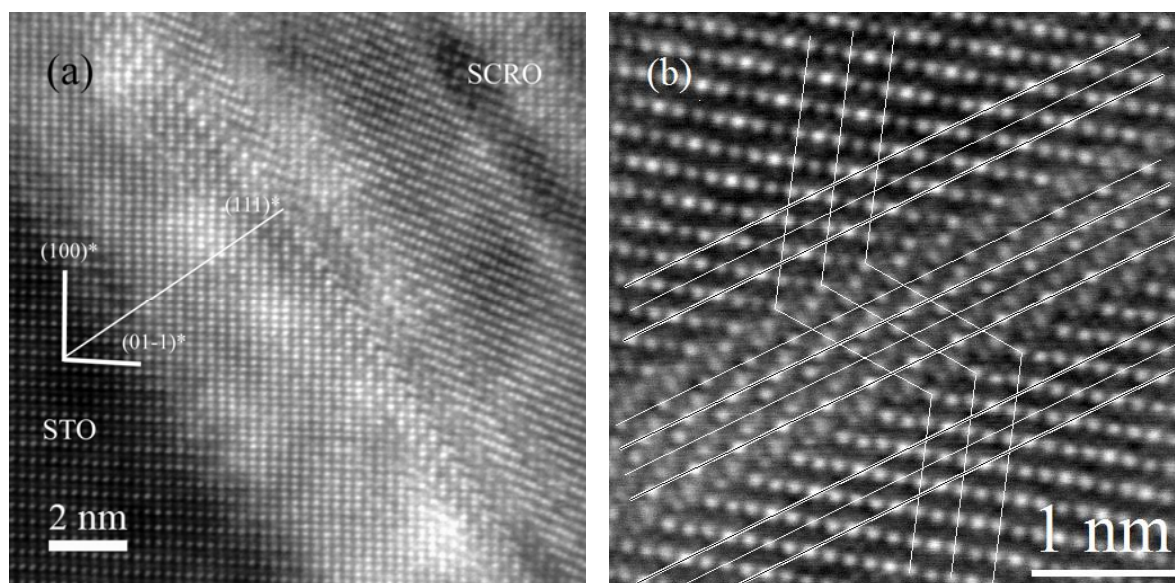


Figure 2. (a) VG 501 High resolution Z-contrast STEM image of a cross section SCRO specimen grown on STO (111) (VG501). (b) Fourier filtered image of a twin boundary in SCRO (VG603).

Effect of nanoparticle volume concentration in jet flow with noise

Taher Armaghani^a, Mohammad Javad Maghrebi^a, Farhad Talebi^b

^aThe Faculty of Mechanical Engineering, Shahrood University of Technology, Shahrood, Iran

^bThe Faculty of Mechanical Engineering, Semnan University, Semnan, Iran,

taherarmaghani@yahoo.com

Jet flow with desired physical conditions thought lots of applications in industrial and scientific scope has been the most important subjects in fluid mechanic and from appearance of fluid mechanic theory; many researchers have attended this subject.

In this paper, direct numerical solution two dimensional incompressible jet flows is performed.

We replaced the base fluid properties with nanofluid that contain nanoparticle and base fluid. Nanoparticle in this study is Al_2O_3 and the basefluid is water.

In this study the following non-dimensional equation are solved :

$$\nabla \cdot \vec{U} = 0 \quad (1)$$

$$\frac{\partial \nabla^2 \vec{U}}{\partial t} = -\nabla \times (\nabla \times \vec{H}) + \frac{1}{Re} \nabla^4 \vec{U} \quad (2) \text{ in there } \vec{H} = (H_1, H_2, H_3) = \vec{U} \times \vec{\omega} \quad (3)$$

$$\frac{\partial T}{\partial t} + \vec{U} \cdot (\nabla T) = \frac{1}{Pe} (\nabla^2 T) \quad (4)$$

The equation (2) used by many investigators including Maghrebi[1] is the vorticity form of Navier stokes equation.

The governing equations are discretized in the streamwise direction (x), using a sixth order compact finite difference scheme, and in the cross-direction (y) using a mapped compact finite difference scheme[2]. A cotangent mapped of $y = -\beta \cot(\pi\zeta)$ [3] is used to relate the computational domain $0 \leq \zeta \leq 1$ to the physical domain in the double infinit interval of $-\infty \leq y \leq \infty$. The compact third order of Runge-Kutta method [4] is used for the time-advancement of the simulation. The inlet boundary condition is the Dirichlit and Neumann condition; The convective outflow boundary condition is employed to create a non-reflective type boundary condition at the outlet[1]. An inviscid (Stuart flow)[5] and a completely viscose solutions of the Navier Stokes equations are used for verification of the numerical simulation. The numerical results show a very good accuracy and agreement with exact solution of the Navier Stokes equation[1]. A noise in the form of periodic perturbations at the inlet is used for the forced simulation. The inlet perturbation were studied by salmani[6]

For nanofluid(Al_2O_3 -water) the following equation are used. these equations, introducing the effective properties, were used by maiga[7]

$$\rho_{nf} = (1 - \phi)\rho_{bf} + \phi\rho_p \quad (5) \quad (cp)_{nf} = (1 - \phi)(cp)_{bf} + \phi(cp)_p \quad (6)$$

$$\mu_{nf} = (123\phi^2 + 7.3\phi + 1)\mu_{bf} \quad (7) \quad k_{nf} = (4.97\phi^2 + 2.72\phi + 1)k_{bf} \quad (8)$$

In these equation ρ, μ, cp, k refers to density, viscosity, specific heat, conductivity respectively where ϕ refers to nanofluid volume concentration. and sub scrips nf, bf, p refers to nanofluid, base fluid and particle respectively.

Figure (1,2) show the validity the result with Stuart flow and Navier Stokes equation.

Figure (3) show the velocity time histories for U component without noise and without nanoparticle.

Figure (4) show the temperature time histories without noise and without nano particle. Figure (5) velocity time histories for the v component with noise. Figure (6) show the effect of nanoparticle volume concentration in U-time it is obsened that ϕ increase the noise amplitude decrease because the Reynolds number decrease. Figure (7) show the effect of nanoparticle volume concentration in T-time the figure result that when ϕ increase the noise amplitude decrease because the amplitudes of U decreased.

References:

- 1- M.J. Maghrebi, "A Study of Evolution of Intense Focal Structures in Spatially-Developing Three-Dimensional Planer Wake", PhD thesis, Department of Mechanical Engineering, Monash University, Melbourne, Australia, 1999.
- 2- S.K. Lele, "Compact Finite Difference Scheme with Spectral-Like Resolution", Journal of Computational Physics, 103, 16-12, 1992.
- 3- M.J. Maghrebi, "Orr Summerfield Solver Using Mapped Finite Difference Scheme for Plane Wake Flow",.
- 4- A. Wray & M.Y. Hussaini, "Numerical Experiments in Boundary Layer Stability", Proc. R. Soc. Lond. A, vol. 392, pp 373-389, 1984.
- 5- J. T. Stuart. On finite amplitude oscillations in laminar mixing layer. Journal of fluid mechanics. 29.(3) pp 417-440. 1967.
- 6- A. salmani, "Numerical study of linear stability of jet flow". Department of Mechanical Engineering Shahrood University of Technology, Shahrood, IR.IRAN, 2005.
- 7- S.E.B. maiga et all, "Heat transfer enhancement by using nanofluids in forced convection flows". Internal Journal of Heat and Fluid flow 26(2005)530-546

Figures:

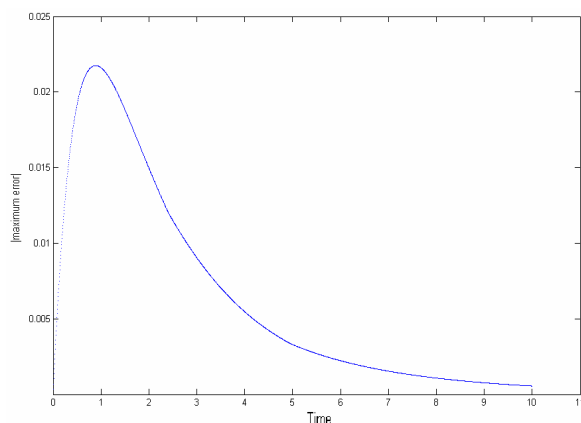


Figure 1. maximum error in 2D solution

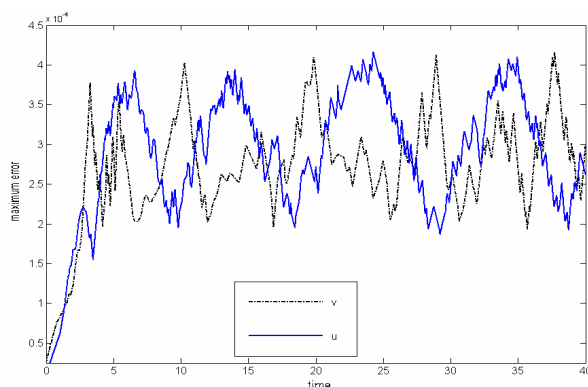


Figure 2. maximum error for Stuart flow

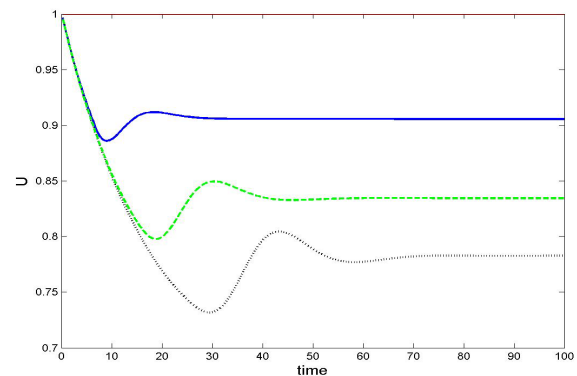


Figure 3. U velocity time history of numerical simulation

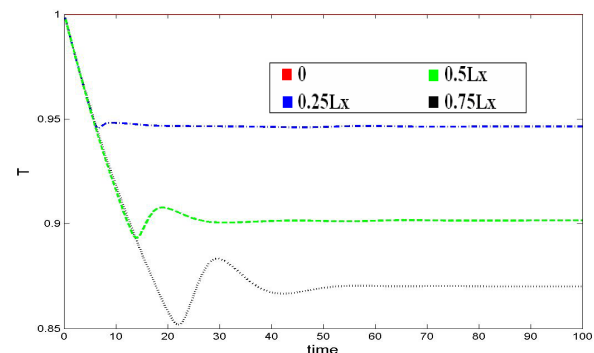


Figure 4 temperature time history of numerical simulation

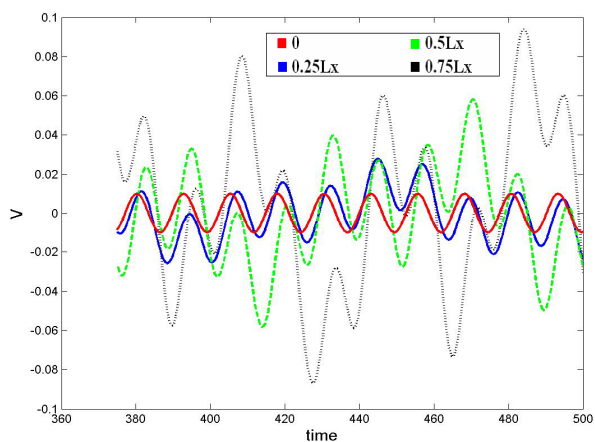


Figure5. V velocity time history with noise at $y=0, L(x)$

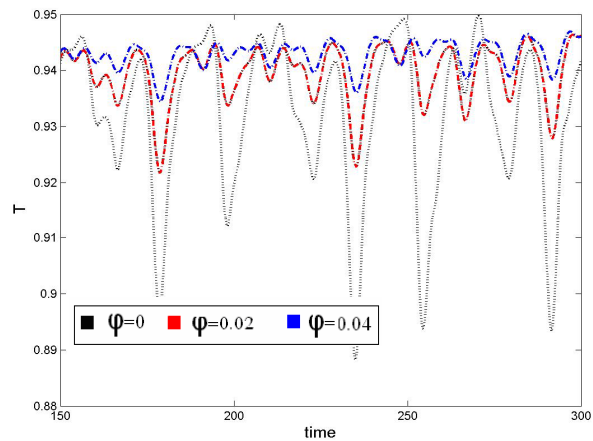


Figure7. temperature w time history with noise and nanoparticle at $y=0, x=0.75Lx$

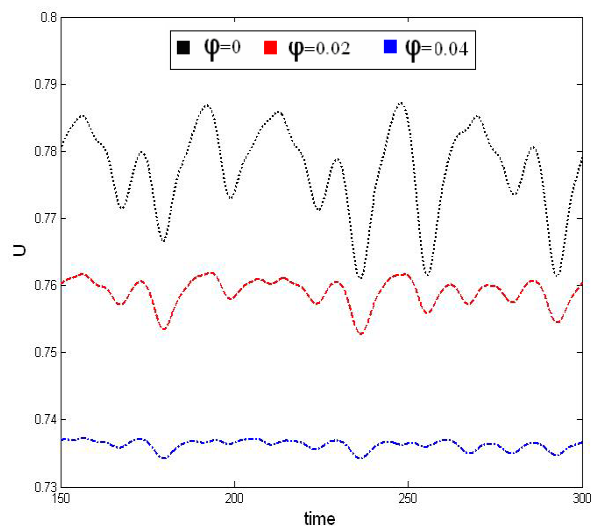


Figure6. U velocity time history with noise and nanoparticle at $y=0, x=0.75Lx$

Transport properties of individual Bi nanowires contacted by Dual Beam

N. Marcano^{a,b}, S. Sangiao^{a,b}, M. Plaza^c, R. Córdoba^b, A. Fernández-Pacheco^{a,b}, L. Pérez^c,
J. M. De Teresa^a, L. Morellón^a, M.R Ibarra^{a,b}

^a Dpto. Física de la Materia Condensada, Instituto de Ciencia de Materiales de Aragón,
Universidad de Zaragoza-CSIC, Facultad de Ciencias, Zaragoza, 50009, Spain

^b Instituto de Nanociencia de Aragón, Universidad de Zaragoza, Zaragoza 50009, Spain

^c Dpto. Física de Materiales, Universidad Complutense de Madrid, Madrid 28040, Spain

marcanon@unizar.es

Semimetallic Bi, with a rhombohedral structure, exhibits many unique electronic properties due to the small effective mass, the low density and the long mean free path of the carriers. Due to these unique features, Bi has attracted much attention for applications involving field sensing due to its extremely high magnetoresistance (MR) relative to those reported for giant-and colossal-magnetoresistive materials [1]. Recently, there has been a long-standing interest in Bi nanostructures for both fundamental understanding and device applications. However, most of the Bi nanostructures are in thin film form. Nanowires of Bi offer a new medium for exploring novel low-dimensional transport phenomena. Since the diameter is smaller than the mean free path of the electrons, they will be confined by the boundary of the nanowire, thereby resulting in a reduction in mean free path as the wire diameter decreases. Also, the small effective masses of Bi ($\sim 0.001 m_e$) result in very pronounced quantum size effects [2].

In this contribution we describe four-probe transport measurements of individual Bi nanowires contacted in a dual-beam system. The Bi nanowires, typically up to 3 μm in length with a diameter ranging from 100 to 150 nm, were fabricated by electrodeposition. A drop of solution containing such nanowires was placed on a substrate consisting of thermally oxidized Si wafer (300 nm SiO_2 on top of Si substrate) where Aluminium micrometric electrodes had been previously patterned by optical lithography. Selected nanowires were connected to the microelectrodes via four nanopads (see figure 1) which consist of ion-beam-induced W deposit (IBID-W) grown in-situ by injecting the precursor gas $\text{W}(\text{CO})_6$ in the proximity of the substrate. This kind of deposit favours low electrical resistance as required in some applications. In-situ current versus voltage measurements indicate ohmic contacts. Ex-situ magnetotransport properties of a single Bi nanowire in the temperature range $5 \text{ K} < T < 300 \text{ K}$, with fields up to 90 kOe are discussed.

References:

- [1] F. Y. Yang et al., Phys. Rev. Lett., **82** (1999) 3328.
- [2] S. B. Cronin et al., Molecular Electronics, 582 (2000) 10

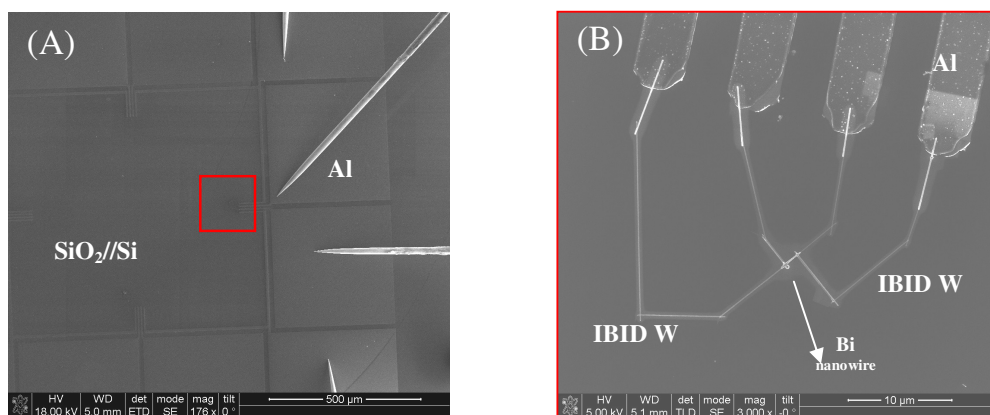
Figures:

Figure 1: A) SEM image of the electrical aluminium micropads patterned by optical lithography. The four microprobes are contacted for in-situ electrical resistance measurements. The red rectangle shows the zone where the Bi nanowire is located. B) Magnification of the region where the Bi nanowire is contacted with the Al micropads via the four W nanodeposits.

Effect of the nature and the particle size on the properties of uniform magnetite and maghemite nanoparticles

Alejandro G. Roca,^a José F. Marco^b, María del Puerto Morales^a and Carlos J. Serna^a

^aInstituto de Ciencia de Materiales de Madrid. CSIC. Cantoblanco. 28049 Madrid, Spain

^bInstituto de Química Física "Rocasolano". CSIC. c/ Serrano, 119. 28006 Madrid, Spain

jfmarco@iqfr.csic.es

Magnetite nanoparticles with two different sizes, 5 and 17 nm (Figure 1), have been prepared by decomposition of organic precursors in an organic media in the presence of oleic acid. The particles have been characterised by TEM, X-ray diffraction, Infrared and Mössbauer spectroscopy in order to clarify their structural and physicochemical properties. The samples consist on non-interacting magnetite nanoparticles in both cases with a more uniform size distribution and higher crystal order degree than particles of similar sizes prepared by coprecipitation. A controlled heat treatment of the samples in air leads to the transformation of magnetite to maghemite which can be followed by the appearance of many IR bands forbidden for a spinel structure. In addition to that, an important reduction of saturation magnetisation and coercivity at low temperature takes place whenever the oleic acid is preserved. Finally Mössbauer spectra at different temperatures clearly shows the effect of the nature of the iron oxide phase, the particle size, particle interactions and structural order at the surface in both, magnetite and maghemite as a consequence of the oleic coating.

Figures:

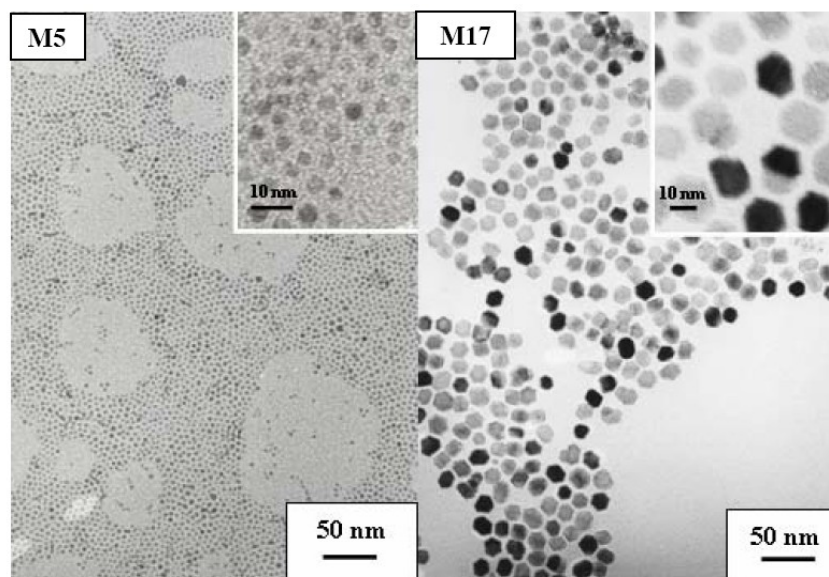


Figure 1. TEM images of magnetite nanoparticles of 5 nm (left) and 17 nm (right).

Fe₃O₄ Nanoparticles for Biomedical Applications.

C Marquina⁵, M A Gonzalez-Fernandez², M A Verges³, R Costo², C J Serna², M P Morales², T.E. Torres¹, M R Ibarra⁴ and G F Goya¹

¹*Instituto de Nanociencia de Aragón y Departamento de Física de la Materia Condensada, Universidad de Zaragoza, Zaragoza, Spain.*

²*Instituto de Ciencia de Materiales de Madrid, CSIC, Madrid, Spain*

³*Departamento de Química Orgánica e Inorgánica, Universidad de Extremadura, Badajoz, Spain*

⁴*Instituto de Nanociencia de Aragón, Universidad de Zaragoza, e Instituto de Ciencia de Materiales de Aragón, CSIC, Zaragoza, Spain.*

⁵*Instituto de Ciencia de Materiales de Aragón (ICMA)& Departamento de Física de la Materia Condensada; CSIC-Universidad de Zaragoza; Zaragoza, Spain.*

clara@unizar.es

Fe₃O₄ nanoparticles with sizes from 5 to 110 nm were prepared by a direct method based on the precipitation of an iron (II) salt (FeSO₄) in the presence of NaOH and a mild oxidant (KNO₃) at 90° C in a mixture of solvents water/ethanol.[1] Particle size was controlled by changing the concentration of the iron salt leading to magnetite nanoparticles with narrow size distributions. Several samples were further coated with silica to obtain a core/shell structure.

The efficiency of the nanoparticles as heating agents was assessed through specific power absorption (SPA) measurements as a function of particle size and shape. The results show a strong dependence of the SPA with the particle size, with a maximum around 30 nm, as expected for a Néel relaxation mechanism in single-domain particles. The SiO₂ shell thickness was found to play an important role in the SPA mechanism by hindering the heat outflow, thus decreasing the heating efficiency. Both good heating efficiency and surface functionality for biomedical purposes were attained for the thinnest SiO₂ coatings of about 1 nm.

In order to test the efficiency of the synthesized nanoparticles as MRI contrast agents NMR relaxation measurements were performed in a top-bench equipment, operating a 1.5 Tesla and 37 °C. T₁ and T₂ relaxation times were determined for several magnetite concentrations in water-stable suspensions. Both spin-lattice and spin-spin relaxation show a monoexponential decay. For some of the samples the obtained values of the r₂ relaxivity are close to those of commercial MRI contrast agents.

References:

[1] Verges M.A., Costo R., Roca A.G., Marco J.F., Goya G.F., Serna C.J. and Morales M.P *J. Phys. D: Appl. Phys.* **41** . (2008) 134003.

Figures:

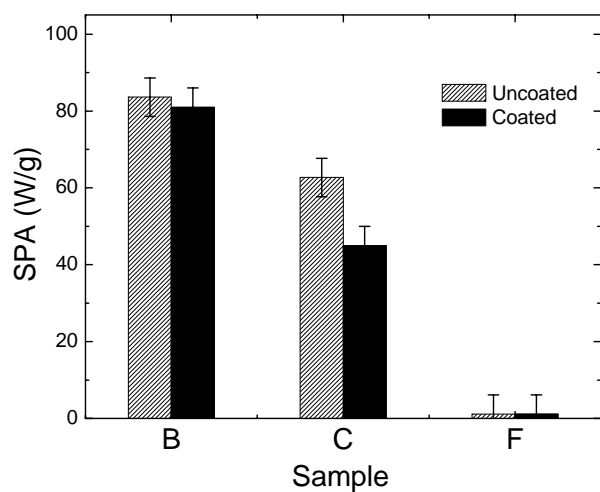


Figure 1: SPA of single domain (BSi and CSi) and multidomain (FSi) silica coated nanoparticles. SPA for pure magnetite was 95 W/g.

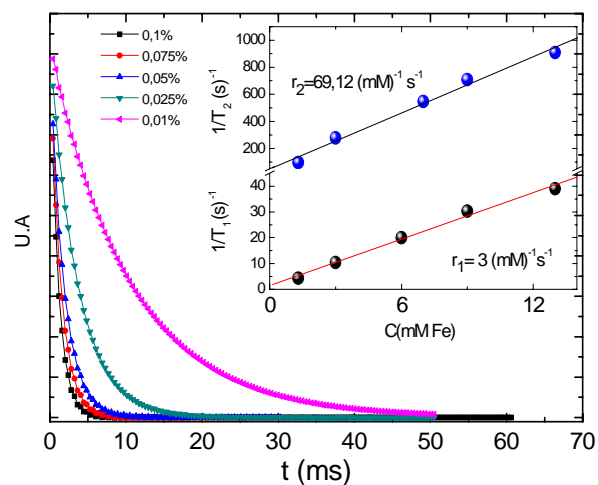


Figure 2: T1 Relaxation time for a sample with $d = 5$ nm. Inset: relaxivity values.

Ultrasensitive microsusceptometer for magnetic AC measurements at very low temperatures and high frequencies

M.J. Martínez-Pérez^a, J. Sesé^b, F. Luis^a, D. Drung^c, C. Assman^c, and T. Schurig^c

*^aInstituto de Ciencia de Materiales de Aragón and Dep. de Física de la Materia Condensada.
Zaragoza, Spain*

*^bInstituto de Nanociencia de Aragón and Dep. de Física de la Materia Condensada.
Zaragoza, Spain*

^cPhysikalisch Technische Bundesanstalt (PTB) Berlin, Germany

pepam@unizar.es

The aim of this work is the fabrication of an ultra sensitive SQUID susceptometer capable of operation under extreme conditions of high frequency and low temperatures. A huge bandwidth of about 1 MHz is expected and the sensor will be placed inside the mixing chamber of a dilution refrigerator ($T \approx 13$ mK). With this instrument, measurements of AC susceptibility will be done to search for quantum phenomena at very low temperatures.

For this purpose 2-stage SQUIDS sensors fabricated at PTB-Berlin will be used [1]. These are 3 mm×3 mm sized chips consisting of an ultra low noise single SQUID read out by a 16-SQUID array (Fig. 1). At $f = 100$ kHz and $T = 4.2$ K, the typical flux noise is about $S_\phi^{1/2} \approx 800$ n Φ_0 /Hz^{1/2}. It turns out that doing one simple modification in the wire scheme of the chip, a susceptometer directly coupled to the SQUID is obtained. This implies an enhancement of the sensitivity since the sample is placed over the sensor and no extra connections or inductive couplings are needed.

Two kinds of sensors can be produced. For the first type, the estimated sensitivity is $s_\mu \approx 10^4$ μ_B /Hz^{1/2} and the pick-up coil is big enough (1mm×360micron) to enable an easy deposition of samples i.e. gluing crystals with vacuum grease. For the second type, the sensitivity is enhanced since there is no inductive coupling between the pick-up coil and the SQUID ($s_\mu \approx 10^3$ μ_B /Hz^{1/2}) and the sample area is much smaller ($\approx 60 \times 180$ micron) so they are ideal for deposition of small magnetic particles using the dip-pen lithography technique.

The modification of the chips is carried out at the Instituto de Nanociencia de Aragón (INA, Zaragoza) by Focused Ion Beam etching and deposition. In both cases, the modification consists in the inversion of the current sense of one of the coils coupled to the SQUID. That turns out to be simple because of the existence of wire crossovers between the washers (Fig. 2).

The sensors have been already tested inside the mixing chamber of a dilution refrigerator (Leiden Cryogenics) down to 15 mK. The base temperature is not significantly

altered by the presence of the devices and the thermalization of samples is ensured since they are immersed in the ^3He - ^4He mixture. In this experiment, a crystal of molecular magnets (ErW_{10}) was used for ac-susceptibility measurements up to 1 MHz applying an ac-field of 5 mOe (Fig. 3). For low frequencies, the resolution is limited by the $1/f$ noise of the SQUID. As follows from the fluctuation-dissipation theorem, measurements of the noise curves also enable us to see the peak associated with the superparamagnetic blocking of the susceptibility (Fig. 4).

References:

- [1] D. Drung, C. Aßmann, J. Beyer, A. Kirste, M. Peters, F. Ruede, and Th. Schurig, IEEE Transactions on Applied Superconductivity, **17**, 699-704 (2007).
- [2] E. S. Sadki, S. Ooi and K. Hirata, Applied Physic Letters, **85**, 6206 (2004).

Figures:

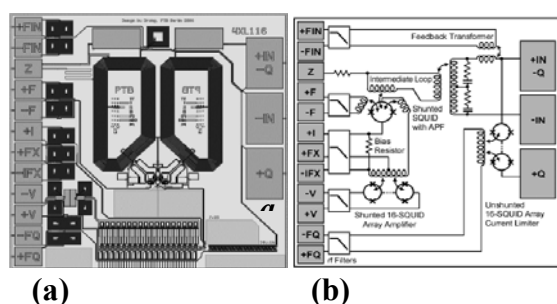


Fig. 1: (a) Chip layout (b) Simplified scheme of the circuit [1]. Modifications in order to obtain the susceptometer are carried out within the Intermediate loop.

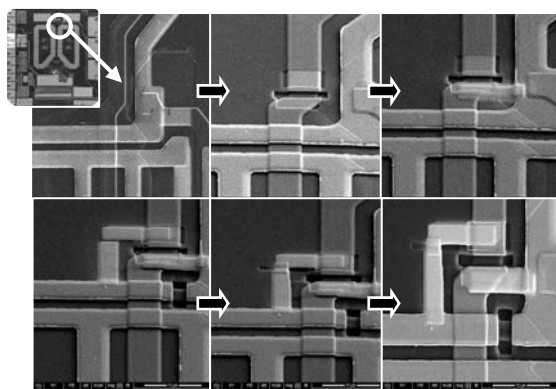


Fig. 2: SEM images of the modification process. The crossover between the two transformer coils is inverted by FIB etching and deposition of W. The material deposited is actually a composite material of W, C and Ga, and it is superconducting below 5.2 K [2].

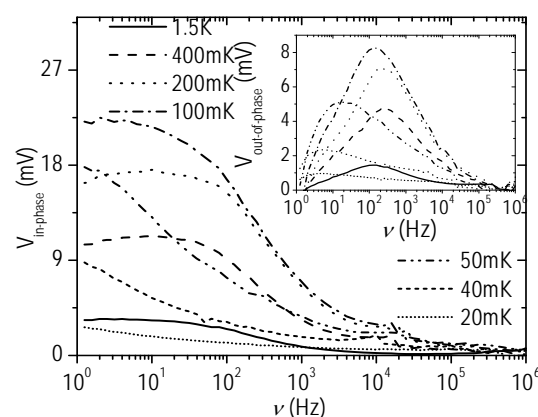


Fig. 3: In-phase and Out-of-Phase (inset) frequency response of the ErW_{10} crystal.

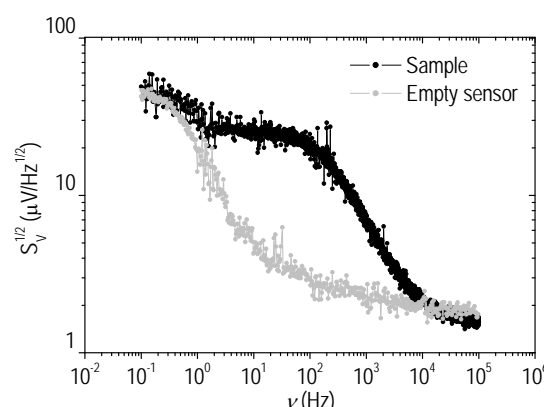


Fig. 4: Voltage noise of the system (grey line). When the ErW_{10} crystal is present (black line) the peak associated with the superparamagnetic blocking of the susceptibility is visible.

SIZE CONTROLLED DEPOSITION OF PARTIALLY OXIDIZED FE AND TI NANO-CLUSTERS BY A HIGH VACUUM SPUTTERING GAS AGGREGATION TECHNIQUE.

R. Martínez- Morillas, J. Sánchez-Marcos, A. de Andrés and C. Prieto.

Instituto de Ciencia de Materiales de Madrid, Consejo Superior de Investigaciones Científicas. Cantoblanco, 28049 - Madrid (Spain).

In the field of nanomaterials research, the common objective for different metallic and non metallic elements is to understand the evolution from atoms or molecule to materials with bulk properties. So, it is interesting the identification of various size-control parameters to allow controlled preparation of nanoclusters with tailored size and shape distribution.

Nowadays the study of magnetic granular systems, such as magnetic nanoparticles embedded in a matrix and core-shell structures, is a very intriguing area in the field of the materials science at the nanometric scale [1]. The magnetic properties are greatly determined by structural features, such as particle size. Thus, the control of the particle dimensions will allow us to 'tune', to some extent, the magnetic behaviour of the system. Nevertheless, sizes below a critical value lead to superparamagnetic behaviour, which limits the application of these materials. Exchange anisotropy between a antiferromagnetic and a ferromagnetic materials overcomes this limitation.

On the other hands, the development of new optoelectronics devices based on organics materials has promote the study among the properties of nanomaterials, the movement of electrons and holes in semiconductor nanomaterials is primarily governed by the well-known quantum confinement, and the transport properties related to phonons and photons are largely affected by the size and geometry. The high surface area brought about by small particle size is beneficial to many TiO₂ based devices, as it facilitates interaction between the devices and the interacting media. Thus, the performance of TiO₂ based devices is largely influenced by the sizes of the TiO₂ building units at the nanometer scale [2].

In previous works, we have prepared nanocrystalline iron thin films by sputtering at very low substrate temperatures during growth. The shrink in the grain size observed by using x-ray absorption and diffraction techniques [3], while lowering the temperatures, is decisive in the interpretation of the changes of magnetic properties of the samples. Films prepared at near-room temperatures present a common thin film magnetic behaviour, whereas the films prepared at lower behaves like a granular system formed by a distribution of particle blocking temperatures [4].

Partially oxidized iron and titanium thin films were prepared by using a magnetron sputtering source placed inside a high pressure aggregation chamber. This preparation technique involves typical magnetron sputtering vaporization with aggregation in a high pressure (1e-1 mbar) gas to form cluster. After that process, channelling the clusters, through an aperture to the low pressure main deposition chamber, it is possible to fabricate films form made up by nanometric clusters (Fig. 1 shows an iron film deposited under these conditions) and even to combine it with another deposition technique or with an in situ controlled oxidation after deposition.

The distribution of the cluster size can be changed by controlling the residence time within the aggregation zone [5]. In order to study the physical and morphologic properties of the nanometric clusters, films of clusters with different sizes have been

deposited after varying systematically some parameters. Such parameters are the aggregation length, distance between the aggregation chamber magnetron and aperture between chambers, the He/Ar atmosphere ratio and its pressure in the aggregation region. Clusters size distribution has been characterized by Atomic Force Microscopy as a function of different deposition parameters. Finally, a study of the nanometric clusters size dependence of optical properties, in titanium oxide, and magnetic properties, in iron oxide, has been carried out.

References

- [1] F.J. Himpsel, J.E. Ortega, G.J. Mankey and R.F. Willis, *Adv. Phys.* 47, 511 (1998).
- [2] Xiaobo Chen, Samuel S. Mao, *Chem Rev* 107, 2891-2959 (2007)
- [3] F. Jiménez-Villacorta, A. Muñoz-Martin and C. Prieto, *J. Appl. Phys.* 96, 6224 (2004).
- [4] F. Jiménez-Villacorta, Y. Huttel, A. Muñoz-Martín, E. Román and C. Prieto, *J. Appl. Phys.*, 101, 113914 (2007); and F. Jiménez-Villacorta and C. Prieto, *J. Phys. Condens. Matter.*, 20, 085216 (1-10) (2008).
- [5] H. Haberland, M. Karrais, M. Mall, *Z. Phys. D* 20, 413 (1991)

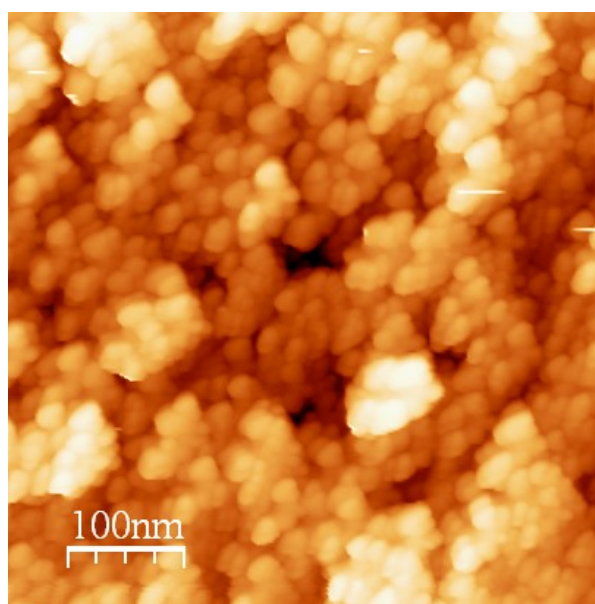


Fig 1.

Influence of gamma irradiation on carbon nanotube/reinforced ultra high molecular weight polyethylene

P. Castell^{1}, M.J.Martínez-Morlanes², V. Martínez², A. Benito¹, W. Maser¹, M.T. Martínez¹, J.A. Puértolas³*

¹Dept. of Carbon Nanostructures and Nanotechnology. Instituto de Carboquímica-CSIC. Zaragoza. Spain

²Dpto. Materials Science and Technology. I3A- University of Zaragoza. Zaragoza. Spain

³Instituto de Ciencia de Materiales de Aragón. Universidad de Zaragoza-CSIC. Spain.

**castell@icb.csic.es*

Ultra high molecular weight polyethylene (UHMWPE) is a polymer with good mechanical and tribological performance used in industrial applications such as bearings, gears and seals. UHMWPE remains also as the most relevant material used in total joint replacement, due to its biocompatibility in addition to its high wear resistance, low friction coefficient and suitable stiffness, toughness and fatigue resistance [1]. In the search for a method to improve the former properties, the incorporation of reinforces to UHMWPE such as carbon fibers, glass, etc has been used to enhance the performance, without reasonable success. The initial biocompatibility of the nanotubes (CNTs) and its exceptional properties allows considering the nanotubes reinforcement like a good option. From an orthopaedic point of view, the improvement in the mechanical properties and tribological properties of UHMEPE could extend the lifespan of the prostheses and reduce the thickness of some polyethylene components with a better function. On the other hand, gamma irradiation is a technique used by the orthopaedic manufacturers for introducing crosslinking among the polymeric chains, by means of the free radical arisen during the irradiation process. Our approach in this work is that these radicals might react with the nanotubes present in the polymer matrix improving the transfer of properties from the CNTs to the matrix. This way we keep the benefit of the gamma irradiation concerning to the improvement of the wear resistance associated to the crosslinked matrix together with a better interaction between the nanotubes and the UHMWPE, that interaction may improve the load transmission with the subsequent increase in the mechanical properties. The assessment of this hypothesis is the content of this abstract.

UHMWPE/MWNTs composites were prepared in a two way approach, first dispersing the nanotubes in either ethanol or vitamin E using ultrasonication and later incorporating the UHMWPE using a ball milling process. UHMWPE/CNT probes were obtained by hot pressing in a thermo-compression cell (Perkin Elmer) during 15 minutes at 175 °C under 10 MPa. The non irradiated composites were denoted like PE (raw material), PE-CNT (blending without dispersant), PE-CNT-VE (vitamin E like dispersant) and PE-CNT-ET (ethanol like dispersant). Several PE and PE-CNT-ET specimens were gamma irradiated at 90 kGy doses.

The crystallinity and the glass transition temperatures of the obtained nanocomposites were calculated by DSC (Table 1). Uniaxial tensile test were carried out at 5 mm/min for obtaining the mechanical parameters, the stress-strain curves up to the fracture are plotted in Figure 1 for each material group (n=4). Analysis of the fracture surface was also obtained by SEM.

The results point out that the presence of CNTs increases up to 10 % the crystallinity of the matrix, in accordance with the idea that the nanotubes act like gens of nucleation. This fact does not agree with the recent Zoo's work [2], where the CNTs provide reinforcement without significant structural changes.

Table 1. Thermal parameters for the raw UHMWPE and NCT's/UHMWPE composite with 1% CNT's concentrations made using different dispersant for 1% CNT's.

Material Group	Tf	Hf (J/g)	Tc (°C)	Hc (J/g)	Cristalinidad (%)
PE	136	155.9	114.9	128.7	44.4
PE-CNT	133.9	142.7	118	143.8	49.6
PE-CNT-VE	136.4	159.3	115.9	158.5	54.7

Stress-strain curves were obtained for all the prepared materials and no significant differences appear in the non irradiated specimens with CNTs at exception of the fracture strain. However, PE-CNT material presents lower values of yield stress and the reinforced specimens are less stiffness than the virgin material due probably to the consolidation defects arisen during the thermo-compression, such as observable in the SEM microfractographies. Gamma irradiated composites at 90 kGy were also measured in uniaxial tensile test and the results compared to the virgin UHMWPE. The irradiated nanocomposites showed a higher elastic modulus and an increase in the yield stress, as expected, nevertheless there are no significant differences between the irradiated samples with and without CNTs. The observed increase in the modulus and yield stress is associated with the crosslinking induced by the gamma irradiation. Although no significant differences are noticed it is expected that the generated radicals may react with the CNTs. In order to proof that, nanocomposites containing higher loadings of CNTs will be prepared, irradiated and their properties evaluated.

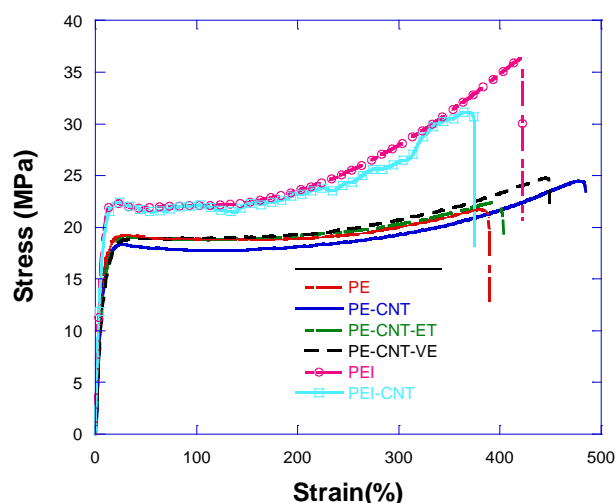


Figure 1. Stress-strain curves for virgin and NCT's/UHMWPE composites at 1%.

References:

- [1] E. Gómez-Barrena, J.A. Puértolas, L. Munuera, Y.T. Konttinen. Acta Orthopaedica 79 (2008) 832-840.
- [2] Y-S. Zoo, J.W. An, D.P. Lim, D.S. Lim, Tribological letters 16 (2004) 305-309.

CARBON NANOTUBE INTEGRATION FOR BIO-SENSING APPLICATIONS

I. Martin-Fernandez, G. Gabriel, G. Rius, R. Villa, E. Lora-Tamayo, F. Perez-Murano, P. Godignon

Insto. de Microelectrónica de Barcelona, Campus UAB, Cerdanyola del Vallès, Spain
inigo.martin@cnm.es

In this contribution we present a technology for batch fabrication of high density of chemical vapour deposition (CVD) grown carbon nanotube (CNT) modified bio-compatible Pt electrodes by using Pt as the CNT catalyst material.

Bio-compatible impedance needles and multi electrode arrays (MEAs) were simultaneously fabricated by using standard microtechnologic technologies at wafer scale as described in ref. [1]. Selective growth of the CNTs was performed in two steps. A 15 nm SiO₂ layer and a 4 nm Pt layer were respectively deposited at wafer scale and selectively on the electrodes as CNT catalyst bi-layer. CNTs growth took place at a rapid thermal CVD system at 800 °C in a H₂ and CH₄ ambience. Device final fabrication step consisted in removing the 15 nm SiO₂ layer on the connection pads with a HF based solution.

Photographs in Fig. 1 showing homogeneous selective growth of CNTs at a 4-inch wafer scale and SEM imaging (Fig. 2) confirm high density growth and vertical alignment of the CNTs. TEM characterization of the CNTs demonstrated they were multi-walled and that there were covered by an amorphous carbon layer.

Two different electrical measurements on the electrodes were performed. Two probe measurements between the different layers forming the electrode (Fig. 3) demonstrate the CNT layer constitutes the main part of the series resistance since directly contacting the electrode in areas where the CNTs had been removed provides lower series resistance. Impedance measurements comparison for bare Pt electrodes and a CNT modified electrodes (Fig. 4) do not show an impedance improvement with respect to bare electrodes.

Based on the electrode improvement when directly depositing single-walled CNTs on the electrode [2] and because of the amorphous carbon surrounding the CNTs inhibits electron transfer from the electrolyte to the CNT layer, we believe that by optimizing CNT synthesis conditions we will achieve an improvement of the characteristic of the electrode.

Despite the fact that the impedance of the modified electrodes has not been improved, the technological process for CNT integration into devices for bio-sensing is demonstrated.

[1] Gabriel, G., I. Erill, J. Caro, R. Gómez, D. Riera, R. Villa, and P. Godignon, **Microelectronics Journal** 38 (2007),406-415.

[2] Gabriel, G., R. Gomez, M. Bongard, N. Benito, E. Fernandez, and R. Villa, **Biosensors and Bioelectronics** (2008), doi:10.1016/j.bios.2008.09.036.

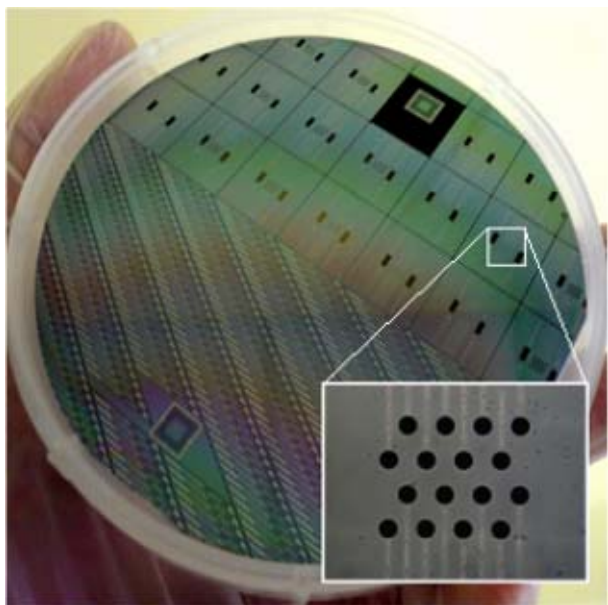


Fig. 1: Impedance needles and MEA 4 inch wafer after CNT integration. Dark areas are the places where CNT have been selectively grown.

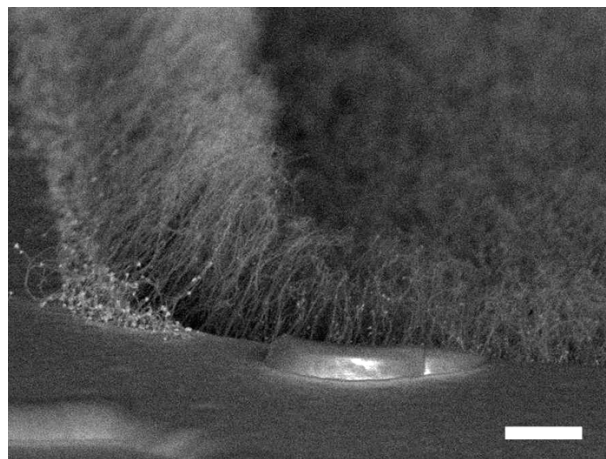


Fig. 2: Tilted SEM image of an electrode. Vertically aligned CNTs grow from inside the electrode

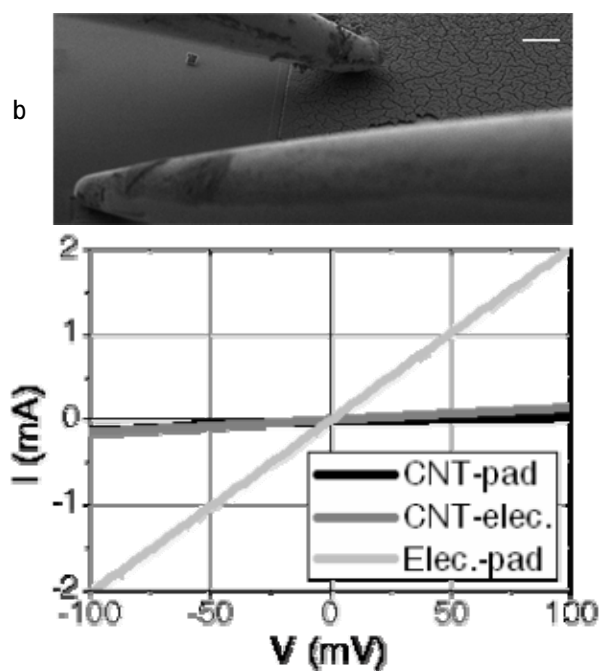


Fig. 3: Two probe electrical measurements between the different layers forming the electrode - CNT layer-SiO₂ layer (CNT-pad); CNT layer-electrode (CNT-elec.); electrode-SiO₂ layer (Elec.-pad) - were performed inside an SEM chamber in order to control the positioning of the probes not to damage the layers.

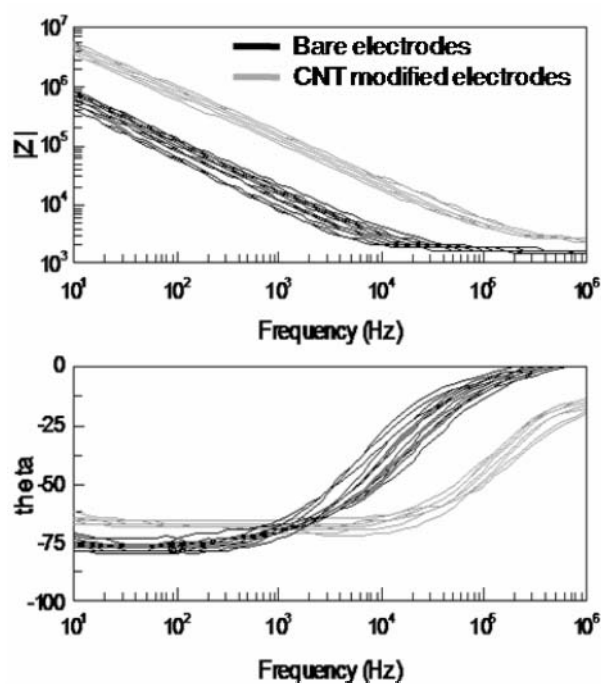


Fig. 4: Impedance measurements on the CNT modified electrodes show an impedance increase with respect to bare electrodes.

USE OF RED-EMITTING OLEDs FOR ILLUMINATION OF PLANTS GROWING IN THE GREENHOUSE

*J. Martín-Gil, L.M. Navas-Gracia, S. Hernández-Navarro,
P. Martín-Ramos, P. Chamorro-Posada*

*Department of Agricultural and Forestry Engineering, ETSIA, Avda de Madrid 57, 34004 Palencia
and Department of Signal Processing, ETSIT, Campus Miguel Delibes, Valladolid*

jesusmartingil@gmail.com

Resume: An OLED with a configuration of [glass/ITO/PEDOT:PSS/PVK:Ln³⁺(fluorinated β -diketonate)₃(*polypy*)/Ca/Al] which emits red light has been proposed for illumination of plants growing in greenhouse

Detailed description:

In horticultural plant production greenhouses are often equipped with artificial light sources to expand the day length in order to grow plants over an extended time period of the year. This allows the producer to bring plants to the market on demand. Since room in greenhouses is limited, it is desirable to grow some plants or seeds in compact racks, in which plants are grown in shelves where several shelves may be arranged on top of each other. Since such an arrangement shields most of the daylight from the plants in the lower shelves, artificial lighting is necessary. Today several types of plant lamps are used in greenhouses: incandescent light bulbs, Sodium high-pressure light bulbs, fluorescent gas discharge lamps, etc. All these light sources have the drawback of being punctual sources and not distributing light as homogeneously as sunlight.

In our method for growing plants, light sources using an organic electroluminescence sheet (OLEDs) have the advantage of being suitable of large area manufacturing. To achieve a generous growth of the plant, the light emitted by the group of OLEDs should consist of approximately 80% to 90% red light and 10% to 20% blue light.

In our Project we carried out I+D+i on new red-emitting OLEDs with lanthanide(III) complexes as electroluminescent materials. With the new materials, based on eight-coordinated praseodymium(III), neodymium(III), erbium(III) and ytterbium(III) β -diketonate complexes of the type [Ln³⁺(fluorinated β -diketonate)₃(*polypy*)], where *polypy* is either 2,2'-bipyridine, 5-nitro-1,10-phenantroline or bathophenanthroline, OLEDs with the following configuration: [Glass/ITO/PEDOT:PSS/PVK:Ln³⁺(fluorinated β -diketonate)₃(*polypy*)/Ca/Al] have been manufactured. For the Er³⁺ device we evidenced excitation maximum at 472 nm y emissions at 700 nm y 1538 nm.

Market:

Since 2004 three foreign patents have explored the use of OLED in the horticultural plant production greenhouses market. They are the entitled: Illuminating device (ref WO 2008078277 20080703); Controlling device for a greenhouse (ref. WO 2008068699 20080612 and US 2005/0252078 A1); and Plant growth device (ref WO 2008047275 20080424 and JP 2004/321074 A). Nevertheless, none of them has claimed, as we have, the syntheses of a specific red-emitting OLED for above purposes. We hope that commercial firms pay attention to our research results in this field

References:

- [1] Chamorro-Posada P, Martín-Gil J, Martín-Ramos P, Navas-Gracia LM: “Fundamentos de la tecnología OLED”. Universidad de Valladolid, 2008. Dep. Legal: VA-932-2008.
- [2] Martín-Ramos P, Chamorro-Posada P, Ramos-Silva M, Matos-Beja AM y Martín-Gil J: “Lanthanide complexes containing fluorinated diketonates and polypyridyl ligands as promising materials for use in NIR-OLED devices” al 2nd Meeting on Organic Photovoltaic and Optoelectronic Devices. Institut Català D’Investigacion Química and Universitat Rovira i Virgili. Tarragona, 14-15 April 2008.
- [3] Martín-Ramos P. “Nuevos dispositivos NIR-OLEDs en electrónica de telecomunicaciones”. Proyecto Fin de Carrera. Ingeniería de telecomunicación, ETSII, Universidad de Valladolid, 16 de julio de 2008.

Figures:



Red-emitting device, suitable for large area manufacturing, promising for use in illumination of plants in greenhouses.

Synthesis, characterization and optical properties of luminescent nanocrystals

Rosa Martin-Rodríguez, Rafael Valiente

Departamento de Física Aplicada. Universidad de Cantabria.
Avda de los Castros s/n 39005, Santander (SPAIN)

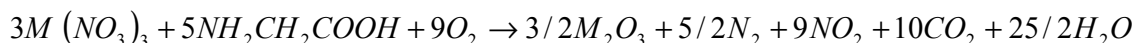
rosa.martin@unican.es

Introduction

Upconversion (UC) is an efficient way to convert two or more low energy photons to obtain higher energy emitted light from excited energy levels. UC materials have attracted significant attention as potential solid state visible lasers, biological fluorescence labels or in order to improve solar cells efficiency [1,2]. It is well known that Yb^{3+} is an excellent UC sensitizer. The ability of this ion to induce UC is based on the high oscillator strength of the $\text{Yb}^{3+} {}^2\text{F}_{7/2} \rightarrow {}^2\text{F}_{5/2}$ transition, which is located in the NIR just in the range of inexpensive diode lasers.

Experimental

Rare earth ions doped nanocrystalline oxide materials have been prepared using different synthesis procedures. Nanosized cubic Y_2O_3 : Er^{3+} , Yb^{3+} crystals have been obtained by both mechanochemical synthesis in a planetary ball mill [3] and the following combustion reaction [4],



$\text{Gd}_3\text{Ga}_5\text{O}_{12}$ (GGG) and $\text{Y}_3\text{Al}_5\text{O}_{12}$ (YAG) nanocrystalline powders doped with different Yb^{3+} and rare earth combinations have been prepared by Pechini's method [5]. The SiO_2 coating of the as-synthesized nanoparticles has been carried out following the Stöber method [6].

The nanocrystalline size has been estimated from X-ray diffraction (XRD) diagrams and transmission electron microscopy (TEM) measurements. Optical properties such as emission and excitation spectra or lifetime measurements have been studied. A detailed investigation of the spectroscopy and the excited state dynamics is extremely interesting in order to determine the mechanisms involved in the UC processes.

Results

From XRD and TEM measurements it can be seen that with all synthesis procedures, ball milling, combustion and Pechini's method, nanoparticles of about 50 nm in size are obtained (Fig 1). All prepared samples show intense UC emission after IR excitation (see Fig. 2 as an example). The UC processes involved in Y_2O_3 : Er^{3+} , Yb^{3+} can be ascribed to GSA/ESA (Ground-State-Absorption / Excited-State-Absorption) or GSA/ETU (Ground-State-Absorption / Energy-Transfer-Upconversion). However, the

situation is completely different for Tb^{3+} and Eu^{3+} ions which have no intermediate levels resonant with Yb^{3+} . SiO_2 coating preserves the nanoparticles from surface contamination and does not affect the optical properties. This is relevant for the eventual functionalization of the nanocrystals.

References

- [1] M. Nyk, R. Kumar, T. Y. Ohulchanskyy, E. J. Bergey, and P. N. Prasad, *Nano Lett.*, **8** (11) (2008) 3834.
- [2] T. Trupke, A. Shalav, B. S. Richards, P. Würfel, M. A. Green, *Solar Energy Mat. & Solar Cells*, **90** (2006) 3327.
- [3] S. Morup, J. Z. Jiang, F. Bodker and A. Horsewell, *Europhys. Lett.*, **56** (3) (2001) 441.
- [4] T. Ye, Z. Guiwen, Z. Weiping, X. Shangda, *Mater. Res. Bull.*, **32** (5) (1997) 501.
- [5] M. P. Pechini, US Patent No 3.330.697, July 11 (1967).
- [6] Q. Lü, A. Li, F. Guo, L. Sun and L. Zhao, *Nanotech.*, **19** (2008) 205704.

Figures

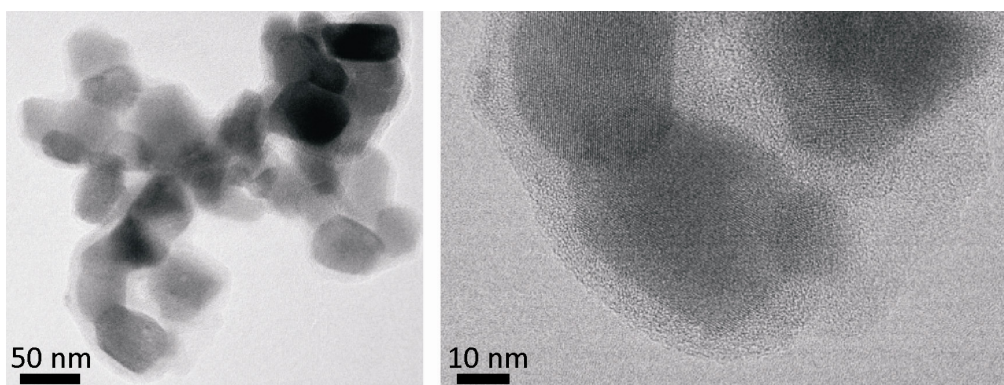


Fig. 1: TEM image of Y_2O_3 : 2% Er^{3+} , 1% Yb^{3+} prepared by combustion after SiO_2 coating.

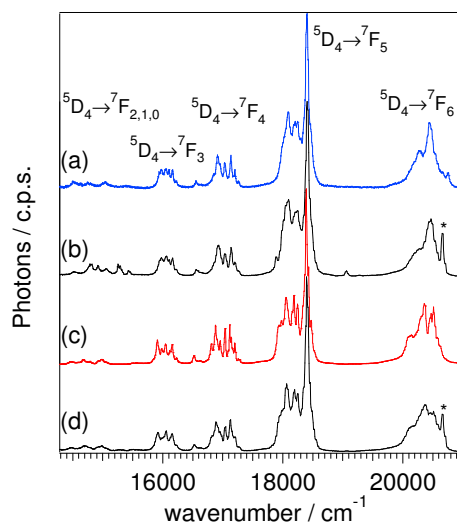


Fig. 2: RT luminescence spectra of GGG: 2% Tb^{3+} 5% Yb^{3+} exciting at 37040 cm^{-1} (a) and 10250 cm^{-1} (b). RT emission spectra of YAG: 2% Tb^{3+} 5% Yb^{3+} exciting at 37040 cm^{-1} (c) and 10250 cm^{-1} (d).

CANCER CRUSADE-USE OF NANO-TARGETTED DELIVERY OF CaMK II IN SPECIFIC LUNG EPITHELIAL CELLS OF THE LUNG.

M. Sri Harsha¹, Srideepika.S

¹harshameghadri@gmail.com

Rajalakshmi Engineering College

Rajalakshmi Nagar, Thandalam, Chennai 602105

INDIA

Abstract:

Nanotechnology holds the key for crusade against lung cancer, which is a prominent disease amongst varied age groups. This article gives a brief hypothesis on cancer cure using fullerene C₆₀ or Colloidal Gold nano-particles for targeting CamKII towards cancer cells. **p53** (also known as **protein 53** or **tumor protein 53**), is a transcription factor encoded by the *TP53* gene. p53 is important in multicellular organisms, where it regulates the cell cycle and thus functions as a tumor suppressor that is involved in preventing cancer. When the p53 is bound to certain proteins for e.g. MDM2 protein gets nonfunctional which leads to cancer and tumor. **Pirh2**, a gene regulated by p53 that encodes a RING-H2 domain-containing protein with intrinsic ubiquitin-protein ligase activity. Pirh2 physically interacts with p53 and promotes ubiquitination of p53 independently of Mdm2. Expression of Pirh2 decreases the level of p53 protein and abrogation of endogenous Pirh2 expression increases the level of p53. Phosphorylated Pirh2 is far more unstable than its unphosphorylated form. **Calmodulin-dependent kinase II** (CaMK II) phosphorylates Pirh2 on residues Thr-154 and Ser-155. Phosphorylation of Pirh2 appears to be regulated through cell cycle-dependent mechanism. CaMK II-mediated Pirh2 phosphorylation abrogates its E3 ligase activity toward p53. This Pirh2 expression was higher in 27 of 32 (84 percent) of **human lung cancers**. Thus, by using specifically targeted nano-particles containing CaM KII encapsulated to the lung epidermal cells the ligase activity of Pirh2 can be effectively tackled thereby improving the levels of p53 protein.

Keywords: human lung cancers, CaM KII, p53, fullerene C₆₀, colloidal gold nano-particles, Pirh2, TP53, RING-H2

COMBINED METHODS IN MAXIMIZING DNA LOADING ON TO GOLD NANOPARTICLES

Megson, Z.; Vázquez, S.; Casals, E; Comenge, J.; Puentes, V.F.

Collaborators: Department of Organic Chemistry (UAB)

Institut Català de Nanotecnologia (ICN), Inorganic Nanoparticles Group

08163 Campus UAB Bellaterra Spain

93 581 48 65 – 93 592 99 65

icn@uab.es

An enormous amount of effort is being put into the development of effective ways of conjugating biomolecules on to the surface of nanoparticles (NP). Our design of NP - organic molecule conjugates pretends to control both properties of the inorganic core and those of the coating molecules. Conjugation refers to the attachment achieved by a chemical reaction between function groups of the inorganic nanomaterial and those of the biomolecules.

For biomedicine the nanomaterial used must be biocompatible and nontoxic, for which colloid gold is generally preferred to synthesize small spherical-like particles. These are then functionalized with the different biomolecules, which could be proteins, such as enzymes or antibodies; sequences of nucleotides, such as DNA or RNA; lipids and sugars, or a combination of these molecules. Possible applications range from simple analytical tools to complicated drug delivery, control of the immune system, and use in therapies. In the case of nucleotids, the characteristic base pairing could be used in diagnostic in the detection of specific sequences and mutations¹; in determining DNA binding proteins and intercalators; control of gene expression using antisense RNA²; DNA scaffolds³; amongst others.

The conjugation of DNA to gold nanoparticles is mediated by a thiol group synthetically added on to the 5'end of the single strand sequence. This is the commonly known way of achieving conjugation to gold surfaces. However conjugation of DNA is not as straightforward as simply adding these modified strands to a nanoparticle solution.

Following the work of A.Paul Alivisatos and Chad A. Mirkin on DNA loading onto gold nanoparticles, our procedure is a combination of the two, the main objective being to maximize the coverage of the particles with single strand DNA and to follow the loading process using agarose gel electrophoresis.

The conjugation of nucleotides to AuNPs is specially challenging due to the high affinity of the phosphate DNA backbone for the gold surface which compete with the thiol groups leading to an undesirable wrapping of the NP with the DNA strands, rather than the intended radial conjugation (see figure 1A).

By combining experimental procedures we are optimizing the process as everything is done to minimize non-specific interactions between the DNA strand and the gold surface, by coating with Bis(p-sulfonatophenyl) phenylphosphine dihydrate dipotassium salt, or to break these interactions if they are formed. Ultimately NaCl is used to stretch the strands and allows further conjugation to the exposed surface.

DNA is added once at the beginning and salt is added gradually. After each salt addition, aliquots are taken and characterized by UV-VIS spectrophotometer and ζ -potential to study the increased loading on the surface and the stretching of the strands which increase the particle size. These aliquots are analyzed in agarose gel electrophoresis where

visualization of the progressive coverage is achieved and appears as less migration in the gel every time the salt concentration is increased (see figure 1B).

The kinetics of the loading, followed by a simple electrophoresis where no staining is needed thanks to the presence of high optically active AuNPs, could have straight forward applications in determining interaction of molecules to DNA, and how, and to what extent, they interact affecting the functionalization process. Our hypothesis is that the interaction of DNA binding molecules should modify the process in a simple and reproducible manner.

This work is a presentation of the different procedures used in the synthesis of monodisperse particles of the required size, their functionalization with single strand DNA using a combined method of the different pre-existing experimental procedures, and completed with a selection of experiments using DNA binding molecules.

Amongst the DNA binding molecules tested is cisplatin, a platinum-based chemotherapy drug that works cross-linking DNA strands, used to treat various types of cancers, such as sarcomas, some carcinomas, lymphomas and germ cell tumours.

The project is also a preliminary study in understanding control of the number of strands conjugated, as achieved by Alivisatos, to develop DNA probes.

References:

- [1] Gerion,D.; Chen, F.; Kannan, B; Fu,A.; Parak, W.J.; Chen, D.J.; Majumdar, A.; Alivisatos, A. P.; Anal. Chem. 2003, 75.
- [2] Rosi, N.L.; Giljohann, D.A.; Thaxton, C.S.; Lytton-Jean, A.K.R.; Min Su Han; Mirkin,C.A.; SCIENCE, vol 312, 2006.
- [3] Zanchet, D.; Micheel, C.M.; Parak, W.J.; Gerion,D; Williams, S.C.; Alivisatos, A.P.; J. Phys. Chem B., 2002, 106

Figures:

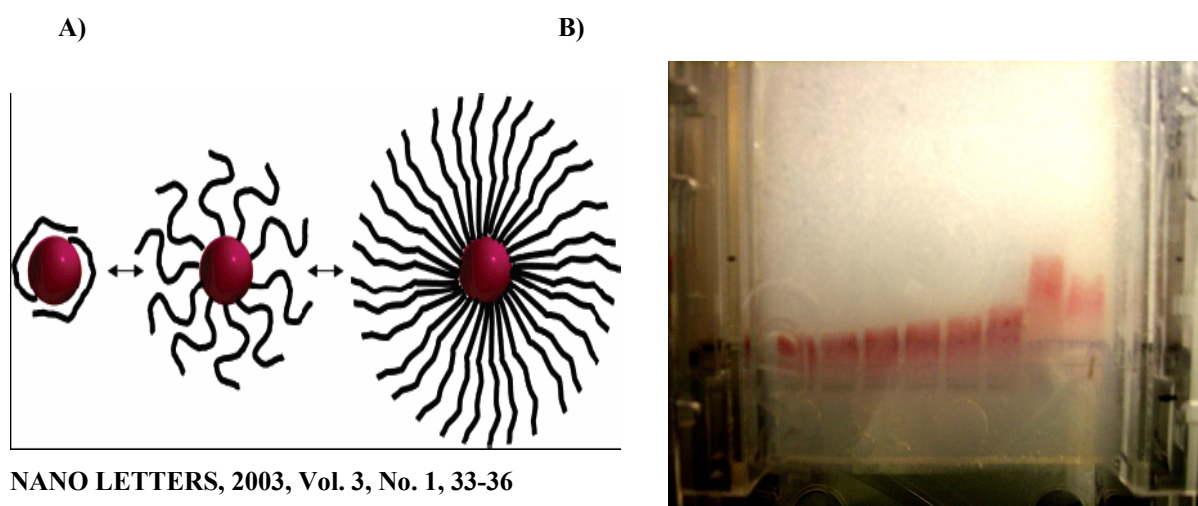


Fig.1. A) The DNA loading protocol minimizes the undesired interactions that stop further conjugation. Avoiding DNA wrapping around the nanoparticle is critical when wanting to maximize coverage. B) From right to left, each aliquot run in the gel (3% agarose) represents an increase in salt concentration during the conjugation process, consequently they migrate less due to an increase in size.

NANOPOROUS SILANE-CONTAINING POLYIMIDES FILMS WITH LOW-DIELECTRIC CONSTANT AND HIGH HEAT-RESISTANT

Shahram Mehdipour-Ataei, Asghar Mohammadpour*

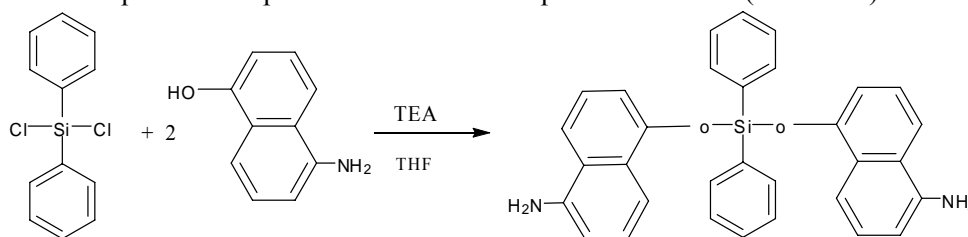
Iran Polymer and Petrochemical Institute, P.O. Box 14965/115, Tehran, Iran, Email:

s.mehdipour@ippi.ac.ir

Polyimide (PI) materials are noted for their high thermal stability, solvent resistance, excellent insulating integrity, good mechanical strength, excellent dimensional stability, low coefficient of friction, high dielectric strength, low dielectric constant, low outgassing, and resistance to creep and wear [1,2]. However, their dielectric constants are not low enough to meet the specifications of intermetal dielectric layers. An approach to lower polymer dielectric constant is to introduce nanoscopic porosity into the polymer film [3,4].

In this research a means of preparing different polyimide nanofoams with pore sizes in the nanometer regime was demonstrated. Microphase separated graft copolymers comprised of a polyimide as the thermally stable matrix and dominant phase with a thermally labile material, PPG, were prepared.

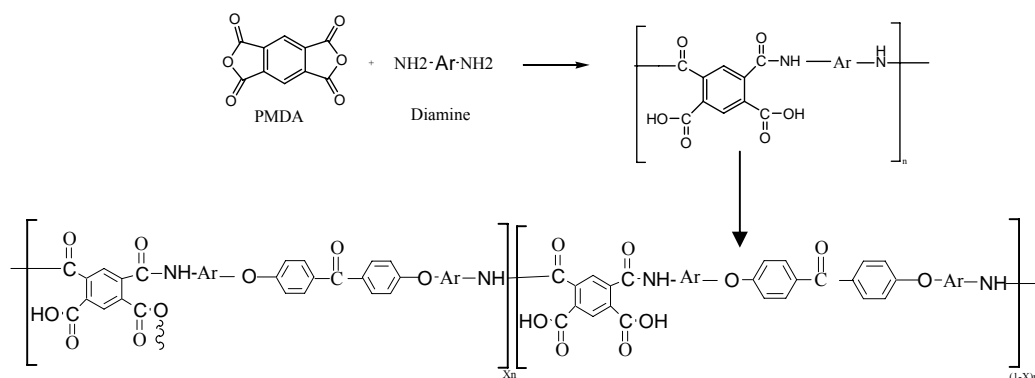
Silicon diamine named bis(5-amino-1-naphthoxy)diphenylsilane was synthesized in one step via a nucleophilic substitution reactions. Diphenyl dichlorosilane was reacted with 5-amino-1-naphthol in the presence of potassium carbonate to produce diamine (Scheme 1).



Scheme 1. Structure of diamine

On the other hand, the functionalized PPG (Mw of 1000 and 2500 g/mol) as a labile oligomer was prepared via reaction of poly(propylene glycol) monobutyl ether with 2-bromoacetyl bromide in the presence of triethylamine (Scheme 2).

The graft copolymers (PAAE-g-PPG) were prepared via poly(amic acid) precursor. Solution polycondensation of pyromellitic dianhydride with the diamine led to preparation of related poly(amic acid)s. Then PPG-Br oligomers were added to the poly(amic acid) solutions in the presence of K_2CO_3 .



Scheme 2. Synthesis of PAAE-g-PPG

After solution casting, the samples were subjected to a heating cycle for effective solvent removal and subsequent imidization. Typically, the samples were heated from 50 °C to 180 °C under nitrogen atmosphere and held at this temperature for 1h to complete the imidization.

The generation of the foam structures was accomplished through decomposition of the PPG by subjecting the copolymer films to the thermal treatment in air. Nanofoams were formed by heating the copolymers at 230 °C in air for 18 h.

The prepared polymers showed high heat-resistant according to the TGA method. To obtain an estimation about the dielectric properties of the thin films, the refractive indices of thin films of foamed samples were measured based on the Maxwell equation ($\varepsilon = \eta^2$, $\Delta \varepsilon = + 0.3$). The dielectric constants of nanofoams were tabulated in Table 1. The smaller dielectric constants of nanofoams in comparison with the related polyimide were mainly due to the incorporation of pores into the final structures.

Tab.1. Refractive indices and dielectric constants of polymers

Polymer ¹	η_i ²	η_o ³	$\Delta\eta$	ε_o ⁴
Si-diamine (h)	1.60	1.56	0.04	2.73
Si-diamine -1000 (n)	1.50	1.45	0.05	2.40
Si-diamine -2500 (n)	1.52	1.46	0.06	2.43

¹h: homopolymer; n: nanopolymer; ² η_i : in-plane refractive index

³ η_o : out-of-plane refractive index; ⁴ ε_o : out-of-plane dielectric constant

The morphology of the prepared nanofoams was studied using SEM and TEM techniques. According to the micrographs the size of the spherical particles was found to be in the nanometer scale (10-40 nm) with a uniform distribution of nanopores and also little interconnectivity between the pores (Fig 1).



Fig. 1. TEM micrographs of Si-diamine -2500 foam

References:

- [1] Kricheldorf, H.R. ; Pakull, R. ; Macromolecules **21**(1998) 551.
- [2] Mehdipour-Ataei, S. ; Sarrafi, Y. ; Hatami, M. ; Eur. Polym. J. **40** (2004) 2009.
- [3] Hedrick, J.L. ; Russell, T.P. ; Labadie, J. ; Lucas, M. ; Swanson, S. ; Polymer **36** (1995) 2685.
- [4] Hedrick, J.L. ; Russell, T.P. ; Hofer, D. ; Wakharker, V. ; Polymer **34** (1993) 4717.

Millifluidic characterizations for the production of macroscopic super tough nanotube fibers.

C. Mercader, A. Lucas, S. Moisan, M. Maugey, A. Derré, C. Zakri, P. Poulin

Centre de Recherche Paul Pascal – CNRS 33600 Pessac, France

mercader@crpp-bordeaux.cnrs.fr

Fibers and yarns are among the most promising forms for using carbon nanotubes (CNTs) on macroscopic scale [1-8]. In analogy with high-performance polymers, fiber spinning allows nanotubes to be preferentially oriented along the main axis of the fibers and then weaved into textile structures or used as cables. A coagulation process was proposed to produce super tough nanotube fibers [2, 8, 9], with a toughness that exceeds that of spider silk or Kevlar®. The process consists of injecting a nanotube dispersion in the co-flowing stream of an aqueous solution of poly(vinyl alcohol) (PVA). As shown on Fig. 1, this can be achieved by injections in co-axial pipes. Coagulation of the nanotubes results from the bridging and adsorption of PVA chains at the interface of the nanotubes. The obtained fibers have a composite structure with large fraction of oriented CNTs. In spite of the exciting properties of the fibers, this process was so far only demonstrated on lab scale and at small production rates.

Up-scaling the method and achieving greater production rates in a continuous process requires a better fundamental understanding of the CNT coagulation mechanisms. In particular, it is critical to know how efficiently the fiber solidifies when the CNTs are in contact with the polymer. Unfortunately, the properties of the coagulating fibers evolve rapidly as they circulate along the pipe of the spinning line. This makes their *in-situ* characterization particularly challenging.

We develop a new method to overcome this challenge and characterize the mechanical properties of the fiber during its solidification. This method consists in stretching the fiber in the elongational flow of the coagulating liquid. The resultant hydrodynamic stress experienced by the fiber can be controlled and used to determine the breaking strength of the fibers.

The elongational flow is achieved by using a pipe with a diameter reduction at a given location (Fig. 2). The diameter reduction induces an acceleration of the surrounding fluid which stretches the fiber. Depending on the geometry of the pipes, flow rates, viscosities of the fluids and residence time of the fiber in the coagulation pipe, we observe distinct behaviours. When the fiber is not yet sufficiently solidified, we found that it breaks regularly into small pieces of uniform length. Analysis of the length as a function of various factors (polymer molecular weight, presence of salt, viscosity, residence time, etc) allows the strength of the fiber to be estimated.

These results provide a better fundamental understanding of the behaviour of nanotubes in polymer solutions. From a technological point of view, they will be of critical help to develop a continuous process for the production of super tough nanotube fibers. Indeed, they will allow the determination of the minimum residence time for the fiber production, the suitable size of the spinning line and the possible production rates.

References:

1. H. Gommans et al., 2000, *Journal of Applied Physics*, 88, 2509.
2. B. Vigolo et al., 2000, *Science*, 290, 1331.
3. H. Zhu et al., 2002, *Science*, 296, 884.
4. K. Jiang et al., 2002, *Nature*, 419, 801.
5. Y. Li et al., 2004, *Science*, 304, 276.
6. L. Ericson et al., 2004, *Science*, 305, 1447.
7. M. Zhang et al., 2005, *Science*, 306, 1358-1361.
8. A. B. Dalton et al., 2003, *Nature*, 423, 703.
9. P. Miaudet et al., 2005, *Nano Letters*, 5(11), 2212-2215.

Figures:



Fig. 1 : Injection of a nanotube dispersion in the co-flowing stream of a PVA.

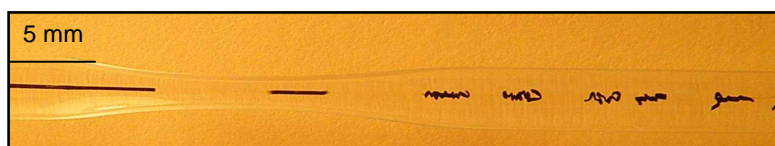


Fig. 2 : Pipe with a diameter reduction , inducing the stretching of the fiber and its breaking.

PROTEIN PATTERNING ON THE MICRO AND NANOSCALE BY THERMAL NANOIMPRINT LITHOGRAPHY ON A NEW FUNCTIONALIZED COPOLYMER

S. Merino^a, A. Retolaza^a, V. Trabadelo^a, A. Cruz^b, P. Heredia^b, J.A. Alduncin^c, D. Mecerreyes^c, I. Fernández-Cuesta^d, X. Borrixe^d, F. Pérez-Murano^d

^a *Fundación Tekniker. Avda. Otaola, 20. 20600 Eibar. Spain*

e-mail: smerino@tekniker.es

^b *Centro Tecnológico Gaiker. Parque Tecnológico Zamudio. Bizkaia. Spain*

^c *Cidetec. Centro de Tecnologías Electroquímicas. San Sebastián. Guipuzkoa. Spain*

^d *Centro Nacional de Microelectrónica, CNM-IMB. Barcelona. Spain*

E-mail: smerino@tekniker.es

The ability to immobilize proteins on sub-micro to nanometric sized areas has become a major challenge for the development of bioengineered surfaces. The ongoing technological advances are partially driven by the aim for broadening the understanding of a variety of surface mediated biological recognition events. Many applications of patterned biomolecules can be enhanced by improving the resolution of the protein features. Smaller feature sizes enable, for example, the fabrication of high density protein arrays for biosensors or proteomic screening, or facilitate studies of cellular interactions with small precisely located clusters of extracellular matrix proteins. A major advantage of nanoimprint lithography (NIL) is that the feature size can be reduced to the nanoscale to create high density arrays, or to control placement of individual proteins, while still retaining high throughput and reproducibility. NIL was used for protein patterning combining high resolution and high density of proteins [1, 2, 3]. L.J. Guo et al [1] developed a technique based on NIL and fluoropolymer surface passivation to avoid protein adsorption and an aminosilane passivation to form a covalent layer with biotin, exploiting later the specificity of the biotin/streptavidin linkage. M. Textor et al. [2] developed a technique for protein patterning combining NIL and molecular assembly patterning by lift-off. H. Schiff et al [3] used NIL and aminosilane deposition followed by lift-off of the sacrificial printable polymer to get streptavidin patterning at the nanoscale. However all these three processes described require the use of a sacrificial printable polymer and vapour deposition of aminosilane, which lead to make the process more complex. The present work shows a new approach: a new bio-functionalized copolymer based on 80% benzyl methacrylate and 20% succinimidyil methacrylate is used as a printable polymer with a great affinity to proteins through the covalent binding between the succinimidyil group and the amino groups of the proteins. It has been used to develop a patterning in the micro and nanoscale of streptavidin protein. Following this approach an enzymatic sandwich immunoassay has been proposed to detect the presence of rabbit IgG protein as analyte. Besides an in situ sandwich, fluorescence based immunoassay has been developed in order to perform specific detection of the analyte using the patterning of the surface.

Stamps with five different gratings in the microscale (ranging from 3.3 μm to 11.3 μm periods and equal line width and space) and in the nanoscale (200 nm lines width spaced some micrometers) were fabricated by UV-Lithography and e-beam Lithography respectively and etched by a combined $\text{SF}_6/\text{C}_4\text{F}_8$ plasma to reach 270 nm in depth. The stamps were imprinted on silicon substrates coated with a 270 nm thick film of the functionalized polymer at 160°C (glass transition temperature of 86°C) and the residual layer was etched by an O_2 plasma. An antiadhesive coating was applied by evaporation of tridecafluoro-(1,1,2,2)-tetrahydrooctyl-trichlorosilane (F_{13} -TCS) to avoid protein adsorption on the silicon areas. These substrates were soaked in a solution of streptavidin (small concentrations of BSA protein were added to avoid non-specific binding) containing the enzyme HRP and streptavidin marked with the fluorescent label Alexa Fluor 488 for ELISA type tests and fluorescence detection

respectively. Figure 1 includes fluorescence detection showing the streptavidin protein patterning on the micro and nanoscale and the low background fluorescence signal.

With the aim of showing the biological functionality of the streptavidin protein once it is bound to the polymer, an immunoassay is proposed to detect the presence of rabbit IgG protein. Different dilutions of rabbit IgG concentration of a stock of 1 mg/ml were used in microstructured samples for fluorescent detection of the fluorescence-labelled antibody specific for IgG, aiming to establish a correlation between IgG concentration and fluorescent signal intensity. The stock was diluted up to 1:5000 (200 ng/ml) in volume and a photomultiplier was used to detect the light emitted by the fluorescent label in order to show the threshold concentration of the IgG that can be detected. A sample without analyte was used as negative control. Figure 2 shows the average values measured of the fluorescence intensity and from these data it can be concluded that the threshold detection is better than 200 ng/ml.

References:

- [1] J.D. Hoff, L.J. Cheng, E. Meyhofer, L.J. Guo, A.J. Hunt. *Nanoletters* 4, **5** (2004) 853.
- [2] D. Falconnet, D. Pasqui, S. Park, R. Eckert, H. Schiff, J. Gobrecht, R. Barbucci, M. Textor. *Nanoletters* 4, **10** (2004) 1909.
- [3] S. Park, S. Saxer, C. Padeste, H.H. Solak, J. Gobrecht, H. Schiff. *Microelectroning Engineering* **78** (2005) 682.

Figures:

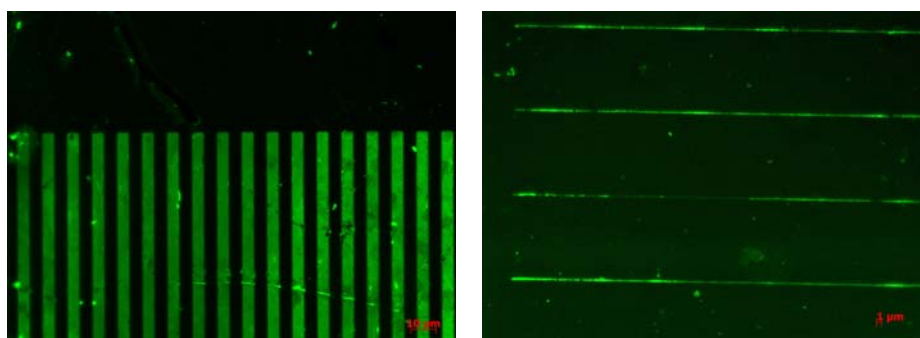


Figure 1. Fluorescence micrographs of patterned samples for a streptavidin concentration of 20 $\mu\text{g/ml}$ containing 0,05 $\mu\text{g/ml}$ of BSA protein. a) Grating with 10 μm period and equal lines and spaces. b) 200 nm width lines.

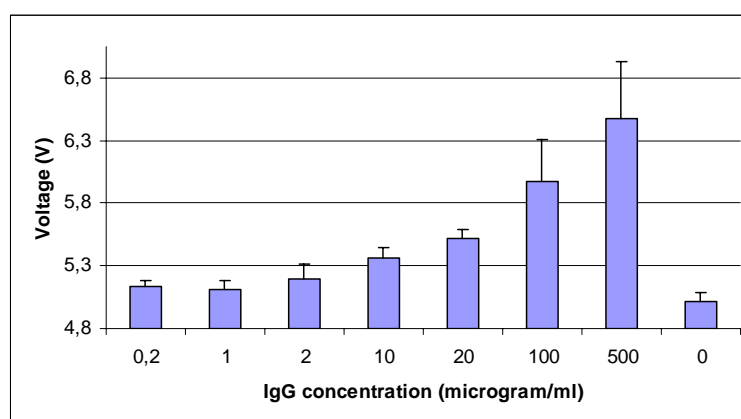


Figure 2. Averaged fluorescent signal measurements as a function of the concentration of the rabbit IgG protein.

Nanofibrillar $\text{Al}_2\text{O}_3\text{-ZrO}_2\text{-Er}_3\text{Al}_5\text{O}_{12}$ eutectics processed by the laser floating zone method

M.C. Mesa, P. B. Oliete, A. Larrea, V. M. Orera
Instituto de Ciencia de Materiales de Aragón (UZ-CSIC)
María de Luna 3, 50018 Zaragoza, Spain
[*mcmesa@unizar.es*](mailto:mcmesa@unizar.es)

Ceramic composites are attracting increasing attention because of the broader diversity and improvement in the properties that can provide as compared with those of the conventional ceramics. Directional solidification of ceramic oxide eutectics allows in-situ composites to be produced. Full density materials are obtained when eutectics are grown from the melt. Moreover, the eutectic growth allows a homogeneous mixing of the phases and a control of the phase size with the solidification rate, following the Hunt-Jackson law: $\lambda \propto v^{-1/2}$, with λ the interphase spacing and v the growth rate. Reduction of the microstructure characteristic size can lead to unusual structural and functional properties.

In the field of structural materials, directionally solidified eutectics based in Al_2O_3 appear as candidates for thermo-mechanical applications at high temperature due to their good creep resistance and microstructure stability [1]. Recently, a strong dependence of the flexural strength of $\text{Al}_2\text{O}_3\text{-Y}_3\text{Al}_5\text{O}_{12}$ eutectic rods with the phase size was reported [2], outstanding mechanical properties being achieved in nanostructured $\text{Al}_2\text{O}_3\text{-Y}_3\text{Al}_5\text{O}_{12}\text{-ZrO}_2$ eutectics [3].

The application field of these materials can be extended with the addition to the eutectic composition of rare earth oxides as Er_2O_3 . Rare earth ions in crystals emit radiation in narrow bands, allowing their use as selective emitters even at high temperature. In particular, the spectral matching of the Er^{3+} emission band with the sensitive region of the GaSb photoconverter makes the $\text{Al}_2\text{O}_3\text{-Er}_3\text{Al}_5\text{O}_{12}$ eutectic selective emitter an adequate material for thermophotovoltaic systems [4]. The efficiency of the rare earth oxide emitters can be increased by reducing the emitter characteristic dimension [5].

Both structural and functional application involves the microstructure fineness. Increasing the number of components to the melt and the use of high solidification rates can result in a highly reduced phase-sized material. Among the different directional solidification procedures to grow ceramic eutectics, the techniques based on floating zone appear as excellent methods as no crucible is needed, the thermal gradients at the liquid/solid interface are very large ($\approx 6000^\circ\text{C}/\text{cm}$) and, consequently, high growth rates can be used. Hence, the control of the crystal microstructure is possible in a wide variety of growth parameters; in particular, very fine microstructure ($\lambda \sim 100$ nm) can be achieved with high growth rates in these systems.

In this work, eutectic $\text{Al}_2\text{O}_3\text{-Er}_3\text{Al}_5\text{O}_{12}\text{-ZrO}_2$ rods were processed by directional solidification using the laser floating zone method at growth rates ranging from 25mm/h to 1200 mm/h. Homogeneous and defect-free microstructures were observed for all the solidification rates. The microstructure was examined by Scanning and Transmission Electronic Microscopy and presented three different phases that were identified by electron and X-ray diffraction as $\alpha\text{-Al}_2\text{O}_3$, $\text{Er}_3\text{Al}_5\text{O}_{12}$ (EAG), and cubic Er-stabilized ZrO_2 . The Er_2O_3 solubility in ZrO_2 was determined by Electron Dispersive Spectroscopy. At rates below 1000 mm/h, the eutectic microstructure consisted of a homogeneous interpenetrating network of the three eutectic phases. However, when higher solidification rates were used, the microstructure adopted a fibrous pattern. The phase-size was strongly dependent on the solidification rate, decreasing at the nanometre range for the samples grown at the highest rate. Figures 1a and 1b show TEM

and SEM images of the transverse and longitudinal sections of an $\text{Al}_2\text{O}_3/\text{Er}_2\text{O}_3/\text{ZrO}_2$ ternary eutectic rod processed at growth rates of 1200 mm/h. The microstructure consists of bundles of single crystal $\text{Er}_3\text{Al}_5\text{O}_{12}$ and Al_2O_3 whiskers (~ 200 nm in width) with smaller ZrO_2 whiskers (< 50 nm in width) between them. Al_2O_3 crystals were c-oriented and presented the typical triangular shape.

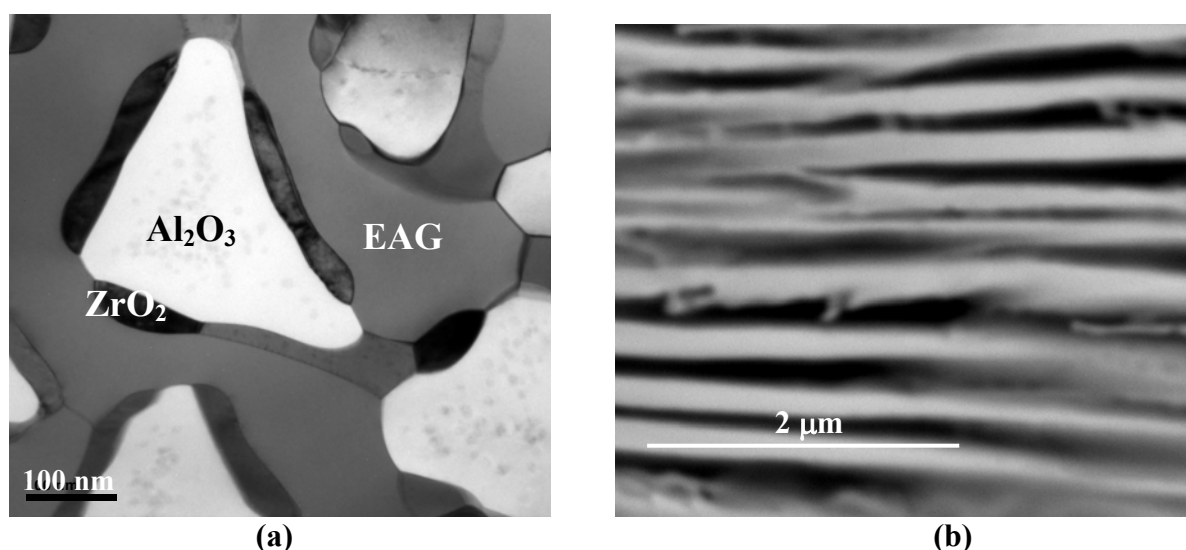
The thermal expansion mismatch between the three constituent phases of the eutectic led to residual stresses in the material. The hydrostatic component of the stress tensor of the Al_2O_3 crystals was measured with the technique of piezospectroscopy using the fluorescence from trace Cr^{3+} impurities. The residual stress in alumina was found to be compressive, varying from -270 MPa to -100 MPa at room temperature, depending on the growth rate.

The mechanical properties were investigated as a function of the growth rate at room temperature. Hardness and fracture toughness were measured from the microhardness Vickers test and mean values of 15.7 GPa and $4.2 \text{ MPam}^{1/2}$ were obtained, respectively. Both properties were not dependent on the phase size. Flexural strength was measured from three-point flexural tests. The mechanical strength showed a large dependence on the growth rate, raising from 1.2 GPa for rods grown at 25 mm/h up to 3.4 GPa for samples solidified at 1200 mm/h. The high flexural strength obtained for this material was explained in terms of its microstructure as the nanometric size of the phases reduces the critical crack length and, as a result, a large strengthening of the material is obtained.

References:

- [1] J. Llorca and V. M. Orera, *Prog. Mat. Sci.*, **51** (2006) 711
- [2] J. Y. Pastor, J. Llorca, A. Salazar, P.B. Oliete, I. de Francisco, and José I. Peña J. Am. Ceram. Soc., **88** [6] 1488–1495 (2005)
- [3] P. B. Oliete, J. I. Peña, A. Larrea, V. M. Orera, J. Llorca, J. Y Pastor, A. Martín, and J. Segurado, *Advanced Materials*, **19** (2007) 2313
- [4] N. Nakagawa, H. Ohtsubo, Y. Waku and H. Yugami, *J. Eur. Ceram. Soc.*, **25** (2005) 1285
- [5] D. L. Chubb, A. T. Pal, M. O. Patton and P. P Jenkins, *J. Eur. Ceram. Soc.*, **19** (1999) 2551

Figure 1: (a) TEM micrograph of the transverse cross-section of the Al_2O_3 -EAG- ZrO_2 nanofibrillar eutectic. b) SEM micrograph of the longitudinal cross-section in the same material.



PRODUCTION OF DISPERSIONS FORMED BY ISOLATED MAGNETIC NANOPARTICLES FOR BIOMEDICAL APPLICATIONS

N. Miguel, O. Bomati-Miguel, J. Santamaría

*Dpto. Ingeniería Química y TMA, Centro de Investigación Biomédica en Red (CIBER-BBN),
C/ P. Cerbuna, 12 50009 numiguel@unizar.es.*

In the last decade, nanoscaled magnetic particles have shown great potential as magnetic functional probes in tumour imaging by Magnetic Resonance (MRI)[1].

MRI is a non-invasive technique routinely used as a very important diagnostic tool in medical practice. Although paramagnetic gadolinium compounds (chelates) have been developed as useful as T_1 contrast agents causing positive contrast enhancement [2], with their increasing use for MRI, some important shortcomings have been found, such as fast elimination in tissue; non-specific distribution in vivo and limited effect in improving MR imaging.

On the other hand, superparamagnetic Fe_3O_4 magnetic nanoparticles (MNPS) are suitable for MRI contrast since the MNPs can enhance the alterations of proton relaxation in the tissue microenvironment and thus provide better MR imaging and longer life time in the bloodstream than Gd-chelate compound [3]. However these materials present two main limitations for their application: 1) magnetic nanoparticles are usually hydrophobic moieties and are therefore easily recognizable for the immune system; this problem can be solved by coating with a hydrophilic polymer; and 2) the usual synthesis methods of magnetic nanoparticles often do not allow to obtain colloidal grade pharmaceutical suspensions formed by isolated magnetic nanoparticles. Therefore, in this study we explored and optimized a facile synthetic route to obtain stable suspensions mostly formed by isolated hydrophilic magnetic nanoparticles.

This synthesis method is based on the thermal decomposition of iron organic compounds in presence of triethylene glycol (TREG) [4,5]. The role of TREG is to provide a biocompatible, water-dispersible coating, which also acts during the synthesis process as a reagent, reducing partially the iron precursor. Furthermore, TREG is absorbed on the magnetic nanoparticles surface forming a hydrophilic coating, retards oxidation of the particle surface, reduce toxicity, and delays detection by the immune system. In a typical preparation a TREG solution (30ml) containing $(Fe(acac)_3)$ (2mmol) was prepared. After being purged with argon, the reaction mixture was kept at 180°C for 30 min followed by 30min at 280°C. After that, Fe_3O_4 nanocrystals were obtained after a posttreatment that included precipitation, decantation and washing in water. The process has been optimized controlling diverse parameters as mechanical stirrer, heating rates and time of reaction.

Fig.1 presents a representative high resolution transmission microscopy (HR-TEM) image of Fe_3O_4 nanocrystals finally obtained in a water suspension. It can be seen from the figures that the morphology of the reaction products obtained under different conditions are quite different. Depending on the heating rate, the HR-TEM images (Fig 1a, 1b), show that individual and uniform magnetic nanoparticles have already formed, however most of the nanoparticles are aggregated even after sonication forming nanorod-like structures. In contrast, when heating rates were increased to 10°C/min y 15°C/min (Fig 1c, 1d) non-agglomerated magnetic particles with uniform shape and narrow size distribution can be observed.

Fig.2 shows the X-ray diffraction (XRD) patterns of the nanoparticles that were synthesized in TREG. The nanoparticles are well-crystallized, showing the spinel cubic structure (fcc) and the diffraction peaks match well with the XRD patterns for bulk magnetite (JCPDS file No 19-0629), though it is not possible to reject the existence of the maghemite phase.

In summary, we have demonstrated that the synthesis of magnetic nanoparticles from $\text{Fe}(\text{acac})_3$ precursor in a TREG environment can be tailored to obtain non-aggregated nanoparticles, which form a stable dispersion in water. The control of the rate of heating seems to be the key parameter in the balance of nucleation/growth processes and therefore in the control of the final morphology of the particles. Because of this, the optimized synthesis is a good candidate to prepare contrast agents for NMR imaging.

References:

- [1] E.X. Wu, H.Y.Tang, J.H. Jensen. *NMR Biomed* **17** (2004) 478-483.
- [2] R.C. Semelka, T.K.G.. Helmberger. *Radiology* **218** (2001) 27-38.
- [3] R.N. Low. *Mag. Reson. Imag.Clin. N.Am.* **9** (2001) 717-743.
- [4] F. Fievet, J.P Lagier, *Solid State Ionics*, **32-33** (1989) 198.
- [5] J. Wan, W. Cai, *Chem. Commun.* **47** 5004-5006 (2007)

Figures:

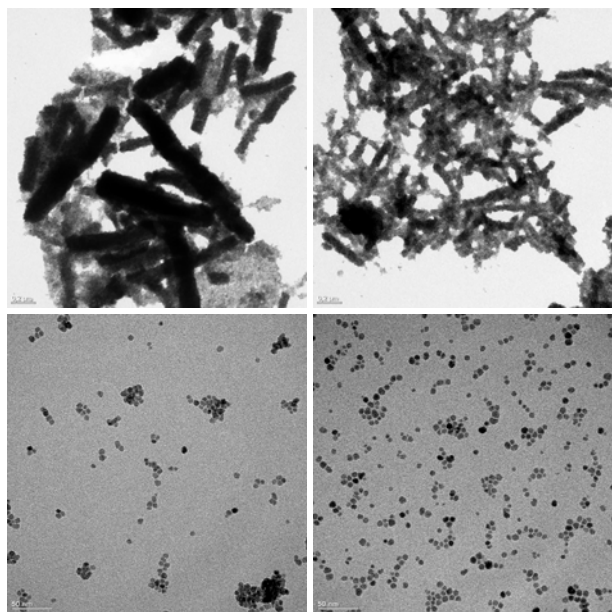


Fig.1 HR-TEM image of the Fe_3O_4 nanoparticles dispersed in water. Rate of heating: 2°C/min (a), 5°C/min (b), 10°C/min(c), 15°C/min(d).

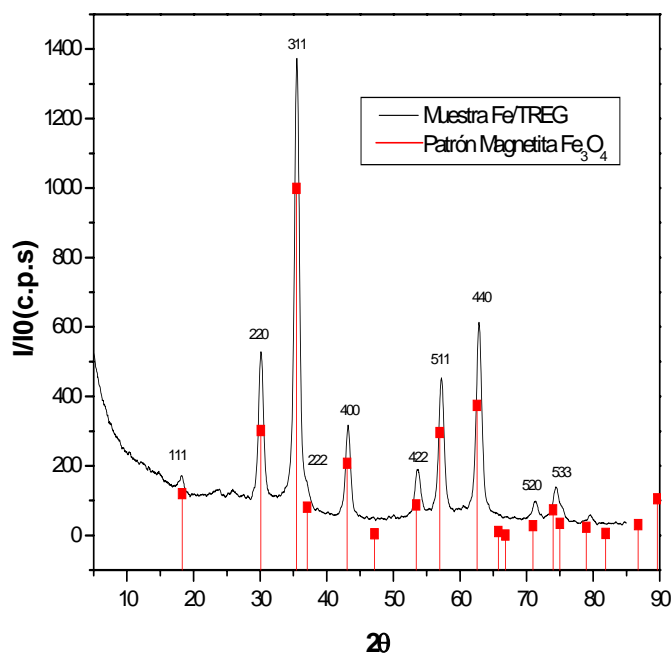


Fig.2. XRD for the Fe_3O_4 nanoparticles and standard XRD for magnetite (JCPDS19-0629)

SYNTHESIS OF CARBON NANOTUBES AND WAX FROM POLYPROPYLENE BY CHEMICAL VAPOR DEPOSITION SYSTEM.

Neeraj Mishra¹, Bhushan Patil¹, Sunil Bhardwaj¹, Shrikant S. Kawale³, Arvind Gupta¹, Sunil Pandey¹, Goldie Oza¹, Pravin Jagadale¹, Sandesh Jaybhaye¹, B.T. Mukharji⁴, Madhuri Sharon², Maheshwar Sharon¹.

¹ Nanotechnology research centre, Birla college, Kalyan, India.

² MONAD Nanotech, Pvt.Ltd.

³ Shivaji university ,kolhapur.

⁴ K.V. Pendharkar College,Dombivali,Maharashtra,India.

Corresponding e-mail: Mishra_neeraj1234@yahoo.co.in

Carbon nanotubes of diameter 20-40 nm and soft wax has been synthesized by simple Chemical Vapor Deposition Technique from polypropylene in the temperature range of 500°C to 800°C. To synthesize CNT's and wax of better quality and quantity Taguchi Optimization technique has been applied. It optimizes various parameters of CVD system like deposition temperature, carrier gas, catalyst and duration within short numbers of experiments. From taguchi calculation best parameters are found for CNT's to be Temperature 800°C, catalyst Nickel, 1 hrs of duration and Nitrogen as a carrier gas. Percentage wise effect study of each parameter level shows temperature affects up to 55% and catalyst up to 33% on results. Other two parameters as Duration and carrier gas are found to be less effective. SEM and XRD study was done for confirmation the structure and size of CNT's and for Wax TG-DTA, GCMS and FTIR has been been done.

Keywords: - CNT, Taguchi optimization, Chemical Vapor Deposition System.

OUTLINE

INTRODUCTION

EXPERIMENT

Taguchi optimizing technique

Experimental setup

Synthesis of CNTs

Characterizations of materials

THE EFFECT OF EPOXIDIZED NATURAL RUBBER (ENR) ON THE MORPHOLOGY AND CURING CHARACTERISTICS OF NATURAL RUBBER / ORGANOCCLAY NANOCOMPOSITE SYSTEMS

M.Mokhtari¹, M. Kokabi^{*1}, A. Bahramian¹
*mehrir@modares.ac.ir**

1. Polymer Engineering Group, Chemical Engineering Department, Faculty of Engineering, Tarbiat Modares University, P.O. Box: 14115-143, Tehran, Islamic Republic of Iran.

Introduction

Polymer / layered silicate nanocomposites exhibit enhanced modulus and strength, heat resistance, gas barrier properties and decreased flammability relative to the polymer matrices [1]. Although clay nanocomposites have been prepared based on many thermoplastic and thermosetting polymers, rubber nanocomposites constitute only a minor proportion [2].

Compatibility of natural rubber (NR) with organoclay is poor due to the polarity of organoclay and lack of polar groups in NR backbone. ENR, obtained by epoxidation of 1, 4-polyisoprene, has polar groups in its backbone, so can increase the polarity of the system and overcomes the disadvantages. It causes better dispersion of organoclay in NR matrix, also provides superior curing characteristics in nanocomposite systems. In this work 25 phr of two types of epoxidized natural rubber were used as compatibilizer in the system and the effect of ENR on morphology and curing characteristics of NR/ENR/organoclay ternary nanocomposite systems was investigated.

Experimental

The elastomers used were NR (SMRL), ENR25 and ENR50 (The ENR contained 25 and 50 mol % epoxidized denoted as ENR25 and ENR50, respectively) with money viscosities of ML (1+4)100 °C = 60, ML(1+4)100 °C =71 and ML(1+4)100 °C = 80, respectively. All purchased from Kumpulan Guthrie Sdn.Bhd., Seremban, Malaysia.

Organoclay cloisite 15A (C15A) with 3.15 nm intergallery spacing, ion exchanged by dimethyl dehydrogenated tallow ammoniums bromide, was provided by Southern clay products. The other compounding ingredients listed in Table 1, are obtained from local manufactures.

Table1: Formulation of various nanocomposite systems.

Ingredients(phr)	Nanocomposite Systems		
	NR/C15A	NR/ENR25/C15A	NR/ENR50/C15A
Natural Rubber	100	75	75
ENR25	0	25	0
ENR50	0	0	25
Organoclay	3	3	3
Carbon black	40	40	40
Zinc oxide	5	5	5
Stearic acid	2	2	2
Vulcagit D	0.5	0.5	0.5
Vulcagit M	0.5	0.5	0.5
Sulfur	2	2	2

The natural rubber /ENR/organoclay were made by melt mixing in an internal mixer at 130°C and 60 rpm rotor speed for 15 minutes. Other ingredients were then added on a laboratory model two roll mixer. The mixtures were cured at 140 °C under an electrically heated hydraulic press for the required curing time (t_{90}).

Results and Discussion

Morphology

Table 2 shows the results of x-ray analysis performed on nanocomposite systems.

Table 2 Morphology of various nanocomposite systems

Sample	2θ Peak Angle (°)	spacing(nm)	Morphology
C15A	2.75	3.15	---
NR/C15A	2.015	4.38	Intercalated
NR/ENR25/C15A	2.00	4.7	Intercalated
NR/ENR50/C15A	-----	-----	Exfoliated

The diffraction peak of C15A in the NR/C15A shifted to a lower angle, corresponding to an interlayer distance of 4.38 nm, providing thus the existence of layered/polymer intercalates. With addition of ENR25 the diffraction peak slightly shifted to lower angle which shows no more pronounced intercalation. By addition of ENR50, the diffraction peak disappeared. This suggests that enough polymer chains have been introduced into the galleries so that increase interlayers distance more than 8nm and the layered silicates show an exfoliated morphology. The polarity of ENR favours the intercalation of this elastomer into the galleries and the dispersion of layered silicates in the matrix.

Curing Characteristics

The Scorch Time (t_{s2}), Maximum Torque (MH) and Minimum Torque (ML) of the nanocomposite systems at 140 °C are compiled in Table3.

Table 3 Curing characteristics of various nanocomposite systems.

Sample	T_{s2} (min)	MH(Ib.in)	ML(Ib.in)
NR\C15A	1.43	52.06	2.16
NR/ENR25/C15A	1.15	62.92	2.73
NR/ENR50/C15A	1.05	67.13	4.09

The scorch time of NR/organoclay changes effectively by addition of ENR. It is attributed to the activity effects of epoxy and amine groups on the ring opening pathway of sulphur.

In the presence of ENR as a compatibilizer, the maximum and minimum torques of NR/ENR/organoclay nanocomposite systems increases effectively. This is due to the better interfacial adhesion between NR and organoclay which could be confirmed by XRD data.

Conclusions

According to this study, exfoliated nanocomposites based on NR/ENR50 blend have been successfully developed. Due to ENR polar character, the higher interaction with organoclay improves the dispersion of the filler in the matrix and curing characteristics of the compounds.

References

- [1] Y.P. Wu, Y. Ma, Y.Q. Wang, L.Q. Zhang, *J. Macromolecular Materials and Engineering*, 2004, 289, 890-894.
- [2] M. Arroyo, M.A. Lopez-Manchado, J.L. Valentin, J. Carretero, *J.Composites Science and Technology*, 2007, 67,1330-1338.

CoFe₂O₄ nanoparticles: ball milling (assisted by NaOH) vs. polymerized complex

D. A. Sánchez-Ramírez¹, A. A. Rodríguez-Rodríguez¹, Sagrario M. Montemayor¹, E. M. Múzquiz-Ramos¹, O. S. Rodríguez-Fernández²

¹Universidad Autónoma de Coahuila, V. Carranza esq. J. Cárdenas s/n Col. República, Saltillo, Coahuila, 25000, México

²Centro de Investigación en Química Aplicada, Blvd. Enrique Reyna Hermosillo No. 140, Saltillo, Coahuila, 25253, México

smmontemayor@gmail.com, sagrario.martinez.montemayor@mail.uadec.mx

1. Introduction. Nanostructured materials have been intensively studied in recent years, particularly because the physical and chemical properties of these materials are quite different from those of the bulk [1]. Metal oxides have important applications, such as magnetic storage media, solar energy transformation, electronics, catalysis and biological applications such as tags in sensing, imaging and delivery [2, 3]. In this work, we studied the feasibility of synthesizing CoFe₂O₄ nanoparticles by the ball milling (assisted by NaOH) method and, in addition, we compared the results with those obtained by the polymerized complex route of sol-gel method.

2. Experimental. The starting chemicals used in this work were high purity cobalt (II) nitrate hexahydrate, iron (III) nitrate nonahydrate, sodium hydroxide, citric acid monohydrate and ethylene glycol purchased from Aldrich and used without further purification. *2.1 Ball milling, assisted by NaOH, method:* The appropriate amounts of Co(NO₃)₂·6H₂O, Fe(NO₃)₃·9H₂O and NaOH, in a 1:2:8 molar ratio respectively, were mixed by ball milling. Milling was performed in a planetary ball mill (Fritsch Pulverisette), the milling time was 4 hours at speed of 300 rpm with a ball-to-powder mass ratio of 10:1. *2.2 Polymerized complex route of sol-gel method:* The experimental details of this part are widely presented in a previous work [4]. *2.3 Characterization:* XRD spectra were obtained using a Siemens D5000 X-ray diffractometer (Cu K α , λ = 1.5418 Å) in a 2 θ range of 10 to 80° with a step size of 0.02 °/s. SEM micrographs were obtained by using a Jeol JFM-7401F instrument. TEM micrographs were obtained in a Jeol JEM 1200EXII microscope operated at 60 KV. Magnetic properties of the samples were measured with a Lake Shore 7300 vibrating sample magnetometer in applied fields from -12.5 to 12.5 KOe.

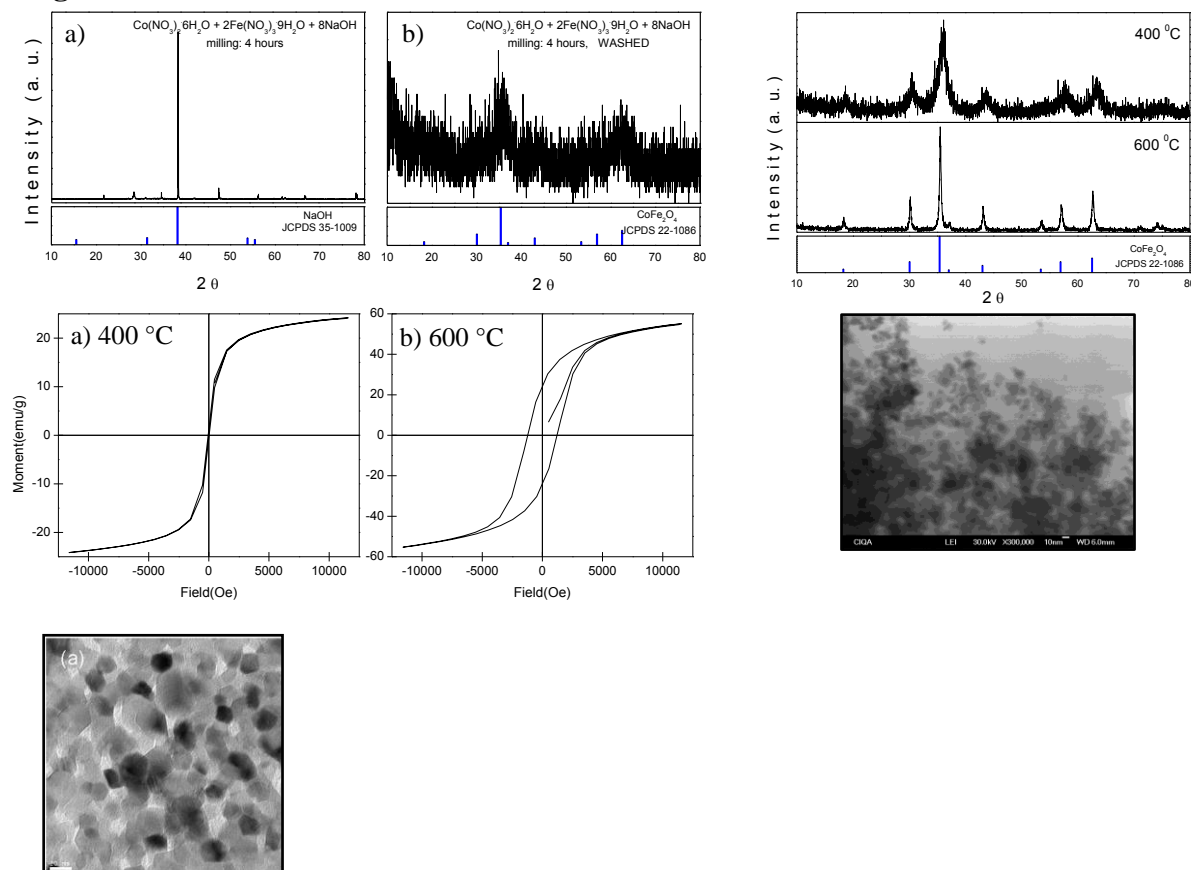
3. Results and discussion. The as-obtained product, after 4 hours of milling, was analysed by XRD. The spectrum, in Figure 1a, shows the presence of NaOH [JCPDS 35-1009] as the main crystalline phase. After repeated washing with distilled and deionised water, the XRD pattern shows the presence of the main reflections of CoFe₂O₄ [JCPDS 22-1086] (Figure 1b), although they are broad. Figure 2 illustrates the XRD patterns of the same sample after two hours thermal treatments at 400 and 600 °C. The diffractograms show that all reflections of the crystalline phase concern to a pure cubic phase of CoFe₂O₄ with a spinel-type structure, represented as bars in the figure. It is possible to observe an improvement in the crystallinity of magnetic phase with increasing temperature. The average size of crystallites in the two samples was calculated using the Debye-Scherrer [4] and the most intense diffraction peaks. The growth of crystallites with increasing sintering temperature is from 5 to 26 nm. The hysteresis loops of the samples treated at 400 and 600 °C are showed in the figure 3a and 3b respectively. It is known that the magnetic properties are influenced by many factors such as size, shape and defects in crystal structure [5]. In this case, is easy to observe, the clear difference between the magnetic behavior, at room temperature, of the CoFe₂O₄ with respect to a drastic difference in particle size from superparamagnetic (for 5 nm) to ferrimagnetic (for 26 nm). The superparamagnetic phase, on one hand, reaches a maximum magnetization value of 24.2 emu/g, a remnant magnetization of 0.919 emu/g and a coercivity of 42.25 Oe. On the

other hand, the ferrimagnetic phase in which the nanocrystals are bigger the maximum magnetization value, reached up to maximum applied magnetic field, was of 55.2 emu/g, with a remnant magnetization of 24 emu/g and a coercivity of 1,218 Oe. This trend, similar to those reported in references 5 and 6, is consequence of that the particle size obtained at 400 °C, 5 nm, is around the critical size for the CoFe_2O_4 , where the typical magnetic behavior is superparamagnetic. It is important to mention that the same procedure, without NaOH during the milling, leads to CoFe_2O_4 only after thermal treatments at temperatures above 800 °C. In a previous work we reported the synthesis of CoFe_2O_4 by sol-gel method, where the cobalt iron oxide is obtain as a unique crystalline phase after sintering the polymerized complex at 400 °C. However, the particle size is of ~20 nm and, as a consequence of this size, the typical ferrimagnetic behavior is obtained [4]. SEM images of the CoFe_2O_4 obtained by ball milling (assisted with NaOH) and sintered at 400 °C, as the presented in figure 4, show spherical nanoparticles homogeneously dispersed on the grid. The size of the particles is, presumably, less than 10 nm. A TEM micrograph of the phase sintered at 600 °C shows uniform nanoparticles of sizes around 20 nm, Figure 5.

References:

- [1] A.S Edelstein, *Nanomaterials: Synthesis, Properties, Applications*, IOP Publishing, 1996.
- [2] R.D. McMichael, et al., *J. Magnetism and Magnetic Materials*, **111** (1992) 29.
- [3] C.H. Cunningham, et al., *Magn. Reson. Med.*, **53** (2005) 999.
- [4] S.M. Montemayor, et al., *Materials Letters*, **59** (2005) 1056.
- [5] R. Valenzuela, *Magnetic Ceramics*, Cambridge University Press, Cambridge 1994.
- [6] O. Ersen, et al., *Nanoletters*, **8** (2008) 1033.

Figures:



OPTIMIZATION OF THE PROCESS PARAMETERS ON THE PRODUCTION OF MWCNTS AND ITS POTENTIAL APPLICATION IN PROTEIN PURIFICATION

Mubarak N. M.¹, Faridah Y.¹, Alkhatib M. F.¹, Muataz A. A.², Qudsieh I.Y.³, Mohammed A. Al Saadi¹, and Khalid M.¹

¹Nanoscience and Nanotechnology Research Group (NANORG),
Department of Biotechnology Engineering, Faculty of Engineering
International Islamic University Malaysia, PO Box 10, 50728 Kuala Lumpur,
Malaysia

Email: mubarak_chem@yahoo.com /yfaridah@iiu.edu.my

Tel: +603 8946 5004, Fax: +603 8946 4862

²Department of Chemical Engineering, Head of Nanocarbon Research Unit
Centre of Research Excellent in Nanotechnology, King Fahd University of
Petroleum and Minerals, P.O. Box 5050, Dhahran-31261, Saudi Arabia

³Faculty of Applied Medical Sciences, Jazan University, P.O.Box 114,
Jazan-45142, Saudi Arabia

Abstract

Carbon nanotubes are in great demand for their fascinating mechanical, physical and chemical properties. Carbon nanotubes (CNTs) have been synthesized by a gas phase Double Stage Chemical Vapor Deposition (DS-CVD) technique with acetylene and hydrogen as a precursor. Optimizing the process parameters such as reaction temperature, reaction time, and gas flow rate of acetylene and hydrogen respectively. The morphology and the structure of CNTs were characterized by using FSEM, TEM, and TGA. These produced CNTs were purified and functionalized. Further these functionalized CNTs were used as column chromatographic media to be used in skim latex protein purification.

CARBON NANOTUBE/ β -CROSS SHEET PEPTIDE DISPERSIONS AND ASSEMBLIES: PREPARATION, CHARACTERIZATION, AND POTENTIAL BIOSENSOR APPLICATIONS

W. J. Goux,^a A. Sreelatha,^a E. Muñoz,^b R. Garriga,^c R. H. Baughman^d

^aDepartment of Chemistry, The University of Texas at Dallas, Richardson, TX 85083-0688, USA.

^bInstituto de Carboquímica (CSIC), Miguel Luesma Castán 4, 50018 Zaragoza, Spain.

^cDepartamento de Química Orgánica y Química Física (Área de Química Física), Facultad de Ciencias, Universidad de Zaragoza, 50009 Zaragoza, Spain.

^dThe Alan G. MacDiarmid Nanotech Institute, The University of Texas at Dallas, Richardson, TX 85083-0688, USA.

edgar@icb.csic.es

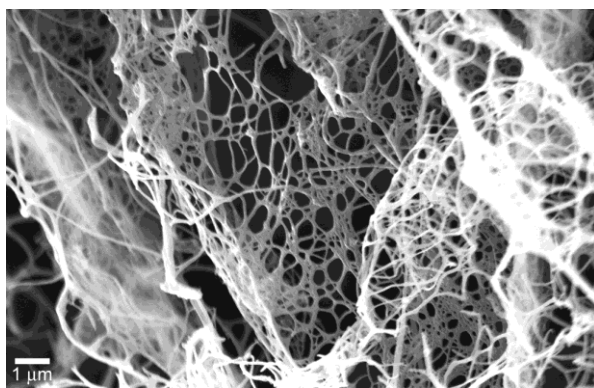
The ability of a variety of different proteins and peptides to bind to carbon nanotubes leading to stable nanotube aqueous dispersions offers wide opportunities for nanotube processing in biological systems and in the development of carbon nanotube-based bio-devices. It has been thus demonstrated that peptide coating facilitates carbon nanotube uptake by cells.[1] On the other hand, these nanotube dispersions have efficiently been employed in the coagulation spinning of macroscopic carbon nanotube biocomposite fibers.[2] Moreover, peptide-coated carbon nanotubes can self-assemble into supramolecular architectures and hierarchical structures such as microfibers,[3] fractal-like structures,[4] and liquid crystal ordered domains.[5].

We here report on the interactions between single-walled carbon nanotubes (SWNTs) and a short hexapeptide homologous to a portion of the tau, a protein known to form amyloid helical filaments in the brains of Alzheimer's diseased patients. We here show that the employed hexapeptide is capable of efficiently dispersing SWNTs. The ability of various single site mutants to disperse SWNTs in water and the resulting strong peptide/SWNT interaction was characterized using electron microscopy, NIR and CD spectroscopies, and mechanical and electrical properties of peptide-impregnated SWNT free-standing films. In order to more thoroughly understand the nature the binding interaction we used optical difference spectroscopy to study the adsorption kinetics of several proteins and peptides onto these SWNT films. The results indicate that the hexapeptide ability to disperse SWNTs is a function of the hydrophobicity of the introduced side-chains. Further processing of stable hexapeptide/SWNT dispersions led to the formation of supramolecular bionanocomposite networks. For most proteins adsorption follows a first order kinetic model. We attempt to correlate rate constants and equilibrium loadings of the proteins onto the SWNT films with surface hydrophobicity, measured using a fluorescent probe. We demonstrate that peptide-coated SWNT films may be used as substrate for immunochemical ELISA assays.[6]

References:

- [1] S. F. Chin, R. H. Baughman, A. B. Dalton, G. R. Dieckmann, R. K. Draper, C. Mikoryak, I. H. Musselman, V. Z. Poenitzsch, H. Xie, P. Pantano, *Exp. Bio. Med.* **232** (2007) 1236.
- [2] C. Lynam, S. E. Moulton, G. G. Wallace, *Adv. Mater.* **19** (2007) 1244.

- [3] G. R. Dieckmann, A. B. Dalton, P. A. Johnson, J. Razal, J. Chen, G. M. Giordano, E. Muñoz, I. H. Musselman, R. H. Baughman, R. K. Draper, J. Am. Chem. Soc. **125** (2003) 1770.
- [4] A. B. Dalton, A. Ortiz-Acevedo, V. Zorbas, E. Brunner, W. M. Sampson, L. Collins, J. M. Razal, M. M. Yoshida, R. H. Baughman, R. K. Draper, I. H. Musselman, M. Jose-Yacaman, G. R. Dieckmann, Adv. Funct. Mater. **14** (2004) 1147.
- [5] S. E. Moulton, M. Maugey, P. Poulin, G. G. Wallace, J. Am. Chem. Soc. **129** (2007) 9452.
- [6] W. J. Goux et al., submitted.



SEM micrograph of a hexapeptide/SWNT composite network.

Hydrothermal preparation of highly photoactive TiO₂ nanoparticles

J.A.Navío, C.Hidalgo, M.Maicu, M.Aguilar, G.Colón

*Instituto de Ciencia de Materiales de Sevilla. Centro Mixto CSIC-Universidad de Sevilla.
C/. Américo Vespucio, nº 49, 41092-Sevilla (Spain)*

navio@us.es

The impact of nanostructure on the properties of high surface area materials is an area of increasing importance for understanding, creating and improving materials for diverse applications. A unique property of nanoparticles is their extremely high surface area. The synthesis of nanoparticles with controlled size and composition is of technological interest. As a consequence, there has been a lot of highlighting on the production of nanoparticulated TiO₂ for a wide range of applications.

TiO₂ nanoparticles have been prepared by amine assisted sol–gel precipitation of Ti⁴⁺ aqueous solutions and further hydrothermal treatment. The effect of different starting acidic solution (nitric, chlorhydric and acetic acids; series A, B and C in Figures) as well as the addition of triethylamine (TEA) at different pH has been widely investigated. It has been stated that different amounts of TEA could have interesting effects upon hydrothermal treatment¹.

The different TiO₂ series were prepared from initial aqueous Ti⁴⁺ stock solutions by precipitation by means of triethylamine at different pH values and further hydrothermal treatment. We have studied the effect of different types of acid in the Ti⁴⁺ aqueous solution as well as the precipitation pH with TEA.

Systems prepared by using different acids show surface area values in the range of 150–250 m²/g depending on hydrothermal conditions and the final pH of the Ti⁴⁺ solution. It is worthy to note that as TEA is added, and pH values increase, it seems that a slight diminution in S_{BET} value is observed in all systems.

The different synthesis studies also produce significant differences under the structural point of view. Hydrothermal synthesis at 120°C for 24 h, leads to mainly anatase structure in all systems independently of the pH value. Systems prepared with HNO₃ and HCl exhibit small rutile fraction in addition to the anatase one. On the contrary, samples prepared with HAc only in the anatase phase with higher crystallinity.

From XPS data it can be stated the presence of adsorbed species (N and C probably coming from TEA) not eliminated in the washing procedure. Series obtained from HAc show the lowest content of the adsorbed species. The position of N (1s) peak around 400 eV clearly indicates that the nature of the nitrogen present at the surface would corresponds to NO or CN. While from C1s spectrum a complex situation is expected with different kinds of carbonaceous species.

The high surface area values obtained for hydrothermally treated samples could explain the important photoactivities of these samples. In this sense, it would be interesting to establish the surface area influence on the photocatalytic activity for the studied systems. For this reason, we have plotted the conversion rate per surface area unit (Fig. 1).

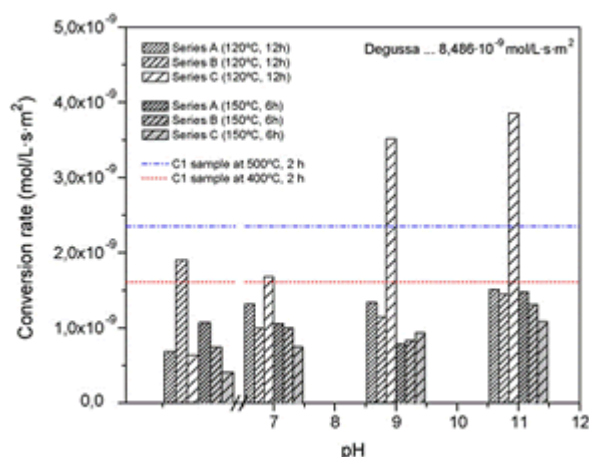


Figure 1

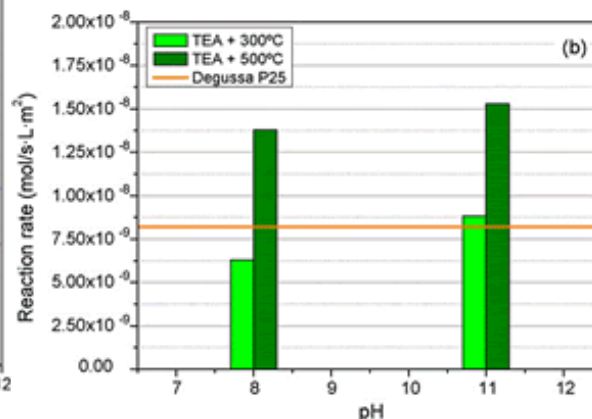


Figure 2

From results reported in Fig.1, it is clear that for most of the hydrothermally prepared systems, the conversion rates appear similar, with a clear exception series prepared with HAc and precipitated in the presence of TEA and treated at 120 °C. That means that surface area values are not responsible of the high difference in reactivities.

It might be said, from the surface and structural characterization performed, it can be inferred that the preparation with HAc leads to well crystallized anatase structure with low crystallite size (ca. 10 nm), with high surface area values and the cleanest surface situation after hydrothermal treatment. The conjunction of all these features would lead to highly active TiO₂ anatase particles. This high photoactivity is explained by considering an improvement in the different steps in the photocatalytic mechanism, though taking apart the surface area contribution the best photocatalyst in our series do not reach the specific rate exhibited by Degussa P25. Thus, the structural features affecting to the electronic transfer and diffusion of charge carriers might be improved in order to compete with Degussa photocatalyst. In Fig. 2 we show the photoactivity results for systems prepared with HAc, hydro-treated and further calcined at 300°C and 500°C. As it can be noticed, the further calcination produces a significant improvement with respect to uncalcined systems (Fig. 1). At the same time, reaction rates observed for catalysts calcined at 500°C clearly overcome the Degussa P25 one.

This further calcination treatment would provide an optimal structural situation, reducing the number of defects or amorphous domains but keeping at the same time a relatively low crystallite

References:

- [1] M.C. Hidalgo, M. Aguilar, M. Maicu, J.A. Navío, G. Colón, *Catalysis Today* 129 (2007) 50–58
- [2] G. Colón, M.C. Hidalgo, J.A. Navío, E. Pulido Melián, O. González Díaz, J.M. Doña, *Applied Catalysis B: Environmental* 78 (2008) 176-182

Synthesis and Characterisation of ZnO-Au Bifunctional Nanocomposites

Cristina S. Neves^{a,*}, Pedro Quaresma^{a,b}, Patrícia A. Carvalho^c, Peter Eaton^a and Eulália Pereira^a

^a REQUIMTE/Faculdade de Ciências, Universidade do Porto, R. Campo Alegre 687, 4169-007 Porto, Portugal

^b CIGMH/Departamento de Ciências da Vida, FCT-UNL, 2829-516 Caparica, Portugal

^c Departamento de Engenharia de Materiais, IST, Av. Rovisco Pais 1049-100 Lisboa, Portugal

* Corresponding author: cristina.neves@fc.up.pt

Fluorescent semiconductor nanocrystals, also known as quantum dots (QDs), have evolved over the past two decades from electronic materials science to biotechnological applications, such as luminescence tagging, immunoassay, drug delivery and cellular imaging [1]. As a fluorescent semiconductor material, ZnO can form nanocrystals exhibiting higher chemical stability and safety relative to the toxic Cd-containing semiconductor nanocrystals [2, 3].

The addition of gold to ZnO particles to form bifunctional water-soluble ZnO-Au nanocomposites (NCs) may confer additional useful capabilities. For example, the SPR band of gold in the UV-vis absorption spectrum allows further modes of detection, and in addition, the ease of further functionalisation of gold can simplify the modification of the QDs for sensor applications. In order to develop nanocomposites QDs for biosensor applications, we have been studying the modification of ZnO QDs with gold nanoparticles.

Quantum dots were synthesised by a sol-gel method based on the condensation of zinc acetate [4]. The nanoparticles were characterized by Transmission Electron Microscopy (TEM), Dynamic Light Scattering (DLS), UV-Vis and fluorescence spectroscopy. This was followed by a gold coating procedure using $[\text{AuCl}_4]^-$ and sodium citrate. The results show the production of a population of photoluminescent ZnO nanocrystals of approximately 5 to 10 nm diameter, according to hydrodynamic radius measurement by DLS (R_h). Reduction of the gold salt in the presence of the ZnO QDs led to the appearance of the expected surface plasmon resonance (SPR) in the UV-vis spectrum from the Au^0 crystals in solution, along with an increase in R_h from the DLS measurements (see figure 1). TEM results indicated co-existence of semiconductor and metal phases but did not unequivocally prove the binding. Therefore we attempted to extract the gold component of the samples to a new phase to test the Au-ZnO binding.

Quantum dots were functionalized with a non polar thiol (1-decanethiol) and were extracted to an organic phase. This phase was characterized by UV-Vis and fluorescence spectroscopy showing the presence of both fluorescence from the ZnO and the SPR band from the gold which indicates the existence of a bifunctional quantum dot nanostructure.

References:

- [1] X. Michalet, F. F. Pinaud, L. A. Bentolila, J. M. Tsay, S. Doose, J. J. Li, G. Sundaresan, A. M. Wu, S. S. Gambhir and S. Weiss, *Science* **307**(5709) (2005) 538.
- [2] Y. C. Liu, M. Y. Zhong, G. Y. Shan, Y. J. Li, B. Q. Huang and G. L. Yang, *J. Phys. Chem. B* **112**(20) (2008) 6484.
- [3] X. Wang, X. G. Kong, Y. Yu and H. Zhang, *J. Phys. Chem. C* **111**(10) (2007) 3836.
- [4] L. Spanhel and M. A. Anderson, *J. Amer. Chem. Soc.* **113**(8) (1991) 2826.

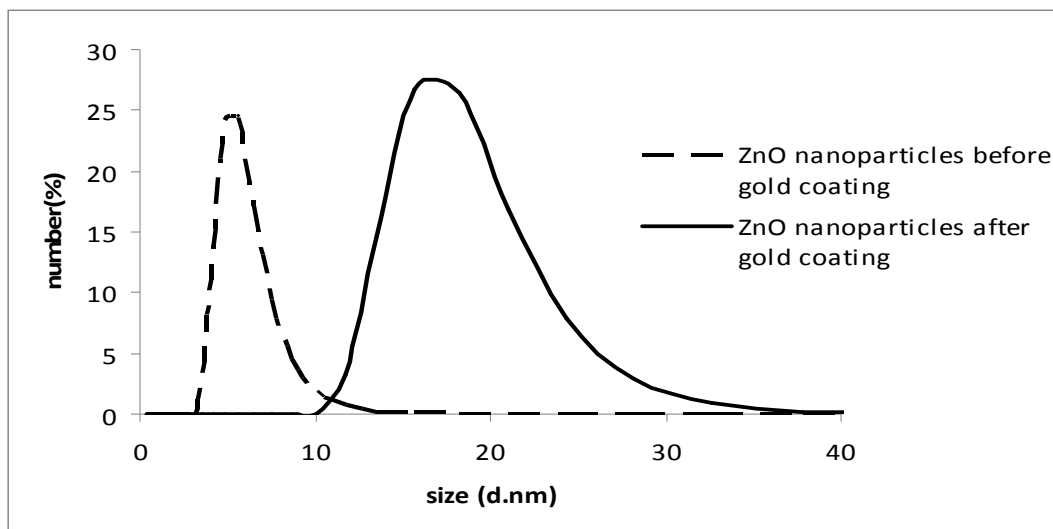
Figures:

Figure 1 – Dynamic light scattering (DLS) of ZnO nanoparticles before and after gold coating.

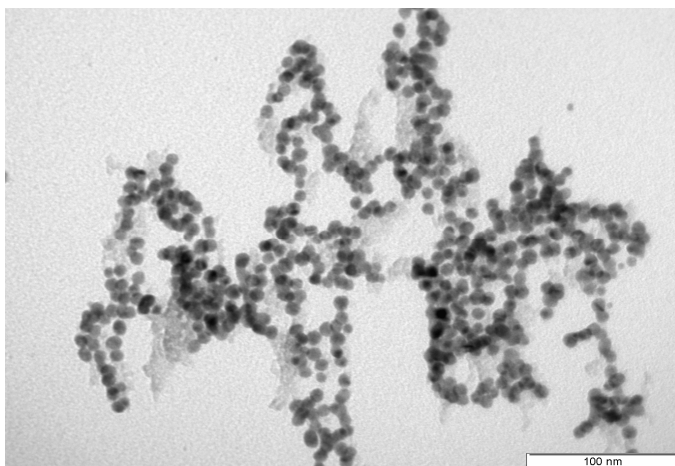


Figure 2 – Transmission electron microscopy (TEM) image of ZnO-Au NCs.

Acknowledgments: Fundação para a Ciência e a Tecnologia, Portugal for financial support through project PTDC/QUI/64484/2006. P. Quaresma thanks FCT for PhD grant SFRH/BD/28209/2006.

PRECISE MEASUREMENT OF ELECTROSTATIC TIP-SAMPLE INTERACTION USING 3D-SFM MODE

I. Nieto, J. Abad, J. Colchero

*Centro de Investigación en Óptica y Nanofísica (CIOyN), Dept. de Física,
Universidad de Murcia Campus Espinardo, E-30100 Murcia*

inc2@alu.um.es

For development of nanotechnological devices the precise determination of local electronic properties will play an important role. A very powerful tool for this kind of studies is the Scanning Force Microscope (SFM). A variety of SFM modes, in particular Electrostatic Force Microscopy (ESFM) as well as Kelvin Force Microscopy (KFM), have been developed to investigate nanoscale electrical properties in a variety of systems [1,3].

It has been shown that interpretation of data obtained by ESFM or KPM is not an easy task, accordingly, a variety of models have been proposed to describe electrostatic tip-sample interaction. Using appropriate models is a fundamental requisite for quantitative interpretation of data acquired by ESFM or KPM. In particular, in previous works our groups have proposed a model system for typical SFM setups that assumes a cantilever-tip system that is composed of three basic units: a macroscopic cantilever, a mesoscopic tip cone and a nanometer sized tip apex. For this geometry the electrostatic forces as a function of the distance d between the surface and the components of the tip-sample system can be calculated for the different units, leading to well-defined relations of the forces (F_{ev} , F_{cone} , F_{apex}) induced by each unit.[4]

An additional problem encountered in the quantitative evaluation of nanoscale electrostatic properties stems from the fact that different materials may have different contact potentials, which induce electrostatic fields that are “build into” the system. Moreover, in addition to electrostatic forces, also other forces, in particular Van der Waals type, will contribute to tip-sample interaction to further complicate data interpretation.

Recently a spectroscopic technique based on the simultaneous measurement of cantilever deflection, oscillation amplitude and frequency shift as a function of tip-sample voltage and tip-sample distance has been presented and shown to yield very promising results [4]. In this method, data is acquired at a fixed lateral position as interaction images with the bias voltage as fast scan and tip-sample distance as slow scan. Due to the quadratic dependence of the electrostatic interaction with tip-sample voltage the Van der Waals force can be separated from the electrostatic force. Using appropriate data-processing the Van der Waals interaction, the capacitance as well as the contact potential can be determined as a function of tip-sample distance. In order to describe experimental results, two different tip-radii R_{vdW} and R_{estat} as well as two different tip-sample distances d_{vdW} and d_{estat} are introduced, which describe how the tip interacts with the surface: electrostatically and due to Van der Waals forces.

In the present work, this spectroscopic technique is applied to study the electrostatic interaction between model surfaces –Platinum-Iridium as model for a metal surface and silicon as model for a semiconductor surface– in order to compare the experimental results with the behaviour that follows from the model discussed in Ref. [3] (see also fig. 1). Differences of between d_{vdW} and d_{estat} on the one side, and between R_{vdW} and R_{estat} on the other will indicate deviations from the ideal behavior described in ref.[3] and can be interpreted as due to band bending in the case of semiconducting surfaces, or due to the presence of (molecularly thin) dielectric films on the tip or on the sample.

References:

- [1] K. L. Sorokina and A. L. Tolstikhina, *Crystallography Reports*, Vol.**49**, No.3 (2004) 476-499.
- [2] B. Pérez-García, J. Abad, A. Urbina, J. Colchero and E. Palacios-Lidón, *Nanotechnology* **19** (2008) 065709
- [3] E. Palacios-Lidón, B Pérez-García and J Colchero, *Nanotechnology* **20** (2009) 085707.
- [4] J. Colchero, A. Gil, and A. M. Baro, *Physical Review B*, **64** (2001) 245403.
- [5] E. Palacios-Lidón and J. Colchero, *Nanotechnology* **17** (2006) 5491–5500.

Figures:

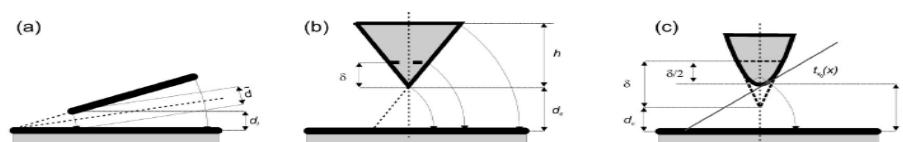


Fig 1. Model for a metal tip-sample system as proposed in Ref. [3] Auxiliary sketches of (a) the lever-sample, (b) the cone-sample, and (c) the tip apex-sample system showing the parameters that are relevant for the calculation of the corresponding forces.

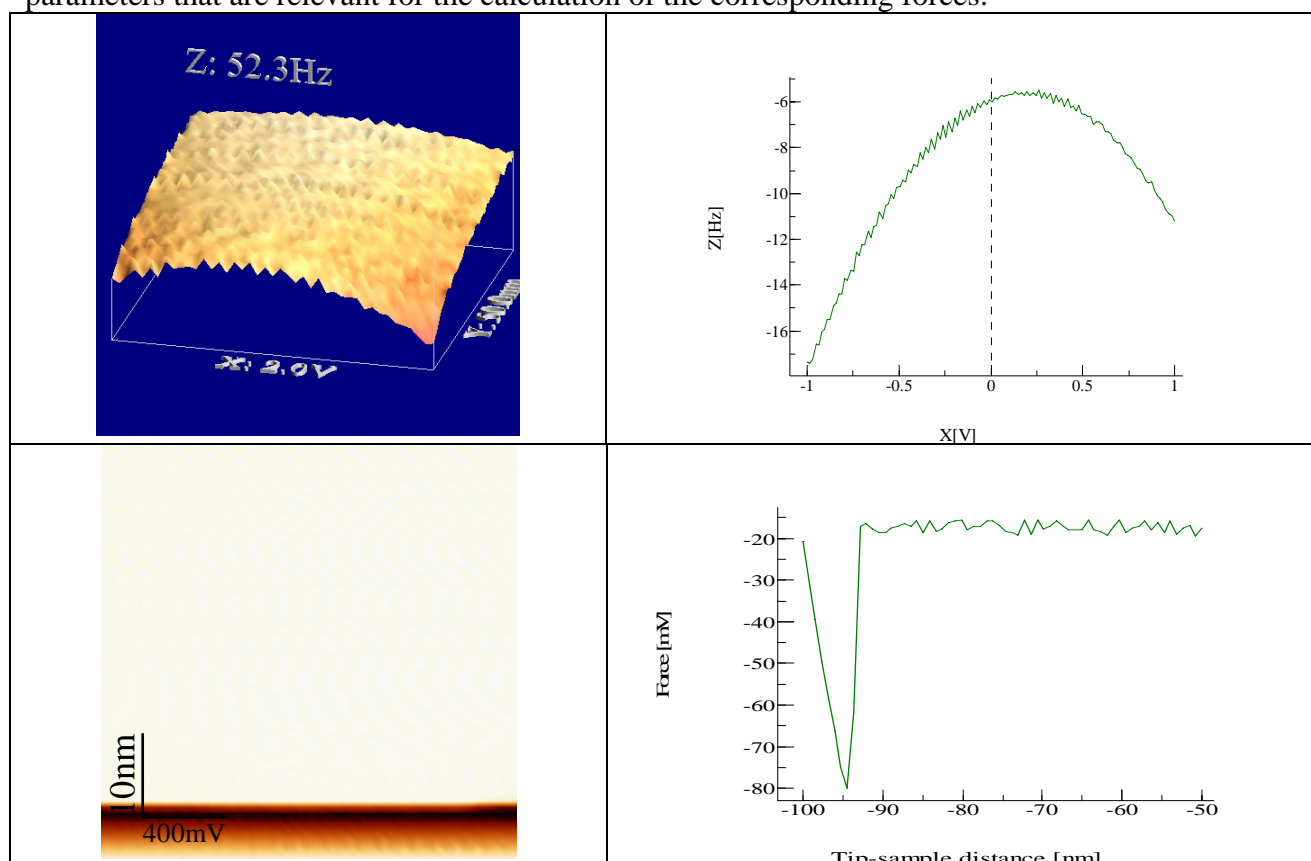


Fig 2. Top Left: Frequency “interaction” image taken using 3D-mode (fast scan “X”: bias voltage; slow scan “Y”: tip sample distance), where the quadratic dependence with the voltage is clearly appreciated. Also, as the tip-sample distance is reduced (smaller “Y” values, front of image) the curvature of the “interaction” image is larger, due to larger tip-sample interaction. Top Right: horizontal line through the “interaction” image (=interaction at constant tip-sample distance, but variable tip-sample voltage).

From an adjustment of the parabolic curves the precise tip sample interaction can be determined. Down Left: Normal force “interaction” image. Down Right: typical force vs. distance curve calculated from the force “interaction” image shown down left.

Epitaxial growth of Fe₃O₄ Thin Films and Fe₃O₄/MgO/Fe heteroepitaxial structures for magnetic tunnel junctions

J.Orna^{1,2}, L. Morellon^{1,2}, P.A. Algarabel², J. A. Pardo^{1,3}, S. Sangiao¹, C. Magen,⁴ J.M. De Teresa², M. R. Ibarra^{1,2}

¹*Instituto de Nanociencia de Aragón, Universidad de Zaragoza, 50009-Zaragoza, Spain.*

²*Instituto de Ciencia de Materiales de Aragón, Universidad de Zaragoza-CSIC, 50009-Zaragoza, Spain.*

³*Departamento de Ciencia y Tecnología de Materiales y Fluidos, Universidad de Zaragoza, 50018- Zaragoza, Spain.*

⁴*Materials Science and Technology Division, Oak Ridge National Laboratory, P.O. Box 2008, ML 118 Oak Ridge, TN 37831-6030, USA*

juliao@unizar.es

Magnetite (Fe₃O₄) is a half-metallic ferromagnet with a high Curie temperature (860 K) that is expected to exhibit suitable properties for its implementation in spintronic devices [1-3]. In addition, the interest in spintronic structures based on magnetic oxides has increased recently [4]. MgO is a serious candidate as tunnel barrier because of the small lattice mismatch with the Fe₃O₄ (0.3%) electrode [5-7]. We believe that prior to application in real devices, the epitaxial growth of heterostructures with Fe₃O₄ and MgO should be further optimized. Additionally, recent magnetization studies on epitaxial Fe₃O₄ thin films grown on MgO [100] show that the ultrathin films (<5 nm thickness) are ferromagnetic and their magnetic moments are much greater than those of bulk magnetite, particularly at a thickness of 20 nm or below [8]. The observation of a ferromagnetic nature in ultrathin magnetite films is in contrast to the previously accepted dead layer interface model or a superparamagnetic behavior for ultrathin films of magnetite.

In this work we report the growth of epitaxial Fe₃O₄ thin films and Fe₃O₄/MgO/Fe heterostructures on MgO (001) substrates by means of pulsed laser deposition (PLD) and their structural and magnetic properties.

Fe₃O₄ and Fe thin films have been grown on single-crystal MgO (001) substrates by PLD using a KrF laser (248 nm). All layers have been deposited in ultra-high vacuum (base pressure < 5 × 10⁻⁹ Torr) at substrate temperatures of 400°C for Fe₃O₄ and between room-temperature (RT) and 400°C for Fe and MgO layers. Individual thin films and Fe₃O₄/MgO/Fe heterostructures on MgO (001) have been characterized by x-ray diffraction (θ-2θ, ω scans, φ scans, and reciprocal space maps) and x-ray reflectivity (XRR), high-resolution transmission electron microscopy (HRTEM) and VSM and SQUID magnetometry. Previous magnetoresistance and anomalous Hall effect measurements in our epitaxial Fe₃O₄ thin films have been published elsewhere [9, 10].

In Figure 1 we show the dependence of the magnetization with the nominal thickness of the films, which show a similar behavior as the observed by Arora et al [8]. For thickness below 20 nm the magnetization reaches values higher than the obtained for Fe₃O₄ single crystals (498 emu/cm³) and for ultrathin films (< 5nm) values higher than 1000 emu/cm³ can be observed. The origin of this unexpected behavior is still unclear. The non-compensation of spin moments between the tetrahedral and octahedral sublattices at the surface and antiphase-domain boundaries are inferred to be the main factor contributing to the observed enhanced magnetic moment [9].

After optimizing the growth conditions and fully characterizing the single Fe_3O_4 and Fe layers onto MgO (001), we undertook the growth of the full $\text{Fe}_3\text{O}_4/\text{MgO}/\text{Fe}$ heterostructures by PLD. HRTEM data (not shown here) demonstrate a high crystallinity of the MgO (001) tunnel barrier and sharp interfaces. From the XRR analysis in a selected heterostructure where both MgO barrier and Fe counterelectrode have been deposited at RT, a rms roughness relatively low, ~ 0.2 nm, is obtained, this being indispensable for future MTJs. The RT hysteresis loop in a sample grown in similar conditions, Fig. 2, reveals an independent switching of both Fe_3O_4 and Fe electrodes, this also being required for tunnel magnetoresistance. The low field (500 Oe) temperature dependence of the magnetization of the same heterostructure (not shown here) displays a clear and sharp drop at the Verwey transition, $T_V=115$ K, demonstrating the high quality of the Fe_3O_4 layer.

We have produced high quality epitaxial $\text{Fe}_3\text{O}_4/\text{MgO}/\text{Fe}$ heterostructures by PLD. To our knowledge, this type of heterostructure has not been grown before by PLD. Microfabrication of MTJs from these is in progress.

References:

- [1] K. Gosh et al., Appl. Phys. Lett. **73** (1998), 689.
- [2] X. W. Li et al., Appl. Phys. Lett. **73** (1998), 3282.
- [3] P. Seneor et al., Appl. Phys. Lett. **74**, 4017 (1999)
- [4] M. Bibes and A. Barthélémy, IEEE Trans. on Electron Devices **54**, 1003 (2007)
- [5] T. Kiyomura et al., J. Appl. Phys. **88**, 4768 (2000)
- [6] W. Kim et al., J. Appl. Phys. **93**, 8032 (2003)
- [7] X. Jin et al, J. Magn. Magn. Mater. **286**, 128 (2005)
- [8] S. K. Arora et al, Phys. Rev. B **77**, 134443 (2008)
- [9] J.M. De Teresa et al, Microelectr. Eng. **84**, 1660 (2007)
- [10] A. Fernandez-Pacheco et al., submitted to Phys. Rev. B (2008)

Figures:

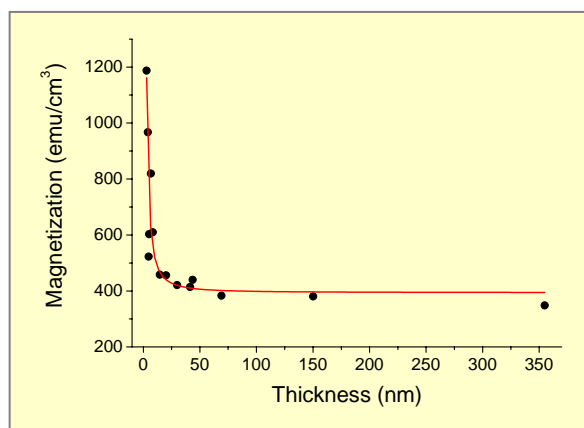


Figure 1. Dependence of the magnetization on the nominal thickness for the Fe_3O_4 thin films. The line is a visual guide.

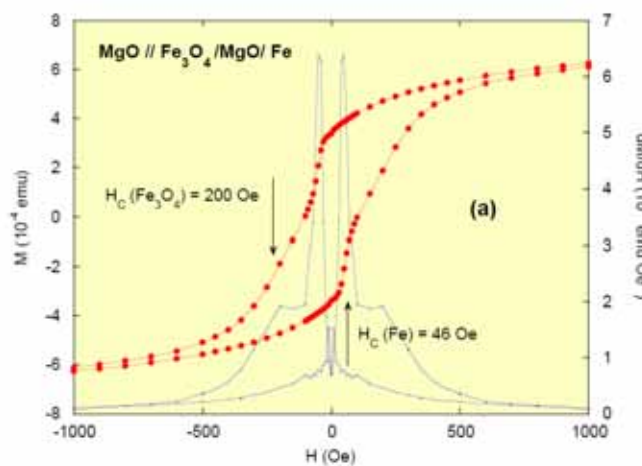


Figure 2. Room-temperature hysteresis loop of a Fe_3O_4 (70.9 nm)/MgO (3.7 nm)/Fe (5.6 nm)/Au (5.3 nm) heterostructure. The switching fields of both electrodes have been marked.

NANO GAL: GALICIAN TECHNOLOGICAL PLATFORM ON NANOTECHNOLOGY.

M. Otero-Leal, H. González-Jorge, J. L. Prieto.

Laboratorio Oficial de Metroloxía de Galicia, Parque Tecnolóxico de Galicia- San Cibrao das Viñas 32901, Ourense, Spain.

nanogal@nanogal.org

Nowadays, it is assumed that the nanotechnology will be one of the engines of economic growth in the XXI century. The Galician Technological Platform on Nanotechnology, Nanogal, was launched from the Laboratorio Oficial de Metroloxía de Galicia in July of 2008 with the financial support of Dirección Xeral de I+D (Xunta de Galicia). Nanogal is the framework of companies, technological centers, and university research groups which interest in nanoscience and nanotechnology.

Nanogal wants to build a new model of relationships in which are involved, companies with scientific, technological, political and social partners from inside and abroad Galician community. A model that will consolidate the exchange of knowledge and support create new business opportunities. A model based on intensive collaboration of all stakeholders.

Moreover, Nanogal wants to address technological challenges that can potentially contribute to a number of key objectives which are essential for Galicia's future competitiveness, including the timely development and deployment of nanotechnologies, nanotechnology development with a view of sustainable development, new technology-based public goods and services, technological breakthroughs necessary to remain at the leading edge in high technology sectors and the restructuring of traditional industrial ones.



XUNTA DE GALICIA
CONSELLERÍA DE INNOVACIÓN
E INDUSTRIA
Dirección Xeral de Investigación,
Desenvolvemento e Innovación



in.ci.te
Innovación, Ciencia e Tecnoloxía



Rede de Plataformas
Tecnolóxicas Galegas

TOUGHENING MECHANISM OF POLYMER/ LAYERED SILICATE NANOCOMPOSITES

Azin Paydayesh, Mehrdad Kokabi*, Ahmad Reza Bahramian

^aPolymer Engineering Group, Chemical Engineering Department, Faculty of Engineering, Tarbiat Modares University, P.O. Box: 14115-143, Tehran, Islamic Republic of Iran.

mehrir@modares.ac.irCorresponding author e-mail;

Phenolic resin (PR) have been widely used as coating, adhesives, composites, and so on due to their excellent flame resistance, heat resistance, insulativity, and dimensional stability[1]. However, their brittleness has significantly limited their widespread applications. High performance composites used for structural applications require excellent mechanical properties. The most widely used toughening agents are elastomers due to their high efficiency and low cost. However the phenolic network is subjected to deterioration in heat resistance, strength and modulus after incorporation with elastomers and flexible compounds [2]. Recently, studies on PR modification by addition of nanoparticles, such as layered silicate were reported [3]. But Report on modification of PR with high content of layered silicate and toughening investigation of these systems has not been found yet.

In this research, highly filled clay nanocomposites based on asbestos- phenolic system(adjusted to 40, 50, 60 and 70 phr clay of resin) are prepared and investigated by XRD, 3 point bending test, SEM and OM microscopy.

Investigation of samples by XRD, Exhibited the typical pattern of well-dispersed and exfoliated structure (fig.1).

Analysis of 3point bending test result, showed improvement of fracture toughness of highly filled nanocomposites by adding clay loading in nanocomposite (fig. 2).

OM images(fig.3) and SEM photographs (fig.) of fracture surface of composite na 60phr nanocomposite, indicated the toughening mechanism of nanocomposite:

clay sheets are too strong to break during crack growth, thus they try to impede the growth of the crack in the polymer matrix, which leads to crack front trapping. In fact clay bundles act as obstacles, forcing the crack to bow and cause deflection of the crack path, which can be one of the main toughening mechanisms for these clay reinforced nanocomposites.

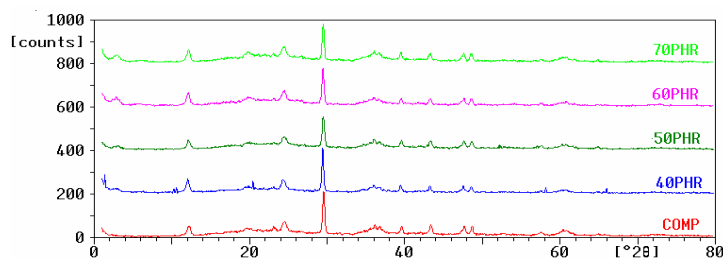


Fig.1

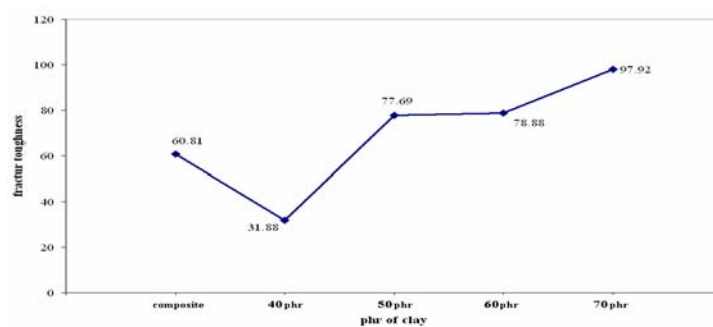
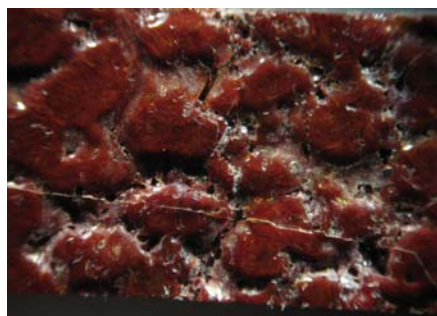
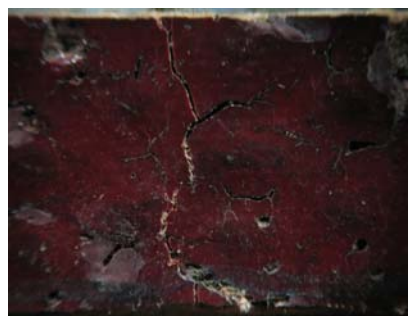


Fig.2

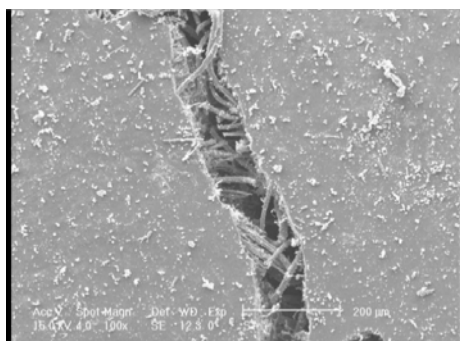


composite

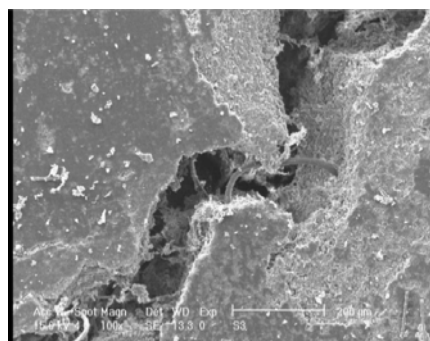


60phr nanocomposite

Fig.3



composite



60phr naocomposite

Fig.4

References:

1. C. Nirmal, S.N. Maithi, High performance Polymer, 18, 57-69, 2006.
2. H. Ma, G. Wei, polymer, 46, 10568-10573, 2005
3. B. Akbari, R.Bagheri, European polymer journal, 43, 782-788, 2007

MECHANICAL PROPERTIES STUDY OF SILICALITE MICROCANTILEVERS

*Ismael Pellejero*¹, Miguel A. Urbiztondo¹, Javier Sesé¹, María Villarroya-Gaudó¹, M.P. Pina¹, Jordi Agusti², Gabriel Abadal², Nuria Barniol², Jesús Santamaría¹

¹*Instituto Universitario de Investigación de Nanociencia de Aragón (INA), Pedro Cerbuna 12, Zaragoza 50009, Spain.* ²*Department of Enginyeria Electrònica, Universitat Autònoma de Barcelona, E-08193 Bellaterra, Spain.*

E-mail: ismapel@unizar.es

Zeolites constitute a family of highly interesting technological materials, on account of their framework structure, with pores of subnanometric size, and their remarkable properties in catalysis and adsorption [1]. Given the interesting properties of zeolite coatings, a significant effort has been carried out to combine the experience gathered in growing zeolite films and the fabrication methods used in the electronic industry to prepare microstructured supports, especially on Si substrates [2].

The final target of this work is the development of a highly selective and sensible nanoporous resonator for the early detection of explosives. The specific and tunable adsorption properties of zeolites combined with their chemical, thermal and elastic properties make them suitable candidates as sensible coatings. However, the mechanical properties of well-intergrown zeolite polycrystalline membranes must also fulfil the transducer requirements in order to develop a resonator with a good quality factor. Indeed, the resonant behaviour of zeolitic layers has not been previously attempted in the literature.

In this work c-oriented silicalite (Sil-1) polycrystalline layers have been synthesized on Si wafers and used as structural layers for micropatterning [3] to develop bulk Sil-1 cantilevers (see Figure 1). To the best of our knowledge this is the first time that a zeolite-only cantilever is proposed. Then, the resonance of these cantilevers excited with a piezoelectric material has been optically detected and characterized. Table 1 compiles the experimental results obtained. From these data, the intrinsic value of Young Modulus for well defined uncalcined SIL-1 polycrystalline cantilevers have been estimated (30.09 ± 5.29 GPa).

The microporous framework structure release by the organic template removal has been attempted by several methods. In addition to standard calcinations at 480°C under controlled atmosphere, ozone oxidation, oxygen plasma, and sulphuric acid leaching has also studied. Thermogravimetric analysis (see Figure 2) of free standing Sil-1 membranes indicates that O₃ oxidation at 200°C during 6 hours enables the complete organic removal. SEM analysis is being carried out to ensure the structure integrity (see Figure 3), before the estimation of the new young modulus.

Acknowledgments

Funding from Regional (PM050/2007 CTU-DGA), (PI 110/08 CTU-DGA) and National Government (CTQ2006 7159/PPQ (DGI-MEC) is gratefully acknowledged.

References:

- [1] Corma, A. State of the art and future challenges of zeolites as catalysts. J. Catal., 216 (1-2) (2003) 298-312.
- [2] Urbiztondo, M.A.; Valera, E.; Trifonov, T.; Alcubilla, R.; Irusta, S.; Pina, M.P.; Rodríguez, A.; Santamaría, J., J. Catal., 250, 190-194, (2007)
- [3] Pellejero, I.; Urbiztondo, M.; Villarroya, M.; Sesé, J.; Pina, M.P.; Santamaria, J.. Micropor. Mesopor. Mater. (2008), Materials 114 (2008) 110–120

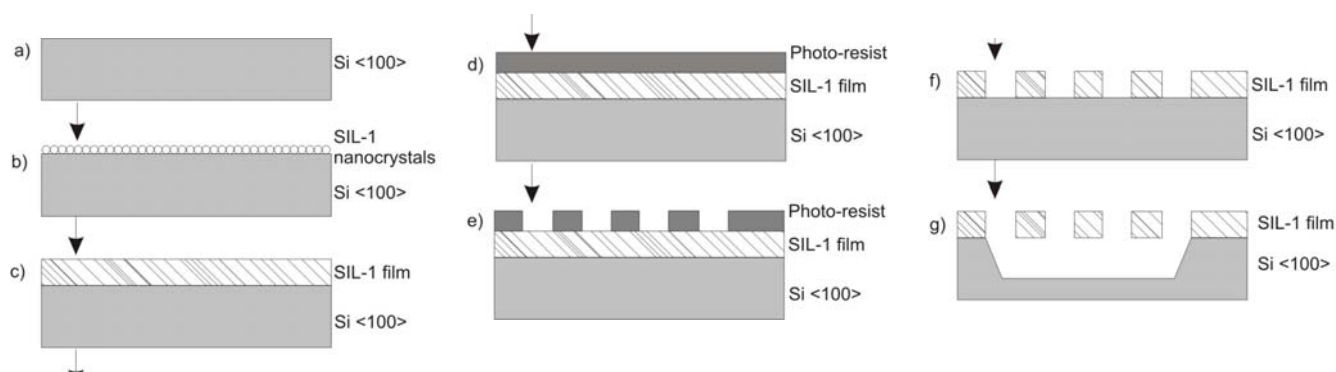


Figure 1. a) Starting Si wafer; b) spin coating of SIL-1 nanocrystals (4% wt. in ethanol); c) hydrothermal synthesis of SIL-1 film; d) deposition of a TI-35 ES reversal photo-resist; e) UV photolithography, reversal bake process and resist development, f) BHF etching of the SIL-1 layer; g) TMAH etching of Si underneath and bulk Sil-1 500 μm length cantilever released as shown in the SEM micrograph.

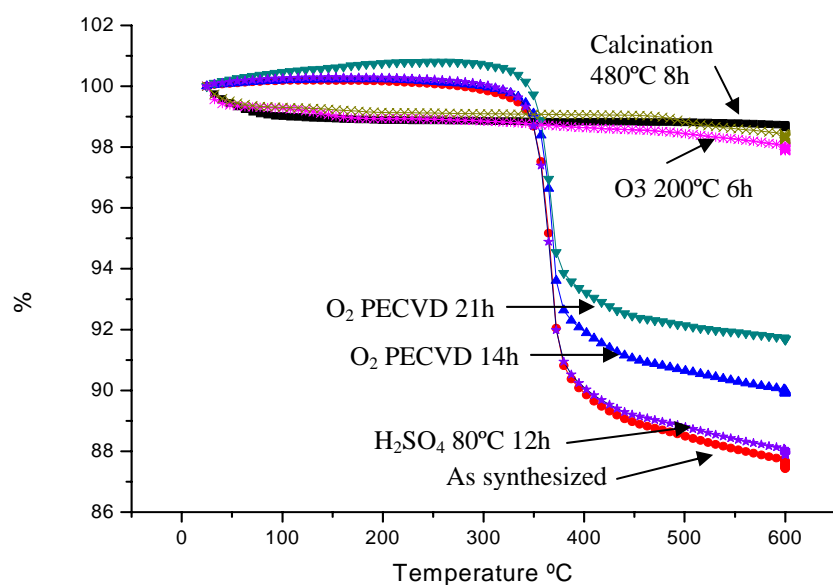


Figure 2. Thermo-gravimetric analysis of SIL-1 free standing membranes subjected to different organic template removal methods

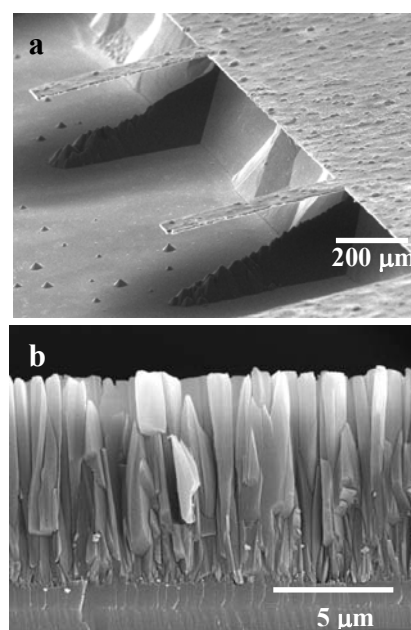


Figure 3. (a) As synthesized $\mu\text{cantilevers}$ 500 μm length. (b) Sil-1 layer, crystal orientation "c".

Table 1. Resonant frequency measurements for cantilevers resonating perpendicular to the SIL-1 surface (parallel to "c" crystallographic axis).

Sample	Length (μm)	Width (μm)	Thickness (μm)	f_0 (kHz)	Young Modulus GPa
1	500	90	8	18.03	30.27
2	1000	90	8	4.83	34.75
3	400	90	8	28.80	31.61
4	1000	60	8	4.54	30.75
5	400	60	8	26.60	26.97

ASSEMBLING MONOLAYERS OF MAGNETIC NANOPARTICLE ONTO TECHNOLOGICAL SUBSTRATES

Luis Peña, Miriam Varón,[†] Lluís Balcells,* Victor Puentes,[†] and Benjamín Martínez**

**Institut de Ciència de Materials de Barcelona, Bellaterra, Spain*

[†] CIN2, Universitat Autònoma de Barcelona, Bellaterra, Spain

lpena@icamab.es

Obtaining monolayers of highly ordered magnetic nanoparticle onto technological substrates is a very interesting issue from both basic research and technological points of view. Long range ordered arrays of magnetic nanoparticles have a great potential for applications in magnetic and electronic devices, thus making this field of research a very active one in the past few years. An ordered array of such nanoparticles can be used in novel tunnel magnetoresistance device or spin-torque nano-oscillators. Nevertheless, obtaining highly ordered monolayers of magnetic nanoparticles on top of on technological substrates has revealed to be a hard attainable issue. The common method to produce ordered two-dimensional arrays of nanoparticles is self-assembling. Self-assembling is a complex process in which several interactions between nanoparticles, substrate, and solvent are involved. As a result of the complexity of the process, a mixture of mono- and bi-layers with order in the few nanometres range is usually obtained when dealing with substrates with technological interest, such as complex oxides. Here we propose an alternative method to obtain highly ordered magnetic nanoparticle monolayers on these technological substrates. The method consists of depositing on the substrate an amorphous carbon membrane that previously has been covered with nanoparticles by spin coating. This new method is reproducible, robust and scalable, and is insensitive to the substrate material and topography. Here we present some preliminary results depositing highly ordered monolayers of cobalt superparamagnetic nanoparticles on top of silicon substrates.

Figures:

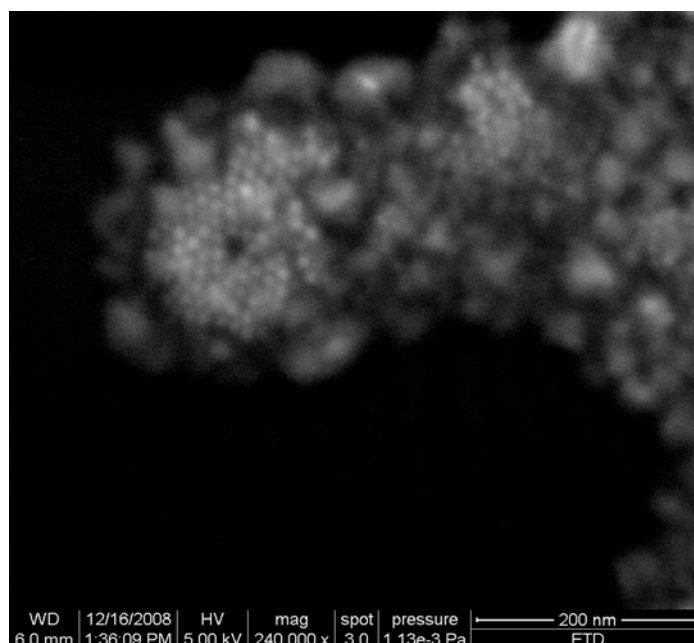


Fig. 1._ Secondary electrons SEM image of highly ordered self-assembled monolayer of Cobalt nanoparticles (white circles) on Silicon substrate. The average nanoparticles diameter is 6 nm.

MAGNETOSTRICTIVE DRIVE OF AFM CANTILEVERS FOR LIQUID OPERATION

M. Penedo, I. Fernández-Martínez, J. L. Costa-Krämer, M. Luna, F. Briones
Instituto de Microelectrónica de Madrid, c/ Isaac Newton 8, 28760 Tres Cantos, Spain
mapenedo@imm.cnm.csic.es

Tapping mode atomic force microscopy (AFM) has proven to be a powerful technique for imaging soft biological samples with AFM [1]. In liquid environments, small oscillation amplitude tapping mode images can have 1 nm lateral resolution or less [2]. AFM cantilevers are often driven in liquid by either mechanical (with a piezoelectric ceramic) or magnetic excitation (applying an alternating magnetic field to a cantilever coated with a magnetic material) methods. It has been also shown that in liquid environments magnetic actuation allows easier identification of the cantilever resonant frequency [3].

In this work, a novel magnetostrictive drive of dynamic AFM cantilevers has been developed to obtain topographic images and force spectroscopy in liquid environment. This method overcomes some of the limitations inherent to operation in liquids: low quality factor (Q) and the shift of the resonant frequency to lower frequencies due to the large damping and the added inertial mass of the liquid. Commercial silicon nitride cantilevers were one side coated with sputtered thin magnetostrictive iron-boron films, opposite to the tip side. These amorphous magnetic alloys present excellent magnetic properties [4], good corrosion resistance in liquid environments, and nearly zero accumulated stress [5] when properly deposited.

A new AFM liquid cell, with a set of miniature solenoids, has been built that creates an AC magnetic excitation field. It is demonstrated that the field drives the mechanical resonance of the coated cantilever through the film magnetostriction. Due to the even effect of the magnetostriction, we can excite the cantilever with an AC current with the same frequency that the resonant frequency (f_0) of the cantilever or with half of this resonant frequency ($f_0/2$). As an operational example, topographic images of a gold surface obtained in water solution are presented, which show lateral and topographic resolution comparable with operation in air.

References:

- [1] S. Kasas et al., *Biochemistry*, 36, (1997) 461.
- [2] D. J. Müller et al., *Biophys. J.*, 76, (1999) 1101.
- [3] S. M. Lindsay et al., *Jour. Vac. Sci. Technol. A*, 11, (1993) 808.
- [4] I. Fernández-Martínez et al., *JMMM*, 320, (2008) 68.
- [5] I. Fernández-Martínez et al., *JAP*, (2008) 103.

Figures:

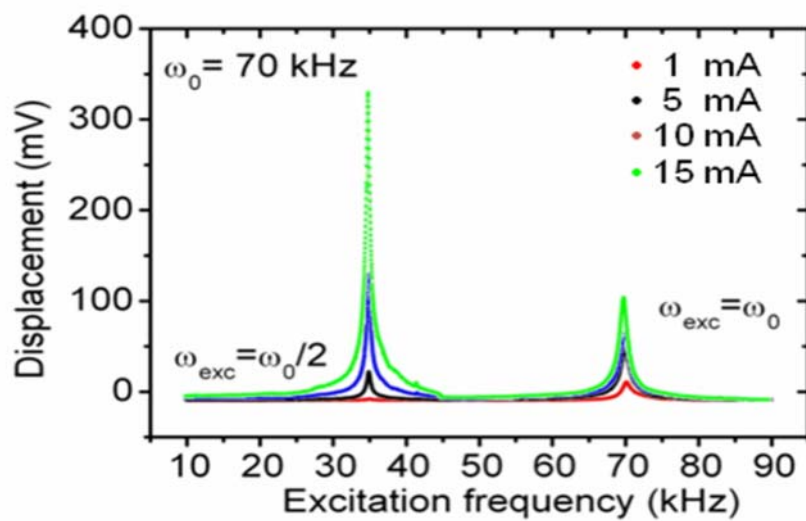


Fig. 1 Amplitude oscillation at different drive currents in air

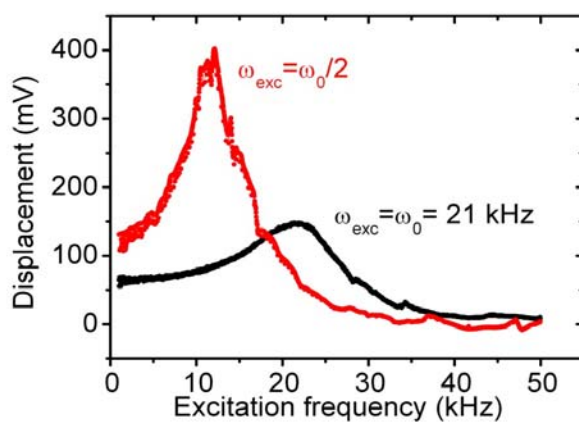


Fig. 2 Amplitude oscillation in liquid

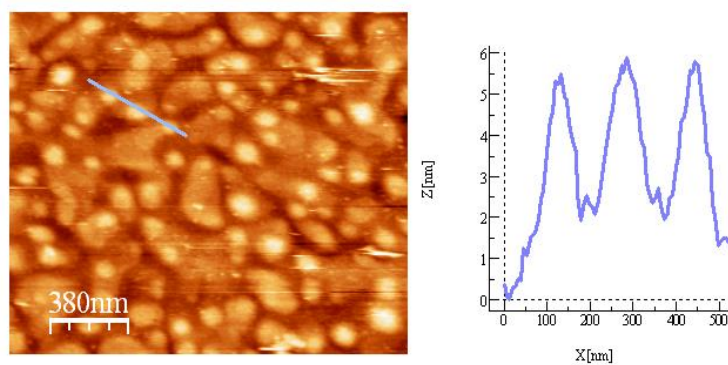


Fig. 3 Topographical image of a gold surface in water obtained with the magnetostrictive drive method. A topographic scan profile is shown.

INFLUENCE OF THE CONCENTRATION OF CTAB AND PHOTOCATALYST ON THE SIZE OF AU NANOTRIANGLES SYNTHESIZED BY A PHOTOCATALYTIC METHOD

Adelaide Miranda^{a)}, Eliana Malheiro^{a)}, Patrícia A. Carvalho^{b)}, Eulália Pereira^{a)}

a) REQUIMTE/Faculdade de Ciências, Universidade do Porto, Rua do Campo Alegre, 687, 4169-007 Porto, Portugal; b) Departamento de Engenharia dos Materiais do Instituto Superior Técnico, Av. Rovisco Pais, 1049-001 Lisboa, Portugal

eulalia.pereira@fc.up.pt

Shape-controlled synthesis of Au nanoparticles has received considerable attention, mainly due to the interesting optical properties of anisotropic Au nanostructures, namely a strong plasmon band in the NIR region. In particular, several methods for the preparation of Au nanoplates have been reported, including the use of plant extracts,¹ seed mediated synthesis,² use of polymers as capping agents,³ and thermal reduction.⁴ Nevertheless, the control over the size of the nanoplates is still a major challenge, with most of the methods yielding nanoplates with widths from a few hundred nanometers to a few micrometers, and large size dispersion.

We report a method for the preparation of Au nanoplates based on a photocatalytic approach⁵ to reduce the Au(III) precursor, in aqueous solution, in the presence of CTAB and a weak reducing agent. Changing the concentration of the photocatalyst it was possible to prepare samples with average side length 50 nm; 80 nm; 140 nm; and 250 nm (Fig. 1). Further control of the size of the nanotriangles can be achieved by changing the concentration of CTAB for each of the photocatalyst concentrations used. For instance, it was possible to prepare nanotriangles with average size length of 90 nm, 65 nm, and 35 nm, by increasing the concentration of CTAB (Fig. 2). In order to further understand the mechanism of formation of the nanoplates, we have followed the reaction by UV-vis spectrometry and TEM. The results obtained show that the reduction of the gold precursor is relatively fast, and after a few minutes of irradiation spherical nanoparticles are formed with diameters in the range 5-10 nm. These nanoparticles tend to fuse and grow by deposition of Au, until depletion of the Au precursor that, under the typical experimental conditions used, takes place within 2 hrs. The nanoplates formed after 2 hrs of irradiation are usually quite irregular, but after 48 hrs the samples contain well formed nanotriangles (Fig. 3).

Acknowledgments: Fundação para a Ciência e a Tecnologia, Portugal, PTDC/QUI/64484/2006, for financial support; A. Miranda thanks FCT for PhD fellowship SFRH/BD/17566/2004.

References:

- [1] Shankar, S. S.; Rai, A.; Ankamwar, B.; Singh, A.; Ahmad, A.; Sastry, M., *Nature Materials*, **3** (2004), 482-488.
- [2] Millstone, J. E.; Metraux, G. S.; Mirkin, C. A., *Adv. Funct. Mater.*, **16** (2006), 1209-1214.
- [3] Xiong, Y. J.; Washio, I.; Chen, J. Y.; Cai, H. G.; Li, Z. Y.; Xia, Y. N., *Langmuir*, **22** (2006), 8563-8570.
- [4] Huang, W. L.; Chen, C. H.; Huang, M. H., *J. Phys. Chem. C*, **111** (2007), 2533-2538.
- [5] Song, Y. J.; Yang, Y.; Medforth, C. J.; Pereira, E.; Singh, A. K.; Xu, H. F.; Jiang, Y. B.; Brinker, C. J.; van Swol, F.; Shelnutt, J. A., *J. Am. Chem. Soc.*, **126** (2004), 635-645.

Figures:

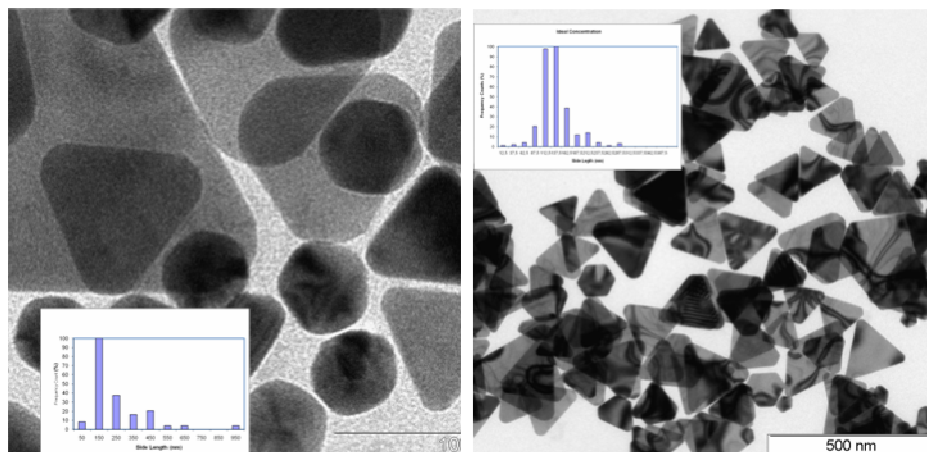


Figure 1. TEM images of nanotriangles obtained with a photocatalyst concentration of 1 nM (left) and 10 nM (right) Size distribution plots are shown as insets.

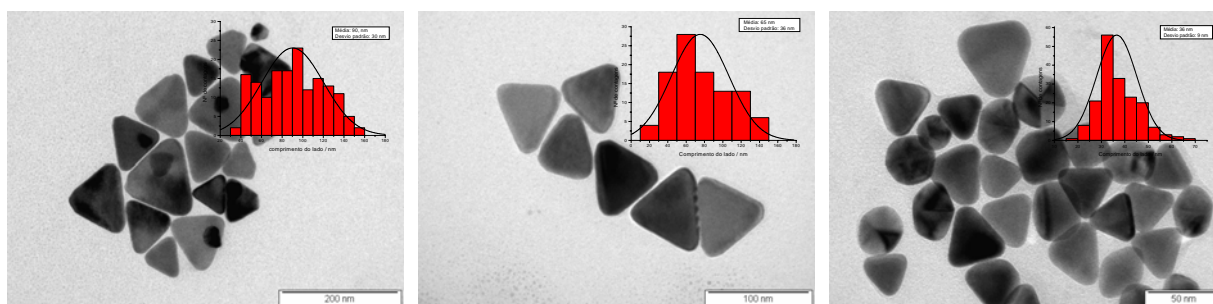


Figure 2. TEM images of nanotriangles obtained with a photocatalyst concentration of 50 nM and CTAB concentration of 0.8 mM (left, average length 90 nm), 1.6 mM (center, average length 65 nm) and 2.3 mM (right, average length 36 nm). Size distribution plots are shown as insets.

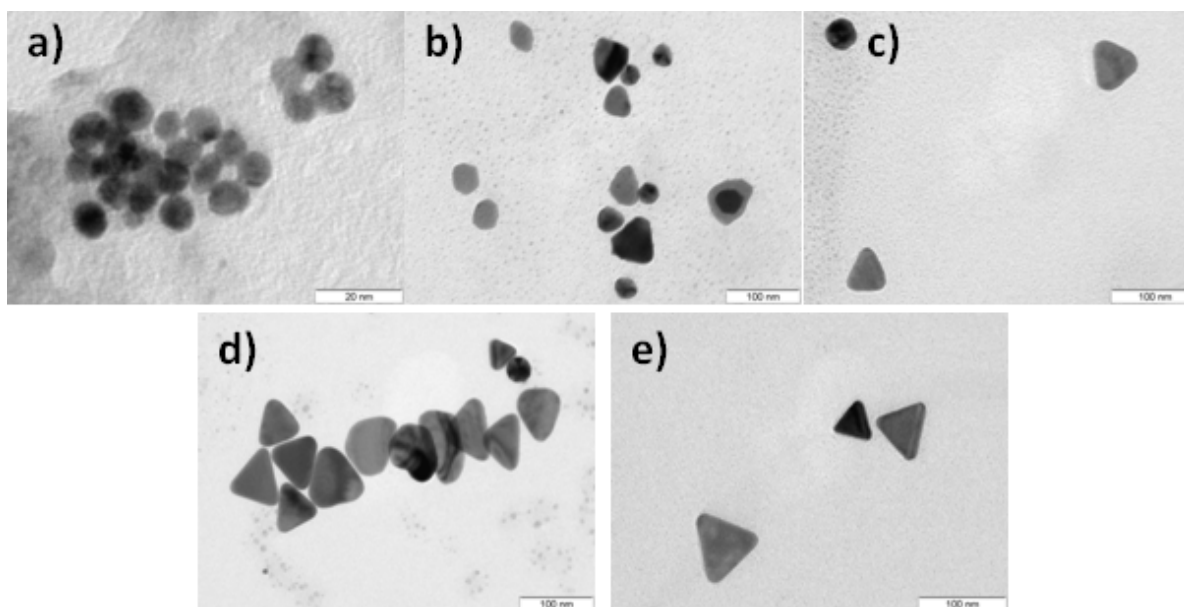


Figure 3: Representative TEM images of products collected after a) 30 min. irradiation; b) 60 min. irradiation; c) 90 min. irradiation; d) 120 min. irradiation; e) 120 min. irradiation and after 24 hrs in solution.

NANOMECHANICAL MASS SENSOR FOR SPATIALLY RESOLVED ULTRASENSITIVE MONITORING OF DEPOSITION RATES IN STENCIL LITHOGRAPHY

*Francesc Pérez-Murano¹, Julien Arcamone¹, Marc Sansa¹, Jaume Verd², Arantxa Uranga²,
Gabriel Abadal², Núria Barniol², Marc van den Boogaart³ and Juergen Brugger³*

¹ *Instituto de Microelectronica de Barcelona CNM-IMB (CSIC), Campus UAB, 08193 Bellaterra (Barcelona),
Spain.*

² *Dept. Electronics Engineering, Universitat Autònoma de Barcelona, ETSE-UAB, 08193-Bellaterra
(Barcelona), Spain*

³ *Microsystems Laboratory (LMIS1), EPFL, EPFL, CH-1015 Lausanne (Switzerland).
Francesc.perez@cnm.es*

Shadow masking (also known as nanostencil lithography, SL) is a well known technique to fabricate patterns on a surface. It is a versatile method that can be used in a variety of applications. There has been recently a strong interest regarding the use of shadow masks, mostly related to combinatorial materials science, organic based device fabrication, as well as rapid prototyping of nanoscale structures using dynamic or quasi dynamic stencil deposition [1]. From the study of almost all reported variants of SL, a series of intrinsic generic advantages emerges. Its main features are its 'cleanliness', its flexibility, its parallelism and its high resolution. This exclusive characteristic makes that ultra-clean surfaces with high purity deposits can be obtained. From that, mechanically fragile and chemically functionalized surfaces can be structured, due to the absence of cyclic process steps seen in lithography and the absence of etching processes. Its parallelism makes it much faster than charged particle techniques (FIB or eBL). Recently it has been demonstrated its implementation at full-wafer scale while providing 150 nm resolution [2].

Here, we report on a novel application for NEMS mass sensing, which allows in situ monitoring and characterization of material fluxes flowing through nano- or micro-apertures in vacuum deposition systems, enabling the development of a new generation of micro- and nano-SL systems for sequential multilevel patterning [3]. A dedicated sensor with spatial resolution is used to characterize the deposition rate (or flux) profile after the material has passed through the stencil membrane apertures. A mechanical mass sensor is developed based on a resonating mechanical structure whose resonance frequency shifts down when a small quantity of material is deposited on top of it. By tracking the change of resonance frequency, the mass deposition can be monitored in real time by computer. In particular, we use a CMOS integrated NEMS mass sensor. [4]

The NEMS mass sensor used here is an 18 μm long, 600 nm wide, 850 nm thick (nominal dimensions) resonant doubly clamped beam whose metallic structure is fabricated with the top metal layer of a commercial 0.35 μm CMOS technology (Figure 1). The electromechanical resonator is monolithically integrated with a CMOS oscillator circuit [5]. This sensor presents the following specific features: (i) a high mass resolution (around $3.4 \times 10^{-11} \text{g} \cdot \text{cm}^{-2} \cdot \text{Hz}^{-1}$), which allows detecting deposition rates below $10 \text{ pm} \cdot \text{s}^{-1}$ for silver deposition; (ii) very good spatial resolution, in the range of hundreds of nanometers, due to the small dimensions of the sensor, which allows a position-dependent detection; (iii) device portability, because the sensor actuation and readout are completely electrical (CMOS integration), simplifying the detection set-up.

We have modeled the local material deposition rate in the sensor surface and compared the modeling results with the experimental measurements employing the sensor. We found that the material flux through confined apertures can be described by taking into account two geometrical effects: (i) The pattern widening effect, which causes the pattern on the sensor

plane to be smaller than the aperture on the shadow mask, due the presence of a gap between stencil and, and because the source is not perfectly punctual; (ii) the penumbra effect, which obscures part of the whole source area, causing the maximum flux on the sensor plane to be smaller than the maximum flux provided by the source. The model was validated with experimental data obtained by displacing the stencil laterally in a given direction while monitoring the change of resonance frequency of the sensor (Figure 2).

Regarding future applications, we have evaluated the minimum squared aperture size (W_{ST_MIN} , defined as the width of a square aperture) that still would be sensed, using the geometrical model of the flux on the sensor plane passing through confined apertures. W_{ST_MIN} has been calculated as a function of the stencil-sensor gap G for a minimum detectable deposition rate by the sensor F_{MIN} of 0.01 nm s^{-1} (value based on the previous experimental observations) and considering a constant stencil scanning speed of 3 mm s^{-1} . In addition, as further miniaturization of the sensor will result in an increase in its mass sensitivity, W_{ST_MIN} is calculated for several sensor beam lengths, L_S (Figure 3). Our analysis suggests the possibility of detecting sub-100-nm apertures in future developments, which would require reducing the gap between stencil and sensor and reducing the sensor length.

References:

- [1] J. Brugger, V. Savu, K. Sidler, M.A.F. van den Boogaart, O. Vazquez Mena, G. Villanueva, E-Nano Newsletter, **vol 8** (2007), pp 22-28
- [2] J. Arcamone, M. A. F. van den Boogaart, F. Serra-Graells, J. Fraxedas, J. Brugger, F. Perez-Murano, Nanotechnology, **vol 19** (2008), 305302
- [3] J. Arcamone, M. Sansa, J. Verd, A. Uranga, G. Abadal, N. Barniol, M. van den Boogaart, J. Brugger, F. Pérez-Murano, Small, **vol 5**, No 2, (2009), pp 176-180
- [4] J. Verd, A. Uranga, J. Teva, J.L. López, F. Torres, J. Esteve, G. Abadal, F. Pérez-Murano, N. Barniol IEEE Electron Device Lett., **vol 27** (2006), pp 495-497
- [5] J. Verd, A. Uranga, J. Teva, J.L. López, F. Torres, J. Esteve, G. Abadal, F. Pérez-Murano, N. Barniol IEEE Electron Device Lett., **vol 29** (2008), pp 146-148

Figures:

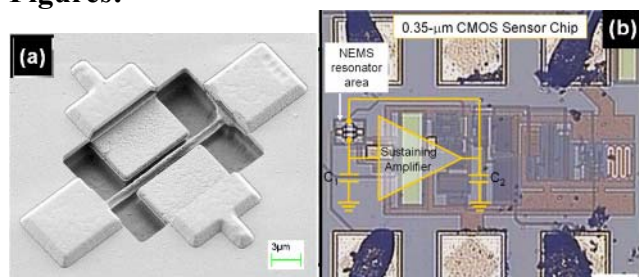


Figure 1. SEM image of the Nanomechanical resonator (left) and optical image showing the sensor + CMOS circuit

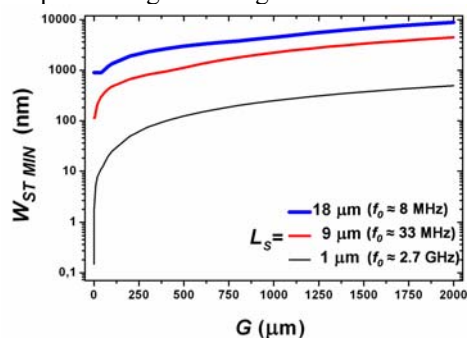


Figure 3. Evaluation of the minimum detectable stencil aperture W_{ST_MIN} as a function of the stencil-sensor gap G for a relative minimum detectable flux of 0.05 and a scan speed of 3 μm/s

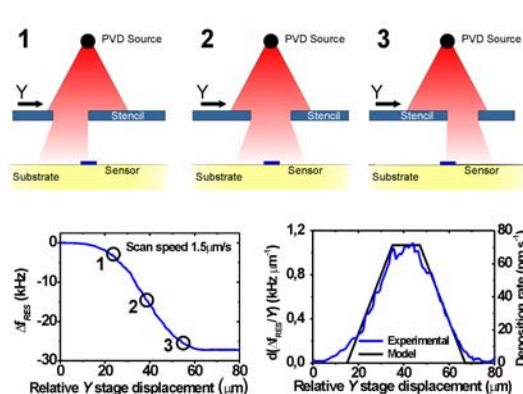


Figure 2. Experimental determination of the evaporation rate of an atom beam after passing through a stencil hole

SYNTHESIS AND CHARACTERIZATION OF MULTIPODAND CALIX[4]ARENE-PROTECTED GOLD NANOPARTICLES

Luca Pescatori,^a Arturo Arduini,^a Andrea Pochini,^a Andrea Secchi^a, Alice Boccia,^b Valeria Di Castro,^b Valeria Lanzilotto,^b and Robertino Zanon^b

^a*Dipartimento di Chimica Organica e Industriale, Università degli Studi, V. le G.P. Usberti 17/a, 43100 Parma, Italy*

^b*Dipartimento di Chimica, Università degli Studi di Roma 'La Sapienza', p.le Aldo Moro, 5 - I 00185 Roma, Italy*

lpescatori@yahoo.com

Monolayer-protected Au clusters^[1] (MPCs) have aroused significant scientific interest because these structures are known to be useful in many fields such as optoelectronics, catalysis and molecular sensing.^[2] Small MPCs (core < 2 nm) are particularly enticing owing to their quantum size effects.^[3] Indeed, it is known that as the core size decreases under the nanometer limit, the particles attain discrete electronic states and thus can show semiconductor-like electronic properties. The preparation of these compounds through direct methods has been, however, restricted to nanoparticles in which the gold passivation has been obtained with specific ligands such as tripeptides (glutathione), mercaptosuccinic acid and thiphenylphosphine derivatives.

Despite the large amount of data present in the literature on the synthesis of MPCs prepared with several thiol-based ligands, using the two phase method developed by Brust,^[4] the role played by the ligand "sulphur denticity" on the gold clusters size has not been yet systematically studied.

In this context we have recently explored the possibility to use multidentate calix[n]arene derivative **1** (see Figure 1), characterized by the presence of two convergent undecanthiol chains onto its lower rim, for the preparation of Au MPCs. The particular multidentate structure of the calixarene derivatives allows the preparation of rather monodispersed and size controlled clusters as shown by TEM measurements (see Figure 2). In particular, when the calixarene is used in excess with respect the aurate salt AuCl₄⁻, clusters with very smaller core were obtained. These new MPCs were compared with gold nanoparticles stabilized by monodentated ligand **2** and dodecanthiol. The MPCs synthesized were also characterized with XPS to analyze the oxidation state of gold in the inorganic core. These results open new possibilities for the synthesis of MPCs with controlled and reduced size to be employed in the emerging field of the nanotechnology.

References:

- [1] Love, J. C.; Estroff, L. A.; Kriebel, J. K.; Nuzzo, R. G.; Whiteside, G. M. *Chem. Rev.* **2005**, *105*, 1103-1169.
- [2] *Nanoparticles: From Theory to Application*; Schmid, G. Ed.; Wiley-VCH:Weinheim, **2004**.
- [3] Volokitin, Y.; Sinzig, J.; de Jongh, L. J.; Schmid, G.; Vargaftik, M. N.; Moiseev, I. I. *Nature* **1996**, *384*, 621-622.
- [4] Brust, M.; Fink, J.; Bethell, D.; Schiffrin, D. J.; Kiely, C. J. *Chem. Soc., Chem. Commun.* **1995**, 1665-1656.

Figures:

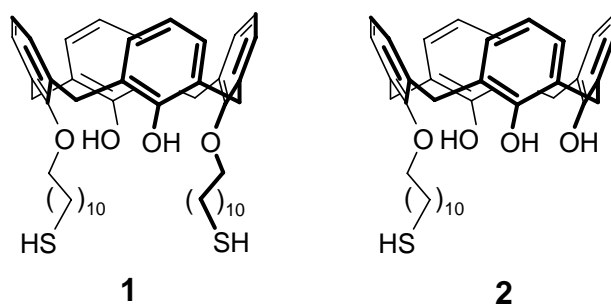


Figure 1. Polyalkylthiols lower rim functionalized calixarene derivatives for the preparation of Au MPCs.

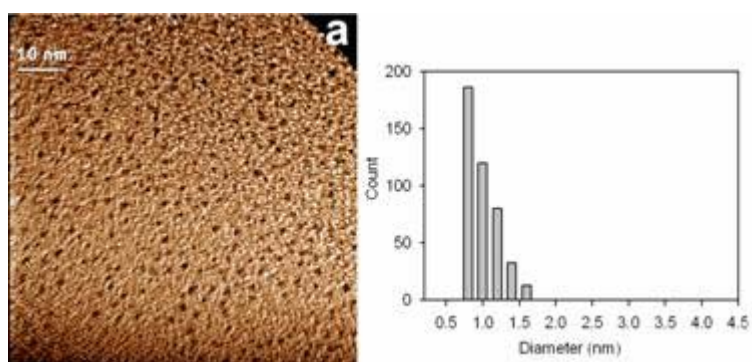


Figure 2. TEM image and core size distribution diagram of MPCs coated with calix[4]arene 1.

Pharmaceutical Characterization of (P53) Gene-loaded chitosan Nanoparticles

Payam Peymani^{1, 2}, Mansoureh Jaberipour³, Ali-Mohammad Tamaddon¹

And Mehrdad Hamidi^{1, 4}

1. Department of Pharmaceutics, Faculty of Pharmacy, Shiraz University of Medical Sciences, Shiraz, Iran.

2. Medicinal and Natural Products Chemistry Research Center& Medical Biotechnology Student Research Group, Shiraz University of Medical Science, Shiraz, Iran.

3. Shiraz Institute for Cancer Research, Medical School, Shiraz University of Medical Sciences, Shiraz, Iran.

4. Department of Pharmaceutics, School of Pharmacy, Zanjan University of Medical Sciences, Zanjan, Iran

Objectives & Background: Gene transfer for cancer gene therapy requires carriers for the plasmid DNA which can efficiently carry the gene into the nucleus of the desired cells. Biodegradable nanoparticles formulated using a biocompatible polymer, Chitosan, have the potential for sustained gene delivery. Since the p53 tumor suppressor gene has been found to be mutated in more than 50% of human cancers, it has attracted the interest of numerous researchers. The capacity of p53 for multiple biological functions can be attributed to its ability to modulate various cellular processes, including apoptosis, cell cycle arrest and DNA repair. Based on p53's critical role in carcinogenesis, scientists have developed multiple effective strategies for treating cancer by enhancing function of wild-type p53.

Materials & methods: Nanoparticles containing plasmid DNA (P53) were formulated using an ionotropic gelation technique. The objective of the present study is consideration of some factors such as Chitosan Molecular weight and concentration, chitosan to Tripolyphosphate amount ratio, solution pH and their effects on size and size distribution of nanoparticles. Fractional factorial design by definition These 4 factors in 4 levels was used for optimization of nanoparticles fabrication. Morphological property, zeta potential, particle size and physicochemical properties of the prepared chitosan-TPP/ nanoparticles were investigated various analytical equipments such as using Electron Microscope, Zetasizer, Dynamic light scattering, and Fourier-transform infrared spectroscopy.

Results: The nanoparticles obtained had a mean particle size of 79 ± 10 nm, indicating a narrow size distribution but in total the nanoparticles size was between 62-193 nm. The P53-loaded chitosan-TPP nanoparticles formed are of a diameter inferior to 110 nm.

Discussion & Conclusion: The formation of high yield chitosan–TPP nanoparticles with predetermined nano-metric size and surface charge density can be simply manipulated and controlled by varying the key processing conditions of chitosan concentration, chitosan to TPP weight ratio, and solution pH value. Within the tested range of conditions, the increase in particle size showed a simple linear relationship with increasing chitosan to TPP weight ratio.

Keywords: Chitosan, Nanoparticles, Gene Delivery, P53, Cancer gene therapy

Figure 1

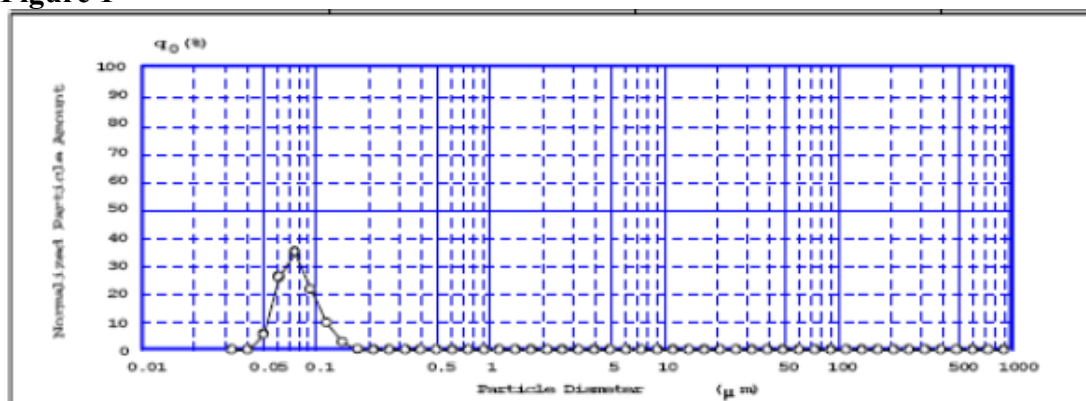
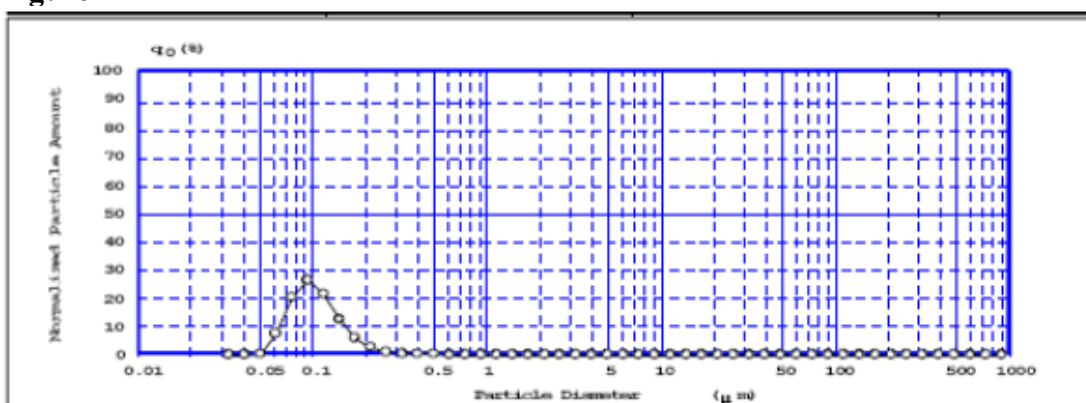


Figure 2



References:

- [1] Tae HK, In KP, Su IK, Hwan JJ, Hee SB and Chong SC. Chitosan Derivatives as Gene Carriers, *Key Engineering Materials* 2005; 288-289: 97-100.
- [2] Sunil AA, Nadagouda NM, Tejjraj MA. Recent advances on chitosan-based micro and nanoparticles in drug delivery, *Journal of Controlled Release* 2004; 100: 5–28.
- [3] Kathleen FP, Xu L, Esther HC. Non-viral gene delivery p53. *Current Opinion in Molecular Therapeutics* 2000; 2:168-175.
- [4] Swayam P and Vinod L. Nanoparticles-Mediated Wild-Type p53 Gene Delivery Results in Sustained Antiproliferative Activity in Breast Cancer Cells. *Molecular Pharmaceutics* 2004; 1: 3- 211-219.

GOLD NANOPARTICLES FUNCIONALIZED WITH ANTIBODIES: STUDYING THE STOICHIOMETRY BETWEEN ANTIBODIES AND PARTICLES.

E. Polo, V. Grazú, M.P. Pina, J.M. de la Fuente, J. Santamaría.

Instituto de Nanociencia de Aragón, University of Zaragoza, Edif. Inter II. C/ Pedro Cerbuna 12, 50009 Zaragoza Spain

esterpol@unizar.es

Gold nanoparticles (AuNPs) have been used for analytical and biomedical purposes for many years. Rapid and simple chemical synthesis, optical and electrochemical properties, a narrow size distribution, a large surface-to-volume ratio, and efficient coating by thiols and other bioligands has enabled gold nanoparticles to be used for several biorecognition binding applications.¹ These biomolecular recognition events occurring at the nanoparticles surface have an influence on the optical and/or electrical properties of the system allowing the development of more sensitive and flexible sensing systems.

The availability of versatile chemistry for functionalizing gold nanoparticles surface, allows preparation of various bioconjugates and these bioconjugates are generally stable in aqueous solution in a wide range of pH values, and ionic strength, providing a particularly useful platform for the application in biodetection. For example, signal enhancement of gold nanoparticles functionalized with capture antibodies has been used for immunoassay detections of analytes.²

In this work, water-soluble gold clusters protected by monolayers of tiopronin (N-2-mercaptopropionylglycine) were synthesized, using the method reported by *Murray et al. in 1999*,³ with a core diameter size between 2 and 3 nm (**Au@Tiopronin**). These **Au@Tiopronin** NPs have been functionalized with antibodies by a covalent strategy binding directly to the nanoparticle surface.⁴

The stoichiometry between **Au@Tiopronin** NPs and antibodies has been studied by assays based on the aggregation of gold nanoparticle (AuNPs) with a bigger size and coated with the corresponding antigen.⁵ 14 nm size-gold nanoparticles were synthesized by citrate method⁶, and antigens were absorbed on the AuNP surface via electrostatic interactions. Antibody-labelled **Au@Tiopronin** NPs bind to the antigen adsorbed onto AuNPs to generate a sandwich system.

The antibody-antigen molecular event occurring at the surfaces of these nanoparticles, results in measurable changes and shifts of nanoparticle surface plasmon absorption band (*Figure 1*). Gold nanoparticle exhibit a strong surface plasmon band in the visible region of the electromagnetic spectrum, at 520 nm, and this SP band depends on the shape, size and the surrounding medium of the particles.⁷ The aggregation of AuNPs leads to the formation of a new absorption band at longer wavelengths, and causes a characteristic transition in solution colour from red to purple-violet.⁸

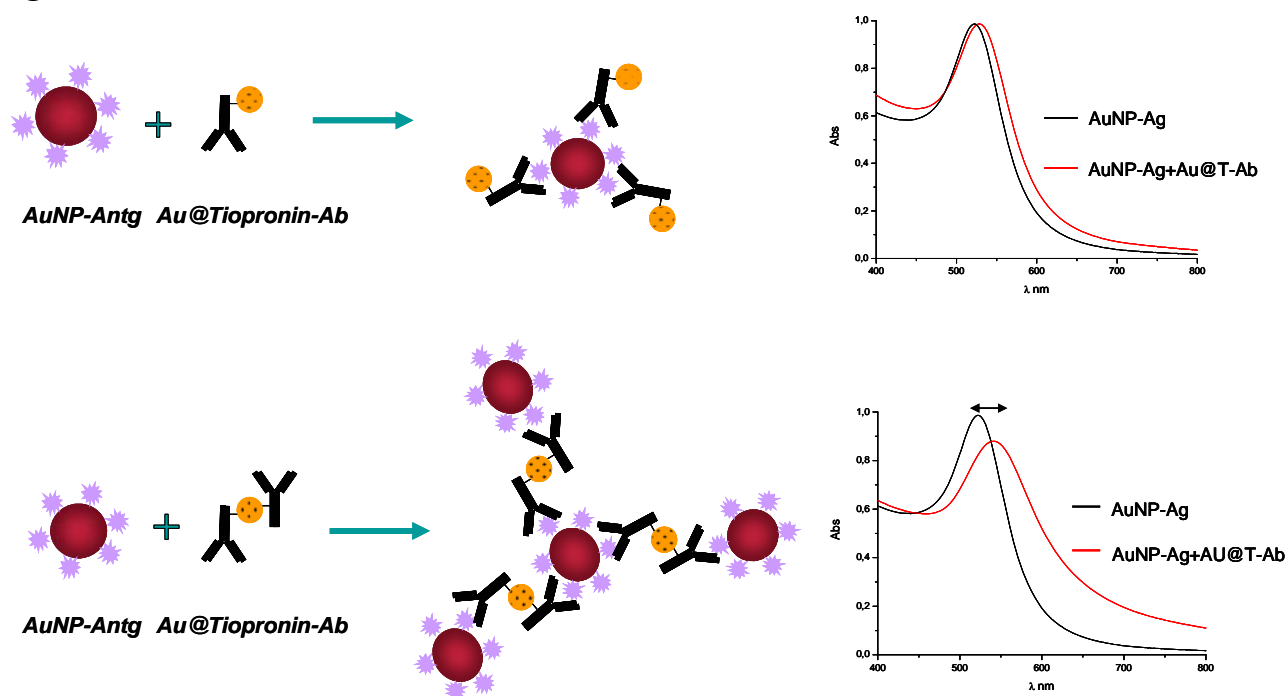
The rate of aggregation of antigen-**AuNPs** in the presence of antibodies-**Au@Tiopronin** NPs was measured by monitoring the absorption change of the AuNPs upon aggregation. The aggregation process was also monitored by transmission electron microscopy.

References:

- [1] Rosi N.L.; Mirkin C.A.; *Chem.Rev.*, (2005), 105, 1547-1562.
- [2] Baptista, P.; Pereira, E.; Eaton, P.; Doria, G.; Miranda, A.; Gomes, I.; Quaresma, P.; Franco, R.; *Anal. Bioanal. Chem.* (2008), 391, 943-950.
- [3] Templeton, A.C.; Chen, S.; Gross, S.M.; Murray, R.W.; *Langmuir* (1999), 15, 66-76.
- [4] Bonroy, K.; Frederix, F.; Reekmans, G.; Dewolf, E.; de Palma, R.; Borghs, G.; Declerck, P.; Goddeeris, B.; *Journal of Immunological Methods* 2006, 312, 167-181.
- [5] Thanh, K.; Rosenzweig, Z.; *Anal. Chem.* (2002), 74, 1624-1628.
- [6] Enüstün, B.V.; Turkevich, J.; *J. Am. Chem. Soc.* (1963), 85, 3317.
- [7] Zhong, Z.; Patskovskyy, S.; Bouvrette, P.; Luong, J.H.T.; Gedanken, A.; *J.Phys. Chem.*; (2004), 108, 4046-4052.
- [8] Schneider, G.; Decher, G.; *Langmuir* (2008), 24, 1778-1789

Figures:

Figure 1



ULTRA HIGH QUALITY FACTOR ON PHOTONIC CRYSTAL MICROCAVITIES AND LATTICES: A PATH FOR ULTRA LOW THRESHOLD LASING AND OBSERVATION OF CAVITY-MEDIATED STRONG COUPLING

L.J. Martínez, I. Prieto, B. Alén, D. Fuster, Y. González, L. González, M.L. Dotor and P.A. Postigo

Instituto de Microelectrónica de Madrid, Centro Nacional de Microelectrónica, Consejo Superior de Investigaciones Científicas, Isaac Newton 8, PTM Tres Cantos, 28760 Madrid, Spain

aitor@imm.cnm.csic.es

Laser emission of a compact surface-emitting microlaser, optically pumped and operating around 1.55 μm at room temperature is presented. The two-dimensional photonic crystal is conformed in a hybrid triangular-graphite lattice designed for vertical emission. The structures have been fabricated on InP slabs. The heterostructure consists of four $\text{In}_{0.65}\text{As}_{0.35}\text{P}/\text{InP}$ quantum wells grown on an InP substrate by molecular beam epitaxy and it is transferred onto a silicon-on-silica substrate by wafer bonding (SiO_2 thickness = $0.9 \pm 0.1 \text{ mm}$). Standard techniques of electron-beam lithography, reactive ion beam etching and reactive ion-etching have been used for the patterning. The optical characterization was performed by micro-photoluminescence spectroscopy. Single-mode, strongly polarized laser emission has been achieved with quality factors Q exceeding 15000.

We show laser emission from the hybrid triangular-graphite lattice at the Γ point. This lattice was introduced with the aim of combined the good properties of the triangular and graphite lattice [1]. The structure has several bands with slow curvature close to the high symmetry points. The lattice was fabricated in III-V semiconductor slab [2]. The structure presents a strong photoluminescence around 1500 nm. The hybrid triangular-graphite lattice was fabricated with lattice parameters $R/a=0.12$, $R_g/a=0.17$, and several values of $a=840\text{-}1050\text{nm}$ at steps of 20nm. Guide-mode expansion method for band calculation [3] has been used. The structures are fabricated on squares with sides around 30 μm . Polarization resolved micro-photoluminescence spectroscopy was used for optical characterization. The samples were optically pumped with a 780nm laser diode through a $\text{NA}=0.14$ (5x) objective placed at normal incidence. The PL emission was collected by a fiber coupled to a optical spectrum analyzer. Several lasing devices operating around 1.55 μm with thresholds of a few of hundreds of microwatts showing polarized emission have been measured.

Moreover, room temperature lasing at 1.5 μm has been obtained in photonic crystal microcavities with self-assembled quantum wire nanostructures. Ultra low threshold values of 10 μW along world-record quality factors exceeding $Q=32000$ have been measured using L7-type photonic crystal microcavities. The results open the way to the observation of strong coupling at room temperature and ultra low threshold laser emission.

References

- [1] L.J. Martínez, A. García-Martín, and P. A. Postigo “Photonic band gaps in a two-dimensional hybrid triangular-graphite lattice” *Opt. Express* 12 (23), 5684-5689 (2004).
- [2] C. Monat, C. Seassal, X. Letartre, P. Regreny, M. Gendry, P. Rojo Romeo, P. Viktorovitch, M. Le Vassor d'Yerville, D. Cassagne, J. P. Albert, E. Jalaguier, S. Pocas, and B. Aspar, Two-dimensional hexagonal-shaped microcavities formed in a two-dimensional photonic crystal on an InP membrane, *J. Appl. Phys.* 93, 23 (2003),.
- [3] L. C. Andreani and D. Gerace, “Photonic-crystal slabs with a triangular lattice of triangular holes investigated using a guided-mode expansion method,” *Phys. Rev. B*, 73, 235114, 2006.

Figures:

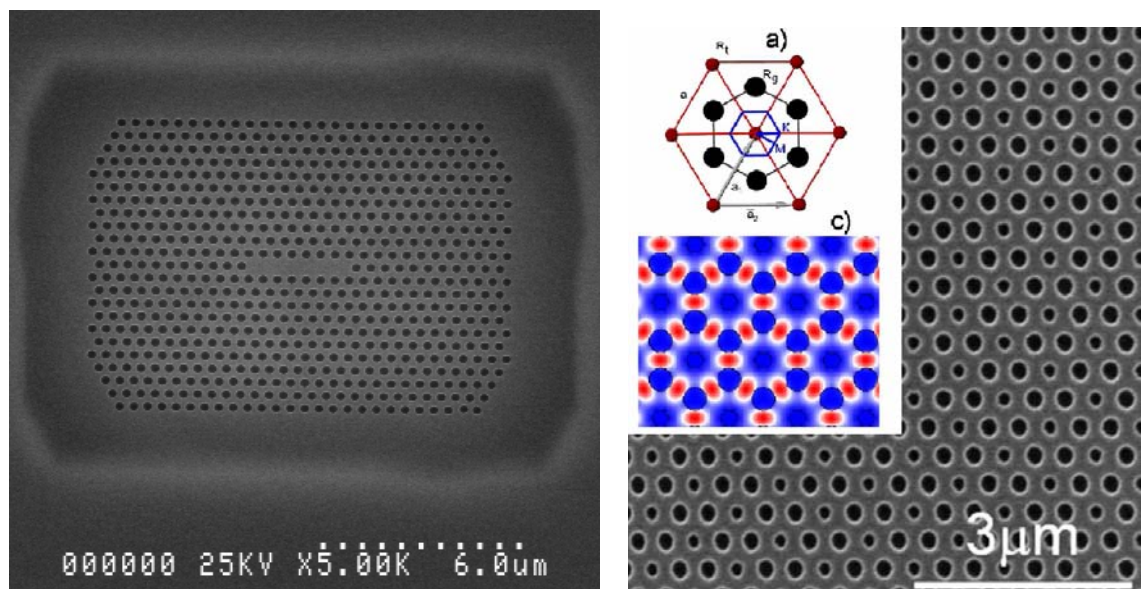
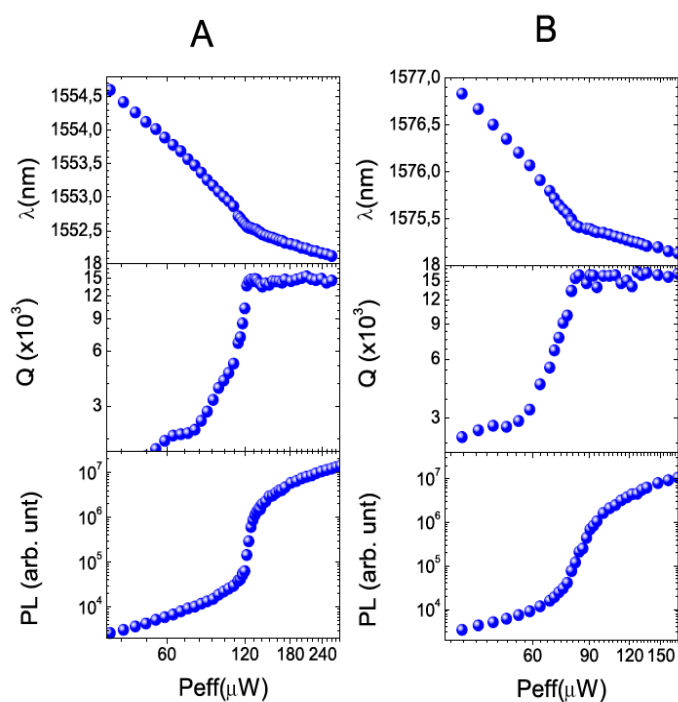


Fig.1. Left: SEM picture of a L7 cavity made on InP-based material with Q-factor exceeding 32000. Right: SEM picture of the hybrid triangular-graphite photonic crystal lattice. Inset: a) layout of the lattice. C) normalized E-field intensity profile at the G3 point.



Evolution with the excitation effective power for two (A and B) hybrid triangular-graphite photonic crystal lattices like the shown in Fig.1. Qs up to 15000 have been observed.

THE IMMUNE RESPONSE INDUCED BY TOLL-LIKE RECEPTOR LIGANDS IS DIFFERENTIALLY REGULATED BY TIOPRONIN MONOLAYER-PROTECTED SILVER NANOPARTICLES

David Pozo¹, Paula M Castillo², Juan L Herrera¹, Rebecca Klippstein¹, Rafael Fernandez-Montesinos¹, Ana P Zaderenko²

¹CABIMER-Andalusian Centre for Molecular Biology and Regenerative Medicine (CSIC-University of Seville-UPO-Junta de Andalucía), Americo Vespucio Ave, Parque Científico y Tecnológico Cartuja 93, 41092, Seville, Spain

*²Department of Physical, Chemical and Natural Systems, UPO-Pablo de Olavide University, Carretera de Utrera Km 1, 41013 Seville, Spain
david.pozo@cabimer.es*

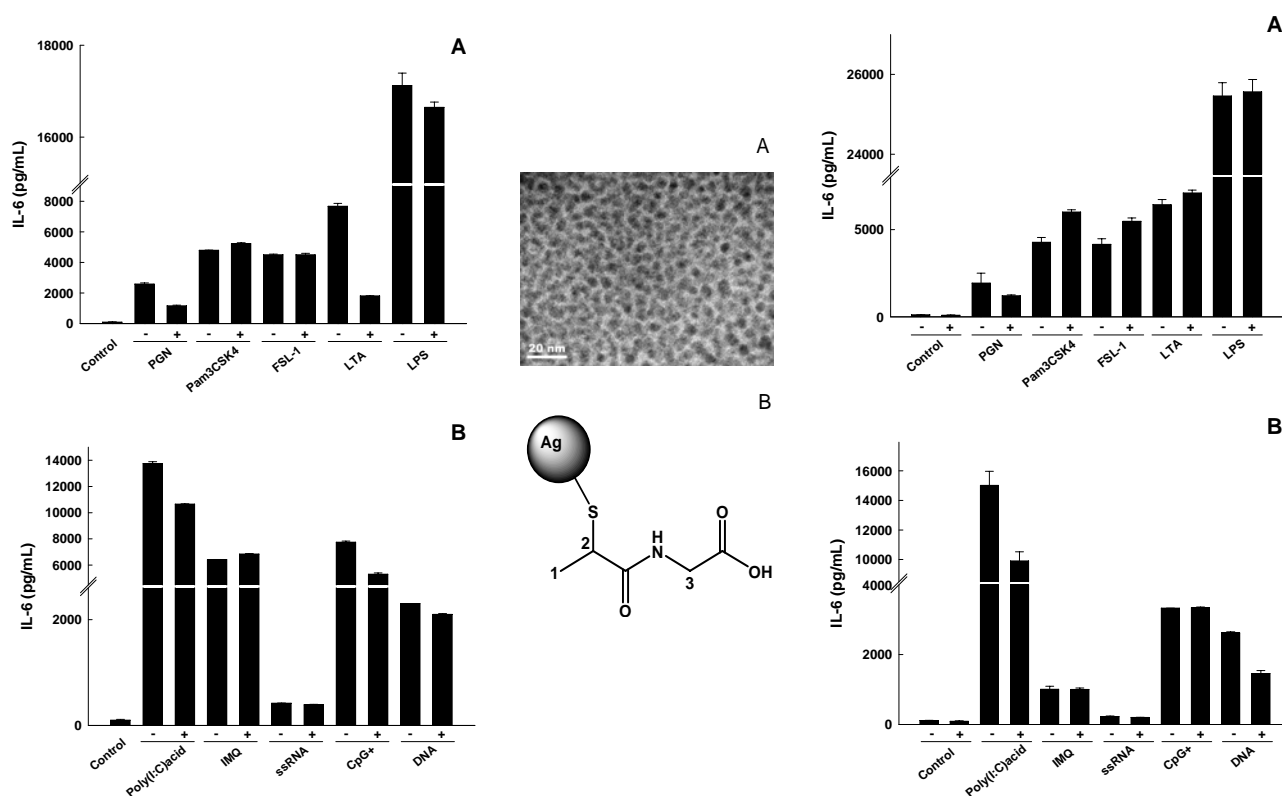
The immune system is one of the most dynamic body components in determining our state of health or disease {Pozo, 2008 #2908}. Capped silver nanoparticles that can be coupled to a variety of molecules and biomolecules are of great interest due to their potential applications in biomedicine. However, there are no data about their toxicity or functional effects on a key innate immune response –such as IL-6 secretion– after the engagement of the main group of pathogen-associated molecular patterns receptors, i.e., the Toll-like receptors. Tiopronin capped silver (Ag@tiopronin) nanoparticles of a narrow sized distribution (≈ 5 nm) were synthesised and characterised by TEM, FTIR, Raman, ^1H -NMR and TOCSY. Cytotoxicity was determined by LDH and MTT assays in Raw 264.7 macrophages. IL-6 was measured by ELISA. Ag@tiopronin nanoparticles have a narrow size distribution (≈ 5 nm), high solubility and stability in aqueous environment with no cytotoxicity in terms of mitochondrial function or plasma-membrane integrity at concentrations as higher as $200 \mu\text{g}/10^6$ cells. Ag@tiopronin nanoparticles were not pro-inflammatory agents, but remarkably they specifically impaired the IL-6 secretion mediated by TLR2, TLR2/6, TLR3, or TLR9 stimulation in co-treatment experiments. However, in pre-treatment experiments, nanoparticles enhanced the susceptibility of macrophages to inflammatory stimulation mediated by TLR2/1 and TLR2/6 specific ligands while severely impaired the IL-6 secretion activated by the TLR3 or TLR9 ligands. Therefore, contrary to what is found for bare silver nanoparticles, Ag@tiopronin nanoparticles are non-cytotoxic to macrophages. Ag@tiopronin nanoparticles showed direct and indirect effects on TLR signalling of a high degree of specificity, without pro-inflammatory effects by themselves {Castillo, 2008 #3055}. These effects have to be born in mind when using bioconjugates of Ag@tiopronin nanoparticles for future medical applications.

References:

- 1 Pozo, D. (2008) Immune-based disorders: the challenges for translational immunology. *J Cell Mol Med* 12, 1085-1086

- 2 Castillo, P. M., Herrera, J. L., Fernández-Montesinos, R., Caro, C., Zadarenko, A. P., Mejias, J. A. and Pozo, D. (2008) Tiopronin monolayer-protected silver nanoparticles modulates interleukin-6 secretion mediated by Toll-like receptor ligands. *Nanomedicine* 3, 627-635

Figure 1 (left & right panels)



Differential regulation of TLR-mediated IL-6 production in Raw 264.7 macrophages in the presence of tiopronin silver nanoparticles. *A. Left.* TLRs located on the cell surface. *B. Left.* TLRs located in the endocytic compartment. Tiopronin silver nanoparticles exposure modulates the TLR-mediated IL-6 responsiveness in Raw 264.7 macrophages. *A. Right.* TLRs located on the cell surface. *B. Right.* TLRs located in the endocytic compartment. *A. Center.* EM image of Ag@tiopronin particles. The image was obtained with a high resolution CM200 Philips-FEI microscope. The sample was prepared by drying a drop of an aqueous solution of nanoparticles (1 mg/mL) on a copper grid. *B. center.* Scheme of a tiopronin molecule adsorbed on an Ag nanoparticle (not to scale) with the numbers of the tiopronin atoms used for the NMR interpretation. Patent Nr. P2008-2831.

CHEMICAL SYNTHESIS AND FUNCTIONAL CHARACTERIZATION OF VASOACTIVE INTESTINAL PEPTIDE (VIP) SILVER-PROTECTED NANOPARTICLES

David Pozo¹, Paula M Castillo², Rebecca Klippstein¹, Rafael Fernandez-Montesinos¹, Ana P Zaderenko²

¹CABIMER-Andalusian Centre for Molecular Biology and Regenerative Medicine (CSIC-University of Seville-UPO-Junta de Andalucía), Americo Vespucio Ave, Parque Científico y Tecnológico Cartuja 93, 41092, Seville, Spain

*²Department of Physical, Chemical and Natural Systems, UPO-Pablo de Olavide University, Carretera de Utrera Km 1, 41013 Seville, Spain
david.pozo@cabimer.es*

An important limitation to the therapeutic use of endogenic peptides is their short half-life due to the attack of endopeptidases or the lack of smart-delivery options [1]. An efficient way of protecting peptides of biomedical interest from endopeptidases consists in their covalent binding to nanoparticles. In spite of VIP interest in therapeutic applications few examples are known that improve its administration by means of nanoparticle functionalization, and to the best of our knowledge none of these examples correspond to metal nanoparticles. The aim of the current study was to functionalize silver nanoparticles with VIP and investigate their function as an anti-inflammatory agent. In this case, we report in here the IL-6, IL-10, and TNF- α regulation mediated by different VIP-nanoparticles as well as their effects on LDH release as a readout of cellular viability. In conclusion, we have prepared for the first time silver nanoparticles with a narrow size distribution, protected with a monolayer of adsorbed tiopronin, derivatized with poly(ethylene glycol)bis(3-aminopropyl) terminated (PEG) and functionalized with Vasoactive Intestinal Peptide (VIP). This will open new avenues for smart design of VIP-based immunotherapies in chronic and/or autoimmunity disorders.

References:

- 1 Pozo, D. and Delgado, M. (2004) The many faces of VIP in neuroimmunology: a cytokine rather a neuropeptide? *FASEB J.* **18**, 1325-1334

Figures

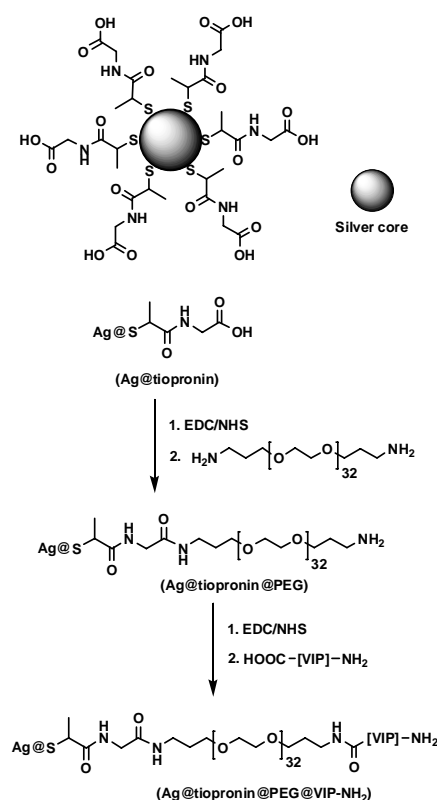
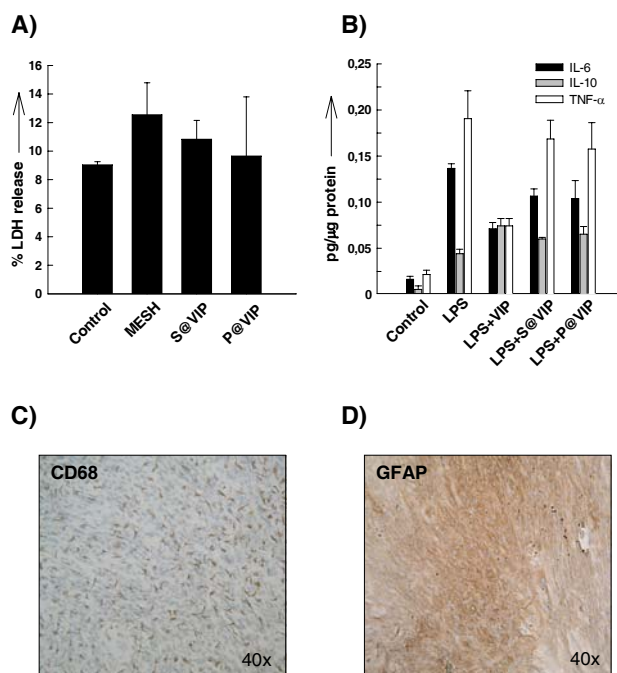


Fig. 1. Top. Schematic representation of Ag@tiopronin@PEG@VIP-NH₂ preparation (Figure not at scale) (Patent P2008-00451). Bottom. C57 mice microglial cultures treated with VIP-based nanoparticles in the presence or absence of LPS.



HYDROTHERMAL SYNTHESIS OF ULTRAFINE PARTICLES OF HEXAGONAL FERRITES ($\text{BaFe}_{12}\text{O}_{19}$, $\text{SrFe}_{12}\text{O}_{19}$) AND THE PREPARATION OF THEIR STABLE SUSPENSIONS

Darinka Primc¹, Darko Makovec¹, Miha Drofenik^{1,2}

¹*Jožef Stefan Institute, Material Synthesis department, Ljubljana, Slovenia*

²*Faculty for Chemistry and Chemical Engineering, University of Maribor, Maribor, Slovenia*
darinka.primc@ijs.si

Ferrofluids are colloidal suspensions of superparamagnetic nanoparticles. They are widely used in many applications in technology, for example, in sealing, damping and heat transfer [1], and recently also in biomedicine. Here, the ferrofluids are being tested for MRI contrast enhancement, targeted drug delivery, as mediators for the hyperthermia treatment of cancer, and for other applications [2]. In addition, ferrofluids are used as precursors for the preparation of some magnetic materials, such as magnetic nanocomposites and magnetic coatings.

For the preparation of ferrofluids, the size of the nanoparticles has to be small enough to be close to the superparamagnetic state. When the size of ferri/ferromagnetic particles is reduced below a critical value, their magnetic moments are relaxed due to thermal energy and they become superparamagnetic. These superparamagnetic particles exhibit zero coercivity and there are no magnetic interactions that would cause their agglomeration. For the successful preparation of their stable suspensions, the particles' surfaces have to be modified in order to prevent aggregation due to the Van der Waals and electrostatic attractive forces. For the suspensions in nonpolar carrier liquids, the repulsive forces are provided by the absorption of surfactants, such as oleic acid [3].

Today several spinel magnetic oxides (Fe_3O_4 , $\gamma\text{-Fe}_2\text{O}_3$, CoFe_2O_4 , NiFe_2O_4 , etc) can be prepared in the form of superparamagnetic nanoparticles. Due to their specific, intrinsic properties, superparamagnetic nanoparticles of hexaferrites would also be of great importance. In this work, the preparation of ferrofluids from two different hexagonal ferrites, barium hexaferrite and strontium hexaferrite, has been studied.

The critical volume below which the nanoparticles become superparamagnetic is reversible and proportional to the magnetic anisotropy of the magnetic material. Since both the hexagonal ferrites exhibit a high intrinsic magnetocrystalline anisotropy ($\text{BaFe}_{12}\text{O}_{19}$, $K_1 = 3.3 \cdot 10^5 \text{ J/m}^3$, $\text{SrFe}_{12}\text{O}_{19}$, $K_1 = 3.8 \cdot 10^5 \text{ J/m}^3$) the critical volume is approximately 300 nm^3 , i.e., much smaller than in the case of soft spinel ferrites like magnetite (Fe_3O_4 , $K_1 = 1.4 \cdot 10^4 \text{ J/m}^3$), reaching 7200 nm^3 . Therefore, for the preparation of stable suspensions of hexaferrite nanoparticles, they have to be extremely small.

However, in contrast to spinel ferrites, which can be easily synthesized even at low temperatures, relatively high temperatures, usually above 700°C , are required for the hexaferrite crystallization, which usually results in the formation of the large particles.

The temperature of hexaferrite formation can be decreased when using hydrothermal synthesis. In this case, a water suspension of precursor particles containing the constituting ions, i.e., a mixture of the corresponding hydroxides, is treated in a sealed reactor at elevated temperature and pressure, usually the equilibrium water pressure. Temperatures above 200°C are usually required to synthesize hexaferrites, resulting in relatively large particles. Recently, Drofenik et al. [4] showed how the crystallization temperature of hexaferrites during a hydrothermal treatment can be decreased. The main factor determining the crystallization

temperature is the concentration of hydroxyl ions relative to the concentration of the metal ions. The high concentration of the hydroxyl ions favours the association of $[\text{Fe}(\text{OH})_4]^-$ ions into iron-rich aggregates $[\text{Fe}(\text{OH})_4]_n^{n-}$, thus improving the kinetics of hexaferrite formation. The increase in the concentration of the hydroxyl ions enabled a decrease in the formation temperature, to as low as 150°C, where superparamagnetic nanoparticles of hexaferrite can be synthesized. The nanoparticles appeared in a disc-like shape, less than 10 nm wide and only approximately 3 nm thick. When the temperature of the hydrothermal treatment was increased to 160°C, large platelet crystals appeared as a consequence of secondary re-crystallization (Ostwald ripening).

The aim of this study was to determine the reaction conditions where uniform, ultrafine hexaferrite nanoparticles can be prepared. We found that the synthesis of uniform nanoparticles is only possible over a narrow range of experimental conditions, where the Ostwald-ripening process is absent. To expand the range over which the uniform nanoparticles can be synthesized, the Ostwald ripening was completely suppressed by the addition of oleic acid to the reaction mixture prior to the hydrothermal treatment. The nanoparticles synthesized in the presence of oleic acid were hydrophobic and can easily be dispersed in non-polar carrier liquids to form relatively concentrated ferrofluids. The ferrofluids were also prepared by the adsorption of oleic acid onto the nanoparticles in a separate step.

The synthesized nanoparticles were characterised using X-ray diffractometry (XRD) and transmission electron microscopy (TEM). The magnetic properties of the nanoparticles were measured using a vibration sample magnetometer.

References:

- [1] R. E. Rosenweig, *Ferrohydrodynamics*, Cambridge University Press, 1985
- [2] Q. A. Pankhurst, J. Connolly, S. K. Jones, J. Dobson, *J. Phys. D: Appl. Phys.* **36** (2003) R167.
- [3] P. Tartaj, M. P. Morales, S. Veintemillas-Verdaguer, T. Gonzáles-Carreño, C. J. Serna, *J. Phys. D: Appl. Phys.* **36** (2003) R182.
- [4] M. Drogenik, M. Kristl, A. Žnidaršič, D. Hanžel, D. Lisjak, *J. Am. Ceram. Soc.* **90** (2007) 2057.

Deposition of gold nuclei on magnetite nanoparticles and growth to a core-shell system

Pedro Quaresma^{a,e,*}, Ricardo Franco^b, Patrícia Carvalho^c,
João Pedro Araujo^d, Pedro Baptista^e and Eulália Pereira^a

a REQUIMTE/Faculdade de Ciências, Universidade do Porto, R. Campo Alegre 687, 4169-007 Porto, Portugal

b REQUIMTE/Departamento de Química, CQFB, FCT-UNL, 2829-516 Caparica, Portugal

c Departamento de Engenharia de Materiais, IST, Av. Rovisco Pais 1049-100 Lisboa, Portugal

d IFIMUP, R. Campo Alegre, 678, 4169-007 Porto, Portugal

e CIGMH/Departamento de Ciências da Vida, FCT-UNL, 2829-516 Caparica, Portugal

* Corresponding author: pedro.quaresma@fc.up.pt

Magnetic nanoparticles for selective capture of biomolecules in complex mixtures is gaining momentum in bionanotechnology by providing significant advantages over traditional methods of separation¹. A magnetite-gold core-shell structure would grant researchers with an integrated detection and “gene fishing” platform by means of the detection properties of gold nanoparticle systems combined with a magnetic component².

A deposition-precipitation procedure was employed for formation of gold nuclei on the surface of magnetite nanoparticles. The conditions for deposition of the gold nuclei were studied and were found to be critically dependant on pH and gold concentration. The growth of the gold nuclei on the magnetite to a gold shell layer was achieved by an iterative addition of gold precursor and reducing agent. The growth of the gold layer was followed by TEM (Fig.1), UV-Vis and EDS. Several parameters, such as gold precursor concentration, rate of reagents addition and initial nanoparticle concentration were analysed. Also, different chemical reductants were evaluated for their ability to produce a gold shell. Magnetic properties of the nanoparticles before and after gold coating were analysed by SQUID (Fig. 2).

In addition, we have studied the replacement of the capping agent used in the synthesis by several different thiol capping agents and the replacement was assessed zeta-potential measurements.

References:

1. Ito, A.; Shinkai, M.; Honda, H.; Kobayashi, T., Medical application of functionalized magnetic nanoparticles. *Journal of Bioscience and Bioengineering* **2005**, 100, (1), 1-11.
2. Xu, C.; Xie, J.; Ho, D.; Wang, C.; Kohler, N.; Walsh, E. G.; Morgan, J. R.; Chin, Y. E.; Sun, S., Au-Fe₃O₄ dumbbell nanoparticles as dual-functional probes. *Angewandte Chemie-International Edition* **2008**, 47, (1), 173-176.

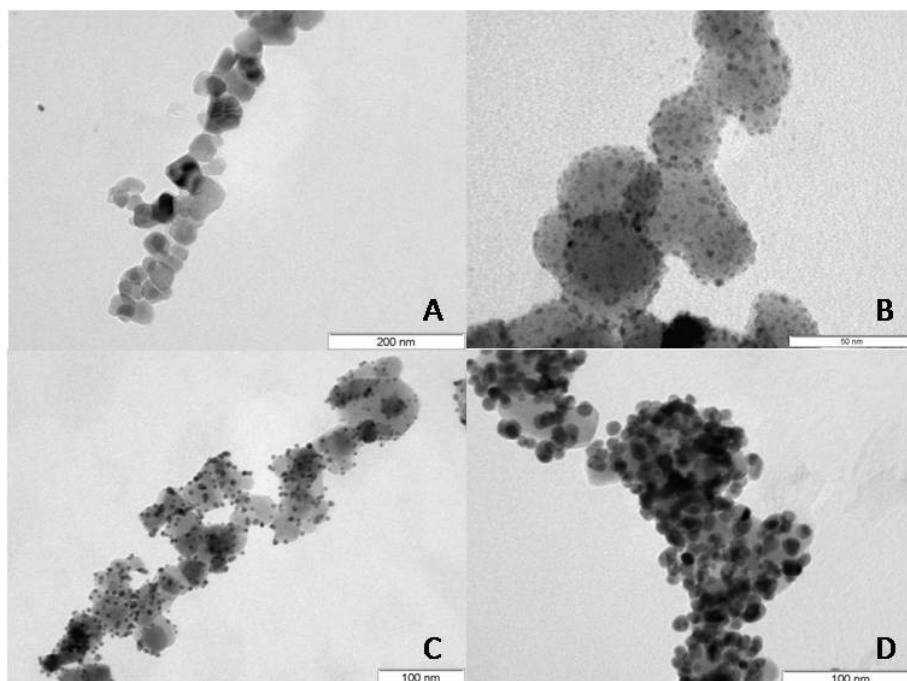
Figures:

Figure 1 – TEM images of the several steps of the synthesis. A) Images of the original magnetite nanoparticles; B) Magnetite nanoparticles after gold hydroxide priming; C) Magnetite-gold nanoparticles after the 4th iterative gold addition; D) Magnetite-gold nanoparticles after the 12th iterative gold addition.

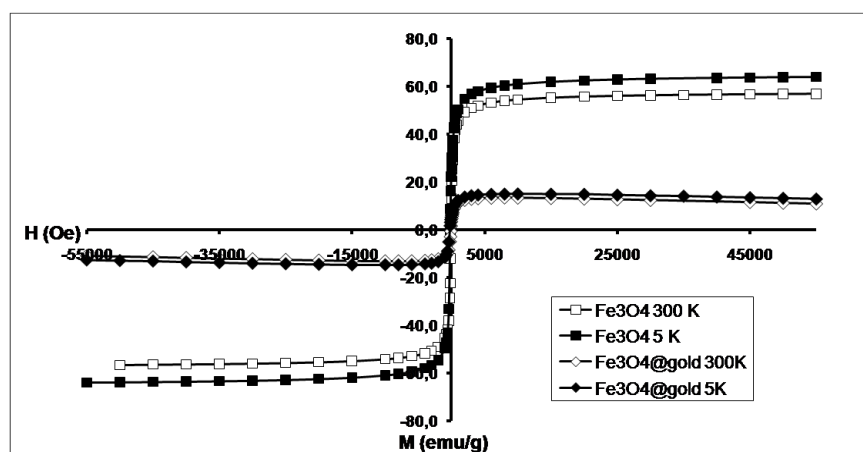


Figure 2 – SQUID measurements of original magnetite nanoparticles and after gold coating at 300K and 5K.

Acknowledgments

The authors would like to thank FCT (Fundação para Ciência e Tecnologia) through projects PTDC/BIO/66514/2006; PTDC/QUI/64484/2006 and PTDC/SAU-BEB/66511/2006, and SFRH/BD/28209/2006 to Pedro Quaresma.

Preparation and Optical Properties of Porphyrin Nanoparticles using Microwave Method

Rahmatollah Rahimi, Marziye Javaheri Kachousangi

Department of chemistry, Iran University of Science and Technology, Narmak, Tehran, Iran

marzieh.javaheri@gmail.com

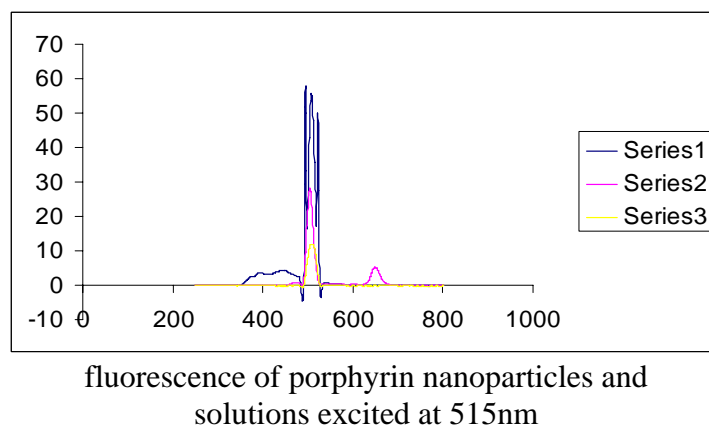
Fabrication techniques of organic molecular nanoparticles have been one of topics in nanoscience and nanotechnology. Kasai et al. have been established a strategy to control the size of organic particles in nano level by reprecipitation method. They have succeeded in making organic nanoparticles such as aromatic compounds, organic dyes and polydiacetylene derivatives[1]. Alternatively Tamaki et al. proposed a laser processing technique to generate organic nanoparticles by laser ablation of organic dyes in microcrystal dispersion[2]. It is possible to downsize the porphyrin crystal to nano level by these techniques and some groups have succeeded in preparing porphyrin nanoparticles[3-5].

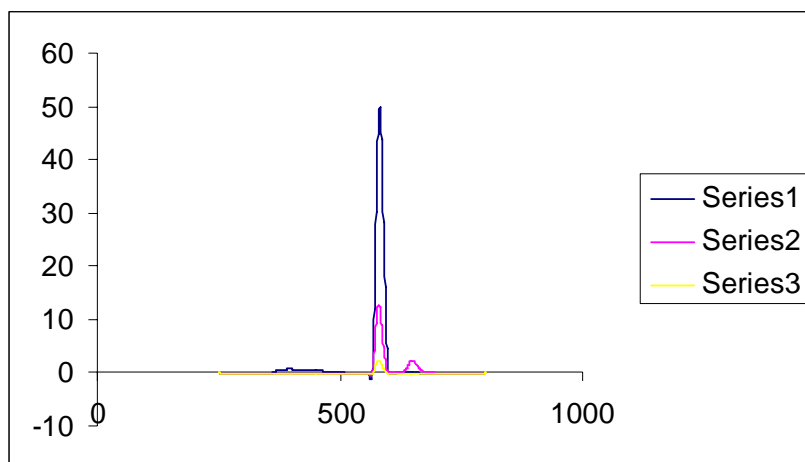
We report a method for the fabrication of porphyrin nanoparticles. nanoparticles were produced by a combination of the reprecipitation method and microwave irradiation, termed the "microwave method". The absorption spectra of nanoparticles were investigated. The porphyrin molecule solutions and nanoparticle dispersions were also used for emission spectroscopy Using a luminescence spectrometer.

References:

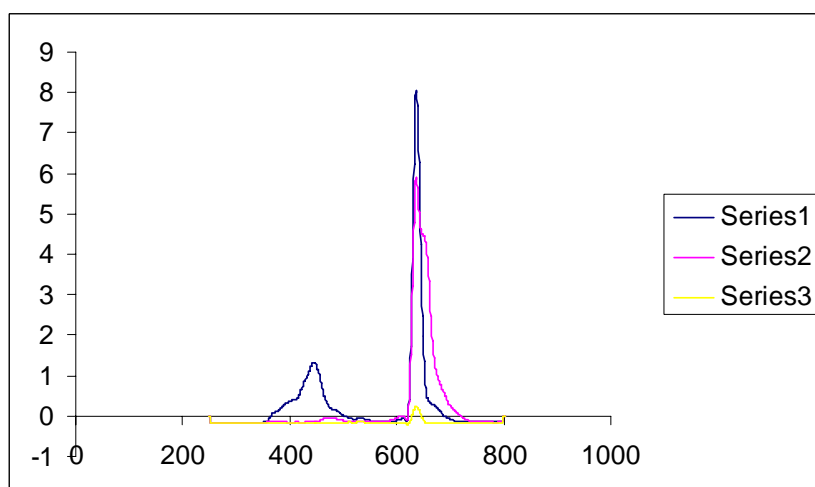
- [1]H. Kasai, H. Kamatani, S. Okada, H. Oikawa, H. Matsuda, and H. Nakanishi, "Size-dependent colors and luminescences of organic microcrystals," *Jpn. J. Appl. Phys.*, **35**, (1996), 221-223.
- [2]Y. Tamaki, T. Asahi, H. Masuhara, "Nanoparticle formation of vanadyl phthalocyanine by laser ablation of its crystalline powder in a poor solvent," *J. Phys. Chem. A*, **106**, (2002), 2135 - 2139.
- [3]X. Gong, T. Milic, C. Xu, J. D. Batteas, C. M. Drain, "Preparation and characterization of porphyrin nanoparticles," *J. Am. Chem. Soc.*, **124**, (2002), 14290-14291.
- [4]C. M. Drain, G. Smeureanu, S. Patel, X. Gong, J. Garnod, and J. Arijeloyea, "Porphyrin nanoparticles as supramolecular systems," *New J. Chem.* **30**, (2006), 1834-1843.
- [5]Z.-M. Ou, H. Yao, K. Kimura, "Preparation and optical properties of organic nanoparticles of porphyrin without self-aggregation," *J. Photochem. Photobiol. A*, **189**, (2007), 7-14.

Figures:

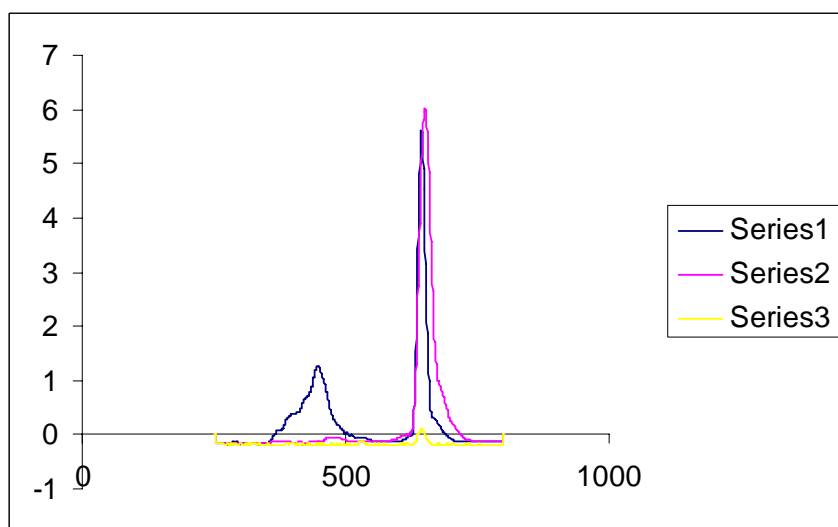




fluorescence of porphyrin nanoparticles and solutions excited at 590nm



fluorescence of porphyrin nanoparticles and solutions excited at 646nm



fluorescence of porphyrin nanoparticles and solutions excited at 653nm

OPTIMIZATION OF CULTURE CONDITIONS FOR BIOSYNTHESIS OF SILVER NANOPARTICLES USING *ASPERGILLUS FUMIGATUS*

Zahra Ranjbar Navazi, Mohammad Pazouki, Farah sadat Halek
 Environmental Group, Energy Department, Materials & Energy Research Center,
 MeshkinDasht, Karaj, IR Iran
Mahsa_ranjbar@merc.ac.ir

ABSTRACT

Synthesis of metal nanoparticles using a reliable and eco-friendly process is an important step in the field of application of nanotechnology [1]. Using biological systems is one of the options in order to achieve this purpose [2,3]. In this study we have investigated and optimized the variables affecting the biosynthesis of silver nanoparticles. The independent variables studied were initial pH and number of spore which affect the cell mass, cell morphology, size, shape and amount of synthesized silver nanoparticles. The culture conditions of 13 designed experiments were according to Table 1. The formation of silver nanoparticles is confirmed using UV-visible spectrophotometer. UV-vis spectrum of aqueous medium containing silver nanoparticles showed a peak around 420nm corresponding to the plasmon absorbance of silver nanoparticles [4]. Initial pH and the number of spores affect the intensity of absorbance in UV-vis spectrum. Figure 1 shows the UV spectrum of 3rd and 6th samples which had the desirable spectrum. The size and morphology of the particles is investigated using transmission electron microscope (TEM). According to Figure 2, there is some agglomeration between the particles in 6th sample, so the optimum culture condition was selected according to 3rd sample. As shown in Figure 2 the size range of 3rd and 6th samples are sequentially 3- 17 nm and 3- 30 nm. The time course of cell mass and sugar assimilation in the culture medium have been investigated.

Keywords: silver nanoparticles, biosynthesis, fungus.

References:

- [1] Kuber C. Bhainsa, S.F. D'Souza, Extracellular biosynthesis of silver nanoparticles using the fungus *Aspergillus fumigatus*, *Colloids and Surfaces B: Biointerfaces* **47** (2006) 160–164.
- [2] R.M. Bruins, S. Kapil, S.W. Oehme, Microbial resistance to metal in the environment, *Ecotoxicol. Environ. Saf.* **45** (2000) 198–207.
- [3] T.J. Beveridge, M.N. Hughes, H. Lee, K.T. Leung, R.K. Poole, I. Savvaiddis, S. Silver, J.T. Trevors, Metal–microbe interactions: Contemporary approaches, *Adv. Microb. Physiol.* **38** (1997) 177–243.
- [4] J.D. Holmes, P.R. Smith, R. Evans-Gowing, D.J. Richardson, D.A. Russel, J.R. Sodeau, Energy-dispersive-X-ray analysis of the extracellular cadmium sulfide crystallites of *Klebsiella aerogenes*, *Arch. Microbiol.* **163** (1995) 143–147.

Figures:

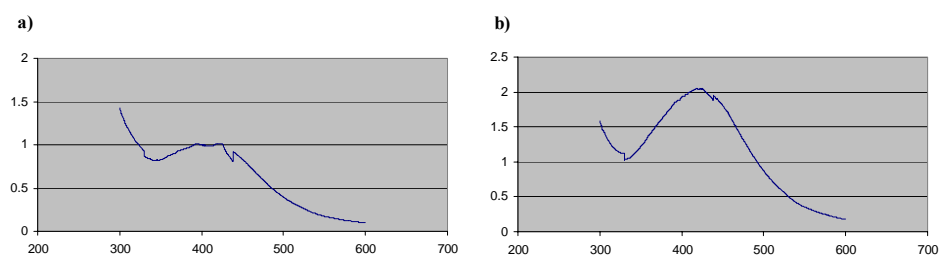


Fig. 1: Uv-vis spectrum of samples: a)3, b)6

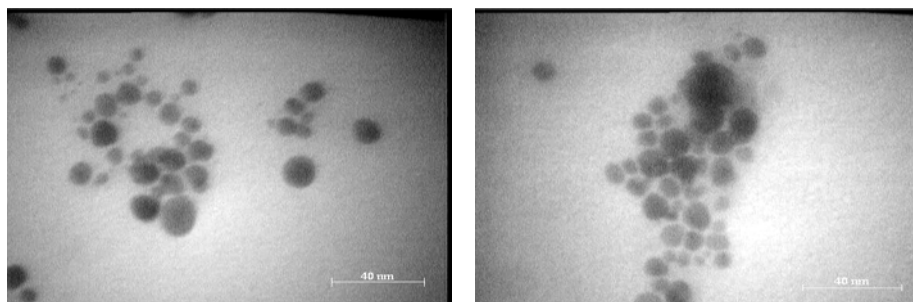


Fig.2: TEM micrograph of 3rd (left) and 6th (right) samples (the scale bars are 40nm).

Tables:

Sample	pH	Spore $\times 10^6/L$
1	2.88	9.5
2	7.12	9.5
3	3.5	16
4	5	9.5
5	5	0.31
6	3.5	3
7	5	18.69
8	6.5	3
9	6.5	16
10	5	9.5
11	5	9.5
12	5.8	9.5
13	5.8	0.75

Table 1: Culture conditions of *Aspegillus fumigatus* for 13 designed experiments

Two and three dimensional polymer devices by means of Nanoimprint Lithography

V. Reboud¹, N. Kehagias¹, M. Zelsmann², M. Striccoli³, M. Tamborra⁴, M. L. Curri³, A. Agostiano^{3,4}, F. Reuther⁵, G. Gruetzner⁵, J. A. Alduncin⁶, D. Mecerreyes⁶ and C. M. Sotomayor Torres¹

1. Catalan Institute of Nanotechnology, Campus de Bellaterra, Edifici CM7, 08193 – Bellaterra (Barcelona), Spain and Catalan Institute for Research and Advanced Studies ICREA, 08010 Barcelona, Spain

2. LTM-CNRS, c/o CEA-LETI, 17 rue des martyrs, F-38054 Grenoble Cedex 9, France

3. CNR IPCF Sezione Bari c/o Dipartimento di Chimica, Università di Bari, Italy

4. Dipartimento di Chimica, Università di Bari, via Orabona 4, I-70126 Bari, Italy

5. micro resist technology GmbH, Koepenicker Str. 325, Haus 211, 1255, Berlin, Germany

6. New Materials Department, CIDETEC-Centre for Electrochemical Technologies, Parque Tecnológico de San Sebastián, Paseo Miramón 196, E-20009 Donostia-San Sebastian, Spain

Email: vincent.reboud.icn@uab.es

Nanoimprint lithography (NIL) is a top-down, parallel lithography technique based on the mechanical deformation of a thin polymer material from a rigid stamp which incorporates micro/nano features or structures. NIL is a feasible, low cost, high resolution and high throughput technique which has been generating increasing interest over the last several years. In this paper we present results in the fabrication and characterization of polymer photonic devices by means of NIL. In particular, two dimensional photonic crystals (PhCs) structures have been studied as efficient light extractors. In this context, new functional materials, able to combine novel tailored physical and chemical properties with versatile and reliable processing capabilities, have been used. An enhancement of the light collection (PL intensity) of up to 2.4 is achieved compared to an unpatterned sample (Fig. 1a). In a second approach to increase even more the light-emission efficiency of imprinted organic thin films, the interplay between PhCs and coupled surface plasmons (SP) was tested. A proof of concept was obtained matching the metal SP energies to the rhodamine 6G emission bands. A 27-fold enhancement of PL intensity at room temperature is achieved in a 2D PhC containing dye in the vicinity of Ag SPs compared to an unpatterned sample on a glass substrate. Finally we discuss the use of NIL for the three dimensional integration of devices for a full plastic photonic circuit. A novel nanofabrication technique, based on ultraviolet NIL and reversal NIL, has been developed to achieve cost efficient and high throughput three dimensional patterning. Figure 1b shows a top view scanning electron microscope image of a three-layer woodpile structure.

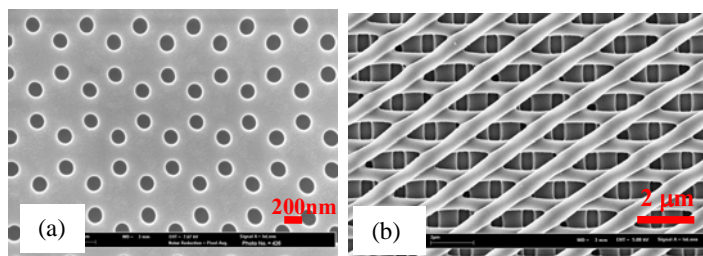


Figure 1 (a) SEM micrographs of an imprint in the composite polymer PMMA₇₀-co-DMEAMA₃₀ with (CdSe)ZnS nanocrystals, (b) SEM images of a three-layer woodpile-like structure fabricated by the reverse contact imprinting technique

Acknowledgments: The support of the EC-funded projects NaPa (Contract No. NMP4-CT-2003-500120), PHOREMOST (FP6/2003/IST/2-511616), and NAPANIL is gratefully acknowledged. The content of this work is the sole responsibility of the authors.

Prediction of Biomolecular Induced-fit Flexibility Through Static Modes

G. Renvez, M. Brut, A. Estève, G. Landa, M. Djafari-Rouhani, D. Estève

Université de Toulouse, LAAS, 7 Avenue du Colonel Roche, F-31077 Toulouse, France

[*grenvez@laas.fr*](mailto:grenvez@laas.fr)

We present a new competitive approach for the treatment of biomolecular flexibility to provide an alternative to the limitations of current methodologies such as molecular dynamics and normal mode analysis. This method, called Static Mode method, is based on the “induced-fit” concept and is aimed at mapping the intrinsic deformations of a biomolecule subject to any external excitations: direct mono or multi-site contact, electrical etc... The algorithm allows obtaining a set of deformations, each one corresponding to a specific interaction on a specific molecular site, in terms of force constants contained in the energy model. Such a process can be used to explore the properties of single molecular intrinsic flexibility, as well as to predict molecular docking or molecule/surface interactions. From a modeling point of view, the interaction problem can be expressed in terms of interaction sites between the interacting entities, the molecular deformations being extracted from the pre-calculated Static Modes of each separated ones. The first applications of our method have focused on the intrinsic flexibility of biomolecules like nucleic acids and proteins (HIV-1 protease, dihydrofolate reductase). We indicate how this new methodology can be pertinent to address some issues of bio/non bio interactions.

MAGNETIC COUPLING BETWEEN ANTIFERROMAGNETIC AND A FERROMAGNETIC MATERIAL STUDIED BY MEANS OF SPIN-POLARIZED SCANNING TUNNELING MICROSCOPY

¹Josefa M. Rodríguez, ¹Bogdana Borca, ¹Juan José Hinarejos, ^{1,2}Amadeo L. Vázquez de Parga
and ^{1,2}Rodolfo Miranda

¹*Departamento de Física de la Materia Condensada
Universidad Autónoma de Madrid, Cantoblanco, 28049, Madrid*
and

²*Instituto Madrileño de Estudios Avanzados en Nanociencia (IMDEA-Nanociencia)
Cantoblanco 28049, Madrid, Spain*

Josefa.rodriguez@uam.es

Spin Polarized Scanning Tunnelling Microscope (SP-STM) uses a tungsten tip covered with magnetic material to study the dependence of the tunnelling current on the relative orientation of the tip and surface magnetization. This dependence makes possible to study magnetic properties of surfaces detecting magnetic contrast [1] and the capability of the STM to get atomic resolved images of the surfaces allow us to correlate the structural and magnetic properties.

Exchange bias is one of the phenomena associated exchange anisotropy created at the interface between an antiferromagnetic (AF) material and a ferromagnetic (FM) one. Exchange-bias is widely used in different electronic devices [2]. The most relevant unknown element in the development of a satisfactory understanding and a comprehensive theory of exchange bias phenomenon, are the atomic features at the interface between the ferromagnetic and antiferromagnetic materials.

In this work we studied by means of SP-STM the atomic and magnetic structure of Mn films deposited on Fe(001) surface. Mn deposited on Fe(001) crystalizes in a bct structure. The Mn atoms are coupled ferromagnetically within an atomic plane and the coupling between atomic planes is antiferromagnetic as can be seen in the model show in Figure 1 [3]. The right panel in Figure 2 shows a topographic image of 4ML of Mn deposited on Fe(001) at RT. The magnetic contrast between layers can be seen in the left panel of Figure 2. We will show results also on the magnetic frustration that takes place when the antiferromagnetic layer is deposited over an atomic step of the Fe(001) substrate. Due to the localized nature of the frustrations, it has not been possible to resolve the spin-configurations until the introduction on the SP-STM.

On the Mn surface we deposited several amounts of Fe at room temperature and low temperature and by means of SP-STM and we studied the degree of intermixing and the magnetic structure depending on the deposition temperature. Figure 3 shows the topography (right panel) and the magnetic contrast (right panel) after depositing on the surface 3.7ML of Fe deposited at room temperature.

References:

- [1] M. Bode, Rep. Prog. Phys. **66**, 523 (2003)
- [2] D. T. Pierce, Phys Scr, **38**, (1988) 291
- [3] T.K. Yamada et al. Phys. Rev. Lett. **90**, 056803 (2003)

Figures:

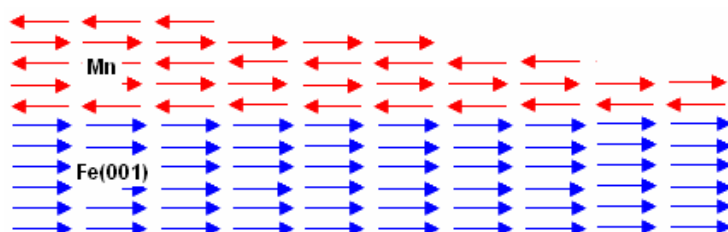


Fig. 1 Atomic magnetizations diagram of different layers in Mn deposited on Fe(001)

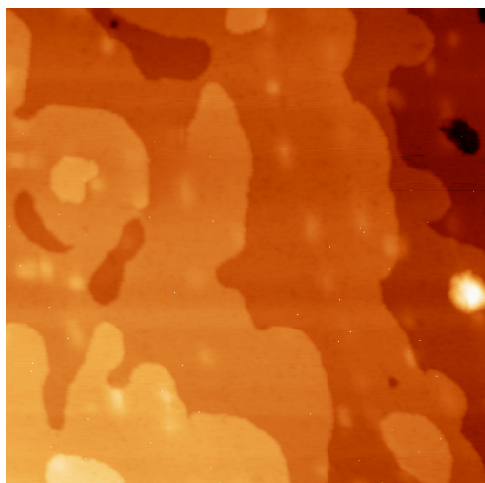


Fig. 2 (a) STM topography of Mn deposited onto Fe(001) at RT. 100nm x 100nm. Setpoint: -0.53 V, 1nA

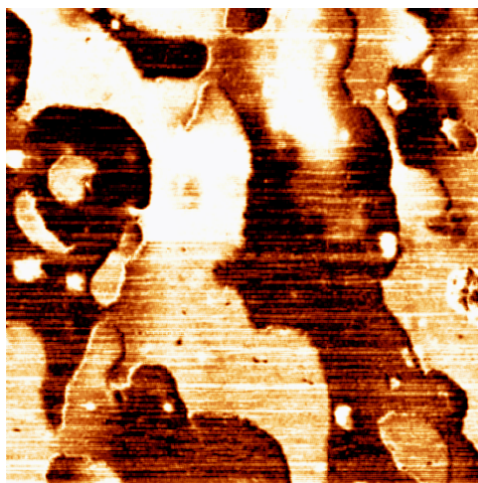


Fig. 2(b) STS magnetic spectroscopy . 100nm x 100nm. 0.2 V. Magnetic contrast between layers due to the layered antiferromagnetic structure of the Mn(001) films.

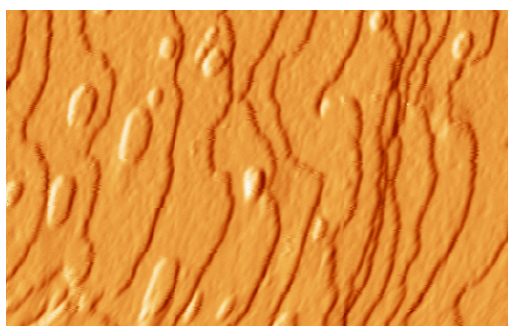


Fig. 3(a) STM topography (I const) of Fe deposited onto Mn/Fe(001). 80nm x 52nm. Setpoint: -0.53 V, 1nA

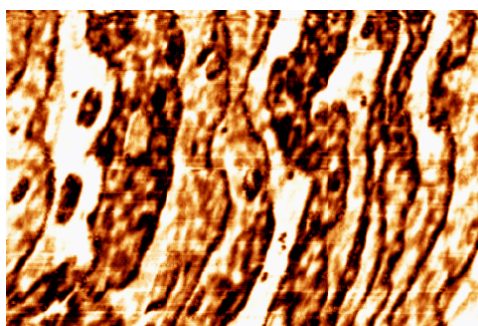


Fig. 3(b) STS magnetic spectroscopy (z const). 80nm x 52nm. 0.2 V. Magnetic contrast between alternated layer in the antiferromagnetic deposition.

ANALYSIS OF UV-FILTERS IN WATER SAMPLES BY SOLID PHASE MICROEXTRACTION WITH COATED-MAGNETIC NANOPARTICLES

Iván Román¹, Dimitar Bozhilov², Veselin Kmetov², Violeta Stefanova², Alberto Chisvert³, Amparo Salvador³, Antonio Canals¹

¹ *Departamento de Química Analítica, Nutrición y Bromatología, Universidad de Alicante, Apdo. 99, 03080 Alicante, España.*

² *Department of Analytical Chemistry, Plovdiv University, 24 "Tzar Assen" St, 4000, Plovdiv, Bulgaria.*

³ *Departamento de Química Analítica, Universidad de Valencia, 46100 Burjassot, Valencia, España.*

Ivan.Roman@ua.es, a.canals@ua.es

In recent years, nanomaterials have become in fashionable promising materials, gathering bulk physico-chemicals properties together with nanoscale structure properties such as magnetic catalytic, optical, sorption and other properties. Spinel ferrite nanoparticles may exhibit the so-called supermagnetic properties when the particle size is of a definite size.

Sample preparation is usually a laborious and time/reagent-consuming step with mainly extraction and preconcentration purposes leading to major sources of error. In the last few years, a considerable scientific interest is focussed on developing miniaturized extraction techniques to avoid these drawbacks. Recently, mixed hemimicelles SPE-based on Fe₃O₄ nanoparticles are proposed to favour mass transfer from sample to the solid extractant phase. The solid phase miniaturized technique reduces considerably the extraction time due to the high surface area/mass ratio and, in addition the strong magnetism of magnetite nanoparticles allows a fast separation from the water sample using a very strong Nd-Fe-B magnet. Afterwards, the particles are chemically desorbed with an appropriate solvent. Coated magnetic nanoparticles were synthesized by Hatton and coworkers for water treatment plant purposes [1]. Basically, FeCl₂ and FeCl₃ were mixed with polyacrylic acid, random copolymer of amino-terminated polyethylene oxide and amino-terminated polypropylene oxide in a hydrothermal media, and then NH₃ was added to leading a Fe₃O₄ coated nanoparticles. Oleic acid coated magnetic nanoparticles were synthesized with oleic acid by aqueous coprecipitation of CoCl₂ and FeCl₃ in basic media at 80 °C. Alternatively, the former copolymer graft was employed for coating CoFe₂O₄ [2].

Nanometer-size particles were measured by high resolution transmission electron microscopy, observing the coating and the stoichiometric ratio was verified by energy dispersive X-ray spectrometry. Nanoparticle surface were characterized by X-ray photoelectron spectrometry (Co, Fe, C and O). Oleic-coated-CoFe₂O₄ exhibits clearly a Type IV sorption N₂-isotherm characteristic of mesoporous materials with a hysteresis type H1. The mesoporous area was 103 m²/g determined by BET plot (r = 99996). Magnetic nanoparticles were characterized by thermogravimetric analysis.

Extraction-preconcentration with surface-modified magnetic nanoparticles for miniaturized SPE are the aims of this work. The magnetic fluid is presented as an interesting and promising alternative to miniaturize solid phase extraction. The nanoparticles were used to extract and preconcentrate UV filters from water samples. High extraction efficiencies and enrichment factors were attained.

Keywords: magnetic nanoparticles, solid phase microextraction, UV-filters, water analysis.

References:

- [1] G.D. Moeser, K.A. Roach, W.H. Green, P.E. Laibinis, T. A. Hatton. Ind. Eng Chem Res., **41** (2002) 4739-4749.
- [2] K. Maaz, A. Mamtaz, S.K. Hasanain. A. Ceylan. J. Magnetism and Magnetic Materials, **308** (2007) 289-295.

Acknowledgments: The authors would like to thank the Spanish Government (project n. CTQ2005-09079-C03-01/BQU), the Generalitat Valenciana (project n. ACOMP07/053) and “Vicerrectorado de Investigación, Desarrollo e Innovación” of University of Alicante (project n. GRE07-1J) for the financial support. I.P.R. also thanks “Caja de Ahorros del Mediterraneo (CAM)”. The authors also thank Huntsman Corp for the kind donation of Jeffamine XTJ-234 and Jeffamine XTJ-507.

Recycling of metallodendritic catalysts by their grafting onto superparamagnetic nanoparticles

D. Rosario-Amorin,^a S. Nlate,^a M. Gaboyard,^b R. Clérac,^c K. Heuzé^{a}*

^a Institut des Sciences Moléculaire, Université Bordeaux I – UMR-CNRS N°5255, 351 cours de la libération, 33405 Talence Cedex, France.

^b Ademtech, SA. Parc Scientifique Unitec 1, 4 allée du Doyen George Brus, 33600 Pessac, France.

^c Centre de Recherche Paul Pascal – UPR-CNRS N°8641, 115 avenue du Dr A.Schweitzer, 33600 Pessac, France.

rosarioamorin.daniel@caramail.com

The homogeneous catalysis offers some major benefits for organic synthesis compared to heterogeneous catalysis. However, the difficulty in separating the catalyst from the reaction media is a limiting factor for their use in industrial processes especially when expensive and toxic complexes are employed.^[1] Because of these economic, health and environmental factors, the development of methods for the recovery and recycling of homogeneous catalysts have been receiving a great attention during recent years, and supported catalysis has been used as an alternative way of recovery. One of the most common way consists in immobilizing the catalysts on organic or inorganic solid supports, and to separate the catalyst from reaction mixture *via* a simple filtration process.^[2] However, a significant decrease in reactivity and selectivity of the catalysts is generally observed due to steric and diffusion effects. The use of small size matrices (< 100 nm) for the immobilization of catalysts may limit the negative impact of the support on the catalytic activity but the recovery processes becomes more difficult. Since few years, magnetic iron oxide nanoparticles (MNPs) have emerged as alternative supports and have opened wide a potential in the field of catalysis. Indeed, superparamagnetic nanoparticles-supported catalysts could be easily isolated and recycled from the reaction medium by simple magnetization with a low magnetic field magnet.^[3] These functionalized superparamagnetic nanoparticles may be synthesized directly at the oxide surface, but the key of their recent success is the tremendous progresses of the surface chemistry on these nanomaterials in particular by their coating with silica or polymer shells. Indeed, these organic or inorganic layers protect the magnetic core from aggregation, and prevent changes in their chemical and physical properties. They also offer widespread and tunable functional surfaces for the immobilization of catalysts.^[4]

In this work, we report the synthesis of metallodendrons bearing pallado phosphine catalysts and their grafting on core-shell γ -Fe₂O₃/polymer MNPs by a convergent approach. In contrast to the divergent grafting approach, that built on the MNPs surface, this method use well-defined dendrons, since the dendritic part are synthesized in homogeneous system and characterized before their grafting on MNPs.^[5] The strategy used for the immobilization has been reported in previous work concerning the positive dendritic effect of dendrons grafting on the surface for the functionalization of these MNPs.^[6] Here we describe the optimization of grafting conditions including various parameters such as solvent, coupling reagents or metallodendron loading. The grafting is based on the covalent coupling between the terminal primary amine of metallodendron and the free carboxyl acid groups at the MNPs polymer shell (see figure 1). Colloidal state and shape of the grafted MNPs remained unchanged especially when aqueous/organic medium with triton/MeOH was used as grafting solvent.

The catalytic activity of grafted MNPs has been investigated in C-C cross coupling reaction such as Suzuki coupling between halogenoarene derivatives and phenyl boronic acid derivatives. The reactivity of these grafted catalysts was studied in middle conditions and revealed a significant activity even towards chloroarenes. Recovery and re-use of grafted MNPs was achieved by magnetization of catalyst by a simple magnet (figure 2). These experiments indicated no decrease of catalytic activity even after 25 runs of recovery, indicating a good stability of the catalyst with this recovery technique.

References:

- [1] J. Hagen, *Industrial Catalysis : A Practical Approach*, Viley-VCH, (1999) .
- [2] (a) N.E. Leadbeater, M. Marco, *Chem. Rev*, **102** (2002) 3217; (b) C.E. Song, S.G. Lee, *Chem. Rev*, **102** (2002) 3495.
- [3] T.J. Yoon, W. Lee, Y.S. Oh, J.K. Lee, *New. J. Chem*, **27** (2003) 227.
- [4] A.K. Gupta, M. Gupta, *Biomaterials*, **26** (2005) 3995.
- [5] N. Tsubokawa, H. Ichioka, T. Satoh, S. Hayashi, K. Fujiki, *Reac. & Funct. Polym.*, **37** (1998) 75.
- [6] K. Heuzé, D. Rosario-Amorin, S. Nlate, M. Gaboyard, A. Bouter, R. Clérac. *New. J. Chem*, **32**(2008) 383.

Figures:

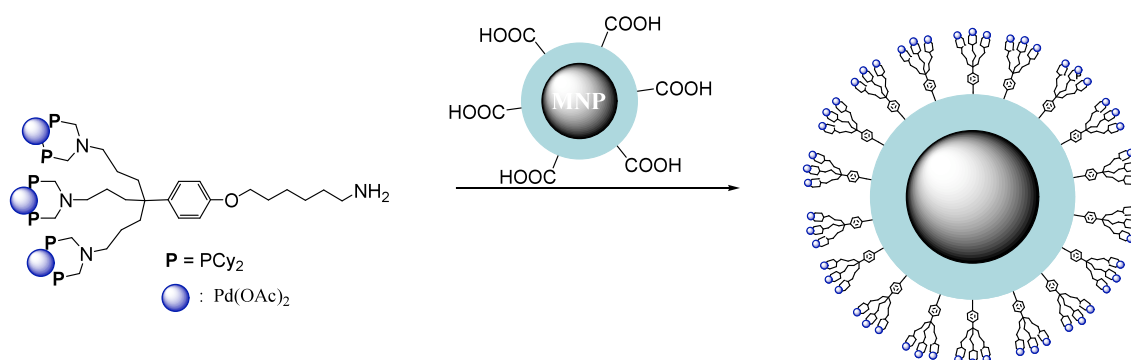


Figure 1 : Grafting of dendron catalyst onto core-shell γ -Fe₂O₃/polymer MNPs

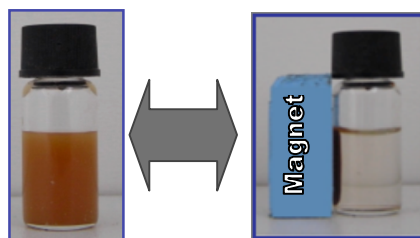


Figure 2 : Magnetization of a grafted MNPs catalyst in solution with an external magnet.

CHARGE TRANSFER EFFECTS ON (ZIG-ZAG) SINGLE-WALLED BORON NITRIDE NANOTUBES (SWBNNTs)

*C. Ruano, Q. Huang, Y. Bando, C. Tang, C. Zhi, D. Golberg,
J.F. Arenas, J.C Otero, J. Soto*

*Department of Physical Chemistry, Faculty of Science,
University of Málaga, E-29071-Málaga, Spain*

cruano@uma.es

One of the most important applications in Nanotechnology is to capture solar energy involving charge transfer (CT) processes. Many of these processes are being developed through modified fullerenes or nanotubes.

A boron nitride (BN) nanotube (NT) is a structural analogue of a carbon nanotube (CNT) in nature which alternates B and N atoms and so entirely substitutes C atoms in a graphitic-like sheet. BNNTs were theoretically predicted and then successfully synthesized in 1995. Primarily, the interest in BNNTs has been due to the undisputed fact that in contrast to metallic or semiconducting CNTs a BNNT is a wide-gap semiconductor. We note that while CNT research is growing exponentially year by year, BNNT research follows a linear-like dependence, in recent years the amount of BNNT-related papers has begun to increase notably.

The group of Q. Huang et al. [1] have studied the properties of Zinc-Phthalocyanine (Zn-Pc) doped SWBNNTs detecting the absorbed photons in the visible region with the possibility of charge separation. These kind of NTs don't absorb in this spectral region but when they are modified with Zn-Pc they exhibit new charge transfer bands in this region which is a very remarkable fact.

In order to detect and confirm the charge transfer character of these new electronic transitions, we have simulated the theoretical Resonance Raman (RR) spectra for a series of models such as the afore mentioned SWBNNTs. These theoretical models have been made by increasing the length and the diameter of the BNNTs (see Figure 1 (a-d)) with the aim of analyzing the effect of these parameters in the RR spectra. The RR intensities have been calculated according to the equations given by Wolde et al. [2],

$$I_j = \Re B_j^2 \omega_j^2$$

where B_j is given by

$$B_j = (2.41 \times 10^6) f \sqrt{M} L_j \omega_j^{-3/2}$$

The intensities are determined by the forces (f) calculated at the Franck-Condon point of the excited states and, therefore, they are related to the respective bands by using the normal modes matrix (L) corresponding to the ground electronic state.

References:

- [1] Q. Huang, A.S.D. Sandanayaka, Y. Bando, C. Zhi, R. Ma, G. Shen, D. Golberg, J. Zhao, Y. Araki, O. Ito, L. Gao, *Adv. Mater.* 19 (2007) 934.
- [2] A. Wolde, H.J.C. Jacobs, F.W. Langkilde, K. Bajdor, R. Wilbradt, F. Negri, F. Zerbetto, G. Orlandi, *J. Phys. Chem.* 98 (1994) 9437.

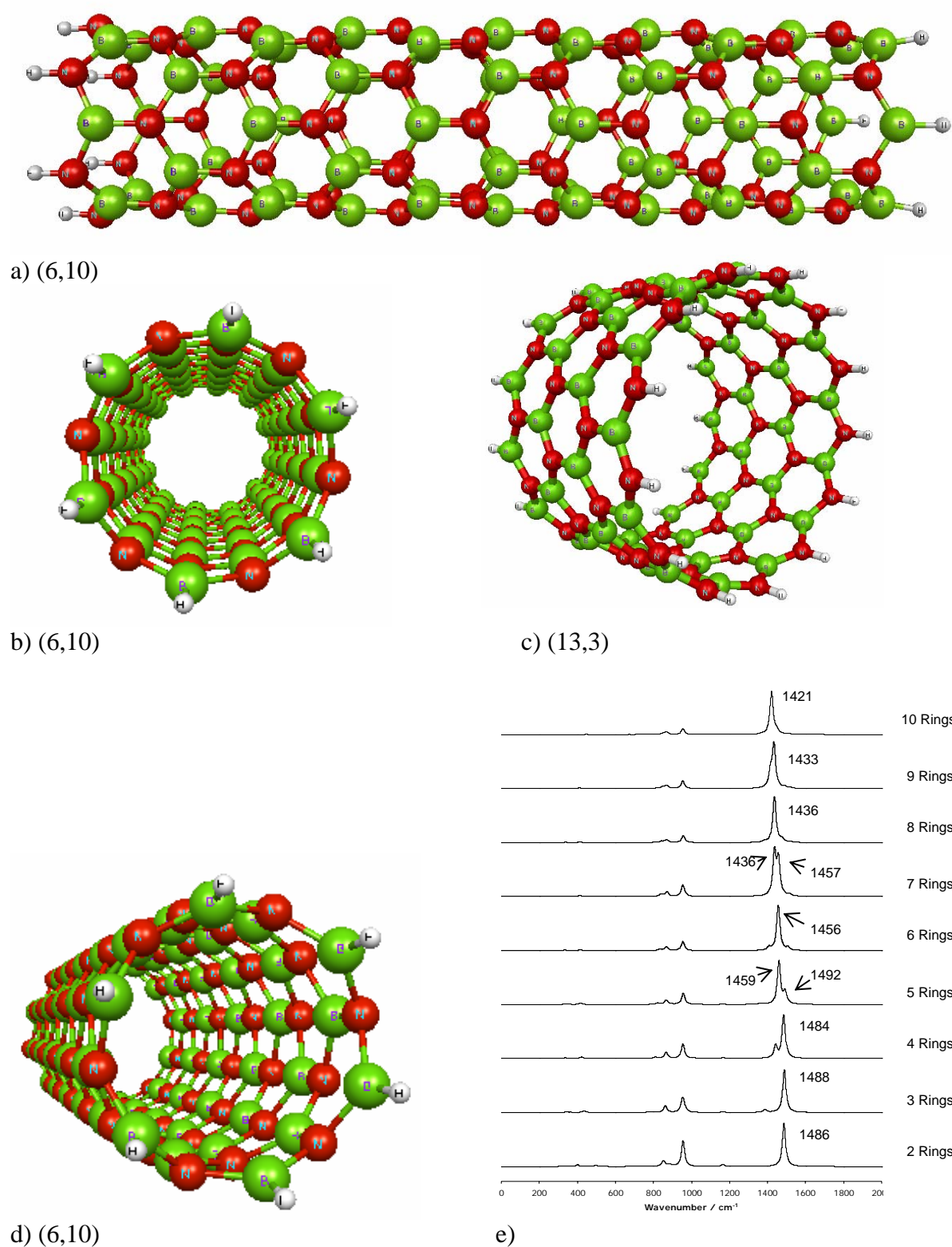


Figure 1: (a-d) Different sizes and views of zig-zag SWBNNT, (n,m)=(diameter, length). (e) Theoretical Resonance Raman (RR) spectra of zig zag SWBNNT increasing the length up to 10 rings.

CEMS STUDY OF THE SUBSTRATE TEMPERATURE DEPENDENCE OF THE MAGNETIZATION IN NANOSTRUCTURED OXIDIZED IRON FILMS

J. Rubin^{1,3}, F. Jiménez-Villacorta², J Bartolomé^{1,4} and C. Prieto².

¹*Instituto de Ciencia de Materiales de Aragón. CSIC-Universidad de Zaragoza, 50009, Zaragoza, Spain.*

²*Instituto de Ciencia de Materiales de Madrid, CSIC, Campus de Cantoblanco, 28049, Madrid, Spain.*

³*Dept. Ciencia y Tecnología de Materiales y Fluidos, CPS, Universidad de Zaragoza, 50018, Zaragoza, Spain.*

⁴*Dept. Física de la Materia Condensada, Facultad de Ciencias, Universidad de Zaragoza, 50009, Zaragoza, Spain.*

jrubin@unizar.es

The transition metal/transition metal oxide (TM/TMO) nanostructures with a ferromagnetic (FM) metal and one or some of its antiferromagnetic (AFM) oxides can show an anisotropic exchange giving rise to enhanced coercivity and low temperature exchange bias, if the oxide has a sufficiently large anisotropy. Furthermore, exchange anisotropy can provide thermal stabilization of the magnetization and increased superparamagnetic blocking temperatures [1]. The oxidized sputtered Fe thin films present such a magnetic behaviour [2]. These films are produced by sputtering Fe on a Si substrate kept at a constant temperature, T_s , and subsequently they are oxidized in O_2 atmosphere at room temperature and capped with a protective layer of Au or SiO_2 . X-ray diffraction and EXAFS experiments have shown that all samples are polycrystalline, but T_s alters the microstructural and magnetic properties: while the in-plane average grain width is almost independent of T_s , the out-of-plane average width decreases from 9 nm for $T_s = 300$ K to 7 nm for $T_s = 200$ K [3,4]. From hysteresis loops and magnetothermal measurements it has been deduced that the $T_s = 300$ K films are formed by strongly interacting grains allowing for a magnetically percolated system behaviour. In contrast, the magnetic data of the films grown at $T_s = 200$ K are consistent with a weakly interacting particle system with random easy magnetic axes [5], in spite of the slight particle non-sphericity and an expected system of particles with easy axes aligned. This different magnetic behaviour has been attributed to differences in the oxidized part, which is larger in the $T_s = 200$ K film than in that of $T_s = 300$ K, and to a broad distribution of the particles size [5]. The oxides are more homogeneously distributed in the $T_s = 200$ K film than in the $T_s = 300$ K one, which has the oxides concentrated in the upper part of the film [5].

Mössbauer spectroscopy can contribute to the study of the magnetic state of these films, in particular to check the behaviour of random distribution of easy magnetization axes. Specifically, Conversion Electron Mössbauer Spectroscopy (CEMS), a spectroscopy method which probes the surface up to about 200 nm, is suitable for this purpose. The measurements were carried out at room temperature (RT). The samples were two oxidized iron films with a nominal Fe thickness of 100 nm, which were prepared at $T_s = 200$ K and $T_s = 300$ K.

The spectra of Fig. 1 show two components: a sextet produced by metal α -Fe and a doublet. For a random distribution of magnetic domains, the relative intensity of the sextet peaks are 3:x:1:1:x:3, with $x=2$. The intensity of the 2nd and 5th peaks with respect that to the inner (3rd and 4th) peaks, x , is related to the relative direction between the magnetization direction and the incident beam (Fig. 2).

$$x = \frac{4 \sin^2 \theta}{1 + \cos^2 \theta} \cdot$$

x goes from 0 to 4 for magnetization directions from parallel to perpendicular to the beam, respectively. In the present films, the fitted x values correspond to $\theta=69^\circ$ and 53° for $T_s=200$ K and 300 K, respectively. The film shape anisotropy, which should produce a magnetization parallel to the film plane, competes with the particles shape anisotropy. This would promote a magnetization perpendicular to the film's plane, because of the columnar growth of the Fe particles. Then, the decrease in the out-of-plane width of the $T_s=200$ K particles is consistent with a decrease in the particle shape anisotropy and a shift of the magnetization directions towards the film plane (increasing θ). The hyperfine parameters of the doublet do not correspond to any paramagnetic Fe oxide or hydroxide. It can be assigned to superparamagnetic oxide layers around the α -Fe cores. The role of the oxides on the anisotropy is to be studied at low temperature.

References:

- [1] Skumryev V., Stoyanov S., Zhang Y., Hadjipanayis G., Givord D. & Nogués J., *Nature* 423, 850-853 (2003)
- [2] Muñoz-Martín A., Prieto C., Ocal C., Martínez J. L. & Colino J., *Surface Science* 482-485, 1095-1100 (2001)
- [3] Jiménez-Villacorta F., Muñoz-Martín A. & Prieto C., *J. Appl. Phys.* 96, 6224-6229 (2004)
- [4] Jiménez-Villacorta F., Muñoz-Martín A. & Prieto C., *Nucl. Instr. Methods Phys. Res. B* 238, 340-345 (2005)
- [5] Jiménez-Villacorta F., Huttel Y., Muñoz-Martín A., Ballesteros C., Román E. & Prieto C., *J. Appl. Phys.* 101, 113914-113921 (2007)

Figures:

Figure 1: RT CEMS spectra of oxidized Fe films, with substrate temperatures $T_s=200$ K and 300 K.

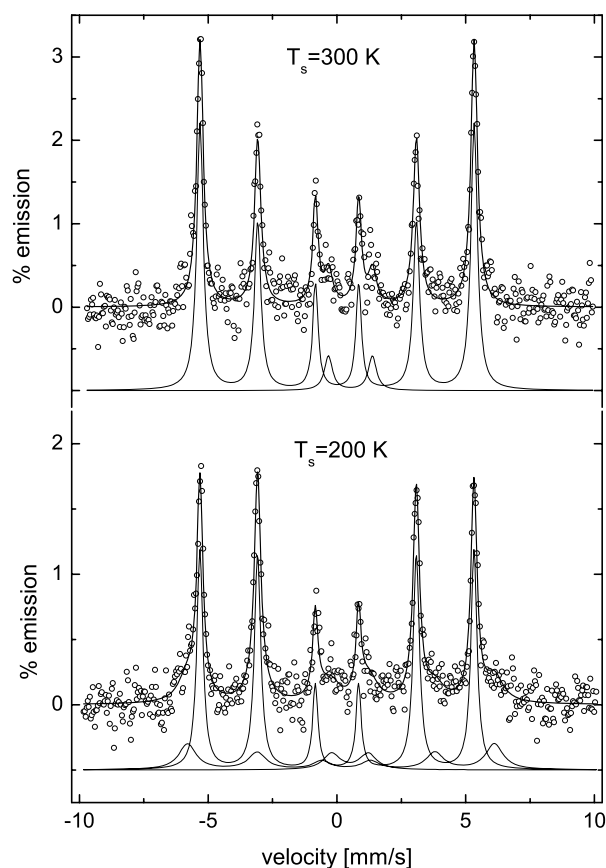
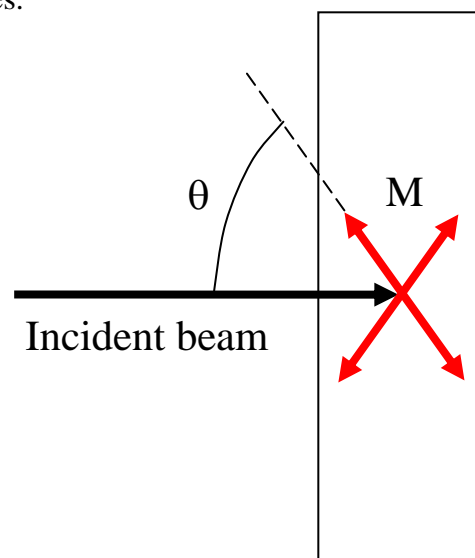


Figure 2: Relative angle between the magnetization and the incident beam direction, derived from CEMS spectra intensities.



Metal-organic spheres as new functional micro- and nanomaterials for encapsulation

Marta Rubio,^a Inhar Imaz,^a Jordi Hernando,^b Daniel Ruiz-Molina,^a Daniel Maspoch^a

^aCentre d'Investigació en Nanociència i Nanotecnologia (ICN-CSIC) and ^bDepartament de Química, Universitat Autònoma de Barcelona, Campus UAB, 08193 Bellaterra, Spain
E-mail: mrubio@cin2.es, daniel.maspoch.icn@uab.es

Encapsulation of functional species into micro- and nanometer sized matrices hold great promise in areas of drug-delivery and cosmetics,^[1] medical diagnostics^[2] and materials science.^[3] Throughout history, big efforts have been dedicated to design and fabricate encapsulating materials that satisfy all specificities and critical properties needed for each intended application. To date, a number of capsules, such as liposomes,^[4] cyclodextrin,^[5] chitosan,^[6] organic polymeric particles,^[7] dendrimers^[8] and carbon or silicate-based hollow spheres,^[9] have been used. Thus far, however, the use of metal-organic micro- and nanoparticles as encapsulating matrices has not been explored. Metal-organic solids created by the association of metal ions and multitopic organic ligands are a very promising type of materials because of their broad compositional and structural diversity, low cost and easy-made production, and their wide range of potential properties and applications that include gas sorption, catalysis, ion exchange, sensing, drug-delivery, magnetism, fluorescence, non-linear optics, etc.^[10] Because of this rich range of properties, we envisage the use of conventional metal-organic chemistry for fabricating functional matrices that display the intrinsic properties of such molecular materials.

Prior to this work, advances have been done on the miniaturization of metal-organic materials down to the micro- and nanometer scale. For instance, Gd(III) nanorods that can act as potential multimodal contrast enhancing agents and sub-50 nm Prussian blue- and triazol-based magnetic particles have been obtained by means of microemulsion-based techniques.^[11,12] More recently, an alternative promising methodology has been reported by Mirkin's and Wang's groups.^[13,14] This strategy, which is based on infinite coordination polymerization followed by precipitation in a poor solvent, allows the straightforward fabrication of cross-linked sub-micron functional metal-organic spheres. For example, this approach has been exploited to synthesize fluorescent metal-organic spheres that show selective cation-exchange and hydrogen storage properties, as well as others with an interesting valence tautomeric behaviour.^[15]

Inspired by this fabrication process, herein we show a new and versatile methodology for encapsulating desired species into metal-organic polymeric micro- and nanospheres.^[17] This new encapsulation method is based on a one-step strategy, depicted in Figure 1a: blue fluorescent metal-organic spheres (hereafter referred to as **ZnBix** spheres, Figure 1b) can be formed by infinite coordination polymerization of Zn(II) metal ions and 1,4-bis(imidazol-1-ylmethyl)benzene organic ligands followed by a fast precipitation to mechanically trap the desired functional species that are present in the reaction mixture. By using this methodology, a wide range of functional species, such as magnetic nanoparticles, gold nanoparticles, organic dyes, and luminescent quantum dots (QDs), has already been encapsulated (Figure 1c-e). In this way, a new type of multifunctional materials, which combine the inherent properties of both **ZnBix** spheres and the encapsulated substances, can be designed. For example, as shown in Figure 1e, **ZnBix** spheres encapsulating QDs are fluorescent in the blue (fluorescence properties of the metal-organic matrix) and red (fluorescence properties of encapsulated QDs) regions of the spectrum.

Based on these promising results, our current motivation is to study the potential of these micro- and nanomaterials for medical applications. Thus, preliminary studies of encapsulation and further *in vitro* controlled release of several drugs will be presented.

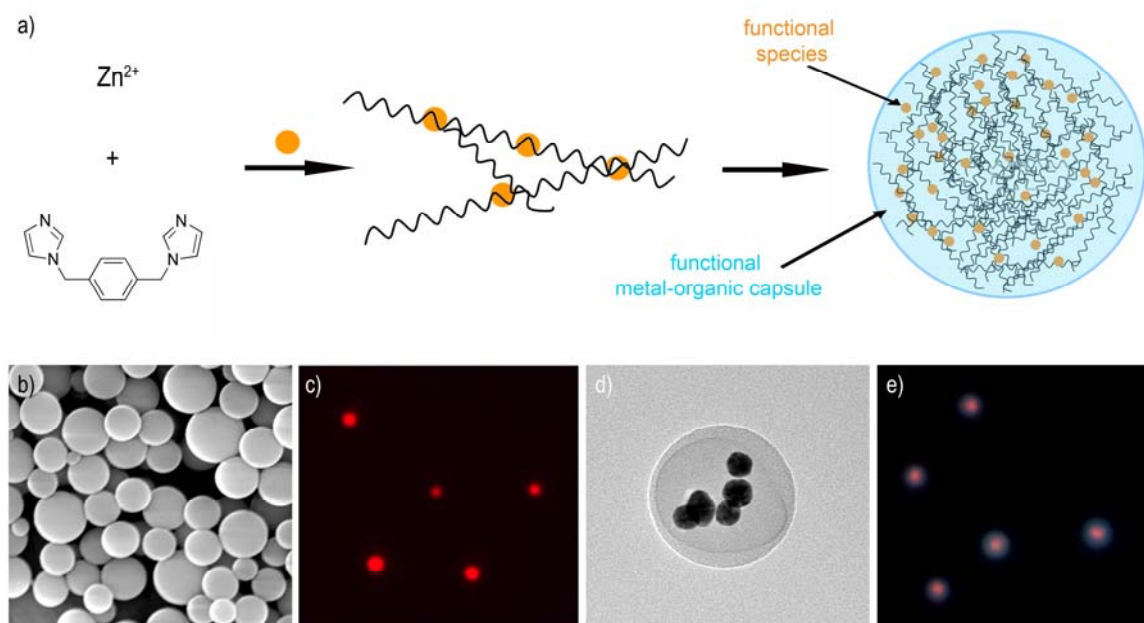


Figure 1. (a) Schematic illustration describing the simultaneous formation and encapsulation of functional species into **ZnBix** spheres. (b) SEM image of **ZnBix** spheres. (c) Fluorescence optical microscope images of Rhodamine@**ZnBix**, (d) Transmission Electron Microscope images of AuNP@**ZnBix**, (e) Fluorescence optical microscope images of QDs@**ZnBix**.

References

- [1] R. Langer, *Nature* **1998**, 392, 5-10.
- [2] J. R. Lindner, *Nat. Rev. Drug Discovery* **2004**, 3, 527-532.
- [3] D. Nguyen, H. S. Zondanos, J.M.Farrugia, A.K. Serelis, C.H. Such, B.S. Hawket, *Langmuir* **2008**, 20, 1292-1298.
- [4] M.Werts, M. Badila, C. Brochon, A. Hébraud, G. Hadziioannou, *Chem. Mater.* **2008**, 20, 1292-1298.
- [5] a) F. M. Muggia, J. D. Hainsworth, S. Jeffers, P. Miller, S. Groshen, M. Tan, L. Roman, B. Uziely, L. Muderpach, A. Garcia, A. Burnett, F. A. Greco, C. P. Morrow, L. J.Paradiso, L.J. Liang, *J. Clin. Oncol.* **1997**, 15, 987-993; b) D.D. Lasic, D. Papahadjopoulos, *Science* **1995**, 267, 1275-1276.
- [6] C. Lucas-Abellán, I. Fortea, J. M. López-Nicolás, E. Núñez-Delicado, *Food Chem.* **2007**, 104, 39-44
- [7] K. A. Janes, M. P. Fresneau, A. Marazuela, A. Fabra, M. J. Alonso, *J. Controlled Release* **2001**, 73, 255-267.
- [8] a) J. Panyam, V. Labhasetwar, *Adv. Drug Delivery Rev.* 2003, 55, 329-347; b) B.J. Nehilla, P.G. Allen, T.A. Desai, *ACS Nano* **2008**, 2, 538-544
- [9] a) J. M. J. Fréchet, *J. Polym. Sci. Part A* **2003**, 41, 3713-3725 ; b) S. Svenson, D.A. Tomalia, *Adv. Drug Delivery Rev.* **2005**, 57, 2106-2129.
- [10] S. Kitagawa, R. Kitaura, S.-i. Noro, *Angew. Chem. Int. Ed.* **2004**, 43, 2334-2375.
- [11]W. J. Rieter, K. M. L. Taylor, H. An, W. Lin, W. Lin, *J. Am. Chem. Soc.* **2006**, 28, 9024-9025.
- [12] S. Vaucher, M. Li, S. Mann, *Angew. Chem. Int. Ed.* **2000**, 87, 1793-1796; b) E. Coronado, J. R. Galán-Mascarós, M. Monrabal-Capilla, J. García-Martínez, P. Pardo-Ibáñez, *Adv. Mater.* **2007**, 19, 1359-1361.
- [13] M. Oh, C. A. Mirkin, *Nature* **2005**, 438, 651-654.
- [14] X. Sun, S. Dong, E. Wang, *J. Am. Chem. Soc.* **2005**, 127, 13102-13103.
- [15] I. Imaz, D. Maspoch, C. Rodríguez-Blanco, J.-M. Pérez-Falcón, J. Campo, D. Ruiz-Molina, *Angew. Chem. Int. Ed.* **2008**, 47, 1857-1860
- [16] I. Imaz, J. Hernando, D. Ruiz-Molina, D. Maspoch, *Angew. Chem. Int. Ed.* **2009** in press.

Thin Film Deposition Study of C₆₀ on Silicon Wafers by Spin Casting

C. R. Zamarreño¹, L. L. Cheong², E. Moon², H. I. Smith², F. J. Arregui¹, I. R. Matias¹,

¹Public University of Navarra, Campus Arrosadia S/N, Pamplona, Spain.

²Massachusetts Institute of Technology, 77 Massachusetts Av., Cambridge, MA.

carlos.ruiz@unavarra.es

Fullerene C₆₀ has raised numerous studies since its discovery in 1985 [1]. Most of these studies have been aimed at the understanding of C₆₀'s chemical and physical properties as well as to purifying the diverse fullerene species [2]. Particularly, C₆₀ thin films exhibit unusual and potentially useful properties, which can lead to technologically valuable applications such as low temperature superconductors or biosensors [3]. Therefore, the understanding of the dynamics and sticking properties of fullerenes is of paramount importance to those interested in the development of fullerene based structures. Most of C₆₀ thin films are fabricated by evaporation and other techniques that require expensive equipment and precise process control. Here, we study the spin-coating deposition technique as a fast, simple and cost effective method to create thin fullerene coatings over pure silicon wafers. It has been previously reported in literature and also corroborated by our experiments that fullerene molecules tend to bundle together, which is mainly associated with the strong three-dimensional hydrophobic interactions between fullerene units [4]. Thus, different parameters such as solvent [5], sonicating and stirring time, post-annealing, spin speed [6], filtering or concentration have been considered in order to obtain a smooth and homogeneous C₆₀ layer.

The solvent used, chlorobenzene, has lower saturation concentration than naphthalene and phenylene derivatives but it has been selected due to the fast evaporation time that allows skipping the post annealing process. The stirring and sonicating processes are required to prevent fullerenes from aggregation in the solution. However, different sonicating times between 5 minutes to 1 hour and stirring times between 2 hours and 24 hours have been explored without major changes. The filtering step is also necessary to keep the bigger aggregates away from being adsorbed directly on the substrate. In our case, two different filters of 200 nm and 20 nm have been probed without significant differences. When the spin speed is varied from 3,000 to 7,000 rpm, the fullerene average cluster height and width are linearly decreased. At the same time, the average cluster density per surface area is linearly increased together with the spin speed as it is shown in Figure 1. Nevertheless, the most important parameter is the concentration of the C₆₀/chlorobenzene solution. In Figure 2, it is shown that the average cluster height and width are exponentially decreased when the concentration is lowered from 4.0 to 0.05 mg/ml. In the same manner, the average cluster density per surface area is exponentially increased from 20 to more than 100 aggregates in a 5 μm² area when the concentration is varied from 4.0 to 0.05 mg/ml. This allows us to obtain a smooth thin fullerene C₆₀ layer formed by small clumps of 8 nm and 150 nm average height and width respectively and homogeneously distributed all over the whole surface. Finally, it should be remarked that the concentration of C₆₀ in the solution is the key parameter in the fabrication process of this coatings without underestimating the others.

[1] H. W. Kroto, A. W. Allaf, S. P. Balm, Chem. Rev., **91** (1991) 1213.

[2] A. W. Jensen, S. R. Wilson, D. I. Schuster, Bioorg. & Med. Chem., **4**(6) (1996) 767

[3] C. A. Mirkin, W. B. Caldwell, Tetrahedron, **52**(14) (1996) 5113.

[4] S. Barazzouk, S. Hotchandani, P. V. Kamat, Adv. Mat. **13**(21) (2001) 1614

[5] V. N. Bezmel'nitsyn, A. V. Eletskiĭ, M. V. Okun', Physics-Uspekhi, **41**(11) (1998) 1091.

[6] I. Belaish, I. Entin, R. Goffer, D. Davidov, H. Selig, J. P. McCauley, N. Coustel, J. E. Fischer, A. B. Smith III, J. Appl. Phys., **71**(10) (1992) 5248.

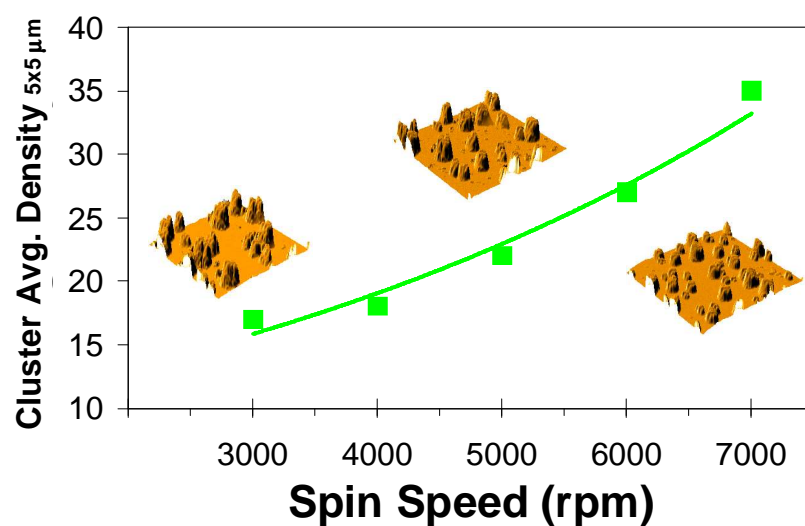


Fig1: Fullerene C₆₀ clusters average density per surface area at diverse spin speed values.
Inset: 5x5μm AFM images

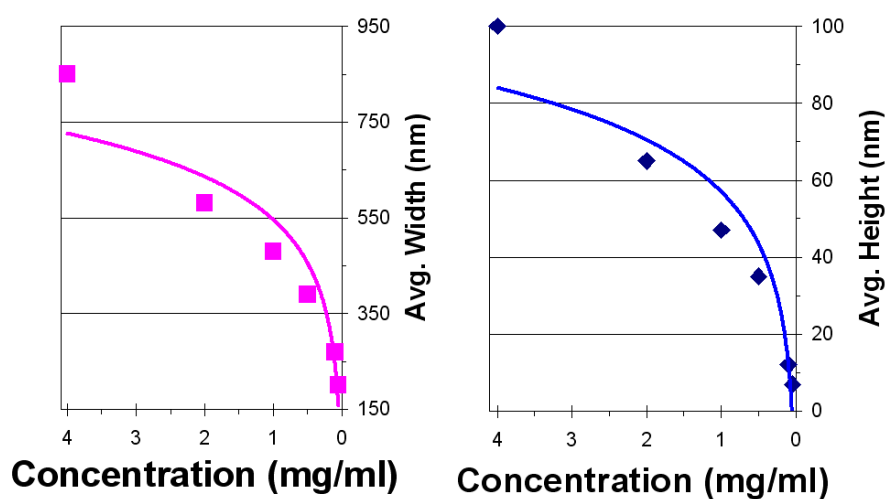


Fig 2: Fullerene C₆₀ clusters average width and height at various concentration values.

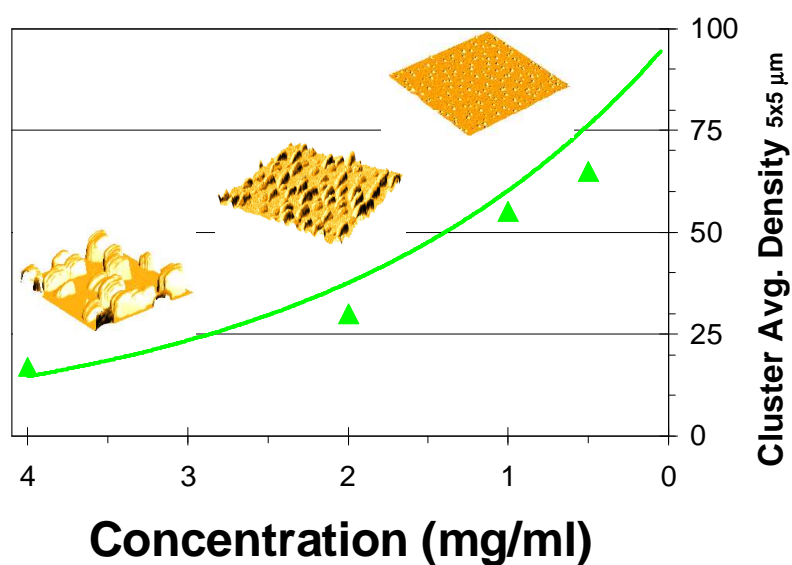


Fig 3: Fullerene C₆₀ clusters average density per surface area at different concentrations.
Inset: 5x5μm AFM images

STABILIZATION OF CARBON NANOTUBES BY POLYELECTROLYTES

Karell Saint-Aubin^a, Maryse Maugey^a, Philippe Poulin^a, P. Gaillard^b, P. Miaudet^b, Cécile Zakri^a

^a*Centre de recherche Paul Pascal, avenue Albert Schweitzer, 33600 PESSAC, France*

^b*Arkema, Groupe de Recherche de Lacq, BP 34, 64170 Lacq France*

saintaubin@crpp-bordeaux.cnrs.fr, zakri@crpp-bordeaux.cnrs.fr

Inclusion of carbon nanotubes in polymer matrices is widely studied to develop multifunctional, strong and light nanocomposites which find application in many fields. Controlling the dispersion and the spatial distribution of the nanotubes in the polymer is a critical for achieving desired properties and functionalities.

In this goal, we study the behaviour of Arkema GraphiStrength multiwall nanotubes (MWNT) in a polymer matrix. This polymer matrix consists of poly(acrylic)acid (PAA). It is a pH responsive polymer which is chosen for its low cost and widely spread use as aqueous dispersant in industrial formulations. As previously reported [1], we show that the stability of MWNT in PAA solutions strongly depends on the pH. At low pH the polymer is neutralized and its adsorption onto the tubes induces their precipitation. At high pH, PAA becomes highly charged and less adsorbing which also causes the aggregation of the nanotubes. In between extreme pH, the nanotubes are homogeneously dispersed and stabilized by electrostatic interactions. This phase behavior and the adsorbing properties investigated by AFM imaging allowed us to develop novel approaches for optimizing the conductivity of PAA composites and coatings. Indeed pH variations during solvent evaporation are used to switch the stability of the nanotubes and promote their structuration in highly conductive networks. Such concepts are potentially useful for achieving applications such as antistatic composites, electromagnetic shielding and conductive inks or paints.

References:

[1] A Liu, I. Honma et al., *Nanotechnology*, **17** (2006) 2845-2849.

[2] J.C. Grunlan, L. Liu et al., *Nanoletters*, **6** (2006) 911-915.

Figure:

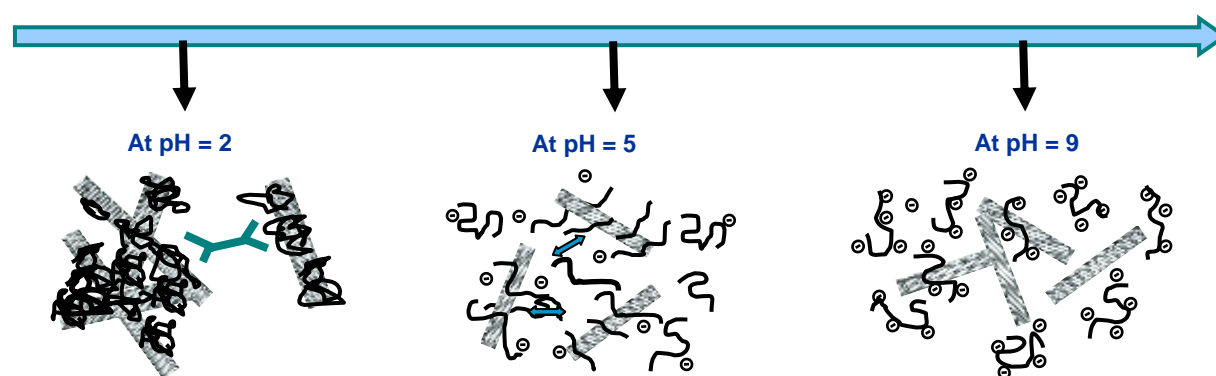


Illustration of the behaviour of the PAA-MWNT system depending on pH

Self-assembly of 4-heptadecylcatechol: thermal symmetry breaking

Javier Saiz-Poseu¹, Félix Busqué², Daniel Ruiz-Molina¹

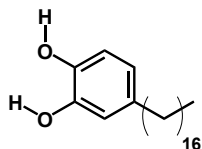
1 Centro de Investigaciones en Nanociencia y Nanotecnología (ICN-CSIC), Edifici CM7, Campus UAB, 08193 Cerdanyola del Vallés, Spain

2 Departament de Química, Universitat Autònoma de Barcelona, Campus UAB, 08193 Cerdanyola del Vallés, Spain

javier.saiz@uab.es

The self-assembly of organic molecules has been widely employed to produce well-defined two dimensional networks on surfaces. These self-assembled monolayers (SAMs) have potential applications in many fields, being of special interest the expression, control and transmission of chirality in these two-dimensional patterns. STM at the solid-liquid interface is a powerful technique in this kind of studies, since it allows the obtaining of submolecular resolution, and therefore, the exact molecular orientation on a given surface.

In this work, the behaviour of 4-heptadecylcatechol (Scheme 1) at the nonanoic acid/ HOPG interface has been studied. Two catechol units form a hydrogen-bonded dimeric structure that in turn self-assembles onto the graphite surface as rows. Most SAMs described in literature are chiral, even when they are generated from prochiral, non-prochiral or non-chiral molecules. Unlike this, the pro-chiral molecule described in this contribution tends to form domains mostly racemic, where every dimer is followed in the row by its non-superimposable mirror image (see Figure 1a, α phase).



Scheme 1 Structure of 4-heptadecylcatechol

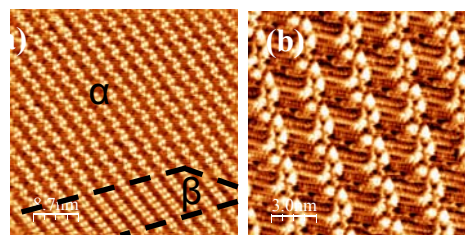


Figure 1 (a) STM image of 4-heptadecylcatechol at the nonanoic acid/ HOPG interface, showing both types of domains, racemic (α) and chiral (β). (b) Zoom area of α phase

Indeed, first experiments carried out at room temperature (20 to 25 °C) and over a wide concentration range lead to the formation in all the cases of the racemate that covers most of the surface as checked over different substrate areas. By contrast with the kinetic control that leads to the unusual formation of the racemic structure, and to favour the formation of chiral domains, which are supposed to be thermodynamically more stable due to a more compact coverage of the surface, the samples were heated from room temperature up to 80°C. As expected, no domains were observed at such temperatures until the system was cooled down to 25 °C. Now, the whole surface was covered by only one enantiomer, giving rise to chiral domains that spread in one direction rows beyond the scan window (see Figure 2). In this way, we have been able to induce for the first time a thermal chiral transition on a racemic 2D pattern that generates spontaneously at room temperature (Scheme 2).

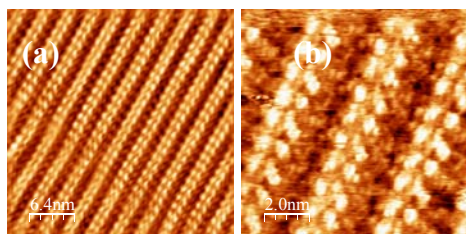
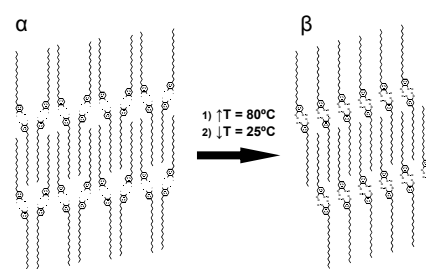


Figure 2 (a) STM image of 4-heptadecylcatechol at the nonanoic acid/ HOPG interface showing the chiral domains obtained after annealing. (b) Zoom area of the same domain.



Scheme 2 Thermal induce phase transition.

References

1. *Molecular chirality at fluid/solid interfaces: expression of asymmetry in self-organised monolayers*, N. Katsonis, E. Lacaze, B. L. Feringa, *Journal of Materials Chemistry* **2008**, 18, 2065-2073.
2. *A thermal-induced chiral transition in self-assembled monolayers*, J. Saiz-Poseu, F. Busqué, D. Ruiz-Molina, *to be submitted*.

Superparamagnetic behaviour of water soluble Fe₃O₄@Au nanoparticles

*J. Salado¹, M. Insausti¹, M. Moros², V. Grazú², J. M. de la Fuente², I. Gil de Muro¹,
L. Lezama¹, T. Rojo¹*

¹ *Kimika Ezorganikoa Saila, Euskal Herriko Unibertsitatea, Apdo. 644, 48080, Bilbao, Spain*

² *Instituto de Nanociencia de Aragón, Universidad de Zaragoza, P.Cerbuna 12, 50009,
Zaragoza
javier.salado@ehu.es*

The preparation of monodisperse magnetic nanoparticles has attracted much attention due to their potential applications in fields such as magnetic storage, drug targeting and delivery, cancer therapy and medical imaging [1]. For these last purposes well defined and water soluble magnetic nanocrystals are desired. By contrast, most of the approaches to obtain highly crystalline and monodisperse nanoparticles take place in organic media, providing particles with a hydrophobic surface. Thus, their transfer into aqueous media with a proper coating is a key issue for their application in areas such as biomedicine. In this contribution, we present the preparation, surface modification and characterization of gold coated Fe₃O₄ nanoparticles.

Gold coated magnetite nanoparticles were synthesized by a two step procedure based on the polyol method [2]. The reduction of Au(OOCCH₃)₃ in the presence of the previously synthesized iron oxide seeds [3], yield gold coated nanoparticles of 5–7 nm, surrounded by organic ligands. The surface modification of the hydrophobic nanocrystals was performed by means of the amphiphilic poly(maleic anhydride-alt-1-octadecene) surfactant [4]. The hydrophobic regions of the polymer intercalates with the alkyl chains of oleic acid surrounding the nanoparticle, rendering the particles water soluble.

The presence of Fe₃O₄ and gold was confirmed by high resolution microscopy. TG-DTA curves measured in argon atmosphere show that depending on the synthetic conditions the organic content varies between 6 and 13 % for unmodified gold coated magnetite nanoparticles.

The expected superparamagnetic behaviour for nanoparticles below the critical size has not been observed in all the unmodified samples. Indeed, at room temperature, coercive fields values in the 30 -130 Oe range and characteristic of ferromagnetic behavior have been obtained from hysteresis cycles. Electron paramagnetic resonance spectroscopy measurements also show strong and broad signals with effective g values ranging from 2.0 to 2.38, depending on the sample.

EPR spectra of water soluble gold coated magnetite nanoparticles, in contrast, show a signal centered at a g value of 2.0, confirming the expected superparamagnetic behaviour for nanoparticles in the observed size range.

References:

- [1] A.K. Gupta, M. Gupta, *Biomaterials*, **26** (2005) 3995.
- [2] L. Wang, J. Luo, Q. Fan, M. Suzuki, I.S. Suzuki, M.H. Engelhard, Y. Lin, N. Kim, J.Q. Wang, C-J. Zhong, *J. Phys. Chem. B* **109** (2005) 21593.
- [3] J. Salado, M. Insausti, I. Gil de Muro, L. Lezama, T. Rojo, *J. Non-Cryst. Solids* **354** (2008) 5207.
- [4] R. Di Corato, A. Quarta, P. Piacenza, A. Ragusa, A. Figuerola, R. Buonsanti, R. Cingolani, L. Manna, T. Pellegrino, *J. Mater. Chem.* **18** (2008) 1991.

Influence of Organo-clay Modifier on Physical Mechanical Properties of Butyl Rubber Nanocomposites

Ali Samadi, Mehdi Razzaghi Kashani

Facility of Engineering, Tarbiat Modares University, Tehran, Iran

a.samadi@modares.ac.ir

Tire curing bladders are important rubber parts used for shaping and curing of tires during molding. These rubber parts are exposed to high temperature, high pressure, large extension, and oxidative aging during their service life. Thermo-mechanical as well as time-dependent properties of bladders are crucial in their quality of performance, duration of service, and possible damages on tires due to their failures. Dimensional stability of bladders guarantees proper shaping and curing of tires. In addition to the crosslinked network of rubber molecules, carbon black filler network can define time-dependent properties of bladders such as creep and permanent set. In order to study the effect of nano-fillers on such properties, montmorillonite nano-clay organically modified with different surfactants were employed in this study. Effect of these modifiers on compatibility between clay and rubber, dispersion of silicate layers in the polymer matrix, and thus mechanical properties of the nano-composite were studied by X-ray diffraction (XRD), mechanical, and rheological investigations. XRD results revealed an intercalated structure for all nono-clays, but with different degree of intercalation. The largest change in interlayer spacing of clays due to intercalation of rubber chains was seen for Cloisite 10A (natural montmorillonite modified with a dimethyl, dehydrogenated tallow, quaternary ammonium). Uniaxial tension tests could also differentiate among nano-composites reinforced with differently modified clays. Rheological properties obtained from dynamic-mechanical-thermal analysis showed more compatibility between bladder compound and the nano-clay modified by Cloisite 10A. As a result, Cloisite 10A was selected as the filler of choice for application in the bladder compound in order to improve its mechanical properties [1-27].

References:

- [1] Michael Alexandre, Philippe Dubois. *Mater Sci Eng* 2000; 28:1–63.
- [2] Suprakas Sinha Ray, Masami Okamoto. *Prog. Polym. Sci* 2003; 28: 1539–641.
- [3] Clay containing polymeric nanocomposites. L.A.Utracki. 2004.
- [4] Franco Cataldo. *Macromol. Symp* 2007; 247: 67–77.
- [5] Paulo Meneghetti, Syed Qutubuddin. *Thermochimica Acta* 2006; 442: 74–77.
- [6] H.S. Jeona, J.K. Rameshwarama, G. Kimb, D.H. Weinkauff. *Polymer* 2003; 44: 5749–58.
- [7] Richard A. Vaia, and Emmanuel P. Giannelis. *Macromolecules* 1997; 30: 8000–8009.
- [8] Qing-Xiu Jia, You-Ping Wu, Yi-Qing Wang, Ming Lu, Jian Yang, Li-Qun Zhang. *J Appl Polym Sci* 2007; 103: 1826–1833.
- [9] Yurong Lianga, Yiqing Wang, Youping Wu, Yonglai Lub, Huifeng Zhanga, Liqun Zhanga. 2005; 24: 1217.
- [10] You-Ping Wu, Qing-Xiu Jia, Ding-Sheng Yu, Li-Qun Zhang. *Polymer Testing* 2004; 23: 903–909.
- [11] C.O. Rohlmann, M.D. Failla, L.M. Quinzani. *Polymer* 2006; 47: 7795–7804.
- [12] W. Lertwimolnun, B. Vergnes. *Polymer* 2005; 46: 3462–3471.
- [13] Jeffrey W. Gilman, Catheryn L. Jackson, Alexander B. Morgan, Richard Harris, Jr. *Chem. Mater.* 2000; 12: 1866–1873.
- [14] Alexander B. Morgan, Jeffrey W. Gilman. *J Appl Polym Sci* 2003; 87: 1329–1338.
- [15] Daniel Fredrick Schmidt. Ph.D. Thesis. Cornell University 2003.
- [16] RICHARD A. VAIA, WEIDONG LIU, HILMAR KOERNER. *J Polym Sci Part B: Polym Phys* 2003; 41: 3214–3236.
- [17] J. KARGER-KOCSIS. *Polym. Eng. Sci.* 2004; 44: 1083–1093.
- [18] Yunfei Xi, Zhe Ding, Hongping He, Ray L. Frost. *Journal of Colloid and Interface Science* 2004; 277: 116–120.
- [19] T.D. Fornesa, P.J. Yoona, D.L. Hunterb, H. Keskkulaa, D.R. Paul. *Polymer* 2002; 43: 5915–93.
- [20] Rajkiran R. Tiwari, Upendra Natarajan. *J Appl Polym Sci* 2007; 105: 2433–2443.
- [21] BP Sreekanth, Bhat Shriharsha, D Raghavendra, GS Ananathapadmanabha, GM Shashidhara. *Polym Int* 2000; 49: 1684–92.
- [22] Samir Majumdar, GR Reddy. EXEL RUBBER LIMITED, HYDERABAD.
- [23] Siljana Lietz, Jing-Lei Yang, Eva Bosch, Jan K. W. Sandler, Zhong Zhang, Volker Altstadt. *Mater. Eng.* 2007; 292: 23–32.
- [24] T. C. Warholid and R. G. Pelle. *Tire Science and Technology, TSTCA* 1988; 16,3:128-145.
- [25] MA Lo´pez-Manchado, B Herrero and M Arroyo. *Polym Int* 2004; 53: 1766–1772.
- [26] Boonstra MM, *Polymer* 1979; 20: 691.
- [27] Madhuchhanda Maiti, Anil K. Bhowmick. *Polym. Eng. Sci.* 2007; 47:1777–1787.

Figures:

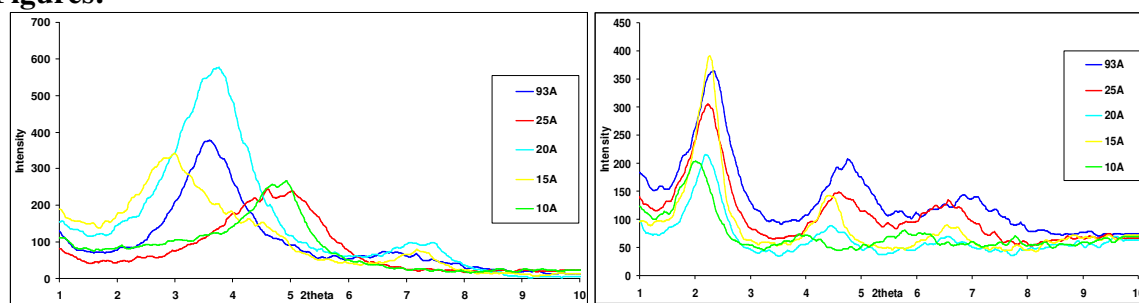


Figure1. X-Ray diffractograms of nanocomposites; from left: original organoclays, nanocomposites after curing

Table 1. D-Spacing of the organo-clays before and after dispersion in the Butyl rubber Nanocomposites

		R 10A	R 15A	R 20A	R 25A	R 93A
Before Mixing (Original Organoclay)	d_{001} (nm)	1.7625	2.9424	2.3515	1.9172	2.4534
After Mixing Before Curing	d_{001} (nm)	4.2777	4.0586	3.9638	3.9095	4.0155
	Δd_{001} (nm) After Mixing - Before Mixing (Rubber Intercalation)	2.5152	1.1162	1.6123	1.9923	1.5621
After Mixing After Curing	d_{001} (nm)	4.3395	3.8430	3.9663	3.8920	3.7335
	Δd_{001} (nm) After Mixing - Before Mixing (Rubber Intercalation)	2.577	0.9006	1.6148	1.9748	1.2801
Effect of curing	Δd_{001} (nm) After Curing - Before Curing	0.0618	-0.2156	0.0025	-0.0175	-0.282

Table 2. Variations in magnitude and position of peak $\tan\delta$ for the nanocomposites

	Ru	R 10A	R 15A	R 20A	R 25A	R 93A
Magnitude of Peak $\tan\delta$	1.334	1.149	1.218	1.220	1.288	1.227
Reduction in Peak $\tan\delta$	0	-1.85	-1.16	-1.14	-0.046	-1.07
Tg ($^{\circ}\text{C}$)	31.2	-27.0	-28.0	-28.3	-29.5	-28.6
Shift in Tg	0	4.2	3.2	2.9	1.7	2.6

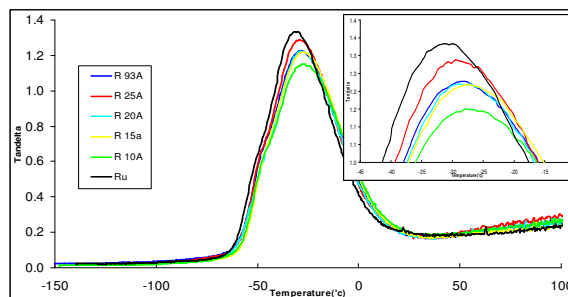


Figure2. Loss factor for the nanocomposites in a temperature sweep

Table 3. Cure characteristics of nano-composites

	Ru	R 10A	R 15A	R 20A	R 25A	R 93A
Minimum Torque (N.m)	2.900	4.141	3.367	3.955	4.146	4.012
Maximum Torque (N.m)	4.172	6.839	5.964	6.092	6.371	8.105
Scorch Time (Min) T2	0.19	1.40	2.59	2.00	2.20	2.00
Optimum Cure (Min) T90	14.60	19.11	15.53	20.90	16.90	27.50

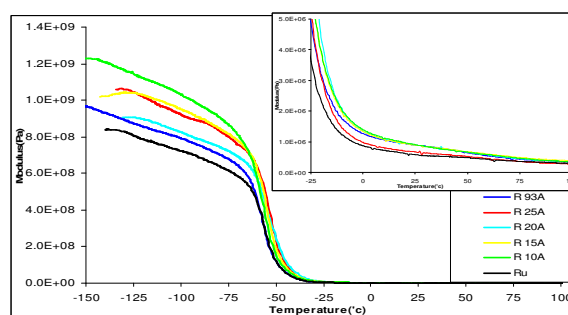


Figure3. Elastic Modulus of nanocomposites in a temperature sweep

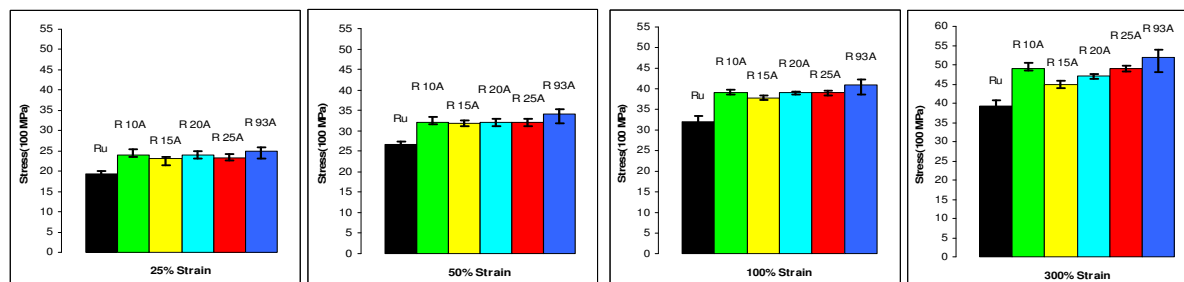


Figure4. Stress-strain figures for nanocomposites and the base compound; from left to right: at 25% strain, at 50% strain, at 100% strain, at 300% strain

NEW ANTICOUNTERFEITING SYSTEM FOR ADHESIVES

M. M. Sánchez Navarro, F. Arán Aís, A. M. Torró Palau, C. Orgilés Barceló

Footwear Technological Institute. 03600 Elda (Alicante), Spain.

Tel. 965395213; e-mail: adhesivos@inescop.es.

Abstract

In the footwear and related industries sector, the illegal market of trademark design (counterfeit), as well as those products that are produced without paying the corresponding copyright fee (piracy), coming from third countries represents a worldwide problem with a significant economic impact. In addition, in some cases, this can affect consumers' health and safety, because these products do not fulfill the current legislation in terms of safety and hygiene requirements, labeling, etc. This is a problem that affects not only the manufacturers of finished products, but also the suppliers of raw materials and components, which emphasizes the necessity of an effective solution in order to fight against forgery of trademarks, fraud and parallel trading.

In this sense, marking or tracing methods are used for "labelling" products, especially in order to closely monitor the potential effects on the market and the life cycle. At present, advanced marking methods are not widely used, mainly because they are supported by emerging technologies and information available regarding those methods is very scarce [1-10]. Many of them have stepped forward from the laboratory to an operative environment and then, to the business network. Meanwhile, there are others that only work at a laboratory scale. Most of the marking systems already available on the market or which are being developed are added as additives to inks or polymeric coatings, which in turn can be used for marking components or finished products. The apparent miscibility of these systems with polymeric materials makes their use feasible for marking adhesives.

Therefore, the main objective of this work has been to research on markers that are applicable to the adhesives used in the footwear industry. In particular, it is focused on the use of coloured codified microparticles, in order to analyze their feasibility to be used for adhesives authentication.

In this research, commercially available coloured microparticles with different properties (electromagnetic, fluorescents, etc.) were used. These samples were analyzed by means of different experimental techniques. The coloured microparticles were incorporated as additives to polyurethane and polychloroprene adhesives. The dispersion capacity of the selected microparticles was analyzed according to their properties, as well as their distribution in the core of the adhesive matrix.

The obtained results indicate that the addition of microparticles to adhesives as additives provide a feasible method for the marking and authentication of adhesives used in the footwear industry, thus providing high added value to these products

References

- [1] J.P. Cox. *Analyst*, **126** (5) 545-547 (2001)
- [2] L.J. Cook, J.P. Cox. *Biotechnol Lett*, **25** (1) 89-64 (2003)
- [3] S.W. Thomas, J.P. Amara, R.E. Bjork, T.M. Swager. *Chem Comm*, (36), 4572-4574 (2005).
- [4] Project G7RT-CT-2000-05014.

- [5] Project G6RD-CT-2002-00849.
- [6] Project QLK1-CT-2000-01658.
- [7] Project QLK1-CT-2001-02202.
- [8] Project QLK1-CT-2002-02386.
- [9] FP6-JRC Project reference: 4315.
- [10] FP6-SOCIETY Project reference: 510235

Acknowledgements. Partial financial support from the Spanish Ministry of Education and Science (project MAT2006-12633) is gratefully acknowledged.

Anomalous Hall effect in Fe (001) epitaxial thin films over a wide range in conductivity

S. Sangiao¹, L. Morellon^{1,2}, G. Simon¹, J. M. De Teresa², J. A. Pardo^{1,3}, J. Arbiol⁴, M. R. Ibarra^{1,2}

¹*Instituto de Nanociencia de Aragón and Departamento de Física de la Materia Condensada, Universidad de Zaragoza, Interfacultades II, Zaragoza, 50009, Spain*

²*Instituto de Ciencia de Materiales de Aragón and Departamento de Física de la Materia Condensada, Universidad de Zaragoza-CSIC, Facultad de Ciencias, Zaragoza, 50009, Spain*

³*Departamento de Ciencia y Tecnología de Materiales y Fluidos, Universidad de Zaragoza, Centro Politécnico Superior, Zaragoza, 50018, Spain*

⁴*TEM-MAT, Serveis Científic tècnics, Universitat de Barcelona, Barcelona, 08028, Spain*

sangiao@unizar.es

We report Hall-effect measurements of epitaxial Fe (001) thin films grown on MgO (001). We have focused on the dependence of the anomalous Hall Effect (AHE) in heteroepitaxial structures MgO (001) // Fe(t) / MgO with $t = 10, 2.5, 2, 1.8$ and 1.3 nm (see Fig. 1). Our results have been interpreted in terms of a recent unified theory of the AHE [1]. We have demonstrated that the thickness and roughness of the Fe layer are control parameters to tune both the longitudinal conductivity σ_{xx} and Hall conductivity σ_{xy} . In this way, we report a crossover from the intrinsic moderately dirty region of conductivities where $\sigma_{xy} = \text{const.}$ to the dirty region of poorly conducting materials ($\sigma_{xx} < 10^4$ S/cm) where we have found that the relation $\sigma_{xy} \propto \sigma_{xx}^n$ with $n = 1.66(4)$ holds, in good agreement, with the expected universal scaling relationship reported in other ferromagnetic compounds.

To our knowledge no single material has been found to span all three regimes proposed in Ref. 1. We show in Fig. 2 that this is possible in pure bcc Fe (001) epitaxial thin films by adequately engineering the conductivity (see Fig. 2). Therefore we provide a comprehensive view and interpretation of the AHE in bcc Fe [4], giving additional support to the unified picture proposed by Onoda et al. [1].

References:

- [1] S. Onoda, N. Sugimoto, and N. Nagaosa, Phys. Rev. Lett. **97** (2006) 086602.
- [2] T. Miyasato, N. Abe, T. Fujii, A. Asamitsu, S. Onoda, Y. Onose, N. Nagaosa, and Y. Tokura, Phys. Rev. Lett. **99** (2007) 086602.
- [3] R. Schad, P. Beliën, G. Verbanck, V. V. Moshchalkov, and Y. Bruynseraede, J. Phys.: Condens. Matter **10** (1998) 6643.

[4] S. Sangiao, L. Morellon, G. Simon, J. M. De Teresa, J. A. Pardo, J. Arbiol, and M. R. Ibarra, Phys. Rev. B **79** (2009), *accepted, in production*.

Figures:

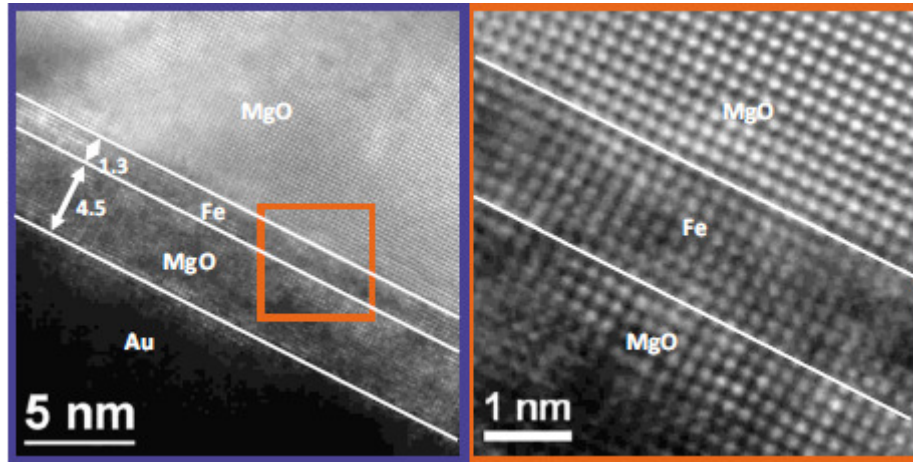


Fig. 1. Cross sectional HRTEM micrograph of a MgO (001) // Fe ($t = 1.3$ nm) / MgO thin film (left). The interface region marked has been zoomed in (right).

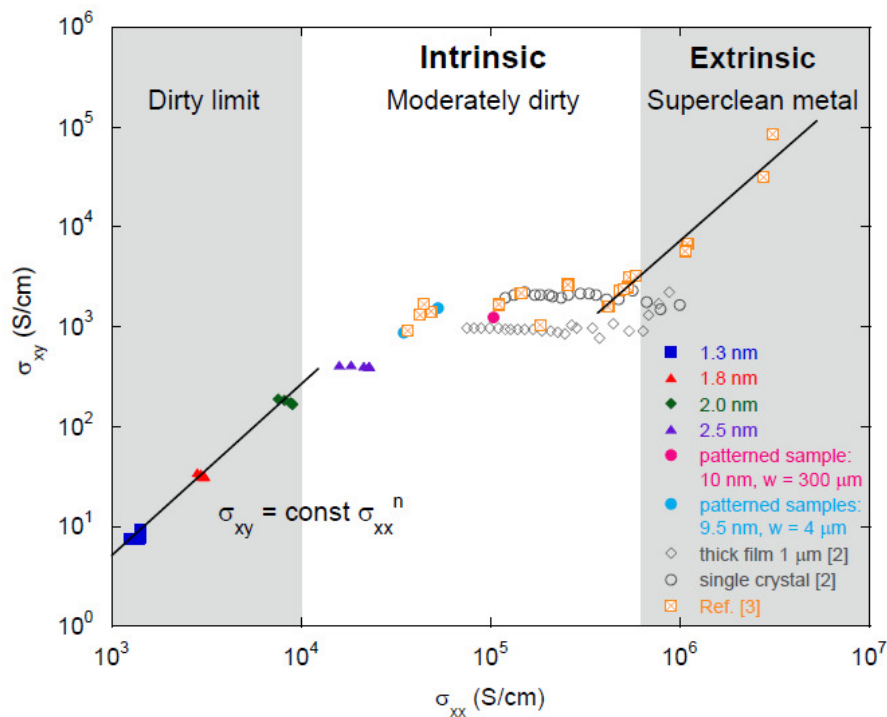


Fig. 2. Anomalous Hall conductivity values $|\sigma_{xy}|$ as a function of longitudinal conductivity σ_{xx} in MgO (001) // Fe (t) / MgO with $t = 2.5, 2.0, 1.8$, and 1.3 nm, and on patterned samples of $t \cong 10$ nm. We have included the results for a $1 \mu\text{m}$ thick film and single-crystal specimen of Fe from Ref. 2 and that of MBE-grown Fe thin films down to 2 nm (Ref. 3). The solid line in the dirty region of conductivities ($\sigma_{xx} < 10^4$ S/cm) is the fit according to the scaling relationship $\sigma_{xy} = \text{const } \sigma_{xx}^n$ with $n = 1.66(4)$.

Hydrogen Incorporation Into Palladium Ultra-Thin-Films By Low Energy Electron Microscopy

B.Santos^{1,2}, J. I. Cerda³, J. M. Puerta³, J. de la Figuera^{1,2}, T. Herranz², K. F. McCarty⁴

¹Universidad Autonoma de Madrid, 28049 Madrid, SPAIN

²Intituto de Química-Física "Rocasolano", CSIC, 28006 Madrid, SPAIN

³Instituto de Ciencias de Materiales de Madrid, CSIC, 28049 Madrid, SPAIN

⁴Sandia National Laboratories, Livermore, CA 9455, USA

benitosantos001@gmail.com

The ability of Palladium to store hydrogen is well known. Nevertheless surface science studies of the exposure of Pd(111) samples to hydrogen have found only a dense hydrogen layer between the last palladium-palladium layers, with additional hydrogen going into the bulk as a solid solution.^{1,2} On Pd films a few atomic layers thick on a substrate which does not accept substantial quantities of hydrogen such as Ru, it should be possible to saturate completely the Pd film, and thus study the formation of PdH hydride with surface science techniques. In particular, as there is a substantial lattice mismatch between Pd and the beta-PdH hydride, the incorporation of H in Pd-interstitial places should induce a significant expansion of the Pd layers. Although H itself is basically invisible to LEED, the change of the Pd-Pd distances should be easily resolved³. In this work, we present a low energy electron microscopy study of the hydrogen exposure of thin films of Pd on Ru(0001) and W(110). We characterize and study the growth and structure of Pd thin films. LEEM is a useful technique to monitor and control the growth of thin films in real space. Furthermore, a LEEM microscope can be used to acquire selected area diffraction (SAD-LEED) to determine the structure of such film.⁴

Our experiments reveals that Pd films 2 to 6 ML thick on Ru(0001) follow the fcc sequence with the Ru in-plane lattice spacing, and present a corresponding expansion in the out-of-plane lattice spacing. Thicker films on Ru(0001) relax to a bulk-like Pd in-plane spacing. Both thick films on Ru(0001) or W(110) show a slight expansion of the last interlayer spacing, in line with reported studies on the surface of bulk Pd. We follow the dosing of atomic H on the Pd films by means of real-time LEED IV curves acquired by LEEM. Figure 1 shows low energy reflectivity curves, this technique can be used as a fingerprint for identification of surfaces changes for example for determination of adatom densities⁵ or local alloy concentration⁶; around 22eV the first Bragg peak is located. During the dose of molecular hydrogen the position of that peak is always in the same indicating that there is no structural change. The curves only show a small change around 8-10 eV which is expected to be due to hydrogen adsorption at the surface.

On the other hand if atomic hydrogen is dosed, we can see a displacement of the Bragg peak to lower energies (Figure2). This shift to lower energies corresponds to an expansion of the Pd layers. To quantify this expansion LEED IV fits were performed, obtaining a expansion only in the last layer, but this expansion is smaller than the one expected for a full PdH beta-hydride formation. A similar result was obtained for films with the Ru in plane lattice parameter. The expansion of the last layer is observed, as shown in Figure2 and also the feature ascribed to hydrogen absorbed on the Pd surface is reversed by heating the sample.

This research was supported by the Office of Basic Energy Sciences, Division of Materials Sciences, U.S. Department of Energy under contract No. DE-AC04-94AL8500, and the Spanish Ministry of Science and Technology Through Project No. MAT2006-13149-C02-02.

References:

- [1] G.E. Gdowski, T.E. Felter and R.H. Stulen Surf. Sci. **181**, (1987) ,L147
- [2] Sampyo Hong and Talat S. Rahman Phys. Rev. B **75**, (2007) ,155405
- [3] T. E. Felter, Eric C. Sowa, and M. A. Van Hove, Phys. Rev. B 40 num. 2, (1989), 891-899
- [4] J. de la Figuera, et al, Surf. .Sci. **600**, (2006), 105
- [5] J. de la Figuera et al. Surf Sci (2006)
- [6] J.B. Hannon et al. Phys Rev Lett **96**(2006),246103

Figures:

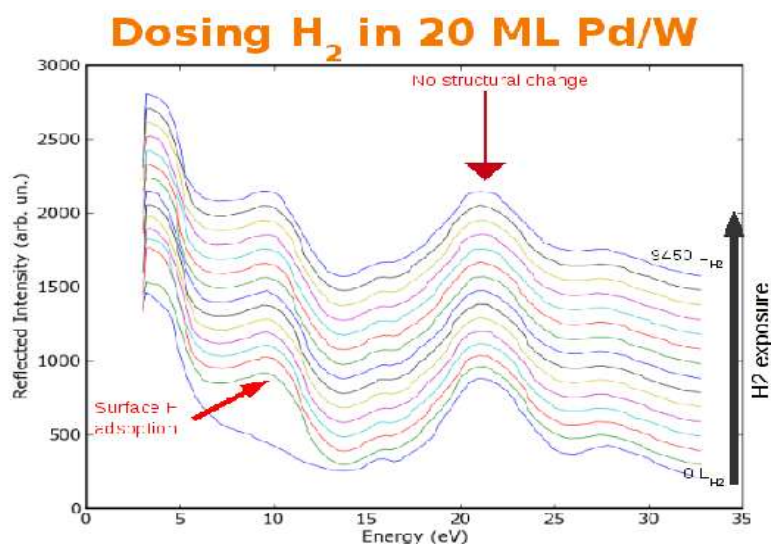


Figure1: Low energy reflectivity curves while dosing molecular hydrogen on 20 ML Pd films

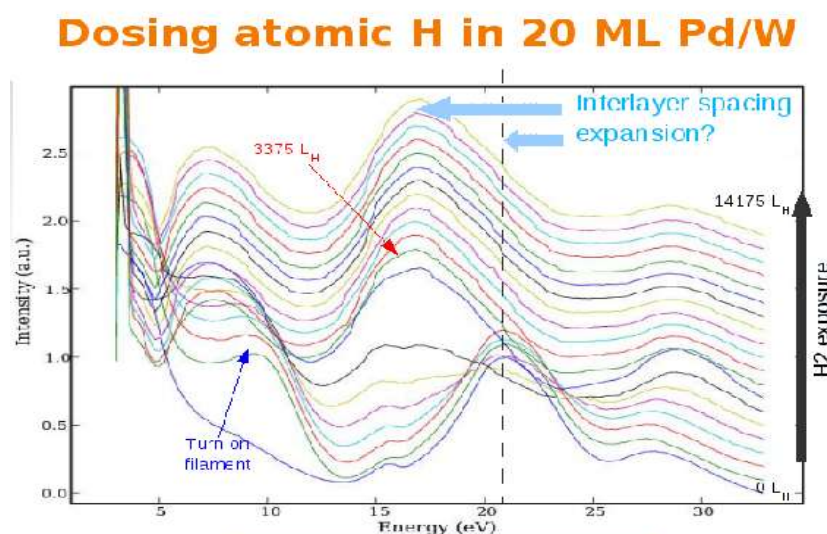


Figure2: Low energy reflectivity curves while dosing atomic hydrogen on 20 ML Pd films

Polar Decomposition and Interference Model Applied to Metallic Nanospheres

J. M. Sanz¹, P. Albella, F. González, J. M. Saiz and F. Moreno

Universidad de Cantabria, Grupo de Óptica, Dpto. Física Aplicada

Facultad de Ciencias, Avda. Los Castros s/n, Santander (Spain)

sanzjm@unican.es

Abstract

We have successfully applied the polar decomposition (PD) to the scattering matrix of coupling metallic nanospheres. The Discrete Dipole Approximation method (DDA) has been used as an intermediate tool to calculate these matrices. We also present a simple model based on the interference to justify the presence of a minimum in the scattered intensity. It is also shown how PD provides us with a frame in which the scattering systems can be characterized by independent parameters representing magnitudes of simple (virtual) elements constituting an alternative to conventional Mueller Matrix analysis methods.

System Geometry and Numerical Method

The scattering system we analyze consists of two silver spheres ($n=0,135+3,988i$, $\lambda=633\text{nm}$) of radius $r=0.1\lambda$, and with gap distances ranging from 0.1λ to 0.8λ . We have considered three different geometries (Fig.1 a, b and c) all illuminated by a monochromatic plane wave of $\lambda=633\text{nm}$. We numerically obtain the elements of the Mueller matrix by using the discrete dipole approximation (DDA) [1], which is a computational procedure suitable for studying scattering and absorption of EM radiation by particles with size of the order or less than the wavelength of the incident light [2].

The scattering matrices obtained from this method have been post-processed in all cases with an algorithm that performs the PD [3]. After testing the purity of the matrices [4], it was found that in the cases analyzed, the Mueller matrices obtained were pure. This means that the system does not produce any depolarization. Therefore, the system matrix can be decomposed as $M_{4 \times 4} = M_A M_R M_D$, where M_A , the *depolarization matrix*, is the *Identity*_{4x4} in our case, M_R is the *retardance matrix* and M_D is the *diattenuation matrix*. Due to the symmetry properties, and as a result of the PD, we can decompose our problem in an equivalent system composed by an ideal diattenuator aligned with the scattering plane, $M_D(t)$, and with the fast axis of a lineal retarder, $M_R(\varphi)$.

If we examine in detail the polarimetric properties of our system and making use of the PD, we can describe the behavior of our system by just considering three independent parameters, the total system transmittance (M_{11}), the transmission along one of the diattenuator axes (t) and the phase shift introduced by the retarder (φ). Once the meaning of the PD parameters is well understood, this polarimetric method provides us with a more handy tool to approach the analysis of the system.

Following the interferencial analysis proposed in Ref. [5], we can carry out a simple model based on two spot scatterers (Fig.1 d), where we can evaluate the angular position of the minimum in t , corresponding to phase shifts and strong changes in the *linear polarization degree* ($P_L = -M_{12}/M_{11}$, and $P_L = 1-2t$ in our case). This model is summarized in equations (1.a) and (1.b), and is a result of the phase lags introduced by the optical path difference (Λ and Ω):

$$(1.a) \quad \text{X-geometries: } (\Omega - \Lambda) = (2n + 1)\pi = \left(\frac{2\pi d}{\lambda}\right)(1 - \cos(\theta))$$

$$(1.b) \quad \text{Z-geometries: } \Lambda = (2n + 1)\pi = \left(\frac{2\pi d}{\lambda}\right)\sin(\theta)$$

where I_T is the *total scattered intensity* in a θ direction, n is the minima order and d is the scatterers separation.

Results and Conclusions

As shown in Fig.2, due to the strong interaction [5], small separations between spheres change the position of the minimum and soften the visibility in both X and Z geometries. However, when separation increases, interaction decreases, and therefore the model provides with more accurate values of minimum positions. Moreover, Y geometries do not introduce any dephase in the light spread along the scattering plane, and only shows a small deviation from the single sphere scatter when the distances between spheres are smaller.

Finally, just remark that PD magnitudes can fully describe the optical system behavior, and can be applied to other geometries, no matter its complexity. The sixteen elements of the Mueller Matrix can be reduced to a smaller number of independent ones, the same number that PD method requires. These parameters are easy to use and also represent magnitudes of simple virtual elements which improve the understanding of the processes involved in complex scattering systems.

Acknowledgements

This research has been supported by the Ministry of Education of Spain under project #FIS2007-60158 and USAITC-A through R&D 1275-PH-01. The authors thankfully acknowledge the computer resources provided by the RES node at Universidad de Cantabria. P. Albella thanks the Ministry of Education for his FPI grant.

References:

- [1] B. T. Draine, P. J. Flatau, User Guide for the Discrete Dipole Approximation Code DDSCAT 6.1, 2004. URL <http://arxiv.org/abs/astro-ph/0409262v2>
- [2] P. Albella, F. Moreno, J. M. Saiz, F. Gonzalez, Backscattering of metallic microstructures with small defects located on at substrates, Optics Express 15 (11) (2007) 6857-6867.
- [3] J.M. Sanz, P. Albella, F. Moreno, J. M. Saiz and F. Gonzalez, Application of Polar Decomposition to Light Scattering Particle Systems, JQSRT Accepted on January 2009.
- [4] J. J. Gil, Polarimetric characterization of light and media, The European Physical Journal of Applied Physics 40 (2007) 1-47.
- [5] P. J. Valle, F. Moreno, J. M. Saiz, and F. González, Electromagnetic Interaction Between Two Parallel Circular Cylinders on a Planar Interface, IEEE (Vol 44, 3) 1996.

Figure 1

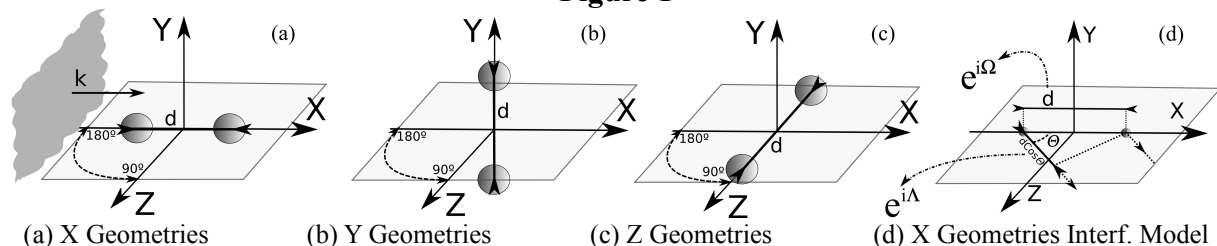
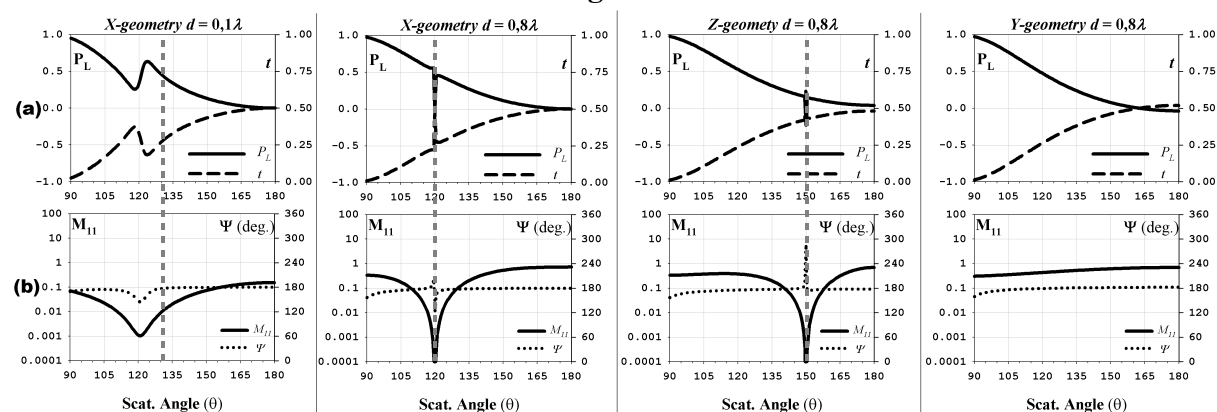


Figure 2



Some graphical results: Dotted Gray Line → Interference Model Predicted Minimum

ADVANTAGEOUS USE OF CARBON NANOFIBERS IN FUEL CELLS AS CATALYST SUPPORT

D. Sebastián, L. Calvillo, I. Suelves, M.J. Lázaro, R. Moliner

Instituto de Carboquímica (CSIC), Miguel Luesma Castán 4, 50018 Zaragoza (Spain)

mlazaro@icb.csic.es

1. Introduction

Fuel cells present unique and favourable advantages over conventional energy converting devices. However, some aspects regarding cost and durability have to be addressed before their widespread commercialization. Great efforts are being carried out to achieve a higher Pt-specific power density, mainly: the reduction of the platinum loading while maintaining high power densities; and the reduction of mass-transport induced voltage losses at high current densities [1]. In this sense, nanotechnology can provide new materials with a great potential to improve currently used electrocatalysts. Carbon nanofibers have attracted interest because of their unique structural, electrical and textural properties, which are expected to offer a great potential in their application as catalyst supports [2]. In this work, carbon nanofibers with different properties have been obtained by methane catalytic decomposition and have been functionalized with acid aqueous solutions under conditions of different severity.

2. Experimental

A co-precipitation method has been used to obtain a Ni:Cu:Al₂O₃ catalyst. Then, a methane flow passes through the catalyst in a fixed bed reactor and decomposes into hydrogen and carbon nanofibers. Reaction conditions such as temperature or gas composition have been varied to study the influence on the carbonaceous material properties. Carbon characterization has been carried out by scanning electron microscopy (SEM), nitrogen physisorption and X-Ray diffraction (XRD). The electrical conductivity has been determined by a two-probe method applying pressure over the powder. Functionalization of carbon nanofibers has been carried out by treatment with nitric acid or a mixture of nitric and sulphuric acid at room or boiling temperature, according to the best results obtained previously [3]. The amount and nature of oxygen surface groups have been determined by temperature programmed desorption (TPD), analyzing CO and CO₂ desorbed by gas chromatography.

3. Results

One of the advantages that carbon nanofibers present as catalyst support for fuel cells is their negligible content in micropores in contrast with commonly used carbon blacks (Vulcan XC-72R). This is due to the morphology of carbon particles, formed by entangled nanofilaments constituted in turn by carbon layers disposed at a determined angle with respect to the growth axis. A SEM micrograph can be observed in Figure 1 as an example. Table 1 shows surface area and pore volume values, determined from nitrogen physisorption isotherms, for Vulcan XC-72R and three selected CNFs obtained at 750°C (CNF-HT), 600°C (CNF-MT) and 550°C (CNF-LT). As can be observed from the table, the highest values of mesoporous surface area (166.4 m²/g) and pore volume (0.712 cm³/g) correspond with CNFs obtained at low temperature (CNF-LT), with a negligible quantity of micropores. However, the highest values of electrical conductivity were observed at CNFs obtained at higher temperatures, showing even higher conductivity than Vulcan XC-72R (sample CNF-HT) as can be observed in Figure 2. This corresponds with a high graphitization degree confirmed by XRD analyses (not shown).

Oxygen surface groups are created by oxidizing treatment. These functional groups decompose into CO₂ and CO at temperatures from 200°C to 1000°C, depending mainly on

their nature. Figures 3 and 4 show the profiles obtained in TPD experiments for three oxidation conditions: a mixture of nitric and sulphuric acids (1:1 v/v) at boiling temperature (F-NS110), nitric acid at boiling temperature (F-N110) and again a mixture of nitric and sulphuric acids (1:1 v/v) at room temperature (F-NS025). On one hand, boiling temperature favors the creation of carboxylic and phenol groups, by the comparison of the peak at 300°C in CO₂ profile and the shoulder at 600°C in CO profile, respectively, in samples F-NS025 and F-NS110. On the other hand, the use of sulphuric acid increases the amount of groups created, by comparison of F-N110 and F-NS110.

Acknowledgments

The authors gratefully acknowledge financial support given by the Spanish MEC and FEDER under the project NAN2004-09333-C05-01. D. Sebastián also acknowledges CSIC for his I3P predoctoral grant.

References:

- [1] H.A. Gasteiger, S.S. Kocha, B. Sompalli, F.T. Wagner, *Applied Catalysis B: Environmental*, **56** (2005) 9-35.
- [2] K. Lee, J. Zhang, H. Wang, D.P. Wilkinson, *Journal of Applied Electrochemistry*, **36** (2006) 507-522.
- [3] L. Calvillo, M. Gangeri, S. Perathoner, G. Centi, R. Moliner, M.J. Lázaro, *Journal of Power Sources*, (2008), doi:10.1016/j.jpowsour.2009.01.005.

Tables:

Sample		Vulcan XC-72R	CNF-HT	CNF-MT	CNF-LT
Surface area (m ² g ⁻¹)	Mesoporous	153.2	93.3	130.2	166.4
	Microporous	65.2	5.8	12.6	18.5
Pore volume (cm ³ g ⁻¹)	Mesoporous	0.370	0.214	0.568	0.712
	Microporous	0.040	0.003	0.007	0.010

Table 1. Textural properties determined from nitrogen physisorption isotherms.

Figures:

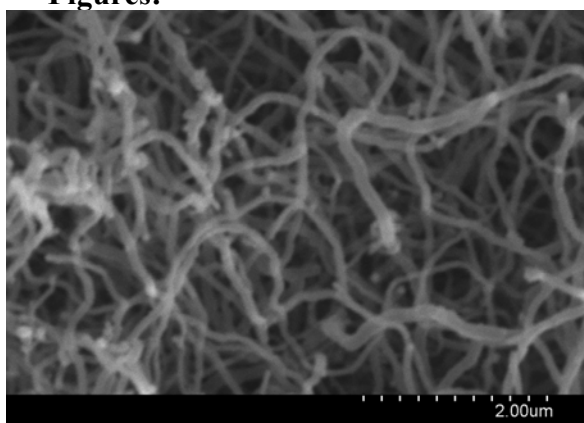


Figure 1. SEM micrograph of carbon nanofibers.

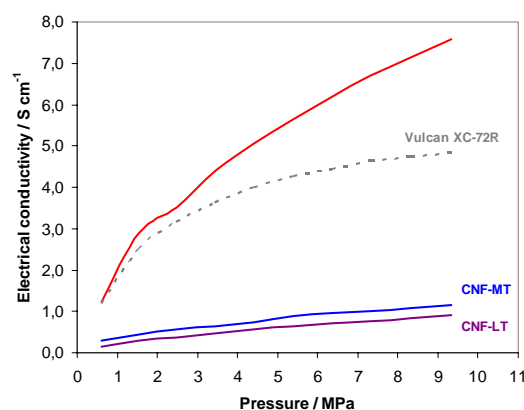


Figure 2. Electrical conductivity of CNFs and Vulcan XC-72R

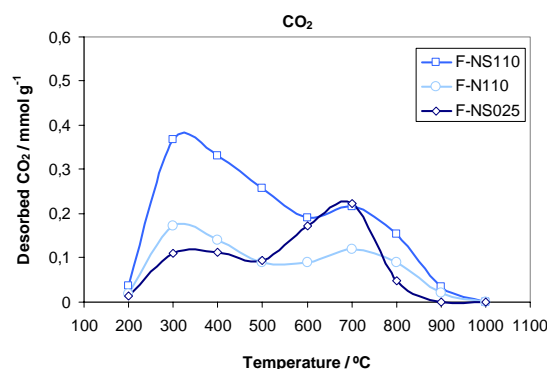


Figure 3. CO₂ desorbed in TPD experiments for CNF-MT

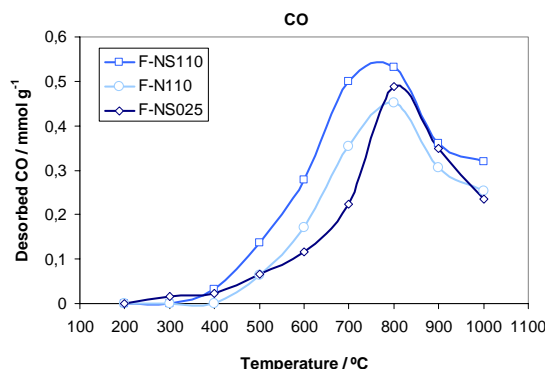


Figure 4. CO desorbed in TPD experiments for CNF-MT

SELF-ASSEMBLED MONOLAYERS OF CALIX[n]ARENE (n=4,6) DERIVATIVES ON SI(100) AND POLYCRYSTALLINE COPPER

Luca Pescatori,^a Arturo Arduini,^a Andrea Pochini,^a Andrea Secchi,^a Alice Boccia,^b Valeria Di Castro,^b Valeria Lanzilotto,^b and Robertino Zanon^b

^a *Dipartimento di Chimica Organica e Industriale, Università degli Studi, V. le G.P. Usberti 17/a, 43100 Parma, Italy;* ^b *Dipartimento di Chimica, Università degli Studi di Roma 'La*

Sapienza', p.le Aldo Moro, 5 - I 00185 Roma, Italy

andrea.secchii@unipr.it

The controlled production of organic monolayers on semiconductor and metal surfaces of technological interest can provide a material with new features in the nanoscale. While numerous examples have been already proposed of functional species, such as redox couples, bio-molecules or selective receptors anchored on silicon or on gold surfaces, very rarely a close comparison has been reported of the behaviour of one class of such compounds on both a semiconductor and a metal surface. In this framework, the first compared study is given here of the distinct anchoring properties on H-Si(100) and polycrystalline Cu of a few members of a class of molecules, chosen among the most representative ones in supramolecular chemistry: calix[n]arenes.[1]

A covalent functionalization on both Si and Cu surfaces requires the molecules to be differently modified: a thiol (-SH) or C=C termination are respectively suitable for copper or H-Si(100). Anchoring on Cu was reached by dipping a clean sample in a calix[n]arene-SH solution (n = 4,6), while a wet chemistry recipe was followed for Si(100), combined with an extra-mild photochemical activation via visible light.[2] Molecular adhesion onto either surfaces has been demonstrated by the presence of XPS signals from specific elements in the molecules: the aromatic nuclei of the calix[n]arene derivatives designed for H-Si were functionalized with Br atoms or NO₂ groups, while the S atom was used as the molecular identifier on Cu. AFM measurements performed on H-Si(100)/calix[4]arene have revealed structures 2-2.5 nm high, consistent with the length of the molecule in a "standing up" conformation. The diameter of these structures suggests that self-assembled calixarenes clusters are formed on Si.

A further extension on Cu is represented by anchoring a rotaxane.[3] A pseudorotaxane species was formed in solution by reacting a calix[6]arene "wheel", functionalized with three *N*-phenylurea groups on its upper rim, with a viologen (4,4'-bipyridinium) axle.[4] The resulting species has been anchored on Cu via the thiol termination of the axle. This two-step reaction has produced a threaded rotaxane covalently bound to Cu surface, as shown by XPS results. This species is ready to respond to external stimuli.

References:

[1] *Calixarenes in the Nanoworld*, J. Vicens and J. Harrowfield Eds., Springer, 2007.

[2] F. Decker, F. Cattaruzza, C. Coluzza, A. Flamini, A. G. Marrani, R. Zanon, E. A Dalchiele, *J. Phys. Chem. B*, **110** (2006), 7374.

[3] V. Balzani, M. Venturi, A. Credi, *Molecular Devices and Machines—Concepts and Perspectives for the Nano World*, 2nd Ed., Wiley-VCH, Weinheim, 2008.

[4] Arturo Arduini, Flavio Ciesa, Marcello Fragassi, Andrea Pochini, Andrea Secchi, *Angew. Chem. Int. Ed.*, **44** (2005), 278.

LASER ABLATION PRODUCTION OF METAL-DOPED NANOSTRUCTURED CARBON FOAM

A. Seral-Ascaso,¹ E. Muñoz,^{2,} M. L. Ruiz-González,³ M. L. Sanjuán,¹ J. M. González-Calbet,³
M. Laguna¹, and G. F. de la Fuente¹*

¹ *Instituto de Ciencia de Materiales de Aragón (Universidad de Zaragoza-CSIC), Zaragoza, Spain.*

² *Instituto de Carboquímica (CSIC), Miguel Luesma Castán 4, 50018 Zaragoza. Spain*

³ *Departamento de Química Inorgánica I, Facultad de Ciencias Químicas, Universidad Complutense, 28040 Madrid. Spain.*

edgar@icb.csic.es

Laser ablation of carbon-containing materials has been demonstrated as a convenient method for the preparation of carbon-based nanostructures [1]. A particular example is the production of single-walled carbon nanotubes by laser irradiation of metal-doped graphite targets [2]. Important laser parameters such as wavelength, pulse repetition rate, laser fluence (pulsed- or cw mode) or irradiance, as well as other experimental conditions (mainly atmosphere composition and pressure, target composition and external or laser-generated heating) strongly affect the recombination of the evaporated species and, therefore, the nature and properties of the produced materials, eventually resulting in efficient carbon nanotube production processes [3].

The present work thus pretends to illustrate the potential of using selected organometallic precursors for the tailored production of metal-doped nanostructured carbon foams. Laser ablation of the employed organometallic precursors leads to the formation of soots exhibiting a spongy texture as a consequence of the aggregation of particles whose diameters range between 20 and 40 nm, as shown in the scanning electron microscopy (SEM) image depicted in Fig. 1 (left). Transmission electron microscopy (TEM) studies reveal that these materials consist of metal nanoparticles embedded in carbon matrices comprising both amorphous carbon and graphitic nanostructures (Fig. 1, right). A new family of carbon nanostructured materials can be thus envisioned by employing the simple, versatile laser ablation technique described in this work [4].

References:

- [1] A.V. Rode, S.T. Hyde, E.G. Gamaly, R.G. Elliman, D.R. McKenzie, S. Bulcock, *Appl. Phys. A*, **69** (1999) S755.
- [2] W.K. Maser, E. Muñoz, A.M. Benito, M.T. Martínez, G.F. de la Fuente, Y. Maniette, E. Anglaret, J.L. Sauvajol, *Chem. Phys. Lett.*, **292** (1998) 587.
- [3] E. Muñoz, W.K. Maser, A.M. Benito, M.T. Martínez, G.F. de la Fuente, A. Righi, J.L. Sauvajol, E. Anglaret, Y. Maniette, *Appl. Phys. A*, **70** (2000) 145.
- [4] E. Muñoz, M. de Val, M.L. Ruiz-González, C. López-Gascón, M.L. Sanjuán, M.T. Martínez, J.M. González-Calbet, G.F. de la Fuente, M. Laguna, *Chem. Phys. Lett.*, **420** (2006) 86.

Figures:

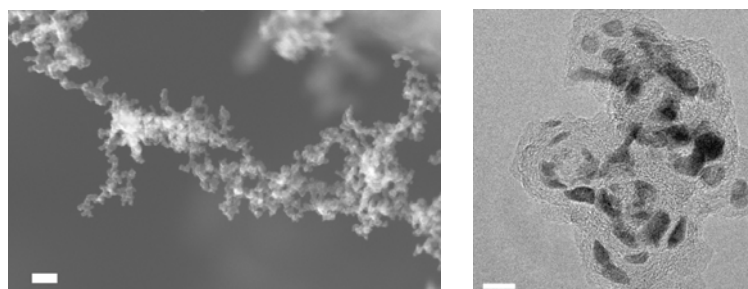


Fig. 1. SEM-(left) and TEM (right) micrographs of laser-ablation produced Au-doped carbon foams [4].

Linear polarization degree of right-angle scattering for silver nanodimmers: changes induced by quadrupolar excitation.

Beatriz Setién, José María Saiz, Francisco González and Fernando Moreno
Grupo de Óptica. Departamento de Física Aplicada. Universidad de Cantabria.
Avda de los Castros s/n, 39005, Santander (SPAIN)
beatriz.setien@alumnos.unican.es

The spectral properties of the linear polarization degree (P_L) at a scattering angle of 90° , are analysed theoretically and numerically for a silver nanodimmer of finite size, characterized by its gap distance, d . We shall focus on the influence that modes of order higher than de dipolar have on parameter P_L , and on the effect of having a size distribution being the asymmetric dimmer an example.

Introduction

The excitation of localized surface plasmon resonances (LSPR) on metallic nanoparticles depends on the physical properties of the system and the surrounding medium [1]. This phenomenon is the basis of some applications in fields like Medicine, Biology or Industry [2,3].

For ideal point-like particles, only the dipolar resonance can be excited. However, for finite-size particles in the nanometric range, although the dipolar mode is still very important, it is possible to efficiently excite modes of higher order and in particular quadrupolar ones.

In this work we analyze the spectral evolution of the linear polarization degree (P_L) of the scattering produced by silver nanoparticle dimmers when measured at 90° respect to the incident direction. Under this configuration the influence of higher orders modes is better shown. These results can have direct application for instance in monitoring nanorulers. [4]

Theory

The linear polarization degree is defined as [5]

$$P_L = \frac{I_{\perp} - I_{\parallel}}{I_{\perp} + I_{\parallel}} \quad (1)$$

I_{\perp} and I_{\parallel} being the scattered intensities when the incident polarization is perpendicular or parallel to the scattering plane, respectively.

For dipole-like particles, the parallel intensity (I_{\parallel}) is zero at $\theta_s=90^\circ$, that is, P_L is always equal 1 at this direction. For larger particles, multipolar orders make $I_{\parallel}(90^\circ)$ different from 0, and P_L different from 1.

Results

In Fig. 1 and Fig.2 we show, as an example of the kind of results produced by this study, the scattered total intensity and the linear polarization degree, both measured at 90° , as a function of the incident wavelength. This is calculated by means of T-Matrix formalism [6]. For a system of two silver particles [7], the centre aligned perpendicularly to the scattering plane, and for different gap distances between them (d). In Fig.1 the system is composed of two identical silver particles of radius $R=50nm$. (The case of an isolated particle is included for comparison).

In Fig.2, we introduce a strong asymmetry in the dimmer by considering two silver particles of different size: $R_1=50nm$ and $R_2=20nm$. When a quadrupolar resonance is excited, P_L reaches a minimum (Fig.1). When the particles of the dimmer approach, the interaction between them increases, and the quadrupolar peak shows some spectral structure where P_L exhibits two minima. For large values of d , P_L tends to that of an isolated particle.

In Fig.2 it can be observed that the asymmetry makes the larger particle dominant, specially for large values of d , and the sensitivity of P_L to the value of d is almost lost. However, there are some interesting features, like the evolution of the scattering at $\lambda=430nm$ when d is reduced.

References:

- [1] P.N. Prasad (Wiley-Interscience, 2004).
- [2] K. Aslan, J.R. Lakowicz and C.D. Gaddes, *Current Opinion in Chemical Biology* **9**, (2005) 538-544.
- [3] X. Wei, X. Luo, X. Dong and C. Du, *Opt. Express* **15**, (2007) 14177-14183.
- [4] B.M.Reinhard, M.Siu,H.Agarwal,A.P.Alivisatos and J.Liphardt, *Nano. Lett.*, **5**(11), (2005)2246-2252.
- [5] C. Bohren and D. R. Huffman (Wiley, 1983).
- [6] M.I.Mishchenko,G.Videen,V.A Babenko,N.G. Khlebtsov and T.Wriedt, *JQSRT*, **88**, (2004) 357-406
- [7] E.D.Palik, *Handbook of Optical Constant of Solids* (Academic Press INC. Florida,1985).

Figures:

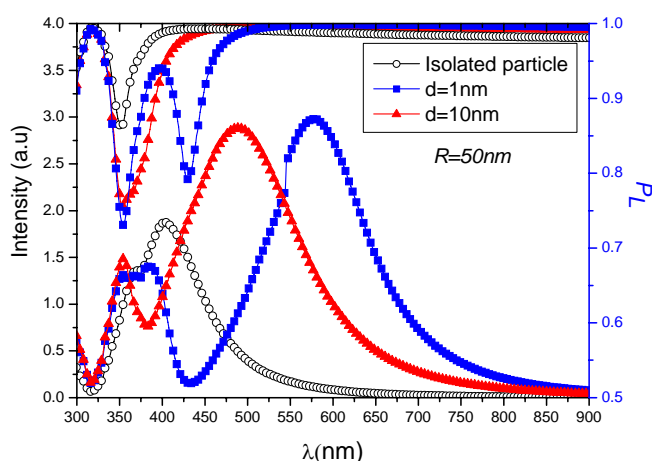


Fig.1

Figure1. Spectral dependence of the scattered total intensity and the linear polarization degree, at 90° , for a dimmer of silver spherical particles ($R=50nm$) oriented perpendicularly to the incident and observation directions, and for two distances between the particles. The isolated case is also included.

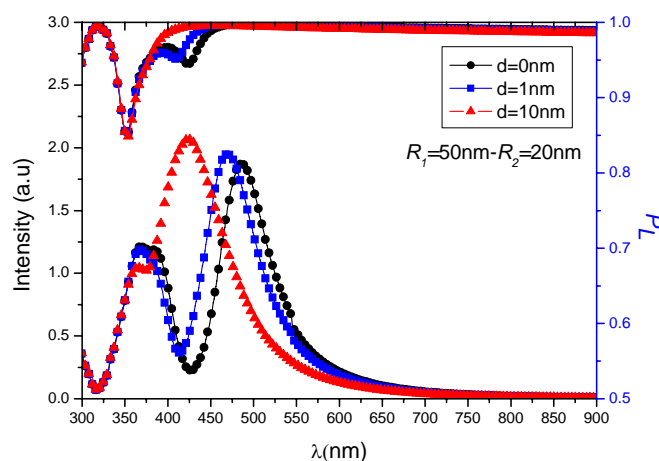


Fig.2

Figure2. Spectral dependence of the scattered total intensity and the linear polarization degree, at 90° , for a non-symmetric dimmer of silver spherical particles ($R_1=50nm$ - $R_2=20nm$) aligned perpendicularly to the incident and observation directions and for three distances between the particles of the dimmer, including the contact case.

Carbon nanotube networks dispersed in a polymer matrix: dielectric properties simulations and experiments

J. Silva^{1,2}, V. Sencadas², P. Costa², J. Gomes^{2,4},
S. Lanceros-Méndez², R. Vaia³ and R. Simoes^{1,5}

¹ IPC – Institute for Polymers and Composites, University of Minho, Campus de Azurem, 4800-058 Guimaraes, Portugal; Tlf. 253510320; Fax. 253510339;

² Department of Physics, University of Minho, Campus de Gualtar, 4710-057 Braga, Portugal.

³ Air Force Research Laboratories, Wright-Patterson AFB, OH 45433-7750, USA

⁴ CeNTI – Centre for Nanotechnology and Smart Materials, Rua Fernando Mesquita, 2782, 4760-034 Vila Nova de Famalicao, Portugal.

⁵ School of Technology, Polytechnic Institute of Cavado and Ave, 4750 Barcelos, Portugal

jaime.silva@dep.uminho.pt, rsimoes@dep.uminho.pt

The addition of carbon nanotubes (CNT) to a polymeric matrix is known to affect its mechanical and electrical properties. The changes can be significant even at small volume fractions of the reinforcement. The CNT concentration, aspect ratio, and dispersion are expected to affect the material response [1]. However, the precise mechanisms responsible for the described effects are not sufficiently understood. This is due to the complex nature of the behavior of polymers, which exhibit a complex structure and a variety of factors that influence the material behavior, such as the thermomechanical processing history, time-dependent behaviour, anisotropy, etc.

For CNT/polymeric composites it is assumed that the mechanism for the composite conduction is formation of conductive channels stretching across the entire length of the system [2]. The later assumption enables the use of the percolation theory where simple power laws can predict the composite conductivity and the effective dielectric constant. One of the fundamental concepts in the percolation theory is the percolation threshold (p_c). The percolation threshold is defined as the concentration (p) at which an infinite cluster appears in an infinite lattice. For a concentration $p > p_c$ a cluster spans the system and for $p < p_c$ the spanning cluster does not exist and the system is made of many small clusters. The value for the percolation threshold depends on the dimensionality of the domain and on the geometry of the filler. At the percolation threshold there are several physical properties that can diverge such as the conductivity and the dielectric constant. The relationship between the composite critical concentration in the conductivity and the dielectric constant was early studied by Bergman and Imry in 1977 [2] for heterogeneous mixtures of a conducting phase in an insulating matrix. Bergman and Stroud [3] used a scaling assumption in order to analyze the critical behavior of the composite dielectric constant, demonstrating that for metallic inclusions in an insulating matrix the real part of the dielectric constant has peak at $\omega = 0$ Hz whose height is proportional to $\varepsilon_{matrix}|p - p_c|^{-s}$, diverging at p_c . The later yields the well known relation that holds for $p < p_c$ and $p > p_c$, $\varepsilon_{eff} \propto \varepsilon_{matrix}|p - p_c|^{-s}$. In the same article [3] Bergman and Stroud also demonstrates, using the same scaling relations, for the composite conductivity that for $p > p_c$ the composite conductivity is given with the following relation, $\sigma_{eff} \propto \sigma_{matrix}(p - p_c)^t$. On the later power laws t and s are called the conductivity – t – and superconductivity – s – critical exponents. The values for the conductivity exponent were determined by Kirkpatrick [4] using three different models. The value in 3D for t was 1.5 +/- 0.2. In more recent works the accepted value is ~1.8. For the superconductivity exponent using a bond percolation model, 3D, in conjugation transfer matrix algorithm, Herrmann and Derrida [5] found that the value is 0.75 +/- 0.04.

The critical values are assumed to be universal; depending only on the dimensionality of the system.

In recent experimental articles for multi wall carbon nanotubes (MWCNT)/polymeric composites were the superconductive exponent – s – and the percolation threshold are reported, a wide range of values have been reported (Table 1).

In this work, a numerical model based on the graph theory is presented which focuses on the effect on the dielectric constant and the dielectric strength of the inclusion of conductive fillers in a dielectric polymer matrix [6]. Experiments have been carried out in carbon nanotubes/poly(vinilidene fluoride) nanocomposites in order to compare to the simulation results Fig. 1. This work shows how the critical concentration is related to the formation of capacitor networks and that these networks give rise to the high variations in the electrical properties of the composites. Finally, based on numerical and experimental results, the origin of anomalous percolation behaviours has been identified.

References:

- [1] Chou T.-W, Thostenson E. T. and Li C., Composites Science and Technology, **65** (2005) 491.
- [2] Bergman D. J. and Imry Y., Physical Review Letters, **39** (1977) 1222.
- [3] Bergman D. J. and Stroud D., Physical Review B, **25** (1982) 2061.
- [4] Kirkpatrick, S., Review of Modern Physics, **45** (1973) 574.
- [5] Herrmann, H. J. and Derrida, B. 7, Physical Review B, **30** (1984) 4080.
- [6] Simoes R., Silva J., Vaia R., Sencadas V., Costa P., Gomes J. and Lanceros-Méndez S., Nanotechnology **20** (2009) 035703.
- [7] Yao S.-H., Dang Z.-M., Jiang M.-J., Xu H.-P., Applied Physics Letters, **91** (2007) 212901.
- [8] Ahmad K., Pan W., and Shi S.-L., Applied Physics Letters, **89** (2006) 133122.
- [9] Zhu B.-K., Xie S.-H, Xu Z.-K and Xu Y.-Y, Composites Science and Technology, **66** (2006) 548.
- [10] Potschkea P., Dudkinb S. M. and Aligh I., Polymer, **44** (2003) 5023.

Figures:

Table 1, Experimental reported values for the percolation threshold in several MWCNT composites types.

Percolation Threshold	Aspect Ratio	s exponent	Composite	Reference
0.0077	62	0.268	MWCNT/PVDF	[7]
0.0114	116	1.007	MWCNT/PVDF	[7]
0.0191	437	1.795	MWCNT/PVDF	[7]
0.0161	833	0.31	MWCNT/PVDF	[7]
0.0079	-	0.35	Alumina/MWCNT	[8]
0.07	300	1.14	MWCNT/Polyimide	[9]
1.44	440	-	MWCNT/Polycarbonate	[10]

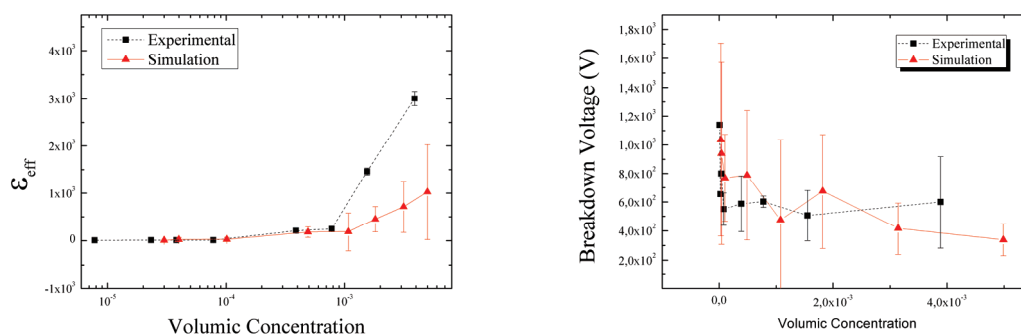


Figure 1, Comparison of the numerical results versus experimental ones.

INTRACRYSTALLINE PORE FORMATION IN NANOCRYSTAL METAL FILMS

Leonid Skatkov¹ & Valeriy Gomoiov

¹ PCB “Argo”, 4/23 Shaul ha-Melekh Str., 84797 Beer Sheva, ISRAEL

²National Technical University “Kharkov Polytechnical Institute”, 21 Frunze Str., 61002 Kharkov, UKRAINE

Creation of novel materials used in metallurgy and alternative industries is to a great extent related to porosity that considerably affects physico-mechanical, physico-chemical, ferromagnetic, and alternative features and working characteristics of materials. Diversified crystal and amorphous condensed systems such as films and coatings are being extensively used in modern science and engineering as the structures that typically comprise pores of differing dispersion, shape, and volume localization nature. The results of previous studies demonstrate that pore formation in such systems results from the regularities and peculiarities accompanying the formation of amorphous and crystal structures during matter condensation. The basic factors determining the nature of condensation pore formation are competition between diffusion and sorption, gas discharge and gas absorption that orient the molecular flux effect, interrelations between overcooling extent, evaporation and condensation rates, structural condition, substrate chemical composition, and surface topology, and the difference between its thermal dilatation and that of the condensate.

The condensation pore formation mechanisms such as diffusion vacancy, “shadowing” effect, growth non-homogeneity, related to the condensation surface topology, pore formation at the growth stages, micro shrinkage, impact and drop mechanisms caused by the condensation mechanisms – all these act in integrity with the relations varying as a function of condensate formation physical conditions, and can be programmed. For such programming, the predominant location of varying-dispersion pore generation under one or another prevailing mechanism is virtually essential. Therefore, the paper discusses the results of submicropore research in single-crystal and poly-crystal condensates in order to define the key factors that are responsible for the processes of prevailing intra-grain pore formation, or limit them. Intra-grain condensation in nanocrystal systems is basically transformed by the concerted action of diffusion vacancy and sorption mechanisms as a function of gas excretion or gas absorption intensity .

Stable Ag and Au Nanospheres Synthesized by Porphyrin-Assisted Photocatalysis

Leonor Soares,^a Pedro Quaresma,^{a,b} Lívia Contar,^a Patrícia A. Carvalho^c and Eulália Pereira^a

a) REQUIMTE/Faculdade de Ciências, Universidade do Porto, R. Campo Alegre, 687, 4169-007 Porto, Portugal; b) CIGMH/Departamento de Ciências da Vida, FCT-UNL, 2829-516 Caparica, Portugal;

c) Departamento de Engenharia de Materiais, IST, Av. Rovisco Pais 1049-100 Lisboa, Portugal

*Corresponding author: leonoririz@gmail.com

Silver and gold nanoparticles have received special attention due to their ease of preparation and their physico-chemical properties.^[1,2] The properties of these nanoparticles grant them a vast applicability in cellular and biomolecular labelling, therapeutical biosensors and also appeared more recently as promising antimicrobial materials.^[1]

A new photocatalytic method for the synthesis of nanospheres was used.^[3] This method involves the reduction of a metallic precursor ($\text{AgNO}_3/\text{HAuCl}_4$) in association with a photocatalyst, a metalloporphyrin of tin (IV), an electron donor agent, triethanolamine (TEA), in the presence of a capping agent. Several capping agents were tested and polyvinylpyrrolidone (PVP) showed to be the most suitable for both metals.^[4] For the optimization of the synthesis, the variation of some parameters was performed, such as the concentration of PVP, metal precursor, and photocatalyst, and their influence was evaluated in order to achieve a greener and more efficient method. The reaction was followed by UV-Vis Spectroscopy, Dynamic Light Scattering (DLS) and Transmission Electron Microscopy (TEM), in order to morphologically characterize the nanoparticles obtained.^[2,7] The stability of the colloidal solutions obtained at several pH and ionic strength was also evaluated.^[5] The ease of exchange of the capping agent was studied by incubation with 11-mercaptopundecanoic acid (MUA).^[6]

References:

- [1] Elechiguerra, L.; Burt, L.; Morones, R.; Bragado, G.; Gao, X.; Lara, H.; Yacaman, M., *J. Nanobiotechnol.*, (2005) 3.
- [2] Eutis, S.; Hsu, H-Y; El-Sayed, M.; *J. Phys. Chem. Lett. B*, **109** (2005), 4811-4815.
- [3] Song, Y.; Yang, Y.; Medforth, C.; Pereira, E.; Singh, A.; Xu, H.; Jiang, Y; Brinker, C.; Swol, F.; Shelnutt, J., *J. Am. Chem. Soc.*, **126** (2004), 635-645.
- [4] Rao, C.; Vivekchand, S.; Biswas, K.; Govindaraj, A., *Dalton Trans* (2007) 3728-3749.
- [5] Wanner, M.; Gerthsen, D.; Jester, SS; Sarkar, B.; Schwederski, B.; *Coll. Polymer Sci.*, **283** (2005), 783.
- [6] Lin, SY.; Tsai, YT; Chen, C-C; Lin, C-M.; Chen, C-H; *J. Phys. Chem.*, **108** (2004) 2134.
- [7] Creighton, A.; Eadon, G.; *J. Chem. Soc., Faraday Trans.*, **87** (1991), 3881-3891.

Acknowledgments: Fundação para a Ciência e a Tecnologia, Portugal for financial support through project PTDC/QUI/64484/2006; P. Quaresma thanks FCT for PhD grant SFRH/BD/17566/2004.

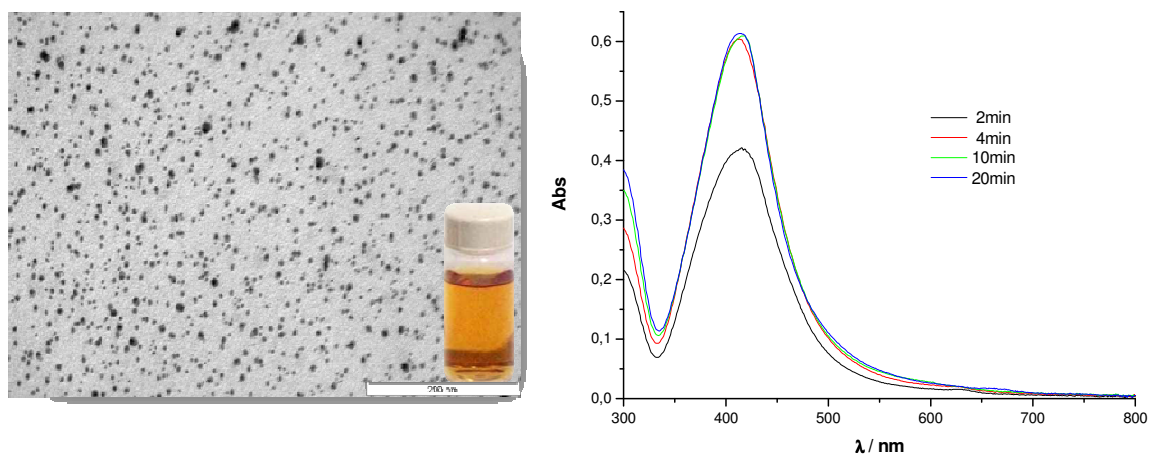
Figures:

Figure 1 – Representative TEM micrograph of Ag nanoparticles ($5\pm 2\text{nm}$) and the UV-Visible spectra, showing the increase of the Ag Plasmon band centered at 420nm.

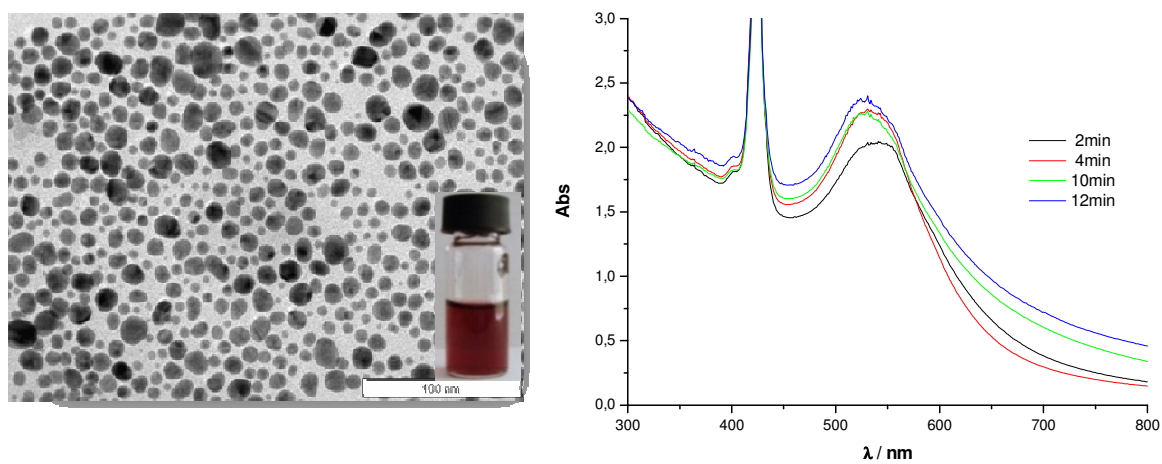


Figure 2 – Representative TEM micrograph of Au nanoparticles ($10\pm 4\text{nm}$) and UV-Vis spectra, showing the increase of the Au Plasmon band at 520nm.

SYNTHESIS OF WATERGLASS BASED SILICA AEROGEL WITH HIGH TEMPERATURE HYDROPHOBIC STABILITY VIA AMBIENT PRESSURE DRYING METHOD

A.Soleimani Dorcheh, M.H. Abbasi

Department of Materials Engineering, Isfahan University of Technology, Isfahan

8415683111, Iran.

ali_sd@ma.iut.ac.ir

Extended Abstract:

Silica aerogel is a nanostructure material with high surface area (400–1200 m²/g), high porosity (~99.8%), low density (0.03–0.35 g/cm³), low dielectric constant (<2.0), and low thermal conductivity (0.01–0.015 W/m·K). Therefore, it has a number of applications such as shock wave studies at high pressures, Cerenkov radiation detectors in high energy physics, inertial confinement fusion (ICF), radio luminescent devices, containers for liquid rocket propellants, micrometeorites, light weight thermal and acoustic insulating systems, adsorption and catalytic supports and for super capacitors [1-4]. However, conventional production of silica aerogel includes expensive raw materials like TEOS and supercritical drying which prohibit commercialization. For successful large scale commercialization of aerogels, it is clear that costs and risks must be dramatically reduced. To achieve this goal, requirements include (1) the use of inexpensive precursors such as sodium silicate (waterglass) and (2) the development of ambient drying technology that does not require high pressure [5-7].

The ambient pressure drying process relies on a modification, usually silylation of the internal gel surface and drying at ambient pressure. Many research works have been directed toward studying the effects of variations in synthesis parameters [1, 7-12].

However, the hydrophobic thermal stability of water glass based aerogels produced were found to be in the range of 223-400°C in air atmosphere which has limited the applications when exposed to humidity or water at high temperature conditions [5,6,12-15].

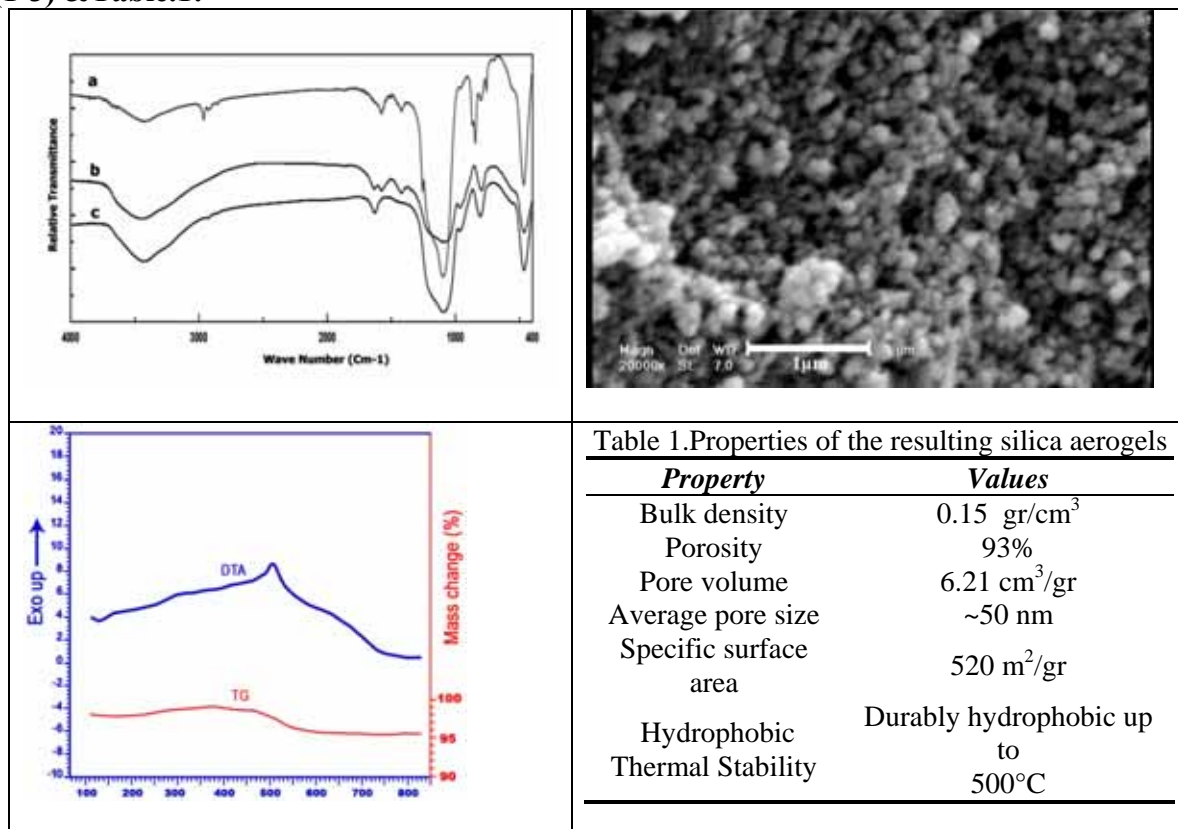
In this research hydrophobic silica aerogel was prepared by a sol-gel technique using waterglass as silicon derivative, n-hexane as solvent, and hexamethyldisilazane (HMDZ) as surface modification agent, followed by drying under ambient pressure. Attempts were made to achieve optimized properties of hydrophobic silica aerogel, especially hydrophobic thermal stability. The chemical bonding state and thermal stability of aerogel was investigated by means of Fourier transform infrared spectroscopy (FTIR) and DTA-TG. The surface characteristic of the aerogel was found to be hydrophobic up to 500°C. The porosity, average pore size, density and surface area of the silica aerogels produced were 93%, ~50 nm, 0.15 gr/cm³ and 520 m²/g, respectively.

References:

1. . Soleimani Dorcheh A, Abbasi MH, J Mater Proc Tech, 199, 2007, p 10-26.

2. Cunha, P. D., J. Neves, F., and Lopes, M. I., Nucl. Instrum. Meth. Phys. Res. A. 452, 2000, p 401.
3. Kim, K., Jang, K.Y., and Upadhye, R. S., J. Am. Ceram. Soc., 74, 1991, p 1987.
4. Reed, S. J., Ashley, C. S., Brinker, C. J., Walko, R. J., Ellefron, R., and Gill, J. , Porous optical composites SPIE, 1328, 1990 , p 220.
5. Schwertfeger, F., Frank, D., Schmidt, M., J. Non-Cryst. Solids, 225, 1998, 24.
6. Lee, CJ, Kim, GS, Hyun, SH, J. Mater Scie, 37, 2002, p 2237.
7. Rao,A.V., Nilsen,E., Einarsrud, M.A., J.Non-Cryst.Solids., 296, 2001, p 165.
8. Wagh, P .B, Begag, R., Pajonk, G.M. Rao, A. Venkateswara, Haranath, D.,Mater. Chem. Phys, 57, 1999, 214.
9. Wagh, P.B., Rao, A. Venkateswara, Haranath, D., Mater Chem Phys, 53, 1998, p 41.
10. Estella,J., Echeverria, J.C., Laguna, M. Garrido, J., J. Micro Meso. Mat., 102, 2007, p 274–282.
11. Einarsrud, M.A., Nilsen, E., Rigacci, A., Pajonk, G. M., Buathier,S., Valette, D., Durant, M., Chevalier, B., Nitz, P., Ehrburger-Dolle, F., J. Non-Cryst. Solids, 285, 2001, p 1.
12. Rao, A.P., Rao, A.V., Pajonk, G.M., Appl. Surf. Sci., 253, 2006, p 6032.
13. Hegde, N. D., Rao, A. V., App. Surf. Sci. 253, 2006, 1566.
14. Lee,S., Cha,Y.C.,Hwang, H.J., Moon, J.W. ., Han, I. S., Mater. Lett., 61, 2007, p 3130.
15. Rao, A.V., Wagh, P.B., Materials Chem. and Phy. 53, 1998, p 13.

Figs (1-3) & Table.1:



FULL QUANTIFYING ORDERING IN SELF-ASSEMBLY OF COLLOIDAL CRYSTALS: TOWARDS NANOMETROLOGY

C. M. Sotomayor Torres^{1,6}, W. Khunsin¹, A. Amann^{1*}, G. Kocher^{1,2}, S. G. Romanov^{1,3}, S. Pullteap⁴, H. C. Seat⁴, E. P. O'Reilly¹ and R. Zentel⁵

1. Tyndall National Institute, Lee Maltings, Cork, Ireland
 2. School of Engineering and Physical Science, Heriot-Watt University, Edinburgh EH14 4AS, UK
 3. Ioffe Physical Technical Institute, 194021, Polytekhnicheskaya ul., 26, St. Petersburg, Russia
 4. Laboratoire d'Optoelectronique pour les Systemes Embarques, ENSEEIHT-INPT, Toulouse Cedex7, France
 5. Institut für Organische Chemie, Johannes Gutenberg Universität, D-55099 Mainz
 6. Catalan Institute of Nanotechnology, Campus Universitat Autònoma de Barcelona, 08193 Bellaterra, Spain, and Institute for Research and Advanced Studies, ICREA, 08010 Barcelona, Spain.
- clivia.sotomayor@cin2.es

Self-assembly is an emerging and highly versatile approach to nanofabrication. However, perfect crystallographic order in the plane is seldom the outcome of a process relying on a myriad of interactions. Here we present a way to obtain crystal ordering in the plane and in the bulk by applying acoustic fields during vertical drawing crystallisation of colloidal mesoscopic and nanoparticles. This spatially coherence resonance-like behaviour in the self-assembly of three-dimensional fcc colloidal crystals results in an improvement of a factor of 10 of the in-plane crystallinity. The process is akin to stochastic resonances [1]. The quantitative analysis is a generic approach to quantify crystal using discrete Fourier Transform analysis of the scanning electron micrograph or AFM images. This approach can be extended to quantify ordering of other self-organised structures, such as micells or self-organised quantum dots. Our study covered also the 3-dimensional ordering of these structures by transmission spectroscopy [2]. We thus have tested a quantitative approach to self-assembly characterisation thereby bring it closer to metrics and standards, which are a prerequisite for uptake in future applications [3].

References:

- [1] A Amann, W Khunsin, G Kocher, C M Sotomayor Torres and E P O'Reilly, *Stochastic Resonances in photonic crystal growth*, Proc. SPIE Vol. **6603** (Noise and Fluctuations in Photonics, Quantum Optics, and Communications, Ed. L Cohen), 660321 (2007)
- [2] W. Khunsin, G. Kocher, S. G. Romanov, C. M. Sotomayor Torres, *Quantitative Analysis of Lattice ordering in thin-film opal-based photonic crystals*, Advanced Functional Materials **18** (17) 2471-2479 (2008).
- [3] W Khunsin et al, in preparation

ELECTRICAL DOUBLE LAYER FORCE MEASUREMENTS ON SINGLE BIOLOGICAL MOLECULES WITH THE ATOMIC FORCE MICROSCOPE

J. Sotres, A.M. Baró

Instituto de Ciencia de Materiales de Madrid, CSIC, E-28049 Madrid, Spain

jsotres@icmm.csic.es

Electrical double layer (EDL) interactions arise from the overlapping of the clouds of ions surrounding charged surfaces brought into proximity in electrolyte solutions. Most theoretical and experimental studies on EDL interaction have been done within the field of colloidal science, from where the DLVO theory was developed. Nevertheless, it is now clear that they also play a crucial role in many biological processes due to its long range and the substantial charge of molecules, like amino and nucleic acids.

Many techniques, like electrophoresis or proton titration, are employed for characterizing average charged states. However, very few allow determining its spatial distribution. Atomic force microscopy (AFM) stands out among these techniques, mainly because it can resolve positions down to the nanometer range and forces down to the picoNewton range. In this technique the force originated by the overlapping of tip sample EDLs it is probed. This is usually done by performing the so-called force distance curves, where the force between the tip and the sample is measured as a function of the separation between them at a fixed lateral position. These curves are well-fitted by the DLVO theory (Butt, 1991). Moreover, from these fits the surface charge density at the sample position, where the force-distance curve is performed, can be estimated (Butt, 1992). Both imaging and force distance measurement can be simultaneously combined by operating in the force spectroscopy imaging (FSI) mode, where a force distance curve is acquired at each pixel of a simultaneously acquired topography image. In this way EDL forces, and thus surface charges, can be mapped along a surface with nanometer resolution. This is of high importance in biological material due to its structural and chemical heterogeneity. One of the main drawbacks attributed to FSI and similar operation modes is the low acquisition time, which results in low lateral resolution, due to thermal drift effects. However, its optimization has recently allowed to map EDL forces on top of single nanometer-sized molecules (Sotres et al., 2008).

The interpretation of EDL force measurements taken on molecules with sizes in the order, or smaller, than the probe tip and/or the characteristic length of the interaction (Debye length) is not an easy issue. We have developed a model where the force from the molecule is superposed to the force from the surrounding substrate. This model is used to fit FSI measurements on avidin and DNA molecules. In this way values for the charge densities of both molecules are obtained in good agreement with expected values, supporting the validity of our model. We also propose the iso-distance representation to map surface charges with nanometer resolution. Finally, the lateral resolution dependence with the solution ion concentration has also studied (Sotres et al., 2009).

References:

- [1] Butt H.J. Biophys. J. **60** (1991) p777.
- [2] Butt H.J. Biophys. J. **63** (1992) p578.
- [3] Sotres J., A.M. Baró. Appl. Phys. Lett. **93** (2008) 103903.

Figures

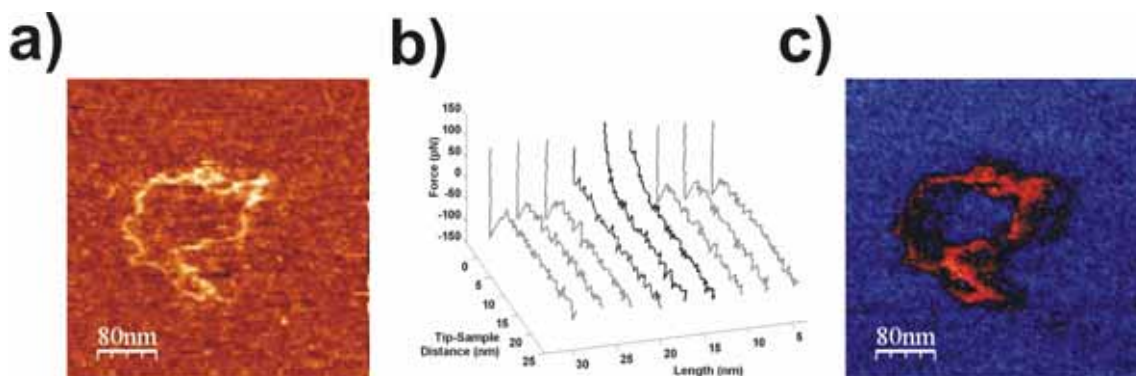


Figure. **a)** Topography image, from a FSI file, of a plasmid DNA molecule deposited on a poly-lysine coated surface in phosphate buffer 10mM. **b)** Successive force distance curves along a direction perpendicular to a strand of the molecule represented in a) (curves are obtained from the same FSI file). The EDL force switches from a repulsive behaviour on top of the molecule (three middle curves) to an attractive behaviour far from it. **c)** Iso-distance map, calculated from the same FSI file, representing the force at a distance of 4nm from the poly-lysine surface.

**FAST TO ULTRAFAST DYNAMICS OF PALLADIUM PHTHALOCYANINE
COVALENTLY BOUND TO MCM-41 MESOPOROUS MATERIAL**

A. Synak¹, M. Gil¹, J. A. Organero¹, F. Sanchez² and A. Douhal^{1}*

¹ *Departamento de Química Física, Facultad de Ciencias del Medio Ambiente
Campus Tecnológico de Toledo, Avenida Carlos III, Sin número,
Universidad de Castilla-La Mancha, 45071 Toledo, Spain*

² *Instituto de Química Orgánica, Consejo Superior de Investigaciones Científicas,
c/ Juan de la Cierva 3, 28006-Madrid, Spain*

** corresponding author: abderrazzak.douhal@uclm.es*

Palladium phthalocyanine (PdPc) covalently bonded within MCM-41 mesoporous structured silicates has been studied by UV-vis steady-state absorption and fluorescence spectroscopy and by pico- and femtosecond time-resolved emission spectroscopy. Caging of PdPc by MCM-41 results in a splitting and a substantial broadening of absorption spectrum. Presence of new absorption band, appearing at 708 nm suggests large distortion of PdPc molecular symmetry inside the channels. For the emission, a bathochromic shift of ~ 40 nm is observed upon linking into the MCM-41 framework. Picosecond data shows an appearance of a new lifetime component of ~ 1.4 ns in comparison to PdPc in solution, which can be due to a specific interaction of guest dye with the host. New conformations inside MCM-41 are unique for covalently linked dye and not present in diffusion encapsulated nanocomplex. The fluorescence up-conversion study shows two time-scales of ultrafast dynamics. The 170 – 500 fs component has been assigned to intramolecular vibrational-energy redistribution (IVR) and S₂-S₁ internal conversion (IC) processes, while time constants of 1.5 – 4.4 ps are due to the vibrational relaxation at the S₁ manifold. We believe that these results can be potentially useful in development of new nanosystems.

Acknowledgements:

This work was supported by the JCCM and MEC through projects PCI08-5868 and CTQ2005-00114/BQU.

A.S. thanks the Marie Curie Actions for the Intra European Fellowship through project PIEF-GA-2008-219856 (FENASY).

OVER-EXPRESSION OF RECOMBINANT PROTEINS BY A SELF-INDUCTION METHOD FOR NANOTECHNOLOGY APPLICATIONS

Edurne Teiletxea Malda¹, Aaron Cabrera², Jose F. Moran²

¹FideNa PrincipiaTech Navarra, Edificio CIDEA, C/ Tajonar s/n, 31006 Pamplona, Navarra, Spain

²Instituto de Agrobiotecnología, Universidad Publica de Navarra-CSIC-Gobierno de Navarra, Campus de Arrosadia s/n, 31006, Pamplona, Navarra, Spain

jose.moran@unavarra.es

The production of high quantities of a pure biological macromolecule is a very important subject in many nanobiotechnological applications, during the investigation phase, as well as, in the posterior industrialization phase. Protein production may be carried out by over-expression of foreign gene in bacteria followed by protein purification and characterization of the recombinant protein. Former bacterial expression systems involved the use of plasmids expressing proteins under the control of constitutive promoter, which we found to render low protein concentration [1], and some authors reported protein expression unable to be characterized [2]. The use of newer inducible plasmids may allow much higher concentrations of expressed proteins. However, these expression systems often result in high formation of insoluble protein into “inclusion bodies” or even, it could lead to unpaired synthesis of protein and prosthetic group as the heme group in hemoglobins. Therefore, when using systems based on the de-repression of an inducible promoter with Iso-propyl thiogalactoside (IPTG) some authors had employed denaturing buffers to isolate the apo-proteins, and at a later stage, prosthetic group was added [3].

In this work we describe the production of recombinant proteins under a self-expression system [4], and report the purification of iron-superoxide dismutase (FeSOD) from cowpea (*Vigna unguiculata*). FeSOD is a metallo-enzyme that catalyzes the dismutation of superoxide radicals into hydrogen peroxide, thus preventing oxidative damage [5]. The over-expression of FeSOD in *Escherichia coli* using self-induction of the bacterium may take between 16-24 hours with optimal results, after which period cells are harvested by centrifugation and either used or stored at – 80° C. FeSOD is over-expressed using plasmid pET28a(+), and the gene has been cloned at the NdeI site of this vector, which implies the synthesis of the protein with a 6(His)-tag [5]. Up to 50 mg of protein can be affinity purified from 1L of bacteria culture in a single chromatography step with a 5 mL NTA-Ni column (Amersham-Pharmacia). The process can be completed with the treatment of the FeSOD with

thrombin to remove the 6(Hys)-tag, and appropriate capture of the thrombin and dialysis with desired buffer. Full process of purification can be easily accomplished in only 3 days.

This expression and purification system produce higher quantities of recombinant protein, reducing the formation of inclusion bodies and contributing to the better purification and characterization of the protein, as well as, minimizing the production cost. In our lab, we have produced several recombinant bacteria with a high effectiveness using this system obtaining improved yields which ranges between 4-10 times higher. We have reported that this system is optimal to over-express and purify flavoproteins which contain FAD as prosthetic groups [6]. For the FeSOD the production has been shown to be 3.5 times higher. The chromatography step renders protein extremely pure and we have produced high quantities that have made possible the crystallization of the protein and the research by X-ray of the protein crystals [7].

Currently, we are using these and other macromolecules in nanodevices for different applications.

References:

- [1] Arredondo-Peter R, Moran JF, SarathG, Luan P, and Klucas RV, *Plant Physiology*, **114** (1997), 493.
- [2] Sikorski MM, Topunov AF, Strozycki PM, Vorgias CE, Wilson KE, Legocki AB, *Plant Science* **108** (1995), 109.
- [3] Hargrove, MS, Barry, JK, Brucker, EA, Berry, MB, Phillips, GN, Jr., Olson, JS, Arredondo-Peter R, Dean, JM, Klucas, RV, and Sarath G, *Journal of Molecular Biology*, **266** (1997), 1032.
- [4] Studier, F. W, *Protein Expression and Purification*, **41**(2005), 207.
- [5] Moran JF, James EK, Rubio MC, Sarath G, Klucas RV, and Becana M, *Plant Physiology*, **133** (2003), 773.
- [6] Urarte E, Auzmendi I, Rol S, Ariz I, Aparicio-Tejo PM, Arredondo-Peter R, Moran JF *Methods in Enzymology* **436** (2008), 411.
- [7] Muñoz I, Moran JF, Becana M, Montoya G., *Protein Science* **14** (2005) 387.

Aqueous phase surfactant selective shape controlled synthesis of lead sulfide nanocrystals

Pankaj Thakur^{a,b}, M. S. Bakshi^c, T. S. Banipal^b

a) Department of Chemistry, Guru Nanak Dev University, Amritsar, INDIA.

b) Department of Applied Chemistry, Guru Nanak Dev University, Amritsar, INDIA.

c) Department of Chemistry, Acadia University, Wolfville, CANADA

chempank@yahoo.com

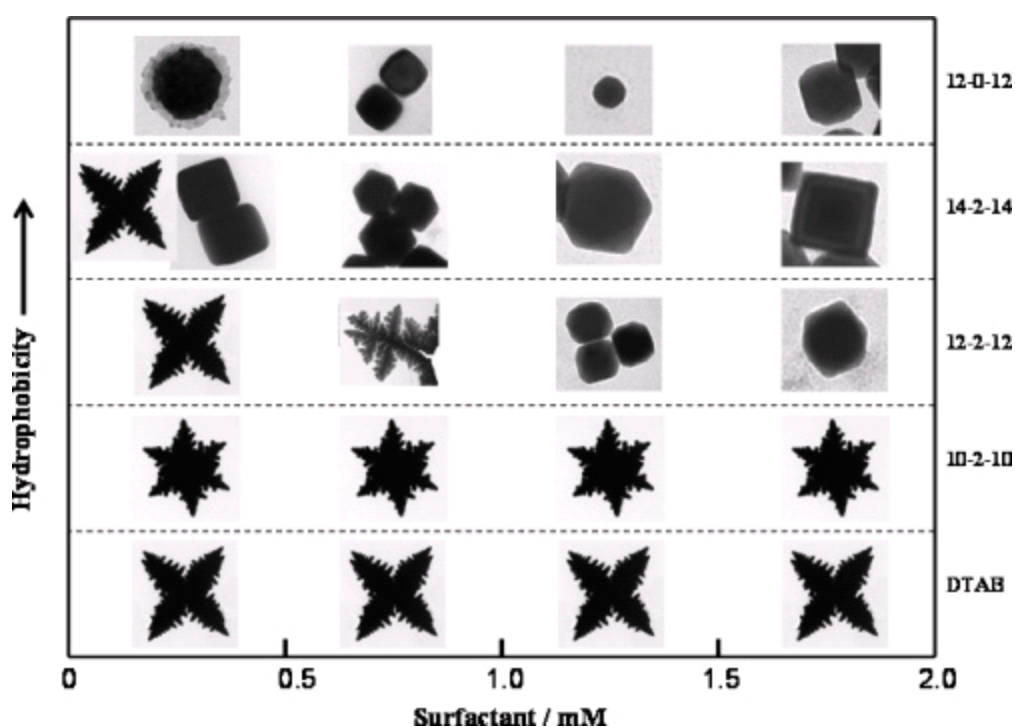
Aqueous phase synthesis at 80 °C was carried out to synthesize lead sulfide (PbS) nano- (NC) and micro-crystals (MC) by using cationic twin-tail surfactants (TTS) such as 12-0-12, 10-2-10, 12-2-12, and 14-2-14 as capping agents in the concentration range from 0.1 – 2mM. The effect of hydrophobicity on the shape and size of PbS NC was evaluated by choosing DTAB as a reference surfactant for all TTS. TEM micrographs of PbS MC synthesized in the presence of DTAB indicated the formation of star shaped MC with size 3 – 5 micron. An increase in the hydrophobicity by introducing another tail in the basic structure of DTAB in order to make 12-0-12, significantly controlled the shape and size, and lead to the formation of well defined nanocubes and spheres of 50 – 100nm in size. Similarly, the effect of hydrocarbon tail length on the shape controlled synthesis of PbS NC was systematically evaluated. Pyrene fluorescence measurements were used to determine the variation in the degree of hydrophobicity with respect to both chemical structure as well as concentration of TTS. It was concluded that stronger hydrophobic character and higher concentration produced well defined geometries of PbS NC. No significant concentration effect within a range of 0.1 – 2mM of DTAB and 10-2-10 was observed on the morphology of PbS NC probably due to much weaker hydrophobicity of these surfactants. An attempt was made to present all TEM results in a schematic phase diagram (Fig. 1). This phase diagram provided a best correlation between the shape and size of PbS NC and the surfactant parameters (i.e., hydrophobicity and concentration effect). Apart from this, a shape dependence UV-visible absorbance was also noted and discussed in context with overall preview of all shapes of PbS NC/MC obtained. The shape controlled synthesis of PbS NC was obtained due to the preferential adsorption of TTS on the {111} crystal planes that directed the overall growth predominantly at {100} planes.

References:

- [1] I. Honma, S. Hirakawa, K. Yamada, J. M. Bae, *Solid State Ionics*, **118** (1999) 29.
- [2] T. S. Phely Bobin, R. J. Muisener, J. T. Koberstein, F. Papadimitrakopoulos, *Synth. Methods*, **116** (2001) 439.
- [3] M. L. Curri, R. Comparelli, P. D. Cozzoli, G. Mascolo, A. Agostiano, *Mater. Sci. Eng. C*, **23** (2003) 285.
- [4] M. Bruchez, Jr. M. Moronne, P. Gin, S. Weiss, A. P. Alivisatos, *Science (Washington, DC, U.S.)* **281**, (1998) 2013.
- [5] W. C. Chan, S. M. Nie, *Science (Washington, DC, U.S.)* **281** (1998) 2016.
- [6] H. Mattoussi, J. M. Mauro, E. R. Goldman, G. P. Anderson, V. C. Sundar, F. V. Mikulec, M. G. Bawendi, *J. Am. Chem. Soc.*, **447** (2000) 12142.

Figure

Schematic phase diagram showing different morphologies of PbS NC/MC with respect to hydrophobicity as well as concentration of each TTS.



SIMULATING OF THE CLUSTER-NATURE SOLVENT FEATURES OF SINGLE-WALL CARBON NANOHORNS

Francisco Torrens, Gloria Castellano

¹*Institut Universitari de Ciència Molecular, Universitat de València, Edifici d'Instituts de Paterna, P. O. Box 22085, 46071, and Instituto Universitario de Medio Ambiente y Ciencias Marinas, Universidad Católica de Valencia San Vicente Mártir, 46003, València, Spain
francisco.torrens@uv.es*

The existence of single-wall carbon nanotubes (SWNTs) in organic solvents, in the form of clusters, is discussed [1]. A theory is developed based on a *bundlet* model for clusters, describing the distribution function of clusters by size [2]. The phenomena have a unified explanation in the bundlet model of clusters, in accordance with which the free energy of an SWNT, involved in a cluster, is combined from two components: a volume one, proportional to the number of molecules n in a cluster, and a surface one proportional to $n^{1/2}$. The bundlet model for clusters enables describing the distribution function of SWNT clusters by size. The droplet model is formally analogous to the one for fullerene clusters. From purely geometrical differences the models predict different behaviours. Single-wall carbon nanocones (SWNCs) of various disclinations are investigated *via* energetic and structural analyses [3]. Several SWNC's terminations are studied, which are different amongst each other because of the type of closing structure and the arrangement of them. The SWNC packing efficiencies, and interaction-energy parameters, are intermediate between the ones of fullerene and SWNT clusters; an in-between behaviour is expected. However, SWNC properties are calculated closer to those of fullerene and more distant from those of SWNT. The equilibrium difference between the Gibbs free energies of interaction of an SWNT with its surroundings, in the solid phase and in the cluster volume or on the cluster surface shows that, on going from C₆₀ (droplet) to SWNT (bundlet) the minimum is less marked (68% of C₆₀), which causes a lesser number of units in SWNT ($n_{\min} \approx 2$) than in C₆₀ clusters (≈ 8). Moreover the abscissa is also shorter in SWNT ($n_{\text{abs}} \approx 9$) than in C₆₀ (≈ 28). In single-wall carbon nanohorns (SWNHs, droplet) the minimum is more marked (122% of C₆₀), but the number of units in SWNH ($n_{\min} \approx 8$) and abscissa ($n_{\text{abs}} \approx 28$) are equal to those in C₆₀. Temperature dependence of SWNT solubility S shows that S decreases with temperature T , because of cluster formation. At $T \approx 260\text{K}$, the C₆₀ crystal presents an orientation disorder phase transition from face-centred cubic (FCC) to simple cubic (SC). The S diminution is less marked for SWNT, in agreement with lesser number of units in SWNT clusters. The T dependence of the heat of solution H in toluene, benzene and CS₂, calculated for saturation concentration (Fig. 1), shows the C₆₀ FCC–SC transition at $T \approx 260\text{K}$. For C₆₀ (droplet) on going from $T = 260\text{K}$ to $T = 400\text{K}$ H increases $3\text{kJ}\cdot\text{mol}^{-1}$. For SWNT (bundlet) and SWNH (droplet) H increases 10 and $4\text{kJ}\cdot\text{mol}^{-1}$, respectively, in the same interval. The results for the dependence of diffusion coefficient D on concentration C in toluene, at $T = 298.15\text{K}$ (Fig. 2), show that the cluster formation in a solution close to saturation decreases D by 58%, 69% and 54% for C₆₀, SWNT and SWNH, respectively, as compared with D_0 for an SWNT. For SWNT D decreases by 27% and for SWNH D increases by 9% with regard to C₆₀. Provisional conclusions follow. (1) Close packings are the tightest way to pack spheres. Atoms and fullerenes being nothing but tiny spheres often arrange in this way. Furthermore it is also possible to deduce atomic structures of metal alloys, salts and oxides by fitting the voids of close-packed spheres. Several criteria have been selected to reduce the analysis to a manageable quantity of packing properties and objects, from the enormous set of equal objects. (2) The single-wall carbon nanocone–nanohorn packing efficiencies, and interaction-energy parameters, are intermediate between those of fullerene and single-wall carbon nanotube clusters. Therefore an in-between behaviour is expected. However, the single-wall carbon nanohorn properties are calculated closer to those of fullerene and more distant from those of single-wall carbon nanotubes.

References:

- [1] F. Torrens and G. Castellano, J. Comput. Theor. Nanosci., **4** (2007) 588 (2007).
 [2] F. Torrens and G. Castellano, Nanoscale. Res. Lett., **2** (2007) 337.
 [3] F. Torrens and G. Castellano, Int. J. Quantum Chem., in press.

Figures:

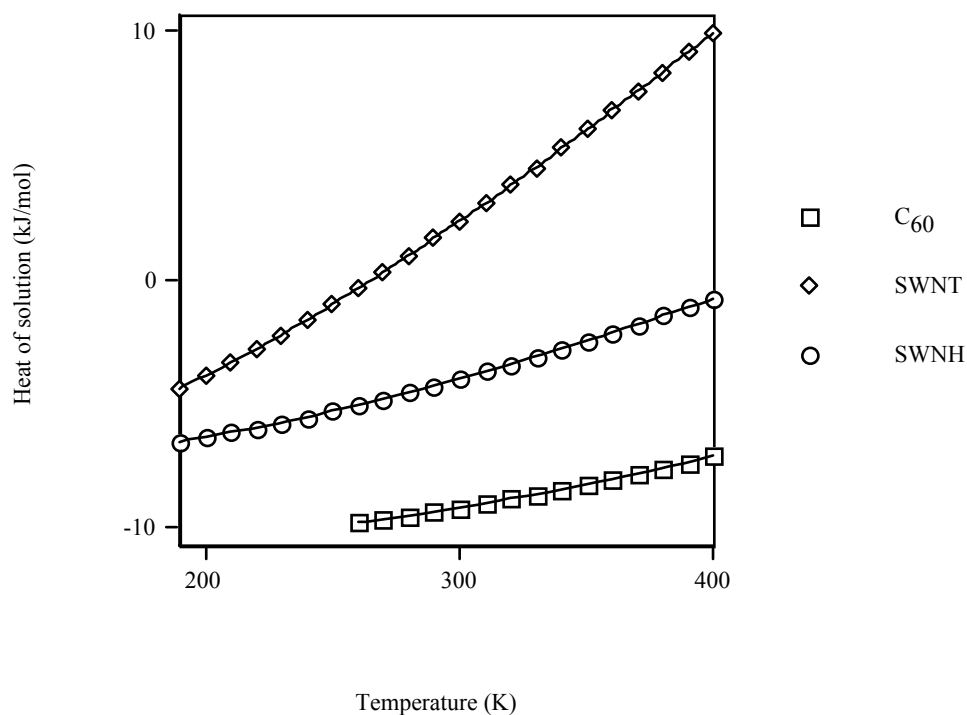


Fig. 1. Heat of solution vs. temperature of C₆₀-SWNH in toluene/benzene/CS₂ for saturation.

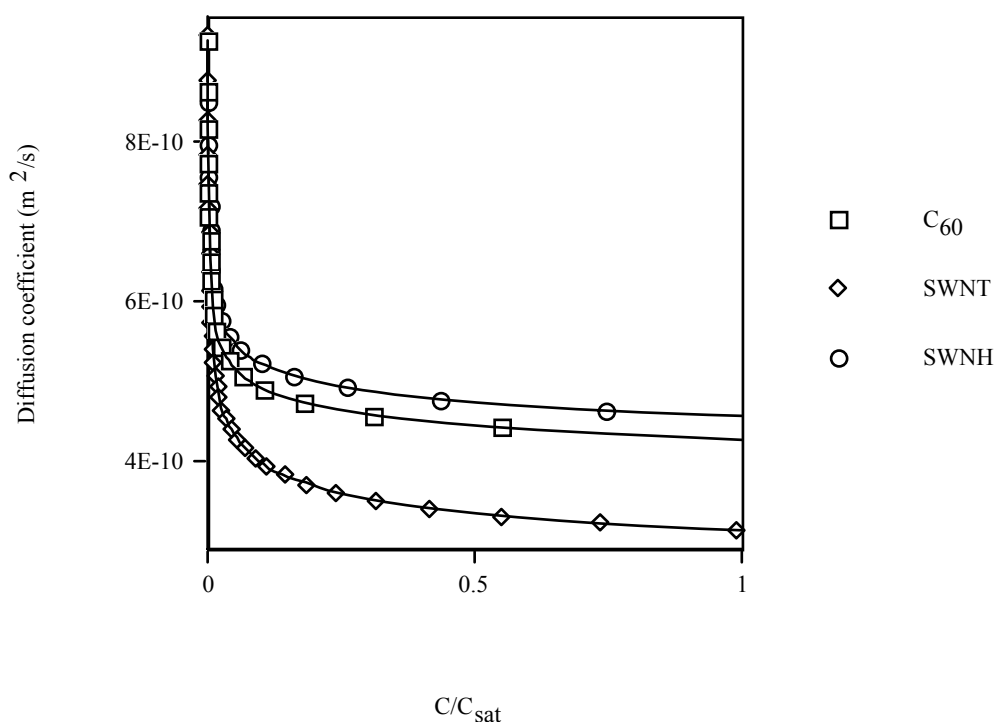


Fig. 2. Diffusion coefficient vs. concentration of C₆₀-SWNH/SWNT in toluene at 298.15K.

BIODISTRIBUTION OF MAGNETIC CORE-SHELL NANOPARTICLES USED AS MRI CONTRAST AGENTS

T.E. Torres^{1,2}, L. Asín-Pardo¹, J. Gómez-Arrue¹, K. Nass¹, G. F. Goya¹, C. Marquina², Miguel Á. Marín³, M. R. Ibarra^{1,2}

¹*Instituto de Nanociencia de Aragón (INA), Universidad de Zaragoza; Edificio Interfacultativo II, C/Pedro Cerbuna 12, 50009-Zaragoza, Spain*

²*Instituto de Ciencia de Materiales de Aragón (ICMA) & Departamento de Física de la Materia Condensada; CSIC-Universidad de Zaragoza; C/Pedro Cerbuna 12, 50009-Zaragoza, Spain*

³*Centro de Diagnóstico por imagen RXd. Félix Lattasa 19. 50006 – Zaragoza, Spain*

teo@unizar.es

Magnetic Resonance Imaging (MRI) is one of the most powerful diagnostic tools in medicine, due to its non-invasive nature and high spatial resolution. Although enormous progress has been achieved in the improvement of the technique itself, the development of MRI contrast agents is still a wide research field. Magnetic core-shell nanoparticles are very promising materials to synthesize biocompatible magnetic fluids, able to modify the longitudinal T1 and transversal T2 proton relaxation of water in body tissues. Moreover, the coating not only helps to make the particles biocompatible but also it can be functionalized in order to link the nanoparticle to a biomolecule of interest (antibody, tumor marker receptor, chemotherapeutic drug, etc.) improving the performance of the MRI contrast agent [1].

In this work the viability of three different biocompatible magnetic fluids, containing three different sets of nanoparticles (arc-discharge synthesized Fe@C [2] and dextran-coated Fe₃O₄), as MRI contrast agents has been studied. The experiments have been carried out in *phantoms* as well as in an *in-vivo* preclinical animal model (New Zealand rabbits). T1 as well as T2-weighted MR coronal and sagittal images of the rabbit abdomen were taken 15 minutes after administration of the dispersion, and periodically repeated along eight months post-injection. The nanoparticles content has been each time evaluated in liver, kidney and muscle tissues. The analysis of the phantoms allowed us to quantify the concentration of nanoparticles in each organ. By means of these experiments the biodistribution of the nanoparticles after injection and its time evolution have been studied. Although in all cases most of the nanoparticles accumulated in the liver, different time-evolution has been observed depending on the type of particle. It has been found that Fe@C particles have longer residence time than the Fe₃O₄ ones.

Our results suggest that the synthesized suspensions can be used as positive as well as negative MRI contrast enhancer agents, mainly for liver MRI.

[1] M. Ferrari, Nat. Rev. Cancer **5** (2005) 161.

[2] J.M. De Teresa, C. Marquina, D. Serrate, R. Fernandez-Pacheco, L. Morellón, P.A. Algarabel, M.R. Ibarra, Int. J. Nanotechnology **2** (2005) 3.

Epitaxial Growth of Organic Nanocrystals on Surfaces

Marta Trelka¹, Anaïs Medina², David Ecija¹, Christian Urban¹, Jose M. Gallego³, Christian G. Claessens², Roberto Otero^{1,4}, Tomás Torres² and Rodolfo Miranda^{1,4}

¹ *Universidad Autónoma de Madrid, Departamento de Física de la Materia Condensada, 28049 Madrid, Spain*

² *Universidad Autónoma de Madrid, Departamento de Química Orgánica, 28049 Madrid, Spain*

³ *Instituto de Ciencia de Materiales de Madrid, CSIC, 28049 Madrid, Spain*

⁴ *Instituto Madrileño de Estudios Avanzados en Nanociencia (IMDEA-Nano), 28049 Madrid, Spain*

rodolfo.miranda@uam.es; tomas.torres@uam.es

Controlling the formation of nanosized organic particles of well-defined size and shape is one of the challenges facing modern chemistry. The optical properties of such organic nanostructures are extraordinary and very different from the properties found for the same materials in bulk form⁴⁻⁶, similarly to the case for their inorganic counterparts¹⁻³. For example, organic nanoparticles show size-dependent absorption and fluorescence bands^{4,5} or single photon emission⁶. Although these size effects in organic nanoparticles might have been expected on the basis of the optical properties of their inorganic counterparts, the current understanding of these effects is hindered by the difficulty in the synthesis of organic nanocrystals, i.e. organic nanoparticles with an ordered molecular arrangement, as compared to the case of inorganic ones.

A possibility that remains mostly unexplored is the synthesis of such nanocrystals on solid surfaces. In the same way in which crystalline inorganic nanodots can be epitaxially grown on suitable substrates under conditions in which 3D Volmer-Weber growth takes place^{7,8}, an organic system could in principle be devised such that the growth of crystalline 3D islands sets in before the completion of the first monolayer. In practice, however, for organic adsorbates deposited on inorganic substrates intermolecular interactions are much weaker than molecule-substrate interactions⁹, thus promoting a layer-by-layer growth mode, and preventing the fabrication of isolated 3D nanocrystals.

Here we show that, upon deposition of cone-shaped subphthalocyanine¹⁰⁻¹² (SubPc, see Figure 1a) molecules on Cu(111), isolated nanocrystallites up to 3 ML high appear on the surface before the completion of the first monolayer. The structure of such nanocrystals can be explained by the joined effect of electrostatic (dipole-dipole) and dispersive (π - π) interactions. Although 1 ML-thick islands can also be found on the surface, the molecular arrangement in these areas is different from the geometry of the 1st-layer molecules in the crystallites. We suggest that the formation mechanism of the organic nanocrystals is related to the existence of two different adsorption geometries, cone-up and cone-down, each of which sits on different molecular layers placed at different distances from the surface upon crystallite formation.

References:

- [1] Alivisatos, A. P., *Science* **271** (1996) 933.
- [2] Lounis B. & Orrit M., *Rep. Prog. Phys.* **68** (2005) 1129.
- [3] Murray, C. B., Kagan, C. R. & Bawendi, M. G., *Annu. Rev. Mater. Res.* **30** (2000) 545.
- [4] Xiao, D. *et al.*, *J. Am. Chem. Soc.* **125**, (2003) 6740.
- [5] Fu, H.-B. & Yao, J.-N., *J. Am. Chem. Soc.* **123** (2001) 1434.

- [6] Masuo, S. *et al.*, *Jpn. J. Appl. Phys.* **46** (2007) L268.
 [7] Stangl, J., Holý, V. & Bauer, G., *Rev. Mod. Phys.* **76** (2004) 725.
 [8] Otero, R., Vázquez de Parga, A. L. & Miranda, R., *Phys. Rev. B* **66** (2002) 115401.
 [9] Barth, J. V. *Annu. Rev. Phys. Chem.* **58** (2007) 375.
 [10] Kobayashi N. *The Porphyrin Handbook*, vol. 15, pp. 161-262, Kadish, K. M., Smith, K. M. & Guillard, R. (eds.), (Academic Press, San Diego, 2006).
 [11] Claessens, C. G., González-Rodríguez, D. & Torres T., *Chem. Rev.* **102** (2002) 835.
 [12] Torres, T., *Angew. Chem. Int. Ed.* **45** (2006) 2834.

Figures:

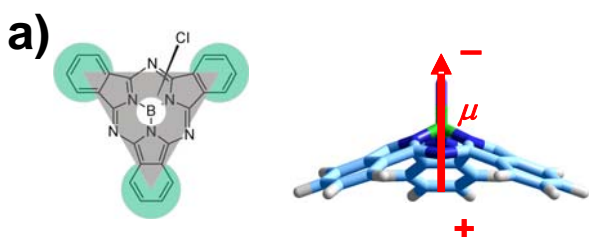


Figure 1. a) Chemical structure of the chlorosubphthalocyanine molecules and side view of its 3D structure showing the dipole moment.

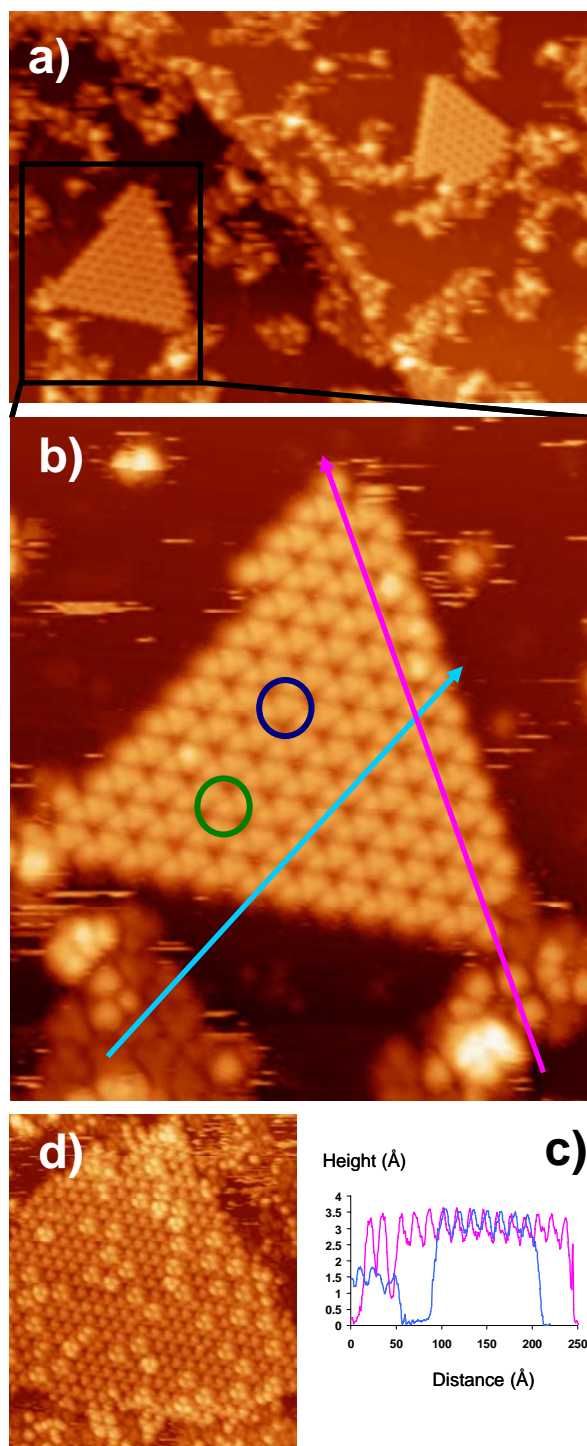


Figure 2. a) $62.4 \times 41.6 \text{ nm}^2$ STM image of 0.4 ML SubPc/Cu(111) ($I = -0.8 \text{ nA}$; $V = -2.9 \text{ V}$). Two triangular islands can be found. As for the 1 ML thick islands, high resolution STM images such as (b, $22.3 \times 26.1 \text{ nm}^2$) show two different molecular features, bright protrusions (green circles) and trefoil shapes (blue circles). The bright protrusions are identical in shape and size to the Cl-up molecules identified in Figure 2, but the trefoil features are 0.2 nm higher (c). Even thicker islands can be found upon further deposition (d, $33.4 \times 39.2 \text{ nm}^2$).

THE FORMATION OF FUNCTIONALIZED SURFACES: THE ADSORPTION OF OXALIC ACID ONTO Cu(111) AND Cu(100)

*Christian Urban*¹, *David Écija*¹, *Marta Trelka*¹, *Carlos Martí-Gastaldo*², *Eugenio Coronado*², *Roberto Otero*^{1,3}, *José M. Gallego*⁴, *Rodolfo Miranda*^{1,3}

¹ *Dpto. de Física de la Materia Condensada, Universidad Autónoma de Madrid, Cantonblanco, 28049-Madrid, Spain*

² *Instituto de Ciencia Molecular, Universitat de Valencia, Dr. Moliner 50, Burjasot E-46100, Spain*

³ *Instituto Madrileño de Estudios Avanzados en Nanociencia (IMDEA-Nanociencia), Cantoblanco, 28049-Madrid, Spain*

⁴ *Instituto de Ciencia de Materiales de Madrid - CSIC, Cantoblanco, 28049-Madrid, Spain*

christian.urban@uam.es

Self-assembly of organic molecules on solid surfaces is nowadays a more than promising bottom-up approach to create functional nanostructures. In particular, the controlled adsorption of suitably tailored carboxylic acids offers a flexible route to the nano-scale engineering of chemically functionalized surfaces. First, the possibility of hydrogen-bond formation between complementary carboxylic groups allows fabricating highly organized 2D structures of flat-lying molecules [2]. In addition, since upright-standing adsorption geometries are also possible (depending on the substrate temperature, molecular coverage, deprotonation of the carboxylic groups...), it is also possible to prepare functionalized surfaces with a carboxylate group interacting with the metal surface and an intact acid group upright at the vacuum interface. These surfaces may have a very wide range of applications, including the immobilization of biomolecules, molecular recognition, biosensors, molecular electronics, and molecule-based magnetic materials [3].

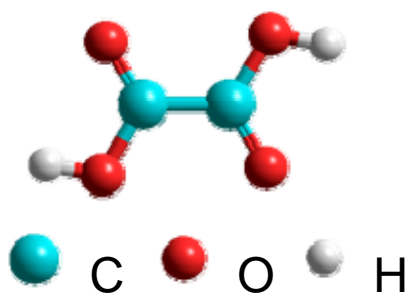
In this work we report on a combined STM and XPS study of the self-assembly, under ultra-high vacuum conditions, of the smallest dicarboxylic acid, i.e. oxalic acid (Figure 1), onto Cu(111) and Cu(100) surfaces. Although a relatively simple molecule, the experimental results show a very rich behavior depending on the surface geometry and the annealing temperature, giving rise to different structures with, probably, very different functionalities.

After depositing 1 ML of C₂O₄H₂ at room temperature, on Cu(111), the molecular overlayer forms a very regular pattern, with hexagonal symmetry, based on the hydrogen bonds between the carboxylic groups of neighboring molecules (Figure 2a). Annealing at high temperatures (~100 °C) causes the decomposition of the molecule, giving rise to a different, also ordered, molecular arrangement now containing two different species (Figure 2b). On the Cu(100) surface, on the other hand, no ordered structure can be observed after room temperature deposition. Only after annealing at moderate temperatures (~50 °C) a rectangular pattern, probably involving metal-ligand coordination bonds, is formed (Figure 3a). Further annealing produces again the decomposition of the oxalic acid, creating a more disordered, labyrinth-type structure (Figure 3b). The origin of the different arrangements, and its relationship to the particular molecular state will be discussed.

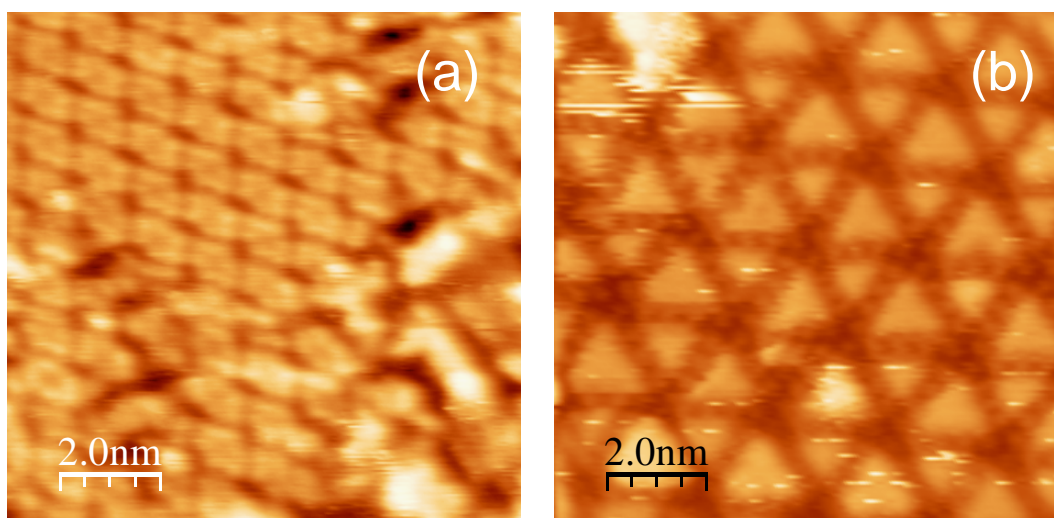
References:

- [1] J. V. Barth, G. Costantini, K. Kern, *Nature* **437** (2005) 671.
- [2] J. V. Barth, J. Weckesser, N. Lin, A. Dmitriev, K. Kern, *Applied Physics A* **76** (2003) 645.
- [3] M. Wühn, J. Weckesser, Ch. Wöll, *Langmuir* **17** (2001) 7605.

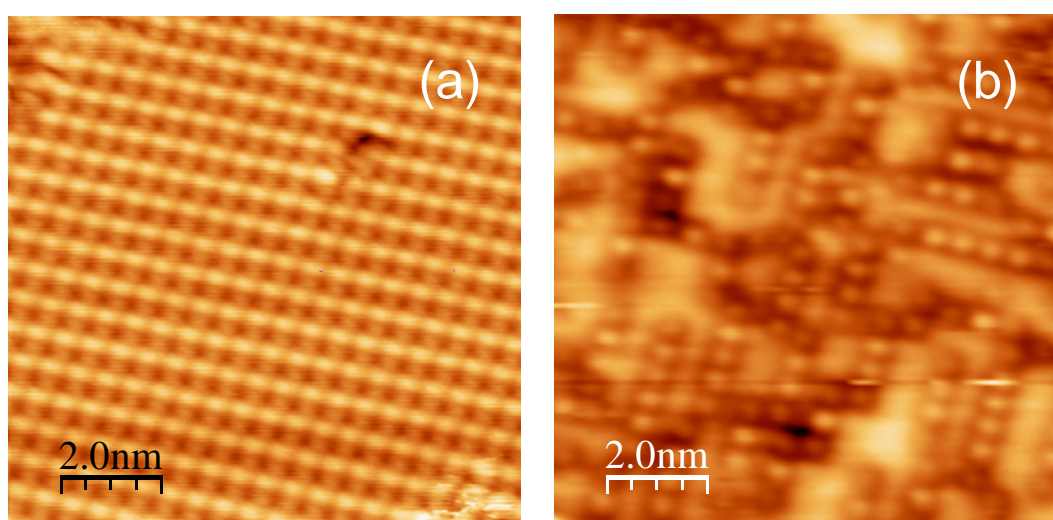
Figures:



Figures 1: Chemical structure of the oxalic acid



Figures 2: STM image of the Cu(111) surface a) after adsorption of ~1 ML of oxalic acid at room temperature; and b) after annealing at 75 °C.



Figures 3: STM image of the Cu(100) surface after adsorption of ~1 ML of oxalic acid at room temperature; b) after annealing at 50 °C; y c) after annealing at 80 °C

SENSING OF AN EXPLOSIVE PRECURSOR WITH ZEOLITE-MODIFIED CANTILEVERS

M. Urbiztondo, I. Pellejero, M. Villarroya, J. Sesé, M.P. Pina, I. Dufour, J. Santamaría
Nanoscience Institute of Aragon (INA), Pedro Cerbuna 12, Zaragoza 50009, Spain
University of Bordeaux, IMS Laboratory, 351 cours de la Libération, 33405 Talence Cedex, France
urbiz@unizar.es

The progress achieved in the field of chemical sensors during the last decade has been truly outstanding, leading to a continuous lowering of sensitivity limits. Regarding sensor selectivity, i.e., the ability of a sensor to discriminate among different analytes, advances have generally been achieved on an ad hoc basis, when a specific target has been identified for a certain analyte. Thus, high sensitivity has been achieved, or seems to be within reach, for many types biosensors, in view of the high specificity of biorecognition events. However, attaining high selectivity still remains a challenging task in many applications, with gas sensing being at the forefront.

A common strategy to attain higher sensitivity levels involves adding materials capable of molecular recognition to existing platforms of sufficient sensitivity, such as surface acoustic wave (SAW) devices, quartz crystal microbalances (QCMs) or cantilevers. For gas sensing this is generally realized using a variety of recognition elements have been used, such as polymer layers, carbon nanotubes and microporous solids. The latter hold considerable promise for gas sensing [1], in view of the intense guest-host force fields that are felt by fluid phase molecules capable of penetrating their cavities, where sizes range from a few angstrom to a few nanometers. These interactions are often selective, and can be used to implement molecular recognition functions.

Zeolites are perhaps the most widely employed silicon-based nanoporous solids. Their well defined pore of subnanometric size have earned them the name of molecular sieves, meaning that operation in the size exclusion regime is possible by selecting, among over 170 structures available, the zeolite whose pores allow the pass of the desired molecule, while keeping larger molecules outside. In addition, the adsorption properties of the zeolites can be fine-tuned by adjusting their Si/Al ratio and their exchange cations.

In view of their molecular sieving and selective adsorption properties, it is not surprising that zeolites have found use in a number of works dealing with gas sensing devices, either as a target or as a barrier to prevent the adsorption of interfering molecules. Thus zeolites have been used in electrochemical sensors, optical sensors, capacitors and of course mass sensors such as QCM and cantilevers [2]. However, the number of works that have coupled zeolites to cantilevers is very small, due in part to the difficulty of attaining homogeneous and reproducible zeolite coatings on cantilevers [3-8].

In the present work we have attempted a deeper study of the preparation of zeolite-modified cantilevers, studying how different methods can be used to obtain zeolite coatings of varied nature on cantilevers. We then proceed to show how the zeolites can be modified to increase the detection selectivity towards nitrotoluene, as an example of an explosives-related molecule. Figure 1 shows paddle-shaped cantilever appearance and dimensions and how the presence of Co in the zeolite improves the detection of nitrotoluene are shown in figure 2.

References:

- [1] M. Urbiztondo, M.P. Pina, J. Santamaría, in: Valtchev, S. and Mintova S. (Eds.), *Ordered Porous Solids: Gas sensing with silicon-based nanoporous solids*, Elsevier, (2008), pp 381-405.
- [2] J. Coronas, J. Santamaría, The use of zeolite films in small-scale and micro-scale applications, *Chem. Eng. Sci.*, 59, (2004) 4789-4785.
- [3] X. Xu, J. Wang, Y. Long, Zeolite-based materials for gas sensors, *Sensors*, 6, (2006), 1751-1764.
- [4] L. Scandella, G. Binder, T. Mezzacasa, J. Gobrecht, R. Berger, H.P. Lang, Ch. Gerber, J.K. Gimzewski, J.H. Koegler, J.C. Jansen, Combination of single crystal zeolites and microfabrication: Two applications towards zeolite nanodevices, *Microporous and Mesoporous Materials*, 21, Issues 4-6, (1998) 403-409.
- [5] R. Berger, Ch. Gerber, H.P. Lang, J.K. Gimzewski, *Micromechanics: A Toolbox for Femtoscale Science: Towards a Laboratory on a Tip*, *Microelectr. Eng.* 35 (1997) 373-379.
- [6] J. Zhou, P. Li, S. Zhang, Y.P. Huang, P.Y. Yang, M.H. Bao, G. Ruan, Self-excited piezoelectric microcantilever for gas detection, *Microelectron. Eng.* 69 (2003) 37-46.
- [7] J. Zhou, P. Li, S. Zhang, Y.C. Long, F. Zhou, Y.P. Huang, P.Y. Yang, M.H. Bao, Zeolite modified microcantilever gas sensor for indoor air quality control, *Sensor. Actuator. B-Chem*, 94 (2003) 337-342.
- [8] T. Wakayama, T. Kobayashi, N. Iwata, Micro-fabrication of silicon/ceramic hybrid cantilever for atomic force microscope and sensor applications, *Sensor. Actuator. A-Phys*, 126 (2006) 159-164.

Figures:

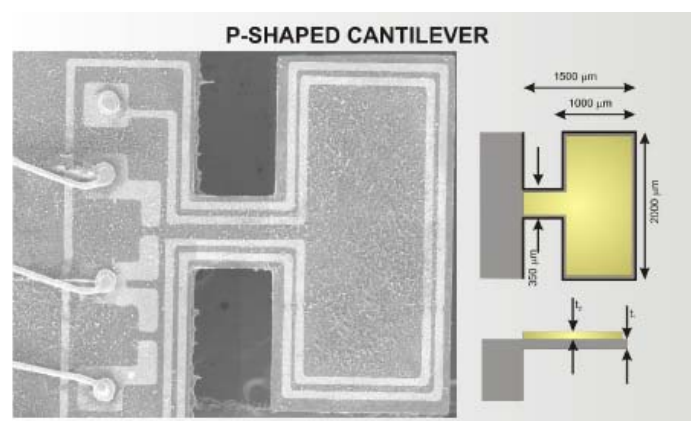


Figure 1: Top view photograph of the paddle-shaped cantilevers used in this work and scheme showing the main characteristic dimensions

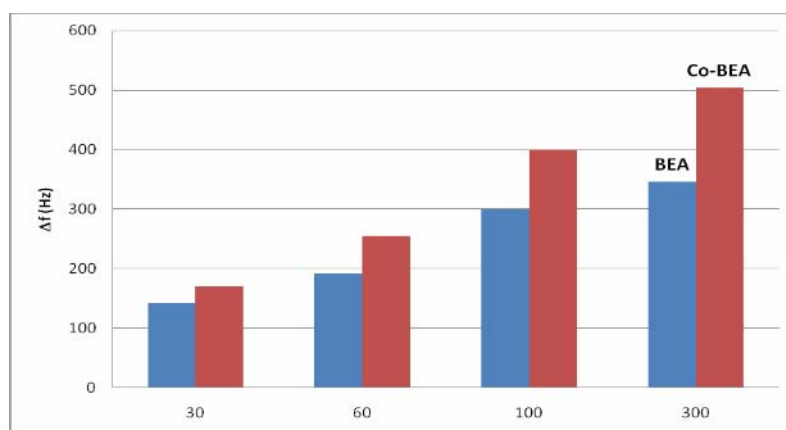


Figure 2: Comparison of o-nitrotoluene detection at room temperature on commercial QCMs loaded with as-received NH₄-BEA and exchanged Co-BEA zeolites, respectively

THERMOINDUCED MAGNETIC MOMENT IN ANTIFERROMAGNETIC NANOPARTICLES

A. Urtizberea, F. Luis, A. Millán, E. Natividad, M. Castro, F. Palacio
Instituto de Ciencia de Materiales de Aragón, CSIC-Universidad de Zaragoza, 50009
Zaragoza, Spain
ainhoa@unizar.es

Antiferromagnetic nanoparticle systems often exhibit an increase of the magnetic moment with the temperature [1-4]. These results have been interpreted by S. Mørup and C. Frandsen as an evidence of the thermal population of uniform spin-precession modes [5]. Alternatively, such increase of the magnetic moment has been questioned and attributed to artefacts of the experimental method followed in the determination of the magnetic moment [6]. A major difficulty to experimentally verify such thermoinduced phenomena is the knowledge of the bulk magnetic properties of the nanoparticles material. For instance, ferrihydrite, in which thermoinduced magnetic moment is usually reported, cannot be found in the form of a massive material. To overcome this problem we have studied the thermoinduced magnetic moment in akaganéite nanoparticles. Bulk akaganéite can be synthesized and then, bulk magnetic properties can be determined in a rather straightforward manner.

We present here the first experimental confirmation of the thermoinduced origin of the observed increase of the magnetic moment with the temperature in antiferromagnetic nanoparticles. We first present the physical properties of the bulk akaganéite. We determine relevant parameters such as the Néel temperature, and the intrinsic antiferromagnetic susceptibility (χ_{AF}). Then, we characterize akaganéite nanocomposites. These composites contain isolated akaganéite nanoparticles embedded in a polymer matrix. Its magnetic relevant properties are compared with those of the bulk material. The Néel temperature and the effective magnetic moment per Fe atom do not seem to depend on size. The dependence with temperature of χ_{AF} is quite similar for bulk and nanoparticles, but the magnitude is larger for nanoparticles.

Finally, as shown in Fig. 1, we determine directly from zero-field susceptibility data how the magnetic moment of the nanoparticles depends with the temperature. We found that it increases with the temperature above the blocking temperature. We calculate the energy of spin waves modes and show that the thermoinduced effect is indeed present in akaganéite nanoparticles and that it accounts well for the experimental results. It is concluded that this thermoinduced moment can be attributed to the population of the homogeneous spin wave mode.

References:

- [1] S. H. Kilcoyne and R. Cywinski, J. Magn. Magn. Mater., **140**, (1995) 1466.
- [2] S. A. Maklout, F. T. Parker, and A. E. Berkowitz, Phys. Rev. B, **55**, (1997) R14717.
- [3] J. G. E. Harris, J. E. Grimaldi, D. D. Awschalom, et al., Phys. Rev. B, **60**, (1999) 3453.
- [4] M. S. Seehra, V. S. Babu, A. Manivannan, et al., Phys. Rev. B, **61**, (2000) 3513.
- [5] S. Mørup and B. R. Hansen, Phys. Rev. B, **72** (2005) 024418.

[6] N. J. O. Silva, V. S. Amaral, and L. D. Carlos, Phys. Rev. B, **71** (2005) 184408.

Figures:

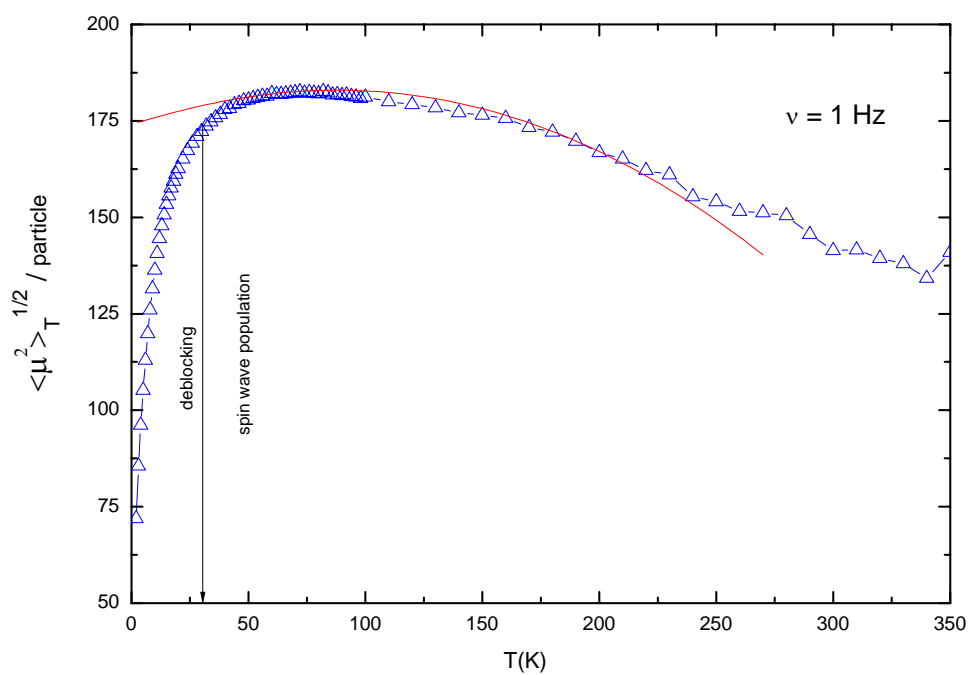


Figure 1. Magnetic moment of akaganéite nanoparticles. The continuous red line is the thermoinduced magnetic moment calculated with the semi-classical procedure.

COMPARED OF ADSORPTION METALS(Ni^{+2} , Cr^{+2} , Co^{+2} , Fe^{+2}) BY ALGAES AND CNT

Mehdi Vadi: Islamic Azad University Fasa Branch;Fasa,Fars,Iran

Nasim Nematollahi : Islamic Azad University Firozabad Branch;Firozabad,Fars,Iran

The adsorption of mean heavy metals as Cr^{+2} , Co^{+2} , Ni^{+2} and Fe^{+2} on two algae Scenedemus and Chorella is compared with carbon nanotube .

The test carried out at room temperture and optimum time 24 hrs with densities 1, 5, 10, 20 , 25 mg/lit .Temperture condition and pH were monitoring during the test. the standard methods is used for appropriate the solutions and the compared methods is used for measuring method .

The results show that the heavy metals adsorption of carbon nanotube is greater than algae.

Keywords:adsorption;metals; Cr^{+2} ; Co^{+2} ; Ni^{+2} ; Fe^{+2} ; **algae**; **CNT**

Exploring the Length of Gold Nanorods

M. Varón-Izquierdo¹, S. Lim¹, I. Ojea¹, J. Arbiol², V. Puntès¹

¹Institut Català de Nanotecnologia, Campus UAB, 08193 Bellaterra, Spain.

²GAEN-CeMARC, Group of Advanced Electron Nanoscopy - Centre de Microscòpia d'Alta Resolució de Catalunya, Universitat de Barcelona, Lluís Solé i Sabaris 1-3,

E-08028 Barcelona, Catalonia, Spain

Miriam.varon.icn@uab.es

In the synthesis of metal nanoparticles (NPs), control over the shape has been one of the most important and challenging tasks. The shape and crystallographic facets are the major factors in determining not only the catalytic and surface activity of the NPs [1] but also its optical and magnetic properties. By suitable choice of experimental conditions and additives, non-spherical shapes such as disks, rods, wires, tubes and concentric core-shell structures have been successfully synthesized and they are found to possess properties which depend not only on NP size but also their shape and other topological aspects [2].

An interesting case is the study of rod-shaped gold NPs or gold nanorods (Au NRs). One of the features of these rod nanoparticles is the presence of two distinct surface plasmon absorption bands. The transverse surface Plasmon (TSP) band, around 520 nm, is due to the excitation across the short dimension of the NRs while the longitudinal surface plasmon (LSP) band is due to the excitation along the long axis [3]. By changing Au NRs aspect ratio (AR), the LSP resonance band can be tuned from the visible to near infrared (NIR) wavelength [2], a region where interesting biologic tissues are relatively transparent (water window) and can be studied.

The two known approaches in the preparation of Au NRs using surfactants are: the electrochemical [4] or photochemical methods [5] and seed-mediated growth methods [6]. In the electrochemical method, the gold ions are reduced on a platinum electrode in the presence of a solution of surfactant mixture [4] while in the seed-mediated method Au seeds are first synthesized and then used as nucleation sites for the anisotropic growth of Au NRs. Besides the methods mentioned above, other approaches have also been attempted to produce Au NRs, such as bio-reduction [7] and growth of Au NRs directly on mica surface [8].

The seed-mediated growth formation mechanism of Au NRs in CTAB (Cetyl Trimethyl Ammonium Bromide) micellar solution remains a subject of debate, but all mechanism for the growth of Au NRs are based on the crystal growth inhibition, which is closely related to the crystalline structure and thermodynamic stability of the face-centered cubic (fcc) structure of the metallic gold. The use of cationic surfactant CTAB is a crucial parameter in the synthesis of Au NRs following a seed-mediated method. However, the trimethylammonium headgroup alone does not efficiently direct NP growth into rods and silver nitrate plays a crucial role in obtaining Au NRs in high yield. In fact, the kinetics of reduction of gold ions to atomic gold showed that the reduction was slower in the presence of silver nitrate.

In this work, we present the synthesis of bimodal metallic systems including Au and Pt. The influence of different parameters that have crucial influence in the final morphology of Au NRs will be discussed. In detail, the control of the length of Au NRs will be studied by systematically varying both platinum ion and seeds content in the growth solution. Besides, the influence of CTAB concentration on the final morphology of Au NRs will be thoughtfully studied.

Previous results of the approach presented in this work are shown in Figure 1. Au rods of 10 μm can be synthesized in the presence of Pt nanoparticles in aqueous solution. AuNRs with AR of 200 were obtained. This is a noteworthy achievement, since in the bibliography AuNR with aspect ratio from 2.9 to 4.5 have been previously reported by standard routes. Further experiments will offer the perspective of to what extent the NRs can grow in the experimental conditions. The concepts of kinkerdall effect, transmetallization, seeded growth, assisted growth and other will be discussed.

References:

- [1] El-Sayed, M.A., Accounts of Chemical Research, 34:4 (2001) p.257-264.
- [2] Kelly, K.L., et al., Journal of Physical Chemistry B, 107:3 (2003) p.668-677.
- [3] Mohamed, M.B., et al., Journal of Physical Chemistry B, 102:47 (1998) p.9370-9374.
- [4] Yu, Y.Y., et al., Journal of Physical Chemistry B, 101:34 (1997) p. 6661-6664.
- [5] Esumi, K., K. Matsuhisa, and K. Torigoe, Langmuir, 11:9 (1995) p. 3285-3287.
- [6] Jana, N.R., L. Gearheart, and C.J. Murphy, Journal of Physical Chemistry B, 105:19 (2001) p. 4065-4067.
- [7] Canizal, G., et al., Journal of Nanoparticle Research, 3:5-6 (2001) p. 475-481.
- [8] Mieszawska, A.J. and F.P. Zamborini, Chemistry of Materials, 17:13 (2005) p. 3415-3420.

Figures:

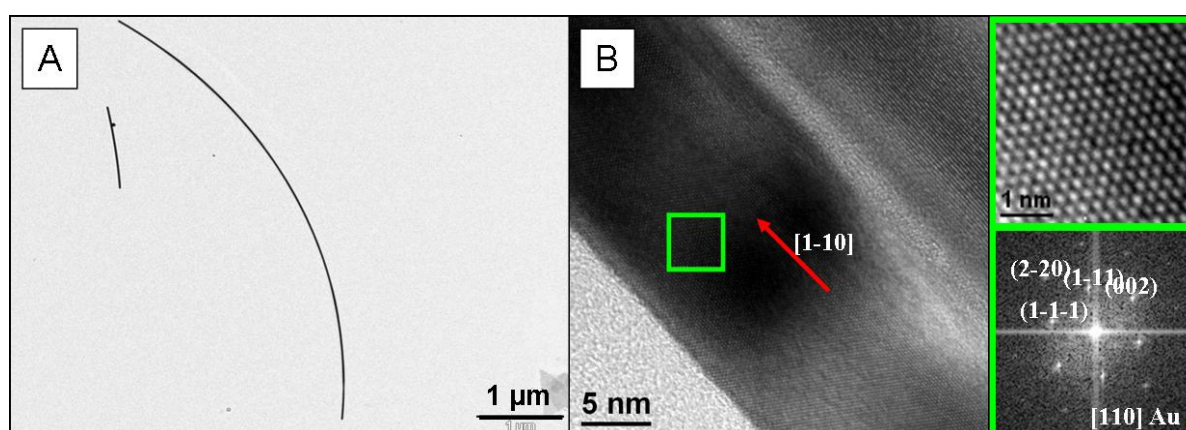


Figure 1: A) TEM image of a 6 μm AuNR. B) HRTEM of AuNR with a growth in the [1-10] direction and without defects.

EFFICIENT FUNCTIONALIZATION OF CARBON NANOHORNS VIA MICROWAVE IRRADIATION

Ester Vázquez,^a Maurizio Prato,^b Noelia Rubio,^a M. Antonia Herrero,^a Moreno Meneghetti^c

^a Departamento de Química Orgánica, Facultad de Química, Universidad de Castilla-La Mancha, 13071 Ciudad Real, Spain. ^b Dipartimento di Scienze Farmaceutiche, Università degli Studi di Trieste, Piazzale Europa 1, 34127 Trieste, Italy. ^c Dipartimento di Scienze

Chimiche, Università di Padova, Via Marzolo 1, 35131 Padova, Italy.

ester.vazquez@uclm.es

The mass production of new carbon nanostructures and their potential applications in many different fields have made these materials the subject of heavy investigations.¹ Carbon Nanohorns (CNHs)² represent a new type of nanostructured carbon-based material, which possess interesting properties for applications in clean-energy technologies as well as biology and medicine.³ A primary CNH particle is a single graphene tube (similar in structure to single-walled carbon nanotubes) with 2-5 nm in diameter and a length of 40-50 nm, with a conically-closed tip. Around 2000 CNHs aggregate with each other to form a spherical dahlia flower-like structure with a rather narrow diameter distribution of 80-100 nm (figure1). The high purity of produced CNHs is their major advantage as compared to carbon nanotubes, they are completely metal-free. Functionalization of CNHs has given scientists the ability to manipulate these structures enhancing their solubility and broadening the spectrum of applications. While different covalent functionalization strategies have been described,⁴ reactions usually proceed with long times, in the presence of highly contaminating solvents and/or under harsh conditions.

In the present work, we explore the efficiency of microwave irradiation for the covalent functionalization of CNHs. Two different reactions have been used, the 1,3-dipolar cycloaddition of azomethine ylides, in solvent-free conditions and the addition of diazonium salts in water, both functionalization methods allow the preparation of CNH derivatives with many functionalities. As a result of the covalent attachments onto the skeleton of CNHs the solubility is highly enhanced in several common organic solvents as well as in water. The differences observed are highly dependent on the polarity and the number of groups covalently attached to the CNHs. (Figure 2).

In addition, a combination of the two reactions has also permitted the preparation of doubly functionalized CNHs with orthogonally protected groups (figure 3). These groups, in principle, can be selectively cleaved and modified with different moieties, broadening the number of derivatives that can be prepared and paving the way to new applications. Finally, the microwave-assisted organic transformations here described proceed with short reaction times and involve two benign alternatives, namely solvent-free or aqueous reaction media.

References:

- [1] *J. Mater. Chem.*, **18** (2008) 1401-1604, Special Issue on Carbon Nanostructures, D. Guldi, N. Martin, M. Prato, Eds.
- [2] S. Iijima, M. Yudasaka, R. Yamada, S. Bandow, K. Suenaga, F. Kokai, K. Takahashi, *Chem. Phys. Lett.*, **309** (1999)165.
- [3] a) K. Murata, K. Kaneko, H. Kanoh, D. Kasuya, K. Takahashi, F. Kokai, M. Yudasaka, S. Iijima. *J. Phys. Chem., B*, **106** (2002) 1132. b) K. Murata, A. Hashimoto M. Yudasaka, D. Kasuya, K. Kaneko S. Iijima, *Adv. Mater.*, **16** (2004) 1520. c) K. Ajima, M. Yudasaka, T.

- ### Figures:

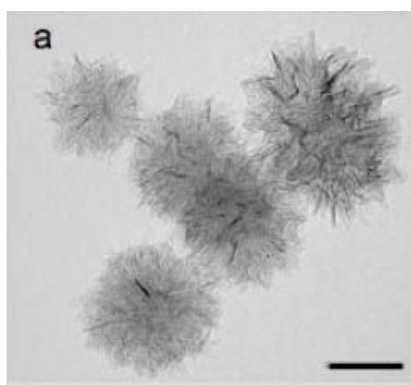


Figure 1

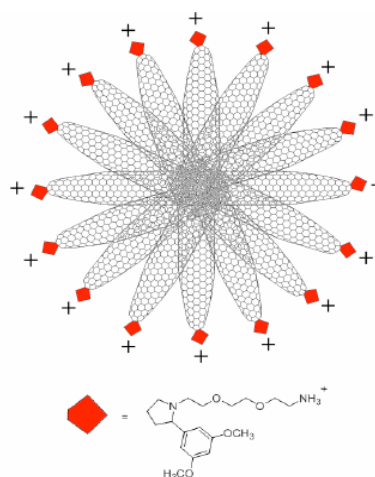


Figure 2

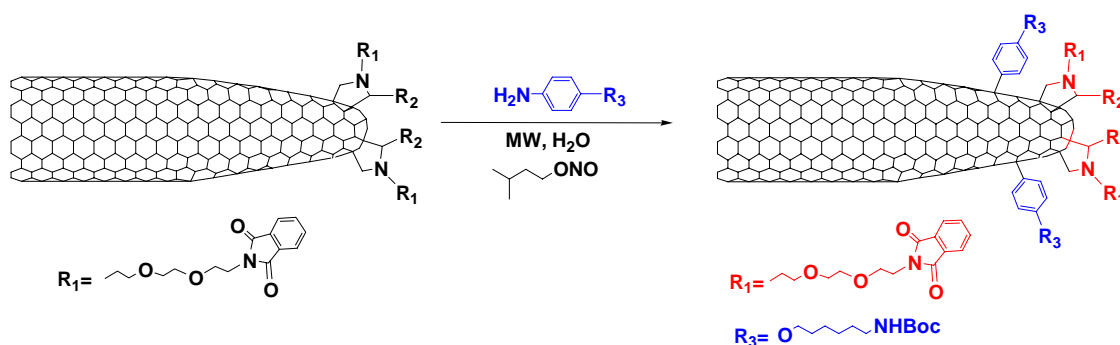


Figure 3

Synthesis and characterization of SiO₂@Au core-shell nanoparticles for biomedical applications

Clara Yagüe, Alfonso Ibarra, Silvia Irusta, Manuel Arruebo, Jesús Santamaría
Department of Chemical and Environmental Engineering and Aragon Nanoscience Institute,
University of Zaragoza, 50009 Zaragoza, SPAIN
clara.yague@unizar.es

Nanoparticles with electrical and optical properties have received a lot of attention in the past few years for their potential application in the field of biomedicine. These particles have unique features that make them very interesting for their use in this field. Metal nanoshells consist of a dielectric core with a metallic shell. Their optical properties can be tuned by changing the ratio between the thicknesses of the core and the shell. Tuning the plasmon resonance into the near-infrared region of the highest physiological transmissivity has led to a variety of applications in biomedicine. These nanoparticles have been used for drug delivery and hyperthermia among other applications [1, 2].

Silica-gold nanoshells can be obtained through an easy procedure. They are made from positively charged surface modified amino-silica nanoparticles onto which it is possible to attach small, negatively charged gold nanoparticles. The gold shell is obtained by the intergrowth of these gold-decorated silica particles. Synthesis of silica nanoparticles is a well-established procedure and it is possible to obtain particles with different sizes using a simple method. The light-absorbing gold shell can be modified by different chemical procedures preserving their light absorbing characteristics [3].

In this work, SiO₂@Au nanoshells were synthesized and characterized in order to study their potential application as gene delivery carriers and as photothermal therapy agent.

First, various batches of silica nanoparticles of different sizes, each batch having uniform particle-size distribution, were synthesized and characterized [4]. A positive functionalization of the nanoparticle surfaces was obtained by using 3-aminopropyltriethoxysilane (APTES) as source of amino groups. These particles were characterized by DLS, SEM and TEM. On the other hand, gold nanoparticles of different sizes were synthesized following the procedures described in the literature [5]. The attachment of gold nanoparticles onto the silica particle surface was obtained by electrostatic interaction between the positively charged silica nanoparticles and negatively charged gold nanoparticles. The resulting gold-decorated silica particles were observed by TEM. Finally, a new regrowth of gold by reduction of HAuCl₄ was made in order to obtain a uniform continuous shell.

The procedure above was used with different combinations of silica-gold particle sizes and the variation of the resulting absorption properties was studied by UV-VIS-NIR spectroscopy.

References:

- [1] Oldenburg S. J., Averitt R. D., Westcott and Halas N. J., Chemical Physics Letters, **288** (1998) 243.
- [2] Bikram M., Gobin A. M., Whitmire R. E., West J. L., Journal of Controlled Release, **123** (2007) 219.
- [3] Fu K., Sun J., Bickford L. R., Lin A. W. H., Halas N. J., Yu T., Drezek R. A., Nanotechnology **19** (2008) 045103.
- [4] Lange P., Schier A., Schmidbaur H., Inorganic Chemistry, **35** (1996) 637.

[5] Duff D. G., Baiker A., Langmuir, **9** (1993) 2301.

[6] London South Bank University (<http://www.lsbu.ac.uk/water/vibrat.html#a>).

Figures:

Figure 1: The UV-VIS-NIR spectra of liquid water [6].

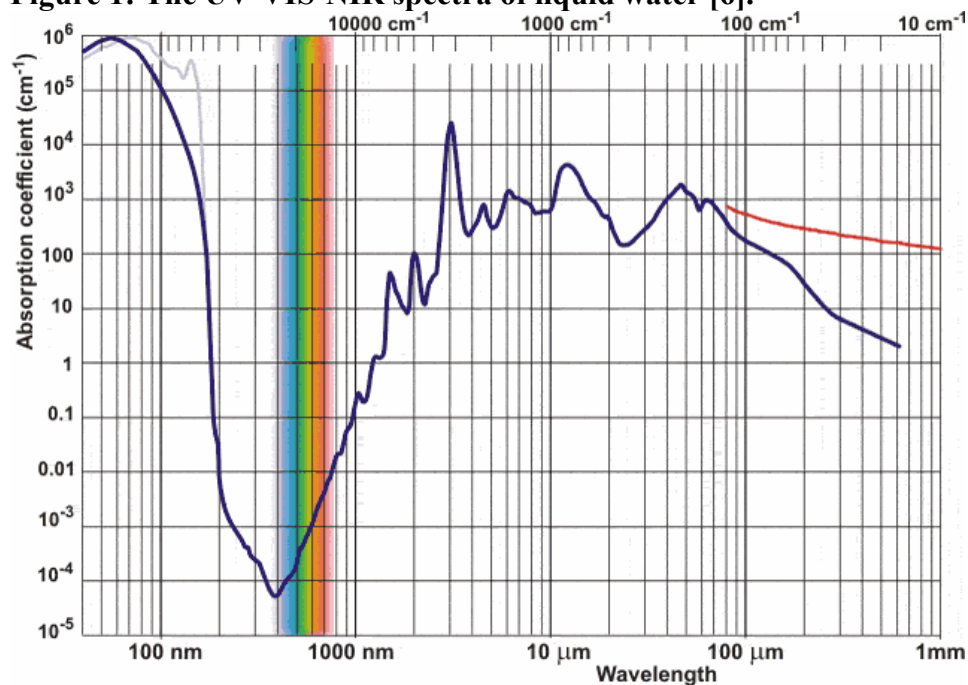


Figure 2: The UV-VIS-NIR spectra of $\text{SiO}_2\text{@Au}$ nanoshells.

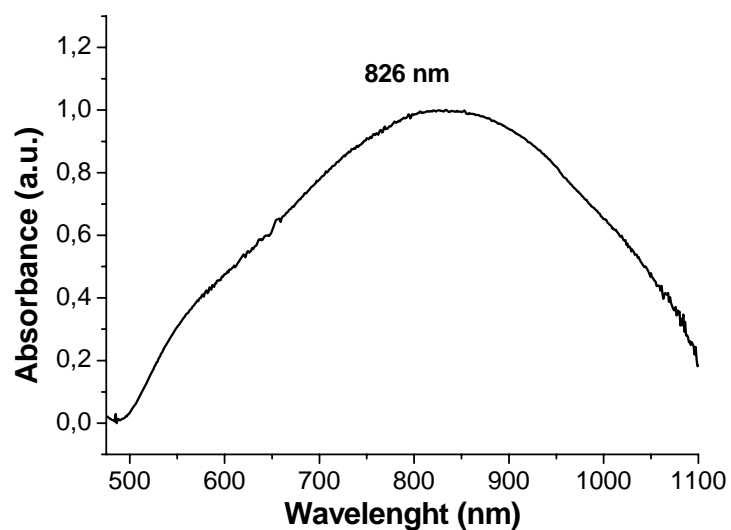


Figure: Pt-Mordenite layer in a MSR.

V. Sebastián, S. Irusta, R. Mallada and J. Santamaría

Department of Chemical and Environmental Engineering and Nanoscience

Institute of Aragon, University of Zaragoza, Zaragoza, Spain

victorse@unizar.es

Figure: SEM micrograph of gelled nanoparticle aqueous dispersions.

P. Kirilov, S. Franceschi-Messant, L. Lukyanova, E. Perez, I. Rico-Lattes

Laboratoire des IMRCP, UMR 5623, 118 route de Narbonne,

31062 Toulouse, France

kirilov@chimie.ups-tlse.fr

Figure: Pt-ZeoliteY layer in MSR.

V. Sebastián, S. Irusta, R. Mallada and J. Santamaría

Department of Chemical and Environmental Engineering and Nanoscience

Institute of Aragon, University of Zaragoza, Zaragoza, Spain

victorse@unizar.es

Figure: TEM micrograph of gold beaded nanochains contained within polymer vesicles of gold-ELP hybrid.

R. Alvarez-Rodríguez, J. Arias, M. Alonso, J.C. Rodríguez-Cabello

CIBER-BBN: Networking Research Center on Bioengineering, Biomaterials and Nanomedicine

BIOFORGE (Group for Advanced Materials and Nanobiotechnology)

University of Valladolid, Valladolid, Spain

cabello@bioforge.uva.es; ralvarez@bioforge.uva.es

Figure: Unprocessed ibuprofen.

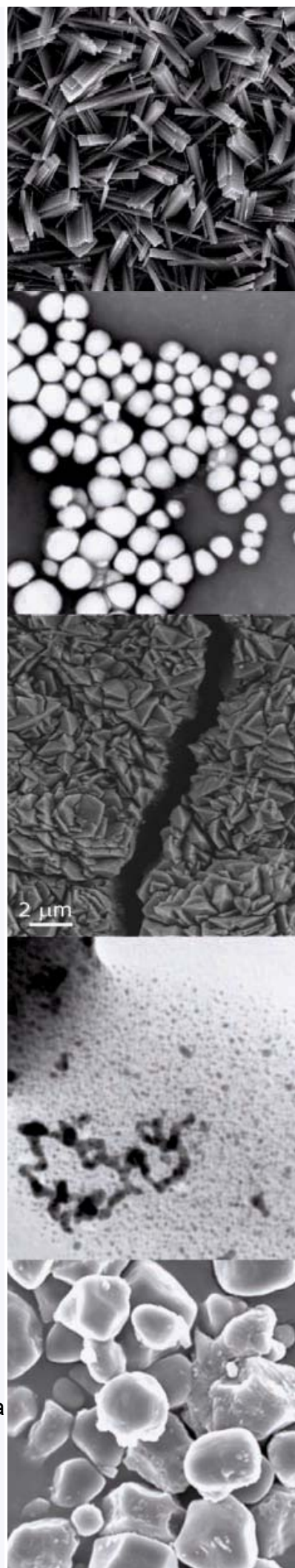
M. Cano-Sarabia^{1,2}, S. Sala^{2,1}, N. Ventosa^{1,2}, J. Veciana^{1,2}

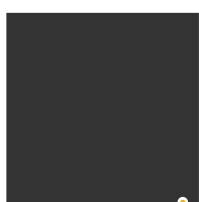
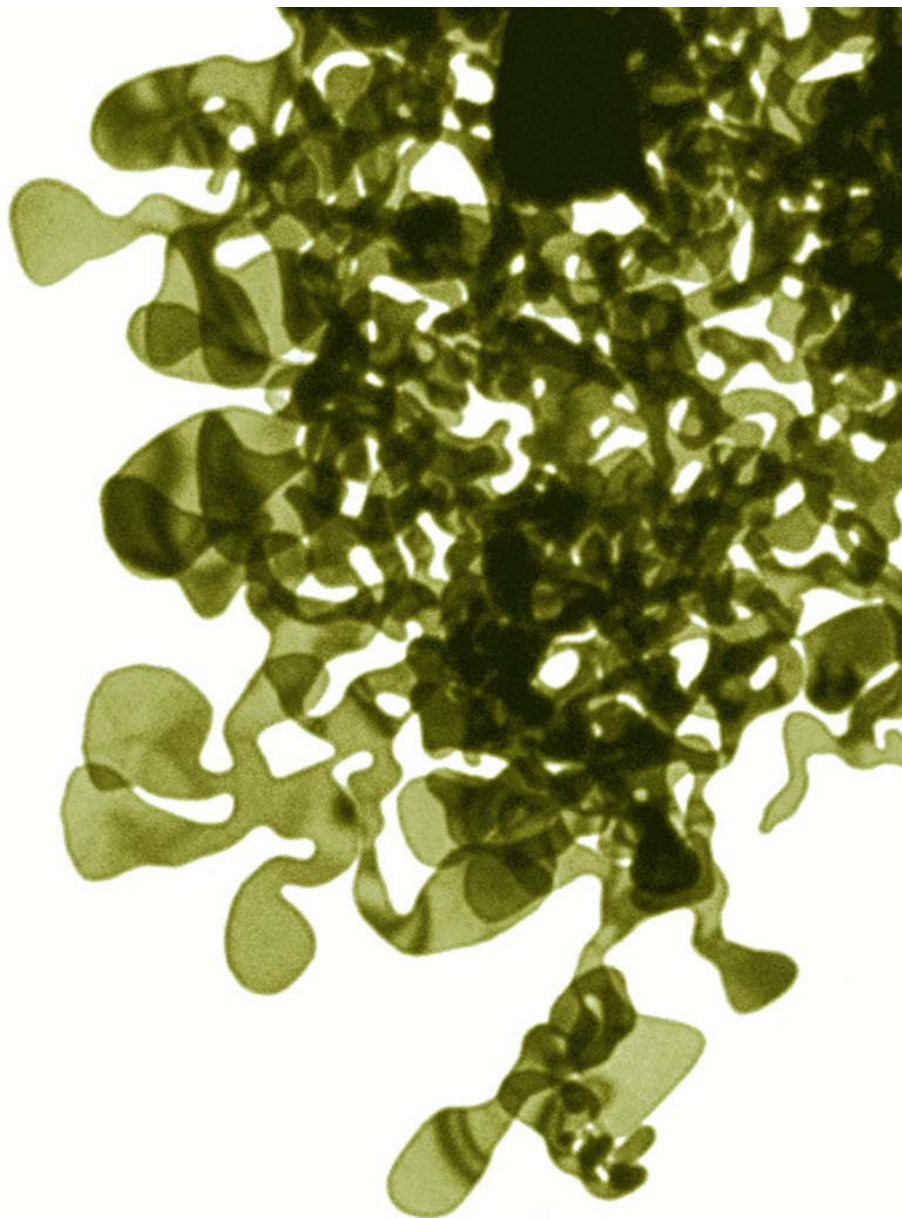
¹ Department of Molecular Nanoscience and Organic Materials, Institut de Ciència de Materials de Barcelona (CSIC), Bellaterra, 08193 Barcelona, Spain

² CIBER de Bioingeniería, Biomateriales y Nanomedicina (CIBER-BBN),

Bellaterra, 08193 Barcelona, Spain

ventosa@icmab.es





NANOGAP
SUBNANOPARTICLES

Are you looking for **Nanoparticles?**

NANOGAP's customized nanoparticles,
on an industrial production basis, will
help you to be innovative and unique.
Your success is our success.

Metallic Nanoparticles
Magnetic Nanoparticles
Atomic Quantum Clusters (AQC_s)

T. +34 981523897
info@nanogap.es
www.nanogap.es

Nanogap is a spin-off from the USC research group 'NANOMAG', with more than 250 publications and several patents. Our cutting edge nanoscience knowledge led to the development of our products, which includes a novel technology to produce subnanoparticles (AQC_s)